TD

Anticancer prodrug nanoscale platform using low-generation dendrimers and/or platinum derivatives

Synthesis, cytotoxicity, and synergetic effects

DOCTORAL THESIS

Cláudia Sofia Camacho
DOCTORATE IN CHEMISTRY

UNIVERSIDADE da MADEIRA
A Nossa Universidade
www.uma.pt

October | 2021

Cofinanciado por:

MADEIRA 14-20 · REGIÃO AUTÓNOMA DA MADEIRA · PORTUGAL 2020 · UNIÃO EUROPEIA Fundo Social Europeu · arditi

Anticancer prodrug nanoscale platform using low-generation dendrimers and/or platinum derivatives

Synthesis, cytotoxicity, and synergetic effects

DOCTORAL THESIS

Cláudia Sofia Camacho
DOCTORATE IN CHEMISTRY

ORIENTATION
João Manuel Cunha Rodrigues

CO-ORIENTATION
Helena Maria Pires Gaspar Tomás

Anticancer prodrug nanoscale platform using low-generation dendrimers and/or platinum derivatives – Synthesis, cytotoxicity and synergetic effects

A thesis presented to the University of Madeira to obtain the Doctoral degree in Chemistry

Cláudia Sofia Camacho

Under the supervision of:
Doctor (PhD) João Manuel Cunha Rodrigues
Doctor (PhD) Helena Maria Pires Gaspar Tomás

Faculdade de Ciências Exactas e da Engenharia
Centro de Química da Madeira
Funchal, Portugal

October 2021

The work presented in this dissertation was performed in the Centro de Química da Madeira (CQM), at the Molecular Materials Research Group (MMRG), University of Madeira under the scope of the PD-F FCT PhD Programmes (Doctoral Program in Nuclear Magnetic Resonance Applied to Chemistry, Materials and Biosciences (PTNMR PhD), supported by ARDITI - Agência Regional para o Desenvolvimento da Investigação, Tecnologia e Inovação through the PhD grant M1420-09-5369-FSE-000001. The support of PROEQUIPRAM - Reforço do Investimento em Equipamentos e Infraestruturas Científicas na RAM (M1420-01-0145-FEDER-000008), project M1420-01-0145-FEDER-000005-CQM^{+} (Madeira 14-20 Program), and FCT-Fundação para a Ciência e a Tecnologia throught the CQM Projects: UID/QUI/00674/2015, Pest-OE/QUI/UI0674/2019. Base Fund UIDB/00674/2020 and Programmatic Fund UIDP/00674/2020, were also acknowledged.

Acknowledgments

Many people have supported me along this path, and without which I could not have achieved this lifetime milestone.

As so, I would like to express my sincere appreciation and gratitude to my supervisor Prof. Dr. João Rodrigues, for his guidance, constant support, motivation, and patience, for sharing knowledge, constructive criticism, and suggestions, and for his availability to help with all the doubts that emerged in the course of this project. Without his support, I would not have gotten this far.

My co-supervisor, Prof. Dr. Helena Tomás, for all the support, encouragement, criticism, and suggestions given during the project's development.

To Prof. Dr. Fernando Lahoz and his group (Departamento de Física, IUdEA, Universidad de La Laguna, Tenerife, Spain) for the photoluminescence and time-resolved fluorescence experiments of the APS-treated and non-treated PAMAM dendrimers and the biological assays related to the visualization of the APS-treated PAMAM dendrimers in cells.

Also, I am very grateful to *Centro de Química da Madeira (CQM)* for all the opportunities and for making me grow as a researcher and person.

The laboratory technicians of the Chemistry Department (University of Madeira, Portugal), Paula Vieira, and particularly Paula Andrade, for the friendship and the support in the difficult moments, being always there for me. Furthermore, for the help provided with laboratory supplies and reagents.

To Dr. Marijana Petkovic (CQM, University of Madeira, Portugal) for helping me with MALDI TOF experiments and analysis.

I want to thank my colleagues at CQM, principally at the Molecular Materials Research Group (MMRG), for their help, support and for making the lab a pleasant place to work. I will remember each of you.

To my colleagues and friends, Dina Maciel, Carla Alves, Nádia Nunes, Mara Gonçalves, Rita Castro, Nilsa Oliveira, Ana Olival and Tomásia Fernandes for their friendship, encouragement and support. To Dina Maciel, Nádia Nunes, Duarte Fernandes, and Lydia dos Órfãos for our fruitful conversations, stimulating discussions, and great ideas. Especially to Dina Maciel, for all the support, help, companionship, understanding, and all the fun we had in the past four years.

My thanks are also extended to ARDITI - Agência Regional para o Desenvolvimento da Investigação, Tecnologia e Inovação through the project M1420-09-5369-FSE-000001 – PhD Grant for the financial support.

Finally, I would like to thank my family, especially my parents and sister, for all their love, unconditional support, encouragement, and sacrifices made to get me here. Last but not least, the love of my life, for your unconditional support, companionship, for being there in difficult times, tireless patience, and encouragement in all the ups and downs of this period of my life. I have no words to express my eternal gratitude.

A heartfelt thanks to you all!

Resumo

Os compostos de platina entraram em uso clínico, há mais de 40 anos, com a aprovação da cisplatina, permanecendo ainda hoje, e apesar dos progressos da medicina e do conhecimento, como uma das classes de medicamentos anticancerígenos mais usados na clínica. Contudo, as abordagens no uso dos medicamentos à base de platina para o tratamento dos diferentes tipos de cancro carecem de melhoramento. Neste projeto de doutoramento descreve-se o desenvolvimento de uma nova família de metalodendrímeros, baseados em dendrímeros aniónicos de poli(amidoamina) (PAMAM), funcionalizados na sua superfície com cisplatina e 1,2-ciclohexanodiaminaplatina explorando-se o seu potencial como plataforma de entrega de fármacos em diferentes tipos de cancro. O fármaco 5-fluorouracilo foi posteriormente encapsulado nos metalodendrímeros preparados com o objectivo de melhorar a sua eficácia, e avaliar o eventual efeito sinérgico. Igualmente foram desenvolvidos estudos para aumentar a fluorescência intrínseca dos dendrímeros PAMAM com terminações amina, através da oxidação com persulfato de amónio. Além disso ensaiou-se também o encapsulamento da doxorrubicina, um conhecido fármaco para o tratamento de vários tipos de cancro. No primeiro capítulo é apresentado o estado de arte dos sistemas de entrega de fármacos, particularmente os dendrímeros e o seu uso como agentes anticancerígenos. Neste capítulo apresentam-se igualmente, os diferentes compostos de platina usados na terapia dos vários tipos de cancro. O segundo capítulo baseia-se na síntese e caracterização de dendrímeros aniónicos PAMAM, coordenados com cisplatina nas formas mono e bidentada, e no estudo do seu potencial como fármacos anticancerígenos em várias linhas celulares cancerígenas. Estes compostos foram também estudados quanto à sua biocompatibilidade face às células de sangue humano e avaliada a ligação ao ADN. Nos metalodendrímeros mais promissores foi encapsulado o 5-fluorouracilo para estudar o efeito sinérgico do fármaco. No terceiro capítulo, os dendrímeros aniónicos foram coordenados com o 1,2-ciclohexanodiaminaplatina e testados em diferentes tipos de cancro. Foram ainda avaliados a ligação ao ADN e a hematoxicidade. O 5-fluorouracilo foi encapsulado no metalodendrímero mais eficaz e, o seu potencial anticancerígeno e possível efeito sinérgico avaliado. No quarto capítulo, três gerações de dendrímeros PAMAM com terminações amina foram oxidados com persulfato de amónio e as suas propriedades fluorescentes, citotoxicidade e hematoxicidade estudadas. A terminar, no quinto capítulo, apresentam-se as conclusões mais importantes e as perspectivas futuras.

Palavras-chave: Dendrímeros PAMAM, cisplatina, 1,2-ciclohexanodiaminoplatina, metalodendrímeros, fluorescência, anticancerígeno.

Abstract

Platinum compounds entered the clinic more than 40 years ago with the approval of cisplatin and remain today among the most widely used anticancer drugs, despite the progress of medicine and the knowledge in the field. Nonetheless, the approaches to the use of platinum-based drugs need to be improved.

This Ph.D. project describes the development of a new family of metallodendrimers based on anionic poly(amidoamine) (PAMAM) dendrimers functionalized on their surface with platinum drugs like cisplatin and 1,2-cyclohexanediamineplatinum (DACHPt). Their potential as an effective drug delivery platform was evaluated against different types of cancer. Furthermore, the chemotherapeutic drug 5-Fluorouracil (5-FU) was encapsulated within the metallodendrimers to study the synergetic effect of the combined drugs. The enhancement of the blue intrinsic fluorescence of amine-terminated PAMAM dendrimers was explored by using an oxidative treatment with ammonium persulfate (APS). The chemotherapeutic agent doxorubicin (DOX) was encapsulated in the prepared dendrimers, and the system was studied for bioimaging and as an anticancer drug. The first chapter elucidates the state of the art of drug delivery systems, particularly the dendrimers and their use as anticancer agents. The current state-of-the-art platinum drugs for cancer therapy were also revised in this chapter. The second chapter, which relies on the synthesis and characterization of anionic PAMAM dendrimers coordinated with cisplatin in mono and bidentate forms, and their potential as anticancer drugs was evaluated against various cancer cell lines. The biocompatibility with human blood cells and DNA binding were also studied. The most promising metallodendrimers as anticancer drugs were encapsulated with the 5-FU to evaluate the potential synergetic effect. In the third chapter, the anionic PAMAM dendrimers were coordinated with DACHPt and tested in several cancer cell lines. Biological studies such as DNA binding and hematoxicity were also assessed. Finally, 5-FU was encapsulated in the best metallodendrimer, and their anticancer potential through a possible synergetic effect of both drugs was studied. In the fourth chapter, three generations of amine-terminated PAMAM dendrimers were oxidized with APS, their fluorescence properties evaluated, and their cytotoxicity and hematoxicity. The fifth chapter focuses on the main conclusions and the future perspectives of the work achieved.

Keywords: PAMAM dendrimers, cisplatin, 1,2-diaminocyclohexanedichloroplatinum(II), metallodendrimers, fluorescence, anticancer.

List of publications

Papers

- Related to this thesis

- Camacho, C.; Tomás, H.; Rodrigues, J. Use of Half-Generation PAMAM Dendrimers (G0.5–G3.5) with Carboxylate End-Groups to Improve the DACHPtCl_2 and 5-FU Efficacy as Anticancer Drugs. *Molecules*, **2021**, 26, 2924. https://doi.org/10.3390/molecules26102924
- Camacho, C. S.; Urgellés, M.; Tomás, H.; Lahoz, F.; Rodrigues, J. New insights into the blue intrinsic fluorescence of oxidized PAMAM dendrimers considering their use as bionanomaterials. *J. Mater. Chem. B.* **2020**, 8, 10314-10326. https://doi.org/10.1039/D0TB01871F

Oral presentations

- Related to this thesis

- International conferences

- C. S. Camacho, H. Tomás, J. Rodrigues. PAMAM Dendrimers as nanocarriers for Platinum anticancer complexes. 11th International Dendrimers Symposium held in Funchal, Madeira (Portugal), from 14 – 18 of July, YSC2, page 88, 2019.
- C. S. Camacho, H. Tomás, J. Rodrigues. Platinated low-generation of PAMAM dendrimers as drug delivery vehicles for cancer treatment. MAD-Nano18: Madeira International Conference on Emerging Trends and Future of Nanomaterials for Human Health held in Funchal, Madeira (Portugal), 30 November to 2 of December, OC8, page 46, 2018.
- C. S. Camacho, H. Tomás, J. Rodrigues. The challenge of designing powerful platinum-based prodrugs based on PAMAM dendrimers as anticancer agents. Biodendrimer 2018: 6th International Symposium on Biomedical Applications of Dendrimers, Urbino, Italy, June 4-7, 2018.
- C.S. Camacho, M. Urgellés, H. Tomás, F. Lahoz, J. Rodrigues. The Blue Fluorescence of PAMAM Dendrimers: Chemical, Biological, and Optical Studies. University of Donghua, Shanghai, China; 26 of June, 2017. (Invited lecture)
- C.S.Camacho, M. Urgellés, H. Tomás, F. Lahoz, J. Rodrigues. The fascinating intrinsic blue fluorescence of PAMAM dendrimers and their biomedical applications. HYMA -5th International Conference on Multifunctional, Hybrid and Nanomaterials, 6-10 March 2017, Lisbon, Portugal.

- ***National conferences***

- C. S. Camacho, H. Tomás, J. Rodrigues. PAMAM dendrimers- a strategy to improve the efficacy of 1,2-diaminocyclohexane platinum(II). 7th CQM Annual Meeting at the University of Madeira, 21-22 of September 2020.
- C. S. Camacho, H. Tomás, J. Rodrigues. Cisplatin the powerful anticancer drug - An improvement using anionic PAMAM dendrimers. 6th CQM Annual Meeting held in Porto Moniz, Madeira (Portugal), from 26 - 27 of April, O25, page 43, 2019.
- C. S. Camacho, H. Tomás, J. Rodrigues. Low generation of metallodendrimers as prodrugs for cancer treatment. Encontro com a Ciência e a Tecnologia em Portugal - Ciência 2018, Lisbon, Portugal: July 2-4, 2018.
- C. S. Camacho, H. Tomás, J. Rodrigues. Low generation of metallodendrimers as anticancer agents-synthesis and characterization by using NMR (^{1}H, ^{13}C, HSQC, and ^{195}Pt). 18-VIII Ibero-American NMR meeting, Lisbon-Portugal, 26-29 of June 2018.
- C. S. Camacho, M. Urgellés, H. Tomás, F. Lahoz, J. Rodrigues. The Blue autofluorescence behavior of three generations of PAMAM dendrimers. 5th CQM Annual Meeting at the University of Madeira, 1-3 of February 2018.
- C. S. Camacho, H. Tomás, J. Rodrigues. Anticancer Prodrugs of Low-generation Metallodendrimers. 4nd CQM Annual Meeting at the University of Madeira, 3-4 of February 2017.

- Related work

- J. Rodrigues, N. Nunes, C. Camacho, D. Maciel, H. Tomás. Metallodendrimers - A Route for New Anticancer Candidates. ICAFPM2019 - The 9th International Conference on Advanced Fibers and Polymer Materials, November 19-23, Shanghai, China, 2019. (Invited lecture).
- D. Maciel, C. Camacho, N. Nunes N., M.A. Muñoz-Fernández, H. Tomás, J. Rodrigues. Metallodendrimers as Anticancer and Antiviral Drug Candidates. IDS10 – 10th International Dendrimer Symposium, Weihai, China, August 5-9, 2017. (Invited lecture) (Biological medicine/Nanodrug Section, Abstract book, page 32).

Poster presentations

- Related to this thesis

- C. S. Camacho, H. Tomás and J. Rodrigues. Improving DACHPt activity by using low generations of anionic PAMAM dendrimers. 2nd International Workshop on Advanced Materials for Healthcare Applications held in Funchal, Madeira (Portugal), 8 - 9 of October, PC18, page 58, 2019.
- Cláudia S. Camacho, M. Urgellés, H. Tomás, F. Lahoz, J. Rodrigues. Characterization of Photoluminiscent PAMAM Dendrimers for Biomedical Applications". 11th International Dendrimers Symposium held in Funchal, Madeira (Portugal), 14 – 18 of July, PC35, page 135, 2019.
- C. S. Camacho, H. Tomás and J. Rodrigues. Cisplatin combined with low generation dendrimers as an anticancer agent. First CA17140 Training School held at the University of Trieste in Trieste, Italy, 8 – 11 of April 2019.
- Cláudia S. Camacho, M. Urgellés, H. Tomás, F. Lahoz, J. Rodrigues. A Stunning intrinsic blue fluorescence from the exceptional class of dendrimers – PAMAM dendrimers. MAD-Nano18: Madeira International Conference on Emerging Trends and Future of Nanomaterials for Human Health held in Funchal, Madeira (Portugal), 30 November to 2 December, PC10, page 60, 2018.
- C. S. Camacho, M Urgellés, H. Tomás, F. Lahoz, J. Rodrigues. Cytocompatible Highly Fluorescent PAMAM Dendrimers for Biological Application. 6th China- Europe Symposium on Biomaterials in Regenerative Medicine CESB2017, Porto- Portugal, 21-24 of May 2017.

Seminars (Doctoral Programme in Nuclear Magnetic Resonance Applied to Chemistry, Materials, and Biosciences –PTNMR PhD*)*

- *Module I* - NMR course entitled "XII Manuel Rico NMR School", geRMN specialized nuclear magnetic resonance group, in Jaca (Huesca) from 18th to 23rd of June 2017.
- *Module II* - Elucidating Biomacromolecular Structure and Function from 18th - 22nd of December 2017, University Nova de Lisboa (FCT-UNL), Portugal.
- *Module IV* - Small Molecules, Drug Discovery and NMR in Industry with the Programme NMR in NMR Focus- NMR in health and disease: From Protein-Ligand Interactions to Small Molecules in Tissues from 7th -11th May of 2018, University of Coimbra, Portugal.
- Module V - Frontiers in NMR incorporated in the conference VIII Ibero-American NMR Meeting- 6th Iberian NMR Meeting- 9th GERMN Meeting- 4th Portuguese RNRMN Meeting from 26th- 29th June 2018, University Nova de Lisboa, Portugal.

Other work

- First CA17140 Training School: COST Action CA17140 “Cancer Nanomedicine from the bench to the bedside” held at the University of Trieste in Trieste, Italy 8- 11 of April 2019.
- Member of the organizing committee of “11th International Dendrimers Symposium” held in Funchal, Madeira (Portugal), 14-18 of July 2019.
- Member of the organizing committee of “MAD-Nano18: Madeira International Conference on Emerging Trends and Future of Nanomaterials for Human Health” held in Funchal, Madeira (Portugal), 30 November to 2 of December 2018.
- Volunteer in the “Portuguese League against Cancer (LPCC) National Peditory”, 31 October 2019.
- Participation in "A Química é Divertida" whose activities were held at the University of Madeira, Centro de Química da Madeira (CQM), 2017-2019.
- NMR Lab manager (from November 2018 until September 2020).

Abbreviations and symbols

A	Adenine
AA	Antibiotic-Antimycotic
ABC	ATP-binding cassette
AG	Alginate
AGT	Glutamyl cysteine synthase
APS	Ammonium persulfate
ATM	Ataxia telangiectasia-mutated
ATP	Adenosine triphosphate
ATP7A and ATP7B	ATP-dependent copper transporters
ATR	Ataxia telangiectasia and RAD3-related
AuDENPs	Gold nanoparticles entrapped in dendrimers
AuNPs	Gold nanoparticles
a.u.	Arbitrary units
A2780	Human ovarian cancer cell line
A2780cis	Resistant-human ovarian cancer cell line
Bcl2	B-cell lymphoma 2
Bis-MPA	2,2-bis(hydroxymethyl)propionic acid
BJ	Normal human fibroblast cell line
C	Cytosine
CACO-2	Human epithelial colorectal adenocarcinoma cell line
CAM-DR	Cell adhesion-mediated drug resistance
Cal-72	Human osteosarcoma epithelial cell line
ChK1 and CHK2	Checkpoints kinases 1 and 2
CH_2THF	5,10-methylenetetrahydrofolate
CMC	Critical micellar concentration
CT-DNA	Calf-thymus DNA
CTLs	Cytotoxic T cells
CTR	Copper transporter
CuAAC	Copper-(I)-catalyzed alkyne-azide cycloaddition
Cys	Cystamine
d	Doublet (NMR)
DACH	1,2-diaminocyclohexane
DACHPt	1,2-(diaminocyclohexane)platinum II
$DACHPtCl_2$	1,2-diaminocyclohexanedichloroplatinum(II)
DAPI	4-6-diamino-2-phenyindole
DISC	Death-inducing signaling complex
D-MEM	Dulbecco's modified eagle's medium
DMPM	Diffuse malignant pleural mesothelioma
DMSO	Dimethylsulfoxide
DNA	Deoxyribonucleic acid
dNTP	Deoxynucleotide
DOX	Doxorubicin
D_2O	Deuterated water
DPD	Dihydropyrimidine dehydrogenase
dTMP	Deoxythymidine
dThdPase	Thymidine phosphorylase
dTTP	Deoxythymidine triphosphate
dUMP	Deoxyuridine monophosphate
DWCNTs	Double-Walled carbon nanotubes
EDA	Ethylenediamine
EPR	Enhanced permeability and retention effect

Eq	Equivalent
ER	Endoplasmatic reticulum
ESI	Electrospray ionization
FADD	Fas associated death domain
FasL	Fas ligand
FBAL	Alpha-fluoro-betha-alanine
FBS	Fetal bovine serum
FDA	Food and drug administration
FdUDP and FdUMP	Fluorodeoxyuridine diphosphate and Fluorodeoxyuridine monophosphate
FdUTP	Fluorodeoxyuridine triphosphate
FID	Free induction decay
FTIR	Fourier-transform infrared spectroscopy
5-FU	5-Fluorouracil
FUDP	Fluorouridine diphosphate
FUDR	Fluorodeoxyuridine
FUMP	Fluorouridine monophosphate
FUTP	Fluorouridine triphosphate
FUR	Fluorouridine
G	Guanine
GEM	Gemcitabine
GEJ	Metastatic or unresectable gastric or gastroesophageal junction
GHFU	Dihydrofluoroutacil
GSH	Glutathione-mediated export
GST	Glutathione-S-transferase
GS-X	Glutathione S-conjugate export
HASLs	Hetero-atomic sub-luminophores
Hb	Hemoglobin
HEPES	(4-(2-hydroxyethyl)-1-piperazineethanesulfonic acid)
HMG	High-mobility group
HPMA	Hydroxyl propylmethacrylamide copolymer
HSA	Human serum albumin
HSF	Hand foot syndrome
IC_{50}	Half maximal inhibitory concentration
IG1	Insulin-like growth factor 1
IONPs	Magnetic iron oxide nanoparticles
IRF	Instrumental response function
JNK	C-Jun N-terminal kinases
LC	Loading capacity
LE	Loading efficiency
LUV	Large uni-lamellar
LTLD	Lysothermosensitive liposomal doxorubicin
m	Multiplet (NMR)
MALDI	Matrix-assisted lase desorption/ionization
MCF-7	Human breast cancer cell line
MCM-41	Mobil Composite Matter number 41
MCM-48	Mobil Composite Matter number 48
MDR	Multiple drugs resistance
MEM	Minimum essential medium
MMR	Mismatch repair protein
MNP	Magnetic nanoparticles
MPT	Mitochondrial membrane permeability transition
MRI	Magnetic resonance imaging
MRPs	Multidrug resistance-associated proteins
mRNA	RNA messenger
MS	Mass spectrometry

MSNs	Mesoporous silica nanoparticles
mtDNA	Mitochondrial DNA
MTD	Maximum tolerated dose
MTT	(3-(4,5-dimethylthiazol-2-yl)-2,5-diphyltetrazolium bromide)
MTX	Metrotrexate
MW	Molecular weight
MWCNTs	Multi-walled carbon nanotubes
NER	Nucleotide excision repair
Neya	Non essential amino acid
NIH 3T3	Mouse fibroblast cell line
NIR	Near infrared spectroscopy
NMR	Nuclear magnetic resonance
NSCLC	Non-small cell lung cancer
NTIL	Non-traditional intrinsic luminescence
OCT	Organic cation transporter
OPRT	Orotate phosphoribosyltransferase
PACA	Poly-alkyl-cyanoacrylates
PAMAM	Poly(amidoamine) dendrimer family
PAMAMOS	Poly(amidoamine-organosilicon) dendrimer family
PBS	Phosphate buffered saline
PD	Pharmacodynamics
PDX	Pancreatic cancer-derived xenograft
PEG	Polyethylene glycol
PET	Positron-emitting
PEG-b-P(Glu)	Polyethylene glycol-poly(glutamic acid)
P(Glu)	Poly(glutamic acid)
PL	Photoluminescence
PLA	Polylactic
PLC	Polycaprolactone
PLGA	Poly(lactic-co-glycolic acid)
PNIPAAM	Poly(N-isopropyl acrylamide)
PPI	Poly(propylene imine) dendrimer family
PPCD	PEG-PAMAM-cis-aconityl-DOX conjugates
PTX	Paclitaxel
PK	Pharmacokinetics
RBC	Red blood cells
RES	Reticuloendothelial system
RF	Resistance factor
RGD	Arginylglycylaspartic acid
RNA	Ribonucleic acid
ROS	Reactive oxygen species
RP	Relative potency
RPMI	Roswell PARK Memorial Institute
s	Singlet (NMR)
SBA-15	Santa Barbara Amorphous number 15
SD	Standard deviation
SI	Selectivity index
SKOV-3	Ovarian carcinoma cells
SMMC-7721	Human hepatocellular carcinoma cell line
SPIONs	Superparamagnetic iron oxide nanoparticles
SUV	Small uni-lamellar
SWCNTs	Single-walled carbon nanotubes
T	Thymine
t	Triplet (NMR)
TBP	TATA binding protein

TLR4	Toll-like receptor 4
TOF-MS	Time of flight mass spectrometry
Tris-HCL	Tris(hydroxymethyl)aminoethane hydrochloride
TS	Thymidylate synthase
TK	Thymidine kinase
UGD	Uracil-DNA glycosylase
U2OS	Human bone osteosarcoma epithelial cell line
UP	Uridine phosphorylase
UPW	Ultrapure water
UrdPase	Uridine phosphorylase
UTP	Uridine triphosphate
UV-vis	Ultraviolet visible
UK	Uridine kinase
VEGF-C	Vascular endothelial growth factor
VSSA	Volume-specific surface area
XPS	X-ray photoelectron spectroscopy
δ	Chemical shift

Contents

Figure Index

Scheme Index

Table Index

CHAPTER I

Introduction

Introduction

In this chapter, a literature review on cancer and topics related, such as, different drug carriers and anticancer drugs will be presented and discussed. More attention will be given to dendrimers as delivery systems and platinum drugs already under use in the clinic to treat cancer.

1. Cancer

Cancer is a leading cause of mortality worldwide[1,2]. According to GLOBOCAN and the International Agency for Research on Cancer - World Health Organization (WHO), in 2020, it was estimated that this disease had caused 10 million deaths and 19.3 million new cases in the world[1]. In Portugal, 30.2 thousand people died, and 60.5 thousand new cases have emerged. Additionally, the three types of cancer with a higher incidence of mortality in Portugal were colorectal, breast, and prostate cancer[3]. Nowadays, cancer is responsible for 1 in 6 deaths, corresponding to more deaths than HIV/AIDS, tuberculosis, and malaria diseases. Reports on the field estimated that in 2040, the global cancer burden will reach 27.5 million new cases and 16.2 million deaths due to aging and population growth[4]. These facts indicate the severity and complexity of cancer. For that reason, new strategies are required to fight this disease.

1.1.Definition of cancer

Cancer is classified as a group of diseases where an abnormal and uncontrolled growth of cells occurs in the body. It is a process that involves multiple stages (Figure 1) in which genetic mutations lead to disturbances in the regulation of cell division and differentiation, causing an imbalance in its proliferation and cell death. Since an abnormal cell cannot repair anomalies in its genetic material, DNA (Deoxyribonucleic acid), or can accept signals that normal cells use to stop dividing or begin a programmed cell death process, a process known as apoptosis[5–7]. For a normal life cycle, when cells become old/defective, they are replaced by cells as they are needed to keep the body healthy. Cancerous cells differ from healthy cells due to a lack of control in their growth, making them invasive. While healthy cells can acquire distinct specializations forming different types of cells, cancerous cells are less specialized, multiplying without stopping (Table 1). The result is that the abnormal growth of cells leads to the mass formation named tumor[5–8]. There are two types of tumors, benign and malignant. Malignant tumors are called carcinogens because they can spread in the body through the blood, lymphatic system, or invading tissues close to them, forming new tumors named metastases[5–9]. When a tumor grows, angiogenic factors (e.g., vascular endothelial growth factor (VEGF)) are synthesized and secreted to induce the formation of a complex blood vessel system. Later, the lymphatic vessels would also extend from host tissues to the tumor, where the tumor also induces the growth of lymphatic vessels (lymphangiogenesis)[10–14].

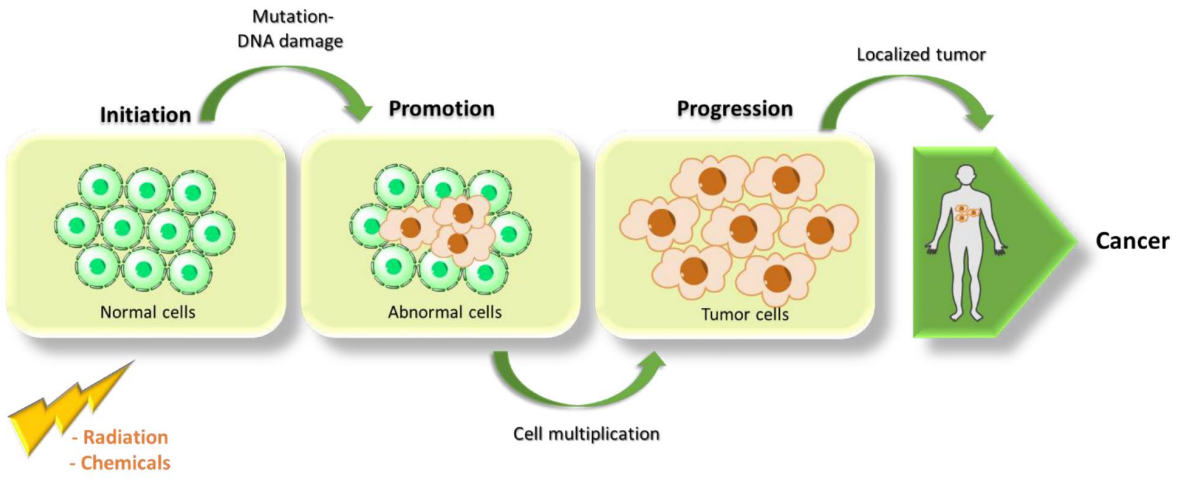

Figure 1: Process of cancer development.

In the initial stage of metastasis, cancer cells spread in the lymphatic circulation. They have a greater probability of survival since the lymphatic capillaries have a slightly larger diameter than the blood capillaries, and the composition of the lymphatic fluid is similar to the tissue fluid. The lymphatic capillaries have a thin wall of lymphatic vascular endothelial cells with weak links between them than blood cells and greater permeability, which is the most common route for the transendothelial migration of cancer cells[10,15,16]. On the other hand, metastasis is also considered a major route to other distant organs, as they can express different receptors to bind to proteins, platelets, red blood cells to prevent the immune system. Although less than 0.01% of cancer cells that enter the bloodstream can form metastases, those that survive are in the capillary beds of the organs and then invade it by extravasation (movement of cells from a blood vessel to tissue). Afterwards, if cancer cells adapt to the new host's microenvironment, they can form new metastases with different biological characteristics than the primary tumors. The most common destinations for metastases are the liver, brain, bones, and lungs. For this reason, it is more challenging to treat metastases than benign tumors. Although, it is important to emphasize that less than 0.1% of cancer cells that enter the bloodstream only survive 24 hours[10]. While benign tumors do not spread or travel to other parts of the body, they can usually be removed without growing back. They grow slowly and in a well-defined area. However, they can be lethal in some cases, depending on where they grow, as they can cause compression on other organs. Nevertheless, some cancers do not form solid tumors, such as hematological cancers in which cancer cells circulate through the body. Cancer cells can influence the environment surrounding them, known as microenvironments, such as cells, blood vessels, fibroblasts, molecules, and other surrounding structures, so that they provide nutrients and oxygen necessary for their growth. They can also avoid the immune system, responsible for eliminating abnormal/damaged cells, protecting the body against infections, and use the immune system to grow and prevent their death[5,6,8].

Usually, the cancer types are classified depending on the body part and tissue where the tumor begins[5].

Table 1*:* Principal differences between normal and cancer cells. Adapted from reference[8].

Normal cells	Cancer cells
Mortal	**Immortal**
Regular, small and uniform shape.	Irregular, large and variable shape.
Single and small nucleus.	Multiple and large nucleus.
Integrity genome.	Lack of integrity genome with multiple mutations.
Growth and proliferation in control.	Non-controllable growth and proliferation.
Normal cell function.	Lose some/all diferenciated functions of their parente cell.
Blood supply- Angiogenesis during repair.	Blood supply- tumor angiogenesis.
Normal polar surface with regular receptors.	Lose polarity, over expression of some proteins/receptors as markers.
Intracellular pH: ~ 7.2 and extracelular pH:~ 7.4.	Higher intracelular pH: >7.4 and lower extracelular pH: ~ 6.7-7.1.
Nutrient source: Glucose.	Nutriente source: Fat, Serine, Ketone, Glycine, Glucose, among others.

1.1. Causes

Cancer is caused by a mutation in the genes of cells essential for their cellular function. These genetic alterations can be due to internal and/or external factors that can act together or in sequence to promote cancer[4,5,7]. External factors include tobacco, alcohol consumption, overweight, physical inactivity, unhealthy diet, ultraviolet radiation (like sun exposure), and infectious microorganisms that can transform cells or cause chronic inflammation. As for internal factors, there are hereditary genetic mutations, hormones, and immunological conditions. Cancer can thus develop during a person's life (increasing the cancer probability with age) due to genetic errors or environmental exposures[4,5,7].

1.2. Treatments

Over the years, there has been a remarkable progression in understanding cancer mechanisms, diagnosis, and therapy, leading to significant advances in its treatment. However, cancer still remains a complicated disease to prevent and treat due to its complexity. It is a disease that evolves and progresses over time and can affect any body part, making its treatment a challenge[5–8,17,18]. Regarding treatment, there are three main processes: surgery (for the role of surgery in triggering metastases, see the interesting review by Samer Tohme *et al.*[19]),

radiation, and chemotherapy. Surgery is used to remove tumors that are well defined as well as radiation. Radiation is a localized therapy, which acts essentially on cancerous tissues, minimizing the death of normal cells by damaging the cell's DNA, blocking their cell cycle, that is, their capacity for cell division and proliferation, ultimately leading to their death[5,7,8,17,18]. These two treatments are effective only for local and non-metastatic cancers[8,20]. On the other hand, chemotherapy is used mainly to treat metastatic cancers and as an adjunctive treatment to surgery and radiotherapy as it can reach all body organs through the bloodstream[5,7,8,17,18].

Chemotherapy is based on the use of drugs that inhibit the proliferation and regeneration of cells with a high capacity to reproduce, such as cells in the skin, hair, bone marrow, and epithelium gastrointestinal tract cells. The inhibition of cancer cells and other normal cells with this high replication capacity causes high undesirable effects in the treatment due to its high risk of toxicity. The effectiveness of drugs is often limited by the low concentration that reaches the therapeutic site since the rest of the medication also goes to other parts of the body. For this reason, the doses administered cannot be high as they reach healthy organs/tissues. Besides, other complications can also occur in the long term, such as pathologies like cardiotoxicity, neurotoxicity, nephropathy, infertility, chronic liver damage, and drug resistance. However, when a treatment is not possible, chemotherapy is used to prevent the progression of the disease or, in terminal cases, to relieve symptoms and improve the quality of life of patients[5,6,8,17,18]. Nonetheless, other treatments have appeared over time to minimize the suffering and death of cancer patients, such as photodynamic therapy, photothermal therapy, drug therapy with nanoparticles, and gene therapy[6,8].

Photodynamic therapy is a non-invasive treatment in which cancer cells are destroyed by a photosensitizing drug activated by specific wavelengths of light[8]. On photothermal therapy, cancer cells are damaged by heat through a photothermal agent activated by light that causes irreversible cell damage and consequently cells death. Despite being more selective for cancer cells once they tolerate light heat, this method is limited because it causes damage to the surrounding healthy tissues. However, non-toxic photothermal agents have recently been used to decrease this unwanted effect with the ability to absorb light and convert it to heat. Being biocompatible, photostable, and with close infrared absorption[8].

Drug therapy with nanoparticles consists of using a carrier to transport the drug or, acting as a drug herself, targeting cancer cells more accurately and reducing the toxicity effect on normal tissues. This therapy maximizes the drug quantity to be transported, thus increasing its bioavailability in the desired location, stability, and efficiency, contrary to systems that only transport a single drug molecule[6,8].

Gene therapy constitutes three different methodologies: immunotherapy, gene transfer, and oncolytic virotherapy that uses genetic materials capable of modifying cancer cells or stimulating immune cells through their suppression[6,8]. Immunotherapy uses cellular debris or viral vectors that stimulate the immune system to destroy cancer cells. For this, vaccines, lymphocytes, cytokines, and monoclonal antibodies are used to improve the effectiveness[6,8].

Gene transfer is another cancer treatment method that introduces new genes into cancer cells to suppress cell proliferation and promote cell death. However, this method presents some controversy and concerns regarding the potential contamination of healthy cells and the exact insertion of genes into the correct location[8].
In contrast, oncolytic virotherapy uses viral conjugates incorporated into the genome of cancer cells, causing cell lysis as the virus spreads or by inducing the expression of some toxic proteins. This therapy minimizes the toxic effects on healthy tissues. However, this method has disadvantages, among which many gaps still need to be overcome concerning its clinical application, like its safety and the unpredictable side effects that make this methodology expensive[8].

1.3. Cancer nanomedicine

Currently, cancer treatment methods such as surgery, radiation, and chemotherapy, despite being widely used, show limitations due to the complexity and heterogeneity of the disease[17,18,21]. Thus, nanomedicine for cancer has emerged as a promising approach to achieving a better response in diagnosing and treating cancer. As the name suggests, nanomedicine uses nanoscale tools to diagnose better, prevent, and treat cancer. It consists of using delivery systems known as nanocarriers, nanodrugs, or nanotherapeutics that aim to improve the therapy efficiency of existing chemotherapeutic agents by combining them with a nanoscale delivery system[17,18,21–23]. However, there are still gaps in the scientific knowledge of these nanomaterials, such as their long-term effects and their safety. Therefore, the nanotherapeutic approach leads to inadequate protocols for increasing production, creating barriers to public acceptance, investors, and commercial approval. Hence, nanomedicine remains a challenge[21,22].

2. Drug delivery systems

Drug delivery systems targeted cancer nanomedicine is an important field as it aims to improve treatment by increasing its effectiveness and reducing side effects since it has tumor specificity compared to conventional chemotherapeutic drugs. The ideal drug delivery system must have a set of features such as stability, present a long-circulating half-life in the bloodstream and low premature release of the drug; go undetected so as not to be captured by the reticuloendothelial system (RES); accumulate inside the tumor either by passive or active targeting; having the ability to cross the blood vessel and tumor stroma barriers; be able to release the drug at the desired location within the cells, improve problems of solubility and stability of the drugs, reduce the drug resistance and be biocompatible and biodegradable. In this way, a drug delivery system not only protects against drug degradation but can cross the biological barrier to deliver the drug to a specific location (the therapeutic target)[24,25]. Indeed, a diverse variety of nanocarriers, including organic and inorganic materials based, has been explored in recent times[10,22,26]

2.1. Nanocarriers for cancer

The improvement of nanotechnology has led to the development of new nanomaterials with excellent properties for cancer therapeutic and diagnostic applications[17,27,28]. Nanomaterials are known for their nanoscale dimension in the range of 1 to 100 nm, making them an ideal system for delivering anticancer drugs[17]. In this sense, when nanomaterials are used to transport other drugs, they are known as nanocarriers[29]. Nanocarriers have then been used to overcome the problems associated with conventional drug delivery systems. As conventional nanocarriers cannot transport and release the drug in the desired location, with the desired concentration, and under either internal or external stimulation, being necessary to functionalize them with the required characteristics[29]. So, nanocarriers are systems of a nanometric scale capable of transporting anticancer drugs such as low molecular weight drugs or macromolecules, including proteins or genes, allowing these agents to avoid healthy tissues and accumulate in tumor tissues in higher concentration[5,6,8,17,26]. In fact, they improve the performance of anticancer drugs concerning safety, specificity, and bioavailability, taking advantage of the properties of the nanoscale range. These drugs can be transported by nanosystems via covalent bonding to the surface of the nanomaterial either by degradable bonds or nondegradable bonds, adsorption, or physical entrapment. The physical-chemical properties of nanocarriers are fundamental in the interactions between the nanomaterial and the environment found during the treatment. Thus, in addition to size being an important factor for internalization into tumor tissue, the shape and characteristics of the surface must be adjustable to allow for better system efficiency and lower toxicity[5,6,8,17,21,26].

As stated before, angiogenesis in cancer induces new tumor blood vessels, typically with irregular forms and architectures, which leads to increased permeability, EPR effect (enhanced permeability and retention effect), and also due to the poor lymphatic drainage of the tumor allows passive accumulation of nanocarriers into tumor tissues with the release of the chemotherapeutic drugs near on the tumor[30–36]. Thus, as previously mentioned, nanocarriers must have certain characteristics. They must have an extended circulation half-life to reach the tumor and avoid the action of the mononuclear phagocytic system, also named the reticuloendothelial system, to release the drug subsequently[5,6,21–23]. Therefore, the nanocarrier size should not be greater than 400 nm, and to escape the immune system and reach the extravasation in tumors by the ERP effect size should be below 200 nm. So, very small particles can extravasate into the surrounding normal tissue, which leads to less specificity, and very large particles tend not to extravasate, as their diffusion is difficult and as the tumor is not homogeneous, its accumulation will not be the same[5,6,21]. Furthermore, the surface of the nanocarriers must be hydrophilic and neutral or slightly anionic to avoid plasma proteins and delay the attack of macrophages. The surface camouflage can also be carried out with the help of hydrophilic polymers such as polyethylene glycol (PEG) or with amphiphilic polymers such as synthetic copolymers of polyethylene oxide (hydrophilic part) and propylene oxide (hydrophobic part). Besides, the surface of blood vessels and cells contains negatively charged components that can repel nanocarriers with negative surfaces. Therefore, nanocarriers with slightly negative or positive surfaces charge should be used[5,6,37]. Nevertheless, once exposure of drugs to the tumor environment depends on many factors than those mentioned, it is also important to highlight the following:

- the type and size of the tumor, as well the anatomical localization, proliferation rate, and necrosis;
- the dense vasculature, the volume, the permeability, and its distribution relative to stromal, tumor cells, and blood flow;
- the architecture, composition, and rigidity of the matrix and the density of the stroma;
- the location and pressure gradients of the interstitial fluid between the tumors;
- the density, function, and lymphatic system location within and around the tumor and the function and number of macrophages[22].

The efficient delivery of nanomaterials occurs selectively with the intracellular accumulation in cancer cells through active, passive, and physical targeting, decreasing the toxicity in healthy tissues as desired and, in a way, overcoming the resistance mechanism of chemotherapeutics[17,21,23,29,38].

As stated before, it is, despite the controversy, commonly accepted that passive accumulation at the tumor site occurs through the EPR effect, which allows nanomaterials to penetrate the tumor and stay longer because of the leaky tumor vasculature and poor lymphatic drainage (Figure 2). In addition, the nanocarrier circulates in the bloodstream for a more extended period. Also, as they are nanometric in size, they can enter the cancer cells by other mechanisms of endocytosis, overcoming resistance mechanisms when compared to conventional chemotherapeutic drugs[17,21,23,29,37,39].

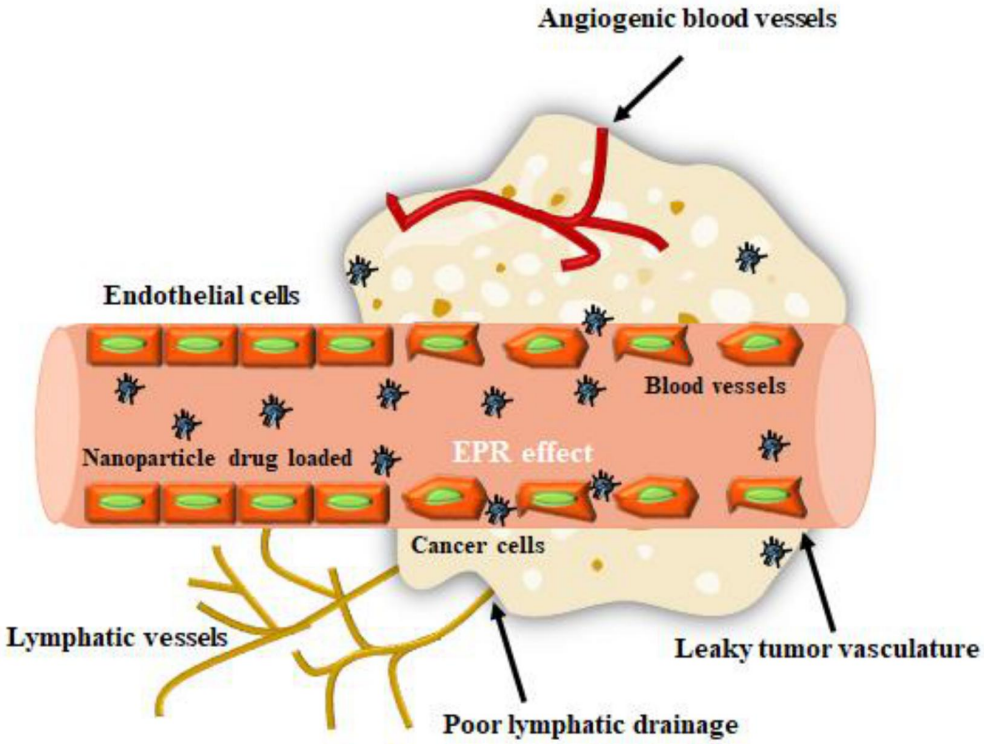

Figure 2: Representation of EPR effect in drug delivery. Adapted from reference[40].

The first nanosystem approved by the FDA (Food and Drug Administration) for cancer treatment was DOXil®/Caelyx® (with a size of 100 nm), pegylated injectable liposomes with encapsulated doxorubicin (anthracycline antibiotic with anticancer activity based on inhibition of topoisomerase II)[41], targeted against HIV-related Kaposi sarcoma tumor, and ovarian cancer. Another example is Abraxane® (size 130 nm), based on paclitaxel (a member of the taxane family of antimitotic agents) linked to albumin in the form of injectable nanospheres[17,21,23]. More recently, in 2017, FDA approved a nanoformulation of liposomal entrapped cytarabine – daunorubicin combination (CPX-351 Vyxeos™) that showed an increase in survival from 6 to 9.6 months for patients with acute myeloid leukemia when compared with the use of the free form of the drug[17]. Other nanosystems have been approved, which has opened new opportunities for cancer treatment[17]. However, the effectiveness of the used therapy is limited by the heterogeneity of the EPR effect seen within and between different tumors[17,42]. Therefore, non-uniform extravasation of nanoparticles may occur in the target area due to variable endothelial gaps resulting from the vigorous growth of tumor cells[17].

Active targeting consists of a ligand-mediated targeted approach that involves recognition by affinity, absorption, and/or retention by target cells. Chemical affinity is based on different specific molecular interactions such as receptor-ligand interactions, charge-based interactions, and facilitated motif-based interactions with substrate molecules[17,21,23]. The ligands can be biomolecules such as proteins, antibodies, nucleic acids, peptides, carbohydrates, and/or vitamins. The target substrates can be surface molecules expressed in proteins, sugars, or lipids present in organs, diseased cells, molecules present or secreted by cancer cells in the diseased cell microenvironment. This approach has been explored to increase the internalization of nanoparticles by the target cells and the effectiveness in drug delivery[17,21,23]. One example is the anti-HER2 targeting ligand moieties functionalized on the surface of the liposome, which has been found to increase the cellular uptake of nanoparticles in cancer cells expressing HER2, a cancer marker. In another example, insulin-like growth factor 1 (IG1) was synthesized and conjugated to magnetic iron oxide nanoparticles (IONPs) with doxorubicin as a therapeutic drug. After intravenous administration of this nanocarrier in the pancreatic cancer-derived xenograft (PDX) prototype, remarkable tumor targeting and internalization were observed. The location and internalization of these nanoparticles were determined using magnetic resonance imaging (MRI), with the nanosystem significantly inhibiting the growth of pancreatic PDX tumors[17,21,23].

The physical targeting or external forces can be used to improve the accumulation of anticancer drugs in tumor tissues. These external forces can be magnetic, heat, ultrasound, light waves, including near-infrared, ultraviolet, and visible. On the other hand, the accumulation of the drug can also be controlled by endogenous factors such as temperature, pH, and even the ROS (reactive oxygen species) of the tumor microenvironment[8]. The surface of magnetic nanoparticles (MNP) can be layered to produce multifunctional nanoparticles to diagnose and treat cancer. Moreover, these multifunctional nanoparticles can be designed to avoid the accumulation of drugs in healthy tissues. For example, MNP can be heated via a high-frequency magnetic field, inducing the death of cancer cells by thermal therapy[8]. Moreover, as the tumor microenvironment is slightly acidic, hypoxic, and mild hyperthermia, these factors can be considered in the previously mentioned therapeutic methods as nanosystems depending on their functionalization to respond to stimuli[8]. An example

of a nanocarrier for treating liver cancer, presently in a clinical trial, is the Lyso-thermosensitive liposomal doxorubicin (LTLD) with physical targeting by hyperthermia and ultrasound[8].

The nanocarriers used in cancer therapy are diversified as well as the anticancer drugs that can be used in the therapy independently or in conjunction with other drugs[6,8,26,29]. Cancer therapy using combinations of various drugs is another method used to minimize the toxic effects on healthy tissues and overcome the drug resistance mechanism[23].

2.1.1. Types of nanocarriers

Nanocarriers are structures that protect drugs from physiological phenomena and, in addition, provide a prolonged release of the drug due to their multivalent properties (Figure 3). The most common nanocarriers used for cancer treatment are liposomes, organic/inorganic nanoparticles (quantum dots, carbon nanotubes, gold nanoparticles, superparamagnetic iron oxides, and mesoporous silica nanoparticles (MSNs)), micelles, dendrimers, and polymers[5,6,8,21,26,29]. Following, the main types of nanocarriers will be described briefly, except for dendrimers, where the approach will be developed in more depth due to the aim of this project.

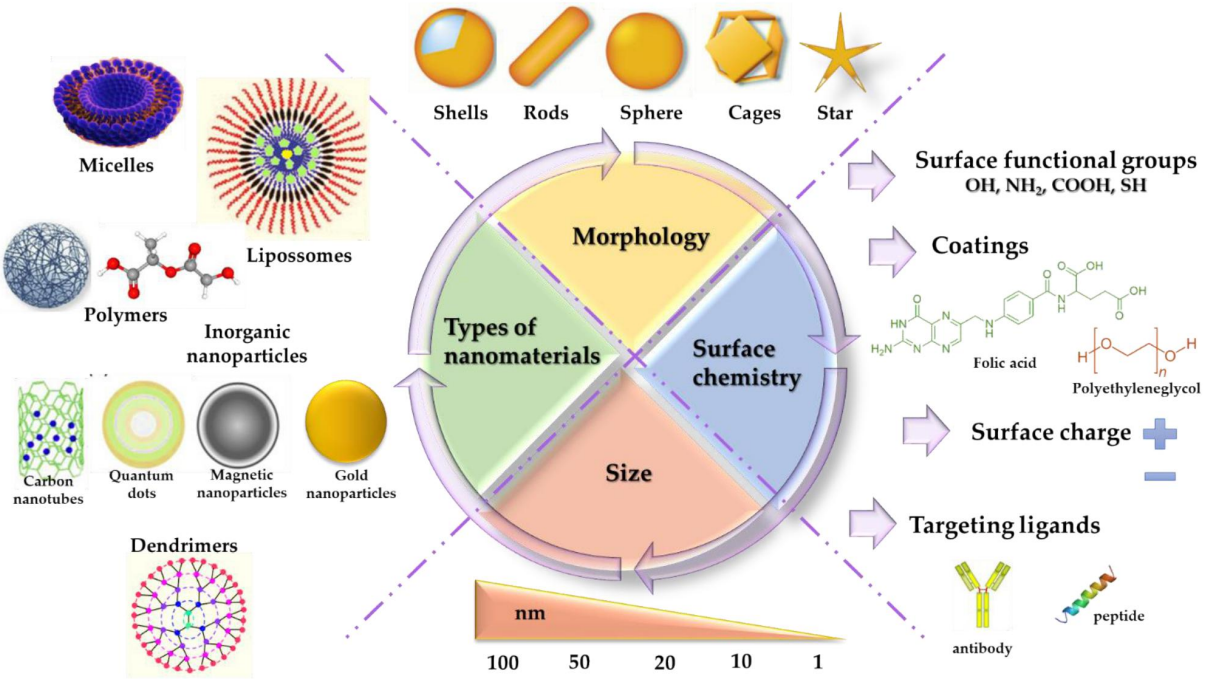

Figure 3: Illustration of different types of nanomaterials used as drug delivery and their properties. Adapted from reference[17].

2.1.1.1. Liposomes

Liposomes are small vesicles based on phospholipids, which are an important component in the cell membrane (Figure 3). Phospholipids consist of a hydrophilic head based on phosphate and a hydrophobic tail based on a hydrocarbon chain of fatty acids. In an aqueous medium, the molecule's head is attracted to water, while the tail is repelled, forming a two-layer vesicle by self-assembly where one part is polar and the other non-polar. Thus, the nucleus formed by this bilayer can retain water or encapsulate hydrophilic drugs. On the other hand, lipophilic drugs can be adsorbed on the membrane. Furthermore, depending on the number of bilayers and the liposome size, there are three types of vesicles: the multi-lamellar, the small uni-lamellar (SUV), and the large uni-lamellar (LUV)[5,6,8,21,26,29]. Liposomes can be prepared by different conventional methods, such as reverse phase evaporation, solvent injection technique, thin-film hydration, also known as method Bangham, and detergent dialysis. However, as these methods have limitations, other methods have been developed with the help of technology, such as supercritical fluid, supercritical reverse-phase evaporation, and the supercritical anti-solvent method[5,29]. In fact, the biggest challenge in using these liposomes is to make them more efficient, functionalizing them with other molecules. The so-called conventional liposomes present problems regarding their mobility, an insufficient amount of drug and faster release of it, and have a shorter circulation time in the bloodstream[5,29]. Molecules such as proteins, vitamins, peptides, carbohydrates, glycoproteins, monoclonal antibodies, and antibody fractions are usually grafted onto liposomes to target the cancer site actively. Which, in turn, can respond to various external or internal stimuli such as pH, redox reaction, enzyme, ultrasound, light, and microwave. They can be used to diagnose and treat the tumor-like radiolabeled liposomes, carry therapeutic and imaging agents, and be designated as theranostic liposomes[5,29]. Overall, liposomes are biocompatible, biodegradable, and non-immunogenic and are therefore versatile for therapeutic applications[5,8]. Liposomes as a nanocarrier of anticancer drugs have been extensively evaluated[43]. Examples of liposome-encapsulated anticancer drugs in the market include Doxil® (BAXTER Healthcare Corporation)[44,45], doxorubicin hydrochloride encapsulated in stealth liposomes* and Marqibo® (ACROTECH Biopharma, LCC)[46,47], a formulation containing vincristine sulfate[5,21].

2.1.1.2. Micelles

Micelles are spherical amphiphilic structures made up of a hydrophilic core and a hydrophobic shell, which, when exposed to a solvent, has the characteristic of self-assembly (Figure 3). This can occur if the solvent is hydrophilic and the concentration exceeds the critical micellar concentration (CMC). The copolymer polar parts are attracted towards the solvent and, the hydrophobic parts move away from the solvent. Therefore, the hydrophilic parts form a shell, and the hydrophobic parts form the nucleus.

***Note:** Stealth technology consists of a liposomal coating that evades detection and destruction by the immune system[44].

This arrangement is known as a direct or regular polymeric micelle. The hydrophilic shell stabilizes the micelle while the nucleus stores the drug[5,6,8,29,48]. However, when exposed to a hydrophobic solvent, they produce another structure, called the reverse micelle, where the nucleus forms the hydrophilic part and the shell the hydrophobic[5,29]. As the micelles have a diameter less than 50 nm and their shell is hydrophilic, circulation time in the bloodstream is increased and, consequently, the ability to release the drug in the target site due to its resistance to elimination by the reticuloendothelial system[5,6,29,48]. Depending on the solubility of the copolymer, the micelles can be prepared in different ways. If the copolymer is soluble in water, the method of direct dissolution and casting the film is used. If the copolymer is not easily soluble in water, dialysis or an oil in water procedure is used[29]. However, there are limitations in the micelles use. Such as the drug's early release due to the CMC, its interaction with blood and, the absorption of unimers to plasma proteins that can disturb the balance between micelle and blood. To overcome these limitations, the micelles usually are cross-linked. That is, two polymer chains are linked through the formation of disulfides. There are two types of crosslinking, shell crosslinked polymeric micelles and core crosslinked polymer micelles[5,29,48]. Different types of ligands are used to functionalize the micelle surface to actively target cancer cells, namely antibodies, peptides, folic acid, aptamers, and carbohydrates, among others. In this sense, anticancer drug release in the correct concentration can be obtained by functionalizing the nucleus and the shell. For the release of the drug, various stimuli such as pH, temperature, oxidation, enzymes, and ultrasound can be used. A multifunctional micelle can also be used for synergistic effects in cancer treatment. In addition, micelles can also be functionalized on the surface with imaging agents to diagnose and monitor cancer[29]. An example of micelles in cancer treatment is the co-delivery of thioridazine and DOX through polymeric micelles, which produced a stronger antitumor activity[5,49].

2.1.1.3. Polymers

Polymers (Figure 3) can be classified into three categories: natural polymers such as peptides, glycans, cellulose, starches, and proteins; synthetic polymers synthesized from monomers, such as poly (lactic-co-glycolic acid) (PLGA) and polylactic acid (PLA); and microbial fermentation polymers such as polyhydroxybutyrate[26]. The natural polymers that are used in the synthesis of nanoparticles are dextran, albumin, chitosan, alginate, gelatin, collagen, and heparin. For example, PLGA nanoparticles coated with chitosan and nanoparticles with chitosan can be used as nanocarriers to deliver proteins in specific organs[5,6,21,26]. On the other hand, synthetic polymers such as N-(2-hydroxypropyl)-methacrylamide copolymers, monomethoxypolyethylene glycol-block-polycaprolactone nanoparticles, PLA-PEG-PLA nanoparticles, PEGylated PLA nanoparticles, and poly-PLGA nanoparticles assist in the transport of proteins within the drug capsules. Furthermore, PEG prolongs the circulation time of the nanoparticles in the bloodstream and improves the stability of the nanoparticles that are exposed to gastrointestinal fluids[5,6,26]. Nevertheless, the most studied polymers are biodegradable polymers, including PLA, PLGA, poly-alkyl-cyanoacrylates (PACA), chitosan, and polycaprolactone (PCL)[5].

PLA is a biodegradable and biocompatible polymer that degrades in the body to monomeric units of lactic acid as a natural intermediate in the metabolism of carbohydrates[5,6,26]. An example is PLA nanoparticles loaded with oridonin (a natural diterpenoid). The results showed greater efficiency in trapping the drug into the PLA nanoparticles and a longer circulation time. Despite the anticancer effect of oridonin, its clinical application is limited due to its poor water solubility and low therapeutic index[50].

PLGA is a biodegradable polymer used to develop nanoparticles because it undergoes hydrolysis in the body producing two monomers of degradable metabolites, glycolic acid, and lactic acid. In that sense, its toxicity is minimal because these two metabolites are already known to the body[5,6,26]. Many anticancer drugs have been encapsulated in PLGA nanoparticles or that have been used to functionalize their surface, including DOX, 5-fluorouracil (5-FU), paclitaxel (PTX), cis-diamminedichloroplatinum(II) (cisplatin), dexamethasone, triptorelin, xanthone, 9-nitrocamptothecin, among others[5,6,26]. The PLGA thus protects drugs against the biological environment, in addition to being able to escape to the endocytose, penetrate the capillaries, and be internalized by the cells due to their small size[5,6,26].

Chitosan is a linear cationic polysaccharide prepared by the partial N-deacetylation of crustacean-derived natural biopolymer chitin through an alkalinization process under high temperatures. An example is the use of self-assembled glycol-chitosan nanoparticles to encapsulate the RGD (Arginylglycylaspartic acid) peptide to increase the *in vivo* half-life of RGD, thereby obtaining a stronger antiangiogenic effect[5,6].

PCL is a biodegradable polyester that has received particular attention due to its ability to be hydrolyzed through its ester bonds in a physiological environment. Anti-cancer drugs such as PTX, tamoxifen, vinblastine, and docetaxel have been encapsulated in PCL nanoparticles to increase their effectiveness[5,6,26].

PACA is a biodegradable and biocompatible polymer that polymerizes in the presence of water, where the ester bond present in the chain is easily hydrolyzed, forming poly-cyanoacrylic acid and alkyl alcohol. It was approved for human use in surgeries such as surgical glues and is being exploited as a potential drug delivery system. An example is chitosan-coated PACA nanoparticles functionalized with folic acid and encapsulated doxorubicin to cancer therapy[51,52]. Another type of polymers are the thermosensitive polymers such as poly(N-isopropyl acrylamide)-based (PNIPAAM) that can respond to a change in the temperature, which can also be used as a drug delivery system[26,53].

Also, our group used alginate-based nanogels to increase the intracellular delivery of DOX. This nanogels system was prepared via a mini-emulsion method through *in situ* alginate (AG) cross-linking using cystamine (Cys) as a cross-linker. DOX was then encapsulated in the nanogels through electrostatic interaction with alginate. The results demonstrated that the nanogels showed a high loading efficiency and an *in vitro* DOX-controlled release of DOX. They have also been shown to be cytocompatible and easily endocytosed by the CAL-72 cells with an increased accumulation of intracellular DOX compared to free DOX[54].

2.1.1.4. Carbon nanotubes and inorganic nanoparticles

Carbon nanotubes are hydrophobic networks with an elongated tubular structure of carbon atoms with a diameter between 1-2 nm. Its diameter depends on the number of graphene layers (Figure 3). They have a structure similar to graphite sheets wrapped around themselves in a cylindrical tube. There are three types of carbon nanotubes, single-walled carbon nanotubes (SWCNTs), double-walled carbon nanotubes (DWCNTs), and multi-walled carbon nanotubes (MWCNTs). They have unique electronic, optical, structural, and mechanical properties. Various methods can be used to synthesize carbon nanotubes, starting from carbon precursors, vaporized from graphite by laser, or by an electric arc in metal particles or chemical vapor deposition. However, carbon nanotubes are completely insoluble in all solvents and consequently lead to toxicity problems. This toxicity can be reduced by limiting its diameter and size and through chemical changes in its structure that increase its biocompatibility. Carbon nanotubes can encapsulate anticancer drugs in their internal cavity and on the surface. The carbon nanotubes can cross the plasma membrane and enter cancer cells by different processes such as penetration or endocytosis. Alternatively, for the specificity of tumor cells, their surface can be functionalized, allowing overcoming the resistance to multiple drugs. Furthermore, carbon nanotubes can be used as a diagnostic tool for the early detection of cancer. However, to date, there are no FDA approvals or clinical trials in the process of using carbon nanotubes to treat cancer. There are clinical pre-results *in vitro* and *in vivo* through passive targeting that show that carbon nanotubes are promising nanocarriers in cancer treatment. An example is a single-walled carbon nanotube modified with chitosan and folic acid in the outer layer to deliver DOX in cancer cells of the SMMC -7721 liver (Human hepatocellular carcinoma cell line)[6,29,48,55].

Inorganic nanoparticles for cancer treatment increase the efficiency of radiotherapy and improve the image of tumors. Among the inorganic nanoparticles, quantum dots, gold nanoparticles, super magnetic iron oxides, and mesoporous silica nanoparticles can be highlighted (Figure 3). Some of these inorganic nanoparticles are small with dimensions between 10-100 nm, which allows them to penetrate the capillaries and be absorbed in different tissues, while others are larger and need to be delivered to specific tumor sites through passive targeting[26,29].

A quantum dot is a semiconductor nanoparticle that limits the motion of the conduction band electrons in the three spatial dimensions confined to the 1 to 10 nm length scale. Due to their exclusive properties, quantum dots have been used for several applications, such as fluorescent semiconducting nanocarriers. The quantum dots are commercially available and generally constituted by 3 parts: the nucleus, the shell, and the covering material. The nucleus consists of a semiconductor material such as CdSe, the shell ZnS, which covers the shells around the nucleus, and the cap by a double layer of different materials used to encapsulate the quantum dots. Quantum dots can be synthesized either by a top-down or bottom-up method. As in other nanocarriers, quantum dots also experience non-specific uptake by the RES. PEG is attached to their surface to overcome this limitation so that quantum dots can accumulate in the tumor through the EPR effect. Specific ligands can also target specific tumor sites such as folic acid, peptides, and large proteins that can be grafted. There are

several studies with the use of quantum dots as nanocarriers, among which, the graphene QD-based targeted drug delivery. Where quantum dots have been linked to biotin because cell tumors have overexpressed biotin receptors, this system, through pH stimulation, can release the drug[26,29,56,57].

Gold nanoparticles (AuNPs) belong to the small group of the most well-studied nanomaterials having, in general, controllable diameters between 1-100 nm. When dispersed in the water, they are called colloidal gold. AuNPs are synthesized from a set of methods, such as chemical, biological and physical methods[29]. Gold nanoparticles have aroused interest as nanocarriers due to their unique characteristics, such as their dimensions on a nanoscale range, having a large surface for functionalization, biocompatibility, optical, electronic, and magnetic properties, and can emit natural radiation[26,29,48,58,59]. These unique optical and electronic properties are due to the interaction of light with the electrons existing on the surface of the gold nanoparticles. At a specific wavelength, "the collective oscillation of conducting electrons" causes a phenomenon called surface plasmon resonance (SPR)[29,58–60]. Furthermore, these properties can be adjusted by changing their shape, size, aggregation state, and surface chemistry[58,59]. Accordingly, these metallic nanoparticles exist in several forms, as nanospheres, nanoshells, nanorods, and nanocages[29,61]. A study using mammalian cells has shown that the size and shape of colloidal gold nanoparticles are important factors in the intercellular uptake process[62]. They are also promising candidates for delivering therapeutic agents, like small drugs or large biomolecules like DNA, RNA (ribonucleic acid), and proteins[29,59]. Therefore, these nanoparticles can generate images of the intracellular location and also transport various drugs. One of the obstacles in the use of gold nanoparticles is their toxicity and poor stability[26,29,59]. PEG has been used to overcome these limitations for its functionalization, demonstrating greater solubility and stability[29,59]. Other ligands can also be used for targeting, such as folic acid and transferrin, as many tumor cells overexpress receptors for these ligands[29,48,58,59]. Several studies have been developed; one of them involves the use of gold nanoparticles entrapped in dendrimers (Au DENPs), for imaging and targeting cancer cells[63].

Superparamagnetic iron oxide nanoparticles (SPIONs) are iron oxide particles with a diameter between 1 to 100 nm. The two main forms are maghemite (Fe_2O_3) and magnetite (Fe_3O_4). Iron oxides mixed with transition metals such as nickel, copper, and cobalt are also considered SPIONs. In addition, when the magnetic particles are reduced in size to 10-20 nm, they present superparamagnetism. That is, when applying a magnetic field, the nanoparticles are magnetized until saturation, but they do not show residual magnetism after removing the magnetic field. For the synthesis of SPIONs, several methods can be used, including thermal, hydrothermal decomposition, co-precipitation, microemulsion, sonochemical, and microwave-assisted. However, chemical synthesis is the most used method. SPIONs have theranostic properties and can, therefore, be used as a magnetic nanocarrier, as an external magnetic field can detect them, and at the same time, be used for specific therapy. For specific therapy, SPIONs need to be functionalized, as it reduces aggregation, allows the conjugation of drugs and ligands on its surface, protects the surface from oxidation, and increases its half-life in the bloodstream as it avoids RES. SPIONs functionalized with stimulus-sensitive polymers are being studied for drug targeting. One study has shown that SPIONs functionalized with polymers have dual responsiveness, not only to changes in pH but also in temperature[26,29,48,64]. SPIONs can be classified according to their size into

large or oral SPIO agents, as Ferumoxsil with 300 nm approved for clinical application; SSIPO or standard agents such as Ferumoxide 80-150 nm also approved for clinical application; USPIO or ultra-small agents such as Ferumoxtran 20-40 nm approved for clinical application and MION agents or monocrystalline iron oxide nanoparticles with 5 to 10 nm still in the experimental phase[48].

MSNs are materials with well-ordered and uniform internal mesoporous with a diameter usually from 2 to 6 nm, have a large surface area of 700-1000 m^2/g and volume 0.6-1 cm^3/g, with a shape, robustness, and adjustable size from 50-200 nm are easy to functionalize the surface, and they are biocompatible and have good hemocompatibility. Its porous silica structure (SiO_2) is similar to a honeycomb. These characteristics make this nanoparticle ideal for drug delivery due to its multifunctionality. There are essentially two types of MSNs, ordered mesoporous silica nanoparticles, including MCM-41 (Mobil Composite Matter number 41), MCM-48 (Mobil Composite Matter number 48), and SBA-15 (Santa Barbara Amorphous number 15) and hollow or rattled type mesoporous silica nanoparticles. These structures are amorphous and consist of pores that form channels. MCM-41 has a two-dimensional (2D) flat hexagonal structure, MCM-48 is three-dimensional (3D) cubic bicontinuous, and SBA-15 has a hexagonal plane with MCM-41, although the pores are larger (9 nm) than the pores of MCM-41 (3 nm). It also has a microchannel system that connects the mesochannels. In the MCM-48, the pores have a size between 1.6 and 3.8 nm with a 3D dimension, in which the longitudinal pores intersect in the 3 directions of the space. In MCM-41 and SBA-15, the pores are longitudinal with a hexagonal cross-section. The most studied MSN for biomedical applications is the MCM-41 (Mobil Composite Matter number 41). MSNs can be synthesized using the flexible method or the rigid model method. Therefore, the pore diameter allows being selective in size to load biologically active molecules into their cavities, as it regulates the release of the drug from diffusion processes to the physiological environment. The surface area determines the nanoparticle's drug capacity and the volume of the pores, which promotes matrix-host interactions and drug-drug interactions. MSNs also have good hemocompatibility. Nonetheless, conventional MSNs have a limited half-life in the bloodstream due to the hemolysis of human red blood cells, phagocytosis of macrophages, and unspecific binding to the protein human serum albumin (HSA). One strategy to minimize these limitations is to bond the PEG polymer to the MSNs. Copolymers can also be grafted onto their surfaces to prevent premature drug release, which acts as gatekeepers. The release of drugs can be carried out through various external or internal stimuli such as temperature, pH, enzymatic transformation, redox reaction, and magnetic field. For active targeting, the approach consists of modifying the outermost surface of the mesoporous silica nanoparticles with molecules capable of interacting with specific membrane receptors overexpressed in tumor cells such as folic acid, transferrin, mannose, and peptides. MSNs can also be used as synergistic cancer treatment therapies to increase selectivity and effectiveness. An example is a theranostic drug delivery system developed to obtain cancer images and simultaneously deliver the drug[29,65,66].

2.1.1.5. Dendrimers

Dendrimers are one of the most versatile polymeric macromolecules that were extensively studied as drug delivery systems, gene transfection, and imaging agents. In 1978 Fritz Vöglet *et al.*[67] synthesized, for the first time, a dendritic structure called a cascade of molecules. However, only low generation dendrimers were obtained due to experimental problems in the synthesis. In 1985, Donald Tomalia *et al.*[68,69] and George Newkome *et al.*[70,71] synthesized dendrimers of higher generations with well-defined structures. However, was Donald Tomalia the first to introduce the term "*dendrimer*". Since then, the synthesis of different families of dendrimers has been studied. The term "*dendrimer*" was named from the Greek word "*dendrons*" which means tree, and the word "meros," which means "part". Dendrimers are characterized by highly branched, three-dimensional globular macromolecules with a nanoscale dimension of 1 to 100 nm. These macromolecules have a uniform branched structure with many arms emanating from a central nucleus and constituting three different domains: a central nucleus consisting of an atom with at least two identical functions or molecules, branches that emanate from the nucleus designated as generations, repeated units with at least one branch junction and many terminal functional groups (Figure 4).

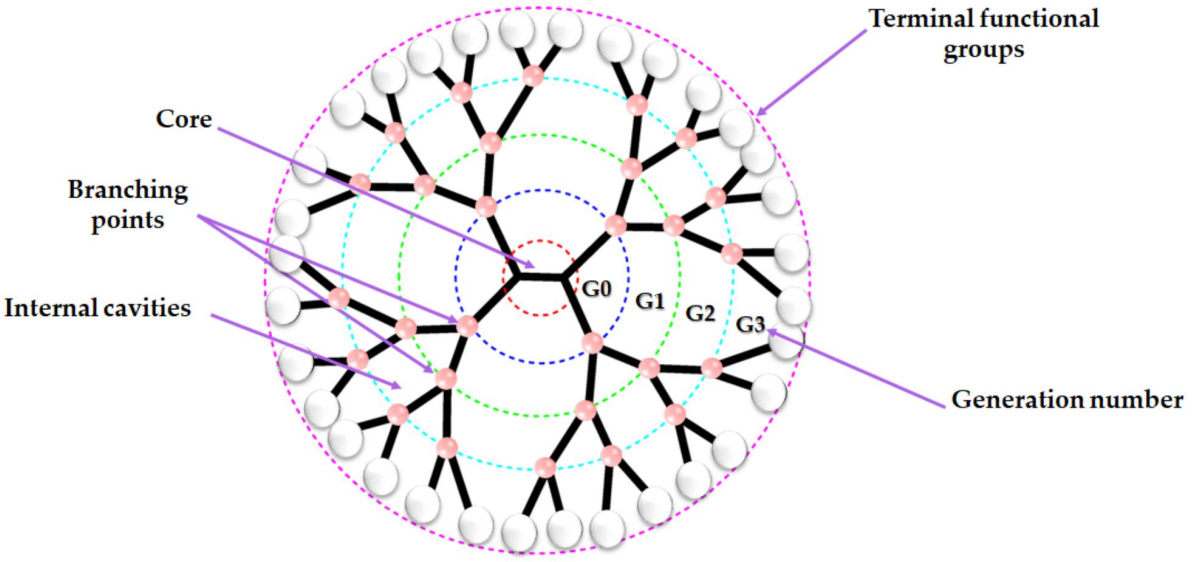

Figure 4: Schematic representation of a general structure of a dendrimer. Adapted from reference[72].

These three domains determine the dendrimer's shape, size, and reactivity. They can be synthesized mainly by convergent and divergent methods through polymeric reactions that allow a high level of control of their architecture and low polydispersity index, making them customizable and versatile. In the convergent method, firstly proposed by Jean Frechet *et al.*[73], the synthesis begins from the periphery where units of the surface of the dendrimer are coupled to form a branched structure. The dendrons which in turn are coupled repeatedly to

a multifunctional nucleus to the center of the dendrimer, while in the divergent method mentioned for the first time by Donald Tomalia *et al.*[68] the dendrimer is synthesized from the core that is the initiator, followed by the coupling of a monomeric unit that extends to the periphery gradually by repeatedly adding monomer units to a multifunctional initiator nucleus. In this sense, the addition of monomers to each functional group results in the next dendrimers generation with increased size. Nevertheless, both methods have advantages and disadvantages[74–80].

Divergent synthesis is the most used because it allows the manufacture of dendrimers on a large scale, but dendrimers may have defects such as lack of arms, especially in those of higher generation, due to increased steric impediment in the periphery. Convergent synthesis, on the other hand, minimizes defects in dendrimers since the dendrons are synthesized and purified individually before being conjugated. Nevertheless, many synthesis steps are required, and a large amount of starting materials are needed and, a low yield is achieved due to the steric impediment at the focal point[81]. Nonetheless, other approaches can also be used but with less frequency, such as hypercores and branched monomers, lego chemistry, double exponential, and click chemistry[74–79].

Dendrimers can be classified depending on their generation into low-generation dendrimers (generation 1 to 4) and high-generation dendrimers (generation 5 to 10). However, low-generation dendrimers are preferably used for biomedical applications because they have advantages such as easy synthesis, purification and characterization and, consequently, better yield; they also have a low level of defects in their branching; they accumulate in higher concentrations in the tumor than in normal tissues due to the EPR effect; they are easily eliminated by endocytosis and renal excretion and play an important role in solubility. Nonetheless, one of the limitations of using dendrimers in therapeutics is its synthesis due to the several steps that are necessary to obtain the dendrimer, which increases the production costs. They have promising characteristics as nanocarriers for use in cancer therapy such as monodispersed size, good water solubility, biocompatible and biodegradable, have several well-defined terminal groups that can be functionalized, enhancing the selectivity of the drug and internal cavities where drugs can be encapsulated, they are non-immunogenic and have an acceptable excretory pathway. Because of the uniform structure, they have the ability to cross the membrane of cancer cells and reduce their elimination by macrophages. However, it is the terminal groups of the dendrimer that determine its physical and chemical properties. The groups can be hydrophilic or hydrophobic molecules. As they are outside the dendrimer, at least in the lower generations, they allow a higher drug encapsulation rate[76,80].

The drug can be physically encapsulated inside the core via hydrogen bonds, electrostatic attraction, hydrophobic, and van der Waals interactions, or it can be chemically covalently conjugated on its surface, or it can be combined in both ways. In this sense, the number of generations influences the drug's carrying capacity[76,77,79].

Dendrimers can directly encapsulate drugs in their internal cavities, as they are hydrophobic and interact with the drug even though it is poorly soluble through hydrophobic interactions. On the other hand, the nitrogen and oxygen atoms present inside the dendritic structure can also interact with the drug through hydrogen bonds

or by electrostatic interactions. This interaction between ionic groups of the drug, with opposite charges of groups on the surface of the dendrimer, also allows the increase of the hydrophobic drug solubility. Drugs such as naproxen, ibuprofen, indomethacin were complexed with dendrimers by electrostatic bonds[76,77].

This physical conjugation has the advantage of being a direct and quick approach without affecting the pharmacological activity of the drug. However, it is not very stable concerning drug release and storage. The encapsulated drug differs from synthesis to synthesis and has a low drug loading capacity[76].

A wide variety of functional groups on the surface of dendrimers make them suitable for covalent drug conjugation. Where the drug is released through chemical or enzymatic cleavage of hydrolytically unstable bonds, drugs can also be covalently conjugated to spacers like PEG, or biodegradable bonds like ester or amide bonds (ester bond is more rapid to cleavage than amide bond) inside the cell can be hydrolyzed by endosomal or lysosomal enzymes. The release of drugs from the dendrimeric conjugate will depend on the type of covalent bond between them. Many anti-cancer drugs such as PTX, DOX, cisplatin, methotrexate (MTX), and epirubicin have been conjugated with dendrimers where they have shown potential in drug targeting[76,77]. Therefore, the smallest drugs are usually encapsulated while the larger drugs are conjugated on the surface. For example, when amphiphilic dendrimers encapsulate the drug with a hydrophobic nucleus and hydrophilic branches, its application is only for local treatments such as intratumoral injections, as an uncontrolled drug release occurs. The covalent bonding of the drugs allows for greater solubilization, which can be hydrophilic and/or hydrophobic, and depending on the ligands, their release can be controlled. Nevertheless, the controlled release of the drug remains a challenge today. Several small molecules with anti-inflammatory, microbial, and anti-cancer activity have been conjugated to dendrimers through physical interactions or chemical bonds. Using dendrimers as nanocarrier allows to improve the solubility of the drug, their stability, increasing its efficiency and diminishing the side effects, in a way to adopt the pharmacodynamics (PD) and pharmacokinetics (PK) behaviors of the drugs. The surface of the dendrimer can also be functionalized by molecules sensitive to stimuli (light, changes in pH and temperature, heat, among others)[76].

The drug delivery systems of dendrimers are based on two different strategies, passive and active targeting[74,79]. We have an EPR effect on passive targeting where dendrimers accumulate essentially in cancer cells due to low lymphatic drainage and high vascularity. In this way, the drug's bioavailability is increased with a reduced side effect. But, this method has some limitations since the EPR effect is not equal in all tumors, and as such, it may affect the accumulation of macromolecules at the tumor site[74]. The anticancer drug delivery for dendrimers includes 5-FU, DOX, cisplatin, camptothecin, adriamycin, tamoxifen, dimethoxycurcumin, MTX, PTX, among others[82]. For the active targeting, the dendrimer with the drug can be incorporated into its surface ligands with a specific affinity that will interact with the overexpressed tumor cell receptors. This method is more effective because the system is internalized by releasing the drug into the cancer cell. These methods can also be used together to increase the efficiency of the system and decrease side effects[74]. The ligands-based targeted drug delivery using dendrimers includes folic acid, biotin, riboflavin, D-glucosamine, etc[82].

Thus, given the type of need for therapeutic action, different approaches to drug loading in dendrimers allow adjusting its release from dendrimers[76]. Nonetheless, combining a dendrimer with an active ligand and drugs could result in a synergistic effect that can trigger a very efficient therapy[83].

So, there are two mechanisms for drug delivery: the release of the drug from the dendrimer through physical changes such as changes in pH, temperature, among others, and the *in vivo* degradation of the covalent bond between the dendrimer and the drug via enzymes[76].

Different types of dendrimers have emerged since then with different functionalities (Figure 5). Among which, polyamidoamine (PAMAM), poly (propyleneimine) (PPI), core-shell tecto, peptide, chiral, liquid crystalline systems, glycodendrimers, hybrid, PAMAM-organosilicon (PAMAMOS), triazine, polyether, carbosilane, polyester, polylysine, metallodendrimers, phosphorous and poly (2,2-bis (hydroxymethyl)propanoic acid) (bis-MPA)[75–77,80,82–84].

The unique properties of dendrimers and the possibility of being adaptable allows them to have various potential therapeutic and biomedical applications as gene delivery, sustained release, cancer therapy, photodynamic therapy, bioimaging, drug solubilization, site-specific delivery, oral, ocular, transdermal, topical, and pulmonary drug delivery, and diagnosis[75,80,83–85]. Apart from this, dendrimers are also used in cosmetics such as hair gels, anti-acne products, sunscreens and shampoos, printing technologies on toners and inkjet cartridges, paint, and textile industry as water repellent coatings[86].

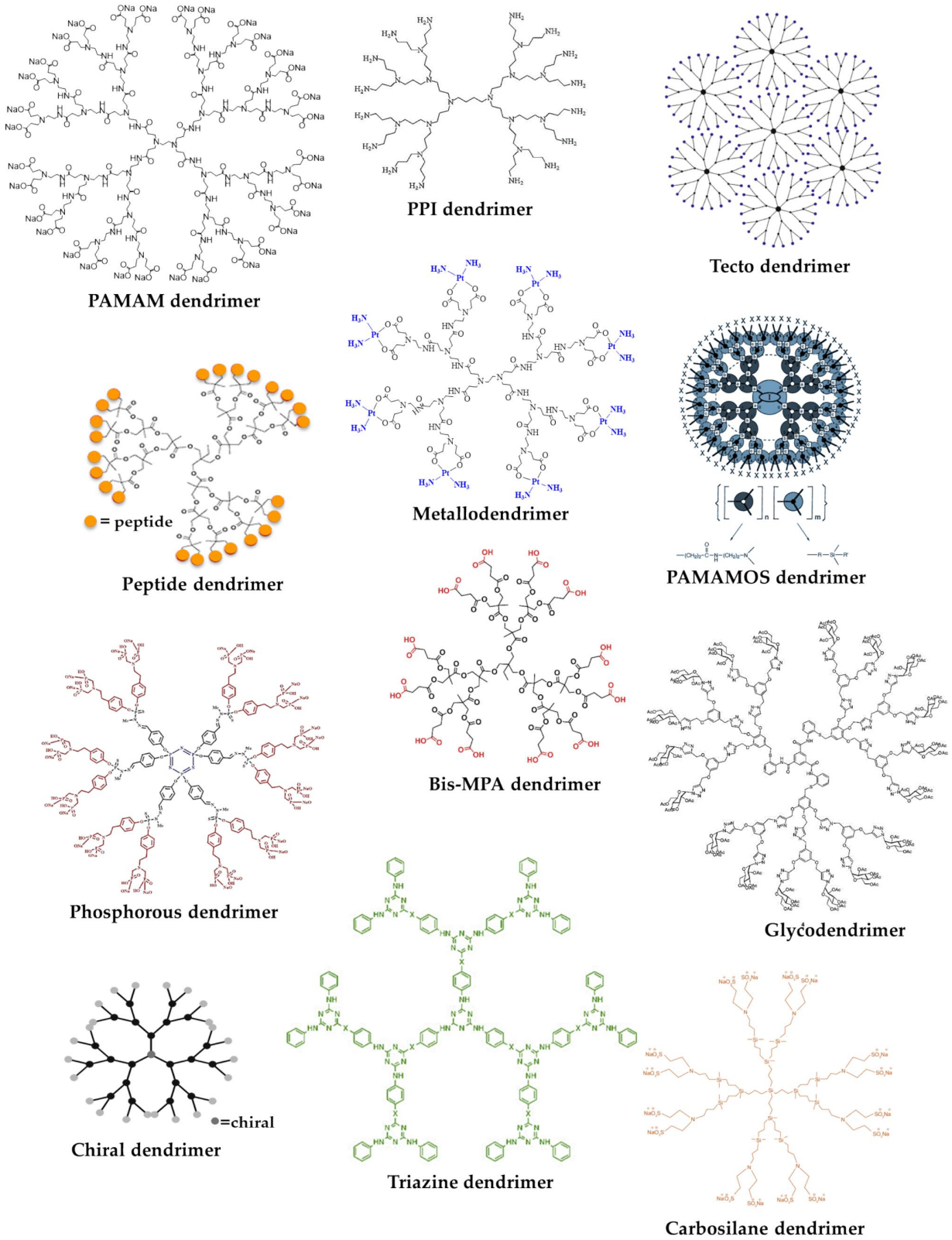

Figure 5: Representation of different types of dendrimers. Adapted from reference[80].

In addition to the potential of dendrimers for biomedical applications, there are some limitations in their use as nanocarriers[81,83]. One of the limitations is its cytotoxicity, which depends on the number of functional groups on the surface, the generation, and the nature of the terminal groups. Thus, cationic dendrimers have high cytotoxicity, while neutral or anionic dendrimers have very low or even no toxic effects. The cytotoxicity in cationic dendrimers is due to the interaction of the surface of the dendrimer that is positively charged with the cell membrane that is negatively charged, which leads to the formation of nanopores in the cell membrane and, consequently, the leakage of the cell content that can lead to cell death[83]. Depending on their physicochemical characteristics, dendrimers can interact with various plasma proteins and blood cells[77]. One of the approaches to decreasing dendrimers' toxicity and increasing their biocompatibility is to modify their surface[83].
So, dendrimers as nanocarriers are promising vehicles capable of transporting the drug and crossing the biological barrier efficiently[76].

2.2. Dendrimers as a nanoscale platform for anticancer drugs

Due to their unique characteristics, dendrimers have been explored for the delivery of various anticancer drugs and diagnoses in cancer therapy[76]. Among the different families of dendrimers, only the PAMAM dendrimers, fluorescence dendrimers, biodegradable dendrimers (bis-MPA dendrimers), and metallodendrimers will be focused on this introduction.

2.2.1. PAMAM dendrimers

The biggest challenges in cancer therapy, more specifically in conventional chemotherapy, are low aqueous solubility, low membrane permeability, non-selective biodistribution, rapid release, lack of selectivity, hypersensitivity reactions, and resistance to multiple drugs (MDR). Thus, the scientific community focuses on developing a system that has reproducibility in its pharmacokinetic behavior, is stable, monodisperse, and well defined. In this sense, these characteristics led to the development of hyperbranched polymers called dendrimers for biomedical applications[78].
The PAMAM dendrimers were the first complete family discovered, synthesized, and commercialized by Donald Tomalia *et al.*[87]. Since then, they have been extensively studied for biomedical applications due to their exceptional properties[84,88]. As presented previously, PAMAM dendrimers belong to the family of hyperbranched nanoscale polymers with defined and uniform size and shape, monodisperse, and multifunctional terminal groups[89]. PAMAM dendrimers compared to linear polymers have significantly improved properties, such as monodispersity: PAMAM dendrimers have a monodispersed globular structure, size, and shape that varies according to the generation where lower generations have an ellipsoidal shape and high generations a spherical shape that is similar in size to several biological molecules (for example generation 3 to the insulin that has 3 nm, generation 5 to hemoglobin that has 5.5 nm, etc.), the charge on its surface that can be modified through functionalization with other molecules, as well as their biocompatibility, once cationic

dendrimers are more cytotoxic and hemolytic even at low concentrations than neutral or anionic ones[90]. PAMAM dendrimers are synthesized by the divergent method because with this approach it is possible to have high yields in all generations[24,91]. It consists of the reaction of the alkyldiamine nucleus like ethylenediamine (EDA) with the methylacrylate monomers through the Michael addition reaction forming a branched intermediate, that reacts with an excess of EDA producing the generation 0 of PAMAM dendrimers with terminal groups that can be transformed into amine (NH_2), alcohol (OH) or carboxylic acid (COOH). Higher generations are synthesized from the sequential Michael addition reaction of methyl acrylate monomers followed by an amidation reaction with ethylenediamine (EDA)[79,87]. This method has some advantages as it allows the direct dendritic growth of dendrons from the nucleus, which can be EDA, ammonia, or cystamine, without the need for another step in anchoring the nucleus occurs with the convergent method, which is stereochemically limited. The monomers (acrylonitrile, acrylates, etc.) used to synthesize these dendrimers are of low cost and are readily available. They produce high organized and monodisperse macromolecules, and it is adaptable to the expansion of large volumes. For example, PAMAM dendrimers are prepared in substantial quantities, in the order of kilograms, and can be used to prepare high generation dendrimers[24,91]. However, two limitations are reported regarding the synthesis of higher generations of PAMAM dendrimers as the terminal groups are not formed properly, and the other is the difficulty of their purification by chromatography separation[24]. Also, as the generations increase, a steric agglomeration of the arms limits their growth to the next generation, producing defective branches known as the Gennes dense packing effect. This effect is observed from generation 7, decreases the synthesis yield, and limits the subsequent generations' synthesis until generation 10[79]. When the generation of dendrimers increases, the number of terminal groups increases exponentially, and the diameter increases linearly by about 1 nm per generation. The full-generation have terminal amine or hydroxyl groups, and the half-generation has carboxylic acids as terminal groups[89]. In this sense, full-generation PAMAM dendrimers amine-terminated have cationic charges in an aqueous medium and are ideal for transporting anionic drugs. In contrast, half-generation dendrimers have anionic charges being ideal for the transport of cationic drugs and reversible coordination of platinum complexes[92].

PAMAM dendrimers can be used as drug nanocarriers either by covalent bonding or electrostatic interactions to the functional groups on their surface or by encapsulation inside their internal cavities by hydrogen bonds or hydrophobic interactions. The primary and tertiary amine groups present on the surface and in the nucleus of the PAMAM dendrimers have pKa values of 10.7 and 6.5 respectively and, consequently, ionizable groups in both the nucleus and on the surface allowing drug interactions. The primary and tertiary amine groups also respond to changes in the pH, being used as a drug delivery system for the release of a drug that is activated at low pH[93,94]. Studies with drugs such as ibuprofen, indomethacin, piroxicam have shown the formation of stable systems through electrostatic interactions with the dendrimer. In other studies, penicillin V, naproxen, venlafaxine, propranolol, and 5-aminosalicylic acid have been covalently conjugated to dendrimer[76].

Different mechanisms have been proposed to describe molecular transport across cell membranes, such as passive diffusion, endocytosis, and paracellular and carrier-mediated transport. In general, PAMAM dendrimers, depending on their surface properties, are transported more effectively through epithelial barriers

compared to many other water-soluble linear polymers. Charged dendrimers have a higher permeability than neutral dendrimers, which at physiological pH do not have charge and, consequently, are unable to perturb or disturb the anionically charged cell membranes. However, the epithelial permeability in cationic dendrimers decreases with increasing the size and, in contrast to anionic dendrimers, which increases with size. Several studies carried out by Kelly Kitchens *et al*. on cationic, anionic, and neutral dendrimers demonstrated that the permeability was enhanced with the increase of the carboxyl groups of the anionic PAMAM dendrimers[95–97]. Although the main mechanisms of drug targeting and intracellular uptake of PAMAM dendrimers are carried out by passive targeting, as previously mentioned, they may also happen by endocytosis. Endocytosis is a process where cells internalize particles across the cell membrane. There are three pathways of endocytosis: phagocytosis, pinocytosis, and receptor-mediated endocytosis, which will depend on the charge, shape, and size of the dendrimer[98]. For instance, studies carried out by Felipe Vidal *et al.* found that the PAMAM generation 4 dendrimer is internalized mainly by the clathrin-mediated endocytosis mechanism[99,100].

As having a nanoscale size and a relatively low molecular weight, the PAMAM dendrimers show a propensity to extravasate. This movement of the molecules that are in the blood circulatory system to the endothelial lining of the capillary walls into the neighboring interstitial tissues can be used as targeted delivery of drugs. The extravasation of different generations of PAMAM dendrimers was studied by Kelly Kitchens *et al.,* and they concluded that the extravasation time is exponentially proportional to the size and molecular weight of the dendrimers in the order G0 <G1 <G2 <G3 <G4, where the overflow was between 143.9- 422.7 s[101]. The greater the molecular weight and size of the dendrimers, the extravasation time through the microvascular endothelium also increases. The selectivity of dendrimers is dependent on their size because when the size increases, it also increases the exclusion of the PAMAM-NH_2 dendrimers from the endothelial pores with a radius of 4-5 nm. As the PAMAM-NH_2 dendrimers have a relatively small molecular size between 1.5-4.5 nm, they can pass by the microvascular endothelium through the endothelial pores. The extravasation observed may be due to electrostatic interactions between the dendrimer with a positive charge and the glycocalyx lining of the endothelium with a negative charge[95]. Moreover, other characteristics such as the geometry and charge of the dendrimer's surface also influence the microvascular leakage of water-soluble dendrimers. This property is important in passive targeting for drug delivery and cancer diagnosis[80,95]. However, the cellular uptake mechanisms of dendrimers vary depending on the generation, concentration, and functionalization, although the role of these factors is not yet well known. Whereas, it is known that cell uptake and cell transport depend on the surface charge of the PAMAM dendrimer and the type of cell under study[102]. Nevertheless, for PAMAM dendrimers to be used in clinical as a drug delivery system, it is necessary to know their biological properties such as toxicity, biocompatibility, and pharmacodynamics (absorption, biodistribution, bioavailability, metabolism, and excretion in function on time), and pharmacokinetics[103]. Despite the innumerable advantages and qualities of PAMAM dendrimers as drug delivery systems, it has some disadvantages limiting its biomedical application[103]. Among them, one of the main obstacles for its use at the clinical level is the cytotoxicity and rapid elimination from the circulation after intravenous administration[104]. However, these disadvantages are due to the presence of amine groups on its surface since they are cationic dendrimers.

However, to overcome such limitations and improve biocompatibility, several strategies can be used, such as the conjugation of carbohydrates, amino acids, peptides, folic acid, acetylation, and pegylation are the most commonly used. On the other hand, anionic or neutral PAMAM dendrimers are more biocompatible and much less toxic. However, the surface modification also increases the capacity to encapsulate anticancer drugs and target cancer cells by binding specific ligands[104]. Due to their nanoscale size, dendrimers can interact with various cellular components such as endosomes, plasma membranes, mitochondria, and the nucleus[104].

A simple method to study the interaction between dendrimer-membrane is through the lysis of red blood cells (RBC), as it provides quantitative information on the release of hemoglobin (Hb) and qualitative information on the damage of RBC[105]. Several studies by N. Malik *et al*.[106] have shown differences in hemolytic behavior depending on the dendrimer. They found that to the amine-terminated PAMAM dendrimers, the hemolysis process depends on the generation. For instance, after 1 h of administration of the dendrimer with low concentrations (10 μg/mL), changes in the morphology of the red blood cells occurred[105,106]. This change in membrane curvature and pore formation may result from electrostatic interaction and disturbing properties of the dendrimer membrane[77]. It was observed that the cationic PAMAM dendrimers of generations 3 and 4 labeled with ^{125}I-labeled and administered intravenously in Wistar rats (10 μg/mL) were rapidly eliminated from the bloodstream, as only <2% was recovered in 1 h. However, the anionic PAMAM dendrimers of generations 2.5, 3.5, and 5.5 had longer blood circulation times, where between 20-40% of the dendrimer was recovered from the blood after 1 h with clearance rates that depend on the generation. For both cationic and anionic dendrimers, blood levels at 1 h correlated with the extent of liver capture verified, about 30-90% of the dose of dendrimer recovered in 1 h[105,106]. Thus, hemolytic activity depends on the dendrimers' concentration and exposure time, being more pronounced in cationic dendrimers than in anionic dendrimers[106]. As for the biocompatibility of PAMAM dendrimers, lower generation dendrimers with anionic or neutral polar terminal groups exhibit higher biocompatibility and less toxicity than high generations and with cationic or neutral apolar groups that exhibit higher toxicity and immunogenic properties[96].

PAMAM dendrimers have also been used as drug delivery due to their internal cavities that allow the encapsulation of small hydrophobic drugs and the possibility to attach on the surface different molecules[102,107]. So, due to their versatile surface and distinctive architecture, PAMAM dendrimers are considered ideal nanocarriers for delivering therapeutic agents, including anti-cancer drugs[79]. One example of the use of PAMAM dendrimer as a drug delivery system for cancer is reported by T. P. Thomas and coworkers that synthesized PAMAM dendrimer generation 5 with riboflavin, a targeting ligand, and the MTX for the human KB carcinoma cells. The results revealed that this system PAMAM-MTX-riboflavin causes cell growth inhibition by blocking the catalytic activity of the dihydrofolate reductase enzyme in cytosol[108]. Saijie Zhu and coworkers have prepared PAMAM dendrimer conjugated with different PEGyalation degrees and DOX. The *in vitro* cytotoxicity studies showed that the PPCD (PEG-PAMAM-cis-aconityl-DOX) conjugates cytotoxicity increased against the SKOV-3 ovarian cancer cells. Furthermore, the *in vivo* fluorescence imaging showed an efficient accumulation of this conjugate in tumor location[109].

2.2.2. Fluorescent dendrimers

Despite the distinctive characteristics that make them ideal candidates for biomedical applications, such as the delivery of drugs and genes and as bioimaging/diagnostic agents, dendrimers have some limitations[84,90,95,98,110–112]. One of them is the toxicity that constitutes the terminal groups of dendrimers because they can interact with various components in the bloodstream and cells. Another important one is the lack of intrinsic fluorescence that allows tracing its location within cells/tissues. Several strategies are available to overcome these issues by modifying their surface[80,83,105,113]. Nevertheless, these modifications should not change either the dendrimer's properties or its biological behavior[114].

A less known and explored strategy is to enhance the intrinsic fluorescence of the dendrimer without labeling it with any kind of dye. This strategy was highlighted recently by Donald Tomalia *et al.* and is based on a phenomenon of non-traditional intrinsic luminescence (NTIL)[115]. Indeed, some studies with PAMAM dendrimers, including from this Ph.D. project (see Chapter IV) show that the NTIL can be significantly enhanced by an oxidative treatment using ammonium persulfate (APS) (Figure 6) or from direct oxygen exposure[116–122]. Thus, as mentioned thereafter, PAMAM dendrimers are a versatile nanomaterial for the bioimaging field[96,123]. For instance, Ya-Ju Tsai and coworkers described the preparation of a fluorescent PAMAM dendrimer, without conjugation of a fluorophore, to deliver antisense oligonucleotides in rat C6 glioma cells. The results showed that this system could be used for delivery, transfection, and bioimaging, particularly as a nanoplatform for cancer imaging and therapy[119].

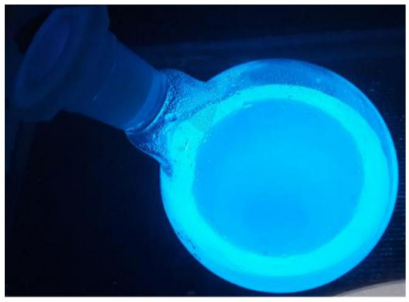

Figure 6: Amine terminated PAMAM dendrimer generation 3 treated with APS under UV light at 366 nm (ref. unpublished figure related to Chapter IV).

2.2.3. Biodegradable dendrimers

Another approach to circumvent dendrimers' cytotoxicity and hemolytic toxicity is to develop less toxic and biodegradable dendrimers, allowing their elimination through urine in a fast and safe way[79,113]. Since the most common dendrimers used are not degradable under physiological conditions, presenting side effects due to the accumulation of non-degradable macromolecules inside the tissues and cells[124]. Biodegradable dendrimers are usually constituted by biodegradable repeating units, which degrade into small molecules through chemical hydrolysis or enzymatic cleavage in a physiological medium. This enzymatic cleavage results from esterases

and can be excreted or eliminated by metabolic routes, minimizing the exposure time-dependent dendrimer toxicity[79,124]. Thus, depending on the type of the repetition unit, biodegradable dendrimers can be classified into three different categories, polyester dendrimers, polyacetal dendrimers (Figure 7), and other biodegradable dendrimers[124].

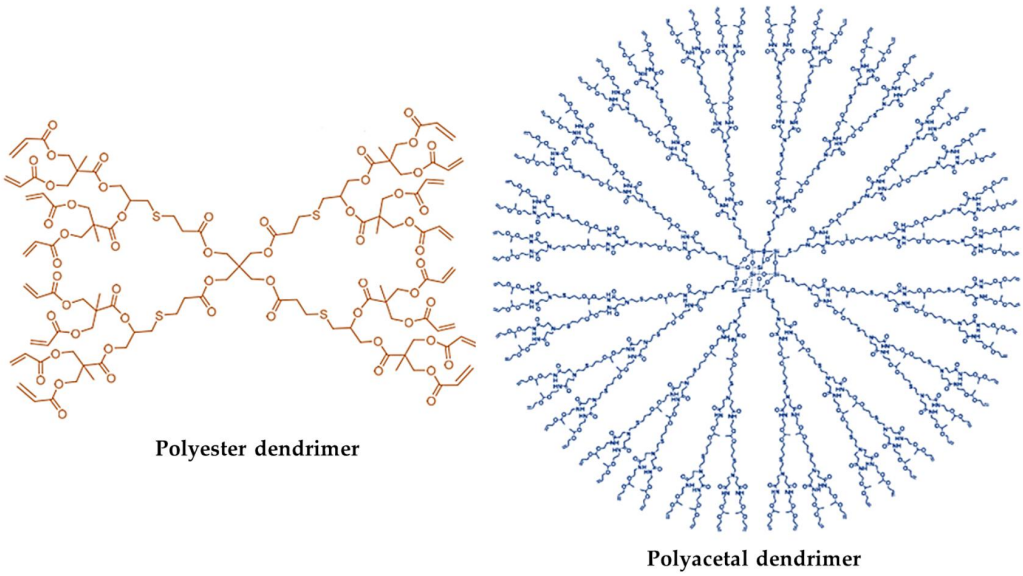

Figure 7: Representation of biodegradable dendrimers. Adapted from references[124,125].

In general, biodegradable dendrimers can be synthesized through the most common approaches used to prepare other dendrimers families[73,124,126,127]. However, most of them are synthesized by the divergent method through an interactive coupling, where biodegradable units are formed during the synthetic process or are derived from biodegradable monomers. Biodegradable units are generally more vulnerable than non-degradable groups, being the synthesis preferably carried out under mild conditions[124].

Compared with other dendrimers families, biodegradable dendrimers are considered promising nanocarriers for drug delivery due to their biodegradation capacity having, like the others, internal cavities and terminal functionalities also able to encapsulate or conjugated drugs to their surface[124]. Nevertheless, the physical encapsulation of drugs has a disadvantage, which is the rapid and uncontrolled release of drugs. A strategy to overcome this limitation is synthesizing biodegradable dendrimers with denser structures, but several reaction steps are necessary, which increase the risk of defect formation and the cost. Chemical conjugation is another strategy for drug delivery as an alternative to encapsulation. However, the linkers used to conjugate the drug to the dendrimer can affect the system's activity and the drug's release profile. Ligands commonly used to covalently link drugs to biodegradable dendrimers include hydrazone, acid-labile acetal/ketal, or cis-aconityl groups. They are easily degraded under acidic conditions in tumor tissues and intracellular lysosomal or

endosomal compartments. More specifically, disulfide groups are reduced by glutathione in the cytosol, and esterase enzymes can hydrolyze ester groups within the cell[124].

The use of biodegradable dendrimers as drug delivery systems present several advantages, among which, the increase the solubility of hydrophobic drugs and protection from the interaction with the physiological environment and its degradation; extension of the circulation time of the drug in the bloodstream, as it protects the drug from being filtered and eliminated by the kidneys, since nanoparticles larger than 5 nm are less likely to be filtered by the kidneys because they exceed the renal threshold; the ability to passively target the drug to tumor tissues due to the EPR effect; possibility of modifying the surface of the dendrimer with other molecules, possibility of deliver different drugs through chemical conjugation and encapsulation designated as synergistic effect to improve therapy; the ability to degrade into small molecules in a physiological environment and be eliminated by the body; reduction of adverse effects and the ability to achieve controlled drug delivery through dendrimers that respond to stimuli or the interaction between dendrimer and drug[124,128].

Many biodegradable dendrimers with distinct properties have been developed and synthesized for various applications, including biomedical applications, particularly polyester dendrimer[124].

Polyester dendrimers have thus attracted attention due to their properties, including their biocompatibility and degradation under physiological conditions. These can be grouped into three categories, polyester dendrimers based on bis-MPA monomers, polyester dendrimers based on alternating monomers, and other polyester dendrimers[124].

The first bis-MPA dendrimer was synthesized in 1996 by Anders Hult *et al.*[131]. Since then, they have attracted interest for biomedical applications, such as the delivery of chemotherapeutic drugs to improve tumor targeting and therapeutic efficacy and as near-infrared (NIR) or positron-emitting (PET) probes for *in vivo* imaging due to their properties, including the solubility, biocompatibility *in vivo* and *in vitro*, easy to functionalize, degradable by hydrolysis or enzymes, non-immunogenic and non-toxic[113,125,126,128–131]. The degradation of polyester dendrimers appears to be controlled by four factors, compared to the amide and ether bonds:

- the nature of the chemical bond that joins the monomer units to the ester bonds are more susceptible to hydrolysis;
- the smaller dendrimers degrade more quickly as they have less tight surface packaging, protecting less the hydrolyzable interior bonds;
- hydrophobicity, they have more hydrophilic polymeric units that degrade faster;
- faster degradation due to the hydrolysis susceptibility of the interior bonds and cleavage of the peripheral and internal dendrimer structure[79].

In the early days, biodegradable polyester dendrimers based on bis-MPA monomers were synthesized by esterification reactions of hydroxyl and carboxyl groups. However, several protection/deprotection steps were necessary during the synthesis, making the synthesis costly and defect formation since the protecting groups can cause the degradation of the ester groups. Recently, and to overcome these limitations, a new approach named bi-functional orthogonally reacting dendritic structure has been used consisting of the orthogonal coupling with biodegradable monomers of type AB_2, where the main step is the formation of the ester bond,

thereby increasing synthetic efficiency[124,131,132]. The synthesis is based on the use of two different branch units with complementing coupling functions that are exchangeable without any activation step. Moreover, both the reagents and coupling products must be inert for subsequent reactions. Accordingly, the designation is orthogonal, meaning that the functionalities are inert in the coupling conditions but can later be activated *in situ* for a subsequent reaction if necessary[133].

Xianghui Zeng and coworkers have prepared a micelle, where their hydrophobic interior layer is composed of bis-MPA polymer and the outer hydrophilic shell of PEG. The DOX was further encapsulated in the interior of this polymer micelle. The results showed an improvement of the cytotoxicity against breast cancer cell lines and exhibited a controlled release of DOX over a long period of time[134].

Hence, biodegradable dendrimers are excellent candidates for drug delivery due to their biodegradable capacity and structural characteristics[124].

2.2.4. Metallodendrimers

In addition to being excellent drug nanocarriers, dendrimers can incorporate metals into their dendritic structure, the so-called metallodendrimers[135,136]. The combination of the properties of dendrimers as a drug delivery system and those of transition metals as anticancer drugs is an alternative strategy for the development of a potent therapy[135,137]. Metallodendrimers can be synthesized through covalent bonding or by non-covalent bonding as hydrogen bonds, ionic interactions, and supramolecular complexation. In the supramolecular complexation, the ligands are coordinated to the central atom by dative bonds, where the electrons came from the same atom, known as coordinate bonds[133,138–143]. Depending on the position occupied by the metal in the dendritic structure can be classified into a) dendrimers with the metal center, b) dendrimers with metal complexes on the periphery, c) dendrimers with metals at the branching points, and d) dendrimers with metals in the dendritic branches[135,138,144].

The diversity of metallodendrimers allows them to be used in a wide range of applications including, catalysis, molecular electronics, sensing, photo-optical materials, and biomedical[136]. However, the field of metallodendrimers is still expanding regarding biomedical applications[138]. Nonetheless, the first metallodendrimer to be synthesized with anticancer properties were those with platinum complexes, such as the compound tetranuclear metallodendrimer DAB(PA-tPt-Cl)$_4$ synthesized by Bart Jansen and coworkers[145,146]. According to the authors, this metallodendrimer showed a moderate antiproliferative action on two mouse leukemia cell lines and different human cancerous breast adenocarcinoma cell lines[135,145]. Our group also contributed to this field by preparing metallodendrimers based on low-generation poly(alkylidenimine) dendrimers functionalized on the periphery with ruthenium (II) for cancer therapy. The results showed a high anticancer activity towards the cancer cell lines studied and a high inhibitory effect on the viability of hMSCs[147]. Other examples involving different types of organic cores and metals/metal complexes are reported in the literature[148–150] and are the object of recent reviews[151,152].

3. Platinum anticancer drugs

Metals, more precisely transition metals, are the most versatile materials with a wide range of applications from the electronics and aerospace industry to health[153]. They play a very important role in biological processes, which are indispensable for living organisms. Metals present unique properties such as redox activity, wide structural diversity, thermodynamic and kinetic characteristics, numbers of variable coordination, and geometry and have reactivity for organic substrates. Compared to organic-based drugs, these advantages can be exploited to develop therapeutic agents[154–157]. In this sense, medicinal inorganic chemistry is an area that allows metal complexes to be used as anticancer agents. However, even though metals have been used for a long time in medicine, their anticancer potential was only explored after the accidental discovery of the biological activity of cis-diamminedichloroplatinum(II), (cisplatin)[156].

Since then, several metal complexes began to be developed as anticancer agents and as antibacterial, inflammatory, anti-rheumatic, and anti-malarial[153]. In terms of anticancer activity, platinum compounds are the most used for cancer treatment. However, other metal based-anticancer drugs, such as palladium (II), ruthenium (II and III), copper (II), gold (I and II), bismuth (III), gallium (III), tin (IV) and rhenium (I) has also demonstrated anticancer activity[158]. Since the discovery of cisplatin in the early 1970s, more than 3,000 platinum derivatives have been synthesized and tested in cancer cells. Nevertheless, only about 30 compounds have entered clinical trials, and more than half of these compounds were rejected due to their high toxicity, low efficiency, and solubility[159,160]. Currently, only a few compounds are clinically approved worldwide as chemotherapeutic drugs, including cisplatin and the derivatives carboplatin and oxaliplatin. While others only have regional approval, such as lobaplatin in China, nedaplatin in Japan, and heptaplatin in Korea (Figure 8)[153,160]. According to M. J. Cleare *et al.*[162] the antitumor activity presented by the platinum complexes is associated with its classical structure. In the 1970s, M. J. Cleare team developed a formula that explains the structure-activity relationship as $[PtA_2X_2]$, where A_2 corresponds to two monodentate ligands or a bidentate amine and X_2 to two monodentate or a bidentate anionic ligand[160–162]. Since then, many platinum compounds have been synthesized from the classical structure-activity relationship formula[160].

Platinum has two main oxidation states, Pt (II) and Pt (IV). Also, platinum (II) is diamagnetic and has a preference for nitrogen atoms and heavy donors (sulfur, phosphorus, etc.) and a low affinity for oxygen and fluorine atoms. Moreover, platinum (II) has a square planar structure with four coordinated ligands, while platinum (IV) is normally an octahedral complex[161].

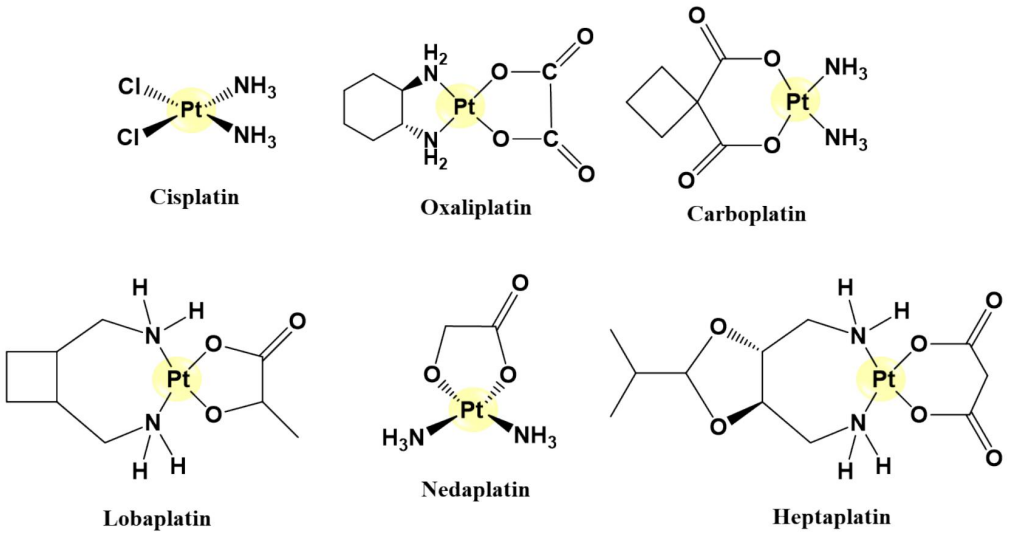

Figure 8: Chemotherapeutic drugs based on platinum compounds. Adapted from reference[153].

However, platinum (II) complexes present some limitations in their use for cancer treatment. Adverse side effects that limit its administration dose and resistance to therapy have led to the development of new strategies such as the incorporation of ligands in order to increase its activity and selectivity. The use of platinum (IV) complexes has high kinetic inertia in the coordination substitution that allows the stability of the drug, reduced reactivity, and side effects, presenting several possibilities of modification of the pharmacokinetic parameters due to the two extra ligands in the octahedral metal center. Furthermore, the reduction inside the cells by cellular reductants once enters cells of platinum (IV) to platinum (II) increases its activation and cytotoxicity. However, this reduction can occur in any part of the body that has a reducing environment, decreasing its bioavailability and selectivity for cancer cells[156,158,163]. In addition to this, platinum complexes have low absorption by the gastrointestinal tract, affecting their bioavailability. Therefore, its administration is carried out intravenously, limiting the amount of drug that reaches the DNA and consequently its efficiency, and also a large part of them has no specificity for tumor cells affecting as well healthy cells. One approach to overcome these drawbacks is using nanocarriers to deliver drugs to the target tumor, either by passive or active transport, depending on the type of ligand, as mentioned in advance[153].

3.1. Cisplatin

As stated before, cisplatin was the first platinum complex to be used as a chemotherapeutic agent, and, today, it remains the most successful therapeutic and effective antitumor drug[164,165]. Cisplatin was first synthesized in 1844 by Michele Peyrone[166] and became known as Peyrone's chloride. However, in the late 1960s, Barnett Rosenberg *et al.*[167] discovered the inhibitory activity of cisplatin in the proliferation of *E. coli* by doing experiments to analyze the effect of the electronic field on the growth of bacteria[159,167–170]. Nevertheless, only in 1971 were initiated several clinical studies that demonstrated its cytotoxic effects and its therapeutic capacity

and safety. However, cisplatin was only approved by the FDA in 1978 to treat ovarian and testicular cancers. Since then, its use has been widened to other different types of cancer such as lung, colorectal, neck and head and bladder[159,168,169,171].

Cisplatin is a neutral inorganic complex with a square planar geometry. Consisting of a platinum (II) metallic center, with two amines and two chlorines in its sphere of coordination with cis configuration. The amine ligands are named non-leaving group ligands since, in the course of intracellular transformations, they remain linked to the metal center, while chlorine ligands are considered good leaving groups, as they leave the sphere of coordination[172].

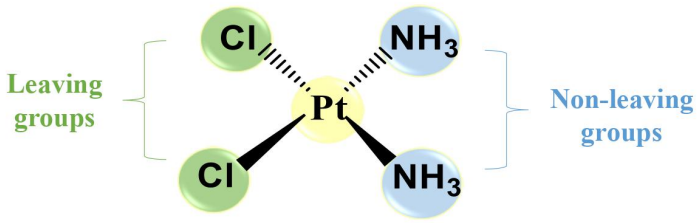

Figure 9: Structure of cisplatin.

The anticancer activity of cisplatin consists of the formation of stable complexes with DNA through intrastrand and interstrand crosslinks, which modifies the structure of DNA, preventing replication and transcription, thus inducing cellular apoptosis. The intermediates that react with DNA are the cationic complexes *cis*-$[PtCl(H_2O)(NH_3)_2]^+$ and *cis*-$[[Pt(H_2O)_2(NH_3)_2]^{2+}$ that are formed by the hydrolysis of cisplatin inside the cell[164,173].

Despite cisplatin is a bestseller drug used to treat several types of cancer alone or in combination, its activity is limited due to adverse effects[153,154,174]. In fact, toxicity is one of the main limitations of using cisplatin because it targets DNA for both tumor and normal cells, making no distinction between them. Furthermore, cisplatin has a high affinity for sulfur and selenium donors that are found in many proteins existing in the cells and plasma. Cisplatin can interact with that donor groups and interrupt proteins and enzymes' functions, reaching the DNA only 1% of the drug administered intravenously[153,163,169,174]. One example is the HSA, one of the most abundant blood proteins, containing the cysteine residue that can interact with metal complexes. Regarding cisplatin, the main interaction with the HSA involves the sulfur donors responsible for the observed toxic side effects when Pt(II) complexes are used as anticancer agents. However, this bond can be broken by so-called "rescue agents", sulfur-containing compounds (*eg.* glutathione (GSH), biotin, etc)[163]. Thus, cisplatin presents severe side effects such as ototoxicity, nephrotoxicity, neurotoxicity, hepatotoxicity, cardiotoxicity, gastrointestinal disorders, nausea, vomiting, anemia, and bone marrow suppression[153,163,169,174]. However, the major dose-limiting of cisplatin is related to nephrotoxicity[175]. Neurotoxicity occurs due to damage to the dorsal root ganglion neurons since cisplatin acts as a calcium channel blocker. Thereby altering the intracellular

calcium homeostasis and leading to apoptosis of the exposed dorsal root ganglion neurons. Symptoms include abnormal sensation, tingling in the extremities, and numbness associated with large fiber sensory loss and reduced or absent muscle stretch reflexes. These effects have a peak in severity between 1 to 4 months after the end of the weekly cisplatin regimen, although the last in many cases are generally reversible effects[175–178].

Cisplatin-induced nephrotoxicity is essentially caused by injury to the renal epithelium, which results in an inflammatory response that induces damage to nuclear and mitochondrial DNA and consequent activation of cell death[176]. This behavior is observed 10 days after the administration of cisplatin[175]. The kidney is the organ that accumulates cisplatin to a greater degree, being the main route of excretion. Thus, the concentration of cisplatin in the proximal tubular epithelial cells is approximately 5 times the serum concentration. Therefore, the unbalanced accumulation of cisplatin in the kidney contributes to nephrotoxicity[179]. This toxicity is triggered by the inhibition of the carnitine synthesis and by its resorption by the proximal nephron tubule due to the decrease in the carnitine production[179]. Carnitine is a fundamental compound in the transport of fatty acids from the cytosol to the mitochondria during the breakdown of lipids to generate metabolic energy and it is produced by the biosynthesis of the amino acids lysine and methionine. Thus, the concentration of cisplatin in the kidney exceeds the blood concentration, indicating an active accumulation by the cells of the renal parenchyma, and it is eliminated through the glomerular filtration and tubular secretion of kidneys[179]. Nephrotoxicity is observed due to increased blood urea nitrogen and creatinine, serum uric acid, and/or a decrease in creatinine clearance and reduced serum magnesium and potassium levels[180]. However, hydration with at least 3-6 L of water per day can decrease the risk of nephrotoxicity, thus decreasing the formation of the more reactive cisplatin monohydrate[180].

A high dose of cisplatin can lead to hepatotoxicity. The hepatotoxicity is mainly caused by oxidative stress, formed by the increase of transaminases and bilirubin in the circulation. Transaminases are the most sensitive biomarkers directly involved in triggering this toxicity, as these enzymes are released into the blood after cell damage. The observed pathological changes consist of necrosis and degeneration of hepatocytes with infiltration of inflammatory cells around the portal area with sinusoidal dilatation[179,180].

Cardiotoxicity is another toxic effect of cisplatin. Cardiotoxicity is due to the leakage of lactate dehydrogenase and creatine kinase from cardiac myocytes, which may be a secondary event after cisplatin-induced lipid peroxidation of cardiac membranes[179].

Cisplatin also induces ototoxicity in 10-90% of patients, affecting more children than adults, leading to deafness. The hearing loss is due to the generation of reactive species of excess oxygen in the cochlea cells, causing cell apoptosis. Symptoms include bilateral symmetrical high-frequency sensorineural hearing loss, tinnitus, and ear pain. Damage starts at the base of the cochlea, where high-frequency sounds are processed and proceed towards the apex, thereby affecting hearing at lower frequencies, with an increase in the cumulative dose. In children and babies, the consequences are devastating due to the delay in language development due to impaired perception of high-frequency consonant sounds[177,180]. However, several approaches to its treatment have been reported as local or systematic administration of antioxidants and anti-inflammatory agents[180].

The effects of gastrointestinal toxicity consist of observed nausea and vomiting that generally occur in almost all patients, despite the routine use of prophylactic antiemetics. These symptoms start after 1 to 4 h after treatment and can last for 24 h. However, late vomiting and nausea are also observed due to high doses that begin or persist more than 24 h after cisplatin administration and last up to 2 weeks. Other symptoms such as loss of taste or metallic taste, diarrhea, mucositis, and pancreatitis are also reported. However, gastrointestinal toxicity may be worse when using combined cisplatin therapies with other anticancer agents[180]. This adverse effect is much more severe compared to other platinum drugs use[175].

Another severe side effect of cisplatin is the induces of profound bone marrow suppression and anemia[175,176]. Leading, in the case of anemia, to the need for a transfusion of erythrocytes or the prophylactic use of erythropoietin[175].

Cisplatin and other platinum drugs are usually administered by intravenous infusion with changeable dosage schedules, generally in combination therapy with other cancer drugs[178]. After administration, 90% of cisplatin binds to plasma proteins such as albumin, transferrin, and γ-globulin[181]. The same is distributed throughout the body tissues, mainly in the liver, kidney, and prostate[182,183]. Their interaction with the serum proteins influences their disappearance in the plasma. Its plasma elimination is biphasic, with a short initial phase and a long second phase[181]. For example, patients who receive more than 1 h of infusion will present a total platinum biphasic clearance with a rapid initial phase of 8.7 to 22.5 minutes and a prolonged second phase of 30.5 to 106 h. Free cisplatin or ultrafilterable platinum was quickly detected and eliminated with a half-life of 22 minutes. The volume of distribution was 50.3 to 65.6 L, and about 26.6 to 50% was excreted in the urine within 48 h, making the urinary tract the main route of cisplatin elimination[181].

Another limitation is resistance. There are two forms of resistance clinically demonstrated, acquired and intrinsic resistance. Acquired resistance occurs from prolonged drug exposure throughout the treatment, while intrinsic resistance is verified without prior exposure to the drug, occurring from the beginning of the treatment[184]. Resistance mechanisms are understood as the primary mechanisms for its occurrence, the increased degradation and detoxification of cisplatin by thiols glutathione, metallothionein, and other cysteine-rich protein inside the cell preventing its interaction with DNA, as cisplatin binds to sulfur groups. In addition, the conjugation of cisplatin with glutathione can be catalyzed by the enzyme glutathione S-transferase (GST), making the compound more anionic, being subsequently eliminated from the cell through the ATP-dependent glutathione S-conjugate export (GS-X) pump. Reduction in the cellular uptake by copper transporters (CTR1 and CTR2) and organic cation transporters (OCT) and upregulate cisplatin efflux from cells which decreases cisplatin accumulation due to ATP-binding cassette (ABC) transporters. As such, the multidrug resistance-associated proteins (MRPs), which are membrane transporters, belong to this subfamily and are responsible for the efflux of ATP-dependent glutathione-platinum conjugates. In addition, the downregulation of ATP-dependent copper transporters (ATP7A and ATP7B), which belong to the P-type ATPases family, where their principal function is to remove excess copper from cells, is also implied in cisplatin resistance. So, these two major pathways (P-type ATPases transporters and ABC transporters) are responsible for removing cisplatin

from the cells. Furthermore, the increased DNA repair pathways and consequently the reduction in the formation of cisplatin DNA adducts contribute to its resistance[153,168,169,184–188].

One more limitation is the lack of selectivity once cisplatin reaches the target site once the DNA is present in small amounts since most are dispersed in cells and plasma. In this sense, several strategies were adopted to overcome these limitations, among which the use of transport systems such as dendrimers, nanotubes, micelles, and the use of ligands with specific affinity for tumor cells to improve the cisplatin efficiency[153].

Another significant drawback is the poor solubility of cisplatin in water (ca. 1 mg/mL). It is known that platinum (II) ions are considered "soft" acids and thus has affinities for moieties that contain elements according to the order S> N> Cl> O. Despite being poorly soluble in water, cisplatin is unstable in water, undergoing the first hydrolysis half time ($t_{1/2}$) approximately in 2 h at 37°C. Therefore, when cisplatin is administered intravenously because it has poor oral bioavailability, it has to be in a saline solution, allowing its charge to remain neutral for entering into cells by passive diffusion or membrane transporters. Well, cisplatin is only stable when the chlorine concentration is high, greater than 100 mM as in blood plasma[164].

Recent studies highlight the importance of the tumor microenvironment in cisplatin resistance[188–190]. The tumor microenvironmental factors that affect cisplatin resistance can be biological and/or physical. The biological components refer to biochemical consequences of tumor growth such as acidity and hypoxia and non-cancerous cells such as immune and stromal cells. On the other hand, the physical components, such as high cell density, extracellular matrix, and fluidic shear stress, also called interstitial fluid pressure, interfere with the delivery and efficiency of cisplatin[188]. The tumor microenvironment inhibits cisplatin from reaching tumor cells due to the physical barrier made up of compact cancer cells. However, the interaction between the rapid growth of the tumor and the disorganization of the surrounding vessels and the extracellular matrix can lead to increased interstitial fluid pressure[188]. The extracellular matrix is the main component of the tumor microenvironment, whose role is to act as a scaffold to maintain the structure and function of the tissue. Thus, changes in its rigidity and elasticity can make it challenging to deliver the drug to cancer cells. For this reason, the extracellular matrix plays a fundamental role both in tumor progression and in resistance to anticancer drugs[188]. The extracellular matrix can also interact with the surrounding cells and promote drug resistance by activating survival proteins, known as cell adhesion-mediated drug resistance (CAM-DR). This resistance mechanism occurs through the receptor-ligand interactions of the tumor cell with the extracellular matrix. Consequently, the contact of the tumor cells with the extracellular matrix or stromal cells triggers integrin-mediating signaling pathways that can produce anti-apoptotic molecules[188]. Another obstacle is the compact aggregation of tumor cells, and reduced blood flow can lead to hypoxia of tumor tissue and, consequently, facilitate the rigidity of cancer cells and multidrug transporter expression. Furthermore, the deficient nutritional supply of disorganized tumor vessels impels tumor cells into glycolysis, leading to the production of more acidic residues. Therefore, this acidic medium can promote the expression of the multiple drug transporter and reduce the accumulation of cisplatin within the cell[188]. The intercellular interactions in the tumor microenvironment between stromal and tumor cells can also modify the extracellular matrix and secrete growth factors, suppress the antineoplastic immune response, and support tumor angiogenesis, producing a favorable

environment for drug resistance[188]. The immune system also plays a role in cisplatin resistance. Indeed, cytotoxic T cells (CTLs), also known as $CD8^+$ T-cells, are T lymphocytes that can secrete cytotoxic enzymes such as granzyme or perforin to induce cancer cell death. However, cancer cells can activate the immune checkpoint signaling pathways and escape attacks by these lymphocytes[188]. Thus, the microenvironmental tumor can impair the efficiency of cisplatin as an anti-cancer agent through its limited delivery, inactivation, and inhibition of cancer cell death[188]. Consequently, combinatorial therapy using nanosystems is a strategy to prevent the formation of cisplatin resistance mechanisms and maintain selective targeting in cancer cells[191].

3.1.1. Mechanism of action

The mechanism of action of cisplatin involves several sequential processes, namely, the cellular uptake of cisplatin, followed by its aquation/activation, DNA binding, and cell process that leads to apoptosis (Figure 10)[192,193].

As stated earlier, for cellular uptake, pass the cell membrane and interact with the target DNA, cisplatin must be administered intravenously in a saline solution[192]. It is speculated that the entry of cisplatin into the cells occurs through the mechanisms of passive diffusion, crossing the lipid bilayer due to steric restrictions that prevent it from entering the cell via ion channels or, by transmembrane transportation system as CTR and OCT, or even by a combination of the two mechanisms[165]. In this sense, as at physiological pH, platinum chlorides are replaced by OH molecules with a neutral charge that allows the transport of cisplatin by passive diffusion across the cell membrane, flowing from high external concentration to low internal concentration inside the cell. On the other hand, the low level of copper transporters and organic cation transporters implies reduced levels of cisplatin within the cell[155,161,184,192]. The membrane transporters that can play a role in cisplatin uptake are copper transporters such as CTR1, organic cation transporters (OCT1 and OCT2), and sodium-dependent transporters. Copper transporters CTR1 are the primary copper transporters being expressed in all tissues and essential in regulating intracellular copper levels. OCTs are located in the plasma membrane and are involved in the absorption and excretion of exogenous and endogenous compounds in various organs. Regarding sodium-dependent transporters, they indirectly influence the transport of cisplatin, as it controls the gradient of sodium ions. Its inhibition decreases the gradient of sodium ions that cross the membrane and consequently affects the passive diffusion or active transport of cisplatin. Since sodium and potassium pump (enzyme Na^+/K^+ ATPase) is responsible for maintaining the gradient of the Na^+ and K^+ ions across the plasma membrane, thereby hydrolyzing the adenosine triphosphate (ATP) at the same time that it pumps sodium into the outside and potassium inside the cells[177,192].

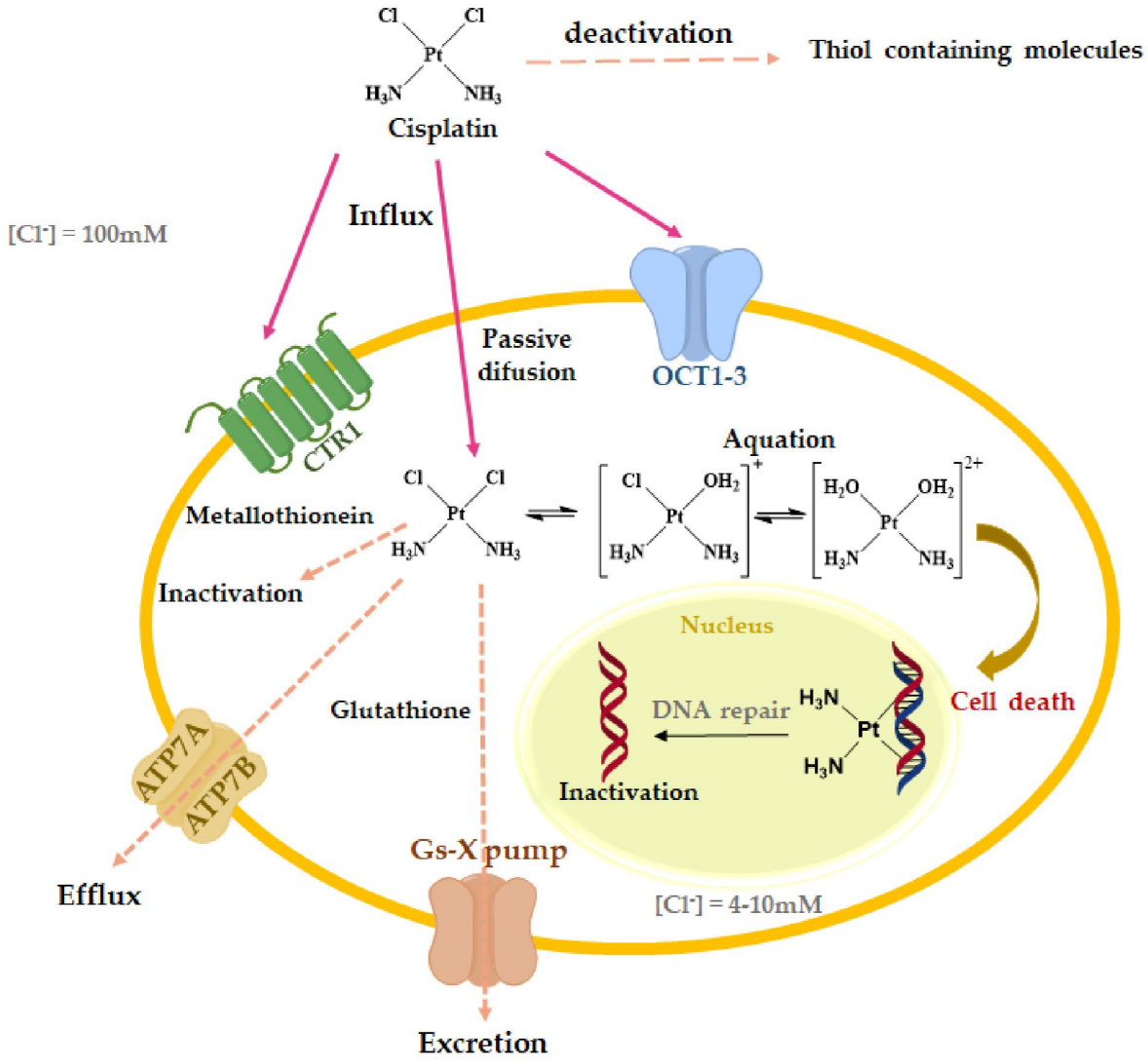

Figure 10: Representation of the cytotoxicity pathway of cisplatin.

When cisplatin is transported into the cell, it can have several ends, such as reacting with several subcellular components, including proteins, RNA, and DNA. It can also bind to thiol groups of the glutathione and metallothionein proteins, being neutralized and exported from the cell by a membrane transport system[184]. Besides, cisplatin can also bind to mitochondria DNA, inhibiting ATP production, which reduces ATPase activity by altering the calcium content within the cell, decreasing cellular respiration, ROS, and cellular lipid peroxidation[182]. Mitochondrial DNA is sensitive to platinum complexes. Additionally, the mitochondria in tumor tissues differ from normal tissues at the functional and structural level, where cancer cells have higher mitochondrial membrane potentials, making them more vulnerable to mitochondrial disturbance than normal cells[153,194]. Once inside the cell, cisplatin is subjected to hydrolysis reactions where becomes activated through the replacement of chloride ligands by water molecules. Hydrolysis of cisplatin is triggered by the concentration of chlorine ions in the cytoplasm being significantly lower between 4-10 mM than in the

extracellular matrix 100 mM[155,192]. Thus, the lower intracellular concentration of chlorine ions facilitates the hydrolysis of cisplatin in mono and diaquated cationic complexes such as cis-$[Pt(NH_3)_2Cl(OH_2)]^+$ and cis-$[Pt(NH_3)_2(OH_2)_2]^{2+}$ due to the loss of one or two chlorine ligands. These complexes are very reactive and therefore can interact with a number of nucleophiles as DNA or cellular structures present in the cytoplasm[192]. The first-order rate constants of the mono and diaquation steps in pure water at 25ºC are $2.5x10^{-5}$ and $3.3x10^{-5}$ s^{-1}, respectively. In the presence of DNA, the monofunctional adducts form at a constant rate of $10.2x10^{-5}$ s^{-1} and bifunctional adducts $9.2x10^{-5}$ s^{-1}. In this sense, the half-life for aquation and binding to DNA is approximately 2 h[192]. It is noteworthy that the exchange rate of ligands is very important, as rapid hydrolysis of the X_2 ligands leads to the formation of more reactive species. Consequently causing severe systemic toxicity and greater binding to biomolecules such as sulfur-containing amino acids, peptides, or proteins in the blood. If hydrolysis is slow, it will have less toxicity, longer plasma half-life, efficient excretion by the kidneys, but there will be a reduction in its anti-cancer properties. This effect can be overcome if the concentration of cisplatin in the target site is maintained for a longer period[161]. It should be noted that when cisplatin or a platinum complex enters the tumor cell, its cytotoxicity is only inevitable when it reaches the nucleus and reacts with DNA. This happens because the active cationic species can react with other molecules than DNA, such as proteins and RNA. In addition to having an affinity for molecules with thiol groups such as cysteine, methionine, and others, and for several enzymes involved in glutathione activity such as GST, gamma-glutamyl transferase (AGT), and glutamyl cysteine synthase (AGGS)[159]. Preferentially, the activated cisplatin complexes bind covalently to the most nucleophilic sites of the DNA at the N7 position of the imidazole ring of the guanine (G) and adenine (A) nucleotide bases in the dinucleotide sequences GG and AG. Where monofunctional adducts in DNA are formed first. Subsequently, bifunctional adducts are formed by linking a second guanine base, forming a crosslink in the DNA. These crosslinks can occur between deoxyguanosines on the same strand or at different strands, giving rise to intrastrand and interstrand DNA crosslinks[154,163,195]. The most prevalent adduct is the 1,2-d (GpG) intrastrand crosslink (65%), although 1,2- (ApG) (25%) and 1,3-d (GpTpG) (10%) intrastrand crosslinks are also formed with small amounts of GG interstrand crosslinks and monofunctional adducts (Figure 11). Furthermore, the GG intrastrand crosslinks cause the bend of DNA double helix about 35 e 40º[163,172,196]. Besides, 1,3-intrastrand adducts are repaired more rapidly by DNA repair enzymes than 1,2-intrastrand adducts[180]. Despite that, and although these changes are rare, the interstrand DNA crosslinks can also cause major changes in the structure of DNA. In this way, the interstrand DNA crosslink produced by cisplatin unwinds the DNA near the platinum site and bends the helix towards the smaller groove where cisplatin is bound[163]. Platinum-DNA adducts are recognized by several protein families associated with DNA repairs, such as high mobility group (HMG) non-histone chromosomal protein, mismatch repair (MMR) proteins, and nucleotide excision repair (NER) proteins and transcription factors as TATA protein and Y-box binding protein, YB-1[169,197]. The 1,2-intrastrand adducts can be recognized by proteins such as HMG non-histone chromosomal 1 and 2 (HMG1 and HMG2) proteins. These proteins bind tightly to platinum-DNA adduct in the broadened minor groove, specifically to the 3′ side of the strand with platinum, protecting cisplatin-DNA adducts from being repaired and contributing to its toxicity[163]. These HMG proteins are mainly

involved in regulating cellular processes involving DNA, such as replication, transcription, recombination, and chromatin remodeling. These recognize cisplatin-DNA intrastrand adducts between adjacent guanines, altering cell cycle events which subsequently leads to apoptosis[169,197].

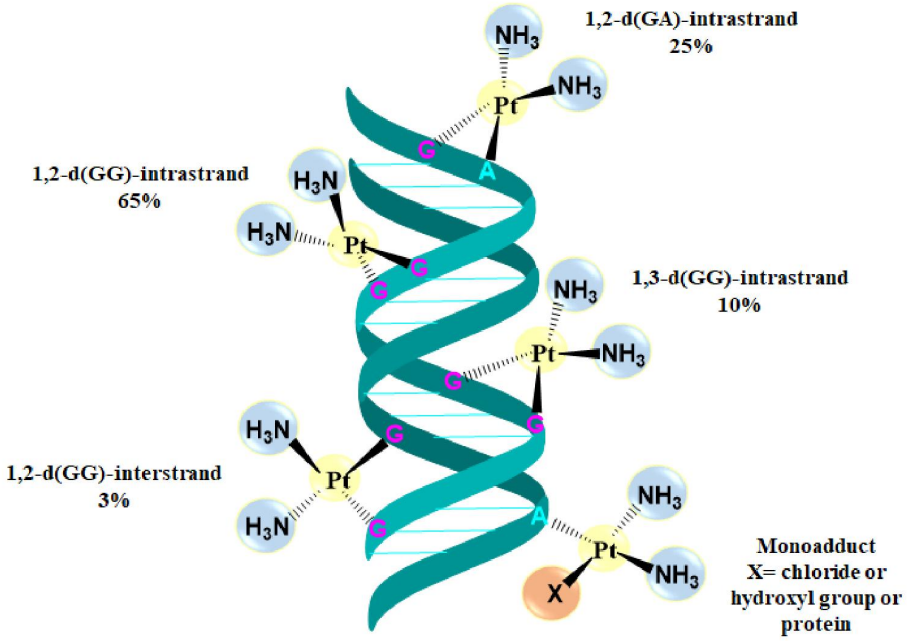

Figure 11: Cisplatin DNA-adducts. Adapted from references[163,196].

The TATA protein is a transcription factor for the RNA polymerases I, II, and II. This protein binds to DNA at the promoter sites in the minor groove by bending the double helix towards the main groove, causing a structural change similar to that of an intrastrand cisplatin crosslink. TATA recognizes the platinum adduct 1,2-[Pt $(NH_3)_2]^{2+}$-d(GpG), and binds to it, inhibiting the initiation of transcription. The affinity of this protein to the cisplatin adduct is similar to that of a link with the promoter[197]. Another transcription factor that binds cisplatin-modified DNA is the Y-box binding protein, YB-1. It is a protein that recognizes an inverted CCAAT sequence called Y-box. The YB-1 protein selectively binds cisplatin cross-links to DNA, 1,2-d (GpG), 1,2-d (ApG) and 1,3- (GpTpG). This protein is important in signaling DNA damage and also in cell proliferation. It is overexpressed in the nucleus of cells resistant to cisplatin[197]. Following this, when cell DNA is damaged, the common response to this event is to interrupt the progression of the cell cycle so that the damage is repaired, preventing mutation-inducing lesions from being transmitted to daughter cells[192]. So, the DNA damage resulting from cisplatin binding induces cell cycle arrest at the G2 stage, mediated by ATM (Ataxia-telangiectasia-mutated) and ATR (ataxia telangiectasia and Rad3-related) pathways via downstream kinases, checkpoint kinases 1 and 2 (Chk1 and Chk2), delaying the cell cycle progression. After activation, both

upregulate cell cycle checkpoint pathways, inducing cell cycle arrest and DNA repair[192,198]. The pathway employed by cancer cells to perform the DNA repair and remove adducts of cisplatin-DNA is by using the nucleotide excision repair (NER) mechanism. This process requires a large number of proteins to remove an oligonucleotide with 30 nucleotides that contain the platinum site where the new single-stranded complementary DNA replaces it, to template the synthesis of a new oligonucleotide and consequently reconstituting integrity of the gene. Amongst the NER associated proteins, the ERCC1 a DNA excision repair protein is one of the components involved in cisplatin resistance. So, the increased NER activity is associated with resistance to cisplatin[165,169,180,192].

The MMR protein complex also recognizes the major cisplatin 1,2-dGG intrastrand adduct in the template strand and binds to DNA to repair in cisplatin-DNA damage[169,180,199,200]. This protein is responsible for recognizing and repairing mismatched base pairs[199]. However, if the damage cannot be repaired, the cells will initiate a programmed cell death process by activating the apoptotic signaling pathway, which can be triggered by two mechanisms, the extrinsic or death receptor pathway or the intrinsic mitochondrial pathway. The extrinsic pathway is activated by extracellular ligands that bind to the death receptors on the cell surface, leading to the formation of the death-inducing signaling complex (DISC). At the same time, the intrinsic mitochondrial pathway is activated by intracellular signals when the cell is under stress, like DNA damage. This pathway is mediated by various mitochondrial intermembrane proteins such as c-Jun N-terminal kinase protein (JNK) signaling cascade, p53 and pro-apoptotic members of the Bcl-2 (B-cell lymphoma 2) family proteins[201]. The c-Jun N-terminal kinase protein is activated by various stress stimuli, including DNA damage. Thus, cisplatin activates the JNK pathway, where the protein p73, a pro-apoptotic member of p53, forms a complex with JNK leading to cell apoptosis[179]. Tumor suppressor protein p53 is a short-lived protein that is activated by ATM and ATR in the DNA damage signal. It can transactivate genes that are involved either in the progression of the cell cycle or the repair of DNA and apoptosis. It is responsible for preventing genome mutation[179,180]. In this sense, the increase in p53-regulated expression of pro-apoptotic genes including BAX (bcl-2-like protein 4) after DNA damage, leads to the loss in membrane potential and release of cytochrome c from mitochondria and subsequent cleavage of procaspase-9 (caspase is cysteine aspartate-specific proteinase) that bind with cytosolic Apaf-1 (apoptotic protease activating factor 1) and ATP to form an apoptosome complex which activates caspase-9. Subsequently, caspase-9 interacts with other caspases to activate the caspases 3, 6, and 7, which degrade the cell components essential to its viability, leading to apoptosis, an ATP dependent cell death mechanism[179,180,192].

On the other hand, cisplatin-DNA adducts inhibit DNA replication and inhibit transcription at the initiation and elongation stages. The discovery of the cisplatin cytotoxicity mechanism reveals that the G2 arrest of L1210 leukemia cells was necessary for apoptosis and that loss of DNA replication viability was not consistent with cell death. Thus, with the arrest in the G2 phase, the cells could not synthesize the messenger RNA (mRNA) necessary for the next stage, the mitosis, leading to inhibition of transcription and consequently to apoptosis[197]. In this sense, the antitumor efficacy of a platinum complex is related to its ability to block RNA synthesis[197].

The mechanism of inhibition of transcription of cisplatin-DNA adducts involves three steps, (1) the binding of transcription factors, where cisplatin-DNA adducts serve as binding sites such as TATA-binding protein (TBP), which have a high affinity for DNA with cisplatin. In this way, interactions with platinum adducts prevent transcription factors from binding to native promoter sites and consequently inhibit transcription in the early stage. (2) Inhibition of RNA polymerases, as cisplatin-DNA adducts inhibit RNA polymerase II at the site of platinum adducts since they prevent the transcription from being extended by the enzyme, with adducts being a physical impediment. (3) Interruption of chromatin remodeling since cisplatin-DNA adducts can interfere with transcription at the level of chromatin reorganization. Where nucleosome positioning and mobility are essential factors for transcription. Thus, cisplatin-DNA adducts can inhibit transcription in the initiation and elongation stages by altering the nucleosome organization of promoter sites and reducing nucleosome mobility[197]. However, the pathways involved from inhibition to apoptosis are not yet elucidated, although some processes that may be involved in cell death have been suggested[197,202,203].

Apart from DNA damage, cisplatin can also induce oxidative stress depending on its concentration and exposure time by ROS formation. The mitochondria is one of the main targets, resulting in the loss of the mitochondrial protein thiol group, reduction of the mitochondrial membrane potential, and inhibition of calcium uptake[179]. So, ROS can affect their respiratory function and cause cellular dysfunction. Together with apoptosis regulator BAX (member of the Bcl-2 gene family) and calcium (Ca^{2+}), they cause damage to the mitochondrial DNA (mtDNA) and decrease the mitochondrial membrane permeability transition (MPT), facilitating the rupture of the mitochondria that leads to the cleavage of the substrates and consequently to apoptosis[180]. On the other hand, cisplatin can induce apoptosis from the cell membrane. That is, the type-II transmembrane protein Fas ligand (FasL) can activate the Fas receptor to form the apoptosome complex from FADD (Fas-associated death domain) and procaspase-8. This procaspase-8 apoptosome complex activates caspase-8, which subsequently activates caspase 3, 6, and 7, cleaving key substrate and leading to apoptosis[180]. In sum, cisplatin-DNA adducts are the major cytotoxic mechanism that leads to the activation of signal transduction pathways, which sequentially kill cancer cells through programmed cell death, apoptosis[161].

3.2. Oxaliplatin and DACHPt (the active part of oxaliplatin)

Although its limitations include toxicity and resistance, cisplatin has been extensively used in cancer treatment. In this sense, these limitations triggered the pursuit of alternative compounds derived from platinum with improved anticancer properties and pharmacokinetics[159]. Among the new platinum compounds of second and third generation developed, those with 1,2-diaminocyclohexane (DACH) ligand have received more attention in recent years[204].

The synthesis of 1,2-(diaminocyclohexane)platinum (DACHPt) complexes (tetraplatin (Tetrachloro (D,L-trans)1,2-diaminocyclohexaneplatinum(IV)),malonatoplatin (1,2- diaminocyclohexanemalonatoplatinum(II)), oxaliplatin([(trans-1R,2R)-cyclohexane-1,2-diamine](ethanedioato-O,O')platinum(II)), dichloro(1,2-diaminocyclohexane)platinum(II) ($DACHPtCl_2$)) was reported in the 1970s, where the 1,2-

diaminocyclohexane (DACH) ligand showed a lack of cross-resistance with cisplatin in resistant L1210 leukemia cells and more effectiveness than others carrier-ligand platinum complexes[204,205]. Other studies have shown that DACHPt compounds are more effective against several cisplatin-resistant cell lines[204].

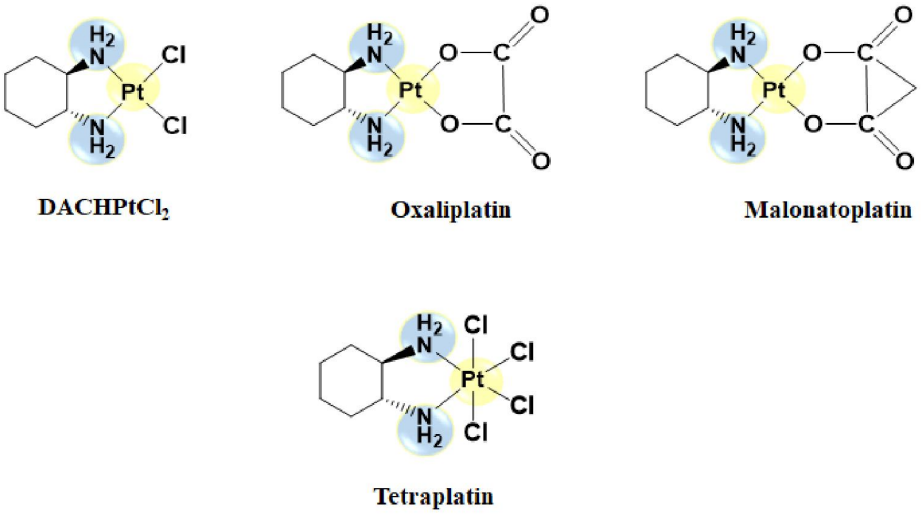

Figure 12: Structures of 1,2-diaminocyclohexane platinum(II) (DACHPt) complexes. Adapted from reference[204].

Yoshinori Kidani *et al.* at the Univesity of Nagoya, Japan was the first to suggest that stereochemical conformations of DACH ligands may affect the interactions of DACHPt compounds with DNA[204,206]. The DACH ligand has two asymmetric centers, which give rise to the trans-R, R-DACH and trans-S, S-DACH enantiomers, and the cis-R, S-DACH diastereomer. These complexes differ in their anticancer activity, which decreases according to the following order: R, R> S, S> R, S[204,205]. Amongst the DACHPt compounds, oxaliplatin, a third-generation platinum anticancer drug, was designed to overcome cellular resistance to cisplatin, being one of the best sale anticancer drugs [160,175]. The strategy used to overcome resistance to cisplatin consisted of exchanging amine ligands for 1,2-diaminocyclohexane and subsequently replacing the chloride leaving groups with an oxalate group to increase the aqueous solubility allowed for further improvement with clinical importance[205].

Oxaliplatin was synthesized by Yoshinori Kidani *et al.* in 1976 (U.S. Patent 4,169,846 in 1979) and developed primarily in France with the support of Roger Bellon Laboratorie and Debiopharm Laboratories and sold now by Sanofi S. A.[159] under the trade name of Eloxatin (patent expired). However, it was only in 1986 that oxaliplatin started the clinical trials phase I[204]. In 1999 it was received European approval and in 2002 the FDA approval[154].

Oxaliplatin is square planar platinum (II) consisting of a chelating and chiral bidentate 1,2-diaminocyclohexane (DACH) stable ligand and an oxalic acid leaving group. The DACHPt ([Pt(*trans*-1R,2R-DACH)]$^{2+}$) unit plays an important role in cytotoxicity, as it has a potent antitumor activity and protects against

cross-resistance to cisplatin. In contrast, oxalic acid significantly reduces the reactivity of oxaliplatin despite limiting the side effects associated with neurotoxicity. Due to its better safety profile than cisplatin, oxaliplatin is used in patients who cannot tolerate cisplatin[157,160,169,195]. Oxaliplatin gave interesting results in some types of cancer such as ovarian, head and neck cancer, breast, malignant melanoma, glioblastoma, non-Hodgkin's lymphoma, and non-small cell lung cancer (NSCLC). However, the best results were obtained in the treatment of colorectal cancer[159]. Accordingly, oxaliplatin is being used as a combination therapy in the frontline with other chemotherapeutic drugs, namely 5-FU and leucovorin, to treat colon cancer and non-small cell lung cancer[157]. It showed synergistic effects with 5-FU, even in tumors resistant to oxaliplatin, presenting only a specific set of toxicities[207]. The exceptional activity in colon cancer has been associated with its ability to act as a substrate for organic cationic transporters since they are overexpressed in large quantities in patients with this type of cancer[172]. Nevertheless, oxaliplatin has some side effects that limit its therapeutic index. The target organs are essentially the hematopoietic and gastrointestinal systems and the peripheral nerves[161,176,208,209].

Oxaliplatin is moderately myelotoxic. The severity of myelotoxicity is proportional to the dose, usually 85-135 mg/m^2 intravenously. Grade 3 and 4 of neutropenia are common, although only 4% have a neutropenic fever. On the other hand, hemolytic anemia and thrombocytopenia are not so serious[176,208]. It probably affects the progenitor cells in the bone marrow as oxaliplatin enters the peripheral blood cells, and therefore the DNA adducts are observed in leukocytes after its administration. However, the real impact is not known. However, the number of oxaliplatin-DNA adducts in patients' blood cells may be related to the severity of thrombocytopenia and leukopenia[176,208]. Other less frequent mechanisms of hematological toxicity have been reported, such as hypersensitivity reactions after successive infusions of oxaliplatin that can cause hemolytic anemia, secondary immune thrombocytopenia, and rare cases of acute secondary leukemia[174,176,208]. The effects of the gastrointestinal system are generally mild to moderate in intensity and include nausea, diarrhea, and vomiting[208]. In contrast, peripheral neuropathy is very common in patients treated with oxaliplatin[176,208].

Experimental data suggest that oxalate, an oxaliplatin metabolite, interacts with voltage-gated sodium channels in complex pathways involving calcium chelation, which can block the conduction pathways leading to peripheral neuropathy involving, essentially, sensory and non-motor fibers[176,208]. Peripheral neuropathy exists in two forms, the acute and the chronic form. Acute peripheral neuropathy is characterized by symptoms such as paresthesia, allodynia, or dysplasia that affects the oropharyngolaryngeal area, extremities, and lips during or just after the administration of oxaliplatin infusion. It is usually triggered by exposure to cold and disappears in a few hours or days[176,208]. Chronic peripheral neuropathy results from cumulative exposure to oxaliplatin and occurs in grades 3 and 4. Incidence is approximately in 15% of patients who received a cumulative dose of 800 mg/m^2. The symptoms are associated with the extremities[176,208]. This adverse effect, initially described as a degenerative process of the axons, in which the sodium channels play a role, is now considered the accumulation of platinum compounds in the dorsal root ganglia cells, which causes atrophy and mitochondria dysfunction being irreversible in less than 5% of patients[176,208]. So, mostly, peripheral neuropathy manifests itself as a decrease in proprioception and distal sensations[176,208]. Nonetheless, it is crucial to understand the mechanism of oxaliplatin chronic peripheral neuropathy in order to prevent and treat it, once dose-limiting

toxicity causes neurotoxicity[163]. Other disadvantages include low selectivity at tumor sites, rapid degradation and/or inactivation after administration, and low bioavailability[210]. Nevertheless, it has several advantages compared to cisplatin: low toxicity, no cross-resistance to cisplatin, and a wide spectrum of anticancer activity[210].

Oxaliplatin is administered intravenously through an infusion. The bioavailability of oxaliplatin is complete after intravenous administration. Thus, when a 2 h intravenous infusion of oxaliplatin is administered at a dose of 130 mg/m^2, the maximum plasma platinum concentration was 2,96 ± 0,57 µg/mL[211]. After 2 h of infusion, about 15% of administered platinum is present in the systemic circulation while the remaining 85% is quickly distributed in the tissues or eliminated in the urine. The platinum volume distribution on plasma ultrafiltrate ranged from 349 ± 132 to 812 ± 369 L. This high volume of distribution may be due to the DACH complex as it has a lipophilic nature and binds irreversibly to proteins, DNA, and other cellular macromolecules[211]. Right after the infusion, oxaliplatin undergoes rapid and extensive non-enzymatic biotransformation in physiological solutions into active derivatives by substituting the oxalate group. In this way, some transient reactive species are formed, among which the mono and diaquo DACH platinum complexes, that can subsequently covalently bond to macromolecules such as plasma proteins, essentially albumin, and gamma-globulins, being an irreversible process and over 95%. It also irreversibly binds to erythrocytes[211]. So, the interaction of oxaliplatin with cellular proteins, tissues, blood, and other plasma constituents, forms inactive species. However, it is expected that these molecules are of no pharmacological interest. Because most pharmacological studies only measured the content of platinum in biological matrices, which complicates the interpretation of pharmacological data[208]. After five days of a single 2 h infusion of oxaliplatin, platinum was eliminated in about 54% by urine and only 2% by fecal excretion. Being the main route of elimination the renal excretion. Furthermore, the clearance of platinum from plasma through the covalent binding to tissues and renal elimination is fast. As the renal clearance of platinum correlated with the glomerular filtration rate, the main mechanism for eliminating platinum from the kidneys is glomerular filtration[211]. The decline in platinum levels after administration of oxaliplatin is described as having a tri-exponential elimination pattern, with two distribution phases at 0.28 h ($t_{1/2}\alpha$) and 16.3 h ($t_{1/2}\beta$). This was followed by a long phase of elimination of 273 h ($t_{1/2}\gamma$)[211]. As the third half-life of oxaliplatin is in the order of hundreds of hours, it is expected to accumulate in the tissues. Thus, a study examined the long-term retention of platinum from 8 to 75 months after its treatment[208]. Platinum was found in both the entire and ultrafilterable (unbound platinum) plasma. Where the risk factors for persistently high levels are, high cumulative dose and decreased glomerular function. According to the authors, the platinum found was still reactive, having the ability to form adducts with DNA *in vitro*. However, the physiological significance of this reactivity is not yet known, but the results are worrying about long-term toxic effects as secondary malignancies[208].

In contrast, the pharmacokinetics of oxaliplatin after the infusion were evaluated in the patient's blood, presenting a half-life of 14.1 minutes[212]. Another 45 minutes half-life was also observed and related to the *in vivo* degradation of oxaliplatin in the blood, suggesting that the oxaliplatin degradation in blood has a role in its elimination[208,212]. However, the dichloro (1,2-diaminocyclohexane) platinum (II) compound ($DACHPtCl_2$)

is a potent anticancer drug with a broader spectrum of activity with less toxicity and no cross-resistance with cisplatin in several types of cisplatin-resistant cancers. But, due to its very low solubility in water (0.25 mg/mL), is very difficult to administer intravenously, limiting their clinical use as an antitumor drug[175,213]. Although compounds containing the DACH group have less solubility in water than cisplatin, this feature can be beneficial in developing drug delivery systems[161].

So why not use a carrier to deliver the drug DACHPt, instead of using oxaliplatin which has disadvantages at the clinical level if the mechanism of action of oxaliplatin is due to the DACH carrier?

3.2.1. Mechanism of action

Oxaliplatin is administered intravenously because it is not orally bioavailable due to its poor absorption, chemical reactivity, and severe gastrointestinal side effects[214]. Compared to cisplatin, oxaliplatin is much more stable to aquation due to the chelating nature of the oxalate group. The aquation of oxaliplatin is also much slower, with a constant rate of 1.2×10^{-6} s^{-1} at 37ºC in 10 mM HEPES ((4-(2-hydroxyethyl)-1-piperazineethanesulfonic acid) buffer[192]. Although the differences in cytotoxicity between oxaliplatin and cisplatin are attributed to the DACH ligand, the bidentate oxalic acid ligand, in turn, alters the drug's activation pathway (Figure 13). The biotransformation of oxaliplatin is based on the nucleophilic substitution of the oxalate ligand by chloride ions followed by hydrolysis. So, at intracellular physiological concentrations, these chloride complexes interact with HCO^{3-} (bicarbonate) and H_2PO^{4-} (dihydrogen phosphate) ions, producing reactive species, then the aqua complex can react with amino acids, proteins, and DNA. However, by reacting with amino acids such as glutathione, L-cysteine, and L-methionine can form inactivated species[205,215].

The reaction of platinum complexes with strong nucleophiles usually results in the formation of inactive platinum complexes. Conversely, the reaction of platinum complexes with weak nucleophiles, such as the N7 of guanines in DNA, requires first the hydrolysis of the complex that occurs through interaction with HCO^{3-} and H_2PO^{4-} at physiological concentrations, which creates the active complex. In this sense, most likely, the reactions with HCO^{3-} in the plasma, with intracellular HCO^{3-} and H_2PO^{4-}, represent the main oxaliplatin activation pathways[204]. Therefore, in plasma, oxaliplatin rapidly undergoes non-enzymatic transformation forming reactive species due to the displacement of the oxalate group, which complicates its pharmacokinetic profile[208].

The cellular uptake of oxaliplatin is carried out through passive diffusion, facilitated, and/or active transport[216]. It is assumed that the organic cation transporters OCT1 and OCT2 mediate the cellular uptake of oxaliplatin since their overexpression significantly increases the cellular uptake of oxaliplatin[216,217]. As for copper transporters, it is known that the CTR1, is involved in the cellular uptake of oxaliplatin, although its role in resistance is still uncertain[169,216]. Furthermore, due to the high lipophilicity of the DACH ligand, there is an increase in the cellular uptake of oxaliplatin compared to cisplatin[169].

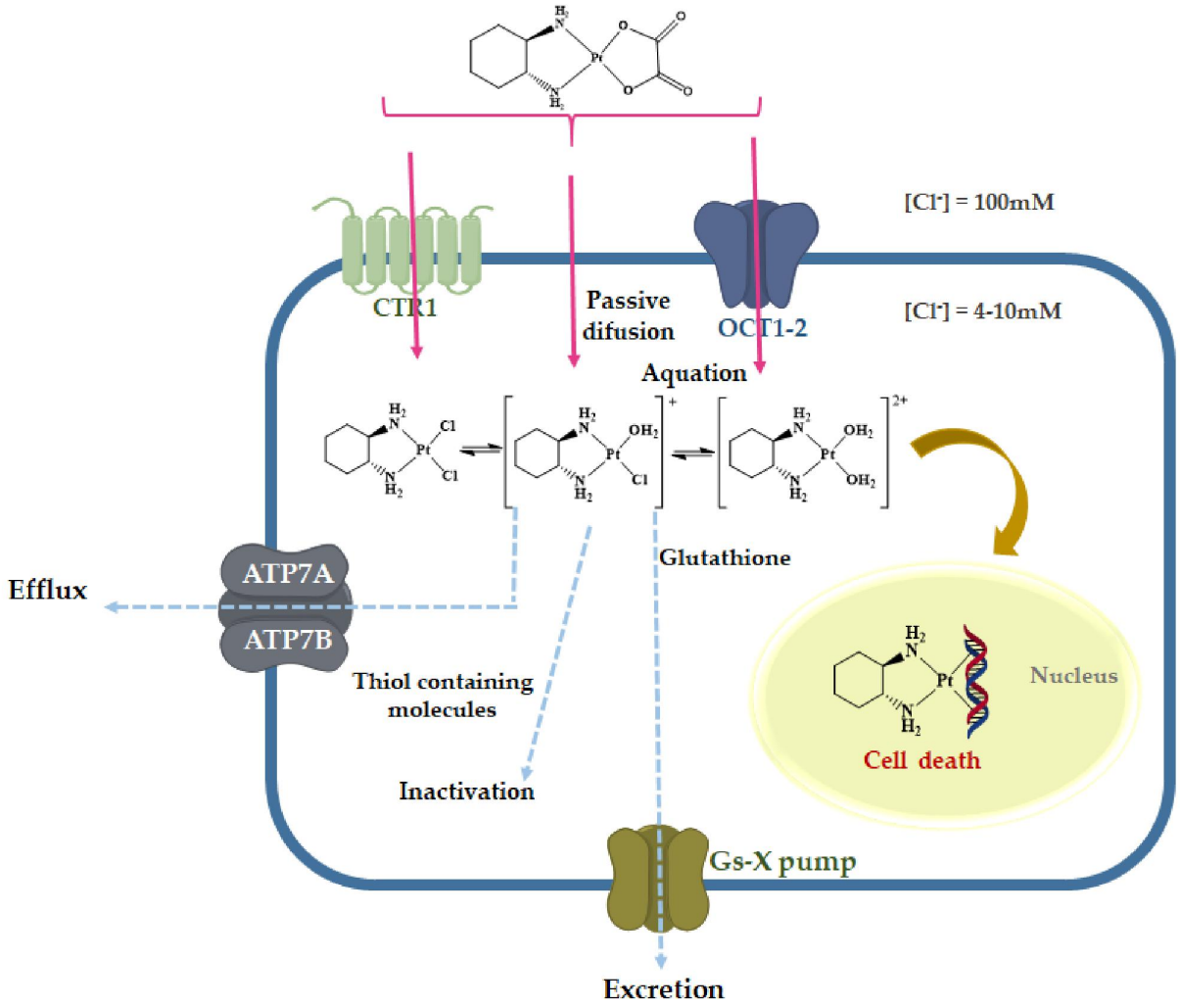

Figure 13: Representation of the cytotoxicity pathway of oxaliplatin.

The main mechanism of action of oxaliplatin is also mediated by the formation of adducts with DNA (Figure 14). Although, it can also bind to RNA and proteins. Thus, when oxaliplatin enters the cell, a chloride ligand dissociates to form a reactive 1,2-DACH monoquamonocloro platinum (II) ($[Pt(R,R\text{-}DACH)(H_2O)(Cl)]^+$) complex, which reacts with the N7 of guanine of the DNA to form monoaducts. The dissociation of the second chlorine ligand forms the reactive specie 1,2-DACH diaqua platinum (II) ($[Pt(R,R\text{-}DACH)(H_2O)_2]^{2+}$) that allows the conversion of monoaducts into several stable diaducts. Thus, the hydrolysis of oxaliplatin through aquation to form reactive species is lower than that of cisplatin. Most adducts formed are with two adjacent purine bases (1,2-GG or AG) intrastrand. These adducts are more effective in blocking DNA replication and transcription, being considered the main cytotoxic lesions. The other types of adducts formed but to a lesser extent are the interstrand crosslinks and DNA-protein crosslinks[204,207,208,218].

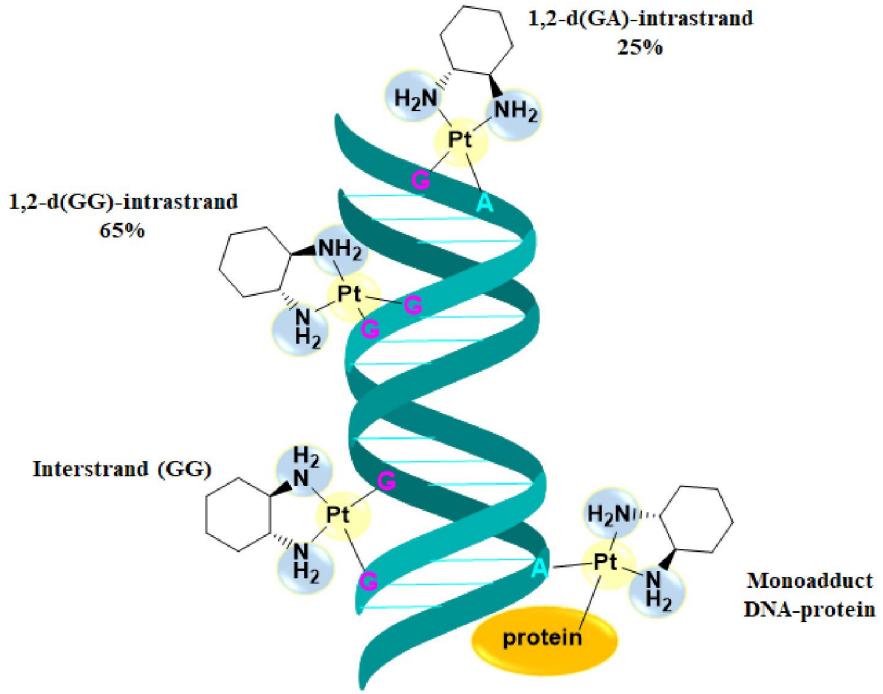

Figure 14: Oxaliplatin DNA-adducts. Adapted from reference[218].

The formation of biaducts between oxaliplatin-DNA inhibits DNA replication and transcription, triggering apoptosis after cell cycle arrest, in case there is no repair by excision of nucleotides[208].

Compared to cisplatin, oxaliplatin is not efficient in inducing adducts, but the modification of the three-dimensional structure of DNA may be more significant and efficient in inhibiting polymerization and DNA repair due to the size of the diaminocyclohexane group[159,219]. Nonetheless, in addition to the formation of the 1,2-intrastrand crosslink, a new feature was identified in the oxaliplatin-DNA adduct, the hydrogen bond between the pseudoequatorial hydrogen atom NH of the trans-R, R-cyclohexane-1,2-diamine ligand, and the C6 atom of the 3-d (GpG) platinated lesion, which demonstrates that chirality influences the interaction of oxaliplatin with DNA[172,207]. However, oxaliplatin requires less DNA damage than cisplatin to achieve an equal level of cytotoxicity[219]. Despite the similarities between cisplatin and oxaliplatin, there are some relevant differences in their mechanism of action, which may be related to their different profiles of anticancer activity. DACHPt adducts are bulkier and more hydrophobic than cisdiaminePt, so DACHPt adducts are more effective in inhibiting DNA synthesis and are more cytotoxic. The conversion of the monoaduct to the diaduct is slower for DACHPt adducts, as the N-Pt-N binding angle is probably more restricted for DACHPt-DNA adducts than for cisplatin-DNA adducts[204]. Since the DACH ligand is bulkier, it induces a different conformational distortion in the DNA, because it fills a large part of the main DNA groove making it narrower and less polar at the intrastrand crosslink site[200]. Thus, its lipophilicity and volume are responsible for the differential formation of oxaliplatin-DNA adducts. Hence, when projecting into the major groove, 3.7 Å more than cisplatin, and exhibiting a non-covalent bond with DNA, the DACH ligand appears to form a helix similar to A-DNA[215]. These adducts are not recognized by the damage recognition complex involved in MMR proteins,

but there is no decrease in cytotoxicity, which makes the antitumor activity of oxaliplatin independent of MMR[169]. In addition, it has been shown that bidentate adducts formed between bifunctional mononuclear platinum (II) complexes and DNA are susceptible to further transformations. That is, the coordination bonds between these platinum complexes and the nucleotide bases of the DNA can be spontaneously cleaved, with a cleavage reaction for each intrastrand crosslink. This process forms an intermediate monofunctional adduct that can restore the intrastrand crosslink or form new adducts such as DNA-DNA or DNA-protein crosslinks[200]. On the other hand, these cleavages can lead to the formation of linkage isomerization reactions between platinum complexes and double-stranded DNA[200]. So, the differences in the thermodynamic destabilization of the DNA and the kinetics of the rearrangement reactions observed in the oxaliplatin-DNA adducts indicate that the chirality of the DACH ligand can significantly affect the structural properties and consequently its biological effects[200].

Following this, the antitumor activity of oxaliplatin is mediated by the recognition of DNA adducts by cellular proteins. Thus, the affinity of the HMGB protein with the 1,2-GG intrastrand adduct of oxaliplatin is comparable with cisplatin. However, the binding of the HMGB1 protein to oxaliplatin-DNA adducts is less strong[220].

Another protein involved in the biological process of oxaliplatin is TBP, which is a transcription factor for RNA polymerases (I, II, and III) that specifically binds to a DNA sequence called the TATA box. This protein is an abundant nuclear protein that binds to modified DNA as tightly as HMGB1. In turn, the platinum DNA can deviate the TATA box from its natural binding site by inhibiting transcription initiation. The affinity of this protein with DNA is less than with cisplatin[220]. The damage induced in DNA by the DACH ligand is poorly recognized by DNA recognition and repair pathways[220]. In this sense, the MMR protein complex can be prevented from binding to adducts due to conformational distortions in the adduct region, which results in greater irreversibility of lesions in DNA[204,208,221]. The MMR is a post-replication repair path responsible for correcting base mispairs and looped intermediate that occurs during replication. It is also involved in the cellular response to DNA damage, playing a role in the signal transduction pathway, cell cycle regulation, and apoptosis. In this way, MMR initiates cellular responses to damage through recognition of DNA adducts, leading to cell cycle arrest and cell death by apoptosis[215]. Thus, tumors with MMR deficiency are sensitive to oxaliplatin, which is the case with colorectal cancer, and others intrinsically resistant to cisplatin[216].

On the other hand, DNA damage by oxaliplatin is repaired with similar efficiency and kinetics by the NER system than cisplatin[200,216]. The NER system targets damaged or inappropriate DNA bases. In this sense, the repair factors XPA and RPA that are involved in the formation of a damage recognition subunit triggers the recruitment of endonucleases responsible for double excision at the 3' and 5' lesion sites, with the excision of the oligomer containing the damage from 22 to 32 nucleotides in length. Subsequently, DNA re-synthesis is carried out, and the linking of the new strand to the parental DNA fills the gap obtained after removing the damage[215].

In addition, tolerance to DNA damage can be achieved through the post-replication repair process, which refers to the ability to replicate DNA past a bulky adduct without introducing gaps in the strand, not being considered

a true repair process, as adducts are not removed. This process is defined as translesion synthesis or replicative bypass. The replicative bypass of DNA lesions can determine the tolerance of the toxic action of the drug. In this sense, replicative bypass and translesion synthesis can be used to indicate the ability of certain polymerases to continue DNA synthesis, even in the presence of bulky adducts such as oxaliplatin in the DNA chain that are ignored by the repair mechanism that continues through them. The tolerance of DNA damage can also occur through the MMR path[215]. Accordingly, an enhanced replication bypass and/or a decrease in MMR are more sensitive to the action of oxaliplatin, suggesting a considerable clinical potential of the drug[215].

Oxaliplatin can also exert its cytotoxic effect by inducing the intrinsic and extrinsic apoptosis pathway, although it is not clear whether it promotes caspase activation[216].

The tumor suppressor protein, p53, detects DNA damage, activate cell cycle control checkpoints, and triggers cell death[216]. So, the intrinsic route is regulated by the Bcl-2 family of proteins, which includes anti-apoptotic members (Bcl-2, Mcl-1, and Bcl-xl) and proapoptotic members (Bak, Bad, and Bax). The extrinsic pathway is mediated by the activation of death receptors (TNFR1, TRAIL, DR4, DR5, and Fas/CD95) after association with specific ligands[216]. Nonetheless, the inhibition of DNA replication is not always sufficient to cause cell apoptosis, and thus the inhibition of transcription also plays a key role. The inhibition of transcription consists of three mechanisms: (1) the binding of transcription factors where the DNA-platinum adducts can be used for transcription factors as binding sites, preventing their binding to their promoter sites and consequently inhibit the initiation of RNA synthesis; (2) nucleosomal DNA adducts that can block RNA polymerase from accessing the DNA template. In addition to adduct in genomic DNA, oxaliplatin can also form adducts in nucleosomes; (3) the inhibition of RNA polymerases, since the formed adducts are not able to enter the active site of an enzyme as polymerase II, preventing the elongation of transcription by the enzyme[197,208].

Oxaliplatin can also induce cell death by immunogenic mechanisms independent of the DNA damage mechanism. Once inside the cells, it can induce tumor cell stress and death that trigger tumor-specific immune responses. Thus, immunogenic cell death depends on three requirements at the cellular level, such as exposure to calreticulin, a calcium-binding chaperone that prevents misfolded proteins from being exported by the endoplasmic reticulum (ER). Oxaliplatin, induce a response to ER stress, which results in the exposure of calreticulin to the cell surface. As a result, in a signal for engulfing the dying cell by dendritic cells and macrophages[222,223]. On the other hand, oxaliplatin can induce the release of ATP from the apoptotic cell in the extracellular medium, recruiting the dendritic cells to the tumor site inducing their activation. This process leads to the release of the HMGB-1 protein from the cell nucleus during secondary necrosis. HMGB-1 protein bind to Toll-like receptor 4 (TLR4) from dendritic cells, leading to enhanced activation and cross-presentation by dendritic cells to the T cells of the immune system. TLR4 is an important protein that leads to activation of the innate immune system[176,222,223]. In that sense, oxaliplatin in colorectal cancer cells causes the expression of immunogenic signals before apoptosis and activate the innate immune system allowing the T cells to produce interferon and interact with TLR4 protein of dendritic cells creating a tumor vaccine[176].

On the contrary, despite cisplatin having a mechanism of action with some similarities with oxaliplatin, the formation of bis-DNA adducts does not induce immunogenic cell death. This fact is attributed to the lack of

calreticulin exposure on the cell surface after treatment with cisplatin. Although it induces the release of ATP and HMGB-1. However, as radiotherapy is a potent inducer of exposure to calreticulin, and since this treatment is frequently performed with cisplatin administration, their effectiveness can be enhanced by the mechanism of immunogenic cell death[222]. Therefore, apoptosis can be caused by several cellular processes such as the formation of DNA damage, inhibition of RNA, interruption of DNA synthesis, and triggering of immunological reactions[208]. Nevertheless, other mechanisms of cell death are associated with oxaliplatin, such as necrosis and autophagy. Regulated necrosis can occur in response to several factors such as DNA damage, binding of death receptors, among others[216]. Normally, necrosis is associated with an inflammation process since the loss of the integrity of the cell membrane occurs, resulting in the release of cytosolic content such as the HMGB-1 protein and other inflammatory molecules to the extracellular environment, which causes an inflammatory response[216].

It has been shown that, depending on the cell type, oxaliplatin can activate apoptosis or necrosis[216,224,225]. Nonetheless, more information is needed to clarify the necrosis mechanism triggered by oxaliplatin, although some studies are reported in the literature[216,224,225].

Autophagy is a cellular catabolic process that occurs in the degradation of cellular components by lysosomes. This mechanism can be initiated in response to cell stress, DNA damage, endoplasmic reticulum stress, or hypoxia. Autophagy in tumor cells can prevent or promote cancer formation and regulate the response to therapy, including drug-induced cell death[216]. It has been demonstrated in different studies that the treatment with oxaliplatin activates autophagy in cell lines and xenografts of hepatocellular carcinoma and colon cancer, contributing to the tolerance of oxaliplatin by decreasing the generation of reactive oxygen species[216,226–228]. However, a recent study has shown that oxaliplatin kills cancer cells by inducing ribosome biogenesis stress[229]. The ribosome biogenesis occurs in the nucleolus, a highly structured organelle located in the nucleus, whose role is to synthesize proteins and produce ribosomes in cells. Thus, a disruption either of the nucleolus or ribosome biogenesis triggers a nucleolar stress response that leads to cell death through the activation of the tumor suppressor p53[229,230].

A study by Michael Hemann *et al.* demonstrated that oxaliplatin induces cell death through the ribosome biogenesis stress, where it was observed that the pre-RNA was upregulated, unlike the RNA polymerase II transcript that remained stable after treatment with this drug. Nevertheless, the molecular mechanism is not yet fully understood[231].

There are several ways to a cell becomes resistant to oxaliplatin, such as the decrease in cellular uptake and an increase in drug efflux contribute to reducing the amount of the drug within the cell available for cytotoxic action. An important resistance mechanism of oxaliplatin is the efflux through glutathione-mediated export, which is interceded by the family of ABC transporters that decreases oxaliplatin within the cell. Once inside the cell, oxaliplatin can also react with molecules containing thiol groups such as glutathione and metallothioneins, causing it inactive. Thus, GST catalyzes the conjugation of molecules with glutathione protecting macromolecules from cell damage. Another is the upregulation of the ATP-dependent copper transporters (ATP7A and ATP7B), which belong to the P-type ATPases family[216]. In addition, the increased

DNA repair by NER and the increase in the replication bypass process, and the decrease in the MMR mechanism can also contribute to oxaliplatin resistance [208,215].

The different antitumor effects to cisplatin are elucidated by the capacity of oxaliplatin to form adducts with DNA of different conformations, thus exhibiting different cytotoxic effects, although having low reactivity with DNA[200]. Thus, the bend of DNA, thermal destabilization, unwinding, and displacement of the conformational change induced by the oxaliplatin interstrand are greater than those observed with cisplatin; the affinity of the HMGB protein for oxaliplatin interstrand bonds is much less than cisplatin, and the chirality of DACH ligand affects structural properties of oxaliplatin interstrand crosslinks[200,232].

These factors determine that oxaliplatin has a different activity extent of the drug compared to cisplatin[169].

Nevertheless, the cellular activation, processing, and the ability to overcome resistance have not yet been fully elucidated[205,215,229].

3.3. Issues of current platinum drugs: combination therapy

Combination therapy was first devised in 1965, where Emil Frei, James Holland, and Emil Freireich proposed the possibility of the first-ever combined chemotherapy for acute leukemia. The proven success of combination therapy in the treatment of acute lymphocytic leukemia in children has been formally known as the POMP regimen (a combination of methotrexate, 6-mercaptopurine, vincristine, and prednisone)[233]. After that, research in cancer therapy focused on investigating combination therapies that target different pathways to create an additive or synergistic effect[233].

Combination therapy is a therapy in which two or more drugs with different mechanisms of action are used, where the drugs can act synergistically, additively, or antagonistically depending on the molar ratios of the individual drugs in the combination[180,234–236].

The synergistic effect is when one drug intensifies the effects of another, resulting in greater activity than the added effect of each drug individually. Meanwhile, the additive effect results in an activity equal to the sum of the effects of each drug. In contrast, the antagonistic effect results in an activity that is less than the sum of individual drugs effect, although it is still beneficial[180,234,235,237]. Drug interactions are generally assessed with a median effect analysis widely applied to calculate a combination index (CI). Thus, if CI =1 the effect is additive, CI <1 the effect is synergistic, and if the CI > 1 the effect is antagonistic[237].

The approval of drugs for combination therapy in recent years fundamentally highlights the potential of conjugating drugs to improve the efficiency of cancer treatment[238]. It was being an appealing alternative treatment due to its potential to overcome the resistance developed by many drugs and decrease the probability of developing cross-resistance[239].

Following this, the selection of the combination therapy was, for decades, based on the subsequent principles, using drugs with clinically proven activity as unique agents, without resistance, without overlapping toxicity, with different mechanisms of action, with different target cell cycles, and able to induce anticancer synergetic effects[237].

Thus, a good combination will lead to a synergistic or additive therapeutic effect due to the combination of drugs with non-overlapping mechanisms of action and toxicity, besides delaying or overcoming resistance to multiple drugs[237]. Nevertheless, despite an excellent initial efficacy that decreases over time due to acquired resistance, the conventional method, monotherapy, is still a widespread treatment modality for treating different types of cancer. However, it is considered less effective than synergistic or additive combination therapy[233,234]. A common issue of these therapies is that they do not distinguish between healthy and cancer cells, which causes toxic side effects and unforeseen risks. In addition, combination therapy could greatly reduce patients' immune systems, increasing the probability of other diseases, drug resistance, severe tumor microenvironment that hinders drug penetration, dose-limiting toxicity, and tumor heterogeneity[233,237]. Although combination therapy can also be toxic, it represents significantly less toxicity, as a reduced dose of each drug is required to achieve the synergistic or additive effect[233].

On the other hand, monotherapy is more susceptible to drug resistance since, with the treatment cyclic, the use of a drug causes cancer cells to recruit alternative ways to escape cell death. In contrast, combination therapy can reduce the incidence of resistance due to a more effective response and fewer treatment cycles[233]. However, one of the concerns of using combination therapy is off-target toxicities. Nonetheless, synergistic combinations of drugs can achieve greater selectivity than individual drugs[239]. Thus, if well designed, these combinations of drugs can allow the targeting of drugs and effective therapies with reduced toxicity, using lower single drug concentrations with non-overlapping dose-related toxicities[239]. Once one of the most significant limitations of the drugs used in cancer treatment is a lack of specificity and, consequently toxicity, anticancer drugs are selected based on their complementary mechanisms and non-overlapping toxic side effects[239].

In combination therapy, compared to monotherapy, determining the optimal dose of each drug is very important[235].

Although combination therapy has shown promising results in patients with some types of cancer, in others, the use of multidrug or drug combinations is not very effective[235].

One limitation to be considered in combination therapy is the toxicity of healthy cells and tissues, the inability to coordinate the pharmacokinetics of drugs, and the exposure of tumors to decrease the development of resistance to multiple drugs. In this sense, it is necessary to effectively inhibit the target[235,238].

Generally, the development of new drug combinations continues to be based on the maximum tolerated dose of each drug individually. Nevertheless, it is necessary to consider that the doses of the drugs used in the combined therapy for the system to be effective may not be equivalent to the maximum tolerated dose of each one and not the doses empirically recommended in clinical trials. Therefore, the molar proportions of drugs in combination therapy play a fundamental role in increasing the effectiveness of the therapy[235].

After administration, it is very difficult to coordinate drug pharmacokinetics simultaneously due to the difference in clearance, tissue uptake, and metabolism[235]. In addition, many drug combinations need simultaneous exposure to have an effective antitumor activity, where the mechanisms of action are interrelated. The concentration of each drug, or rather, the molar proportion of the drugs exposed to the cancer cell, is an important factor[235,237]. The pharmacokinetic differences of the drugs in combination mean that higher doses of

the drugs are used to obtain a simultaneous and prolonged efficacy against the tumor. Such high doses to patients result in unnecessary toxicity that can compromise combination therapy[235].

Alternatively, combination therapy can be ineffective when the exposure of one drug to the tumor cells falls below the therapeutic concentration limit. This situation could happen due to the difficulty of controlling the proportions of the drugs *in vivo* when the pharmacokinetics of the drug combination is uncoordinated, causing the tumor cells to trigger a survival signaling pathway inducing resistance[235].

Hence, the success of clinically tested combination therapy presents a lack of efficacy because of the difficulty of the drugs reaching the desired spatiotemporal distribution when delivered in free form. Since drugs must be delivered to the right place at the right time, the differences in their pharmacokinetic and physicochemical properties prevent this from happening, producing intolerable toxicities, and acquired drug resistance[237,239]. The selection of drugs to be used in combination therapy must be based on their selective and synergistic activity and not based on the success of a single drug[239].

The undesirable effects also present in combination therapy led to the introduction of new strategies, such as the use of nanoparticles to deliver combinations of drugs to increase the drug exposure since they assume the pharmacokinetic characteristics of the carrier. In addition to that, the cellular uptake of the carrier influences the biodistribution of drugs, providing greater access to tumor tissues. Thus, a coordinated pharmacokinetic behavior can allow a targeted delivery with a synergistic proportion of drugs in tumor cells and tissues to decrease the toxic effects during the treatment and improve the sustained release of the drugs[235,238].

Particularly, nanocarriers are suitable for controlling the proportions of drugs during the administration process, which is not achieved with the administration of free drugs due to their uncoordinated biodistribution, metabolism, and elimination[235]. Thus, the nanocarrier can synchronize the drugs' local availability, biodistribution, and accumulation in the tumor tissue due to the ERP effect[237]. In fact, the premature release of drugs into the blood circulation must be avoided once it can reduce the efficiency and increase toxicity in normal cells and tissues due to synergistic toxicity and interfere with their elimination[237]. It follows that the use of nanocarriers is an effective way to improve the effectiveness of cancer treatment since the complexity of cancer requires alternative therapies, such as the use of combination therapy using new nanocarriers[240]. Besides this, due to synergistic effects, combination therapy has been very appealing due to the increased effectiveness against cancer, reduced toxicity, and resistance to multiple drugs due to cyclical treatments[240].

Accordingly, the key points of combination therapy consist of reducing the therapeutic dose and adverse effects and simultaneously increasing the effectiveness of the treatment[240]. Therefore, the amalgamation of the advantages of combined therapy with the nanocarrier approach is expected to provide a more efficient and safe multipotential system[237,240]. In this sense, the use of drug delivery systems has been promising in this type of therapy[240].

In this way, advanced drug carriers may allow synergistic combinations of drugs in the preclinical setting to be translated more predictably clinically. Although, in most cases, it can be directed towards preferential uptake in tissues and tumor cells instead of healthy cells[235].

Thus, there are several ways to deliver multiple drugs. For a combination of two drugs, one drug can be delivered freely while the other by using a nanocarrier ("Free drug + Nanocarrier"); both drugs can be administered by separate nanocarriers ("Nanocarrier + Nanocarrier"), or both drugs are co-encapsulated in the same nanocarrier[237].

Usually, the first two forms of administration are delivered sequentially. In contrast, in the form of co-encapsulation, the delivery is simultaneous, which allows a controlled temporal and spatial distribution of the various drugs, increasing the concentration of drugs within the cell and coordinating drugs synergy against tumor cells[237]. The "Free Drug + Nanocarrier" form is the closest to the current practice in the use of nanoparticle formulations for cancer treatment. However, the "Nanocarrier + Nanocarrier" form can offer more flexibility in dosage and formulation than co-encapsulation, and the latter can be more effective in coordinating drug actions at the cellular level[237]. Obviously, there are advantages and disadvantages for each of these delivery forms, and they must be selected according to each specific situation[237].

Platinum drugs approved for clinical use are rarely administered on monotherapy. They are generally used in combination therapy to obtain a synergistic effect through different mechanisms of action, allowing a reduction of the dose for each drug[169].

Some examples of combination therapies with cisplatin are the conjugation of cisplatin and doxorubicin that is effective in diffuse malignant pleural mesothelioma (DMPM)[180,241], cisplatin combined with Anvirzel™ (a *Nerium oleander* extract composed mainly by oleandrin and oleandrigenin[242]) for breast cancer cell lines, prostate, colon, pancreatic, lung, and melanoma cancer[180,243], and cisplatin, oxaliplatin, quercetin, and thymoquinone for human ovarian cancer[180,244]. Oxaliplatin has also been used in clinical in combination therapy. Some examples are oxaliplatin combined with 5-FU (5-fluoro-2,4-pyrimidinedione/ 5-fluorouracil) and folinic acid as a first and second-line treatment for advanced colorectal cancer as FOLFOX (FOLinic acid-Fluorouracil - OXaliplatin) chemotherapy regimen; a combination of docetaxel, oxaliplatin, and 5-FU (DOF) for the treatment of metastatic or unresectable gastric or gastroesophageal junction (GEJ) adenocarcinoma, oxaliplatin, 5-FU, and leucovorin as adjuvant treatment for colon cancer and bevacizumab in combination with oxaliplatin as first-line in the treatment of metastatic colorectal cancer[245–248].

In this sense, 5-FU is one of the drugs used in combination therapy with other drugs such as cisplatin and oxaliplatin because it has a different mechanism of action. 5-FU is an important anticancer drug with a broad antitumor activity, often used in combination with other drugs to treat different types of cancer, particularly colorectal cancer, due to its synergism effect. It belongs to the group of fluoropyrimidines, antimetabolite drugs. Antimetabolite drugs are responsible for inhibiting essential biosynthetic processes or for being incorporated into DNA and RNA, inhibiting their normal function[249,250]. The development of 5-FU was reported by Charles Heidelberger *et al.* in 1957[251]. However, several important findings have been previously described. In 1954, Robert Rutman *et al.*[252] observed that uracil pyrimidine (one of the four bases found in RNA) had been integrated into rat hepatomas more quickly than normal tissues, indicating that uracil metabolism was a potential target for antimetabolic chemotherapy. Later, in 1956 R. E. Handschumacher *et al.*[253] reported the tumor inhibitory activity by 6-azauracil[249,250]. The 5-FU mechanism of action is through the

incorrect incorporation of the metabolites into DNA and RNA and inhibiting the thymidylate synthase (TS) enzyme [249]. Despite being used to treat different types of cancer, 5-FU has been mainly used to treat advanced colorectal cancer and early-stage, due to its therapeutic effectiveness against this cancer. The first-line treatment for advanced colorectal cancer based on chemotherapy with 5-FU as a single agent is only 10 to 15%. Therefore, in the past 20 years, new approaches have been developed to increase the anticancer activity of 5-FU, overcoming its clinical resistance. For instance, combining other drugs with 5-FU increases the response rates for the same type of cancer to 40-50%. However, despite these significant improvements in treatment, new therapeutic strategies are needed[249].

5-FU, an analog of uracil with a fluorine atom on its structure is administered to patients through intravenous infusion[249,250]. More than 80-85% of the 5-FU administered is catabolized into inactive metabolites by the enzyme dihydropyrimidine dehydrogenase (DPD), being only about 1 to 3% responsible for the anticancer effects through an anabolic pathway[249,250,254]. 5-FU enters the cell *via* facilitated transport, such as uracil, which is first converted into three active metabolites as fluorodeoxyuridine monophosphate (FdUMP), fluorouridine triphosphate (FUTP), and fluorodeoxyuridine triphosphate (FdUTP). These metabolites, as mentioned earlier, are integrated into DNA as the FdUTP and FdUMP metabolites. The FdUTP causes DNA damage and FdUMP the DNA synthesis, because inhibit the TS enzyme due to the formation of a ternary complex with the TS and 5,10-methylenetetrahydrofolate (CH_2-THF or MTHF), and the FUTP metabolite is integrated into RNA, causing changes in its function and processing[249,250,254].

The 5-FU main mechanism of action is the conversion of fluorouridine monophosphate (FUMP) directly by the orotate phosphoribosyltransferase (OPRT), or indirectly by fluorouridine (FUR) using the enzymes uridine phosphorylase (UrdPase) and uridine kinase (UK)[249,250].

Another alternative route of action is the conversion of 5-FU into fluorodeoxyuridine (FUDR) through the catalysis of thymidine phosphorylase (dThdPase), and then into FdUMP through the phosphorylation of FUDR by the thymidine kinase (TK) enzyme[249,250]. However, this conversion causes adverse effects such as gastrointestinal toxicity and myelotoxicity[250].

On the other hand, the DPD enzyme, through the catabolism pathway, converts 5-FU into dihydrofluorouracil (DHFU), giving rise to alpha-fluoro-β-alanine (FBAL) and alpha-fluoro-β-ureidopropionic acid metabolites[249,250]. The DPD is usually found in the intestinal mucosa, liver and also in other tissues. This is a rate-limiting process of catabolism of 5-FU in cancer and normal cells. Where DPD breaks down up to 80% of administered 5-FU in the liver[249,250], cancer patients with a deficiency in the DPD enzyme have a greater risk of severe toxicity consisting of mucositis, diarrhea, neurotoxicity, and may even lead to death[250]. In terms of 5-FU clearance, approximately 60-90% of the drug administered is excreted in the urine in 24 h in the form of FBAL[250]. Nevertheless, FBAL is responsible for observed adverse effects during chemotherapy, such as neurotoxicity and cardiotoxicity in several patients. Additionally, FBAL is also considered to be the leading cause of hand-foot syndrome (HSF) acquired by cancer patients during the 5-FU treatment process[250].

As stated before, FdUMP metabolite forms a ternary complex inhibiting the TS enzyme responsible for converting deoxyuridine monophosphate (dUMP) into deoxythymidine monophosphate (dTMP) by a

reductive methylation reaction using the methyl donor CH_2-THF. This reaction provides the only source of thymidylate, which is necessary for DNA replication and repair[249,250]. The TS protein operates as a dimer, where the subunits contain a nucleotide-binding site, where the active metabolite FdUMP binds, and a CH_2-THF binding site, forming a stable ternary complex. In turn, this complex prevents the dUMP from accessing the TS nucleotide-binding site by competing with the FdUMP, which inhibits the synthesis of dTMP, resulting in a deoxynucleotide (dNTP) pool imbalances and an increase in the levels of deoxyuridine triphosphate (dUTP), which causes DNA damage[249,250]. However, the repair of uracil and DNA with 5-FU by the UDG (uracil-DNA glycosylase) nucleotide excision repair enzyme is useless due to the high ratios of FdUTP/FdTTP, resulting only in the false incorporation of nucleotides, which causes DNA strand breaks and consequently cell death[249]. Nevertheless, the extent of DNA damage caused by dUTP depends on the levels of pyrophosphatase dUTPase that limits the intracellular accumulation of dUTP and UDG[249]. On the other hand, thymidylate can be recovered from thymidine using the TK enzyme, decreasing the effects of TS deficiency, where this rescue pathway represents a potential mechanism of 5-FU resistance[249,250]. Even so, therapy with 5-fluorouracil can be improved with the specific accumulation of this drug in tumor tissues, decreasing its toxicity.

Thus, drug delivery systems are a promising strategy for the delivery of 5-FU, as it allows specific targeting for cancer cells and improves its pharmacokinetic profile, as a short half-life and non-uniform oral absorption. This occurs due to the 5-FU metabolism by the enzyme dihydropyrimidine dehydrogenase. In this sense, the use of delivery systems are an appealing approach to decreased the side effects of anticancer drugs[255].

3.4. Platinum metallodrugs delivery systems under clinical studies and/or commercially available

Currently, more than 99% of approved clinical drugs are organic compounds. Although the percentage of drugs containing metals, metallodrugs, is very low[256]. Metallodrugs are compounds that have metal ions in their structure[164,256,257].

Regarding cancer therapy, platinum coordination compounds are considered crucial anticancer agents against various types of cancer, with a clinically proven efficiency[256]. Among which cisplatin and oxaliplatin are commercially available drugs, is broadly used to treat diverse types of cancer, either individually or combined with other drugs, as mentioned earlier[258]. However, as these platinum compounds used alone have adverse effects that are harmful to health, new metallodrugs delivery systems using these platinum complexes are being developed to improve the therapeutic effects and tested clinically[258].

Some examples of metallodrugs delivery systems that are in clinical trials will be discussed below.

The NC-4016 was developed by Professor Kazunori Kataoka of the University of Tokyo and is currently licensed by NanoCarrier (Japan) to improve antitumor effects and decrease oxaliplatin peripheral neuropathy[258]. The NC-4016 micelle formulation is driven by the polymer-metal complexation between the Pt (II) groups of DACHPt and the carboxylic acid of the polyethylene glycol-poly (glutamic acid) block copolymer, PEG-b-P(Glu). The molar ratio of [DACHPt]/[Glu] is 0.75. The NC-4016 has a hydrodynamic

diameter of 40 nm and a narrow size distribution[258]. DACHPt is the active metabolite of oxaliplatin, hydrophobic, and toxic when administered systemically. Therefore, the use of polymeric micelles can increase cell permeability and improve the retention of these anticancer drugs, allowing a prolonged half-life in the blood circulation and a selective accumulation of platinum at the tumor sites[258]. DACHPt is released from the NC-4016 complex accompanied by the dissociation of the micelles, depending on the pH and concentration of chloride ions, with the replacement of Pt(II) in the center of the micelle by chlorine ions. Thus, with increasing acidity, DACHPt is selectively released in cancer cells during subcellular traffic. After intravenous administration and internalization by cancer cells, DACHPt binds to DNA through inter and intrastrand crosslinks, forming adducts that consequently trigger the cell death mechanism[258].

Preclinical data demonstrated that NC-4016 has high stability, which is attributed to the hydrophobicity of DACHPt and a significantly improved PK profile compared to oxaliplatin alone, which results in superior antitumor effects and reduced peripheral neuropathy. The significant inhibition of tumor growth provided by NC-4016 over the free drug was attributed to the high and prolonged accumulation of platinum in the tumors[258]. Accordingly, the reduced peripheral neuropathy observed is due to the high stability of the micelles and the reduction of platinum exposure to normal tissue. Thus, the combination of the improved safety profile and antitumor efficacy served as the basis for the clinical development of this formulation[258]. A phase I clinical trial (NCT03168035) developed in the USA using the NC-4016 to determine the highest tolerated dose that can be administered to patients with advanced solid tumors or lymphoma and its pharmacokinetics was concluded in 2017. However, the results had not been publicly disclosed[258].

NC-6004, micellar nanoparticle-encapsulated cisplatin, consists of a polymer-metal complex with block copolymers of hydrophilic polyethylene glycol and poly (glutamic acid) attached to the inner core of the micelle consisting of the hydrophobic polyaminoacid polymer. Cisplatin is thus complexed in the P(Glu) block (poly(glutamic acid)) with a molar ratio of [cisplatin]/[Glu] of 0.71. Thus, the micelles form spontaneously between Pt(II) and carboxylic acid groups in the P(Glu) block[258]. This formulation was developed by Kataoka group at the University of Tokyo, reported in 2003, and later licensed to NanoCarrier (Japan). In 2008 NanoCarrier licensed NC-6004 to Orient Europharma (Taiwan)[258]. Compared to other block copolymer-drug aggregates, this formulation showed high stability and provided sustained release of cisplatin for more than 150 h in physiological saline. When incubated in saline solution at 37ºC, the micelle system NC-6004 has a diameter of 28 nm, keeping an approximate diameter of 25 nm up to 50 h[258]. In 2011, an NC-6004 phase I clinical trial tested on 17 patients with advanced solitary tumors was completed. This study was consistent with preclinical observations where toxicities such as neurotoxicity, nephrotoxicity, and cytotoxicity were less frequent and less severe in patients treated with this drug than cisplatin alone[258]. Despite this, unpredictable hypersensitivity reactions have been observed. Although they are not fully understood, it is suggested that the rapid binding of plasma protein to cisplatin and the subsequent prolonged circulation time of protein-bound cisplatin may be an underlying mechanism for sensitivity reactions[258]. In this sense, the maximum tolerated dose (MTD) has not been identified due to serious and unexpected hypersensitivity reactions. But 120 mg/m^2 was considered as the proximate dose of MTD and the recommended dose of 90 mg/m^2 [258]. Another phase I/II

study was conducted to assess the combination of NC-6004 with gemcitabine (GEM) in patients with pancreatic cancer. Patients were pre-medicated with oral steroids before the administration of NC-6004, and no hypersensitivity reactions were reported. The treatment of NC-6004 combined with GEM was relatively well tolerated, despite showing only modest efficacy in this group of patients[258]. Other clinical trials were conducted using this NanoCarrier formulation, including a phase I study for various types of cancer, such as head and neck cancer (NCT02817113) and a phase III study in pancreatic cancer (NCT02043288) in USA and Asia, respectively[258–260]. Nevertheless, no results were available regarding to these studies.

SPI-77 is a metallodrug that completed phase II of clinical trials to treat patients with ovarian cancer (NCT00004083). SPI-77 is a liposomal formulation pegylated with cisplatin, developed to reduce systemic toxicity and increase the availability of cisplatin in cancer cells[261,262]. This study aimed to evaluate the response rates and safety of SPI-77 in patients with recurrent epithelial ovarian cancer. More properly determine the objective response rate in patients with platinum-sensitive ovarian cancer treated with SPI-77. As well as determining the time and the duration of the response, the progression time, survival index and characterizing the safety of this regimen in patients[261]. Phase I studies of clinical trials began in 1995 with doses between 40-420 mg/m^2, where side effects included nausea, vomiting, mild anemia, and muscle weakness in doses above 320 mg/m^2 and an infusion-related reaction. They observed that serum cholesterol levels in patients increased with higher doses of SPI-77, probably related to the number of lipids administered. This safety profile has been confirmed in phase II studies[261]. The phase II study consisted of enrolling patients with recurrent ovarian cancer with a progression-free interval of more than 6 months after the last platinum-based chemotherapy. This study was initiated to test the hypothesis that SPI-77 would be active in a disease selected for sensitivity to platinum drugs[261]. However, the results of this study were inconclusive despite providing important information for the development of similar platinum liposomal agents[261].

BTP-114, is an albumin-binding cisplatin prodrug, currently in phase I of clinical trials to treat patients with advanced solid tumors and BRCA or another mutation in DNA repair (NCT02950064). This clinical study consists of the dose-escalation part 1 and the expansion part 2. Furthermore, it aims to assess the safety, pharmacokinetics, and anticancer activity of BTP-114[263]. This complex is composed of cisplatin and a maleimide fraction, which can bind strongly and selectively to human serum albumin with a potential for anticancer activity[264]. Intravenous treatment of BTP-114 for part 1 consists of 21-day cycles. Where doses will be increased in sequential cohorts until the maximum tolerated dose is determined, which will lead to the recommended dose for phase II[263]. For part 2, 5 patient cohorts will be treated at the RP2D (highest dose with acceptable toxicity) of BTP-114 in 21 day cycles for pancreatic cancer, ovarian cancer, castration-resistant prostate cancer, triple-negative breast cancer, and deoxyribonucleic acid (DNA) repair mutation-positive advanced solid tumors[263]. After intravenous administration, the maleimide group of BTP-114 rapidly conjugates with HSA in the bloodstream, prolonging blood circulation, improving half-life, and altering the biodistribution of BTP-114 compared to free cisplatin[264]. BTP-114 demonstrated greater accumulation in tumor tissue, thereby increasing its effectiveness and reducing systemic toxicities. This study is active[263,264].

BBR 3464 is a new trinuclear platinum compound that exhibited antitumor activity on sensitive and resistant models to cisplatin and the p53 (a tumor suppressor gene) mutant tumor models[265]. Phase I/II of clinical trials consisted of the treatment of patients with small cell metastatic lung cancer who have not responded to previous treatment (NCT00014547)[266]. The purpose of this study was to determine the efficiency of BBR 3464 in terms of response rate to patients with sensitive or refractory metastatic cell lung cancer. Duration of the response and time for progression in patients treated with this drug, including the survival, incidence and the severity of the toxic effects, and the pharmacokinetics of this drug in patients involved, were also evaluated. Two routes were explored in phase I of the clinical trials, an intermittent schedule (day 1 every 21 days), and a continuous schedule (daily x 5). The dose-limiting toxicities in both schedules included diarrhea and neutropenia[265]. A subsequent study was started, analyzing two levels of doses, 0.9 and 1.1 mg/m^2, administered every 21 days[265]. From the obtained results, the 0.9 mg/m^2 dose every 21 days was recommended for phase II tests, due to a greater proportion of patients at 1.1 mg/m^2 requiring a dose reduction or delay[265]. It was concluded that the toxicity profile of BBR 3464 in this phase II is consistent with phase I since patients with lung cancer patients in phase II clinical trials did not show a significant response to BBR 3464. However, due to side effects associated with toxicity such as diarrhea and neutropenia, the clinical development of this drug as a unique agent of this disease was stopped[154,265]. Another phase II study of BBR 3464 consists of treating patients with gastric or gastroesophageal adenocarcinoma[267]. The study objectives were to determine the efficacy and toxicity of BBR 3464 when administered as a first and second-line treatment for advanced disease in patients with gastric and gastroesophageal adenocarcinoma. In this sense, two studies were conducted, one as a first-line study and another as a second-line treatment for metastatic or locally advanced disease[267]. Thus, 19 first-line patients received 74 infusions and 26 second-line patients had 53 infusions[267]. However, due to the low antitumor response and the toxicities found during treatment, the use of BBR 3464 for this type of cancer was not recommended[267].

ProLindac, DACH polymer platinate AP5346, is a DACH platinum prodrug that has concluded the phase II clinical for treating ovarian cancer[268]. This drug delivery system consists of DACHPt coupled to a biocompatible water-soluble hydroxypropylmethacrylamide copolymer (HPMA) *via* a pH-sensitive linker[269]. The phase I study aimed to establish a recommended dose for the phase II clinical trials. In addition, to determine the qualitative and quantitative toxic effects and to study the duration, predictability, intensity, onset, reversibility, and the dose-effect relationship of the toxic side effects[268]. This study included 26 patients who received a total of 104 infusions of ProLindac at doses ranging from 40 mg Pt/m^2 to 1280 mg Pt/m^2 [268]. The PK results obtained indicated that the objective of the specific design of this drug was achieved since its function was to remain inactive in the plasma and to be activated only after entering the environment with low pH of the extracellular fluid of the tumor or inside the cancer cell[268]. Dose-limiting neutropenia was found at the highest dose. However, there was a single episode of neutropenia at another dose level but with grade 1. The main adverse effects were nausea, vomiting, renal toxicity, and possible hypersensitivity reactions[268]. This phase I study demonstrated that high doses could be safely administered to patients when treated with antiemetics and hydration[268]. However, the results also demonstrated that frequent administration of ProLindac

was not appropriate due to the long terminal half-life of platinum observed in patients. In this sense, the dose administered in the phase II study was revised every two or three weeks. The phase II study was designed to include a dose-varying phase, with doses based on the recommended dose intensity in phase I[268]. The objectives of the phase II study consisted of assessing the antitumor activity of ProLindac as a unique agent in chemotherapy in patients with advanced ovarian cancer previously pretreated with organoplatin, taxane, and anthracycline for 6 months or more without platinum and free of progression[268]. Treatment-related adverse effects included gastrointestinal, nervous system disorders, metabolism, and nutrition. Other effects such as nausea, vomiting, and paresthesia occurred in less than 5 patients. The frequency and severity of these effects corresponded to the expected toxic effects known from platinum-based treatments. No cases of acute neurotoxicity were observed, although some patients had some chronic neurotoxicity due to platinum accumulation[268]. This study concluded that ProLindac in patients with recurrent cancer has been demonstrated to be efficient and safe. The results were similar to those reported for oxaliplatin but in a patient population that was more heavily pretreated[268]. The next phase of clinical development of this drug will probably be to evaluate combinations with other drugs such as gemcitabine or paclitaxel for gynecological cancers and even the replacement of oxaliplatin in FOLFOX, a combination of chemotherapy drugs (Folic acid, 5-FU and Oxaliplatin) used in the treatment of colorectal cancer[268].

Another system consists of Dendrimer-Oxaliplatin, which, in a preclinical study developed by Starpharma, demonstrated better anticancer efficacy and less toxicity than oxaliplatin in a model of colon cancer (xenograft)[270]. They observed that the dendrimer-enhanced oxaliplatin nanoparticles substantially reduced neutropenia, an effect of dose-limiting toxicity[270]. This system is being developed as part of Starpharma's internal drug delivery program. The positive results are the subject of a new patent application in addition to the commercial potential[270]. In this sense, Starpharma intends to move forward with dendrimer-enhanced oxaliplatin formulations, where further studies are underway to explore further the positive impact on bone marrow toxicity and the potential to reduce other clinically important toxicities. This dendrimer-enhanced oxaliplatin formulation is protected by a portfolio of registered and granted patents[270]. Due to impressive results, the company intends to promote the development of oxaliplatin derivatives enhanced with dendrimers[270].

4. NMR for platinum drugs

Nuclear Magnetic Resonance (NMR) spectroscopy was discovered in 1945 by Felix Bloch and Edward Purcell[271–273]. At the end of the Second World War, Felix Bloch, seeing the success of the molecular beam magnetic resonance experiments of Isidor Rabi *et al.*, thought as a theory the possibility of measure the magnetic resonance of nuclei in condensed matter. Bloch made several estimates for the ^{1}H signal, but it was only in the fall of 1945 when he returned from service during WWII for Stanford, where he worked on radar scattering and magneton theory who started the experimental work. Later, on Christmas of that year, they found the resonance and that the relaxation of thermal equilibrium T1 was only a few seconds or even less,

contrary to what they thought. After the first successful experience, Felix Bloch received the news that the same discovery related to his work was made by Edward Purcell and his colleagues H. C. Torrey and R. V. Pound at Harvard[272]. The discoveries of both Bloch and Purcell were announced in 1946 in the same issue of the Physical Review. In 1952, Felix Bloch and Edward Purcell received the Nobel Prize for Physics. Where Edward Purcell, in his lecture, described all the basic quantities and processes that control NMR spectra, being the same: "the influence of molecular motion; magnetic dipolar splitting in solids; the influence of electric quadrupole moments; chemical shift; indirect spin–spin coupling and aspects of a general theory of nuclear magnetic relaxation"[272].

NMR spectroscopy is based on the study of a variety of nuclei that have different spin states, which consists of the rotation of the nucleus around its own axis. As the nuclei are electrically charged, the application of an external magnetic field generates two different spin states, one of low energy-oriented with the applied field and the other of high energy with magnetic moment opposite to the applied field, thus occurring a transfer of energy from the lowest level to the highest energy level. For the excitation of the nuclei from the lower energy level to the higher one is applied a short and intense burst of radiofrequency radiation[274,275]. Although the spin states are almost equally populated, the small excess of spins that assume the low energy state is responsible for resonance. Nuclear magnetic resonance is achieved when the nuclei oriented with an applied magnetic field are induced to absorb energy and change the spin orientation in relation to the field. A signal named free induction decay (FID) is obtained when the nucleus relaxes to the ground state. This signal, detected as a function of time, is then converted by the Fourier transform, obtaining a frequency spectrum of the nucleus under study[274–276].

Since then, the applications of NMR have been continually expanded, as it is a versatile and powerful tool for the elucidation of structures of organic and organometallic compounds, degree of functionalization, as well as in the structural and dynamic determination of macromolecules in biology and recently in metabolite profiles in the area of metabolomics and also to medicine[273,274,276]. Its selective detection of elements and the sensitivity of nuclear spin properties to inter and intramolecular environments make this technique a crucial choice for fast structural characterization[273].

In medicine, more specifically in the pharmaceutical industry, NMR was used as an analytical tool to validate and identify synthesized compounds. However, in recent years, NMR has played an essential role in discovering and designing drugs, including platinum drugs, which are among the most used drugs in cancer treatment[276].

The development of platinum drugs with reduced toxic side effects and with a broader spectrum of activity to overcome cisplatin resistance has been a significant focus on the search for anticancer agents, making NMR methods very useful in their investigation[277,278].

The ^{195}Pt and ^{15}N-NMR nuclei as well as the 2D [^{1}H, ^{15}N] NMR have contributed to the study of the molecular mechanism of action involving reactions with DNA and proteins, thermodynamic stability, and the kinetics of dynamic processes, including linker exchange rates, beyond the structures of molecules[277,278]. Although the ^{195}Pt nucleus is reasonably sensitive for NMR detection, with a natural abundance of 33.8%, its detection limit

(5-10mM) prevents observing ^{195}Pt signals of natural abundance in physiological fluids. Nevertheless, its very large chemical shift range (> 15,000 ppm), is an appealing characteristic that allows differentiating between Pt (II) and Pt (IV), which tend to have chemical shifts at the high and low-field ends of the range, respectively[277,278].

Besides, it is important to note that NMR does not always give us detailed information on all reactions, but it has contributed to the understanding of the molecular mechanisms of action of platinum complexes by providing information about their behavior in biological systems[278]. Indeed, the use of the NMR metabolic approach for study the biological systems with metal complexes has been shown to be a useful tool both in the molecular mechanism of action of the drug and in the evaluation of the tumor response to metal complexes[279].

5. Goals of the thesis

The complexity and severity of the cancer disease demand alternative compounds that allow us to overcome the problems presented by commercially available drugs, such as toxicity and acquired resistance. This motivated us to investigate systems that allow maintaining the metallodrugs already used in the therapy, potentially effective but significantly reducing its side effects.

In detail, this Ph.D. work-plan aimed to develop a new family of metallodendrimers based on anionic PAMAM dendrimers (carboxylate terminated half-generations 0.5-3.5) functionalized on their surface with platinum drugs (cisplatin Pt(II) or DACHPt(II)), evaluate their potential *in vitro* as effective drugs delivery platform against different types of cancers, as human ovarian cancer cell lines (A2780 and A2780CisR), human breast cancer cell line (MCF-7), human epithelial colorectal adenocarcinoma cell line (CACO-2) and normal human fibroblast cell line (BJ). Subsequently, study its biocompatibility toward the human blood cells and the DNA binding. The best metallodendrimers were encapsulated with the drug 5-FU and test against two cancer cell lines (A2780CisR and CACO-2).

In another way, but with the same purpose, PAMAM dendrimers were used in the treatment of cancer (*in vitro*), with increased fluorescence of amine-terminated PAMAM dendrimer (generations 3, 4, and 5) decreasing at the same time its toxicity to be used as drug delivery systems and as bioimaging agents. The fluorescence properties of Ammonium persulfate (APS)-treated PAMAM dendrimers were evaluated against a set of cancer cells as well their hematoxicity and cytotoxicity. DOX was then encapsulated in APS-treated PAMAM G4 to study their capability of delivering the drug without losing their fluorescence.

Our purpose with the use of these family of PAMAM dendrimers as a delivery drugs platform is to increase the tumor accumulation of the drug, minimizing the exposure in the normal tissues, and for the metallodendrimers family obtaining a more effective DNA platination and an improved and less-repairable DNA damage by increasing the number of platinum complexes with fewer side effects. For the APS-treated PAMAM dendrimers, the purpose is to increase its fluorescence and use them as an anticancer drug delivery system.

The four main questions to be addressed with this Ph.D. are the following:

1) Can low generations of anionic PAMAM dendrimers surface modified with platinum drugs improve the therapeutic efficacy of the standard metallodrugs?
2) Can APS-treated PAMAM dendrimers be less toxic and deliver the anticancer drug simultaneously without losing its fluorescence?
3) Can the simultaneous co-administration of the prepared metallodendrimers with other standard drugs result in a synergetic effect?
4) How could NMR techniques be useful in the characterization of the synthesized metallodendrimers?

CHAPTER II

Cisplatin-based metallodendrimers as anticancer drugs

1. Introduction

Cisplatin was approved by FDA at the end of 1978 for clinical use and remains today in the frontline for cancer treatment[165]. Nonetheless, the limitations of cisplatin have led to the development of new platinum compounds, intending to decrease the adverse effects and maximize their effectiveness[153,154,174,184,280]. One way to overcome these drawbacks is to use nanodelivery platforms, such as dendrimers to deliver the drug to the target site[22,23,76]. Different groups published studies using PAMAM dendrimers with higher generations. For instance, Gordon Kirkpatrick *et al.*[92] showed the functionalization of high generations (3.5-6.5) of the anionic PAMAM dendrimers with cisplatin in a bidentate form. Navid Malik *et al.*[146] described the conjugation of cisplatin to the G3.5 anionic PAMAM dendrimer. Ismaeil Haririan *et al.*[281] reported the conjugation of cisplatin with PAMAM dendrimers of generations 1 and 2, and Ngoc Tran *et al.*[282] the conjugation of cisplatin with the G2.5 and G3 of PAMAM dendrimers. Hitesh Kulhari *et al.*[283] also used the G3.5 and G4.5 of PAMAM dendrimers with different cores to conjugate cisplatin. Other studies have also reported the conjugation of cisplatin with PAMAM dendrimers but using the amine-terminated PAMAM dendrimers[284,285].

In this context, our strategy uses anionic PAMAM dendrimers as nanocarriers for cisplatin, where two forms of conjugation were studied. Thus, different generations of the anionic PAMAM dendrimers (G0.5-G3.5) were functionalized with cisplatin in mono and/or bidentate forms to determine which conjugation of cisplatin is more effective as an anticancer drug. After complete characterization, the cisplatin-metallodendrimers were tested *in vitro* with several cancer cell lines, and the hematoxicity in human blood and DNA binding were also assessed. Moreover, 5-FU was encapsulated within the cisplatin-metallodendrimers for those that showed better efficacy against cancer cells. The anticancer potential of these combination drugs was then evaluated *in vitro* using two cancer cell lines, the A2780CisR and CACO-2. To the best of our knowledge, this is the first study that compares different conjugation forms of cisplatin using several half-generations of PAMAM dendrimers and the effect of the 5-FU drug, a combination drug in both conjugation forms of cisplatin. Additionally, as far as we are aware, we prepared the first anionic PAMAM dendrimers conjugated to cisplatin in a monodentate form using low generations from 0.5-2.5 and in the bidentate form until generation 1.5.

2. Materials and Methods

2.1. General

Except for the anionic PAMAM dendrimers generations 0.5-3.5, all the other chemicals were used as received. Anionic PAMAM dendrimers G0.5 (19.19 w/w % in methanol), G1.5 (20.03 w/w % in methanol), G2.5 (9.98% w/w in methanol) or G2.5 (3.43 w/w % in water), and G3.5 (10.04 w/w % in methanol) with an ethylenediamine core were acquired from Dendritech® Inc. and purified by dialysis before use to eliminate further impurities. Cis-diaminedichloroplatinum (II) (cisplatin 99.99%) was obtained from Acros Organics. 5-Fluoro-1H-pyrimidine-2,4-dione (5-fluorouracil, 99%) from TCI Chemicals. Deoxyribonucleic acid sodium salt from the calf thymus (CT-DNA) and 4'6-diamino-2-phenyindole dilactate (DAPI) were purchased from

Sigma-Aldrich. Dialysis membranes (MW 100-500 Da, 1000 Da, 2000 Da, 3500 Da, 6000-8000 Da) were bought from SpectrumLabs. The other reagents were acquired from Acros Organics and Fisher Scientific. The ultrapure water (UPW) was obtained with a Milli-Q Direct 8 Water Purification System with a resistivity higher than 18.2 MΩ·cm. All the media, solutions, and reagents used for cell culture manipulation were purchased from Life Technologies (Thermo Fischer Scientific) unless otherwise stated. The healthy human blood was supplied by Hospital Dr. Nélio Mendonça (SESARAM), Funchal under the collaboration between the University of Madeira/Centro de Química da Madeira and the SESARAM hematology service.

2.2. Synthesis

The methodology used to prepare the metallodendrimers with cisplatin was based on the procedure described by Gordon Kirkpatrick *et al.* [92], Hoang Nguyen *et al.*[286], and Ngoc Tran *et al.*[282].Two different approaches were implemented to conjugate cisplatin to the anionic PAMAM dendrimers. In the first approach, cisplatin was directly conjugated to the anionic PAMAM dendrimer in a monodentate form. In the second approach, silver nitrate was used to remove both chloride groups from the cisplatin structure before the addition of the anionic PAMAM dendrimer allowing the bidentate form conjugation.

2.2.1. Preparation of Cisplatin Metallodendrimers in a monodentate form

2.2.1.1. PAMAM dendrimer Generation 0.5 - G0.5(COOPt(NH_3)$_2$Cl)$_8$

Cisplatin (0.12 g, 0.41 mmol; 8.5 equivalent (eq.) mol) was dispersed in 48 mL of UPW. Then, 0.06 g of G0.5COONa PAMAM (0.05 mmol) was dissolved in 3 mL of UPW and added to the mixture. The solution was left for 24 h at 18ºC in the dark under nitrogen atmosphere with constant mild stirring (Scheme 1). After a period of time, it was observed a change in the solution, the cisplatin suspension disappears, obtaining a transparent yellow solution. The resulting solution was then purified by dialysis membrane (MW 100-500 Da) for 4.5 h in distilled water. After freeze-dried, it was obtain a "greenish-yellow" hygroscopic solid (0.14 g) with 91% of yield. ^{1}H-NMR (400 MHz, D_2O) [ppm]: δ= 2.63 (H_c + H_i, t, 23H), 2.66 (H_a, s, 4H), 2.97 (H_g, t, 8H), 3.26 (H_b, t, 10H), 3.34 (H_h, t, 12H) and 3.64 (H_f, t, 8H). ^{13}C-NMR (100 MHz, D_2O) [ppm]: δ= 30.32 (C_c + C_i), 33.64 (C_a), 34.25 (C_f), 48.23 (C_g), 50.30 (C_h), 50.99 (C_b), 174.33 (C_d), 177.53 (C_p). ^{195}Pt-NMR (86 MHz, D_2O) [ppm]: δ= - 1848.15 (PtO). FTIR (KBr pellet): ν = 1576 cm^{-1} (amide II, N-H and C-N), 1631 cm^{-1} (C=O), 2853 cm^{-1} (C-H), 2966 cm^{-1} (C-H), 3277 cm^{-1} (NH_3) and 3418 cm^{-1} (N-H). Fluorescence: λ_{ex} = 380 nm, $\lambda_{em,\ max}$ = 442 nm. TOF-MS (ESI +) *m/z* calc. = 1606.68, *m/z* found = 1606.46 [M+2H$^+$+H_2O] $C_{46}H_{118}Cl_8N_{26}O_{21}Pt_8^{2+}$. EA (%) calc.: C 17.29, H 3.60, N 11.40, found: C 14.96, H 3.92, N 9.20 (hygroscopic compound).

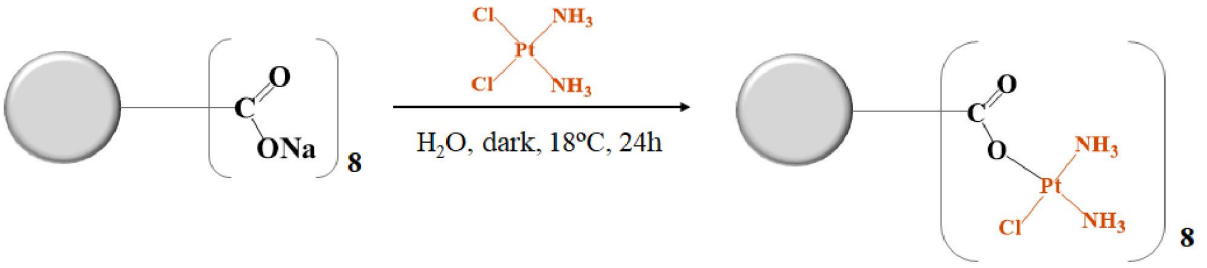

Scheme 1: Representation of the synthesis of the PAMAM dendrimer G0.5 functionalized with cisplatin in monodentate form, G0.5(COOPt(NH$_3$)$_2$Cl)$_8$.

2.2.1.2. PAMAM dendrimer Generation 1.5 - G1.5(COOPt(NH$_3$)$_2$Cl)$_{16}$

Cisplatin (0.29 g, 0.97 mmol; 17.5 eq. mol) was dispersed in 100 mL of UPW. 0.16 g of G1.5COONa PAMAM (0.06 mmol) was dissolved in 8.5 mL of UPW and subsequently added to the cisplatin solution with constant mild stir. The solution was left for 30 h protect from light at 18ºC under nitrogen atmosphere (Scheme 2). A change in the solution was observed after a few hours, the cisplatin suspension disappears, getting a transparent yellow solution. Then, the resulting solution was purified by dialysis membrane (MW 2000 Da) in distilled water for 4.5 h and then freeze-dried. A hygroscopic "greenwish-yellow" solid was obtained with 35% of yield (0.13 g). ^{1}H-NMR (400 MHz, D$_2$O) [ppm]: δ= 2.65 (H$_o$, t, 36H), 2.85 (H$_c$ + H$_i$, t, 19H), 3.20 (H$_a$ + H$_g$, m, 14H), 3.30 (H$_b$ + H$_h$ + Hn, m, 56H), 3.52 (H$_m$, t, 18H) and 3.68 (H$_f$ + H$_l$, m, 23H). ^{13}C-NMR (100 MHz, D$_2$O) [ppm]: δ= 28.68 (C$_e$ + C$_i$), 29.80 (C$_o$), 33.98 (C$_f$ + C$_l$), 48.84 (C$_a$ + C$_g$), 50.22 (C$_n$), 51.02 (C$_m$), 51.50 (C$_h$ + C$_b$), 172.36 (C$_d$) and 177.16 (C$_p$). ^{195}Pt-NMR (86 MHz, D$_2$O) [ppm]: δ= - 1848.02 (PtO). FTIR (KBr pellet): ν = 1587 cm^{-1} (amide II, N-H and C-N), 1658 cm^{-1} (C=O), 2841 cm^{-1} (C-H), 2961 cm^{-1} (C-H), 3251 cm^{-1} (NH$_3$) and 3425 cm^{-1} (N-H). Fluorescence: λ$_{ex}$ = 380 nm, λ$_{em,\ max}$ = 455 nm. TOF-MS (ESI +) *m/z* calc. = 1013.47, *m/z* found = 1013.46 [M+3H$^+$] C$_{110}$H$_{205}$N$_{30}$O$_{44}$Pt$_2^{3+}$. EA (%) calc.: C 19.43, H 4.03, N 11.95, found: C 38.65, H 7.30, N 11.96 (hygroscopic compound).

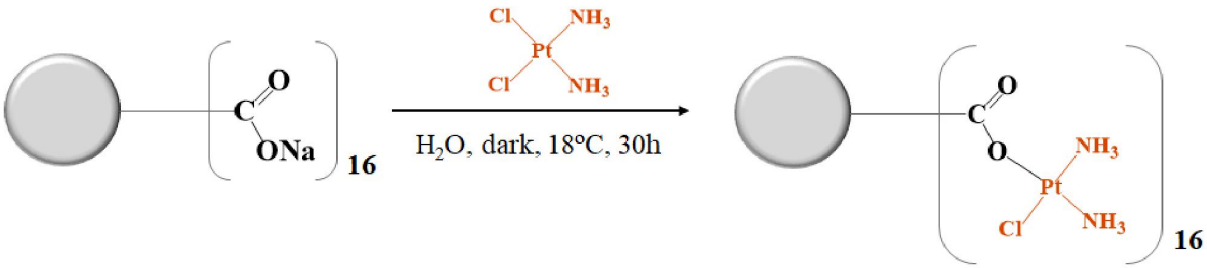

Scheme 2: Representation of the synthesis of the PAMAM dendrimer G1.5 functionalized with cisplatin in monodentate form, G1.5(COOPt(NH$_3$)$_2$Cl)$_{16}$.

2.2.1.3. PAMAM dendrimer Generation 2.5 - G2.5(COOPt(NH_3)$_2$Cl)$_{32}$

Cisplatin (0.094 g, 0.31 mmol; 32 eq. mol) was dispersed in 37 mL of UPW. Subsequently, an aqueous solution of G2.5COONa PAMAM (0.06 g, 0.01 mmol, 3 mL of UPW) was added to the cisplatin solution under constant mild stir. The solution was left for 40 h at 18ºC in the dark under nitrogen atmosphere (Scheme 3). A change in the solution was observed, the cisplatin suspension disappears, obtaining a transparent yellow solution. The obtained solution was purified by dialysis membrane (MW 2000 Da) for 4.5 h in distilled water. A greenish hygroscopic solid was obtained with 55% of yield (0.07 g). ^{1}H-NMR (400 MHz, D_2O) [ppm]: δ= 2.69 (H_c + H_i, H_o + H_u, t, 89H), 2.82 (H_{f+} H_l, t, 37H), 3.18 (H_t, t, 50H), 3.45 (H_a + H_g + H_m + H_s + H_b + H_h + H_n, m, 126H) and 3.74 (H_r, t, 32H). ^{13}C-NMR (100 MHz, D_2O) [ppm]: δ= 29.46 (C_l + C_f), 29.99 (C_c + C_i + C_o + C_u), 34.09 (C_r), 48.83 (C_t), 50.39 (C_n), 51.02 (Ca + C_m + C_s), 51.17 (C_h + C_{h+} C_n), 173.22 (C_d) and 177.20 (C_p). ^{195}Pt-NMR (86 MHz, D_2O) [ppm]: δ= - 1841.86 (PtO). FTIR (KBr pellet): ν = 1581 cm^{-1} (amide II, N-H and C-N), 1647 cm^{-1} (C=O), 2844 cm^{-1} (C-H), 2963 cm^{-1} (C-H), 3263 cm^{-1} (NH_3) and 3423 cm^{-1} (N-H). Fluorescence: λ_{ex} = 380 nm, $\lambda_{em,}$ max = 458 nm. TOF-MS (ESI +) *m/z* calc. = 974.82, *m/z* found = 974.65 [M+H$^+$] $C_{238}H_{562}Cl_{29}N_{116}O_{92}Pt_{29}^+$. EA (%) calc.: C 20.42, H 4.15, N 12.21, found: C 33.73, H 6.56, N 12.01(hygroscopic compound).

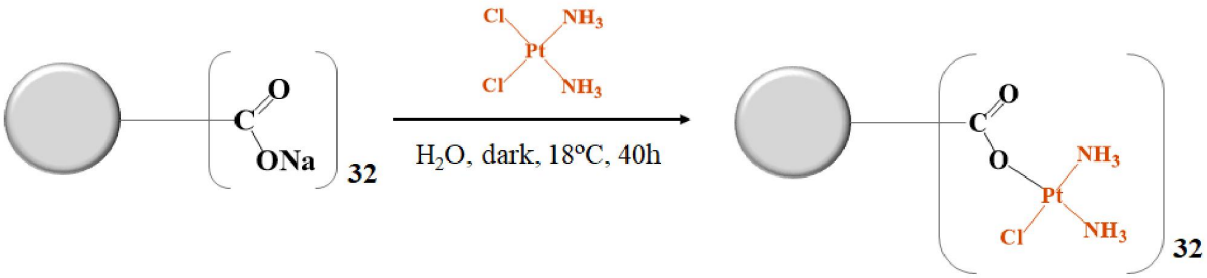

Scheme 3: Representation of the synthesis of the PAMAM dendrimer G2.5 functionalized with cisplatin in monodentate form, G2.5(COOPt(NH_3)$_2$Cl)$_{32}$.

In conclusion, as depicted in Figure 15, three metallodendrimers conjugated with cisplatin in a monodentate form were prepared.

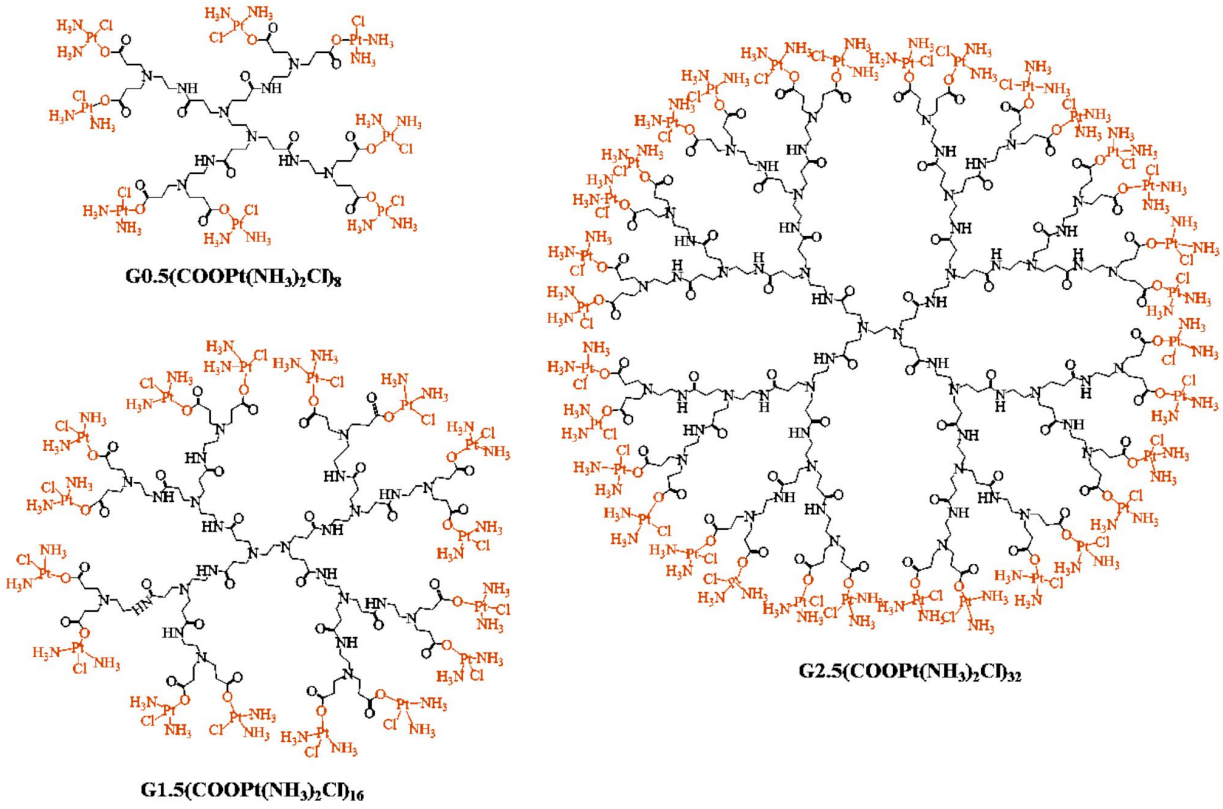

Figure 15: Metallodendrimers functionalized with cisplatin in a monodentate form (G0.5-G2.5).

2.2.2. Preparation of Cisplatin Metallodendrimers in a bidentate form

2.2.2.1. Aquation of cisplatin

For the preparation of cisplatin-metallodendrimers in a bidentate form, cisplatin was firstly hydrolyzed. Accordingly, 0.25 g of cisplatin (0.84 mmol) was dispersed in 100 mL of UPW. Then, an aqueous solution of 0.28 g of $AgNO_3$ (1.69 mmol, 2 eq. mol) in 6.5 mL of UPW was added dropwise to the mixture under stirring. The solution was left for 24 h at r.t. in darkness under a nitrogen atmosphere (Scheme 4). After 24 h, a "milky-white" precipitate (silver chloride precipitate) was observed, indicating the formation of the aquated cisplatin. The silver chloride precipitate was removed by centrifugation at 15000 rpm for 1.5 h at 20ºC. The supernatant was afterward filtrated through a 0.22 µm nylon filter to remove the remaining silver chloride precipitate and freeze-dried. It was obtained a yellow fluorescent powder with a 97% yield (0.22 g).

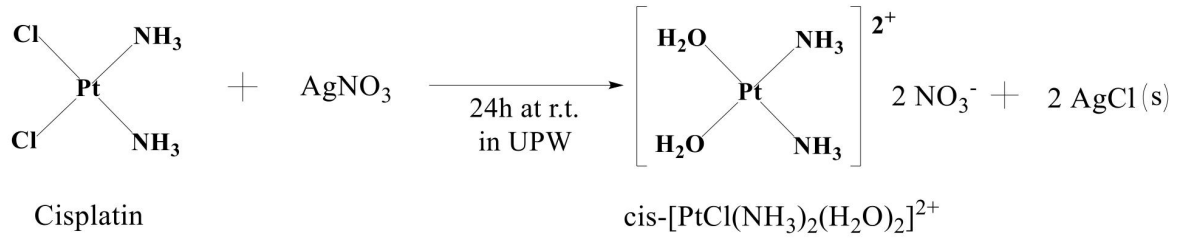

Scheme 4: Synthesis of aquated cisplatin.

2.2.2.2. PAMAM dendrimer Generation 0.5 - G0.5COO(Pt(NH3)2)4

Aquated cisplatin (0.12 mg, 0.42 mmol, 5.5 eq. mol) was dispersed in 46 mL of UPW and an aqueous solution of 5 mL of G0.5COONa PAMAM (0.10 g, 0.08 mmol) was added to the mixture under stirring. The solution was left for 24 h at r.t. in dark under nitrogen atmosphere (Scheme 5). After that time, the resulting solution was purified by dialysis membrane (MW 100-500 Da) in distilled water for 8 h and then freeze-dried, obtaining a green hygroscopic solid with 80% of yield (0.13 g). ^{1}H-NMR (400 MHz, D_2O) [ppm]: δ= 2.57 (H_c + H_i, m, 19H), 2.71 (H_a, 3H), 2.92 (H_g, 9H), 3.19 (H_b, m, 9H), 3.27 (H_b, m, 12H) and 3.58 (H_f, t, 8H). ^{13}C-NMR (100 MHz, D_2O) [ppm]: δ= 31.26 (C_i), 32.07 (C_c), 34.96 (C_f), 48.83 (C_g), 49.93 (C_a), 50.58 (C_h), 51.34 (C_b), 174.99 (C_d) and 178.50 (C_p). ^{195}Pt-NMR (86 MHz, D_2O) [ppm]: δ= - 2119.18 (PtO_2). FTIR (KBr pellet): ν = 1557 cm^{-1} (amide II, N-H and C-N), 1633 cm^{-1} (C=O), 2853 cm^{-1} (C-H), 2923 cm^{-1} (C-H) and 3435 cm^{-1} (N-H). Fluorescence: λ_{ex} = 380 nm, $\lambda_{em,}$ max = 440 nm. TOF-MS (ESI +) *m/z* calc. = 1023.27, *m/z* found = 1023.27 [M+2Na$^+$] $C_{46}H_{96}N_{18}Na_2O_{20}Pt_4^{2+}$. EA (%) calc.: C 27.60, H 4.83, N 12.60, found: C 21.93, H 5.71, N 10.60 (hygroscopic compound).

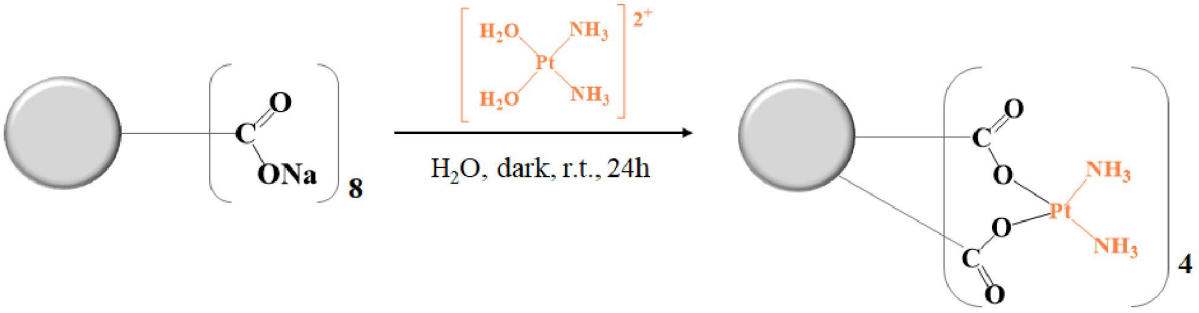

Scheme 5: Representation of the synthesis of the PAMAM dendrimer G0.5 functionalized with cisplatin in bidentate form, G0.5COO(Pt(NH3)2)4.

2.2.2.3. PAMAM dendrimer Generation 1.5 - G1.5COO(Pt(NH3)2)8

Aquated cisplatin (0.19 g, 0.72 mmol, 8.5 eq. mol) was dispersed in 80 mL of UPW. Therefore 0.25 g of G1.5COONa PAMAM (0.09 mmol) was dissolved in 10 mL of UPW and added dropwise to the aquated cisplatin mixture under stirring. The mixture was left for 30 h at r.t. in the dark under nitrogen atmosphere

(Scheme 6). The obtained solution was purified by dialysis membrane (MW 2000 Da) for 8 h in distilled water and then freeze-dried. It was obtained an ivory hygroscopic powder with a yield of 64% (0.24 g). ^{1}H-NMR (400 MHz, D_2O) [ppm]: δ= 2.53 (H_c + H_i, 30H), 2.61 (H_o, 29H), 2.98 (H_a + H_g + H_m, 40H), 3.36 (H_n, H_b + H_h, 56H) and 3.63 (H_f + H_l, 20H). ^{13}C-NMR (100 MHz, D_2O) [ppm]: δ= 30.04 (C_o), 31.53 (C_c + C_i), 34.07 (C_f + C_l), 48.32 (C_a + C_g), 50.28 (C_n), 50.95 (C_h + C_h), 52.97 (C_m), 174.74 (C_d) and 177.37 (C_p). ^{195}Pt-NMR (86 MHz, D_2O) [ppm]: δ= - 2119.38 (PtO_2). FTIR (KBr pellet): ν = 1586 cm^{-1} (amide II, N-H and C-N), 1644 cm^{-1} (C=O), 2856 cm^{-1} (C-H), 2976 cm^{-1} (C-H), 3266 cm^{-1} (NH_3) and 3400 cm^{-1} (N-H). Fluorescence: λ_{ex} = 380 nm, λ_{em}, max = 457 nm. TOF-MS (ESI +) *m/z* calc. = 1466.80, *m/z* found = 1466.83 [M+3H$^+$] $C_{110}H_{227}N_{42}O_{44}Pt_8^{3+}$. EA (%) calc.: C 30.03, H 5.13, N 13.37, found: C 32.43, H 6.34, N 11.72 (hygroscopic compound).

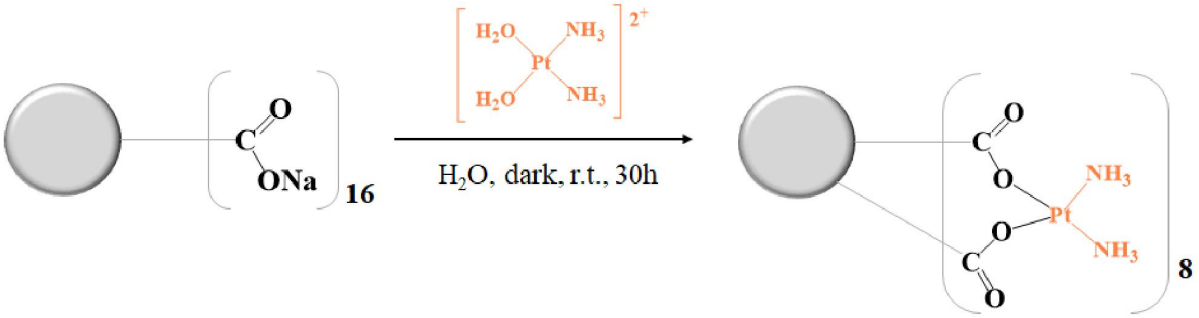

Scheme 6: Representation of the synthesis of the PAMAM dendrimer G1.5 functionalized with cisplatin in bidentate form, G1.5COO(Pt(NH_3)$_2$)$_8$.

2.2.2.4. PAMAM dendrimer Generation 2.5 - G2.5COO(Pt(NH_3)$_2$)$_{16}$

Aquated cisplatin (0.18 g, 0.68 mmol, 16.5 eq. mol) was dispersed in 75 mL of UPW. Separately, 0.26 g of G2.5COONa PAMAM (0.04 mmol) was dissolved in 10 mL of UPW and added dropwise to the aquated cisplatin mixture under stirring. The solution was left for 40 h at r.t. in dark under nitrogen atmosphere (Scheme 7). At the end, the obtained solution was purified by dialysis membrane (MW 2000 Da) for 8 h in distilled water and then freeze-dried. It was obtained a light gray hygroscopic powder with a yield of 56% (0.21 g). ^{1}H-NMR (400 MHz, D_2O) [ppm]: δ= 2.59 (H_c + H_i +H_o, 39H), 2.65 (H_u, t, 67H), 3.05 (H_t, 84H), 3.40 (H_a + H_g + H_m, H_s + H_b + H_h, H_n, m, 112H), 3.58 (H_l + H_f, 17H) and 3.68 (H_r, 32H). ^{13}C-NMR (100 MHz, D_2O) [ppm]: δ= 30.08 (C_c + C_i + C_o + C_u), 34.13 (C_r), 36.01 (C_f + C_l), 48.68 (C_t), 50.41 (C_a + C_g + C_m + C_s), 51.11 (C_b + C_h + C_n), 174.33 (C_d) and 177.30 (C_p). ^{195}Pt-NMR (86 MHz, D_2O) [ppm]: δ= - 2122.82 (PtO_2). FTIR (KBr pellet): ν = 1587 cm^{-1} (amide II, N-H and C-N), 1645 cm^{-1} (C=O), 2847 cm^{-1} (C-H), 2966 cm^{-1} (C-H), 3255 cm^{-1} (NH_3) and 3425 cm^{-1} (N-H). Fluorescence: λ_{ex} = 380 nm, λ_{em}, max = 452 nm. TOF-MS (MALDI) *m/z* calc. = 4598.51, *m/z* found = 4597.5 [M+2H$^+$] $C_{238}H_{482}N_{90}O_{92}Pt_{16}^{2+}$. EA (%) calc.: C 31.08, H 5.26, N 13.71, found: C 35.63, H 6.98, N 12.56 (hygroscopic compound).

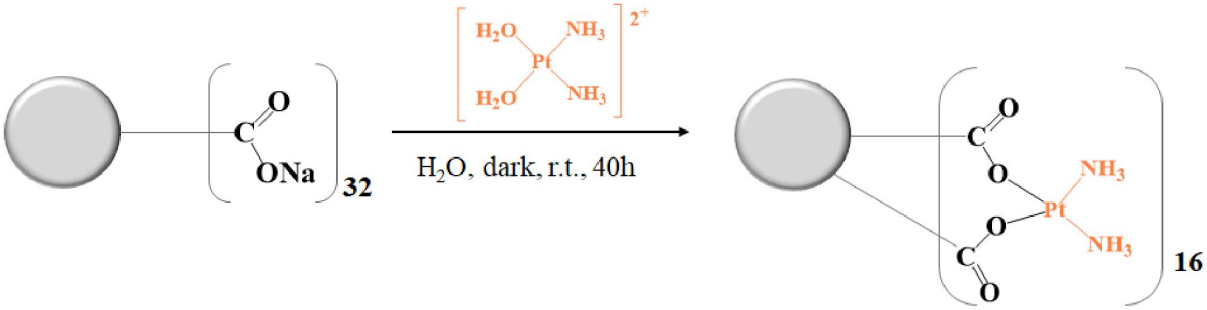

Scheme 7: Representation of the synthesis of the PAMAM dendrimer G2.5 functionalized with cisplatin in bidentate form, G2.5COO(Pt(NH$_3$)$_2$)$_{16}$.

2.2.2.5. PAMAM dendrimer Generation 3.5 - G3.5COO(Pt(NH$_3$)$_2$)$_{32}$

Aquated cisplatin (0.10 g 0.39 mmol, 32.5 eq. mol) was dispersed in 90 mL of UPW. And 0.16 g of G3.5COONa PAMAM (0.01 mmol) was dissolved in 10 mL of UPW and added dropwise to the aquated solution under stirring. The solution was left for 43 h at r.t. in darkness under nitrogen atmosphere (Scheme 8). The mixture was then purified by dialysis membrane (MW 3500 Da) for 1 day in distilled water. After freeze-dried it was obtained a light gray hygroscopic powder with a yield of 58% (0.13 g). ^{1}H-NMR (400 MHz, D_2O) [ppm]: δ= 2.59 (H_c + H_i +H_o + Hu, m 159H), 2.66 (H_Y, m, 145H), 3.05 (H_a + H_g + H_m + H_s, 64H), 3.26 (H_y, 73H), 3.40 (H_z + H_b, H_h, H_n, H_t, m, 253H), 3.59 (H_f + H_l + H_r, 36H) and 3.69 (H_x, 64H). ^{13}C-NMR (100 MHz, D_2O) [ppm]: δ= 29.96 (C_Y), 31.80 (C_c + C_i + C_o + C_u), 34.07 (C_x), 35.51 (C_f + C_l + C_r), 48.62 (C_a + C_g + C_m + C_s + C_y), 50.37 (C_z), 51.07 (C_b + C_h + C_n + C_t), 173.68 (C_d) and 177.20 (C_p). ^{195}Pt-NMR (86 MHz, D_2O) [ppm]: δ= - 2120.93 (PtO_2). FTIR (KBr pellet): ν = 1581 cm^{-1} (amide II, N-H and C-N), 1642 cm^{-1} (C=O), 2850 cm^{-1} (C-H), 2927 cm^{-1} (C-H), 2953 cm^{-1} (C-H) and 3466 cm^{-1} (N-H). Fluorescence: λ_{ex} = 380 nm, $\lambda_{em, max}$ = 454 nm. TOF-MS (ESI +) *m/z* calc. = 974.82, *m/z* found = 974.64 [M+H$^+$] $C_{494}H_{981}N_{180}O_{188}Pt_{29}^+$. EA (%) calc.: C 31.58, H 5.32, N 13.87, found: C 35.01, H 6.87, N 12.89 (hygroscopic compound).

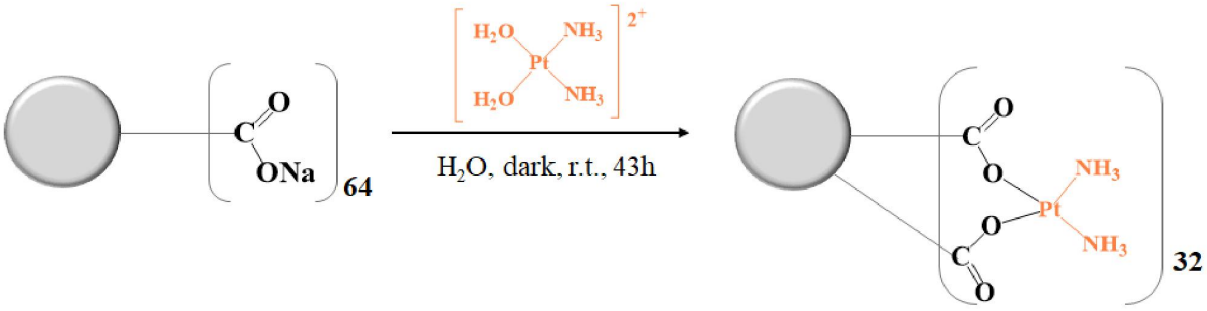

Scheme 8: Representation of the synthesis of the PAMAM dendrimer G3.5 functionalized with cisplatin in bidentate form, G3.5COO(Pt(NH$_3$)$_2$)$_{32}$.

In the bidentate form, was prepared four metallodendrimers (G0.5 to G3.5) as exemplified in the following Figure 16.

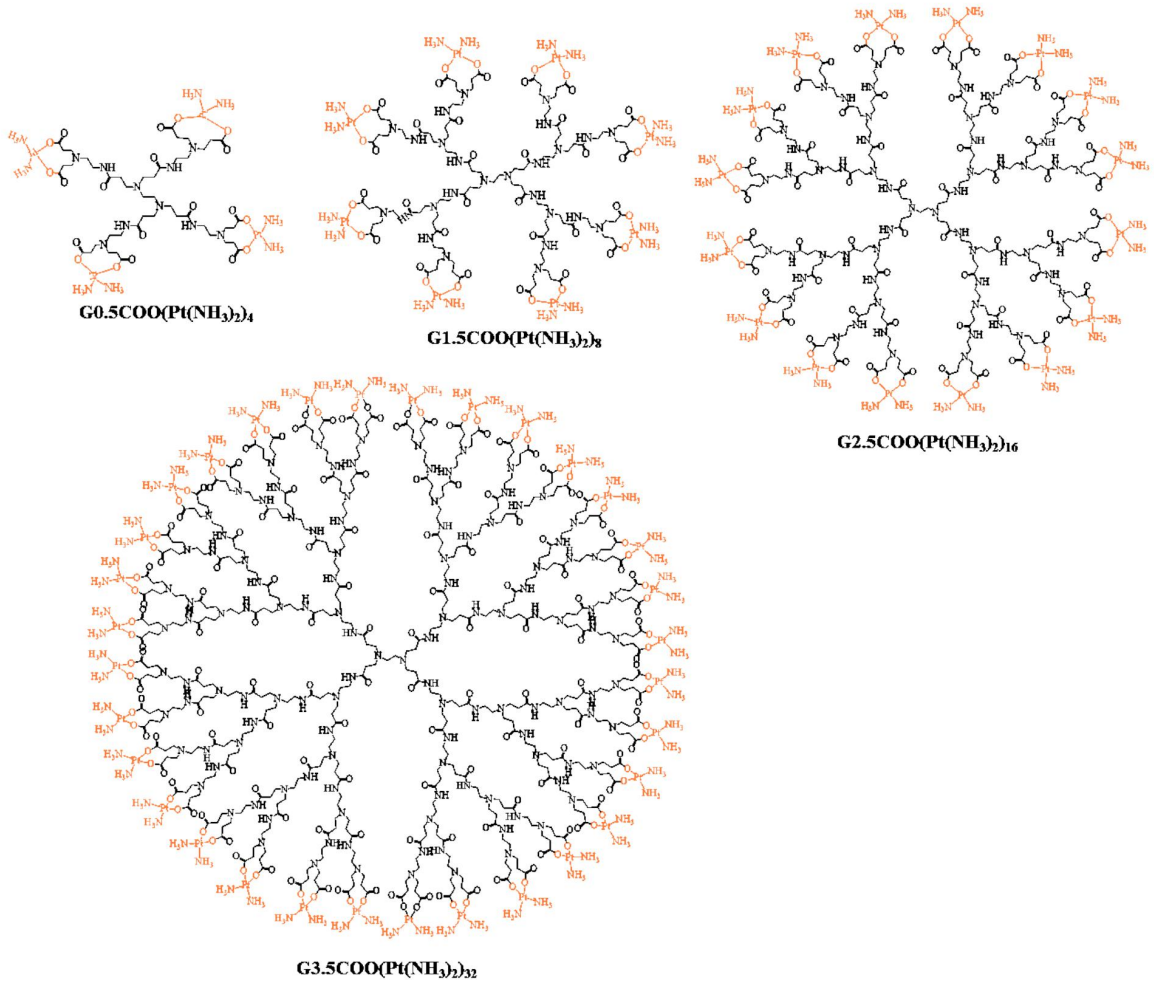

Figure 16: Metallodendrimers functionalized with cisplatin in a bidentate form (G0.5-G3.5).

2.3. Biological studies

2.3.1. Cell culture and cytotoxicity evaluation

For the cytotoxicity evaluation of the prepared mettalodendrimers, several human cell lines were used, such as ovarian cancer cells (A2780), cisplatin-resistance ovarian cancer cells (A2780CisR), colorectal adenocarcinoma cells (CACO-2), breast cancer cells (MCF-7), and fibroblast cells (BJ, a non-cancer cell line). The cell lines were cultured in 96-well plates at a seeding density of 1 x 10^4 cells per well with a specific culture medium supplemented with 10% (v/v) fetal bovine serum (FBS) and 1 % (v/v) antibiotic-antimycotic (AA, 100x solution) at 37ºC in a humidified atmosphere of 5% CO_2. The cell culture media were performed as follows, the A2780 and A2780CisR cell lines were cultured in RPMI 1640 medium supplemented with L-

glutamine (2 mM), and 1% (w/v) of cisplatin (100 mM) and for the A2780CisR cells (cisplatin was only used in the subculturing process before the cytotoxicity assays); the CACO-2 cell line was cultured in MEM medium supplemented with 1% (v/v) nonessential amino acids (NEAA); the MCF-7 cell line was cultured in RPMI 1640 medium supplemented with 1mM sodium pyruvate, 1% (v/v) NEAA (100× solution), and 3.3 μg/mL of human insulin and the BJ cell line was cultured in D-MEM medium. After 24 h, cells were treated with the metallodendrimers G0.5(COOPt$(NH_3)_2Cl)_8$, G0.5COO(Pt$(NH_3)_2)_4$, G1.5COO(Pt$(NH_3)_2)_8$, G1.5(COOPt$(NH_3)_2Cl)_{16}$, G2.5(COOPt$(NH_3)_2Cl)_{32}$, G2.5COO(Pt$(NH_3)_2)_{16}$, G3.5COO(Pt$(NH_3)_2)_{32}$ prepared in nuclease-free water. Then, 100 μL of the compound solution was used for a total volume of 200 μL in the well. The cytotoxicity of the metallodendrimers was evaluated at the concentrations of 0.01, 0.03, 0.1, 0.5, 1, 2.5, 5, and 10 μM. Anionic PAMAM dendrimers half-generations (G0.5-G3.5) as well free cisplatin were used as controls. The cytotoxicity of the G2.5COO(Pt$(NH_3)_2)_{16}$/5-FU and G2.5COO(Pt$(NH_3)_2Cl)_{32}$/5-FU metallodendrimers was evaluated in two cancer cells, the A2780CisR and CACO-2, at concentrations of 0.01, 0.2, 1, 5, 10, and 20 μg/mL. The G2.5$(COONa)_{32}$/5-FU and free 5-FU were used as controls. After 72 h of incubation with the compounds, the culture medium was replaced with fresh culture medium containing 10% (v/v) of MTT (3-(4, 5-dimethylthiazol-2-yl)-2, 5-diphenyltetrazolium bromide) solution (0.5 mg/mL). After 2-3 h of incubation, the culture medium was removed, and the formazan crystals were dissolved in 100 μL of DMSO. Afterward, the absorbance intensity was measured at 550 nm in a microplate reader (Victor^3 1420, Perkin Elmer). Three independent experiments with three replicas each were made. The concentration that inhibited 50% of the cellular metabolic activity (IC_{50}) was determined by linear interpolation between the two experimental points closer to the point correspondent to 50% of the control's cellular metabolic activity. Results are presented as the mean ± standard deviation (SD).

2.3.2. Hemotoxicity evaluation

Human blood from healthy donors was collected in tubes containing EDTA as an anticoagulant. The human blood was used to evaluate the hematoxicity of the compounds under study towards red blood cells by the cyanmethemoglobin method[287]. This method, recommended by the International Committee for Standardization in Hematology, consists of adding C reagent (cyanmethemoglobin reagent) in the samples, which, when mixed with blood, causes the lysis of erythrocytes[287]. Thus, potassium ferricyanide transforms hemoglobin into methemoglobin, which combines with potassium cyanide giving rise to hemiglobincianide, also named cyanomethemoglobin. As a result, all the hemoglobin present in the blood is converted to cyanomethemoglobin, and its concentration is measured by absorbance spectroscopy at a wavelength of 550 nm.

A 250-fold dilution of blood was prepared in C reagent (20 μL of blood in 5 mL of C reagent) to determine the total hemoglobin concentration in the human blood. C reagent was prepared in an amber bottle with 50 mg potassium ferricyanide, 12.5 mg potassium cyanide, 35 mg potassium dihydrogen phosphate in 250 mL of distilled water with 250 μL Triton-X, and the pH adjusted to 7.4. A standard curve of hemoglobin (Hg) was

prepared from bovine blood (see annex Figure B1). For that purpose, a stock solution of Hg (1.5 mg/mL) was prepared in C reagent and diluted to several concentrations (0.2; 0.37; 0.54; 0.71; 0.88; 1.05; 1.22 and 1.39 mg/mL). Then, the absorbance was measured at 550 nm using C reagent as blank. The total hemoglobin concentration was determined with this standard curve, taking into consideration the initial dilution. For the hematoxicity evaluation of the compounds, 10% (v/v) blood solution was prepared in PBS (Mg^{2+}/Ca^{2+} free). Then, 10 µL of blood solution was added to a microtube and subsequently was added 70 µL of compound solutions at concentrations of 0.1, 1 and 5 µM. For the positive and negative controls, 70 µL of distilled water and 70 µL of PBS were used, respectively. After, the microtubes were incubated at 37ºC for 3 h and centrifuged at 3800 rpm for 10 min. Then, 40 µL of each supernatant was transferred to 96-well plates, and 160 µL of C reagent was added to each well. The absorbance was measured at 550 nm in the microplate reader. The concentration of hemoglobin in the supernatants was then determined using the same standard curve. The results are represented as a percentage of hemolysis of three independent assays ± standard deviation (SD).

2.3.3. DNA binding by UV-vis spectroscopy

The absorption spectra were performed at room temperature by varying the concentration of CT-DNA (0, 6.25, 12.5, 18.75, 25, 31.25, 37.5, 43.75 to 50 µM) and keeping constant the concentration of $G0.5(COOPt(NH_3)_2Cl)_8$ (5 µM), $G2.5(COOPt(NH_3)_2Cl)_{32}$ (9 µM) and $G2.5COO(Pt(NH_3)_2)_{16}$ (1.5 µM) metallodendrimers and cisplatin (9 µM). The compound solutions were prepared in UPW and then diluted in a 5 mM Tris-HCl, 50 mM NaCl pH 7.4 buffer. The stock solutions of DNA were also prepared in this buffer. The DNA purity was determined by UV-Vis spectroscopy from the absorbance ratios at 260 nm and 280 nm. The ratio should be between 1.8-1.9 to ensure it is sufficiently protein-free (see annex Figure A17). The obtained ratio was 1.9, meaning that the DNA was pure. The solutions containing the compounds and DNA were incubated for 5 min at r.t. The absorbance was measured by UV-Vis spectroscopy using the buffer as blank. Two independent experiments were carried out for the metallodendrimers and cisplatin. The intrinsic binding constant, K_b, of the compounds with DNA, was determined by the Benesi-Hildebrand equation[288]. The binding constant was obtained from the ratio of the y-intercept to the slope in the plots $A_0/A\text{-}A_0$ vs. 1/[DNA]. The Gibbs free energy (ΔG) that is associated with the DNA interaction process was calculated using the equation:

$$\Delta G = -RTlnKb \quad (1)$$

Where T is the temperature in Kelvin and R is the gas constant.

2.4. Studies with 5-Fluorouracil loaded dendrimers

2.4.1. Loading of 5-FU

5-FU was loaded in the G2.5COO($Pt(NH_3)_2)_{16}$ and G2.5($COOPt(NH_3)_2Cl)_{32}$ metallodendrimers. As such, 25 mg of G2.5COO($Pt(NH_3)_2)_{16}$ (0.003 mmol) was dissolved in 2 mL of UPW, and 5.3 mg of 5-FU (15 eq. mol, 0.04 mmol) was added to the solution. The solution was stirred for 24 h protected from the light. The same procedure was performed for the G2.5($COOPt(NH_3)_2Cl)_{32}$ metallodendrimer. Thus, 25 mg of G2.5($COOPt(NH_3)_2Cl)_{32}$ (0.002 mmol) was dissolved in 2 mL of UPW, and 3.5 mg of 5-FU (15 eq. mol, 0.03 mmol) was added to the metallodendrimer solution. For control, the G2.5$(COONa)_{32}$ dendrimer (7.8 mg, 0.06 mmol) was also loaded with 5-FU (25 mg, 0.004 mmol, 2 mL). After, the G2.5COO($Pt(NH_3)_2)_{16}$/5-FU, G2.5($COOPt(NH_3)_2Cl)_{32}$/5-FU and G2.5$(COONa)_{32}$/5-FU solutions were dialyzed in 50 mL of distilled water using a dialysis membrane with a ct off of 100-500 Da for 20 min to remove the unloaded 5-FU. Then, the G2.5COO($Pt(NH_3)_2)_{16}$/5-FU, G2.5($COOPt(NH_3)_2Cl)_{32}$/5-FU, and G2.5$(COONa)_{32}$/5-FU solutions and the solution from outside the dialysis were lyophilized. The free drug was dissolved in 50 mL of UPW, and its absorbance was measure at 266 nm in a Perkin Elmer UV-Vis spectrometer Lambda equipment to determine indirectly the amount of drug-loaded within the compounds. A standard calibration curve in water was done to quantify the 5-FU in solution (see annex Figure B2. The loading capacity (LC%) and the loading efficiency (LE%) were calculated through the following formulas[289]. The results are expressed as mean ± SD of three independent experiments.

$$\boldsymbol{LC}\ (\%) = \frac{Mass\ of\ loaded\ 5FU}{(Mass\ of\ loaded\ 5FU + Mass\ of\ dendrimer\ or\ metallodendrimer)} \times 100 \quad (2)$$

$$\boldsymbol{LE}\ (\%) = \frac{(Total\ 5FU\ amount - free\ 5FU\ amount)}{Initial\ mass\ of\ 5FU} \times 100 \quad (3)$$

2.4.2. *In vitro* drug release of 5-FU

The release of 5-FU was carried out in PBS at pH 7.4 and pH 5 at 37ºC. For that purpose, were weighted 100 µg of 5-FU loaded in G2.5COO($Pt(NH_3)_2)_{16}$, G2.5($COOPt(NH_3)_2Cl)_{32}$, and G2.5$(COONa)_{32}$ and dissolved in 300 µL of water. The solutions were placed in a SLIDE-A-LYZER™ mini dialysis device with an MW of 2000 Da (volume of 0.1 mL, Thermo Fisher Scientific) and dialyzed with 10 mL of PBS at each pH value in separate tubes. At different time intervals, 1 mL of the dialyzed was taken out from each tube and replaced with an equivalent volume of fresh PBS. The release profile of 5-FU was determined by UV-Vis spectroscopy through absorbance measurement at 266 nm. A standard calibration curve for each pH value was performed (see annex Figures B3 and B4).

3. Results and discussion

3.1.Synthesis and characterization

3.1.1. Monodentate form

To prepare the monodentate cisplatin-metallodendrimers, cisplatin was conjugated directly to the anionic half-generation PAMAM dendrimers (G0.5- G2.5). The prepared metallodendrimers were obtained in general, with good yield (91% for G0.5(COOPt(NH_3)$_2$Cl)$_8$, 35% for G1.5(COOPt(NH_3)$_2$Cl)$_{16}$ and 55% for G2.5(COOPt(NH_3)$_2$Cl)$_{32}$). All the cisplatin-metallodendrimers were then fully characterized by different techniques as NMR (^{1}H, ^{13}C, and ^{195}Pt-NMR), FTIR, UV-Vis, and Fluorescence spectroscopy, zeta-potential, mass spectrometry (MS) and elemental analysis (EA). In the ^{1}H-NMR experiments, the signal of deuterated water (D_2O) was used as an internal reference, and the potassium tetrachloroplatinate (II) was used as an external reference in the ^{195}Pt-NMR experiments. Figure 17 shows the ^{1}H-NMR spectrum of the G0.5(COOPt(NH_3)$_2$Cl)$_8$ with the characteristics signals of the anionic PAMAM dendrimers at 2.65, 2.83, 2.97, 3.26, 3.34 and 3.64 ppm. However, the protons of the NH_3 group of cisplatin are not visible with the solvent used but was visible a downfield shift of the signals compared to the respective pristine PAMAM dendrimer (see annex Figure A1).

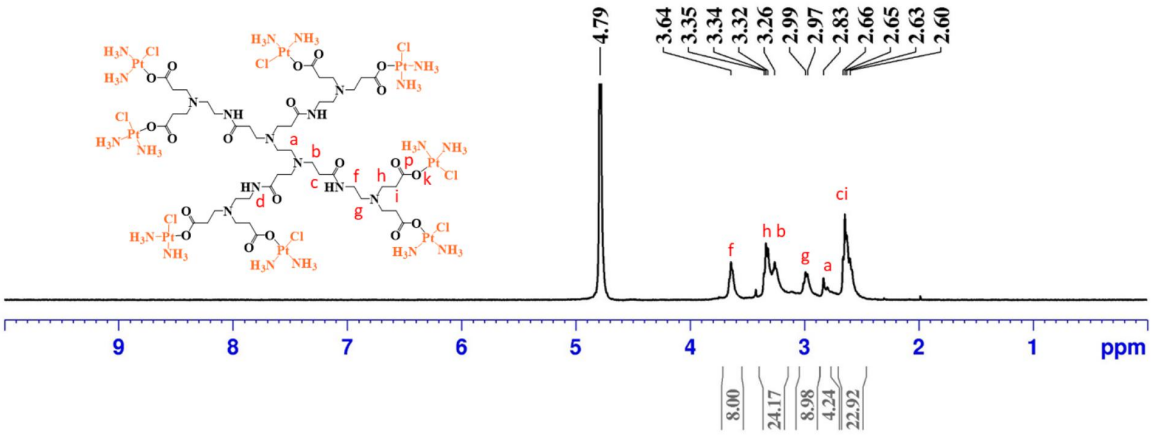

Figure 17: ^{1}H-NMR spectrum of G0.5(COOPt(NH_3)$_2$Cl)$_8$ performed in D_2O.

In the ^{13}C-NMR spectrum (Figure 18) it was possible to observe a downfield shift of the carboxylate signal after the conjugation of cisplatin, from 174.69 to 177.53 ppm, suggesting that the coordination of PAMAM dendrimer to cisplatin was successfully achieved[282,290].

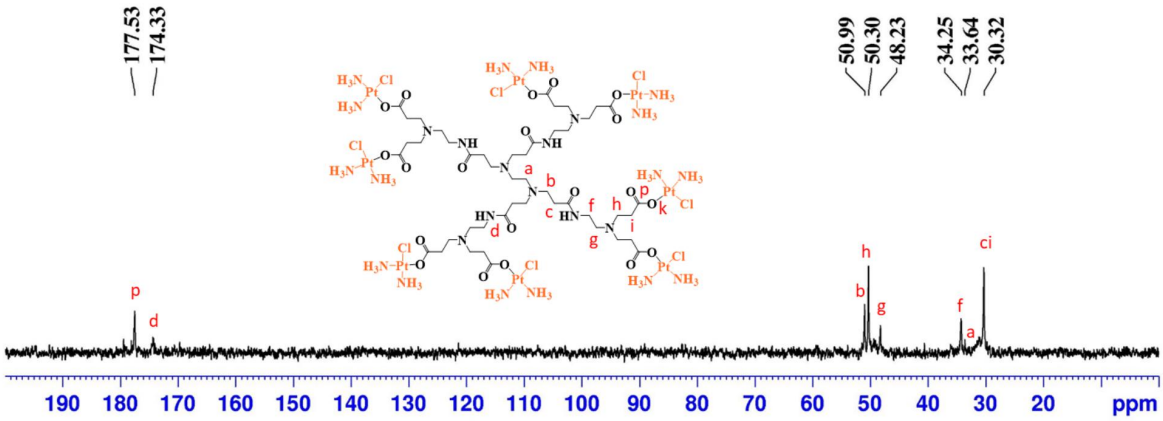

Figure 18: ^{13}C-NMR spectrum of G0.5(COOPt$(NH_3)_2Cl)_8$ performed in D_2O.

Furthermore, the ^{195}Pt-NMR was performed in order to verify how cisplatin was conjugated to the PAMAM dendrimer. As shown in Figure 19, the signal at -1848 ppm suggests the conjugation of cisplatin to the PAMAM dendrimer in a monodentate form[277]. The signal at -2164 ppm was characteristically attributed to free cisplatin (see annex Figure A12), and the signal at -1756 ppm probably corresponded to cis-$[PtCl(NH_3)_2(D_2O)]^+$ fragment due to the interaction between the deuterated solvent (D_2O) and free cisplatin since to obtain the spectrum is necessary a few hours of acquisition[291]. The low-intensity signal obtained in the ^{195}Pt-NMR experiment was due to the sensitivity of the NMR probe for the ^{195}Pt-nucleus.

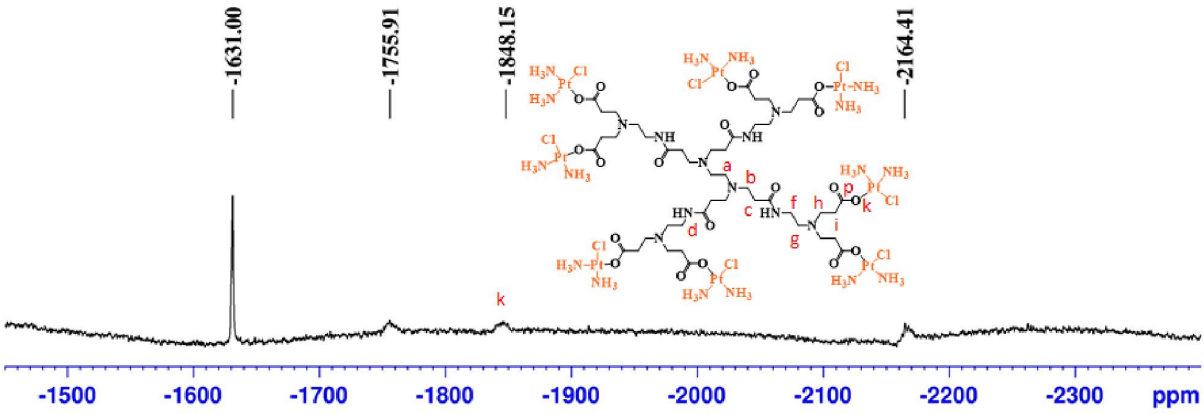

Figure 19: ^{195}Pt-NMR spectrum of G0.5(COOPt$(NH_3)_2Cl)_8$ performed in D_2O, with K_2PtCl_4 as an external reference (-1631 ppm).

Similar results were obtained for the G1.5(COOPt$(NH_3)_2Cl)_{16}$ and G2.5(COOPt$(NH_3)_2Cl)_{32}$ metallodendrimers. In the ^{1}H-NMR spectrum, the G1.5(COOPt$(NH_3)_2Cl)_{16}$ metallodendrimer presented a downfield shift of the characteristics protons of the PAMAM dendrimer structure, of 2.65, 2.83, 3.20, 3.39, 3.52 and 3.68 ppm (Figure 20) compared to the pristine anionic PAMAM dendrimers (see annex Figure A3).

The ^{13}C-NMR spectrum also showed a downfield shift of the carboxylate group from 175.22 to 177.16 ppm, indicating the coordination of cisplatin on its surface (Figure 21). The signal at -1848 ppm in the ^{195}Pt-NMR spectrum (see annex Figure C1) was indicative of the coordination of cisplatin in a monodentate form. The other signal that appeared at – 2162 ppm corresponds to free cisplatin.

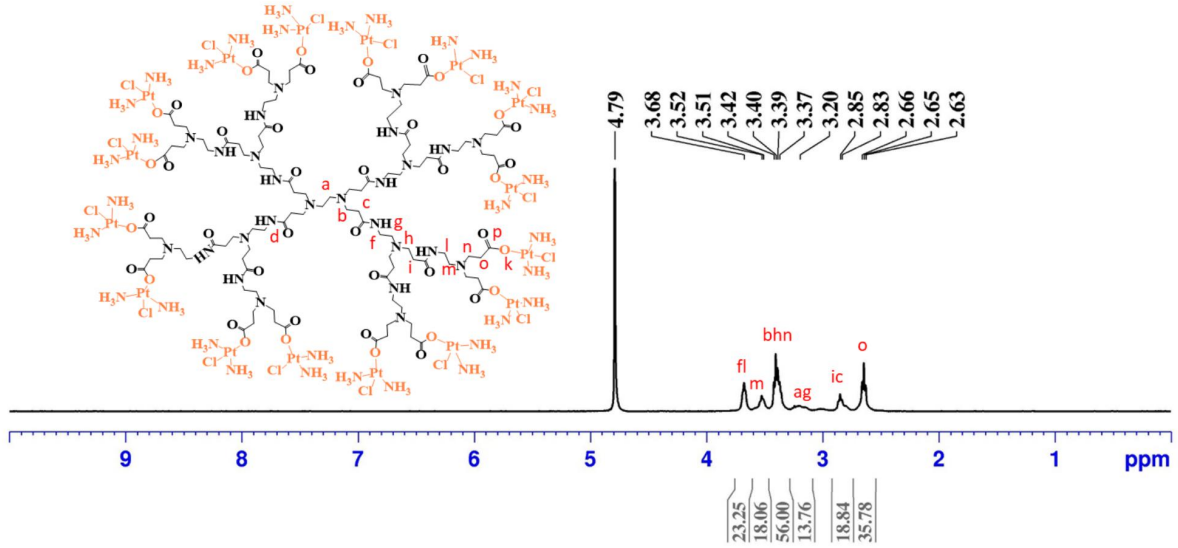

Figure 20: ^{1}H-NMR spectrum of G1.5(COOPt(NH$_3$)$_2$Cl)$_{16}$ performed in D_2O.

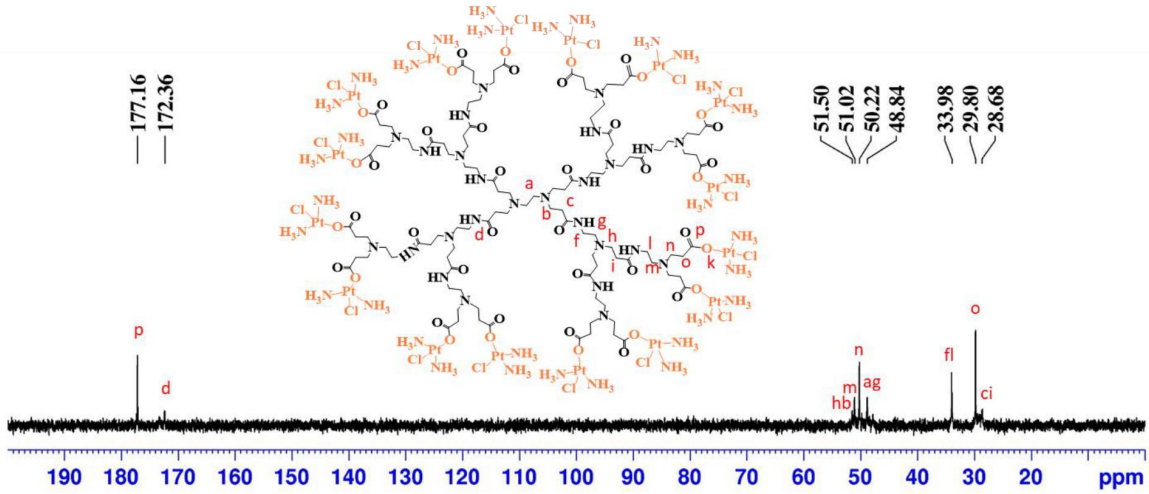

Figure 21: ^{13}C-NMR spectrum of G1.5(COOPt(NH$_3$)$_2$Cl)$_{16}$ performed in D_2O.

Also for the G2.5(COOPt(NH$_3$)$_2$Cl)$_{32}$ metallodendrimer, we were able to observe a downfield shift of the protons signals (Figure 22), regarding the PAMAM dendrimer in the ^{1}H-NMR spectrum. The signals at 271, 2.82, 3.18, 3.45, and 3.74 ppm belong to the structure of the anionic PAMAM dendrimer. The ^{13}C-NMR

spectrum only presented the signals of the structure of the PAMAM dendrimer since cisplatin does not have carbons in its chemical composition. Nevertheless, a downfield shift of the carboxylate group from 174.90 to 177.20 ppm suggests that cisplatin was conjugated on the surface of the dendrimer (Figure 23). The signal at -1842 ppm in the ^{195}Pt-NMR (see annex Figure C2) indicated that cisplatin was conjugated in a monodentate form to the PAMAM dendrimer.

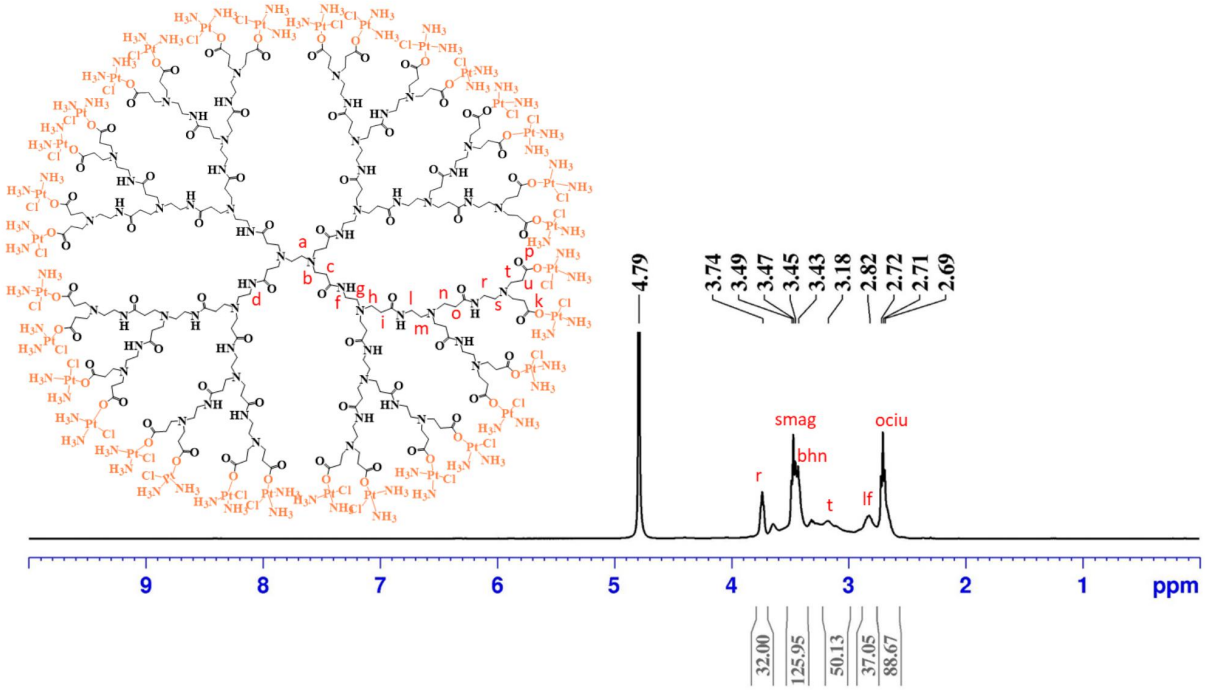

Figure 22: ^{1}H-NMR spectrum of G2.5(COOPt$(NH_3)_2Cl)_{32}$ performed in D_2O.

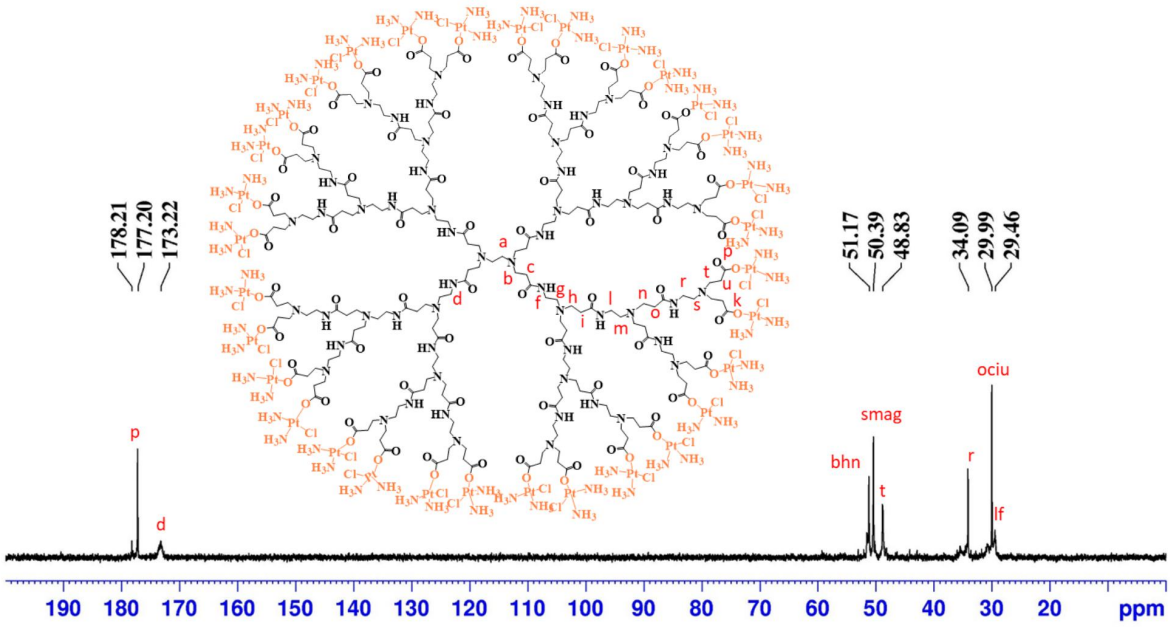

Figure 23: ^{13}C-NMR spectrum of G2.5(COOPt(NH$_3$)$_2$Cl)$_{32}$ performed in D$_2$O.

The prepared monodentate cisplatin-metallodendrimers were also characterized by FTIR. The characteristics bands of cisplatin were the N-H stretch of the amino groups at 1541cm^{-1} and 3267cm^{-1} (see annex Figure A13). When comparing with the pristine anionic PAMAM dendrimers (see annex Figure A9), the cisplatin-metallodendrimers showed a shift in the characteristic carbonyl stretching band from 1639 to 1631 cm^{-1} in the G0.5(COOPt(NH$_3$)$_2$Cl)$_8$, 1633 to 1658 cm^{-1} in the G1.5(COOPt(NH$_3$)$_2$Cl)$_{16}$ and 1638 to 1647 cm^{-1} in the G2.5(COOPt(NH$_3$)$_2$Cl)$_{32}$ (see annex Figure C3). In addition, was observed the presence of a new band related to the N-H stretch of the NH$_3$ groups of cisplatin at 3277 cm^{-1}, 3251 cm^{-1}, and 3263 cm^{-1} in the G0.5(COOPt(NH$_3$)$_2$Cl)$_8$, G1.5(COOPt(NH$_3$)$_2$Cl)$_{16}$, G2.5(COOPt(NH$_3$)$_2$Cl)$_{32}$, respectively.

Additionally, the monodentate cisplatin-metallodendrimers were characterized by UV-Vis spectroscopy (Figure 24a). Cisplatin, UV-Vis spectrum presented a maximum absorbance band at 203 nm attributed to the charge-transfer band and a shoulder at 280 nm assigned to the d-d transitions of the square planar Pt^{2+} ion[292] (see annex Figure A14). After the conjugation of cisplatin to the anionic PAMAM dendrimers, the characteristic band that appears around 280-300 nm from the interior tertiary amines of the PAMAM dendrimer (see annex Figure A10) did not shift significantly, suggesting that cisplatin conjugation has been achieved only at the surface of the dendrimer. However, the cisplatin band in the metallodendrimers spectra showed as a minor shoulder with shifts to 205 nm, 250 nm, and 249 nm for G0.5(COOPt(NH$_3$)$_2$Cl)$_8$, G1.5(COOPt(NH$_3$)$_2$Cl)$_{16}$, and G2.5(COOPt(NH$_3$)$_2$Cl)$_{32}$ respectively, which indicates that the conjugation was achieved successfully. Nonetheless, cisplatin has no fluorescence, contrary to the anionic PAMAM dendrimers that present fluorescence (see annex Figure A11). After the coordination of PAMAM dendrimer to cisplatin, it can be observed that the fluorescence of G0.5(COOPt(NH$_3$)$_2$Cl)$_8$ slightly increased and in the G2.5(COOPt(NH$_3$)$_2$Cl)$_{32}$ decreased, which suggests the conjugation of cisplatin on the surface of the PAMAM

dendrimer. In the case of G1.5(COOPt$(NH_3)_2Cl)_{16}$, the fluorescence increased significantly. Figure 24b were represented the fluorescence spectrum of the cisplatin-metallodendrimers in a monodentate form, where the fluorescence of G1.5(COOPt$(NH_3)_2Cl)_{16}$ compared with the other metallodendrimers is significantly higher. It appears that an enhancement fluorescence effect occurs in this dendrimer after the conjugation of the 16 metals complexes.

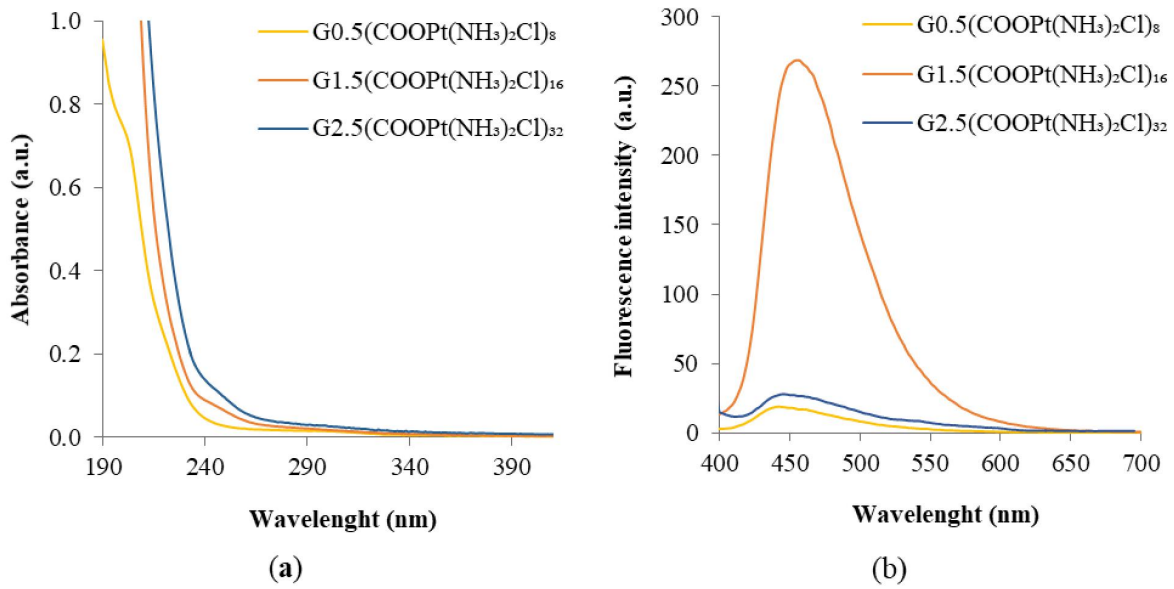

Figure 24: a) UV-Vis spectra of the metallodendrimers conjugated with cisplatin in monodentate form at concentration 40 μM in UPW and b) Emission (λ_{ex} = 380 nm) spectra of metallodendrimers conjugated with cisplatin in monodentate form recorded in UPW at a concentration 500 μM.

After the coordination of the anionic PAMAM dendrimers to cisplatin, the charge of the prepared cisplatin-metallodendrimers increases as expected. These results suggest the functionalization since cisplatin has a positive charge and these dendrimers have a negative charge (Table 2). However, the observed decrease in the zeta-potential values after the conjugation with cisplatin can lead to the aggregation of the metallodendrimers in an aqueous solution, although it is not an absolute indication regarding the stability of the nanoparticles.

Table 2: Zeta-potential of the anionic PAMAM dendrimers (G0.5-G3.5) and their related metallodendrimers after conjugation with cisplatin in a monodentate form (n = 3) in filtered UPW.

Compounds	Zeta-potential (mV)
$G0.5(COONa)_8$	-19.17 ± 1
$G0.5(COOPt(NH_3)_2Cl)_8$	**1.78 ± 148**
$G1.5(COONa)_{16}$	-40.80 ± 0.7
$G1.5(COOPt(NH_3)_2Cl)_{16}$	**-8.8 ± 1.1**
$G2.5(COONa)_{32}$	-47.77 ± 1.46
$G2.5(COOPt(NH_3)_2Cl)_{32}$	**7.99 ± 0.72**

Additionally, these cisplatin-metallodendrimers were evaluated by TOF-MS (ESI positive mode or MALDI) techniques (see the spectra in the annex - Figures C4-C6). Even with difficulties in the characterization, due to the compounds hygroscopic nature, the fragments identified by TOF-MS confirm the functionalization of the anionic PAMAM dendrimers with cisplatin in the monodentate form. Table 3 were summarized the results acquired from MS. The $G0.5(COOPt(NH_3)_2Cl)_8$ had a peak at *m/z* = 1606.46 $[M+2H^+ + H_2O - C_{46}H_{118}Cl_8N_{26}O_{21}Pt_8]^{2+}$. For the $G1.5(COOPt(NH_3)_2Cl)_{16}$ was found only a fragment with two cisplatin without the chlorine groups at *m/z* = 1013.46 $[M+3H^+ - C_{110}H_{205}N_{30}O_{44}Pt_2]^{3+}$. Furthermore, for the $G2.5(COOPt(NH_3)_2Cl)_{32}$ was also found a fragment with PAMAM dendrimer conjugated to twenty-nine cisplatin metals at *m/z* = 974.65 $[M+H^+ - C_{238}H_{562}Cl_{29}N_{116}O_{92}Pt_{29}]^+$.

Table 3: Molecular weight of the cisplatin-metallodendrimers in a monodentate form.

	$G0.5(COOPt(NH_3)_2Cl)_8$	**$G1.5(COOPt(NH_3)_2Cl)_{16}$**	**$G2.5(COOPt(NH_3)_2Cl)_{32}$**
Molecular weight	3201.90	6800.29	13997.08
***m/z* calculated**	1606.68	1013.47	974.82
***m/z* found**	1606.46 $[M+2H^+ + H_2O]^{2+}$ $C_{46}H_{118}Cl_8N_{26}O_{21}Pt_8^{2+}$	1013.46 $[M+3H^+]^{3+}$ $C_{110}H_{205}N_{30}O_{44}Pt_2^{3+}$	974.65 $[M+H^+]^+$ $C_{238}H_{562}Cl_{29}N_{116}O_{92}Pt_{29}^+$

3.1.2. Bidentate form

To prepare the bidentate cisplatin-metallodendrimers, cisplatin was first bis-aquated using silver nitrate as an abstractor of the chlorine groups, with 97% of yield. The aquation of cisplatin is important to assure the removal of the two chlorines and the conjugation in a bidentate form. Actually, the conjugation of cisplatin in a bidentate form involving two bonds should delay the release before the target was achieved, decreasing the side effects. As such, the anionic PAMAM dendrimers were coordinated to the bis-aquated cisplatin. All the synthesized metallodendrimers were obtained with good yields, namely, 80% for G0.5COO($Pt(NH_3)_2)_4$, 64% for G1.5COO($Pt(NH_3)_2)_8$, 56% for G2.5COO($Pt(NH_3)_2)_{16}$ and 58% for the G3.5COO($Pt(NH_3)_2)_{32}$. They were fully characterized by different techniques such as NMR (^1H, ^{13}C, and ^{195}Pt-NMR), FTIR, UV-Vis, and Fluorescence spectroscopy, zeta-potential, MS and EA. As mentioned before, for the ^1H-NMR experiments, the deuterated water (D_2O) signal was used as an internal reference, and the potassium tetrachloroplatinate (II) was used as an external reference for the ^{195}Pt-NMR experiments. Figure 25 showed the ^1H-NMR spectrum of the G0.5COO($Pt(NH_3)_2)_4$ with the characteristics signals of PAMAM dendrimer between 2.57 to 3.58 ppm. Nevertheless, only a downfield shift of the signals was visible as regards the PAMAM dendrimer (see annex Figure A1).

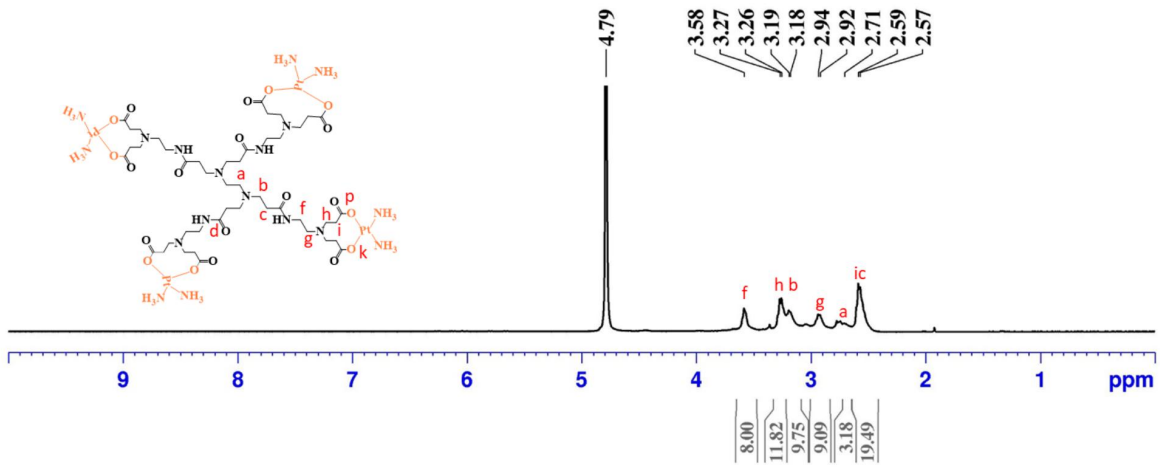

Figure 25: ^1H-NMR spectrum of G0.5COO($Pt(NH_3)_2)_4$ performed in D_2O.

In the ^{13}C-NMR spectrum (Figure 26) a downfield shift of the carboxylate group from 174.69 to 178.50 ppm was visible after cisplatin conjugation to the PAMAM dendrimer.

The ^{195}Pt-NMR spectrum (Figure 27) showed a signal at -2119 ppm from the bidentate conjugation of the anionic PAMAM dendrimer to cisplatin and the signal at -1545 ppm probably corresponds to cis-$[PtCl(NH_3)_2(H_2O)_2]^{2+}$.

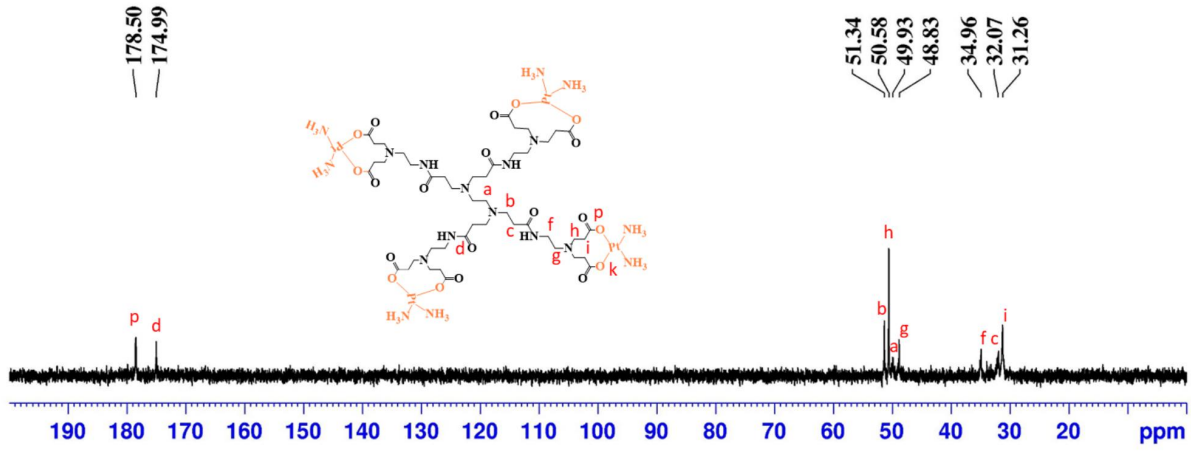

Figure 26: ^{13}C-NMR spectrum of G0.5COO(Pt(NH$_3$)$_2$)$_4$ performed in D$_2$O.

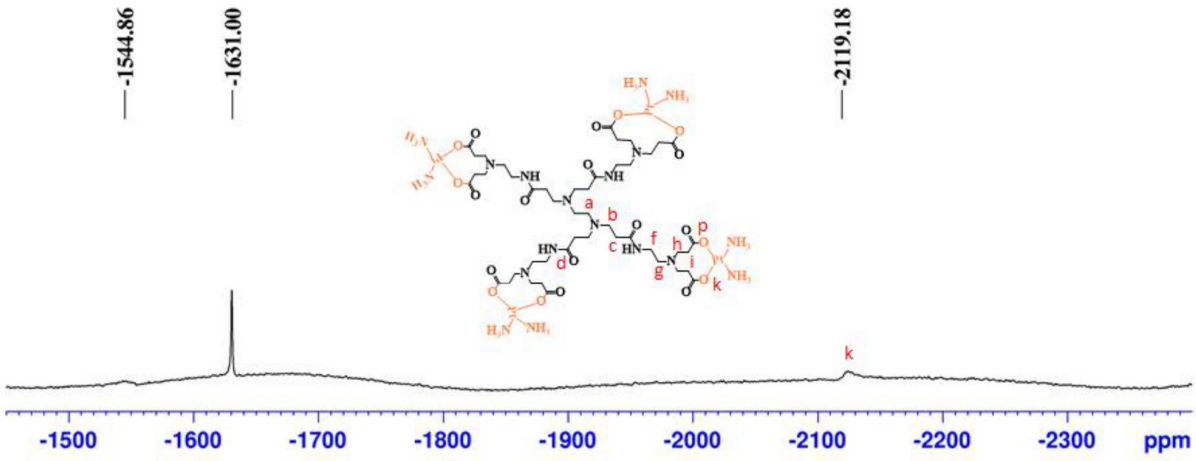

Figure 27: ^{195}Pt-NMR spectrum of G0.5COO(Pt(NH$_3$)$_2$)$_4$ performed in D$_2$O, with K$_2$PtCl$_4$ as an external reference (-1631 ppm).

The G1.5COO(Pt(NH$_3$)$_2$)$_8$ also displayed a downfield shift in the protons in the ^{1}H-NMR spectrum after conjugation with cisplatin (Figure 28). Particularly, the downfield shift in the carboxylate group from 175.22 to 177.37 ppm in the ^{13}C-NMR spectrum (Figure 29) suggests the dendrimer's coordination to cisplatin. The form of how cisplatin was conjugated to the dendrimer was determined by ^{195}Pt-NMR. From the spectrum (see annex Figure C7), the signal at – 2119 ppm suggests that the coordination of the PAMAM dendrimer to cisplatin in a bidentate form was achieved.

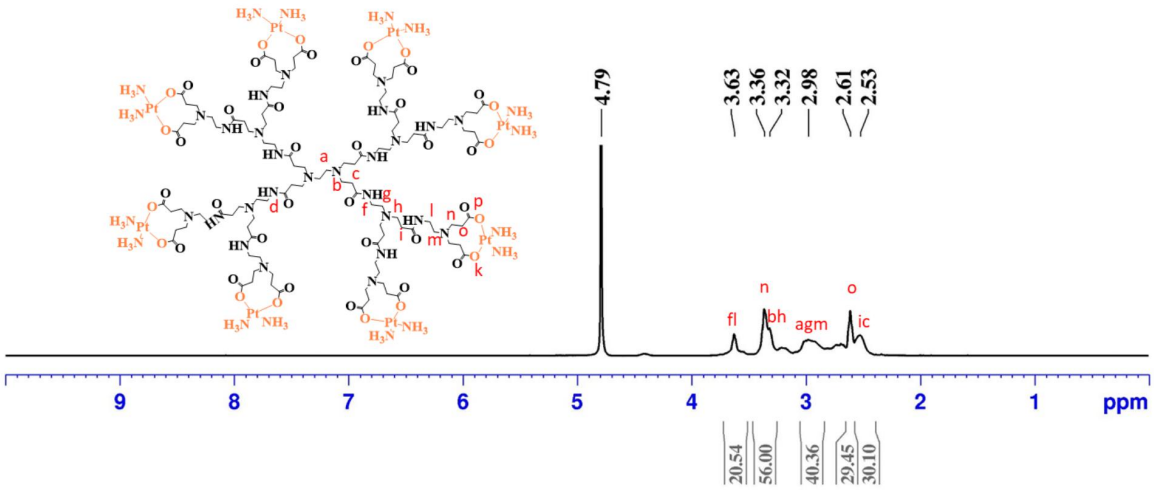

Figure 28: ^{1}H-NMR spectrum of G1.5COO(Pt(NH$_3$)$_2$)$_8$ performed in D$_2$O.

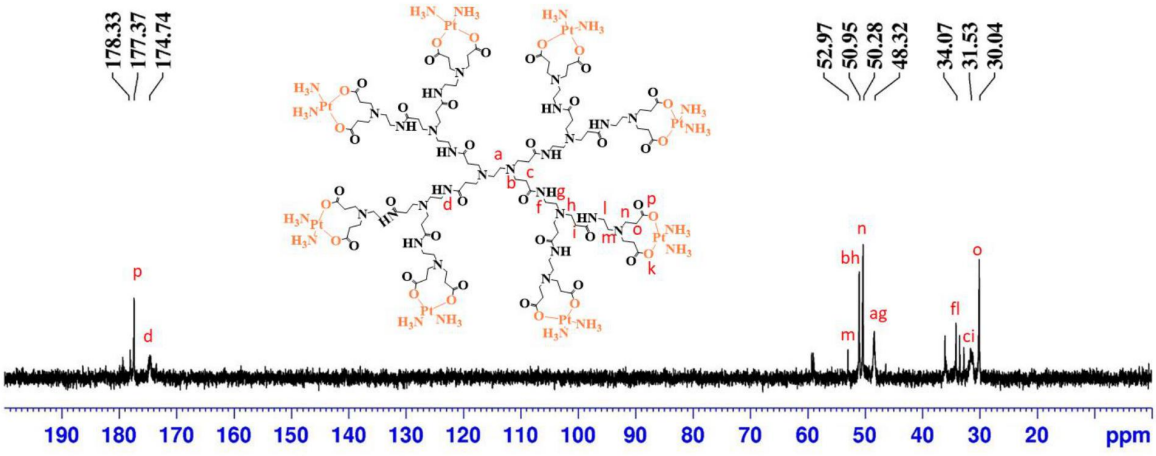

Figure 29: ^{13}C-NMR spectrum of G1.5COO(Pt(NH$_3$)$_2$)$_8$ performed in D$_2$O.

The ^{1}H-NMR spectrum of G2.5COO(Pt(NH$_3$)$_2$)$_{16}$ (Figure 30) also showed a downfield shift in the protons compared to the respective pristine PAMAM dendrimer (see annex Figure A5). In the ^{13}C-NMR spectrum (Figure 31) was visible a downfield shift in the carboxylate group from 174.67 to 177.30 ppm. The signal at -2123 ppm in ^{195}Pt-NMR spectrum suggests the coordination of PAMAM dendrimer to cisplatin in a bidentate form (see annex Figure C8).

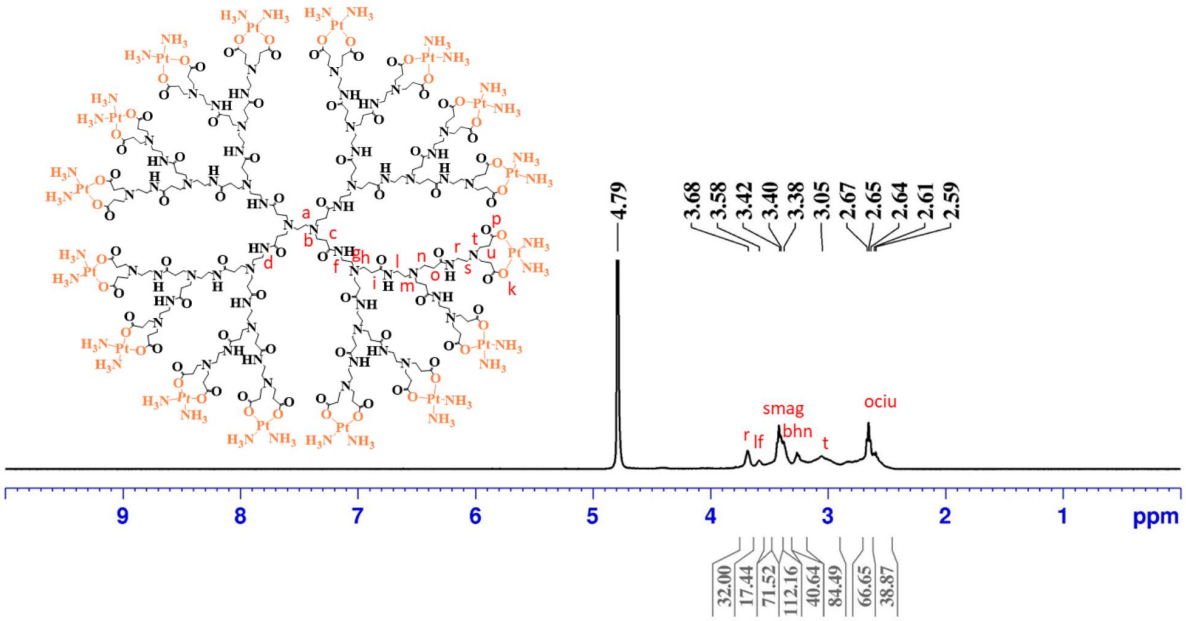

Figure 30: ^{1}H-NMR spectrum of G2.5COO(Pt(NH$_3$)$_2$)$_{16}$ performed in D$_2$O.

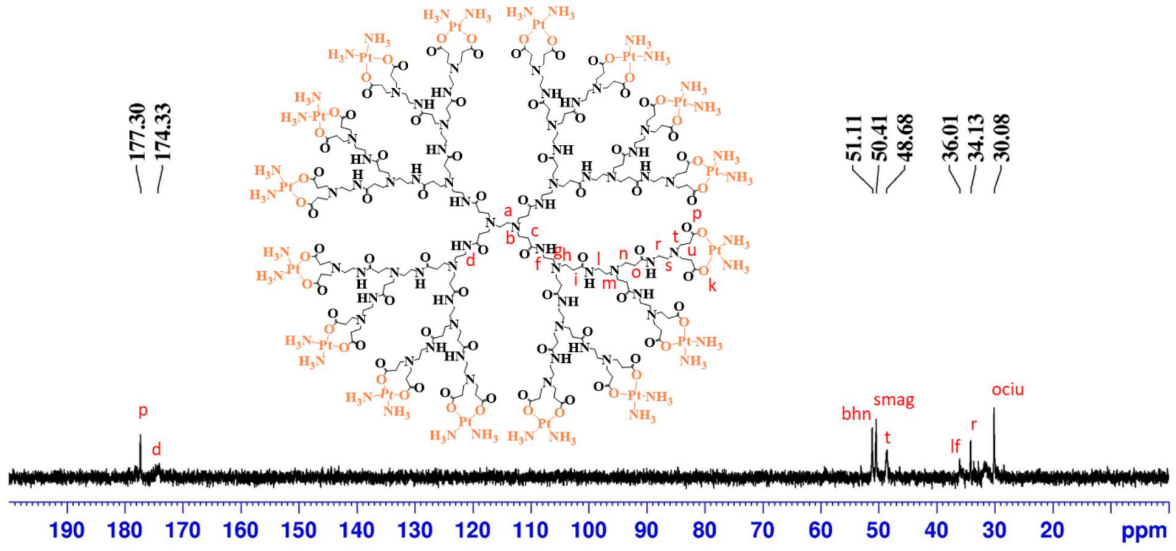

Figure 31: ^{13}C-NMR spectrum of G2.5COO(Pt(NH$_3$)$_2$)$_{16}$ performed in D$_2$O.

In the ^{1}H-NMR spectrum of G3.5COO(Pt(NH$_3$)$_2$)$_{32}$ (Figure 32) is shown the characteristics signals of the PAMAM dendrimer structure that were downfield shifted after the conjugation with cisplatin. A downfield shift was also observed in the ^{13}C-NMR spectrum (Figure 33) of the carboxylate group, from 174.90 to 177.20 ppm, indicating the conjugation of cisplatin. The ^{195}Pt-NMR spectrum (see annex Figure C9) had a signal at -2121 ppm, suggesting the bidentate conjugation of cisplatin.

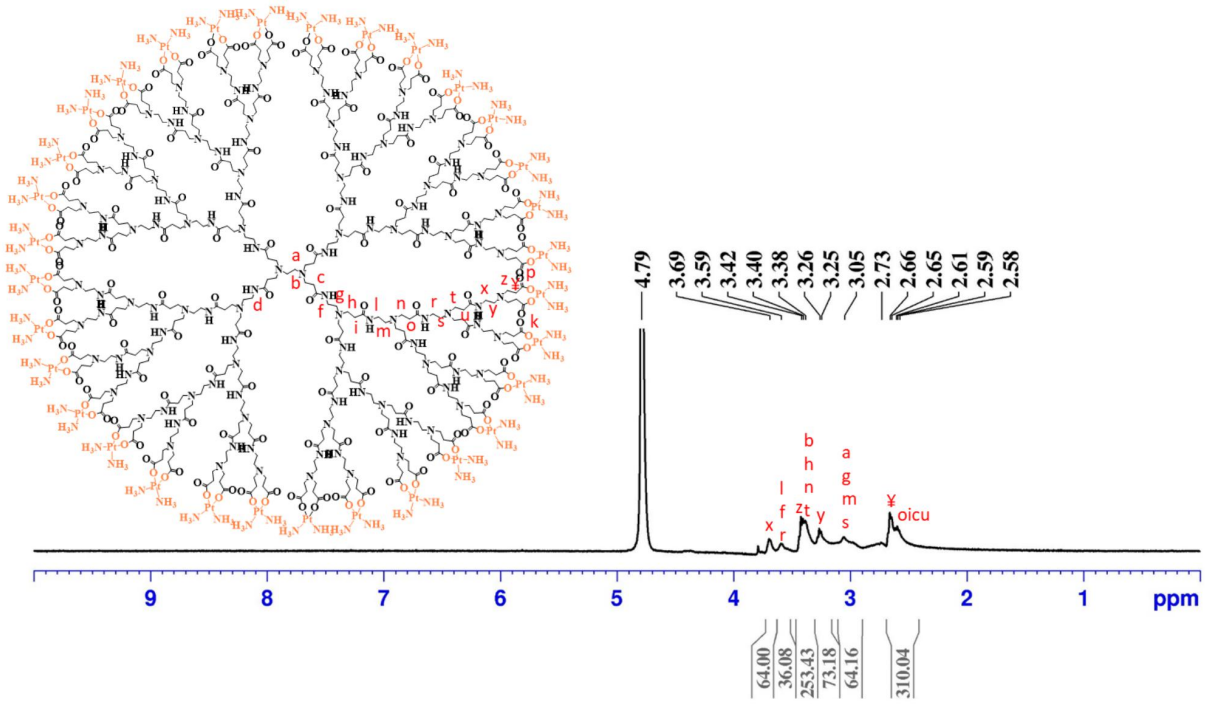

Figure 32: ^{1}H-NMR spectrum of G3.5COO(Pt(NH$_3$)$_2$)$_{32}$ performed in D$_2$O.

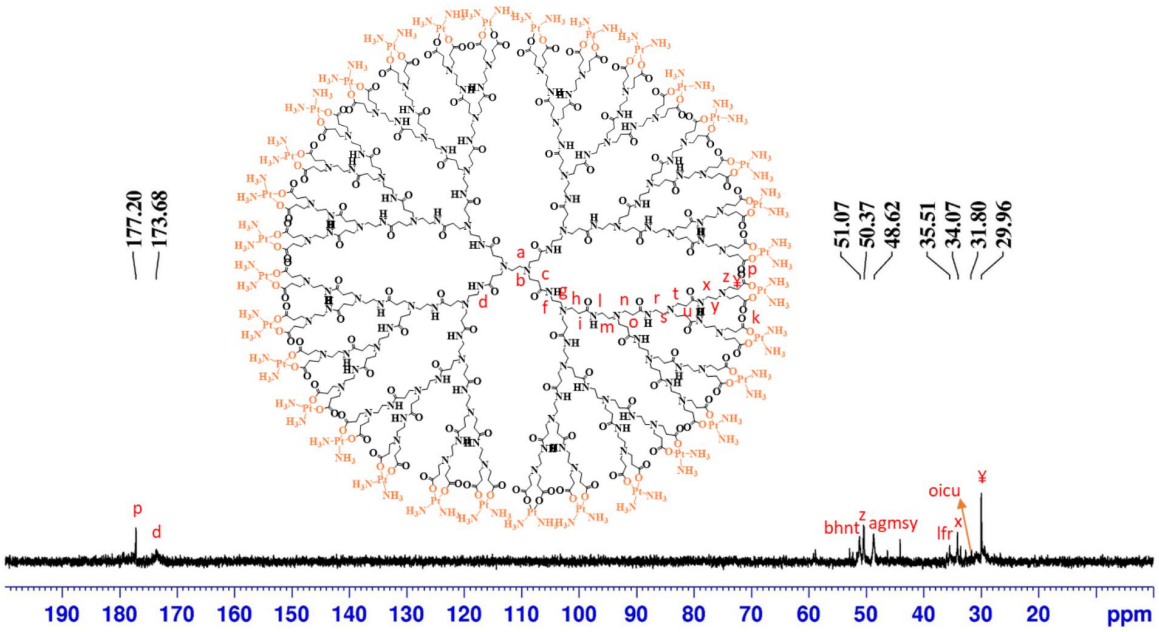

Figure 33: ^{13}C-NMR spectrum of G3.5COO(Pt(NH$_3$)$_2$)$_{32}$ performed in D$_2$O.

The prepared compounds were also characterized by FTIR (see annex Figure C10). In all the cisplatin-metallodendrimers (G0.5COO(Pt(NH$_3$)$_2$)$_4$, G1.5COO(Pt(NH$_3$)$_2$)$_8$, G2.5COO(Pt(NH$_3$)$_2$)$_{16}$ and G3.5COO(Pt(NH$_3$)$_2$)$_{32}$) a shift of the carbonyl stretch band was observed, when compared to the respective

pristine anionic PAMAM dendrimer. In the G0.5COO(Pt(NH$_3$)$_2$)$_4$ the shift was observed from 1639 cm^{-1} to 1633 cm^{-1}, G1.5COO(Pt(NH$_3$)$_2$)$_8$ from 1633 cm^{-1} to 1644 cm^{-1}, G2.5COO(Pt(NH$_3$)$_2$)$_{16}$ from 1638 cm^{-1} to 1645 cm^{-1} and G3.5COO(Pt(NH$_3$)$_2$)$_{32}$ from 1639 cm^{-1} to 1642 cm^{-1}. The slight shifts indicate that the effect of cisplatin was insignificant due to its neutral behavior[293]. For the G1.5COO(Pt(NH$_3$)$_2$)$_8$ and G2.5COO(Pt(NH$_3$)$_2$)$_{16}$ metallodendrimers was also visible the presence of a new band related with the N-H stretch of the NH$_3$ groups of cisplatin at 3266 cm^{-1} and 3255 cm^{-1}, respectively. For the remaining metallodendrimers, although there was not a visible new band, the existent band was significantly shifted, from 3418 cm^{-1} to 3435 cm^{-1} for the G0.5COO(Pt(NH$_3$)$_2$)$_4$, and, from 3421 cm^{-1} to 3446 cm^{-1} for G3.5COO(Pt(NH$_3$)$_2$)$_{32}$. This could probably be explained by the new band overlapping with the N-H band of the amide group of PAMAM dendrimers.

The cisplatin-metallodendrimers in a bidentate form were also characterized by UV-Vis and fluorescence spectroscopy (Figure 34).

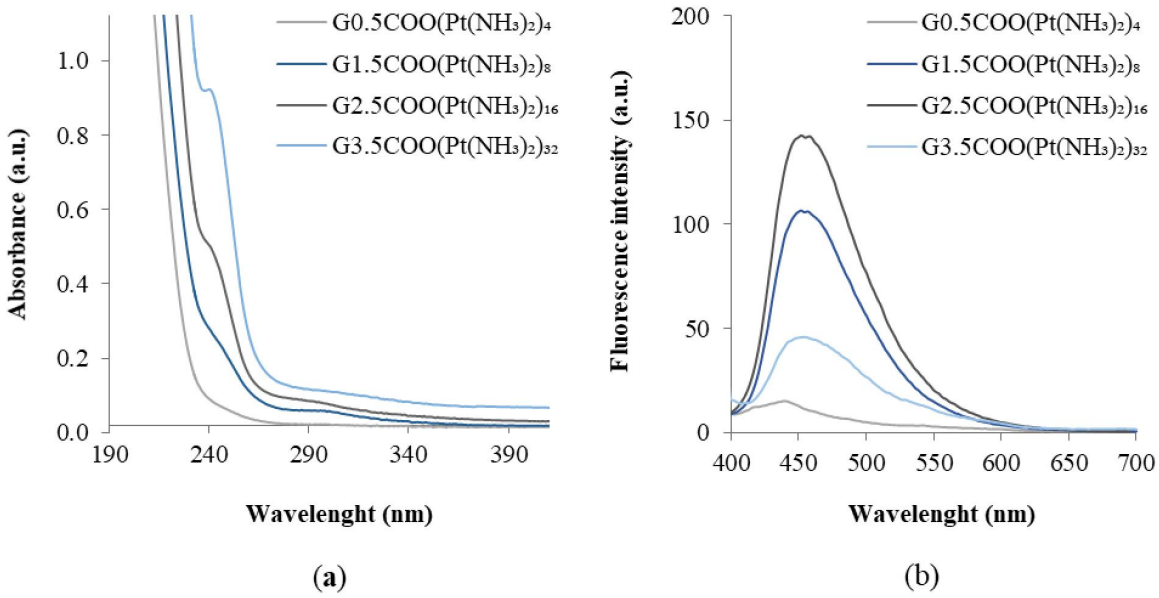

Figure 34: a) UV-Vis spectra of the metallodendrimers conjugated with cisplatin in the bidentate form at a concentration of 40 μM in UPW, b) Emission (λ_{ex} = 380 nm) spectra of metallodendrimers conjugated with cisplatin in the bidentate form recorded in UPW at a concentration of 500 μM.

After the conjugation of the PAMAM dendrimer to cisplatin in a bidentate form, the cisplatin band shifted from 203 to 247 nm, 242 nm and 241 nm for G1.5COO(Pt(NH$_3$)$_2$)$_8$, G2.5COO(Pt(NH$_3$)$_2$)$_{16}$, and G3.5COO(Pt(NH$_3$)$_2$)$_{32}$, respectively. In the spectrum, a shoulder is detected (Figure 34a), which was more evident for the higher generations of the PAMAM dendrimers. However, in the G0.5COO(Pt(NH$_3$)$_2$)$_4$ spectrum, that shoulder was not visible, probably because it has only four metals. In addition, the characteristic absorption band of the anionic PAMAM dendrimers, which appeared around 280-300 nm and was attributed

to the interior tertiary amines, did not shift significantly, suggesting that cisplatin has been conjugated only at the dendrimer surface. In the fluorescence spectrum (Figure 34b), the fluorescence of all cisplatin-metallodendrimers decreased after the coordination of the dendrimer to cisplatin. Nevertheless, the G2.5COO($Pt(NH_3)_2$)$_{16}$ had a greater fluorescence than the remaining metallodendrimers. The same was verified for the G1.5COO($Pt(NH_3)_2Cl$)$_{16}$, where the dendrimer was conjugated to the cisplatin in the monodentate form. These two metallodendrimers have 16 metals conjugated on their surface, which may indicate that a maximum fluorescence is reached with 16 metal. Moreover, the charge of the anionic PAMAM dendrimers increases after the conjugation with cisplatin (Table 4), indicating the coordination of the dendrimer to cisplatin on its surface. Even if the zeta-potential was not an unquestionable indication of the stability of the nanoparticles, the decrease in the zeta-potential values suggests the metallodendrimer aggregation in an aqueous solution.

Table 4: Zeta-potential of the anionic PAMAM dendrimers (G0.5-G3.5) and their related metallodendrimers after conjugation with cisplatin in a bidentate form (n = 3) in filtered UPW.

Compounds	Zeta-potential (mV)
G0.5($COONa$)$_8$	-19.17 ± 1
G0.5COO($Pt(NH_3)_2$)$_4$	**-7.73 ± 0.5**
G1.5($COONa$)$_{16}$	-40.80 ± 0.7
G1.5COO($Pt(NH_3)_2$)$_8$	**-17.37 ± 0.5**
G2.5($COONa$)$_{32}$	-47.77 ± 1.46
G2.5COO($Pt(NH_3)_2$)$_{16}$	**2.49 ± 0.32**
G3.5($COONa$)$_{64}$	- 51.27 ± 1.27
G3.5COO($Pt(NH_3)_2$)$_{32}$	**23.23 ± 0.95**

In addition to this, the conjugation of the anionic PAMAM dendrimers to cisplatin was evaluated by TOF-MS (ESI positive mode or MALDI) analysis (see the spectra in Figures C11-C14). Table 5 summarizes the results obtained for MS analyses. For the metallodendrimers G0.5COO($Pt(NH_3)_2$)$_4$, G1.5COO($Pt(NH_3)_2$)$_8$ and G2.5COO($Pt(NH_3)_2$)$_{16}$ were found the expected structures with peaks at *m/z* = 1023.27 [M+2Na^+ - $C_{46}H_{96}N_{18}Na_2O_{20}Pt_4]^{2+}$, 1466.83 [M+3$H^+$ - $C_{110}H_{227}N_{42}O_{44}Pt_8]^{3+}$ and 4597.5 [M+2H^+ - $C_{238}H_{482}N_{90}O_{92}Pt_{16}]^{2+}$, respectively. For the G3.5COO($Pt(NH_3)_2$)$_{32}$ was only found a fragment with the dendrimer conjugated with twenty-nine cisplatin metals with a peak at *m/z* = 974.64 [M+H^+ - $C_{494}H_{981}N_{180}O_{188}Pt_{29}]^+$.

Table 5: Molecular weight of the cisplatin-metallodendrimers in a bidentate form.

	G0.5COO(Pt(NH$_3$)$_2$)$_4$	**G1.5COO(Pt(NH$_3$)$_2$)$_8$**	**G2.5COO(Pt(NH$_3$)$_2$)$_{16}$**	**G3.5COO(Pt(NH$_3$)$_2$)$_{32}$**
Molecular weight	2001.72	4399.92	9196.34	18789.17
***m/z* calculated**	1023.27	1466.80	4598.51	974.82
***m/z* found**	1023.27 $[M+2Na^+]^{2+}$ $C_{46}H_{96}N_{18}Na_2O_{20}Pt_4^{2+}$	1466.83 $[M+3H^+]^{3+}$ $C_{110}H_{227}N_{42}O_{44}Pt_8^{3+}$	4597.5 $[M+2H^+]^{2+}$ $C_{238}H_{482}N_{90}O_{92}Pt_{16}^{2+}$	974.64 $[M+H^+]^+$ $C_{494}H_{981}N_{180}O_{188}Pt_{29}^+$

3.2.Biological studies

3.2.1. Cytotoxicity assays

The cytotoxicity behavior of cisplatin-metallodendrimers in mono and bidentate forms (G0.5(COOPt(NH$_3$)$_2$Cl)$_8$, G1.5(COOPt(NH$_3$)$_2$Cl)$_{16}$, G2.5(COOPt(NH$_3$)$_2$Cl)$_{32}$ G0.5COO(Pt(NH$_3$)$_2$)$_4$, G1.5COO(Pt(NH$_3$)$_2$)$_8$, G2.5COO(Pt(NH$_3$)$_2$)$_{16}$ and G3.5COO(Pt(NH$_3$)$_2$)$_{32}$) were studied *in vitro* using four cancer cell lines, A2780, A2780CisR, MCF-7, CACO-2 cell lines and one non-cancer cell line, the BJ cells. For the cytotoxicity evaluation, an MTT assay that measures the metabolic activity was used, and the results were obtained after 72 h. The results were presented in Figures C15-C19 (see the annex) and the half-maximal inhibitory concentration, IC_{50}, values in Table 6. The anionic PAMAM dendrimers (G0.5-G3.5) and cisplatin were used for comparison. Our results showed that all the metallodendrimers exhibit cytotoxicity against the tested cancer cell lines, being more effective in at least one of the cancer cell lines studied compared to cisplatin. Nevertheless, the metallodendrimers G0.5(COOPt(NH$_3$)$_2$Cl)$_8$ and G2.5(COOPt(NH$_3$)$_2$Cl)$_{32}$ compared to the remaining metallodendrimers were the most cytotoxic in all the cancer cell lines, as shown by the obtained IC_{50} values. According to the previous studies[281,283,294], the drug cisplatin was expected to be released from the dendrimer due to the concentration of chloride ions in the cell that reacts with the carboxylic groups of dendrimers by an exchange reaction. The aquation of cisplatin gives rise to potent electrophilic cations that bind to DNA, displaying its anticancer activity.

Table 6: IC_{50} values of the prepared cisplatin-metallodendrimers toward various cancer cell lines and non-cancer cell line. Results are expressed as mean ± SD three independent experiments performed in triplicate.

	A2780 IC_{50} ± SD (μM)	***A2780CisR*** IC_{50} ± SD (μM)	***MCF-7*** IC_{50} ± SD (μM)	***CACO-2*** IC_{50} ± SD (μM)	***BJ*** IC_{50} ± SD (μM)
Cisplatin	0.11 ± 0.03	3.51 ± 1.35	1.21 ± 0.45	> 10	0.55 ± 0.23
Monodentate form					
G0.5(COOPt(NH$_3$)$_2$Cl)$_8$	**0.02 ± 0.01**	**> 0.01**	**0.075 ± 0.01**	**2.52 ± 1.7**	0.06 ± 0.01
G1.5(COOPt(NH$_3$)$_2$Cl)$_{16}$	0.20 ± 0.08	6.55 ± 0.15	0.54 ± 0.16	>10	0.50 ± 0.21
G2.5(COOPt(NH$_3$)$_2$Cl)$_{32}$	**0.068 ± 0.03**	**0.04 ± 0.026**	**0.63 ± 0.34**	**6.25 ± 2.7**	0.39 ± 0.22
Bidentate form					
G0.5COO(Pt(NH$_3$)$_2$)$_4$	0.31 ± 0.12	5.21 ± 1.49	2.04 ± 0.16	7.54 ± 2.3	3.28 ± 1.38
G1.5COO(Pt(NH$_3$)$_2$)$_8$	0.07 ± 0.04	6.35 ± 0.19	1.69 ± 0.55	>10	0.53 ± 0.26
G2.5COO(Pt(NH$_3$)$_2$)$_{16}$	0.18 ± 0.03	0.17 ± 0.05	2.35 ± 0.56	>10	0.51 ± 0.27
G3.5COO(Pt(NH$_3$)$_2$)$_{32}$	0.04 ± 0.02	0.06 ± 0.04	3.29 ± 0.69	>10	1.2 ± 0.51

To compare the synthesized metallodendrimers with cisplatin, according to their efficacy, different factors as the relative potency, selectivity, and resistance factor were determined. The cytotoxicity relative potential (RP) value was determined (Table 7), particularly against the A2780CisR cancer cell line, where cisplatin has resistance and, for that reason, presents clinical limitations[295]. This value was obtained by dividing the IC_{50} of the cisplatin by the IC_{50} of the metallodendrimer. Accordingly, the G0.5(COOPt(NH$_3$)$_2$Cl)$_8$ metallodendrimer had an RP value 351 times more toxic than cisplatin, followed by the G2.5(COOPt(NH$_3$)$_2$Cl)$_{32}$ with an RP value of 88, G3.5COO(Pt((NH$_3$)$_2$)$_{32}$ with 59 and finally the G2.5COO(Pt((NH$_3$)$_2$)$_{16}$ with an RP of 20. However, the increase in generation and metallic centers do not significantly influence the cytotoxicity of the metallodendrimer in cancer cells. Nevertheless, the way how cisplatin was conjugated to dendrimer seems to have a role in the anticancer effectiveness of the metallodendrimer to some extent. This can be verified since the two metallodendrimers with the highest RP value, cisplatin was conjugated in a monodentate form. The explanation can be due to the ease of releasing cisplatin compared to the bidentate form, where cisplatin takes longer to be released since it was conjugated to the dendrimer with two bonds.

Table 7: Relative potency (RP) of the cisplatin-metallodendrimers calculated from the division of the IC_{50} value of cisplatin by the IC_{50} value of the metallodendrimers. The obtained value should be higher than 1 to have a relative potency.

Relative potency (RP)	***A2780***	***A2780CisR***	***MCF-7***	***CACO-2***	***BJ***
Monodentate form					
G0.5(COOPt(NH$_3$)$_2$Cl)$_8$	5.5	**> 351**	16	> 4	9.2
G1.5(COOPt(NH$_3$)$_2$Cl)$_{16}$	0.55	0.54	2.2	> 1	1.1
G2.5(COOPt(NH$_3$)$_2$Cl)$_{32}$	1.6	**88**	1.9	> 1.6	1.4
Bidentate form					
G0.5COO(Pt(NH$_3$)$_2$)$_4$	0.35	0.6	0.59	> 1.3	0.17
G1.5COO(Pt(NH$_3$)$_2$)$_8$	1.57	0.55	0.7	> 1	1.03
G2.5COO(Pt(NH$_3$)$_2$)$_{16}$	0.6	**21**	0.5	> 1	1.08
G3.5COO(Pt(NH$_3$)$_2$)$_{32}$	2.75	**59**	0.37	> 1	0.46

As described earlier another limitation of platinum drugs is the selectivity for cancer cells, which leads to undesirable side effects. In this sense, the cytotoxicity of the metallodendrimers in the non-cancer BJ cells was determined to indicate the cancer selectivity of the synthesized metallodendrimers. The selectivity index (SI) is defined as the ratio of the IC_{50} of the normal BJ cells by the IC_{50} of the individual cancer cell line tested, which is presented in Table 8. According to the literature, if the SI value is greater than 2, more selective is the compound for the cancer cells. If the SI values are less or equal to 2, the compound presents only a general toxicity[295–297]. All the cisplatin-metallodendrimers, had a SI greater than 2 in the A2780 cancer cell line, indicating that the compounds were more cytotoxic to this cancer cell line than the non-cancer cell line. Nonetheless, only four metallodendrimers were more selective in this cancer cell line than cisplatin, the G0.5COO(Pt(NH$_3$)$_2$)$_4$, G1.5COO(Pt(NH$_3$)$_2$)$_8$, the monodentate G2.5(COOPt(NH$_3$)$_2$Cl)$_{32}$ and G3.5COO(Pt(NH$_3$)$_2$)$_{32}$. However, in the A2780CisR cancer cells, all the metallodendrimers had a higher SI than cisplatin except for the G1.5(COOPt(NH$_3$)$_2$Cl)$_{16}$ and G1.5COO(Pt(NH$_3$)$_2$)$_8$ metallodendrimers, although some displayed a value less than 2, presenting general toxicity. The metallodendrimers that presented the higher SI were the monodentate G0.5(COOPt(NH$_3$)$_2$Cl)$_8$ with a SI value higher than 6, G2.5(COOPt(NH$_3$)$_2$Cl)$_{32}$ with a SI equal to 9.8, G2.5COO(Pt(NH$_3$)$_2$)$_{16}$ with a SI equal to 3 and G3.5COO(Pt(NH$_3$)$_2$)$_{32}$ with a SI value of 20. These results indicate that they can be considered promising anticancer drugs, with a SI value that is times higher than cisplatin. On the other hand, in the case of MCF-7

and CACO-2 cell lines, the SI was less than 2 for cisplatin, meaning that they have general toxicity for this type of cancer.

Table 8: Selectivity index (SI) of the cisplatin-metallodendrimers calculated from the division of the IC_{50} value of BJ cell line for the IC_{50} value of cancer cell lines.

Selectivity index (SI)	***A2780***	***A2780CisR***	***MCF-7***	***CACO-2***
Cisplatin	5	0.2	0.5	> 0.06
Monodentate form				
G0.5(COOPt(NH$_3$)$_2$Cl)$_8$	**3**	**> 6**	**0.8**	**0.02**
G1.5(COOPt(NH$_3$)$_2$Cl)$_{16}$	**2.5**	0.08	0.9	> 0.05
G2.5(COOPt(NH$_3$)$_2$Cl)$_{32}$	**5.7**	**9.8**	0.6	0.06
Bidentate form				
G0.5COO(Pt(NH$_3$)$_2$)$_4$	**10.6**	0.6	1.6	0.4
G1.5COO(Pt(NH$_3$)$_2$)$_8$	**7.6**	0.08	0.3	> 0.05
G2.5COO(Pt(NH$_3$)$_2$)$_{16}$	**2.8**	**3**	0.2	> 0.05
G3.5COO(Pt(NH$_3$)$_2$)$_{32}$	**30**	**20**	0.4	> 0.1

Since the start of the development of new platinum anticancer drugs, researchers have aimed to overcome the resistance of cisplatin. The A2780 and A2780CisR cancer cells were used to determine the resistance factor (RF) of the metallodendrimers. The RF is defined as the ratio between the IC_{50} value of A2780cisR cells and the IC_{50} value of A2780 cells. The lower the RF value, the better the compound to overcome the cancer cells resistance[92]. As it can be seen in Table 9, except for G1.5(COOPt(NH$_3$)$_2$Cl)$_{16}$ and G1.5COO(Pt(NH$_3$)$_2$)$_8$ metallodendrimers, all the metallodendrimers had an RF significant lower than cisplatin (RF= 31.9). The metallodendrimers with an RF lower than one were more effective in overcoming resistance to cancer cells. G0.5(COOPt(NH$_3$)$_2$Cl)$_8$ with an RF equal to 0.5, followed by the G2.5(COOPt(NH$_3$)$_2$Cl)$_{32}$ with an RF equal to 0.59, and the bidentate G2.5COO(Pt(NH$_3$)$_2$)$_{16}$ with an RF equal to 0.94 were the metallodendrimers that presented lower RF. Thereby these metallodendrimers present attractive advantages once they can surpass cisplatin resistance. Furthermore, the nanocarrier used, the anionic PAMAM dendrimers, can potentially direct the drug for cancer cells.

Table 9: Resistance factor of the cisplatin-metallodendrimers calculated from the division of the IC_{50} value of A2780CiR for the IC_{50} value of A270 cancer cell lines.

		Resistance factor (Rf)
	Cisplatin	31.9
Monodentate form	$G0.5(COOPt(NH_3)_2Cl)_8$	**0.5**
	$G1.5(COOPt(NH_3)_2Cl)_{16}$	32.8
	$G2.5(COOPt(NH_3)_2Cl)_{32}$	**0.59**
Bidentate form	$G0.5COO(Pt(NH_3)_2)_4$	16.8
	$G1.5COO(Pt(NH_3)_2)_8$	90.7
	$G2.5COO(Pt(NH_3)_2)_{16}$	**0.94**
	$G3.5COO(Pt(NH_3)_2)_{32}$	1.5

3.2.2. Hematoxicity assays

The hematoxicity assay was used to study the interaction of the prepared cisplatin-metallodendrimers with red blood cells by measuring the release of hemoglobin through the membrane disruption of these cells.

One of the side effects presented by platinum compounds, such as cisplatin, is the hematological toxicities that affect the function of bone marrow and consequently the production of blood cells, leading to diverse effects such as anemia[174]. Cisplatin forms complexes with the hemoglobin, which releases the Fe (heme group), responsible for transporting oxygen in the body[298]. Following this and based on the results (Figure 35), all the metallodendrimers and cisplatin showed very low hematoxicity levels (less than 5% for all the concentrations), compared with the values of hemoglobin release of the negative control. The low hematoxicity presented by the metallodendrimers was less or quite similar when compared to cisplatin. However, at 5 μM concentration, cisplatin displays hematoxicity values of 1.2 to 1.5 fold higher than the metallodendrimers. This was in accordance with what is found in the literature, that cisplatin induces hematological toxicity dependent on the concentration[175,176] According to a study performed by Mei-Hua Han *et al.*[299], anionic PAMAM dendrimers have a very low generation and concentration-dependent effect on hemolysis compared to cationic PAMAM dendrimers. Furthermore, these results suggest that the number of platinum metal centers and the generation of the anionic PAMAM dendrimers did not interfere with the toxicity in red blood cells at the concentrations used in the experiment since no significant differences are observed in the hematoxicity.

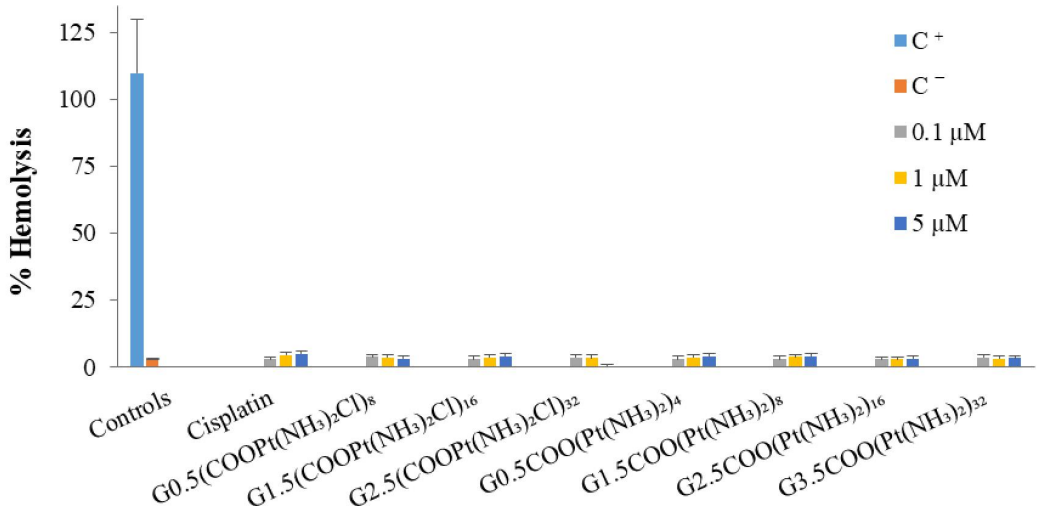

Figure 35: Hematoxicity of the free cisplatin and prepared cisplatin-metallodendrimers in healthy human blood. Blood was treated for 3 h with different concentrations (0.1, 1, and 5 µM) of the metallodendrimers and free cisplatin. The positive and negative control are represented by C^+ and C^-, respectively. The results are expressed as mean ± SD of at least three independent experiments performed in triplicate.

3.2.3. DNA binding studies

Despite the advances in cancer treatment, the main goal of chemotherapy remains to achieve a selective effect between a normal and a cancer cell[288,300]. In this sense, DNA has been the target of many drugs, as it plays an essential role in the replication and cellular transmission of genetic information[288]. The DNA structure is composed of a double helix, where each strand is made up of a combination of four chemical bases: adenine (A), thymine (T), cytosine (C), and guanine (G), linked together by phosphodiester bonds. Each complementary DNA strand is stabilized through hydrogen bonds between the base pairs adenine-thymine and guanine-cytosine[288,300]. The anti-parallel double helix form of DNA results in a region where the two strands are close to each other called the minor groove, and a region where they are away from each other, called the main groove[288,300]. These differences in the DNA conformations provide binding sites for small molecules[288].

Cisplatin binds covalently to the DNA through intra and interstrand crosslinks with the nitrogens on the DNA bases[288]. This binding mode is irreversible, causing the inhibition of DNA processes, leading to cell death[288]. Although the genomic DNA is the primary target of cisplatin, it can react with other cellular components, including proteins, before reaching the target[180,301–304]. Cisplatin firstly binds to DNA through monodentate adducts and then forms bidentate adducts[180,302,303]. This monoadduct has a long lifetime and plays an important role in the cytotoxicity of the drug, where the type of the formed crosslink is crucial[303].

The interactions of the G0.5(COOPt$(NH_3)_2Cl)_8$, G2.5(COOPt$(NH_3)_2Cl)_{32}$, and G2.5COO(Pt$(NH_3)_2)_{16}$ metallodendrimers with calf thymus DNA (CT-DNA) were studied *in vitro* using UV-vis spectroscopy. Cisplatin was also studied for comparison. The G0.5(COOPt$(NH_3)_2Cl)_8$ metallodendrimer was selected

because it has a much lower IC_{50} in all the cell lines studied than the remaining metallodendrimers. While $G2.5(COOPt(NH_3)_2Cl)_{32}$ and $G2.5COO(Pt(NH_3)_2)_{16}$ metallodendrimers were selected because it seems to be the most suitable for loading the 5-FU due to its size. Figure 36 shows the absorbance spectra of solutions containing different CT-DNA concentrations and a constant concentration of cisplatin-metallodendrimers. The CT-DNA spectrum displayed broadband at 260 nm due to the chromophore groups adenine, cytosine, thymine, and guanine. The spectra of the three metallodendrimers in the presence of increasing CT-DNA concentrations presented a hyperchromic effect[305]. The same effect was noticed for cisplatin (see annex Figure C22). It is known that cisplatin forms covalent adducts with DNA, resulting in hyperchromism due to a distortion in DNA conformation from the adduct formation. Indeed, the hyperchromic effect happens from the presence of charged cations, which readily react with DNA through crosslinks, where two bases of DNA are linked together with the drug. For the metallodendrimers, a full release of cisplatin during 5 min incubation probably did not occur, especially for the metallodendrimers in a bidentate form, even in the presence of chloride ions. However, the PAMAM dendrimer also interacts with DNA through electrostatic bonds, leading to a conformational change in the dendrimer-DNA complex that leads to DNA condensation[306]. So, other types of interactions may contribute to the DNA helix disruption, as electrostatic interactions or the cisplatin-metallodendrimers can also bind to DNA via the cisplatin monodentate form.

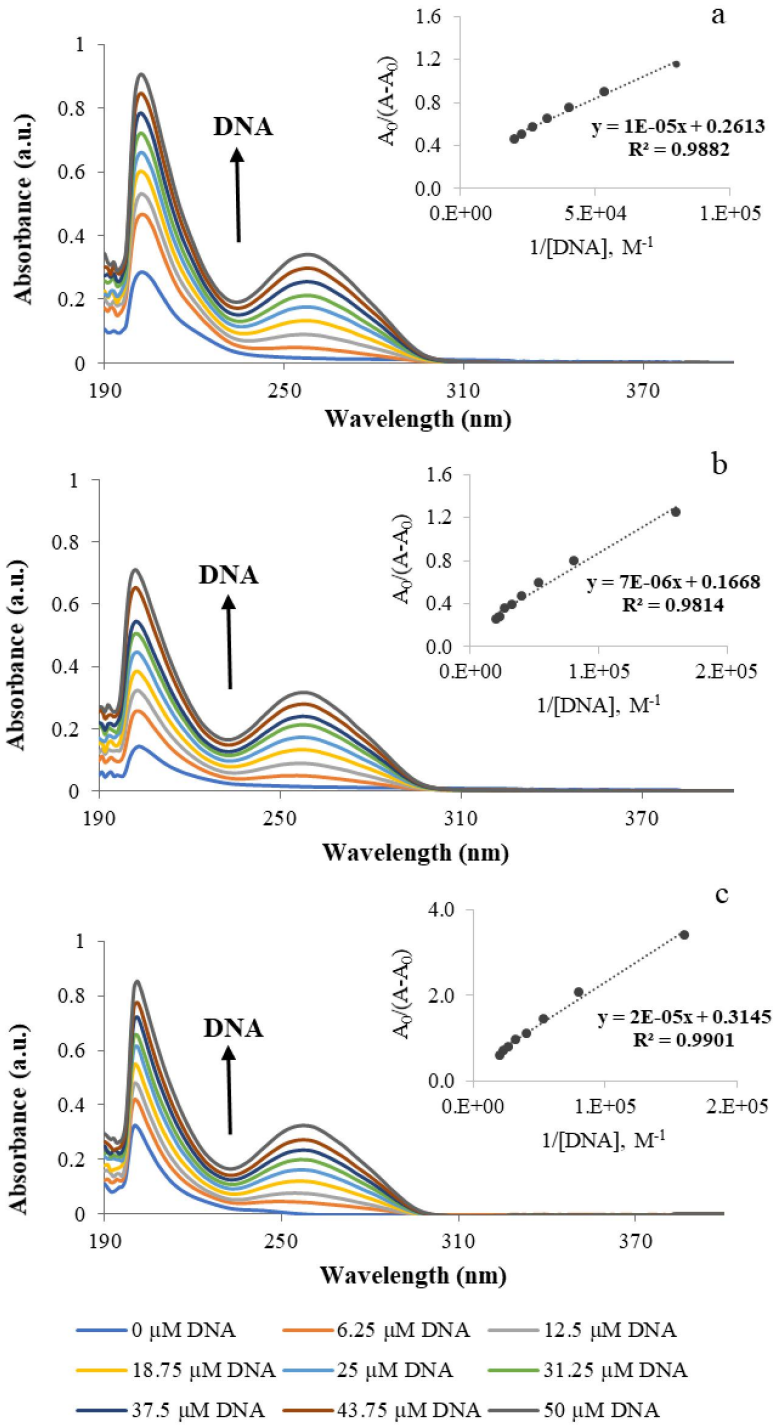

Figure 36: UV-visible spectra of a) G0.5(COOPt(NH_3)$_2$Cl)$_8$, b) G2.5(COOPt(NH_3)$_2$Cl)$_{32}$ and c) G2.5COO(Pt(NH_3)$_2$)$_{16}$ with increasing concentration of CT-DNA (0, 6.25, 12.5, 18.75, 25, 31.25, 37.5, 43.75 and 50 µM) in 5 mM Tris-HCl/50 mM NaCl at pH 7.4. The inset corresponds to the plot of $A_0/(A-A_0)$ versus 1/[DNA], which is used to determine the binding constant. The arrow indicates the direction of increasing the concentration of DNA.

The DNA binding constant (K_b) of the compounds with CT-DNA was determined by UV-Vis spectroscopy through the Benesi-Hildebrand equation, specifically from the ratio of the y-intercept to the slope in the plots $A_0/A\text{-}A_0$ vs. 1/[DNA][288].

The metallodendrimers showed a strong binding affinity with DNA compared to cisplatin (Table 10). However, the G0.5($COOPt(NH_3)_2Cl)_8$ and G2.5($COOPt(NH_3)_2Cl)_{32}$ metallodendrimers had a K_b value higher than bidentate G2.5$COO(Pt(NH_3)_2)_{16}$. Because, probably, this last was conjugated with cisplatin in a bidentate form, being more difficult to release the cisplatin during the incubation time. The conjugation of PAMAM dendrimer with cisplatin increased the K_b values, indicating a strong interaction of the cisplatin-metallodendrimers with the CT-DNA in the *in vitro* experiments. Nonetheless, it is important to emphasize that the interactions observed *in vitro* may not be precisely what happens *in vivo*. In addition to the fact that cisplatin was expected to be released near the target site, that is, in the cancer cells. Moreover, the Gibbs free energy of the binding process was also determined, and the obtained negative values indicate a spontaneous process (Table 10).

Table 10: Values of DNA binding constant (K_b) and Gibbs free energy (ΔG) of the G0.5($COOPt(NH_3)_2Cl)_8$, G2.5$COO(Pt(NH_3)_2)_{16}$ and G2.5($COOPt(NH_3)_2Cl)_{32}$ metallodendrimers and free drug cisplatin. Data are represented as mean ± SD of two independent experiments.

	K_b	- ΔG/ KJ mol^{-1}
G0.5($COOPt(NH_3)_2Cl)_8$	(26.6 ± 0.07) $x10^3$	25 ± 0.07
G2.5($COOPt(NH_3)_2Cl)_{32}$	(19.7 ± 0.006) $x10^3$	24 ± 0.74
G2.5$COO(Pt(NH_3)_2)_{16}$	(13.8 ± 0.003) $x10^3$	23 ± 0.47
Cisplatin	(1.3 ± 0.03) $x10^3$	17 ± 0.58

3.3. Drug loading

3.3.1. Loading of 5-Fluorouracil

The 5-FU drug that was designed, synthesized, and patent in 1957 by Charles Heidelberger[307] was chosen as a second drug to be transported by the metallodendrimers. Also, 5-FU is usually used to treat colorectal cancer and ovarian cancer. Their metabolites intercalate with DNA/RNA damaging the cells during phase S, which involves the replication of DNA and consequently induces cell apoptosis[249,308]. 5-FU also has the particularity of being a hydrophobic drug with low aqueous solubility. Additionally, the PAMAM dendrimer has hydrophobic internal cavities able to interact with poorly soluble drugs through hydrophobic interactions, which makes them suitable for the encapsulation of 5-FU[309]. Furthermore, synergetic effects between cisplatin and 5-FU have been reported in the literature[310,311], leading us to assess the possible existence of a similar effect when 5-FU was encapsulated in our metallodendrimers.

The G2.5COO($Pt(NH_3)_2)_{16}$ and G2.5($COOPt(NH_3)_2Cl)_{32}$ metallodendrimers were selected to load 5-FU because they have an RF value lower than free cisplatin are more selective for the A2780CisR cancer cells, and due to its size, seems to be more appropriate to encapsulate the drug. However, despite the fact that G0.5($COOPt(NH_3)_2Cl)_8$ metallodendrimer was considerably the best candidate since it has a more open structure (due to the lower generation), not allowing it to do so the encapsulation of drugs[309,312,313]. The 5-FU was encapsulated in the metallodendrimers by adapting the method described by Phung Le *et al.*[289]. Briefly, the metallodendrimers were dissolved in UPW, and then 5-FU was added to the solution. The unencapsulated drug was removed by dialysis. The amount of encapsulated drug was subsequently calculated indirectly by UV-Vis spectroscopy at the wavelength of 266 nm. The loading results of the metallodendrimers were compared with the pristine PAMAM dendrimer G2.5($COONa)_{32}$. As expected, the G2.5($COONa)_{32}$/5-FU PAMAM dendrimer has a higher loading efficiency than metallodendrimers since it does not have metal centers coordinated in its terminal groups, allowing 5-FU enters without hindrance (Table 11). Follows by G2.5COO($Pt(NH_3)_2)_{16}$/5-FU metallodendrimer conjugated to cisplatin in a bidentate form that has fewer platinum metal centers (16 metal centers), allowing the drug to enter its cavities since the surface was not densely compacted. The G2.5($COOPt(NH_3)_2Cl)_{32}$/5-FU metallodendrimer conjugated to cisplatin in a monodentate form, on the other hand, has a high surface density of end groups due to the greater number of platinum metal centers (32 metal centers) coordinated in the terminal groups. The same occurs with the loading capacity, which decreased with the increase in the number of metal centers coordinated to the terminal groups of the PAMAM dendrimer. The calculation of the number of 5-FU molecules that were encapsulated in each metallodendrimer/5-FU and the PAMAM dendrimer/5-FU is represented in Table 11. It can be observed that the G2.5($COOPt(NH_3)_2Cl)_{32}$/5-FU system has 12 encapsulated molecules and the G2.5COO($Pt(NH_3)_2)_{16}$/5-FU has 13 encapsulated molecules, which explains the difference in the loading capacity. However, in the G2.5($COONa)_{32}$/5-FU, although the loading capacity was higher compared to metallodendrimers/5-FU (LC = 31.72%) the number of loaded 5-FU molecules is only 13, the same as G2.5COO($Pt(NH_3)_2)_{16}$/5-FU.

Table 11: Loading efficiency (LE%), loading capacity (LC%) of 5-FU into G2.5COO($Pt(NH_3)_2)_{16}$ and G2.5($COOPt(NH_3)_2Cl)_{32}$ metallodendrimers, and into the anionic PAMAM dendrimer G2.5COONa (n=3), and number of encapsulated 5-FU molecules.

	LE%	LC%	Nº of molecules encapsulated[a]
G2.5COO($Pt(NH_3)_2)_{16}$/5-FU	82.25 ± 3.5	26.30 ± 6.63	13
G2.5($COOPt(NH_3)_2Cl)_{32}$/5-FU	77.45 ± 5.09	12.54 ± 1.48	12
G2.5($COONa)_{32}$/5-FU	86.14 ± 1.74	31.72 ± 0.95	13

[a] The number of molecules encapsulated was calculated from the following equation,
i = n (drug)/n (dendrimer), where n (drug) = m (encapsulated drug)/MM (drug) and n (dendrimer) = m (dendrimer)/ MM (dendrimer) and i the number of encapsulated molecules.

It is known that the loading capacity measures the capacity of a nanocarrier to encapsulate the drug. This loading capacity indicates the amount of drug loaded per unit weight of metallodendrimer, which depends on various factors, including their interactions and the number of active sites. At the same time, loading efficiency is defined as the percentage of the drug that is successfully encapsulated[314,315]. The interactions of 5-FU molecules with PAMAM dendrimer in its internal cavities occur mainly through hydrogen bonds due to the presence of oxygen and nitrogen atoms and van der Waals interactions[76,316]. As such, the UV-Vis spectrum of the G2.5COO($Pt(NH_3)_2$)$_{16}$/5-FU and G2.5(COO$Pt(NH_3)_2Cl$)$_{32}$/5-FU were performed (Figure 37a). Except for the G2.5(COO$Pt(NH_3)_2Cl$)$_{32}$/5-FU metallodendrimer, where the absorbance slightly increased, the decrease in the absorbance intensity at 266 nm[317] (the characteristic maximum absorption band of 5-FU) confirmed the encapsulation of 5-FU in the selected compound. Indeed, after the loading of 5-FU, the G2.5(COO$Pt(NH_3)_2Cl$)$_{32}$/5-FU metallodendrimer conjugated with cisplatin in a monodentate form had an absorption more intense than the bidentate G2.5COO($Pt(NH_3)_2$)$_{16}$/5-FU metallodendrimer. This suggests that the type of cisplatin conjugation influences the absorption of the metallodendrimer/5-FU system. Furthermore, suppression of the shoulder was observed in the spectrum of the metallodendrimer, indicating the encapsulation of 5-FU within the dendrimer, although no significant shifting was observed[316,318]. In addition, in fluorescence experiments, no significant changes in the fluorescence intensity were observed for the G2.5COO($Pt(NH_3)_2$)$_{16}$/5-FU, G2.5(COO$Pt(NH_3)_2Cl$)$_{32}$/5-FU and G2.5($COONa$)$_{32}$/5-FU when compared with 5-FU (Figure 37b). However, considerable differences in fluorescence intensity were observed for the G2.5COO($Pt(NH_3)_2$)$_{16}$/5-FU and G2.5($COONa$)$_{32}$/5-FU when compared to the non-encapsulated metallodendrimers (Figure 34 and Figure A11, respectively). Indeed, the fluorescence intensity decreased more than four times, which indicates a possible quenching effect. In fact, a study found in the literature demonstrates that 5-FU induces fluorescence quenching when interacting with human serum albumin[319].

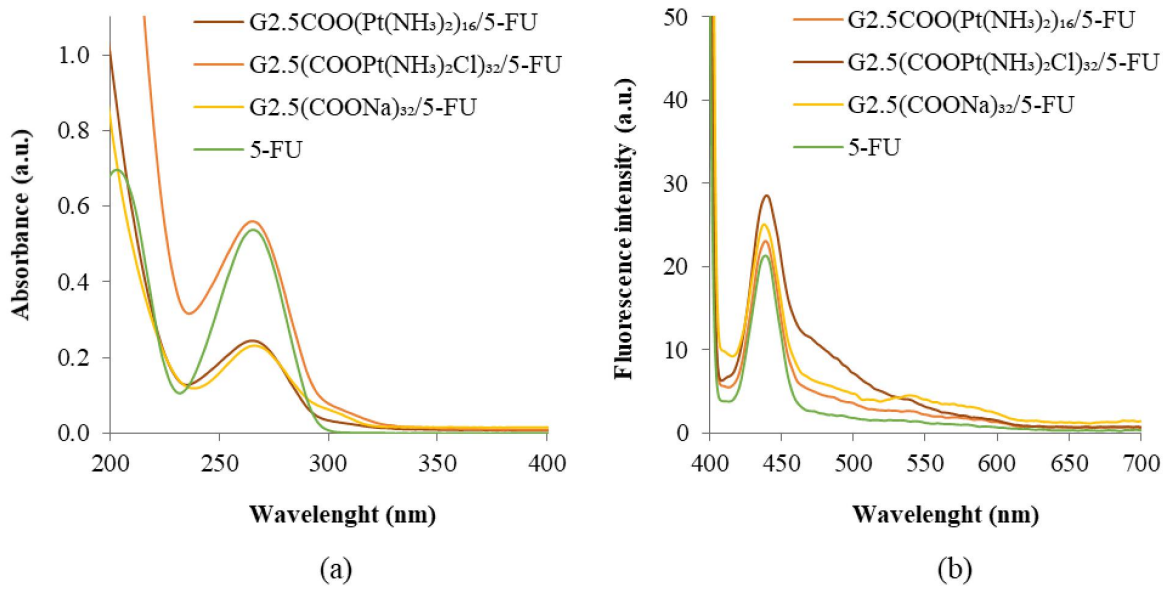

Figure 37: a) UV-vis spectra G2.5COO(Pt(NH$_3$)$_2$)$_{16}$/5-FU, G2.5(COOPt(NH$_3$)$_2$Cl)$_{32}$/5-FU, G2.5(COONa)$_{32}$/5-FU and 5-FU and b) Emission (λ_{ex} = 380 nm) spectra of G2.5COO(Pt(NH$_3$)$_2$)$_{16}$/5-FU, G2.5(COOPt(NH$_3$)$_2$Cl)$_{32}$/5-FU, G2.5(COONa)$_{32}$/5-FU and 5-FU with the same amount of 5-FU (10 µg) in UPW.

As presented in Table 12, the zeta-potential measured for the 5-FU is positive. Nevertheless, in an aqueous solution, the 5-FU charge is dependent on pH. Therefore, at pH values above 8, the 5-FU deprotonates to form anionic structures, while below pH 8 the 5-FU becomes protonated, forming different cationic structures[320]. As the water used in zeta-potential measurements had a pH value around 6.5, and after dissolving the 5-FU the pH of the aqueous solution was 4.9, the 5-FU presented a positive charge. In regards to the 5-FU encapsulation within the metallodendrimers, it can be observed that the zeta-potential for G2.5(COOPt(NH$_3$)$_2$Cl)$_{32}$/5FU and G2.5COO(Pt(NH$_3$)$_2$)$_{16}$/5FU decreased after 5-FU loading, which is in good agreement with the literature[316] while for G2.5(COONa)$_{32}$/5FU the charge slightly increases confirming, in general, the expected encapsulation of the drug.

Table 12: Zeta-potential of 5-FU, G2.5(COOPt$(NH_3)_2Cl)_{32}$/5FU, G2.5COO$(Pt(NH_3)_2)_{16}$/5FU and G2.5$(COONa)_{32}$/5FU (n = 3) in filtered UPW.

Compounds	Zeta-potential (mV)
5-FU	4.48 ± 0.74
G2.5(COOPt$(NH_3)_2Cl)_{32}$	7.99 ± 1.00
G2.5(COOPt$(NH_3)_2Cl)_{32}$/5FU	**-0.52 ± 0.20**
G2.5COO$(Pt(NH_3)_2)_{16}$	2.96 ± 0.72
G2.5COO$(Pt(NH_3)_2)_{16}$/5FU	**-5.29 ± 0.31**
G2.5$(COONa)_{32}$	-47.77 ± 1.46
G2.5$(COONa)_{32}$/5FU	**-41.13 ± 0.49**

The FTIR analysis also supported the encapsulation of 5-FU. The FTIR spectrum of the G2.5(COOPt$(NH_3)_2Cl)_{32}$/5FU and G2.5COO$(Pt(NH_3)_2)_{16}$/5FU systems are shown in Figure C24 (see annex). The characteristics absorption bands of G2.5(COOPt$(NH_3)_2Cl)_{32}$ metallodendrimer, such as the amide I band, C=O stretching at 1647 cm^{-1}, and amide II band N-H bend at 1581 cm^{-1} were shifted to 1644 cm^{-1} and 1586 cm^{-1} in the G2.5(COOPt$(NH_3)_2Cl)_{32}$/5FU, due to the hydrogen bonding between the metallodendrimer and drug[318]. Also, the shift of the 5-FU carbonyl group, from 1658 cm^{-1} to 1644 cm^{-1}, and the C-F stretching band, from 1244 cm^{-1} to 1249 cm^{-1}, indicates the encapsulation of the drug[321]. Similar shifts were also observed in the G2.5COO$(Pt(NH_3)_2)_{16}$/5FU system when compared to the G2.5COO$(Pt(NH_3)_2)_{16}$ metallodendrimer for the amide I and amide II, 1645 cm^{-1} to 1639 cm^{-1} and 1587 cm^{-1} to 1582 cm^{-1}, respectively. The bands of 5-FU shifted from 1658 cm^{-1} to 1639 cm^{-1} for the carbonyl group and the band of the C-F group from 1244 cm^{-1} to 1249 cm^{-1}. A similar result was likewise observed for the G2.5$(COONa)_{32}$/5-FU. A shift of amide I from 1638 cm^{-1} to 1644 cm^{-1} and amide II from 1564 cm^{-1} to 1586 cm^{-1} after the 5-FU encapsulation. The C-F band of 5-FU shifted to 1262 cm^{-1}, as the carbonyl band to 1644 cm^{-1} (see annex Figure C25).

In addition to these characterizations, the G2.5(COOPt$(NH_3)_2Cl)_{32}$/5FU, G2.5COO$(Pt(NH_3)_2)_{16}$/5FU and G2.5$(COONa)_{32}$/5-FU systems were characterized by NMR (^1H, ^{13}C, and ^{19}F). The G2.5(COOPt$(NH_3)_2Cl)_{32}$/5FU (Figure 38), displayed an upfield shift of the protons in the ^1H-NMR spectrum compared to the metallodendrimer G2.5(COOPt$(NH_3)_2Cl)_{32}$. Only the proton signal that is linked to the carbon C-6 in 5-FU is visible, although no significant shift is observed. In the ^{13}C-NMR spectrum (Figure 39), a shift was observed for the carbon signals, being more significant in the carbon signal linked before the amide group from 29.99 to 29.85 ppm and after the amide group from 29.46 to 29.26 ppm. These shifts indicated that the amide groups of the metallodendrimer is the major interaction with 5-FU. The signals related to the carbons C-5 and C-6 of 5-FU also did not shift significantly, and the signals of the carbons C-2, C-4 were not visible in the spectrum. These signals correspond to the carbonyl group, which probably are protonated and bonding

to the metallodendrimer. The fluorine group of 5-FU did not shift (Figure 40) after encapsulation which indicates that this group don´t interact with the metallodendrimer G2.5(COOPt$(NH_3)_2Cl)_{32}$/5-FU.

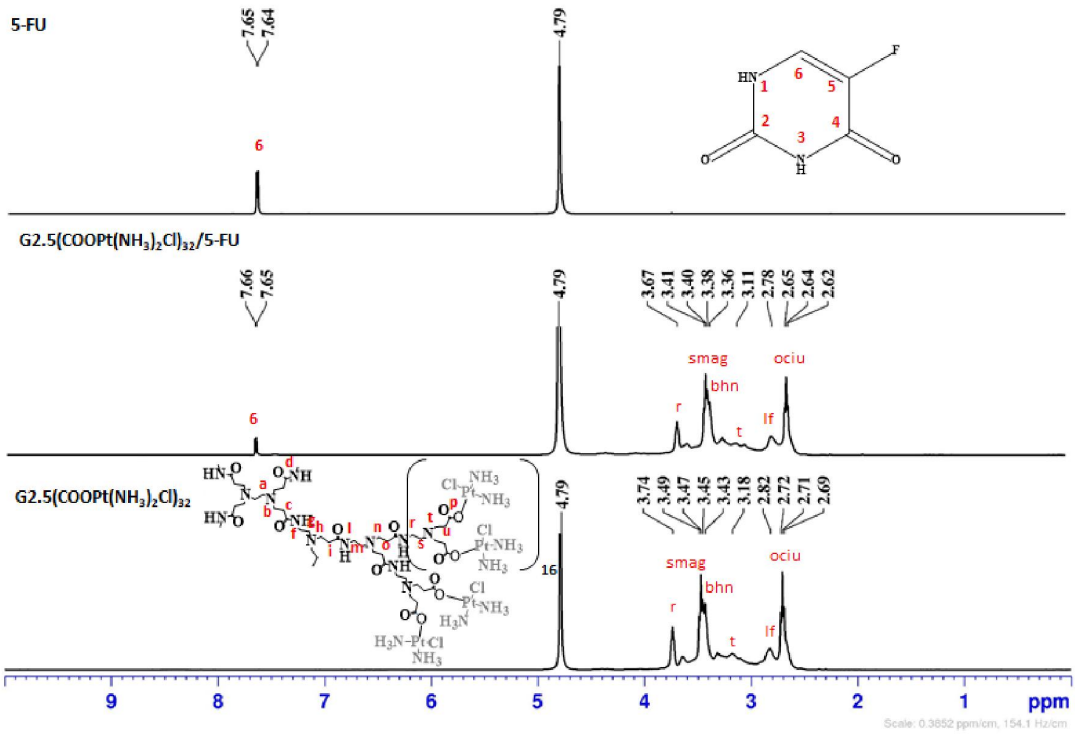

Figure 38: ^{1}H-NMR spectrum of G2.5(COOPt$(NH_3)_2Cl)_{32}$, G2.5(COOPt$(NH_3)_2Cl)_{32}$/5FU and 5-FU in D_2O.

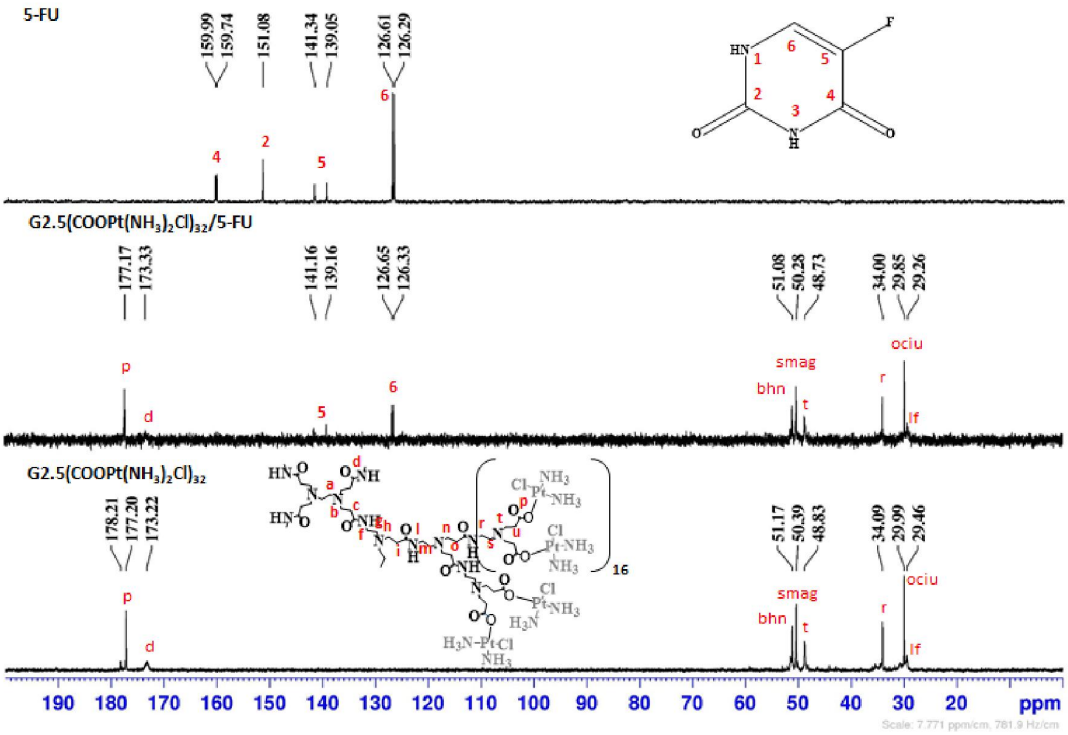

Figure 39: ^{13}C-NMR spectrum of G2.5(COOPt(NH$_3$)$_2$Cl)$_{32}$, G2.5(COOPt(NH$_3$)$_2$Cl)$_{32}$/5FU and 5-FU in D$_2$O.

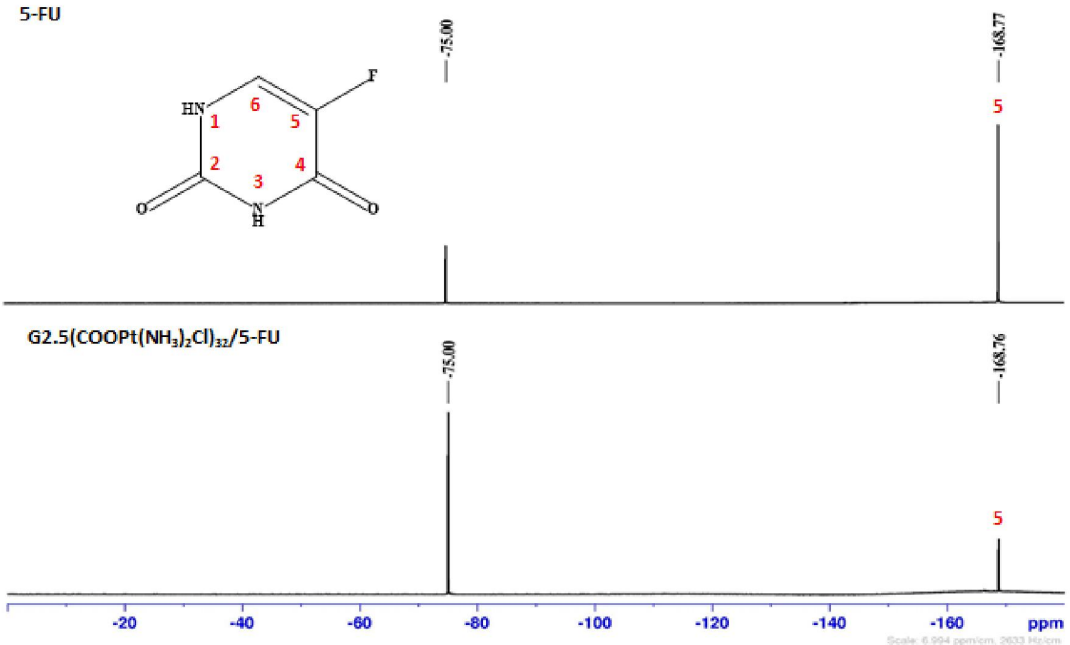

Figure 40: ^{19}F-NMR spectrum of G2.5(COOPt(NH$_3$)$_2$Cl)$_{32}$/5FU and 5-FU in D$_2$O.

In the G2.5COO($Pt(NH_3)_2)_{16}$/5FU system, an upfield shift in the ^{1}H-NMR spectrum was visible (Figure 41). From the ^{13}C-NMR spectrum (Figure 42), the carbon that is bound before the amide carbon shifted from 30.08 to 29.89 ppm, as well the carbons that were bound after the amide group just below the surface shifted from 34.13 to 33.97 ppm. A shift is also observed in the carbons before and after the tertiary amines. As for the signals of the 5-FU, only the peak of the C-6 carbon in the complex was visible. The remaining carbons related to fluorine and the carbonyl group (C = O) are probably protonated and involved in bonding with the complex. In fact, in the ^{19}F-NMR spectrum (Figure 43), a shift of the fluorine group was observed from -168.77 to -168.52 ppm, as well as it was observed the presence of a new signal with lower intensity at -166.23 ppm.

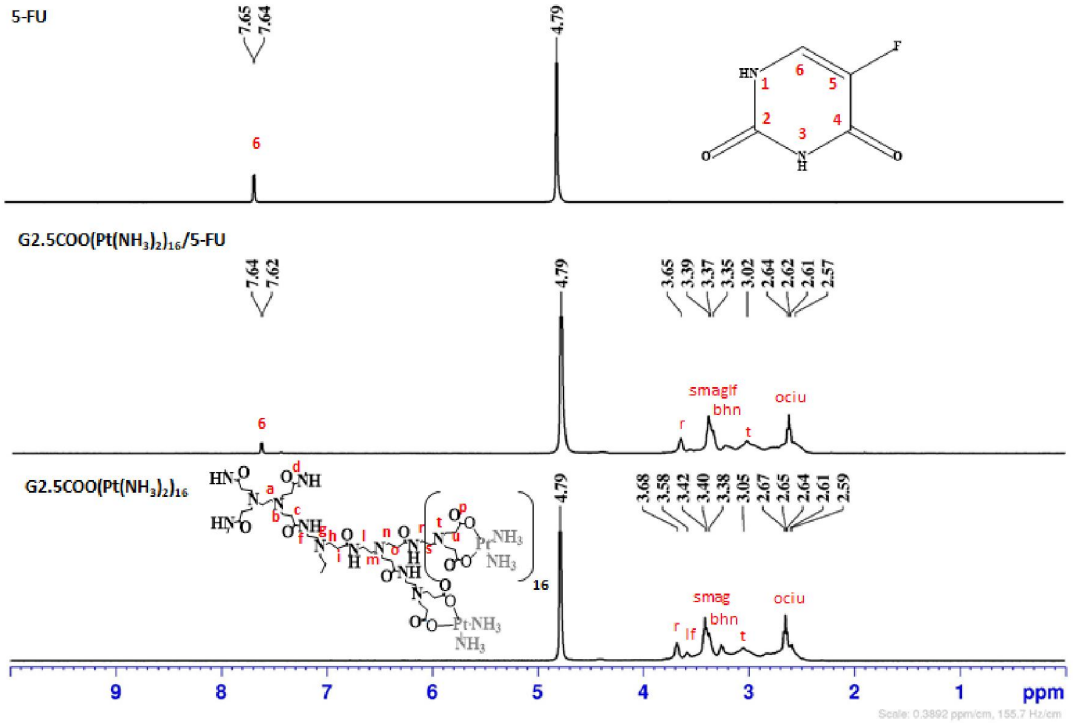

Figure 41: ^{1}H-NMR spectrum of G2.5COO($Pt(NH_3)_2)_{16}$, G2.5COO($Pt(NH_3)_2)_{16}$/5FU and 5-FU in D_2O.

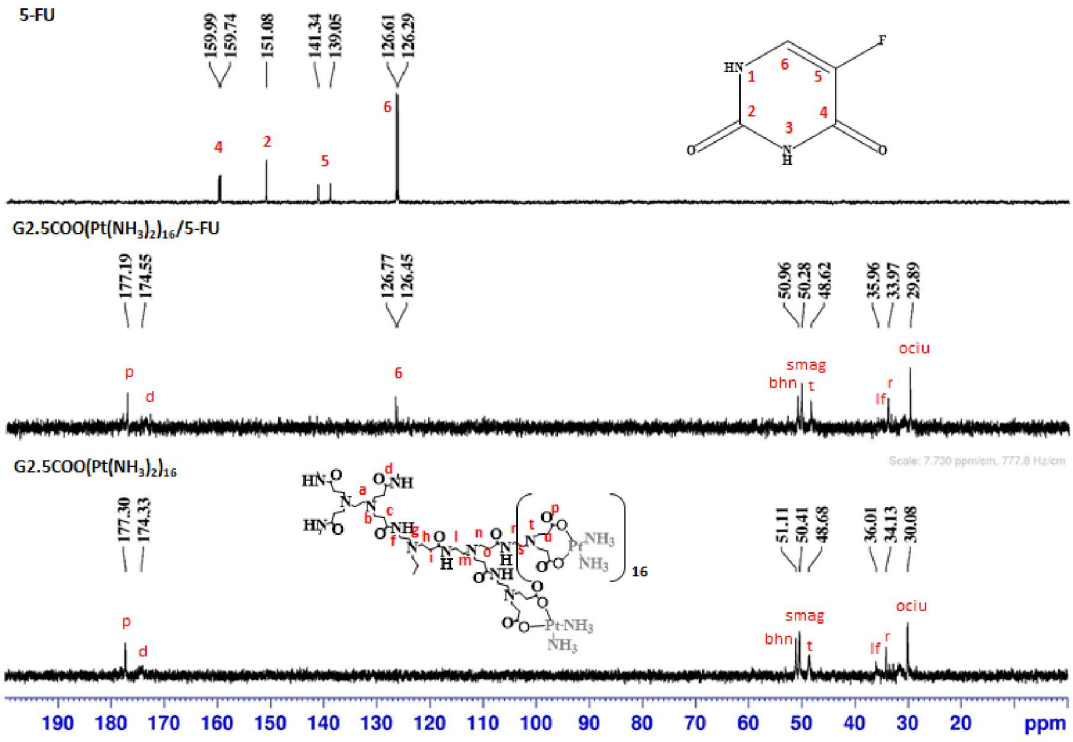

Figure 42: ^{13}C-NMR spectrum of G2.5COO(Pt(NH$_3$)$_2$)$_{16}$, G2.5COO(Pt(NH$_3$)$_2$)$_{16}$/5FU and 5-FU in D$_2$O.

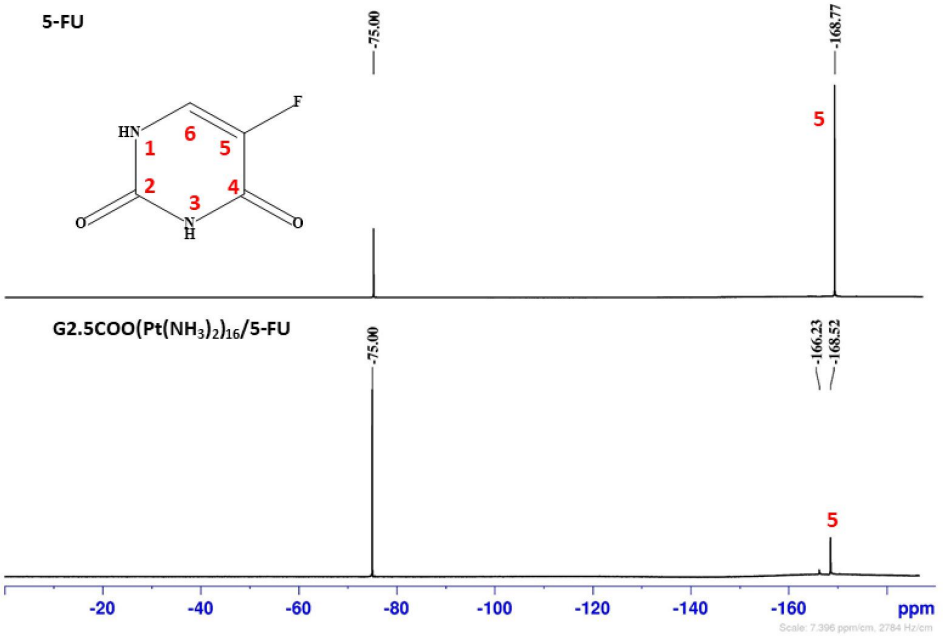

Figure 43: ^{19}F-NMR spectrum of G2.5COO(Pt(NH$_3$)$_2$)$_{16}$/5FU and 5-FU in D$_2$O.

In the ^{1}H-NMR spectrum of G2.5(COONa)$_{32}$/5-FU (Figure 44), a downfield shift of the protons after 5-FU encapsulation was observed, unlike the metallodendrimers. Particularly in the signals of methylene protons present at tertiary amine groups as well as the methylene protons of the amide group. From the ^{13}C-NMR spectrum of G2.5(COONa)$_{32}$/5-FU (Figure 45), a shift in the carbon was observed, being more significant in the carbon signals bonded after to the tertiary amine group from 49.78 to 50.13 ppm in the interior of the complex and in the carbon bonded after the amide group just below the surface from 34.91 to 34.20 ppm. The amide carbons' signals inside the dendrimer shifted from 178.82 to 177.57 ppm and corroborated that the 5-FU is inside the dendrimer and not on its surface. Besides, the carbon signal of the carboxylic end groups did not shift. Also, a shift on the 5-FU carbons was verified, with the carbon signal of C-2 disappearing and the carbon C-4 shifting from 159.74 to 156.78 ppm. These can be explained due to the protonation of the carbonyl groups and their interaction with the dendrimer. Another observation was the downfield shift of the fluorine signal (Figure 46), suggesting its interaction with the dendrimer. In conclusion, the 5-FU was encapsulated inside the metallodendrimers and the PAMAM dendrimer, interacting essentially with the tertiary amine and amide groups of the dendrimer structure and the carbonyl and fluorine groups of 5-FU.

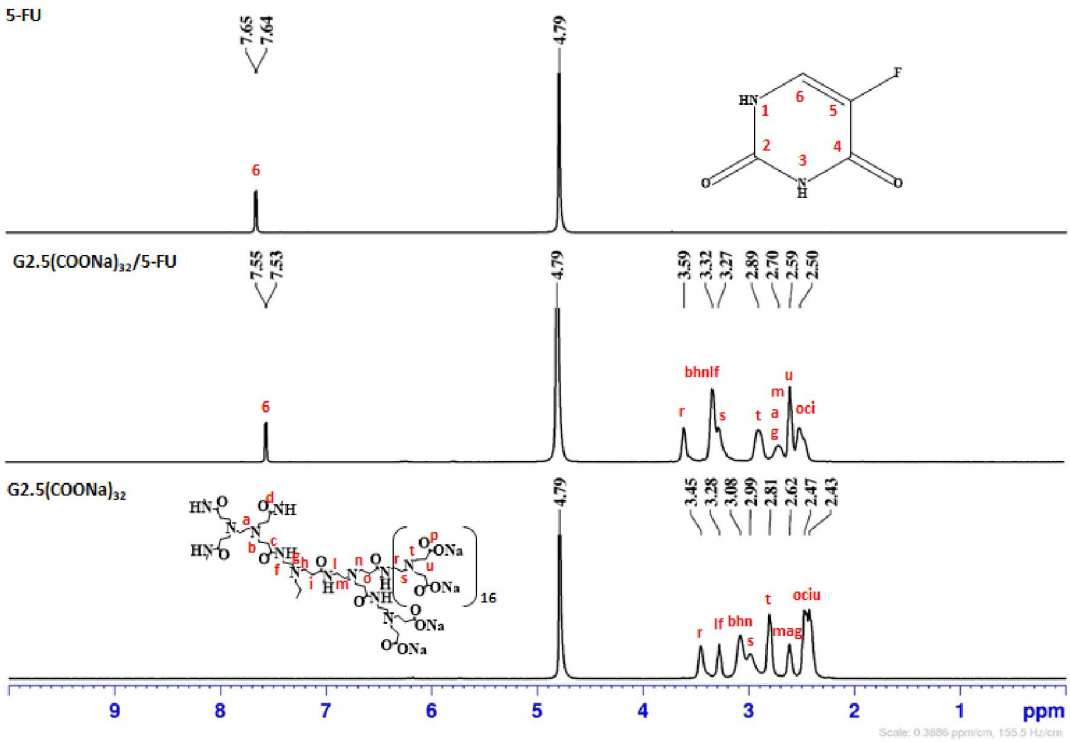

Figure 44: ^{1}H-NMR spectrum of G2.5(COONa)$_{32}$, G2.5(COONa)$_{32}$/5-FU and 5-FU in D_2O.

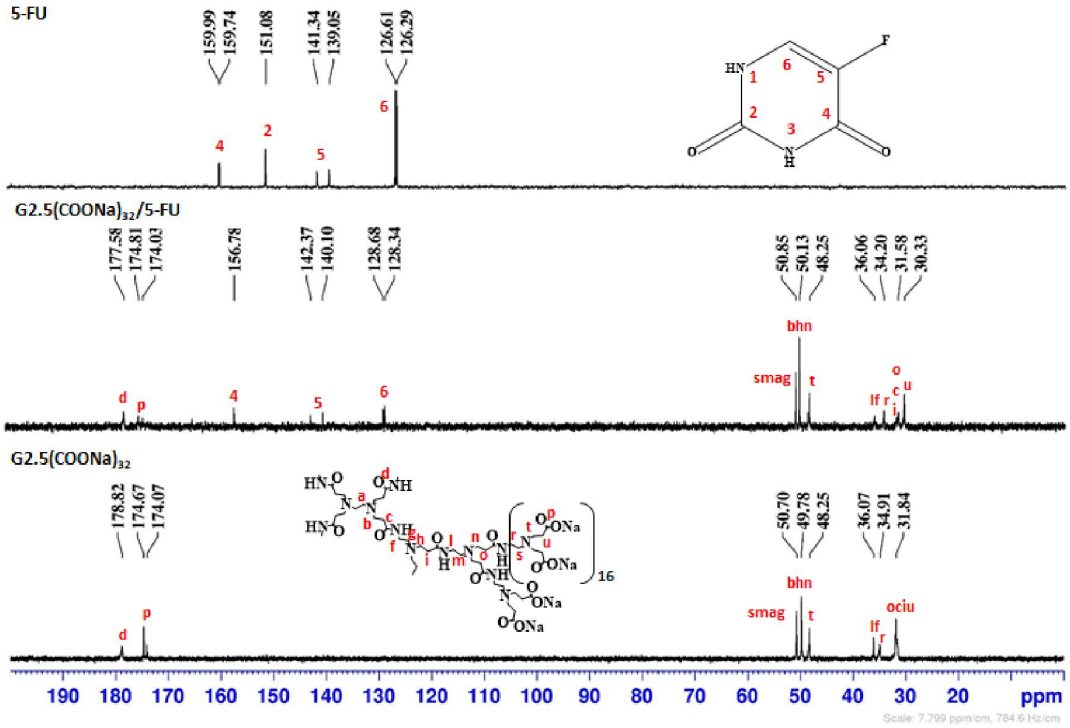

Figure 45: ^{13}C-NMR spectrum of G2.5(COONa)$_{32}$, G2.5(COONa)$_{32}$/5-FU and 5-FU in D_2O.

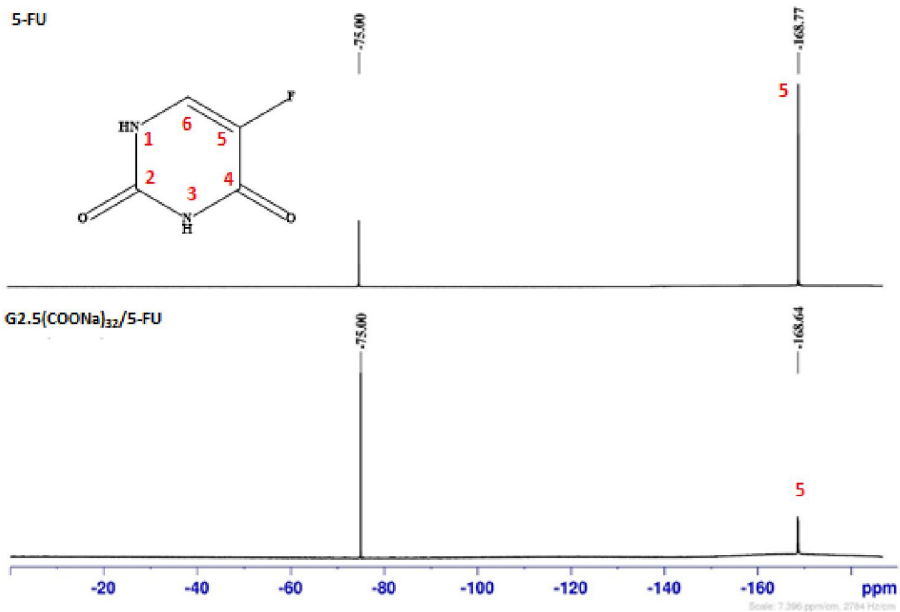

Figure 46: ^{19}F-NMR spectrum of G2.5(COONa)$_{32}$/5-FU and 5-FU in D_2O.

3.3.2. Cytotoxicity of the complex

The A2780CisR and CACO-2 cancer cell lines were used to study the cytotoxicity of the G2.5COO($Pt(NH_3)_2)_{16}$/5-FU and G2.5($COOPt(NH_3)_2Cl)_{32}$/5-FU systems. These two cancer cell lines were selected since 5-FU is used as the first chemotherapeutic line in the treatment of colorectal cancer, although the treatment success is only 15% due to its low bioavailability and causes severe toxic effects[322–324]. The cisplatin-resistant cell line, A2780CisR, was also used because 5-FU is applied to treat ovarian cancer[323]. The results are presented in Figures C20 and C21 (see annex) and IC_{50} values in Table 13. The G2.5COO($Pt(NH_3)_2)_{16}$/5-FU and G2.5($COOPt(NH_3)_2Cl)_{32}$/5-FU systems had an IC_{50} much lower in both cancer cell lines than free 5-FU and G2.5($COONa)_{32}$/5-FU, due to the presence of the metallic fragments that should also be released with time. In the A2780CisR cells, the IC_{50} value increased when comparing the non-loaded with the loaded metallodendrimers. With the CACO-2 cancer cells, the IC_{50} value decreased from >10 μM to 0.61 μM for the G2.5COO($Pt(NH_3)_2)_{16}$ and G2.5COO($Pt(NH_3)_2)_{16}$/5-FU, respectively and from 6.25 μM to 1.07 μM for the G2.5($COOPt(NH_3)_2Cl)_{32}$ and G2.5($COOPt(NH_3)_2Cl)_{32}$/5-FU, respectively. This indicates that cisplatin enhances the effect of 5-FU as a chemotherapeutic agent in this cancer cell line. However, the cytotoxicity of the cisplatin metal dominates over the 5-FU cytotoxicity, as can be observed by the IC_{50} values reported.

Table 13: IC_{50} values of the prepared cisplatin-metallodendrimers toward A2780CisR and CACO-2 cancer cell lines. Results are expressed as mean ± SD three independent experiments performed in triplicate.

	A2780CisR IC_{50} ± SD (μM)	**CACO-2 IC_{50} ± SD (μM)**
5-Fu	> 154	> 154
G2.5($COOPt(NH_3)_2Cl)_{32}$/5-FU*	0.40 ± 0.07	1.07 ± 0.07
G2.5COO($Pt(NH_3)_2)_{16}$/5-FU*	0.39 ± 0.03	0.61 ± 0.2
G2.5($COONa)_{32}$/5-FU*	> 2.5	> 2.5

* For the calculation of the MW, the estimated number of 5-FU molecules carried by the dendrimer was taken into account.

However, comparing both metallodendrimers/5-FU, the G2.5COO($Pt(NH_3)_2)_{16}$/5-FU had a lower IC_{50} than the G2.5($COOPt(NH_3)_2Cl)_{32}$/5-FU, only in the cancer cell line CACO-2, probably because it has one more 5-FU molecule encapsulated in its internal cavity.

On the contrary, although G2.5($COONa)_{32}$/5-FU, has the same encapsulated number of 5-FU molecules, 13, the IC_{50} was higher 2.5 μM, meaning that cisplatin enhances the 5-FU anticancer activity.

Moreover, when compare with the respective metallodendrimer, both G2.5(COOPt$(NH_3)_2Cl)_{32}$/5-FU and G2.5COO$(Pt(NH_3)_2)_{16}$/5-FU had a much lower IC_{50} for CACO-2 cancer cell line, being, respectively, 5 and 14 times more efficient.

3.3.3. Hematoxicity of the complex

The hematoxicity of metallodendrimers encapsulated with 5-FU, the anionic PAMAM dendrimer, and the 5-FU were evaluated using red blood cells from healthy blood. 5-FU, as a free anticancer drug, has hematological toxicity, and in basic medium, undergo degradation. To minimize these undesirable effects, the use of a drug delivery system is a promising strategy[255]. The hematoxicity results (Figure 47) showed that G2.5COO$(Pt(NH_3)_2)_{16}$/5-FU and G2.5(COOPt$(NH_3)_2Cl)_{32}$/5-FU systems at concentrations 0.1 and 1 µg/mL were not hemotoxic, with only 5% of hemolysis. Almost the same result was obtained for the negative control, 4%. The same hemolysis percentage was verified for the 5-FU. However, in the case of the G2.5$(COONa)_{32}$/5-FU system, the hemolysis was slightly higher (*ca.* 7%). Besides, when the 5 µg/mL concentration was used, the hemolysis increased to a value between 24-26% for all the compounds. Nevertheless, the G2.5$(COONa)_{32}$/5-FU continued to be the one with higher hemolysis, even though the difference was irrelative, around 1-2%. In conclusion, the increase observed in the hemolysis % could be attributed to the presence of 5-FU.

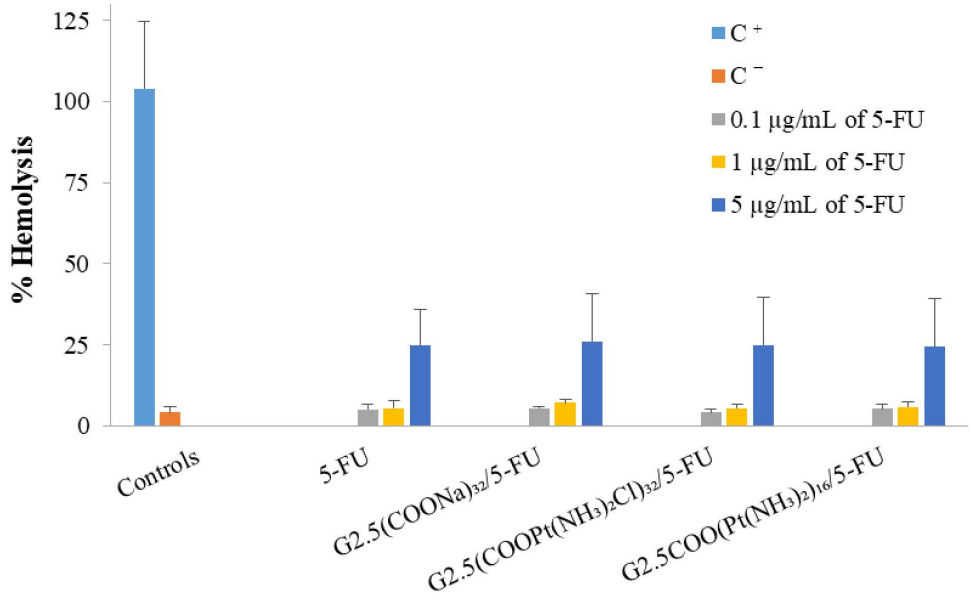

Figure 47: Hematoxicity of the free 5-FU, G2.5$(COONa)_{32}$/5-FU and cisplatin-metallodendrimers/5-FU in healthy human blood. Blood was treated for 3 h with different concentrations (0.1, 1, and 5 µg/mL) of the metallodendrimers and free 5-FU. The positive and negative control are represented by C^+ and C^-, respectively. The results are expressed as mean ± SD of at least three independent experiments performed in triplicate.

3.3.4. *In vitro* drug release

The drug release profile of 5-FU from the metallodendrimers and anionic PAMAM dendrimer was studied in two different pHs media (5 and 7.4) at 37ºC. These pH values were selected because the pH around cancer cells is between pH 5-6.5 and the physiological pH of our body is 7.4. From Figure 48, it can be observed, an initial faster release of 5-FU from G2.5COO($Pt(NH_3)_2$)$_{16}$/5-FU, G2.5(COO$Pt(NH_3)_2Cl)_{32}$/5-FU and G2.5$(COONa)_{32}$/5-FU systems, which started to be a long time sustained-release. However, the G2.5COO($Pt(NH_3)_2$)$_{16}$/5-FU had a lower drug release compared with the other two systems. At pH 7.4 (Figure 48a), the 5-FU achieved 82% cumulative release after 24 h. In G2.5(COO$Pt(NH_3)_2Cl)_{32}$/5-FU and G2.5COO($Pt(NH_3)_2$)$_{16}$/5-FU systems, the drug release reach 53% and 33% respectively in 24 h. The G2.5$(COONa)_{32}$/5-FU system had a cumulative release of 43% at 24 h. Since 5-FU has a short time in circulation blood, where after 1 h of administration 95% is eliminated or metabolized[325], the drug release behavior of the metallodendrimers/5-FU presented a significant advantage because it prolongs the bioavailability of the drug. At pH 5 (Figure 48b), the cumulative release of 5-FU is 80% after 24 h. For the G2.5(COO$Pt(NH_3)_2Cl)_{32}$/5-FU, the 5-FU was released after 24 h in 66%, and for the G2.5COO($Pt(NH_3)_2$)$_{16}$/5-FU, 38%. The G2.5$(COONa)_{32}$/5-FU releases 46% in the same period. As verified in pH 7.4, the G2.5COO($Pt(NH_3)_2$)$_{16}$/5-FU also showed a lower drug release in pH 5 than the other systems. It seems that the way of how cisplatin was conjugated to the dendrimer influences the 5-FU release, which in this case is the bidentate form. On the other hand, at pH 5, 5-FU was released faster from the metallodendrimers than at pH 7.4, making our systems sensitive to the pH. Consequently, the drug is selectively released in a higher amount in the cancer cells, as they have an acid pH microenvironment.

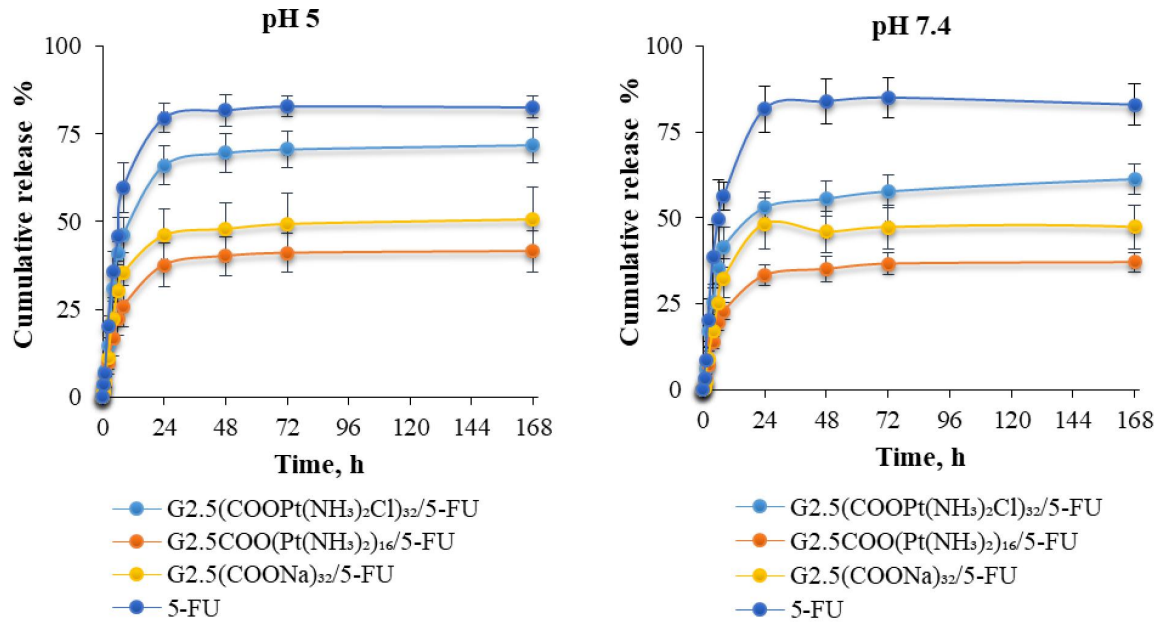

Figure 48: Release profile of 5-FU from cisplatin-metallodendrimers and anionic PAMAM dendrimer at pH 5 and 7.4 at 37ºC.

4. Conclusions

In this work, it was explored the conjugation of the anionic PAMAM dendrimers half-generations (G0.5-G3.5) with cisplatin in mono and bidentate forms. These two forms of cisplatin conjugation were performed to see which one was the most efficient for cisplatin delivery and to overcome the side effects associated with this drug. In addition, the evaluation of the synergetic effect of 5-FU with cisplatin in both conjugated forms was also studied. Our results indicated that the surface of PAMAM dendrimers was conjugated successfully to the cisplatin complex in two different forms, the mono and the bidentate. After their characterization, they were evaluated against four cancer cell lines (A2780Cis, A2780, MCF-7, and CACO-2) and a non-cancer cell line (BJ). The cytotoxicity results show that the monodentate G0.5(COOPt$(NH_3)_2Cl)_8$ and G2.5(COOPt$(NH_3)_2Cl)_{32}$ metallodendrimers were more cytotoxic in all the cancer cell lines tested when compared with the free cisplatin and also with the remaining metallodendrimers. Their compatibility with the blood cells was studied through a hematoxicity assay, and the results demonstrated that the metallodendrimers were not toxic regarding hemolysis at all the concentrations used. For further studies, the G0.5(COOPt$(NH_3)_2Cl)_8$, G2.5COO(Pt$(NH_3)_2)_{16}$, and G2.5(COOPt$(NH_3)_2Cl)_{32}$ were selected to perform DNA binding assays. The DNA binding results showed a strong interaction between the metallodendrimers and CT-DNA compared to free cisplatin. The 5-FU was encapsulated within the G2.5COO(Pt$(NH_3)_2)_{16}$ and G2.5(COOPt$(NH_3)_2Cl)_{32}$ metallodendrimers to investigate if they could increase their anticancer effect using a second drug. Also, their cytotoxicity was evaluated using two cancer cell lines, A2780CisR and CACO-2. In the CACO-2 cancer cells, the G2.5COO(Pt$(NH_3)_2)_{16}$/5-FU and G2.5(COOPt$(NH_3)_2Cl)_{32}$/5-FU systems showed to be 16 and 6 times more efficient, respectively, than the respective metallodendrimers, suggesting that in this case, cisplatin enhances the 5-FU anticancer activity. Nevertheless, the cytotoxicity of cisplatin apparently dominated over the 5-FU cytotoxicity. The *in vitro* release studies demonstrated that the complexes release the 5-FU more slowly than free 5-FU in both pH values. However, when comparing the G2.5COO(Pt$(NH_3)_2)_{16}$/5-FU and G2.5(COOPt$(NH_3)_2Cl)_{32}$/5-FU systems, the G2.5COO(Pt$(NH_3)_2)_{16}$/5-FU retained more the drug, releasing the 5-FU slower than G2.5(COOPt$(NH_3)_2Cl)_{32}$/5-FU and G2.5$(COONa)_{32}$/5-FU. In addition, it was verified that at pH 5, the 5-FU released faster from the metallodendrimers at pH 7.4, suggesting that the systems are sensitive to the pH. In summary, and to confirm the promising results obtained *in vitro*, *in vivo* experiments should be done with the cisplatin-metallodendrimers alone or combined with 5-FU.

CHAPTER III

Improving the efficacy of DACHPt and 5-FU anticancer drugs using anionic PAMAM dendrimer as drug delivery system

This chapter is based on the following publication:

- **Camacho, C**.; Tomás, H.; Rodrigues, J. Use of Half-Generation PAMAM Dendrimers (G0.5–G3.5) with Carboxylate End-Groups to Improve the DACHPtCl_2 and 5-FU Efficacy as Anticancer Drugs". *Molecules,* **2021**, 26, 2924. https://doi.org/10.3390/molecules26102924.

1. Introduction

Nowadays, platinum compounds are the most widely used chemotherapeutic drugs to treat several types of cancer[165]. Amongst the new generations of platinum compounds[187], those with the 1,2-diaminocyclohexane as a carrier ligand has received attention in recent years since it has a different mechanism of action compared to cisplatin[159,169,200,208,215,219]. Oxaliplatin, a third-generation platinum anticancer drug, is a chemotherapeutic drug used in the frontline to treat, particularly, colorectal cancer due to its exceptional activity[159]. The DACHPt unit of oxaliplatin plays an important role in cytotoxicity once the DACH chiral and bulky ligand induces a conformational distortion in DNA different from that caused by cisplatin, forming adducts that are more hydrophobic and distinctively interfere with DNA replication and transcription[204,208,215]. Despite its efficacy in treating colorectal cancer, the associated side effects of oxaliplatin, such as neurotoxicity, can be severe and limit the dose applied to the patient, which may compromise the therapy efficacy[169,326]. Oxalate, the leaving group in oxaliplatin, is a recognized calcium chelator related to its neurotoxicity effects[326]. Furthermore, oxaliplatin is usually used in a combination regimen with other chemotherapeutic drugs to treat stage III of colorectal cancer and their recurrences, as mentioned earlier, such as the chemoprotectant reduced form, usually known as FOLFOX. The combination with 5-FU is often used and showed a synergistic effect in the treatment, even in tumors resistant to oxaliplatin[172,207]. Accordingly, in this work, we explored the possibility of using anionic PAMAM dendrimers as nanocarriers for the DACHPt active fragment. This strategy eliminates the need to use oxalate as a drug component and, in addition, allows us to deliver the 5-FU anticancer drug simultaneously. For this purpose, several half-generation of PAMAM dendrimers (G0.5-G3.5) with carboxylate end-groups were functionalized with 1,2-diaminocyclohexane-platinum(II), DACHPt moiety. The synthesized DACHPt-metallodendrimers were characterized by suitable physicochemical techniques (NMR (^{1}H, ^{13}C, and ^{195}Pt), FTIR, UV-vis and fluorescence spectroscopy, zeta-potential, mass spectrometry (MS) and elemental analysis (EA)). Afterward, their biological behavior was evaluated *in vitro* in different cancer cell lines and the DNA binding and hematoxicity assays were also performed. Then, the metallodendrimer G2.5COO(DACHPt)$_{16}$ was selected to carry 5-FU molecules, and the effect of the combination of the two drugs was likewise evaluated *in vitro* against two cancer cell lines, A2780CisR and CACO-2. As far as we know, this is the first study that integrates the active fragment of oxaliplatin and the 5-FU drug together in a dendrimer scaffold as a new approach for the simultaneous delivery of these two drugs aiming at reducing the side effects, such as neurotoxicity and neuropathy.

2. Materials and Methods

2.1. Materials

All the chemicals were used as received, except the anionic PAMAM dendrimers half-generations G0.5 (19.19 w/w % in methanol), G1.5 (20.03 w/w % in methanol), G2.5 (9.98% w/w in methanol) or G2.5 (3.43 w/w % in water) and G3.5 (10.04 w/w % in methanol) with an ethylenediamine core (purchase from Dendritech®

Inc.) that were purified by dialysis before its use to eliminate further impurities. Trans-1,2-Diaminocyclohexane (99%), and [(1R,2R)-cyclohexane-1,2-diamine](ethanedioato-O,O')platinum(II) (oxaliplatin 99%) were bought from Acros Organics, 5-fluoro-1H-pyrimidine-2,4-dione (5-Fluorouracil, 99%) from TCI chemicals. Deoxyribonucleic acid sodium salt from the calf thymus (CT-DNA) and 4,6-diamino-2-phenyindole dilactate (DAPI) were obtained from Sigma-Aldrich. Dialysis membranes (MWCO 500-1000 Da, 2000 Da, 3500 Da, 6000-8000 Da) were obtained from SpectrumLabs. The remaining reagents were acquired from Acros organics and Fisher scientific. The ultrapure water (UPW) was obtained with a Milli-Q Direct 8 Water Purification System with a resistivity higher than 18.2 MΩ·cm. All the media, solutions, and reagents used for cell culture manipulation were purchased from Life Technologies (Thermo Fischer Scientific) unless otherwise stated. The healthy human blood was supplied by Hospital Dr. Nélio Mendonça, Funchal (SESARAM) under the collaboration between the University of Madeira/Centro de Química da Madeira and the SESARAM hematology service.

2.2. Synthesis

The methodology used for the preparation of trans-(R,R)-1,2- diaminocyclohexanedichloroplatinum(II) ($DACHPtCl_2$) was adapted from the patent USOO8637692B2[327]. The synthesis of DACHPt-metallodendrimers was based on the procedure described by Gordon Kirkpatrick *et al.*[92], Hoang Nguyen *et al.*[286], and Ngoc Tran *et al.*[282]. For the conjugation of the anionic PAMAM dendrimers to the DACHPt moiety, the bidentate form of conjugation was used.

Oxaliplatin was not used, because the leaving group oxalate is a recognized calcium chelator that is associated with neurotoxicity effects[326]. In addition, the purpose of this group is only to increase the solubility of oxaliplatin. So, this strategy eliminates the use of the oxalate group as a drug component, as DACHPt is the active fragment, and at the same time allows us to deliver the 5-FU anticancer drug simultaneously.

2.3.1. Preparation of $DACHPtCl_2$

For the preparation of $DACHPtCl_2$, 0.35g of potassium tetrachloroplatinate (0.84mmol) was dissolved in 17.5 mL of UPW. Then, 0.1g of *trans*-(R,R)-1,2-diaminocyclohexane (0.87mmol; 1.03 eq. mol) in 5.5 mL of UPW was added dropwise to the mixture under stirring. The reaction was left in the dark at r.t. for 7h (Scheme 9). A change in the color of the solution from red to toasted yellow was observed (yellow suspension). The yellow precipitate ($DACHPtCl_2$) was filtrated through a 0.22 µm nylon filter, washed with 40 mL of distilled water, 30 mL of methanol and acetone, and dried in vacuum for 1 h. A yellow powder was obtained with a 59% of yield (0.19 g). ^{1}H-NMR (400 MHz, D_2O) [ppm]: δ= 1.13 (3,3'α-H; m, 2H), 1.26 (2,2' α -H; m, 2H), 1.55 (3,3' β-H; d, 2H), 2.01 (2,2' β-H; d, 2H), 2.40 (1,1'; m, 2H) and 3.39 (NH, broad, 4H). FTIR: ν = 3186 cm^{-1} (N-H amine), 3276 cm^{-1} (N-H amine), 1566 cm^{-1} (N-H amine), 2865 cm^{-1} (C-H), 2935 cm^{-1} (C-H). UV/Vis: 212 nm maximum absorption wavelength. Fluorescence: $\lambda_{em,\,max}$= 429 nm (for λ_{ex} = 380 nm, in UPW).

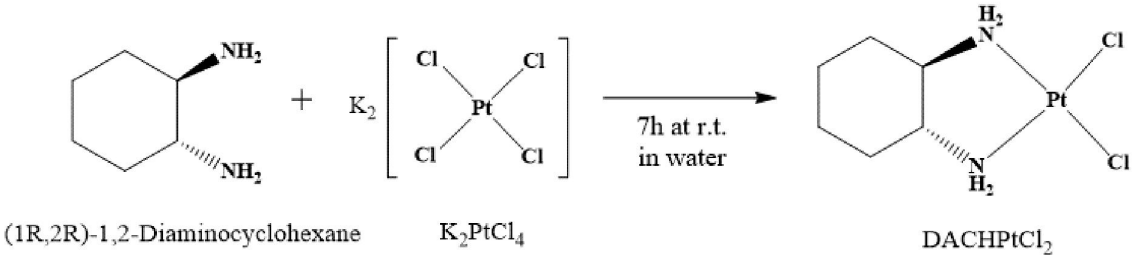

(1R,2R)-1,2-Diaminocyclohexane K_2PtCl_4 $DACHPtCl_2$

Scheme 9: Synthesis of $DACHPtCl_2$ compound, active part of oxaliplatin.

2.3.2. Aquation of $DACHPtCl_2$

In the aquation process, silver nitrate was used to remove both chloride ligands from $DACHPtCl_2$. As such, 0.18 g of $DACHPtCl_2$ (0.48 mmol) was dispersed in 100 mL of UPW. Then, an aqueous solution of 0.16g of $AgNO_3$ (0.9 5mmol, 2 eq. mol) in 6.5 mL of UPW was added dropwise to the mixture under stirring. Then the solution was left under nitrogen atmosphere and stirring for 24 h at r.t. protected from light (Scheme 10). After that time, a "milky-white" precipitate (silver chloride precipitate) was observed, indicating the formation of the $DACHPt(H_2O)_2$ complex. The silver chloride precipitate was removed by centrifugation at 15000 rpm for 1.5 h at 25ºC. The remaining supernatant was filtrate through a 0.22 μm nylon filter and freeze-dried for 3 days. In the end, a sand color powder was obtained with 86% yield (0.14 g). ^{1}H-NMR (400 MHz, D_2O) [ppm]: δ= 1.14 (3,3'α-H; m, 2H), 1.30 (2,2' α -H; m, 2H), 1.56 (3,3' β-H; d, 2H), 2.03 (2,2' β-H; d, 2H) and 2.39 (1,1'; m, 2H). ^{13}C-NMR (100 MHz, D_2O) [ppm]: δ= 23.22 (3,3'), 30.66 (2, 2') and 62.39 (1,1').

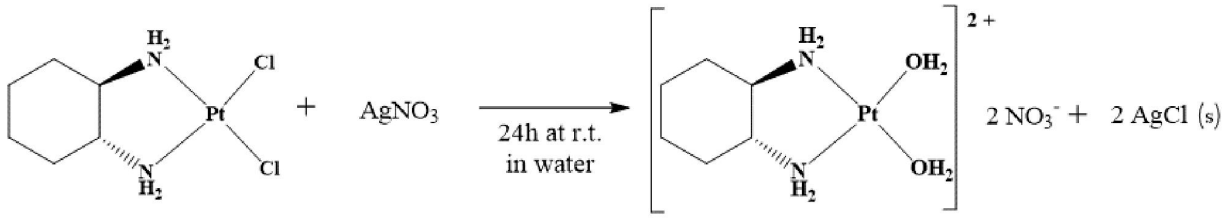

$DACHPtCl_2$ $DACHPt(H_2O)_2$

Scheme 10: Synthesis of $DACHPt(H_2O)_2$ compound.

2.3.3. Preparation of DACHPt Metallodendrimers

2.3.3.1. PAMAM dendrimer Generation 0.5 - G0.5COO(DACHPt)4

The $DACHPt(H_2O)_2$ complex (0.086 g, 0.25 mmol, 4.5 eq. mol) was dispersed in 35 mL of UPW. Then, 0.07g (0.06 mmol) of G0.5COONa PAMAM dendrimer was dissolved in 5 mL of UPW and added dropwise to the mixture under stirring. The mixture was left to react for 24 h at r.t. in dark under nitrogen atmosphere (Scheme 11). The resulting solution was purified using a dialysis membrane (MW 500-1000 Da) for 7 h in distilled water. After freeze-dried, a "greenish-yellow" hygroscopic powder was obtained with 92% yield (0.12 g). ^{1}H-

NMR (400 MHz, D_2O) [ppm]: δ= 1.18 (3,3'α-H; m, 12H), 1.30 (2,2' α -H; m, 8H), 1.61 (3,3' β-H; d, 10H), 2.05 (2,2' β-H; d, 10H), 2.43 (1,1'; m, 10H), 2.63 (H_c + H_i, m, 25H), 2.97 (H_a + H_g, m, 13H), 3.24 (H_b, 8H), 3.31 (H_h, 16H) and 3.61 (H_f, 8H). ^{13}C-NMR (100 MHz, D_2O) [ppm]: δ= 23.32 (3,3'), 30.73 (Cc), 31.01 (2, 2'), 31.40 (C_i), 34.35 (C_f), 48.61 (C_a + C_g), 50.27 (C_h), 50.94 (C_b), 62.02 (1,1') and 177.83 (C_p). ^{195}Pt-NMR (86 MHz, D_2O) [ppm]: δ= - 2313.58. FTIR (KBr pellet): ν = 1584 cm^{-1} (amide II, N-H and C-N), 1618 cm^{-1} (C=O), 2890 cm^{-1} (C-H), 2934 cm^{-1} (C-H), 3231 cm^{-1} (N-H stretch of the amine group of DACHPt) and 3469 cm^{-1} (N-H). Fluorescence: $\lambda_{em,\,max}$= 457 nm (for λ_{ex} = 380 nm, in UPW). TOF-MS (MALDI) calc. *m/z* = 2014.75, found *m/z* = 2014.70 [M+H$^+$] $C_{64}H_{117}N_{16}O_{20}Pt_3^+$. EA (%) calc.: C 36.21, H 5.56, N 10.86, found: C 24.62, H 5.53, N 9.03 (hygroscopic compound).

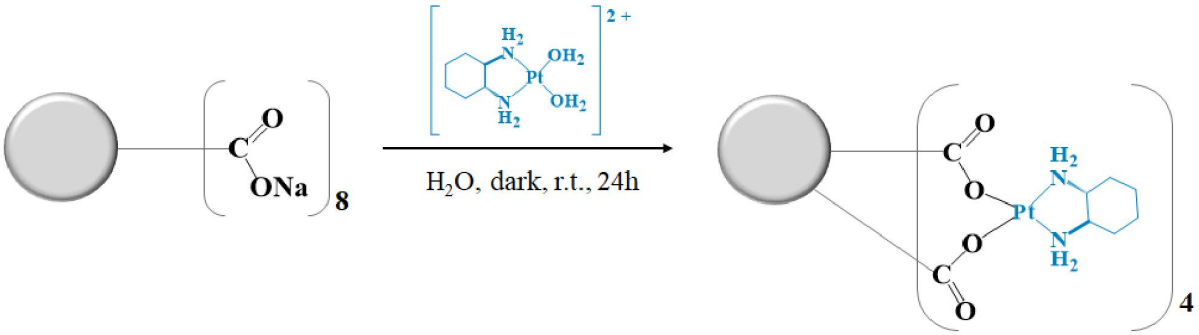

Scheme 11: Representation of the synthesis of the PAMAM dendrimer G0.5 functionalized with DACHPt(H_2O)$_2$ complex, G0.5COO(DACHPt)$_4$.

2.3.3.2. PAMAM dendrimer Generation 1.5 - G1.5COO(DACHPt)$_8$

The DACHPt(H_2O)$_2$ complex (0.05 g, 0.15 mmol, 8.5 eq. mol) was dispersed in 27 mL of UPW. Then, 0.05 g (0.02 mmol) of G1.5COONa PAMAM dendrimer was dissolved in 6 mL of UPW and added dropwise to the solution under stirring. The mixture was left to react for 30 h at r.t. in dark under nitrogen atmosphere (Scheme 12). The resulting solution was then purified using a dialysis membrane (MW 2000 Da) for 6 h in distilled water and freeze-dried. A hygroscopic grey powder was obtained with 77% yield (0.07 g). ^{1}H-NMR (400 MHz, D_2O) [ppm]: δ= 1.20 (3,3'α-H; m, 22H), 1.32 (2,2' α -H; m, 16H), 1.61 (3,3' β-H; d, 18H), 2.07 (2,2' β-H; d, 20H), 2.47 (1,1'; m, 21H), 2.52 (H_c + H_i, m, 38H), 2.62 (H_o, 36H), 2.72 (H_a + H_g, 26H), 2.94 (H_n, 48H) and 3.30 (H_m, 28H), 3.35 (H_b + H_h, m, 44H) and 3.63 (H_f + H_l, m, 16H). ^{13}C-NMR (100 MHz, D_2O) [ppm]: δ= 23.47 (3,3'), 30.38 (C_o), 31.06 (2, 2'), 31.66 (C_i + C_c), 34.24 (C_f + C_l), 48.52 (C_b + C_h), 50.33 (C_n), 50.98 (C_a + C_g + C_m), 61.92 (1,1'), 174.68 (C_d) and 177.55 (C_p). ^{195}Pt-NMR (86 MHz, D_2O) [ppm]: δ= - 2321.68. FTIR: ν = 1582 cm^{-1} (amide II, N-H and C-N), 1639 cm^{-1} (C=O), 2859 cm^{-1} (C-H), 2939 cm^{-1} (C-H), 3278 cm-^{1} (N-H stretch of the amine group of DACHPt) and 3460 cm^{-1} (N-H). Fluorescence: $\lambda_{em,\,max}$= 454 nm (for λ_{ex} = 380 nm, in UPW). TOF-MS (ESI +) calc. *m/z* = 1008.58, found *m/z* = 1008.98 [M+5H$^+$] $C_{158}H_{293}N_{42}O_{44}Pt_8^{5+}$. EA (%) calc.: C 37.65, H 5.76, N 11.67, found: C 32.12, H 5.95, N 10.40 (hygroscopic compound).

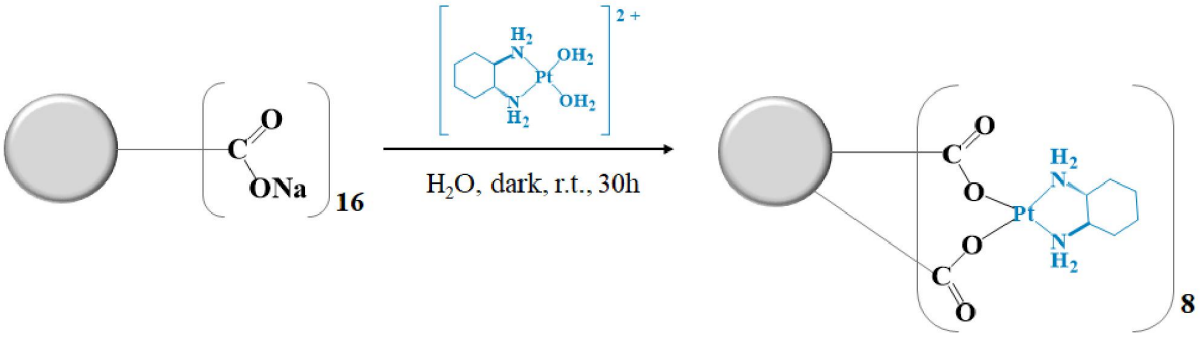

Scheme 12: Representation of the synthesis of the PAMAM dendrimer G1.5 functionalized with DACHPt$(H_2O)_2$ complex, G1.5COO(DACHPt)$_8$.

2.3.3.3. PAMAM dendrimer Generation 2.5 - G2.5COOPt(DACHPt)$_{16}$

The DACHPt$(H_2O)_2$ complex (0.1 g, 0.29 mmol, 16.5 eq. mol) was dispersed in 41 mL of UPW. 0.11 g (0.02 mmol) of G2.5COONa PAMAM dendrimer was dissolved in 10 mL of UPW and added dropwise to the mixture under stirring. The reaction mixture was left to react for 40 h at r.t. in dark under nitrogen atmosphere (Scheme 13). Then, the mixture was purified using a dialysis membrane (MW 3500 Da) for 6 h in distilled water and freeze-dried. A dark brown hygroscopic solid was obtained with 78% yield (0.14 g). ^{1}H-NMR (400 MHz, D_2O) [ppm]: δ= 1.20 (3,3'α-H; m, 23H), 1.34 (2,2' α -H; m, 20H), 1.61 (3,3' β-H; d, 20H), 2.07 (2,2' β-H; d, 20H), 2.38 (1,1'; m, 12H), 2.65 ($H_c + H_i + H_o + H_u$, m, 146H), 3.00 ($H_a + H_m + H_g + H_s$, m, 92H), 3.21 ($H_f + H_l$, 23H), 3.40 ($H_n + H_b + H_h + H_n$, m, 131H) and 3.67 (H_r, 32H). ^{13}C-NMR (100 MHz, D_2O) [ppm]: δ= 23.40 (3,3'), 29.93 (C_u), 30.97 ($C_c + C_i + C_o$), 31.49 (2, 2'), 34.02 (C_r), 48.63 ($C_b + C_f + C_l + C_h + C_n$), 50.31 ($C_t$), 51.02 ($C_a + C_g + C_m + C_s$), 61.84 (1,1'), 173.68 (C_d) and 177.17 (C_p). ^{195}Pt-NMR (86 MHz, D_2O) [ppm]: δ= - 2316.89. FTIR (KBr pellet): ν = 1584 cm^{-1} (amide II, N-H and C-N), 1640 cm^{-1} (C=O), 2855 cm^{-1} (C-H), 2939 cm^{-1} (C-H), 3224 cm^{-1} (N-H stretch of the amine group of DACHPt) and 3410 cm^{-1} (N-H). Fluorescence: $\lambda_{em,\ max}$= 457 nm (for λ_{ex} = 380 nm, in UPW). TOF-MS (ESI +) calc. *m/z* = 1558.71, *m/z* found = 1556.70 $[M+H^+ + 8MeOH]^+$ $C_{342}H_{641}N_{90}O_{100}Pt_{16}^+$. EA (%) calc.: C 38.29, H 5.85, N 12.03, found: C 37.27, H 6.83, N 11.21 (hygroscopic compound).

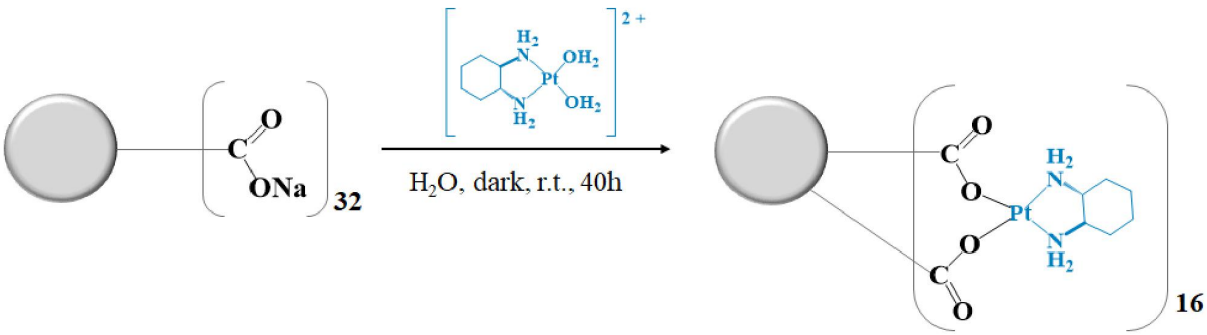

Scheme 13: Representation of the synthesis of the PAMAM dendrimer G2.5 functionalized with DACHPt$(H_2O)_2$ complex, G2.5COO(DACHPt)$_{16}$.

2.3.3.4. PAMAM dendrimer Generation 3.5 - G3.5COO(DACHPt)$_{32}$

The DACHPt(H_2O)$_2$ complex (0.13 g, 0.38 mmol, 32.5 eq. mol) was dispersed in 53mL of UPW. 0.15 g (0.01 mmol) of G3.5COONa PAMAM dendrimer was dissolved in 13 mL UPW and added dropwise to the mixture under stirring. The mixture was left to react for 43 h at r.t. in dark under nitrogen atmosphere (Scheme 14). After, the resulting solution was purified using a dialysis membrane (MW 6000-8000Da) for 6 h in distilled water. After freeze-dried, a dark brown hygroscopic solid was obtained with 60% yield (0.15 g). ^{1}H-NMR (400 MHz, D_2O) [ppm]: δ= 1.19 (3,3'α-H; m, 27H), 1.34 (2,2' α -H; m, 27H), 1.61 (3,3' β-H; d, 26H), 2.07 (2,2' β-H; d, 26H), 2.48 (1,1'; m, 22H), 2.59 (H_c + H_i + H_o + H_u, m, 84H), 2.65 (H_Y, t, 164H), 3.08 (H_a + H_m + H_g + H_s, 162H), 3.26 (H_y, t, 71H), 3.44-3.38 (H_z + H_n + H_b + H_h + H_n, m, 262H), 3.59 (H_l + H_f + H_r, t, 40H) and 3.69 (H_x, 64H). ^{13}C-NMR (100 MHz, D_2O) [ppm]: δ= 23.40 (3,3'), 29.88 (C_Y), 31.56 (C_o + C_i + C_c + C_u), 32.77 (2,2'), 34.00 (C_x), 35.39 (C_l + C_f + C_r), 48.65 (Ca + Cg + Cm+ Cs + Cy), 50.29 (Cz), 51.07 (Cb + Ch + Cn + Ct), 60.09 (1,1'), 173.21 (C_d) and 177.11 (C_p). ^{195}Pt-NMR (86 MHz, D_2O) [ppm]: δ= - 2312.63. FTIR (KBr pellet): ν = 1588 cm^{-1} (amide II, N-H and C-N), 1638 cm^{-1} (C=O), 2855 cm^{-1} (C-H), 2937 cm^{-1} (C-H), 3244 cm^{-1} (N-H stretch of the amine group of DACHPt) and 3417 cm^{-1} (N-H). Fluorescence: $\lambda_{em,\ max}$= 452 nm (for λ_{ex} = 380 nm, in UPW). TOF-MS (MALDI) calc. *m/z* = 388.9, *m/z* found = 388.2 [M] $C_{632}H_{1140}N_{168}O_{188}Pt_{23}$. EA (%) calc.: C 38.59, H 5.89, N 12.20, found: C 41.33, H 7.17, N 12.78 (hygroscopic compound).

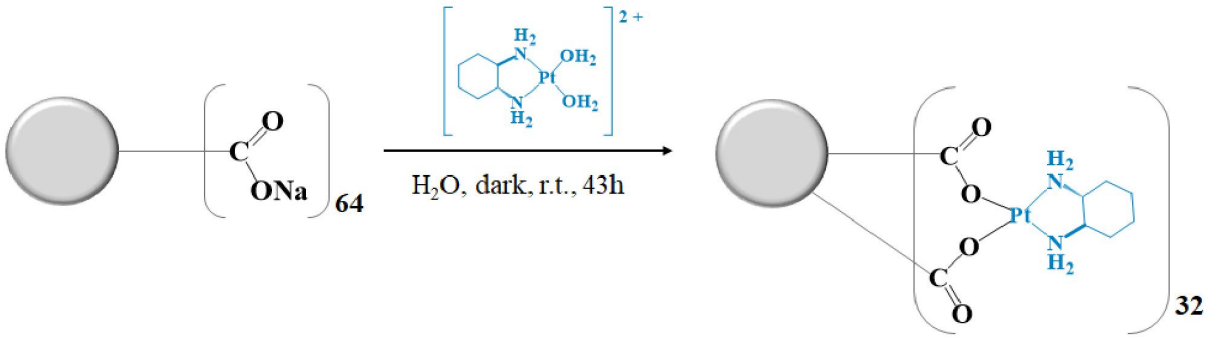

Scheme 14: Representation of the synthesis of the PAMAM dendrimer G3.5 functionalized with DACHPt(H_2O)$_2$ complex, G3.5COO(DACHPt)$_{32}$.

Figure 49 illustrates the prepared dendrimers conjugated with DACHPt in bidentate forrm.

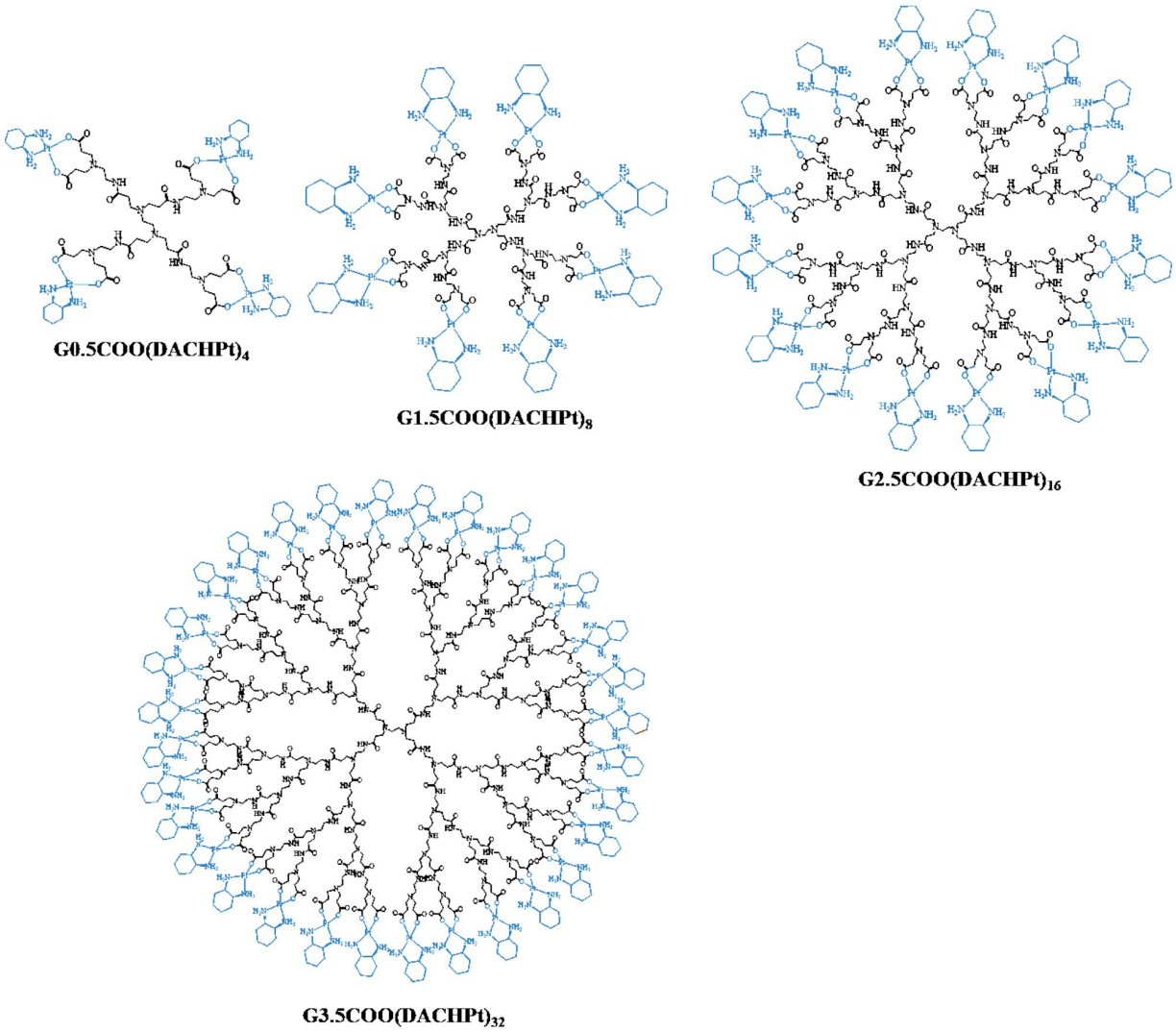

Figure 49: Metallodendrimers functionalized with DACHPt (G0.5-G3.5).

2.4. Biological studies

2.4.1. Cell culture and cytotoxicity evaluation

Several human cell lines were used in the cytotoxicity evaluation studies, namely: ovarian cancer cells (A2780), cisplatin-resistant ovarian cancer cells (A2780CisR), breast cancer cells (MCF-7), colorectal adenocarcinoma cells (CACO-2), and fibroblast cells (BJ, a non-cancer cell line). All cell lines were cultured in 96-well plates at a seeding density of 1 x 10^4 cells per well with a specific culture medium supplemented with 10% (v/v) fetal bovine serum (FBS) and 1% (v/v) antibiotic-antimycotic solution (AA, 100× solution) at 37ºC, in a humidified atmosphere and 5% CO_2. Specific cell culture media were used for each cell line as follows: the A2780 and A2780CisR cell lines were cultured in RPMI 1640 medium supplemented with L-glutamine (2 mM) and 1% (w/v) of cisplatin (100 mM) in the case of A2780CisR cells (cisplatin was only used in the subculturing process before the cytotoxicity assays); the MCF-7 cell line was cultured in RPMI

1640 medium supplemented with 1mM sodium pyruvate, 1% (v/v) nonessential amino acids (NEAA, 100× solution), and human insulin 3.3 μg/mL; the CACO-2 cell line was cultured in MEM medium supplemented with 1% (v/v) NEAA; the BJ cell line was cultured in D-MEM medium. After 24 h in culture, cells were incubated with the compounds under testing prepared in nuclease-free water. In all cases, 100 μL of the compound solution was used for a total volume of 200 μL in the well. The metallodendrimers cytotoxicity was evaluated using all the mentioned cell lines at the concentrations of 0.01, 0.03, 0.1, 0.5, 1, 2.5, 5, and 10 μM. Pristine anionic PAMAM dendrimers (G0.5-3.5) were used as controls. The cytotoxicity of the metallodendrimer G2.5COO(DACHPt)$_{16}$/5-FU was evaluated using A2780CisR and CACO-2 cells at the concentrations of 0.01, 0.2, 1, 5, 10 and 20 μg/mL, and G2.5(COONa)$_{32}$/5-FU and free 5-FU were used as controls. After 72 h of incubation with the compounds under testing, the culture medium was replaced by fresh medium containing 10% (v/v) of a MTT (3-(4,5-dimethylthiazol-2-yl)-2,5-diphenyltetrazolium bromide) solution (0.5 mg/mL). After 3 h of incubation, the culture medium was aspirated, and the formed formazan crystals were dissolved in 100 μL DMSO. Absorbance intensity was measured at 550 nm in a microplate reader. Three independent experiments with three replicas each were carried out. The concentration that inhibited 50% of the cellular metabolic activity (IC_{50}) was determined by linear interpolation between the two experimental points closer to the point correspondent to 50% of the control's cellular metabolic activity. Results are presented as the mean ± standard deviation (SD).

2.4.2. Hematoxicity evaluation

Human blood from healthy donors was collected in tubes containing EDTA and used to evaluate the compounds' hemotoxicity under testing towards red blood cells by the cyanmethemoglobin method[287]. The total hemoglobin concentration in the original blood was determined starting from a 250-fold dilution of blood in cyanmethemoglobin reagent (the C reagent was prepared in an amber bottle with 50 mg of potassium ferricyanide, 12.5 mg of potassium cyanide, and 35 mg of potassium dihydrogen phosphate in 250 mL of distilled water with 250 μL of Triton-X; its pH was adjusted to 7.4). A standard curve for hemoglobin was then prepared with hemoglobin from bovine blood (see annex Figure B1). Briefly, a stock solution of the protein (1.5 mg/mL) was first prepared in C reagent, from which serial dilutions were performed to obtain standards of known concentration (in the range 0.20 to 1.4 mg/mL). Absorbance was then measured at 550 nm, and the C reagent was used as blank. The total hemoglobin concentration was determined using this standard curve, taking into consideration the initial dilution. For hemotoxicity evaluation of the compounds under testing, a 10% (v/v) blood solution was prepared in PBS (Mg^{2+}/Ca^{2+} free). Then, 10 μL of this blood solution was added to several microtubes containing 70 μL of compound solution (at the concentrations 0.1, 1, and 5 μM); for controls, microtubes with 70 μL of distilled water (positive control) and 70 μL of PBS (negative control) were also prepared. After, the microtubes were incubated at 37 °C for 3 h and subsequently centrifuged at 3800 rpm for 10 min. In the end, 40 μL of each supernatant were transferred to 96-well plates, 160 μL of C reagent was added, and absorbance was measured at 550 nm. The concentration of hemoglobin

in the supernatants was then determined using the same standard curve and considering the performed dilutions. The results are presented as a percentage of hemolysis (mean of three independent assays) ± SD.

2.4.3. DNA binding studies by UV-vis spectroscopy

Absorption spectra were performed at room temperature for varying concentrations of CT-DNA (0, 6.25, 12.5, 18.75, 25, 31.25, 37.5, 43.75 to 50 μM) and constant concentrations of G2.5COOPt(DACHPt)$_{16}$ metallodendrimer (2 μM), DACHPtCl$_2$ (9 μM), or oxaliplatin (9 μM). The metallodendrimer, DACHPtCl$_2$, and oxaliplatin solutions were prepared in UPW and then diluted in a 5 mM Tris-HCl, 50 mM NaCl pH 7.4 buffer. The stock solutions of DNA were directly prepared in this buffer. DNA purity was assessed by UV-Vis spectroscopy using the absorbance values ratio at 260 nm and 280 nm (it should be between 1.8-1.9 to make sure it is sufficiently protein-free) (see annex Figure A17). The obtained ratio was 1.9, indicating that the DNA was pure. The compounds and the CT-DNA were incubated at r.t. for 5 min. The absorbance was measured in a PerkinElmer UV-vis spectrometer Lambda equipment, using the buffer as blank. Two independent experiments were carried out for the metallodendrimers, DACHPtCl$_2$, and oxaliplatin. The intrinsic binding constant, K_b, of the compounds with DNA, was determined using the Benesi-Hildebrand equation[288]. Binding constant values were then obtained from the ratio of the y-intercept to the slope in the plots $A_0/A\text{-}A_0$ vs. 1/[DNA]. Additionally, the Gibbs free energy (ΔG) associated with the process of DNA binding was calculated using the Benesi-Hildebrand equation[288].

2.5. Studies with 5-Fluorouracil loaded dendrimers

2.5.1. Loading of 5-FU

G2.5COO(DACHPt)$_{16}$ metallodendrimers were loaded with 5-FU. For that purpose, 25 mg (0.002 mmol) of G2.5COO(DACHPt)$_{16}$ was dissolved in 2 mL of UPW, and 4.7 mg of 5-FU (15 eq. mol, 0.04 mmol) was added to the solution. As a control, the G2.5(COONa)$_{32}$ dendrimer (25 mg, 0.004 mmol, 2 mL) was also loaded with 5-FU (7.8 mg, 0.06 mmol) in similar conditions. Then, the G2.5COO(DACHPt)$_{16}$/5-FU and the G2.5(COONa)$_{32}$/5-FU solutions were dialyzed in 50 mL of distilled water using a dialysis membrane in the MW range of 100-500 Da for 20 min to remove the unloaded 5-FU. Later, the G2.5COO(DACHPt)$_{16}$/5-FU and G2.5(COONa)$_{32}$/5-FU solutions and the solution outside the dialysis membrane were lyophilized. The free drug was dissolved in 50 or 60 mL of UPW, and its absorbance was measured at 266nm in a PerkinElmer UV-Vis spectrometer Lambda equipment to determine the amount of drug-loaded into both dendrimer types indirectly. For the quantification of 5-FU in solution, a standard calibration curve was first established using standards of known concentration of 5-FU in water (see annex Figure B2). The loading capacity (LC%) and the loading efficiency (LE%) were calculated through the formulas described in *Chapter II section 2.4.1. Loading of 5-FU*[289]. The results are expressed as mean ± SD of three independent experiments.

2.5.2. *In vitro* drug release of 5-FU

The release of 5-FU was made in PBS in acid conditions (pH adjusted to 5) and at physiologic pH (pH adjusted to 7.4), at 37ºC. For this aim, 100 µg of 5-FU loaded in G2.5COO(DACHPt)$_{16}$ and to G2.5(COONa)$_{32}$ were weighted and dissolved in 300 µL of water. The solutions were placed in SLIDE-A-LYZER™ mini dialysis devices with a MW cutoff of 2000 Da (0.1mL, Thermo Fisher Scientific) and dialyzed in 10 mL of PBS, in separate tubes, at each pH value. At different time intervals, 1 mL of the dialyzed was taken out from each tube and replaced with an equivalent volume of fresh PBS. The release profile of 5-FU was then determined by UV-Vis spectroscopy. Standard calibration curves were established for each PBS pH value (see annex Figures B3 and B4). Absorbance was measured at 266 nm with a PerkinElmer UV-vis spectrometer Lambda.

3. Results and discussion

3.1. Synthesis and characterization of DACHPt metallodendrimers

For the preparation of DACHPt-metallodendrimers, the trans-(R,R)1,2-diaminocyclohexanedichloroplatinum(II), DACHPtCl$_2$, was first synthesized with 59% yield and characterized by different techniques, such as NMR, FTIR, UV-visible, and fluorescence spectroscopy. The characteristics signals of DACHPtCl$_2$ corresponding to the cyclohexyl and amine protons[210,328,329] can be seen in the ^{1}H-NMR spectrum (Figure 50). The FTIR spectrum (see annex Figure D1) also presents the characteristics bands of the DACHPtCl$_2$ compound, namely the symmetrical and asymmetrical N-H stretch of the primary amine group at 3186 cm^{-1} and 3276 cm^{-1}, respectively and the N-H bending vibration band of the primary amine group at 1566 cm^{-1}. Bands corresponding to the C-H stretch were also observed at 2865 cm^{-1} and 2935cm^{-1} [330].

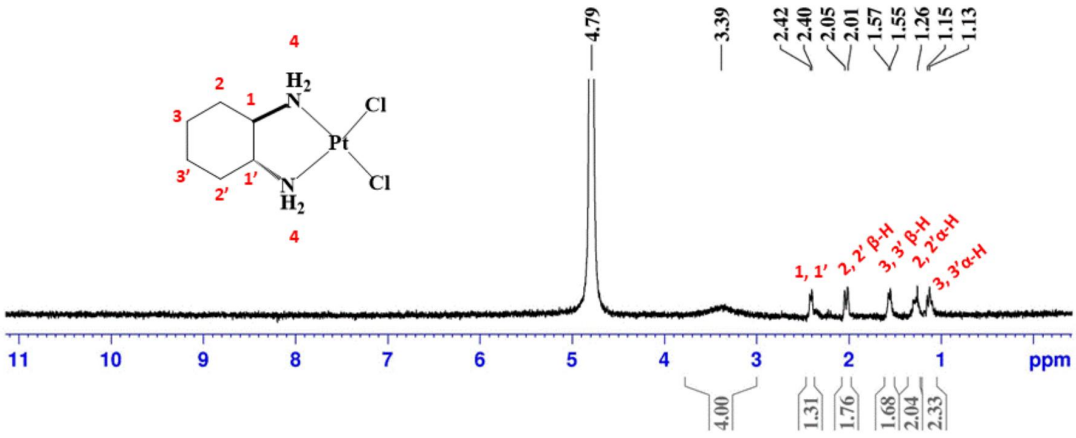

Figure 50: ^{1}H-NMR spectrum of DACHPtCl$_2$ performed in D$_2$O.

In the UV-vis spectra (Figure 51a), a shoulder with a maximum in the UV region (212 nm) appears, due, probably, to a mixture with the characteristic charge transfer transitions of the halide platinum (II) complexes with shifted d-d transitions[331]. The fluorescence emission spectrum (Figure 51b) shows a band at around 429 nm due to the cyclohexyl group of $DACHPtCl_2$.

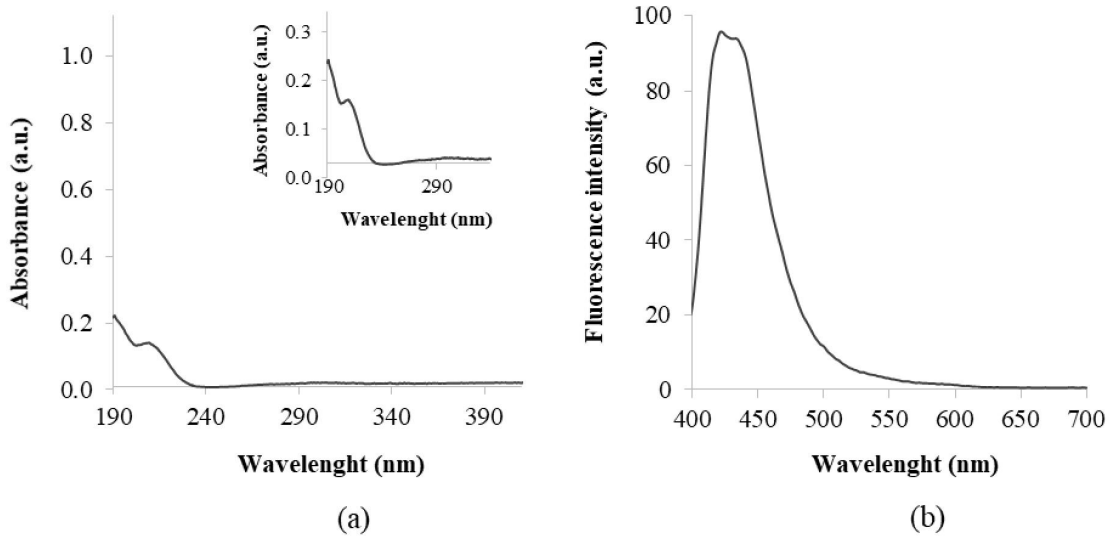

Figure 51: a) Absorption spectra of $DACHPtCl_2$ recorded at a concentration of 40 μM of in UPW and b) Emission (λ_{ex} = 380 nm) spectra of $DACHPtCl_2$ recorded at a concentration of 500 μM in UPW.

Afterward, to attach the DACHPt fragment to the PAMAM dendrimers, the aquation of $DACHPtCl_2$ was necessary to form reversible coordinated bonds with the carboxylate end groups of PAMAM dendrimer half-generations. The aquation of $DACHPtCl_2$ is also important to guarantee the removal of the two chlorines and assure the conjugation of the DACHPt moiety to the anionic PAMAM dendrimer in the bidentate form. Indeed, the conjugation of the DACHPt fragment to the dendrimer involving two bonds (bidentate form) should delay drug release before the target is achieved, thus decreasing the side effects. As so, bis-aquated $DACHPtCl_2$ was synthesized through a reaction of $DACHPtCl_2$ with silver nitrate, an abstractor of chloride ligands, with 86% yield. The product was characterized by ^{1}H and ^{13}C-NMR (see annex Figures D2 and D3).

After, four half-generations of anionic PAMAM dendrimers (G0.5-G3.5) were successfully coordinated to the bis-aquated $DACHPtCl_2$ in a bidentate form. The prepared metallodendrimers were obtained with a good yield ($G0.5COO(DACHPt)_4$: 92%, $G1.5COO(DACHPt)_8$: 77%, $G2.5COO(DACHPt)_{16}$: 78% and G3.5COO(DACHPt)32: 60%). The products were fully characterized by different techniques that included NMR (^{1}H, ^{13}C, and ^{195}Pt-NMR), FTIR, UV-Vis, and fluorescence spectroscopy zeta-potential, MS and EA, although the prepared metallodendrimers are hygroscopic. In the ^{1}H-NMR experiments, the signal of deuterated water (D_2O) was used as an internal reference, whereas potassium tetrachloroplatinate (II) was used as an external reference in the ^{195}Pt-NMR experiments. Figure 52 shows the expected ^{1}H-NMR spectrum of

G0.5COO(DACHPt)$_4$, with the characteristics signals of the anionic PAMAM dendrimer structure between 2.62 and 3.61 ppm and the signals of the cyclohexyl group of DACHPt fragment between 2.43 and 1.18 ppm.

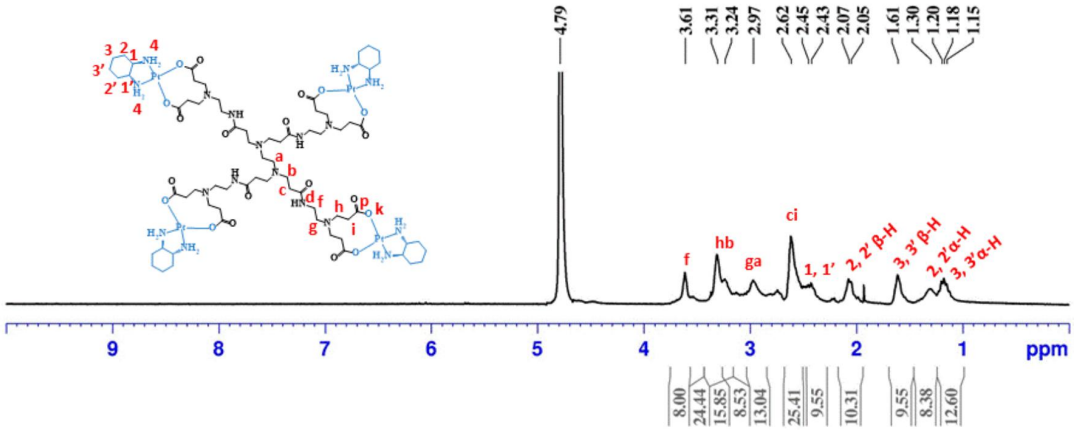

Figure 52: ^{1}H-NMR spectrum of G0.5COO(DACHPt)$_4$ performed in D_2O.

The ^{13}C-NMR spectrum (Figure 53) also presents the characteristic signals of the anionic dendrimer's structure and those corresponding to the cyclohexyl of the DACHPt moiety. The signals at 30.73, 31.40, 34.35, 48.61, 50.27, and 50.94 ppm are from the anionic PAMAM dendrimer scaffold. The signals observed at 23.32, 31.01, and 62.02 ppm are from the cyclohexyl group of DACHPt. Compared to pristine half-generation anionic PAMAM dendrimers, a downfield shift in the carboxylate group's signal (174.69 to 177.83 ppm) indicates metal complex coordination[332].

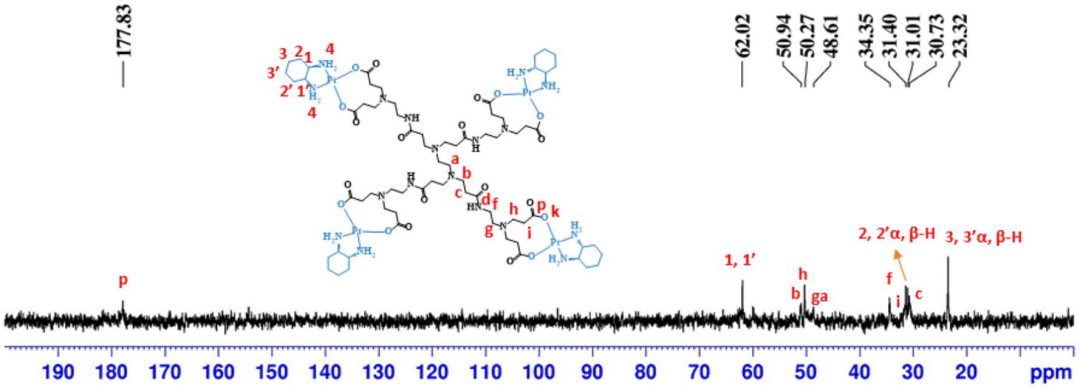

Figure 53: ^{13}C-NMR spectrum of G0.5COO(DACHPt)$_4$ performed in D_2O.

Furthermore, the signal at -2314 ppm in the ^{195}Pt-NMR spectrum (Figure 54) has low intensity and high noise due to the sensitivity of the NMR probe for the ^{195}Pt-nucleus. They suggested that the PAMAM dendrimer was

conjugated to the DACHPt moiety in a bidentate form[291,333]. Similar results were observed for the other dendrimer generations (G1.5-G3.5).

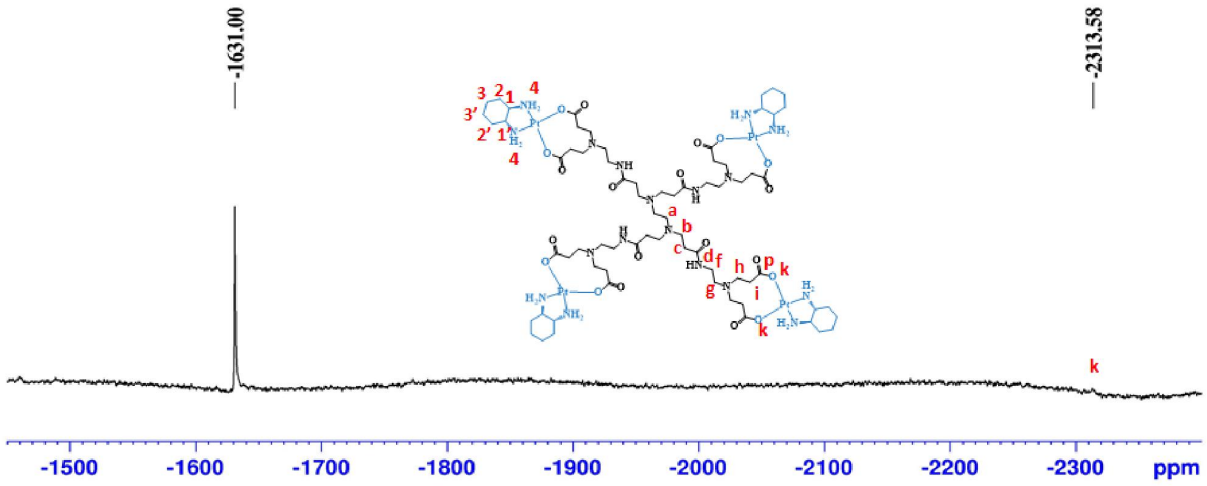

Figure 54: ^{195}Pt-NMR spectrum of G0.5COO(DACHPt)$_4$ performed in D_2O, with K_2PtCl_4 as an external reference (-1631 ppm).

The G1.5COO(DACHPt)$_8$ metallodendrimer presents in the NMR spectrum the expected signals of its structure. In the ^{1}H-NMR spectrum (Figure 55) the signals between 2.47 and 3.77 ppm correspond to the anionic G1.5-PAMAM dendrimer scaffold and the signals between 1.20 and 2.47 ppm to the cyclohexyl group of DACHPt moiety. These last signals are overlapped with the methylene protons of the amide group of PAMAM dendrimer.

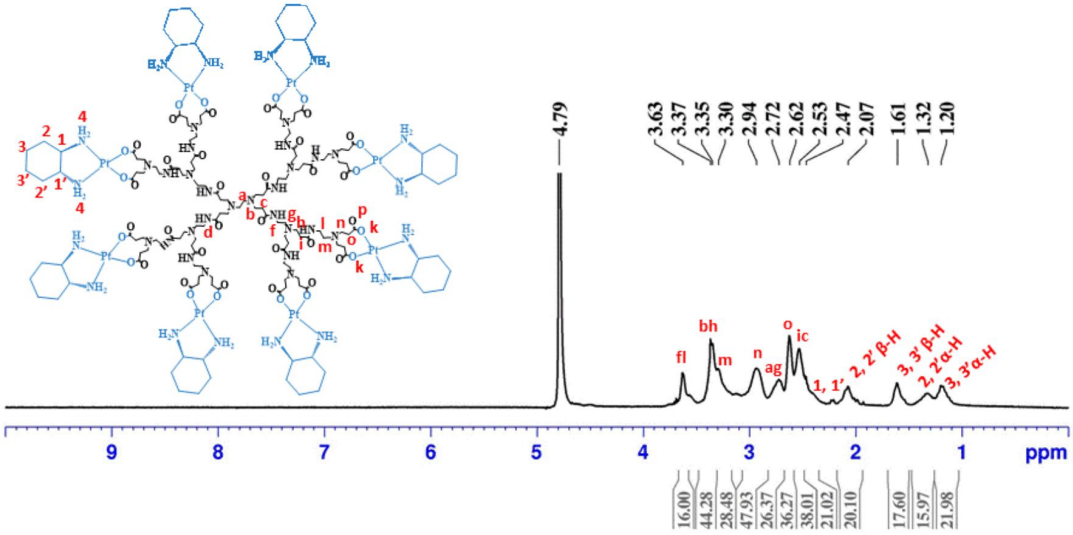

Figure 55: ^{1}H-NMR spectrum of G1.5COO(DACHPt)$_8$ performed in D_2O.

In the ^{13}C-NMR spectrum (Figure 56) is also observed the characteristic signals of the prepared metallodendrimer. Moreover, a downfield shift of the signal corresponding to the carboxylate group compared to pristine anionic G1.5-PAMAM dendrimer from 175.54 ppm to 177.55 ppm (see annex Figure A4), which indicate the conjugation of PAMAM dendrimer to the DACHPt moiety. Moreover, the signal at -2321.68 ppm in the ^{195}Pt-NMR spectrum also suggests the coordination to the dendrimer surface by the DACHPt in a bidentate form (see annex Figure D4). Nevertheless, since $[(DACH)Pt(OH_2)_2](NO_3)_2$ is bulky in size and DACHPt is hydrophobic, it inhibits its entry into the dendrimer due to the sterically agglomerated surface[290]. The other signals at -1467 ppm probably correspond to trans-$[Pt(cyclohexanediamine)(D_2O)_2]$ [291].

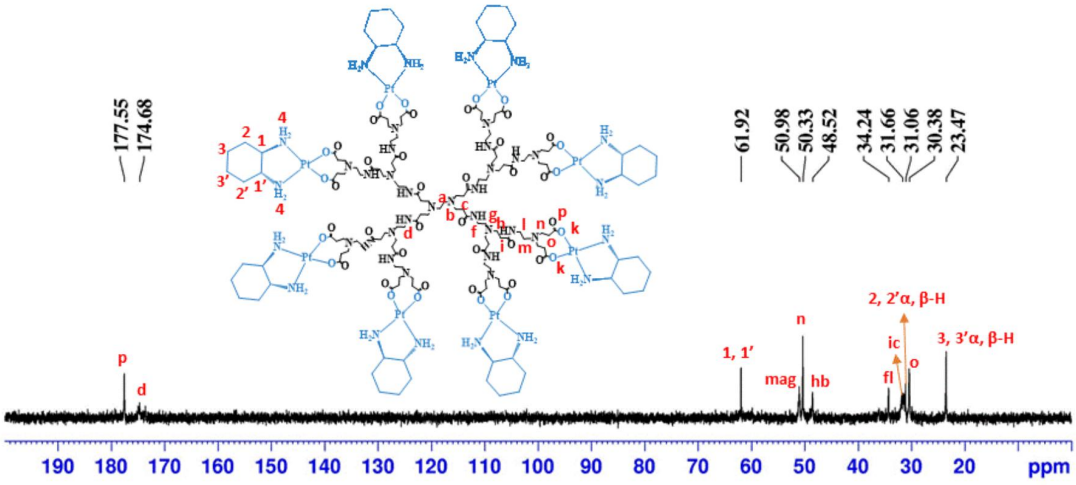

Figure 56: ^{13}C-NMR spectrum of G1.5COO(DACHPt)$_8$ performed in D_2O.

The G2.5COO(DACHPt)$_{16}$ metallodendrimer also has the signals of the expected structure. In the ^{1}H-NMR spectrum (Figure 57), the signals of the anionic G2.5-PAMAM dendrimer are visible between 2.65 and 3.67 ppm. At 1.20, 1.34, 1.61, 2.07, and 2.38 ppm are the signals of the cyclohexyl group of DACHPt. In the ^{13}C-NMR spectrum (Figure 58), the downfield shift (174. 67 to 177.17 ppm) of the carboxylate end group indicates the conjugation of PAMAM dendrimer to the DACHPt moiety. From the ^{195}Pt-NMR spectrum (see annex Figure D5), the signal at -2317 ppm also suggests the conjugation of PAMAM dendrimer to the DACHPt in a bidentate form.

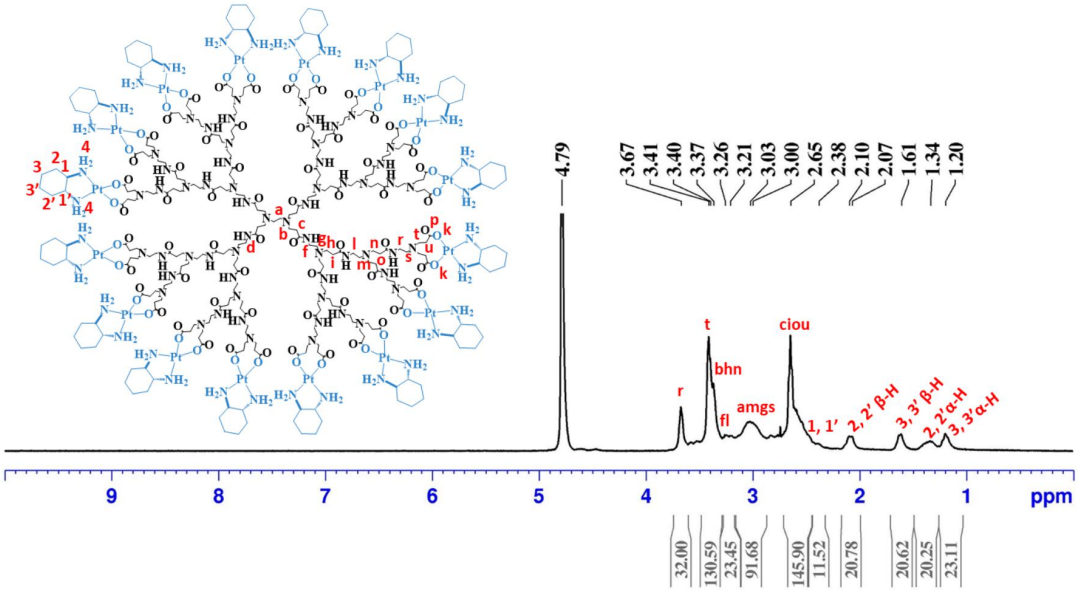

Figure 57: ^{1}H-NMR spectrum of G2.5COO(DACHPt)$_{16}$ performed in D_2O.

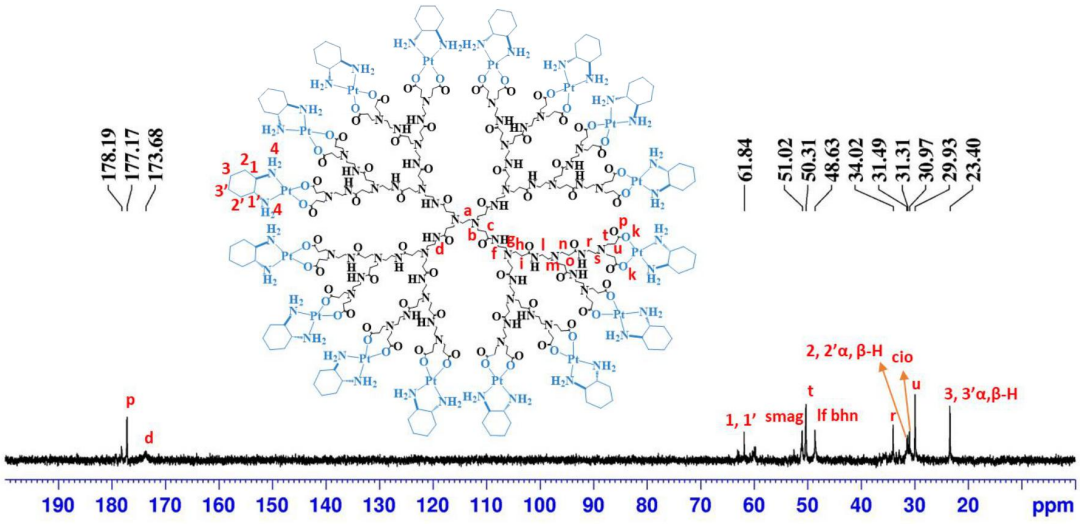

Figure 58: ^{13}C-NMR spectrum of G2.5COO(DACHPt)$_{16}$ performed in D_2O.

For the G3.5COO(DACHPt)$_{16}$ metallodendrimer, in the ^{1}H-NMR spectrum (Figure 59) is observed the signals of the expected structure of the anionic G3.5-PAMAM dendrimer and the cyclohexyl group of DACHPt. A downfield shift in the ^{13}C-NMR spectrum (Figure 60) of the carboxylate end groups from 174.90 to 177.11 ppm is indicative of the coordination of the dendrimer surface by the DACHPt moiety. The signal at -2312 ppm in the ^{195}Pt-NMR spectrum (see annex Figure D6) also corroborates the coordination of the dendrimer to the DACHPt.

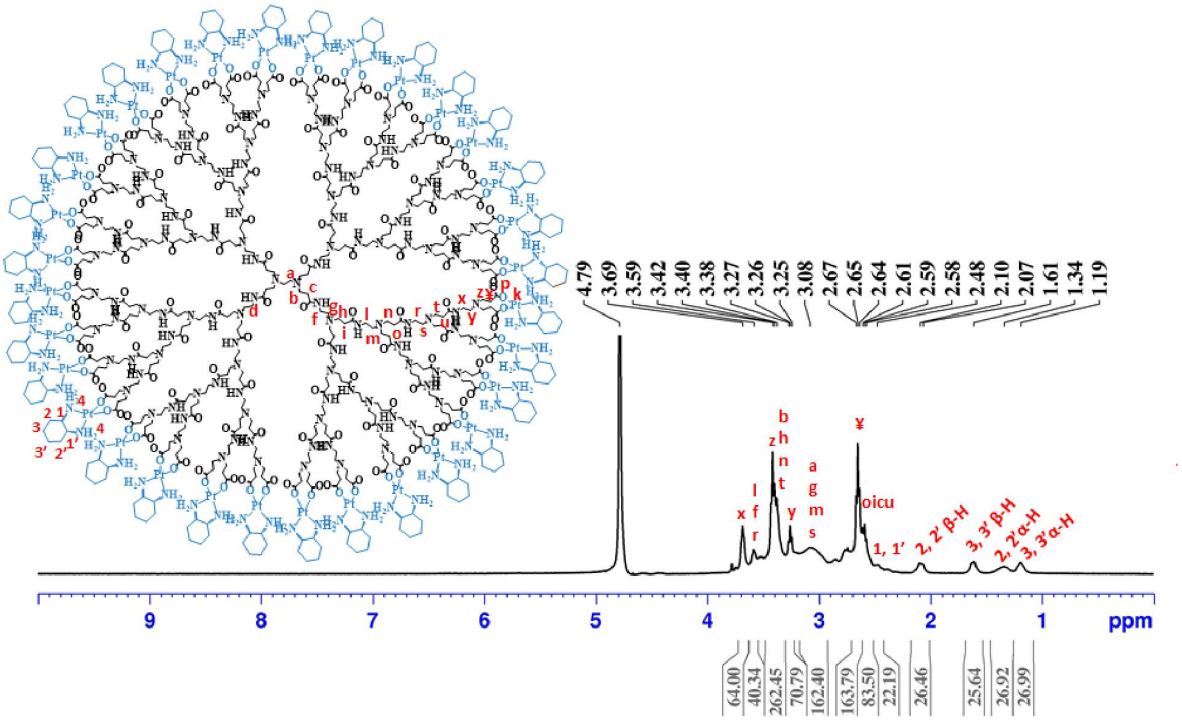

Figure 59: ^{1}H-NMR spectrum of G3.5COO(DACHPt)$_{32}$ performed in D_2O.

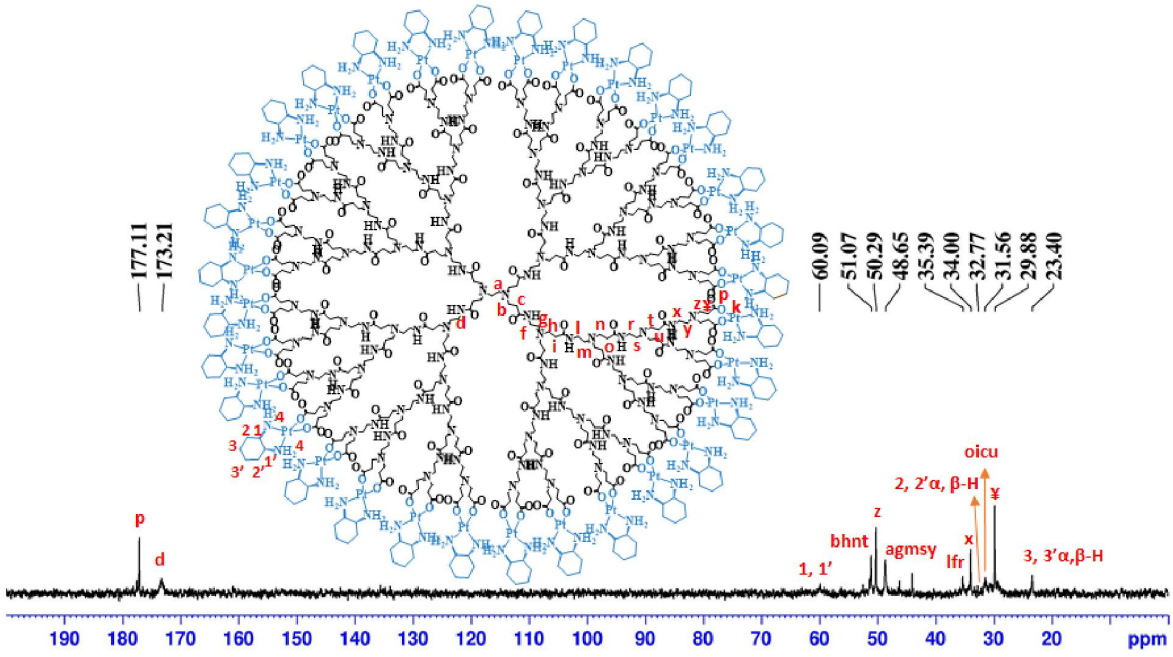

Figure 60: ^{13}C-NMR spectrum of G3.5COO(DACHPt)$_{32}$ performed in D_2O.

In addition to the characteristic signals observed in the NMR spectra of the chemical structure of the prepared DACHPt-metallodendrimers, they were also characterized by FTIR to confirm the dendrimer conjugation of DACHPt moiety in a bidentate form. When compared with the respective pristine anionic PAMAM dendrimer

(see annex Figure A9), the DACHPt-metallodendrimers (G0.5COO(DACH)Pt_4, G1.5COO(DACH)Pt_8, G2.5COO(DACH)Pt_{16}, and G3.5COO(DACH)Pt_{32}) show the characteristic carbonyl stretching band in the range 1618 cm^{-1} to 1640 cm^{-1} (see annex Figure D7) with the N–H stretch of the NH_2 groups of the DACHPt fragment appearing in the range 3388 cm^{-1} to 3470 cm^{-1}. In the G0.5COO(DACHPt)$_4$ spectrum, a shift to a lower wavenumber on the carbonyl group band (C=O stretch) from 1639 cm^{-1} to 1618 cm^{-1}, is observable, being indicative of the bidentate complexation of the DACHPt fragment via the dendrimer carboxyl terminal groups[334]. At 3388 cm^{-1}, a new band appears related to the NH_2 group of DACHPt fragment. In the other DAHPt-metallodendrimers, this shift is difficult to observe, but the conjugation could be confirmed due to the N–H stretch of the NH_2 groups of DACHPt fragment. In the G1.5COO(DACHPt)$_8$ spectrum is visible, a slight shift from 1637 cm^{-1} to 1639 cm^{-1} of the carbonyl stretch and a new band of the NH_2 stretch of the DACHPt fragment appeared at 3409 cm^{-1}. The G2.5COO(DACHPt)$_{16}$ and G3.5COO(DACHPt)$_{32}$ spectra also present a slight shift of the carbonyl group from 1638 cm^{-1} to 1640 cm^{-1} and 1639 cm^{-1} to 1638 cm^{-1}, respectively. And the appearance of a new band at 3470 cm^{-1} (G2.5COO(DACHPt)$_{16}$) and 3459 cm^{-1} (G3.5COO(DACHPt)$_{32}$) of the NH_2 stretch group of DACHPt fragment.

As mentioned earlier, the DACHPtCl_2 complex has a maximum absorption at 212 nm. After the conjugation of the dendrimer to the DACHPt moiety, a shoulder around this wavelength is observed in the UV-vis spectra, more evident for the higher generation dendrimers. The maximum absorbance wavelength suffers a deviation for higher wavelengths as the dendrimer generation increases, which is additional evidence of the success of the coordination process (Figure 61a). Moreover, the characteristic absorption band of the half-generation anionic PAMAM dendrimers, which appears around 280-300 nm and is attributed to the interior tertiary amines (see annex Figure A10), remains visible, without any significant shift, indicating that DACHPt has been conjugated only at the surface of the PAMAM dendrimers. As the generation of the dendrimers increases, absorbance values become higher due to the increase in the number of tertiary amines.

It is known that PAMAM dendrimers possess intrinsic fluorescence properties[335]. Indeed, the emission spectra presented by the pristine anionic PAMAM dendrimers show maximum wavelengths of fluorescence in the range 440-455 nm (see annex Figure A11). Interestingly, after the dendrimers' coordination of the DACHPt fragment, the fluorescence intensity decreased considerably in this wavelength range (Figure 61b). This effect occurs notwithstanding the DACHPtCl_2 compound also shows fluorescence in an aqueous solution with a maximum emission band at 433 nm (Figure 51). This result may be due to a decrease in the intrinsic fluorescence of dendrimers upon coordination with the increased number of DACHPt moieties conjugated to the dendrimer. The bidentate coordination that occurs may affect the distance among branches within the dendrimer scaffold interfering with the overall rigidity in the dendrimer scaffold or/and to quenching effects[336] related to the proximity of the DACHPt peripheral groups.

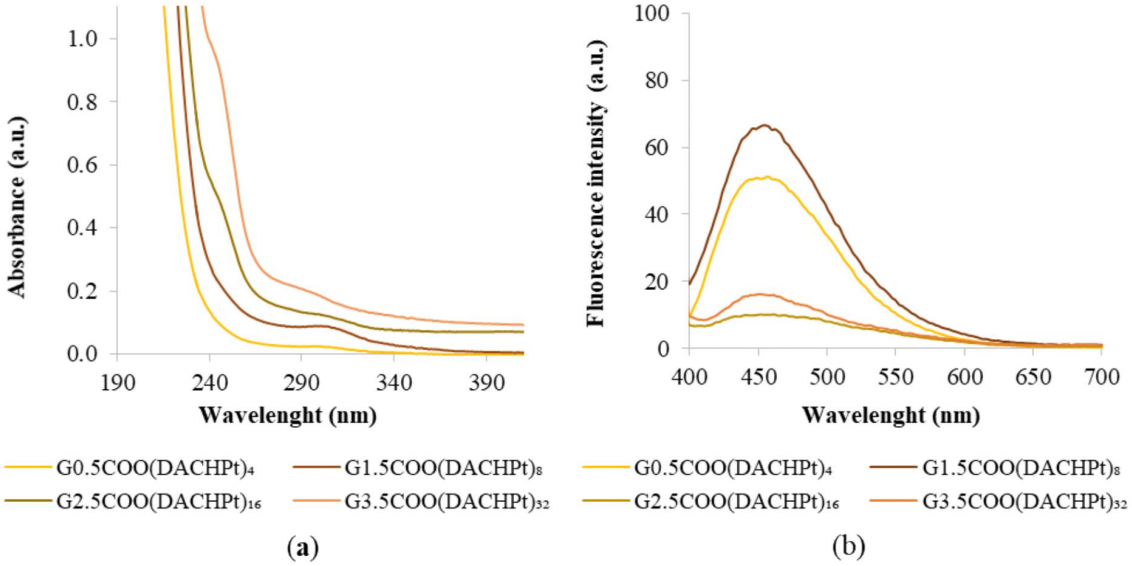

Figure 61: a) UV-Vis spectra of DACHPt-metallodendrimers at a concentration of 40 μM and b) Emission (λ_{ex} = 380 nm) of DACHPt-metallodendrimers at a concentration of 500 μM in UPW.

Furthermore, after coordinating the half-generation anionic PAMAM dendrimers to the DACHPt moiety, the zeta-potential values become less negative for all the prepared metallodendrimers (Table 14). This observation was expected since the dendrimers are anionic, and the DACHPt cation fragment has an associated double positive charge. Nevertheless, it is important to stress that, even if the zeta-potential is not an absolute indication regarding the stability of nanoparticles, the observed reduction in its absolute value after functionalization of the dendrimers with the DACHPt unit may trigger dendrimers' aggregation in an aqueous solution.

Table 14: Zeta-potential of anionic PAMAM dendrimers (G0.5-G3.5) and their related metallodendrimers after conjugation with DACHPt (n = 3) in filtered UPW.

Compounds	Zeta-potential (mV)
$G0.5(COONa)_8$	-19.17 ± 1.01
$G0.5COO(DACHPt)_4$	**-2.34 ± 0.53**
$G1.5(COONa)_{16}$	-40.8 ± 0.70
$G1.5COO(DACHPt)_8$	**-17.3 ± 1.57**
$G2.5(COONa)_{32}$	-47.77 ± 1.46
$G2.5COO(DACHPt)_{16}$	**-10.8 ± 0.26**
$G3.5(COONa)_{64}$	-51.27 ± 0.95
$G3.5COO(DACHPt)_{32}$	**4.03 ± 0.61**

Moreover, the coordination of the anionic PAMAM dendrimers to DACHPt was evaluated by TOF-MS (ESI positive mode or MALDI) analysis, depending on the metallodendrimer (see the spectra in Figures D8-D11). Despite the characterization difficulties experienced since DACHPt-metallodendrimers are, in general, hygroscopic, several fragments from the parent metallodendrimers were identified by TOF-MS, confirming the functionalization with DACHPt. Table 15 summarizes the results obtained from MS. For the G0.5COO(DACHPt)$_4$ metallodendrimer, a peak was found at *m/z* = 2014.7 [M+H - $C_{64}H_{117}N_{16}O_{20}Pt_3^+$]$^+$ that corresponds to three DACHPt moieties conjugated to the PAMAM dendrimer. The G1.5COO(DACHPt)$_8$ has a peak at *m/z* = 1008.58 [M+5H]$^{5+}$ and the G2.5COO(DACHPt)$_{16}$ a peak at *m/z* = 1556.7 [M+H$^+$+8MeOH]$^+$. And the peak at *m/z* = 388.2 [M - $C_{632}H_{1141}N_{168}O_{188}Pt_{23}$]$^+$ was found for G3.5COO(DACHPt)$_{32}$, which is a fragment with PAMAM dendrimer conjugated to twenty-three DACHPt metals.

Table 15: Molecular weight of the DACHPt-metallodendrimers.

	G0.5COO(DACHPt)$_4$	**G1.5COO(DACHPt)$_8$**	**G2.5COO(DACHPt)$_{16}$**	**G3.5COO(DACHPt)$_{32}$**
Molecular weight	2322.24	5040.96	10478.42	21353.33
***m/z* calculated**	2014.75	1008.58	1558.71	388.93
***m/z* found**	2014.7 [M+H]$^+$	1008.98 [M+5H]$^{5+}$	1556.7 [M+H$^+$+8MeOH]$^+$	388.2 [M]
	$C_{64}H_{117}N_{16}O_{20}Pt_3^+$	$C_{158}H_{293}N_{42}O_{44}Pt_8^{5+}$	$C_{342}H_{641}N_{90}O_{100}Pt_{16}^+$	$C_{632}H_{1141}N_{168}O_{188}Pt_{23}$

3.2. Biological studies

3.2.1. *In vitro* cytotoxicity assays

The cytotoxicity of the metallodendrimers G0.5COO(DACHPt)$_4$, G1.5COO(DACHPt)$_8$, G2.5COO(DACHPt)$_{16}$, G3.5COO(DACHPt)$_{32}$, and the free drugs $DACHPtCl_2$ and oxaliplatin were studied *in vitro* using four cancer cell lines (A2780, A2780CisR, MCF-7, and CACO-2 cells), and one non-cancer cell line (BJ cells). The cytotoxicity was evaluated after 72 h through a metabolic activity assay (MTT assay). As a control it was used the pristine half-generation anionic PAMAM dendrimers (G0.5-G3.5). The results are presented in Figures D12-D16 (see annex) and the half-maximal inhibitory concentration, IC_{50}, values in Table 16. All the studied metallodendrimers, were toxic against the tested cancer cell lines. Furthermore, the metallodendrimers were more cytotoxic than oxaliplatin and $DACHPtCl_2$ for all the cancer cell lines considered, as reflected by the obtained IC_{50} values. This can be explained by the available amount of DACHPt that is cleavage from the PAMAM dendrimers, due to the presence of chloride or phosphate ions in the media.

DACHPt is released from the PAMAM dendrimer by an exchange reaction between chloride/phosphate ions and the carboxylic groups of dendrimer[337]. All the DACHPt-metallodendrimers have a lower IC50 in the A2780 and A2780CisR cancer cells compared to cisplatin. In addition, the IC_{50} values obtained for the metallodendrimers in the study cancer cell lines are lower than the IC_{50} values obtained for the non-cancerous cell (BJ), with the exception of MCF-7 cancer cells. Meaning at the studied concentrations the metallodendrimers are not toxic for the normal cells, except for the tested concentrations for the MCF-7 cancer cells.

Table 16: IC_{50} values of the prepared DACHPt-metallodendrimers toward various cancer cell lines and non-cancer cell line. Results are expressed as mean ± SD three independent experiments performed in triplicate.

	A2780 ***IC_{50} ± SD (μM)***	***A2780CisR*** ***IC_{50} ± SD (μM)***	***MCF-7*** ***IC_{50} ± SD (μM)***	***CACO-2*** ***IC_{50} ± SD (μM)***	***BJ*** ***IC_{50} ± SD (μM)***
Cisplatin	0.11 ± 0.03	3.51 ± 1.35	1.21 ± 0.45	>10	0.55 ± 0.23
Oxaliplatin	0.48 ± 0.03	3.47 ± 0.46	> 10	0.91 ± 0.03	>10
$DACHPtCl_2$	0.28 ± 0.2	1.73 ± 0.41	5.38 ± 2.37	>10	>9
$G0.5COO(DACHPt)_4$	**0.03 ± 0.01**	**1.66 ± 0.27**	**1.56 ± 0.75**	**0.18 ± 0.08**	3.1 ± 0.97
$G1.5COO(DACHPt)_8$	**0.04 ± 0.02**	**0.59 ± 0.19**	**1.6 ± 0.68**	**0.25 ± 0.13**	1.25 ± 0.24
$G2.5COO(DACHPt)_{16}$	**0.04 ± 0.03**	**1.08 ± 0.18**	**2.96 ± 1.38**	**0.35 ± 0.09**	1.84 ± 0.72
$G3.5COO(DACHPt)_{32}$	**0.08 ± 0.02**	**1.2 ± 0.47**	**4.12 ± 0.77**	**0.39 ± 0.09**	2.59 ± 1.34

This increase in cytotoxicity can be more easily understood by analyzing the cytotoxicity relative potential (RP) of the metallodendrimers regarding oxaliplatin. This RP parameter was determined from the division of the oxaliplatin IC_{50} by the metallodendrimers IC_{50} (Table 17). As can be seen, RP values were consistently higher than 1, thus revealing a higher anticancer activity of the metallodendrimers concerning oxaliplatin. However, since oxaliplatin is used to treat colorectal and ovarian cancer, as it is a platinum derivative, a particular emphasis is given to CACO-2 and A2780CisR cancer cells. In the CACO-2 cancer cells, the $G0.5COO(DACHPt)_4$ has an RP value 5 times more cytotoxic than oxaliplatin. But, with the increase in generation, the RP value decreases to 3.6 < 2.6 < 2.3. On the other hand, in the A2780CisR, the generation does not influence the RP value. In this cancer cell the $G1.5COO(DACHPt)_8$ and $G2.5COO(DACHPt)_{16}$ are those with the higher RP value, 5.9 and 3.2, respectively. Nonetheless, when comparing the RP value determined as regards $DACHPtCl_2$ (see annex Table D1) is observed the same conclusions for these two cancer cell lines, because DACHPt is the active fragment of oxaliplatin, responsible for the anticancer effect. In general, the A2780 and the MCF-7 cells were the most sensitive to the metallodendrimers. The higher cytotoxicity of the metallodendrimers must be due to the higher number of metallic fragments transported by

the dendrimer scaffold compared with the single metallic fragment present in the oxaliplatin molecule. However, apparently, an effect of dendrimer generation was not observed in the cytotoxic behavior of the metallodendrimers.

Table 17: Relative potency (RP) of the DACHPt-metallodendrimers calculated from the division of the IC_{50} value of oxaliplatin by the IC_{50} value of metallodendrimers.

Relative potency (RP)	A2780	A2780CisR	MCF-7	CACO-2
$DACHPtCl_2$	1.7	2	> 1.9	> 0.1
$G0.5COO(DACHPt)_4$	16	2.1	> 6.4	5
$G1.5COO(DACHPt)_8$	12	5.9	> 6.3	3.6
$G2.5COO(DACHPt)_{16}$	12	3.2	> 3.4	2.6
$G3.5COO(DACHPt)_{32}$	6	2.9	> 2.4	2.3

Selectivity for cancer cells is another important characteristic of a chemotherapeutic agent, and, as such, the cytotoxicity of the metallodendrimers was also studied using non-cancer BJ cells. The selectivity index (SI) of the DACHPt-metallodendrimers is presented in Table 18 for the different cancer cell lines used in the experiment. The selectivity index (SI) value is defined as the ratio between the IC_{50} for BJ cells and the IC_{50} for each cancer cell line. If the SI is greater than 2, then the more selective the compound is towards cancer cells. SI values less or equal to 2 means that the compound has only general toxicity[295–297]. The results show that the metallodendrimers are especially selective regarding A2780 cancer cells. In the A2780 cancer cells, the SI values of all the metallodendrimers are greater than 2, being the $G0.5COO(DACHPt)_4$, the one with the highest selectivity index (SI = 103). In the A2780CisR cancer cells, the free drugs (oxaliplatin, $DACHPtCl_2$) are more selective than metallodendrimers, although the selectivity index of the metallodendrimers is 2, which means that they are selective for these cancer cells. The metallodendrimers also show selectivity for CACO-2 cancer cells. The metallodendrimers are more selective compared to $DACHPtCl_2$ (SI >0.9), which presents general toxicity but compared with oxaliplatin, only the $G0.5COO(DACHPt)_4$ have a SI higher (SI = 17) than the free drug (SI >11). The MCF-7 cancer cells are the cell line that the metallodendrimers are less selective.

Table 18: Selectivity index (SI) of the DACHPt-metallodendrimers calculated from the division of the IC_{50} value of BJ cell line for the IC_{50} value of cancer cell lines.

Selectivity index (SI)	A2780	A2780CisR	MCF-7	CACO-2
Oxaliplatin	>20.8	>2.9	>1	>11
$DACHPtCl_2$	>32	>5.2	>1.7	>0.9
$G0.5COO(DACHPt)_4$	103	1.9	2	17
$G1.5COO(DACHPt)_8$	31	2	0.8	5
$G2.5COO(DACHPt)_{16}$	46	1.7	0.6	5
$G3.5COO(DACHPt)_{32}$	32	2	0.6	6.6

The development of new platinum-based anticancer drugs also aimed to overcome the resistance to cisplatin (the first of this class of drugs that was introduced in the clinic) developed by some cell types. For this reason, we carried out the experiments with the A2780 cell line and, with its corresponding variant resistant to cisplatin, the A2780CisR cell line. The resistance factor (RF), which is the ratio between the IC_{50} value for A2780cisR cells and the IC_{50} value for A2780 cells, was then used as a parameter to evaluate the capacity to surpass cisplatin resistance (Table 19). Thus, the lower the RF value, the better the compound to overcome the resistance[92]. However, when compared to free drugs oxaliplatin and $DACHPtCl_2$, our metallodendrimers showed high RF values, which means that they have no advantages in this regard. The metallodendrimers $G1.5COO(DACHPt)_8$ and $G3.5COO(DACHPt)_{32}$ have a lower RF value than the others metallodendrimers. All things considered, the synthesized metallodendrimers are more cytotoxic in the tested cancer cell lines than the free drugs, although having, in general, a relative potential value and selectivity index lower than oxaliplatin and $DACHPtCl_2$. However, it could be interesting to use another drug in combination to study its potential as anticancer drug as they are more cytotoxic than free drugs.

Table 19: Resistance factor of the $DACHPtCl_2$-metallodendrimers calculated from the division of the IC_{50} value of A2780CisR for the IC_{50} value of A2780 cancer cell lines.

	Resistance factor (Rf)
Oxaliplatin	7.2
$DACHPtCl_2$	6.2
$G0.5COO(DACHPt)_4$	55.3
$G1.5COO(DACHPt)_8$	14.8
$G2.5COO(DACHPt)_{16}$	27
$G3.5COO(DACHPt)_{32}$	15

3.2.2. Hematoxicity assays

The hemolysis assay was used to evaluate the interaction of the free drugs and DACHPt metallodendrimers with red blood cells. The obtained results (Figure 62) show very low hemotoxicity levels for all situations studied if we compare the values of released hemoglobin with those of the negative control. In the case of oxaliplatin, hemotoxicity slightly increases with concentration with a release of hemoglobin around 12% at the maximum concentration used (5 μM), which is in line with the reported oxaliplatin hematological toxicity[208]. At this concentration, the $DACHPtCl_2$ and the metallodendrimers also present a low hemolysis percentage (7–10%). In fact, at least in the concentration range studied, an increase in dendrimers generation and, consequently, an increase in the number of metallic centers does not induce a significant variation in hemotoxicity values. However, these hemotoxicity studies were carried out *in vitro* and, of course, do not reflect the totality of events that may occur *in vivo*, such as selective dendrimers aggregation on atheromatous carotid tissues[338], platelets aggregation[339], and toxic effects in hippocampal neurons that may lead to a significant reduction in viability[340] as reported by others regarding dendrimer-based nanomaterials.

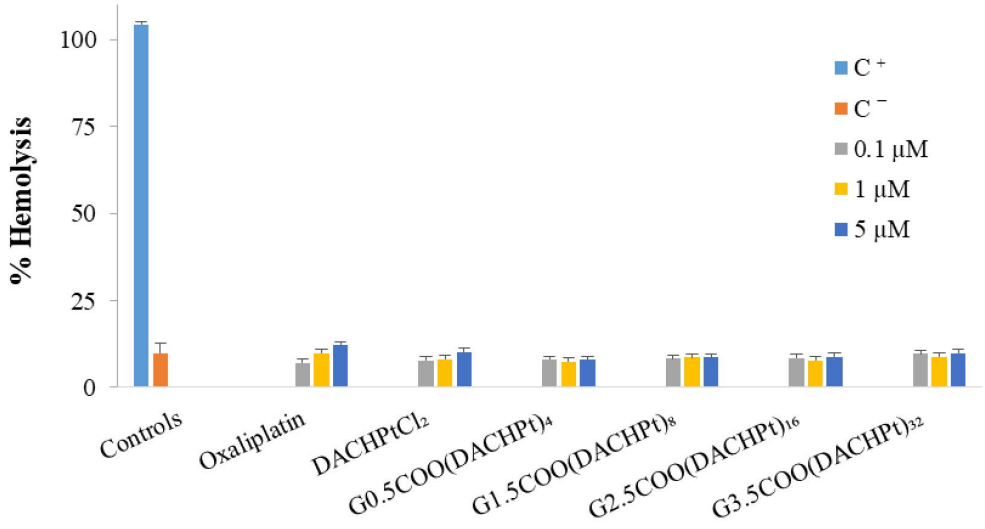

Figure 62: Hematoxicity of the free $DACHPtCl_2$, oxaliplatin and prepared DACHPt-metallodendrimers in healthy human blood. Blood was treated for 3 h with different concentrations (0.1, 1, and 5 μM) of the metallodendrimers and free drugs. The positive and negative control are represented by C^+ and C^-, respectively. The results are expressed as mean ± SD of at least three independent experiments performed in triplicate.

3.2.3. DNA binding assays

Since DNA is the pharmacological target of platinum-based drugs[288,300,341], UV-Vis spectroscopy was used to study the *in vitro* interaction of the metallodendrimers with calf thymus DNA (CT-DNA). For comparison purposes, the DNA binding studies were performed for the $G2.5COOPt(DACHPt)_{16}$ metallodendrimer,

$DACHPtCl_2$ as well as for oxaliplatin. This metallodendrimer was selected as a model for this metallodendrimers family once due to its size, it seems to be the most appropriate for the loading of 5-FU, which was later performed (*See section 3.3.1. Loading of 5-Fluorouracil*). Figure 63 shows the effect on the absorption spectra of solutions containing a varying CT-DNA concentration and a constant concentration of the metallodendrimer. The CT-DNA spectrum shows a broadband in the UV region with a maximum absorption wavelength at 260 nm (see annex Figure A17). This absorption is due to the chromophoric groups of adenine, guanine, cytosine, and thymine. It has been described in the literature that whereas binding to DNA through intercalation results in hypochromism (a decrease in DNA absorption), binding by electrostatic interactions gives rise to a hyperchromic effect (an increase in DNA absorption). Hyperchromism may also arise from other causes that culminate in a disruption of the hydrogen bonds that keep the DNA double helix in place and limit the aromatic rings' resonance (limiting their absorption as well)[288]. Clearly, the spectra of the $G2.5COO(DACHPt)_{16}$ metallodendrimer in the presence of increasing CT-DNA concentrations present a hyperchromic effect (Figure 63a). The same was also observed for the $DACHPtCl_2$ moiety (Figure 63b) and oxaliplatin (see annex Figure D19). Since it is known that the active fragment of oxaliplatin forms covalent adducts with DNA, the observed hyperchromism in $DACHPtCl_2$ and oxaliplatin should be due to a distortion in DNA conformation caused by adduct formation that exposes the DNA bases and results in higher absorbance values. These results are consistent with other studies regarding the interaction of oxaliplatin with linear DNA[342]. In fact, DACHPt adducts are more bulky and hydrophobic than cisplatin adducts, which are more effective in the inhibition of DNA synthesis, as they can cause distortion of the DNA skeleton by affecting its transcription and replication[204,205,288,301]. Besides, the conversion of monoadduct into diadduct is slower, possibly due to the binding angle, which is more restricted for DACHPt-DNA than for cisplatin[204]. In the case of the $G2.5COO(DACHPt)_{16}$ metallodendrimer, one should not expect a full release of the coordinated metallic fragments from the dendrimer scaffold during the 5 min incubation period used in the assay, even in the presence of chloride ions[337]. If that happened, the dendrimeric scaffold was always present in the solution, leading to interaction with DNA. Moreover, it is known that PAMAM dendrimers interact with DNA, through electrostatic bonds, followed by a conformational change in the dendrimer-DNA complex that leads to DNA condensation[306]. For the metallodendrimer, other types of interactions may occur, like those of a solely electrostatic nature that may further contribute to the DNA helix's disruption. Alternatively, the metallodendrimer can bind to DNA via monodentate form with DACHPt.

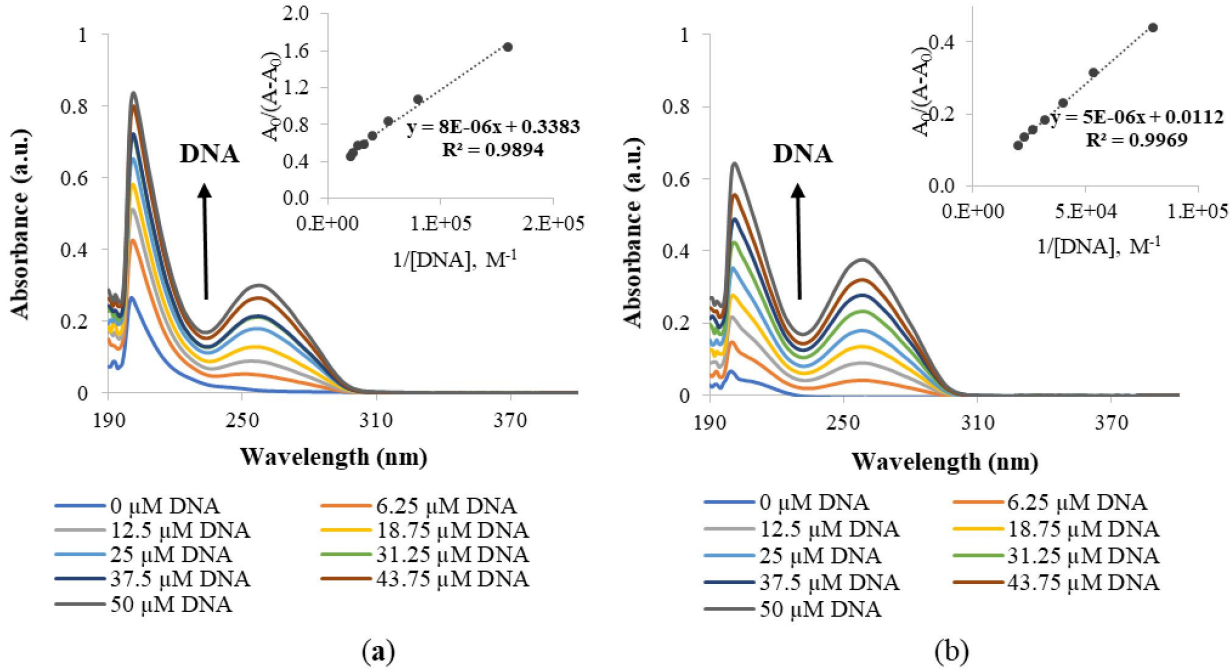

Figure 63: UV-visible spectra of a) G2.5COO(DACHPt)$_{16}$ metallodendrimer b) DACHPtCl$_2$ with increasing concentration of CT-DNA (0, 6.25, 12.5, 18.75, 25, 31.25, 37.5, 43.75 and 50 µM) in 5 mM Tris-HCl/50 mM NaCl at pH 7.4. The inset corresponds to the plot of $A_0/(A-A_0)$ versus 1/[DNA], which is used to determine the binding constant. The arrow indicates the direction of increasing the concentration of DNA.

The DNA binding constant (K_b) of the compounds with CT-DNA was determined by UV-vis through the Benesi-Hildebrand equation, namely from the ratio of the y-intercept to the slope in the plots $A_0/A-A_0$ vs 1/[DNA] [288]. The found K_b were similar for DACHPtCl$_2$ and oxaliplatin ($\simeq 3 \times 10^3$), but much higher for the metallodendrimer (Table 20). The coordination of PAMAM dendrimer to the DACHPt increased the K_b for $(3.6 \pm 0.9) \times 10^4$, reflecting a strong interaction of the metallodendrimers with the CT-DNA in the performed *in vitro* experiments. As mentioned above, additional electrostatic interactions may contribute to strengthening these interactions. However, one should have in mind that the type and extent of electrostatic interactions between the metallodendrimer and the CT-DNA established *in vitro* cannot directly correlate with what will happen *in vivo*. *In vivo*, the release of the metallic fragments is expected to occur near the target site as in the tumor environment or even inside cancer cells. In addition, the Gibbs free energy of the binding process was also estimated, indicating a spontaneous process as negative values were obtained (Table 20).

Table 20: Values of DNA binding constant (K_b) and Gibbs free energy (ΔG) of the G2.5COO(DACHPt)$_{16}$ metallodendrimer and free drugs DACHPtCl$_2$ and oxaliplatin. Data are represented as mean ± SD of two independent experiments.

	K_b	- ΔG/ KJ mol^{-1}
G2.5COO(DACHPt)$_{16}$	$(3.6 \pm 0.9) \times 10^3$	25 ± 0.64
DACHPtCl$_2$	$(3 \pm 1) \times 10^3$	19 ± 1.06
Oxaliplatin	$(3.1 \pm 0.6) \times 10^3$	19 ± 0.51

3.3. Drug loading

3.3.1. Loading of 5-Fluorouracil

As stated in chapter I, 5-FU is part of the chemotherapy regimen used to treat colorectal cancer[246,248,343], and, as such, it was chosen as a second drug to be transported by the anionic PAMAM dendrimers. Furthermore, the metabolites of 5-FU can intercalate with DNA and consequently lead to cell apoptosis mechanism[249,308]. Another reason is the fact that PAMAM dendrimer has hydrophobic internal cavities that enable the interaction with poorly soluble drugs, as 5-FU, by hydrophobic interactions[309]. The metallodendrimer G2.5COO(DACHPt)$_{16}$ was selected to load 5-FU due to its size, which seemed adequate for drug encapsulation[309,313]. The encapsulation of 5-FU within the G2.5COO(DACHPt)$_{16}$ was adapted from the method describes by Phung Le *et al.*[289]. In brief, G2.5COO(DACHPt)$_{16}$ was dissolved in UPW, and then 5-FU was added to the solution. The amount of encapsulated 5-FU was determined indirectly by UV-Vis at 266 nm, from the amount of 5-FU that was not encapsulated. The G2.5(COONa)$_{32}$ was used as a control. Drug loading results were compared with those of the pristine dendrimer G2.5(COONa)$_{32}$. The G2.5COO(DACHPt)$_{16}$ had a loading efficiency of 75%, which was slightly lower compared to the G2.5(COONa)$_{32}$ that had a loading efficiency of 86% (Table 21). These results could be explained by the fact that G2.5(COONa)$_{32}$/5-FU doesn´t have metal centers coordinated on its surface, so the drug enters the internal cavities without constraint. Unlike G2.5COO(DACHPt)$_{16}$/5-FU that has 16 aromatic metal centers on its surface, limiting the entry of the drug, because the surface is densely compacted. In addition, the loading capacity in the G2.5COO(DACHPt)$_{16}$/5-FU system was also lower (14%), which corresponds to a lower number of encapsulated 5-FU molecules (11). The loading capacity of the pristine G2.5(COONa)$_{32}$ dendrimer was more than two times that shown by the metallodendrimer (*ca.* 32%). 5-FU interacts with PAMAM dendrimer in the internal cavities through hydrogen bonds due to the presence of nitrogen and oxygen atoms and van der Waals interactions[76,316].

Table 21: Loading efficiency (LE%) and loading capacity (LC%) of 5-FU in G2.5COO(DACHPt)$_{16}$ metallodendrimer and anionic PAMAM dendrimer G2.5COONa (n= 3), and the number of 5-FU encapsulated molecules.

	LE%	LC%	N° of molecules encapsulated[a]
G2.5COO(DACHPt)$_{16}$/5-FU	74.83 ± 7.66	14.43 ± 1.17	11
G2.5(COONa)$_{32}$/5-FU	86.14 ± 1.74	31.72 ± 0.95	13

[a]The number of molecules encapsulated was calculated from the following equation,
i= n (drug)/n (dendrimer), where n (drug) = m (encapsulated drug)/MM (drug) and n (dendrimer)= m (dendrimer)/ MM (dendrimer) and *i* is the number of encapsulated molecules.

Moreover, the UV-Vis spectrum of the G2.5COO(DACHPt)$_{16}$/5-FU system was recorded. The 5-FU encapsulation in the metallodendrimer was confirmed (Figure 64a) by a decrease observed in the absorbance intensity at 266 nm, which is the maximum absorption wavelength of 5-FU[317]. The decrease in the absorbance was also observed for the G2.5(COONa)$_{32}$/5-FU system. However, when comparing both systems, the G2.5COO(DACHPt)$_{16}$/5-FU has a higher absorbance, although both have the same amount of 5-FU (10 μg). These results suggest that the combination of the metal DACHPt and 5-FU increase the absorption of the metallodendrimer. Also, the disappearance of the shoulder related to the metallodendrimer suggests that 5-FU was encapsulated inside the compound, even though no significant shifting was observed[316,318]. Furthermore, fluorescence emission spectra were also performed. As can be seen in Figure 64b, 5-FU and G2.5(COONa)$_{32}$/5-FU present similar fluorescence intensity, whereas it is much higher for the G2.5COO(DACHPt)$_{16}$/5-FU system (in this case, fluorescence intensity is five times greater than in the G2.5(COONa)32/5-FU system). This means that the combination of 5-FU and DACHPt increases the fluorescence, not observing any quenching effect. Because they are aromatic drugs, the fluorescence probably presents an increase when combined with the two.

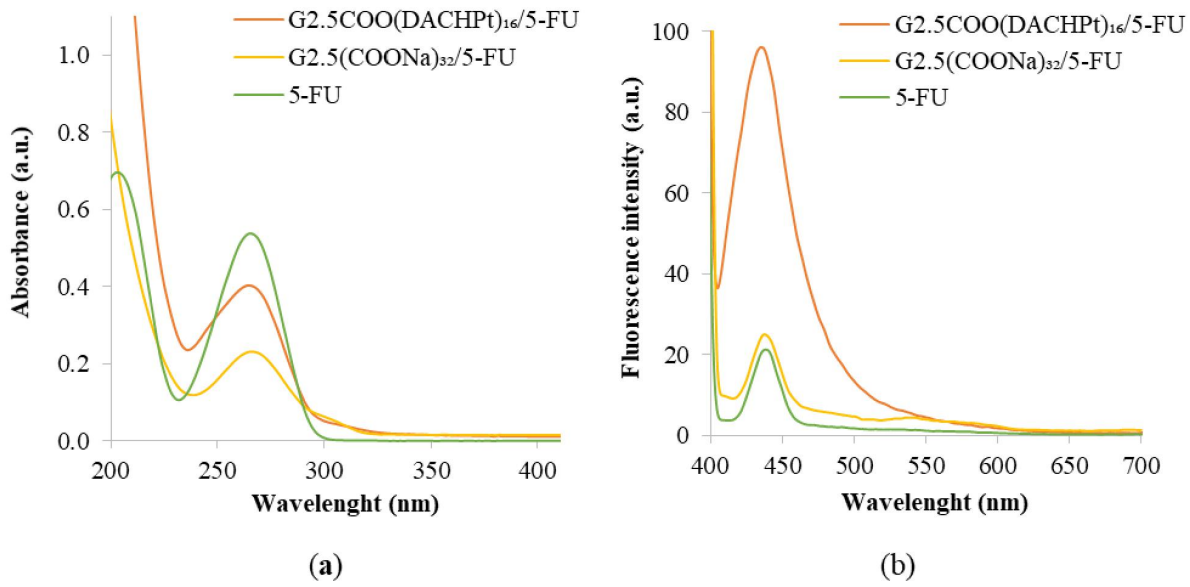

Figure 64: a) UV-vis spectra of G2.5COO(DACHPt)$_{16}$/5-FU, G2.5(COONa)32/5-FU, and 5-FU b) Emission spectra (λ_{ex} = 380 nm) of G2.5COO(DACHPt$_{16}$/5-FU, G2.5(COONa)$_{32}$/5-FU and 5-FU. In UPW spectra were recorded at the same 5-FU concentration ([5-FU] = 10 µg).

As can be observed from Table 22, the zeta-potential increases from -10.8 mV in the metallodendrimer G2.5COO(DACHPt)$_{16}$ to 0.82 mV in the G2.5COO(DACHPt)$_{16}$/5-FU system, corroborating the loading of 5-FU in the G2.5COO(DACHPt)$_{16}$. A similar trend was observed in the zeta-potential when the G2.5(COONa)$_{32}$ dendrimers were loaded with 5-FU. This difference suggests that 5-FU was encapsulated inside the metallodendrimers, also because the measured charge of the 5-FU was 4.48 mV. The positive charge of 5-FU is because, at lower pHs values (below than pH 8), the 5-FU becomes protonated, forming different cationic structures[320]. And the pH of the water used for the measurements was 6.5.

Table 22: Zeta-potential of G2.5COO(DACHPt)$_{16}$/5-FU and G2.5(COONa)$_{32}$/5FU (n=3) in filtered UPW.

Compounds	Zeta-potential (mV)
G2.5COO(DACHPt)$_{16}$	-10.8 ± 0.26
G2.5COO(DACHPt)$_{16}$/5FU	**0.82 ± 0.11**
G2.5(COONa)$_{32}$	-47.77 ± 1.46
G2.5(COONa)$_{32}$/5FU	**-41.13 ± 0.49**

The FTIR spectrum of G2.5COO(DACHPt)$_{16}$/5-FU is shown in Figure D21 (see annex). A shift in the characteristics absorption bands of G2.5COO(DACHPt)$_{16}$ metallodendrimer is observed after encapsulation of 5-FU. The amide I band C=O stretching at 1640 cm^{-1} moves to 1644 cm^{-1} and amide II band, due to the N-

H bending from 1560 cm^{1-} to 1586 cm^{-1}. This shift is due to hydrogen bonding between the 5-FU and metallodendrimer[318]. Furthermore, shifts in the signals of 5-FU carbonyl group C=O (from 1658 cm^{-1} to 1644 cm^{-1}) and of the C–F stretching band (from 1244 cm^{-1} to 1262 cm^{-1}) are visible[321]. Likewise, a shift of amide I band, from 1638 cm^{-1} to 1644 cm^{-1}, and amide II band from 1564 cm^{-1} to 1586 cm^{-1} is observed for the G2.5(COONa)32/5-FU after the drug encapsulation (see annex Figure D22). In addition to the characterizations carried out, the complexes G2.5COO(DACHPt)$_{16}$/5-FU and G2.5(COONa)$_{32}$/5-FU were characterized by NMR (^{1}H, ^{13}C, and ^{19}F). The G2.5COO(DACHPt)$_{16}$/5-FU has an upfield shift of the protons in the ^{1}H-NMR spectrum (Figure 65). The characteristics protons of 5-FU are visible in the spectrum after encapsulation (shifting only 0.1 ppm). For the ^{13}C-NMR spectrum, a shift is observed for the carbons bonded just after to the amide groups inside the metallodendrimer, and the carbons bonded after to the tertiary amine groups from 48.63 ppm to 48.86 ppm (Figure 66). The carbon signals of the amide groups inside the metallodendrimer also shift from 173.68 ppm to 173.08 ppm. Regarding to the 5-FU carbon signals, the only signal visible in the spectrum is the signal related to the C-6 carbon, meaning that the carbonyl groups and amide groups are involved in the interaction with the metallodendrimer. The ^{19}F-NMR spectrum (Figure 67) reveals a non-significant shift (0.08 ppm), probably because the fluorine group is not involved in the interaction with the metallodendrimer. Based on the previous results, we suggest, that 5-FU molecules should be bonded through the amide and tertiary amines groups of the metallodendrimers.

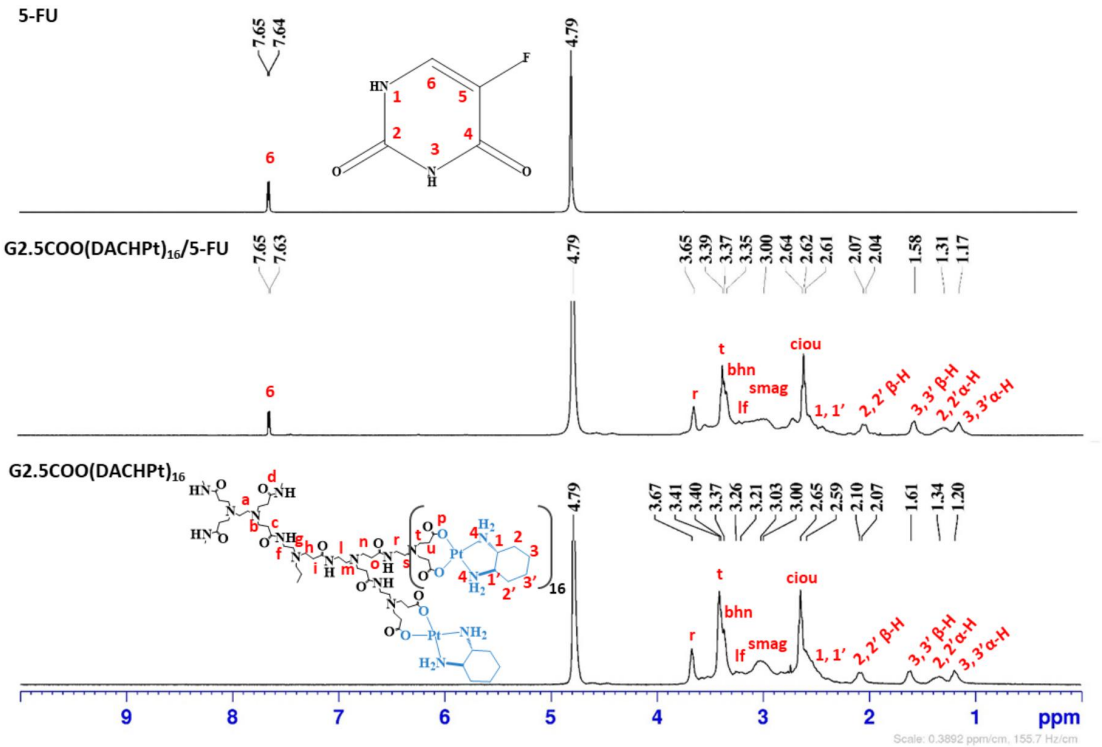

Figure 65: ^{1}H-NMR spectrum of G2.5COO(DACHPt)$_{16}$, G2.5COO(DACHPt)$_{16}$/5-FU and 5-FU in D_2O.

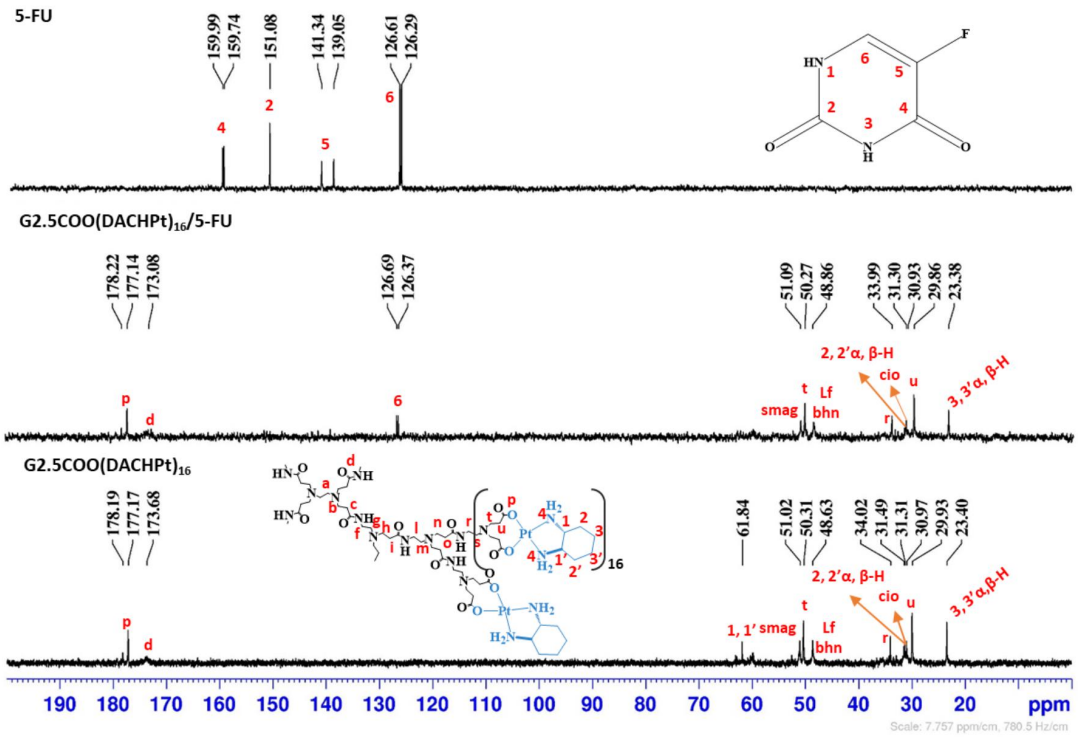

Figure 66: ^{13}C-NMR spectrum of G2.5COO(DACHPt)$_{16}$, G2.5COO(DACHPt)$_{16}$/5-FU and 5-FU in D_2O.

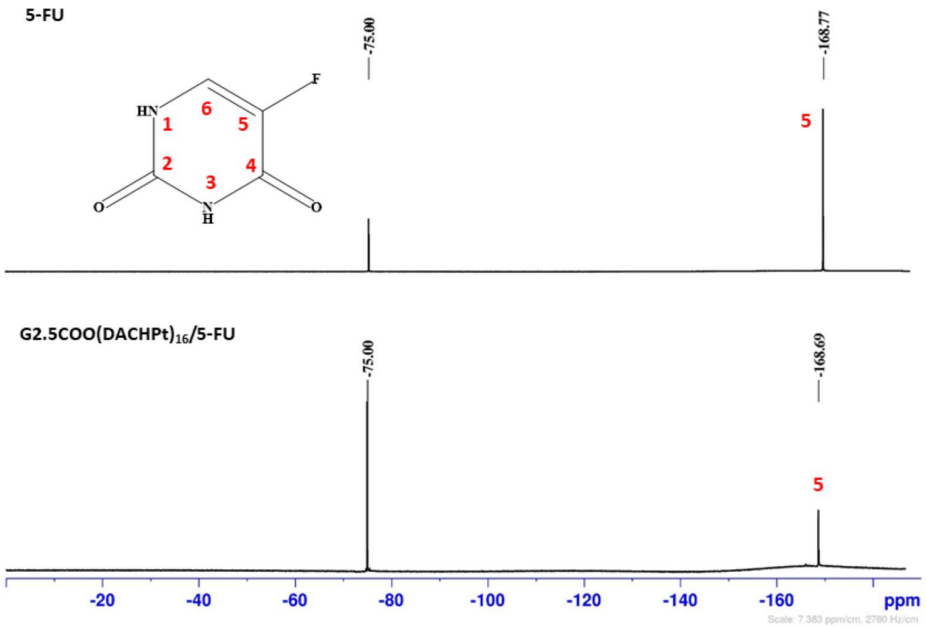

Figure 67: ^{19}F-NMR spectrum of G2.5COO(DACHPt)$_{16}$/5-FU and 5-FU in D_2O.

As described in Chapter II, in the ^{1}H-NMR spectrum of G2.5(COONa)$_{32}$/5-FU (Figure 44) it is possible to observe a downfield shift in all the characteristic signals of the G2.5(COONa)$_{32}$ PAMAM dendrimer after encapsulated 5-FU molecules, which is prominent in the signals of methylene protons present at tertiary amine groups and of the amide groups. Even though it is not so significant, this evidence is also perceptible in the ^{13}C-NMR spectrum (Figure 45), particularly in the carbons bonded after the tertiary amine group (from 49.78 to 50.13 ppm) located in the complex's interior and also in the carbon bonded after the amide group located just below to the surface (from 34.9 ppm to 34.2 ppm). The corresponding signal of the amide carbons, located inside the dendrimer, shifts from 178.82 ppm to 177.57 ppm, corroborating the presence of 5-FU inside the dendrimer and not attached to its surface. Moreover, the carbon signal from the carboxylic end groups does not shift. Regarding 5-FU, in general, a slight shift of the carbons was observed, with the signal of carbon C-2 absent after encapsulation and the C-4 carbon presenting a significant shift (from 159.74 ppm to 156.78 ppm), suggesting that the carbonyl group is protonated and this is the main group that interacts with the PAMAM dendrimer. Besides, the fluorine signal in the ^{19}F-NMR spectrum is shifted downfield (Figure 46), indicating that it is also involved in the interaction with the PAMAM dendrimer.

3.3.2. Cytotoxicity of the complex

A2780CisR and CACO-2 cancer cell lines were used to evaluate the cytotoxicity of G2.5COO(DACHPt)$_{16}$/5-FU system and were selected because 5-FU is used in the treatment of colorectal cancer, but also in the cases of other cancer types, such as ovarian cancer[322–324]. The results are presented in Figures D17 and D18 (see annex) and the IC_{50} in Table 23. From the IC_{50} values, we observe that G2.5COO(DACHPt)$_{16}$/5-FU system, compared to free 5-FU and G2.5(COONa)$_{32}$/5-FU, has an IC_{50} much lower in both cancer cell lines, which is due to the presence of the metallic fragments in the dendrimers that should be released a long time and exert their anticancer activity. When using the A2780cisR cells, the IC_{50} value decreases from 1.1 μM to 0.2 μM for the non-loaded and the loaded metallodendrimer, respectively. The G2.5COO(DACHPt)$_{16}$/5-FU system seems to be more effective 5.5 times than G2.5COO(DACHPt)$_{16}$ metallodendrimer. But when compared with G2.5(COONa)$_{32}$/5-FU system and 5-FU is more efficient in these cancer cells. However, when using CACO-2 cells, the IC_{50} slightly increases when 5-FU molecules are loaded into the metallodendrimer. As such, it seems that the metallic fragments-induced cytotoxicity dominates over the cytotoxicity of 5-FU. This is evident when we compare the IC_{50} values for the free drugs oxaliplatin and 5-FU as IC_{50} (oxaliplatin) << IC_{50} (5-FU). Indeed, the G2.5COO(DACHPt)$_{16}$/5-FU has less encapsulated 5-FU molecules (11 molecules) than G2.5(COONa)$_{32}$/5-FU (13 molecules), and it is more cytotoxicity in both cancer cells. *In vivo*, however, one should expect beneficial effects of the co-delivery of DACHPt and 5-FU, as happens when combined therapy is used in the patients.

Table 23: IC_{50} values of the prepared DACHPt-metallodendrimers toward A2780CisR and CACO-2 cancer cell lines. Results are expressed as mean ± SD three independent experiments performed in triplicate.

	A2780CisR IC_{50} ± SD (µM)	**CACO-2 IC_{50} ± SD (µM)**
5-FU	> 154	> 154
G2.5COO(DACHPt)$_{16}$/5-FU*	**0.2 ± 0.1**	**0.65 ± 0.06**
G2.5(COONa)$_{32}$/5-FU*	> 2.5	> 2.5

*For the calculation of the MW, the estimated number of 5-FU molecules carried by the dendrimer was taken into account.

3.3.3. Hematoxicity of the complex

The hematoxicity of G2.5COO(DACHPt)$_{16}$/5-FU was evaluated by the release of hemoglobin from blood cells. The results of hemolysis (Figure 68) show that G2.5COO(DACHPt)$_{16}$/5-FU system and the 5-FU are not hemotoxic at concentrations 0.1 and 1 µg/mL, only achieving *ca.* 5% of hemolysis. Nonetheless, when we increase the concentration to 5 µg/mL, the percentage of hemolysis significantly increases to a value between 24-26% for all the compounds, which should be attributed to 5-FU presence.

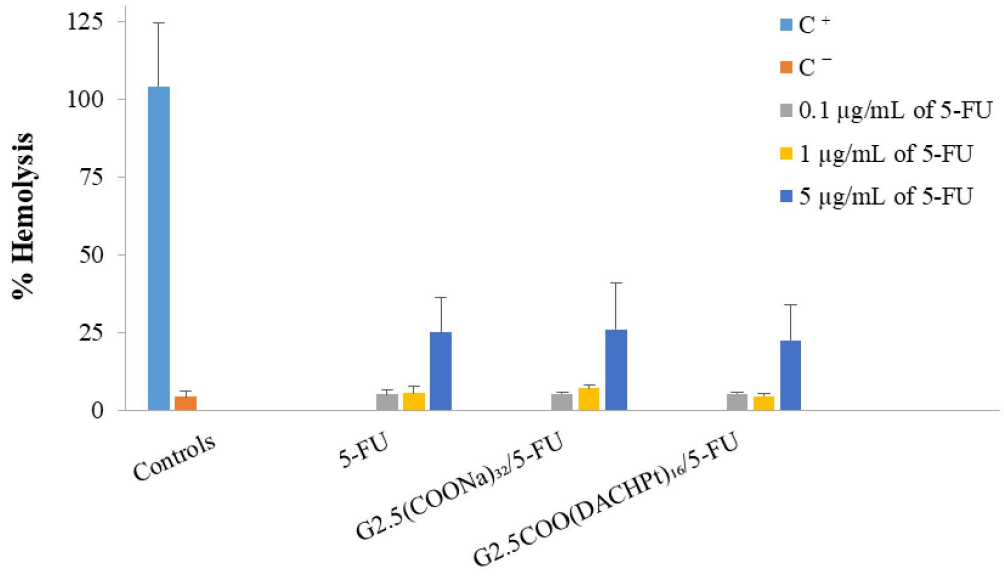

Figure 68: Hematoxicity of the free 5-FU, G2.5(COONa)$_{32}$/5-FU and G2.5COO(DACHPt)$_{16}$/5-FU in healthy human blood. Blood was treated for 3 h with different concentrations (0.1, 1, and 5 µg/mL) of the metallodendrimers and free 5-FU. The positive and negative control are represented by C^+ and C^-, respectively. The results are expressed as mean ± SD of at least three independent experiments performed in triplicate.

3.3.4. *In vitro* drug release

From Figure 69, we can conclude that, after an initial faster release of the 5-FU drug from G2.5COO(DACHPt)$_{16}$/5-FU and G2.5COO(COONa)$_{32}$/5-FU systems, drug release starts to be sustained a long time, achieving maximum values of 57% and 46% of cumulative release after 24 h, respectively. That is, drug release seems to be higher for the metallodendrimer than for the G2.5(COONa)$_{32}$ dendrimer. On the other end, decreasing the pH value does not affect drug release, which means that our system is not sensitive to the pH, which, as it is known, may change towards more acidic values in the microtumor environment. However, comparing the release of the free drug, it is observed that metallodendrimer releases 5-FU more slowly, allowing the bioavailability of the drug to be prolonged in the circulation of blood. This behavior is important, because 5-FU has a short time bioavailability in blood circulation[325].

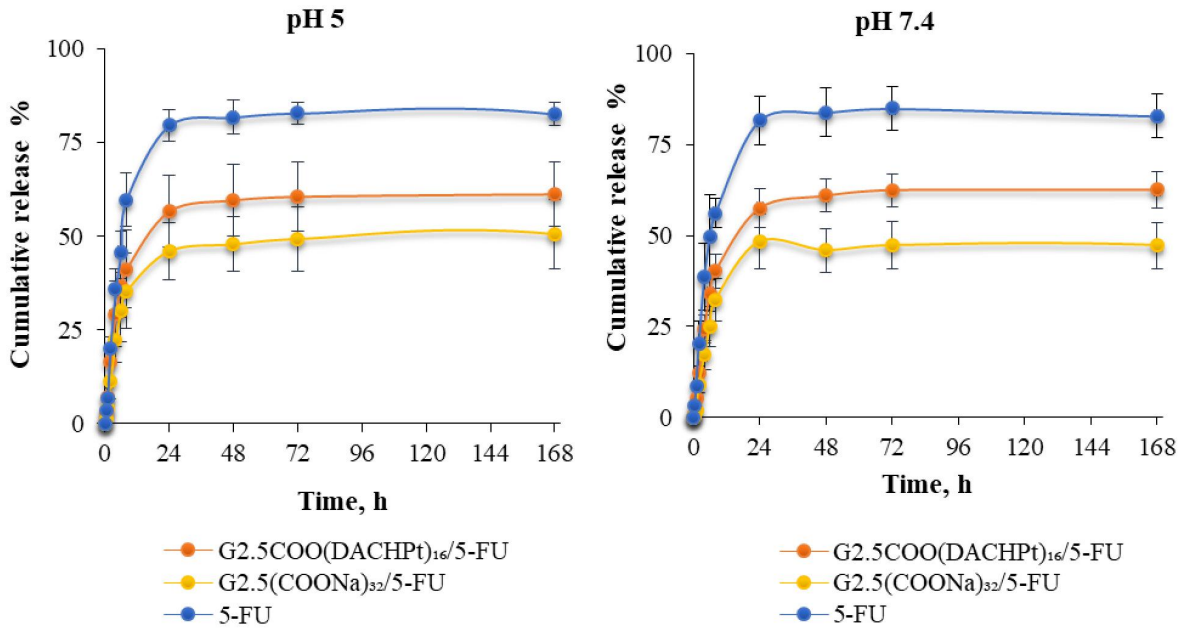

Figure 69: Release profile of 5-FU from DACHPt-metallodendrimer and anionic PAMAM dendrimer in pH 5 and 7.4 at 37ºC.

4. Conclusions

Half-generation PAMAM dendrimers (G0.5-G3.5) with carboxylate end-groups were used as nanocarriers of the active metallic fragment DACHPt to take advantage of its good anticancer activity and to overcome some of the associated problems of the free drug DACHPtCl$_2$, such as its low water solubility. All things considered, we can conclude that DACHPt-metallodendrimers were successfully synthesized in a bidentate form. Furthermore, the DACHPt moiety was coordinated on the surface of the anionic PAMAM dendrimers. As far as we know, these metallodendrimers were prepared for the first time in these generations. Previous studies have only shown the use of generation 4.5 anionic PAMAM dendrimer and generation 3 amine-terminated

PAMAM dendrimer and other polymers[290,337,344–346]. The coordination of DACHPt fragment in the bidentate form, where the metal is linked with two bonds to the dendrimer, should increase its retention, preventing it from being released into the bloodstream and thus interacting with other cellular components until reaching the target site. In this sense, the aquation of $DACHPtCl_2$ was carried out before its conjugation to the PAMAM dendrimers (G0.5-G3.5). After the characterization of the DACHPt-metallodendrimers by various techniques (NMR, FTIR, UV-Vis and fluorescence spectroscopy, zeta-potential, MS, and EA), their cytotoxicity in different cancer cell lines (A2780, A2780CisR, MCF-7 and CACO-2) were evaluated. The cytotoxicity assay showed that DACHPt-metallodendrimers have an *in vitro* cytotoxic effectiveness higher than oxaliplatin in several cell lines. The toxicity toward the red blood cells was also evaluated, revealing a low hemotoxicty of the DACHPt-metallodendrimers. For the further assay, $G2.5COO(DACHPt)_{16}$ metallodendrimer was used to evaluate the DNA binding. DNA binding studies in the presence of increasing CT-DNA concentrations revealed a hyperchromic effect indicating a disruption in the DNA double helix. The prepared DACHPt-metallodendrimers were also shown to be able to load and release the anticancer drug 5-FU, although the cytotoxicity of the metallic fragment DACHPt dominated over 5-FU cytotoxicity. However, in the A2780Cis cancer cells, the $G2.5COO(DACHPt)_{16}$/5-FU system showed to be 5.5 times more cytotoxic than $G2.5COO(DACHPt)_{16}$ metallodendrimer. The *in vitro* release studies showed that the 5-FU is released slower from the $G2.5COO(DACHPt)_{16}$/5-FU compared to the free 5-FU in both pH media (5 and 7.4). Nevertheless, the release of 5-FU from $G2.5COO(DACHPt)_{16}$/5-FU system is not sensitive to pH. In conclusion, promising results on the use of DACHPt-metallodendrimers alone or combined with 5-FU were obtained *in vitro*, and further studies, including *in vivo* experiments, should be done in the future to confirm the full potential of these systems. Indeed, we believe that it will be possible to optimize the DACHPt-metallodendrimer/5-FU systems (preparation, scale-up, and integration of a third drug) to act as an alternative for the current FOLFOX chemotherapy regimen used to treat stage III of colorectal cancer and its recurrences.

CHAPTER IV

Intrinsic blue fluorescence of oxidized PAMAM dendrimers

This chapter is based on the following publication:

- **Camacho, C. S.**; Urgellés, M.; Tomás, H.; Lahoz, F.; Rodrigues, J. New insights into the blue intrinsic fluorescence of oxidized PAMAM dendrimers considering their use as bionanomaterials. *J. Mater. Chem. B.* **2020**, 8, 10314-10326. https://doi.org/10.1039/D0TB01871F.

1. Introduction

In the biomedical field, PAMAM dendrimers have been studied as potential nanocarriers for drugs, genes, and/or bioimaging contrast agents[80,84,107,110,128,347–350]. Nevertheless, their application in the treatment and/or diagnosis of diseases or other medical conditions may be limited by the inherent toxicity associated with their amine termini and the lack of a strong intrinsic traceable signal that would allow their localization within cells or tissues[83,105,351]. To overcome these limitations, different strategies have been used, e.g., decreasing or masking the amine groups at the dendrimer's surface and labelling the dendrimer with fluorescent molecules, which often imply important modifications in dendrimer's properties and unwanted changes in their biological behavior[114,352]. For instance, the labelling of dendrimers with fluorescent probes may impact their cytotoxicity profile and modify their mechanisms of cellular internalization[114,352].

A less known strategy relies on exploring PAMAM dendrimers' intrinsic fluorescence[117,118,120,122,353], which was recently attributed by Donald Tomalia *et al.* to a non-traditional intrinsic luminescence (NTIL) phenomenon [115] that does not involve aromatic or extended π-systems but rather electron-rich hetero-atomic sub-luminophores (HASLs) confined within macromolecular architectures. This NTIL phenomenon is associated with a fluorescence emission that is often amplified by the rigidification of molecular structures or by HASLs clustering[115,354]. Indeed, several experiments indicate that the observed weak intrinsic fluorescence of PAMAM dendrimers does not arise from their surface chemical groups but, instead, stems from chemical entities present in their internal ordered dendritic structure, like the interior amide and tertiary amine moieties that possess electron-rich heteroatoms[115,117,122,354]. In fact, NTIL emission can be observed in PAMAM dendrimers with the amine, hydroxyl, or carboxylate groups termini[117] and can be drastically enhanced through an oxidative treatment, such as direct oxygen exposure[116] or by using ammonium persulfate (APS, $(NH_4)_2S_2O_8$)[118]. Another important feature that should be referred to is that the fluorescence intensity shown by the APS-treated dendrimers was significantly pH-dependent, increasing in acidic conditions[119,121] like already observed for pristine dendrimers[117].

The cumulative evidence of the existence of the NTIL phenomenon in the case of dendrimers, the interesting seminal works of Imae Toyoko *et al.*[116,117,119,122,355,356], and our previous work in the application of dendrimers in the biomedical field[110,128,347,348,357–360], led us to study in more detail the non-intrinsic fluorescence presented by APS-treated dendrimers. Here, three generations of amine-terminated PAMAM dendrimers (G3, G4, and G5) were oxidized with APS and, after characterization by proton nuclear magnetic resonance (^{1}H-NMR) and Fourier transformed infrared (FTIR) spectroscopies, their fluorescence properties were evaluated in solution and lyophilized forms for a better understanding of the possible mechanism underlying the observed enhanced intrinsic fluorescence. As far as we know, this is the first study of the NTIL phenomenon in APS-treated dendrimers without the interference of the solvent. Furthermore, since the ultimate purpose of these dendrimers is their potential application in the biomedical field, the effect of pH on their fluorescence intensity was studied, as well as their cytotoxicity, hematoxicity, and visualization inside cells. In addition, the anticancer drug doxorubicin was loaded to the APS-treated G4 PAMAM dendrimer and its release study in different pH media.

2. Experimental

2.1. General

Except for PAMAM dendrimers, all the reagents were used as received. Amine-terminated PAMAM dendrimers G3 (26.80 w/w %), G4 (9.99 w/w %), and G5 (19.13 w/w %) with an ethylenediamine core were acquired from Dendritech Inc. having methanol as solvent. Before use, they were dialyzed to remove impurities. Ammonium persulfate (APS, $(NH_4)_2S_2O_8$) was supplied by PANREAC (puriss. p.a., ACS reagent, reag. Ph. Eur.), potassium dihydrogen phosphate by Merck, potassium ferricyanide by Riedel-de-Haën, potassium cyanide by Aldrich and Triton-X by Merck Millipore. Fluorescence grade pyrene was purchased from Sigma-Aldrich. The ultrapure water (UPW) used in the synthesis was obtained with a Millipore Milli-Q with a resistivity higher than 18.2 MΩ·cm. All the media, solutions, and reagents used for cell culture manipulation were purchased from Life Technologies (Thermo Fischer Scientific) unless otherwise stated. The hemoglobin used in the hemotoxicity assays was from bovine blood and was purchased from Sigma-Aldrich. The healthy human blood was supplied by Hospital Dr. Nélio Mendonça (SESARAM) under a collaboration between the University of Madeira/Centro de Química da Madeira and the SESARAM haematology service.

2.2. APS-treatment of PAMAM dendrimers and structural characterization

The same methodology was used for the three generations of PAMAM dendrimers. Briefly, an aqueous solution of the PAMAM dendrimer (0.2 mM) and an aqueous solution of APS (0.1 M, 20 eq. mol) were stored in the fridge for 30 min. Afterward, the APS aqueous solution was dropwise added into the PAMAM dendrimer solution. The mixture was allowed to react under magnetic stirring at room temperature for three days. The solution was then lyophilized, always leading to a pale-yellow viscous liquid. Proton nuclear magnetic resonance (^{1}H-NMR) spectra were recorded with a Bruker Avance II+ UltraShield^{TM} 400 Plus Ultra Long Hold NMR spectrometer at room temperature using D_2O as a solvent. Chemical shifts (δ) were reported in ppm and referenced relatively to the residual proton of the deuterated solvent. The Fourier transformed infrared spectra (FTIR) of lyophilized samples were recorded in KBr pellets using a PerkinElmer Spectrum Two spectrometer at the 4000-400 cm^{-1} range.

2.3. UV-Vis spectroscopy and photoluminescence studies

The obtained pale-yellow viscous liquids containing the oxidized PAMAM dendrimers were dissolved in ultrapure water, irradiated using UV light (366 nm) to collect the images of Figures 74 and E7 (see annex). UV-Vis spectroscopy studies in solution were performed in the range of 200-600 nm using a PerkinElmer Lambda 25 UV-Vis spectrometer. Photoluminescence (PL) studies in solution were done using a PerkinElmer LS 55 fluorescence spectrometer in the range 300-700 nm using a 10-mm-path quartz cell and excitation and emission slit widths set at 12 nm and 5 nm, respectively. Emission spectra were recorded using an excitation

wavelength of 380 nm (λ_{ex}), and excitation spectra were recorded, setting the emission wavelength at 450 nm (λ_{em}). Studies at different pH values were conducted in a universal buffer solution (6 g of citric acid, 3.9 g of monopotassium phosphate, 1.8 g of boric acid, and 5.3 g of diethyl-barbituric acid in 1 L of UPW) by adjusting the pH of solutions with HCl or NaOH 1M solutions. Relative quantum yields for the APS-treated PAMAM dendrimers were calculated using the single point method[361]. The following equation was used:

$$\mathbf{Q} = \boldsymbol{Q_R} \frac{\boldsymbol{I}}{\boldsymbol{I_R}} \frac{\boldsymbol{OD_R}}{\boldsymbol{OD}} \frac{\boldsymbol{n^2}}{\boldsymbol{n_R^2}} \quad (4)$$

where Q is the fluorescence quantum yield, *I* the integrated fluorescence intensity, *n* the refractive index of the solvent (water), and *OD* the optical density. The subscript *R* denotes the value for the reference, that is, for the fluorophore of known quantum yield. The reference fluorophore used was pyrene in cyclohexane, which presents a quantum yield of 32% (λ_{ex} = 317 nm)[362]. The concentration used for pyrene and APS-treated PAMAM dendrimers was $1x10^{-5}$M. The absorbance value used was the value at the wavelength of 380nm (the excitation wavelength used in fluorescence emission studies).

The diffuse reflectance of the lyophilized material was measured in the 250 – 500 nm spectral range using an Agilent Cary 5000 spectrophotometer equipped with an integrated sphere. The PL spectra of the lyophilized material were conducted using a 405 nm picosecond pulsed diode laser (Edinburgh Instruments EPL-405) with a typical pulse width of 80 ps. The emission spectra and the fluorescence decays were recorded using a fluorescence spectrometer with a single photon counting multichannel plate photomultiplier and dedicated acquisition software (Edinburgh Instruments LifeSpec II and F900 software). Fitting of the fluorescence decays to multi-exponential decay functions were performed using the reconvolution of the instrumental response function (IRF) of the equipment (Edinburgh Instruments FAST software).

2.4. Cytotoxicity evaluation

CAL-72, a human osteosarcoma cell line, and NIH 3T3, a mouse fibroblast cell line, were purchased from DSMZ. Both cell lines were cultured in Dulbecco's Modified Eagle's medium (D-MEM) containing 1% (v/v) antibiotic-antimycotic 100x solution (AA, containing penicillin, streptomycin, and amphotericin B) and 10% (v/v) foetal bovine serum (FBS), at 37°C, in a humidified atmosphere with 5% carbon dioxide. For CAL-72 cells, the medium was also supplemented with 1% (v/v) insulin-transferrin-selenium 100x solution (ITS) and 1% (v/v) L-glutamine solution 100x.

Both cell lines were cultured in 48-well plates at a seeding density of 10 x 103 cells per well for cell culture experiments. After 24 h, the medium was replaced with a fresh one, and the cells were incubated with the APS-treated PAMAM dendrimers (G3, G4, and G5) prepared in PBS buffer (pH 7.4) within a range of concentrations 0.25 – 20 µM. Pristine PAMAM dendrimer solutions were used as controls. The cytotoxicity of APS-treated dendrimers was indirectly evaluated by measuring the metabolic activity of cells through the

resazurin reduction assay. After a 48 h incubation period, the cell culture medium was replaced with a new medium containing resazurin at a concentration of 0.1 mg/mL, and cells were further incubated for more 3 h at 37°C. Afterwards, aliquots of cell medium were transferred to the wells of 96-well opaque plates, and the fluorescence of resorufin was measured using a PerkinElmer VICTOR³™ microplate reader (λ_{ex} = 530 nm, λ_{em} = 590 nm). The metabolic activity is presented as a percentage of the control (cells culture in the absence of dendrimers). The results are expressed as the mean ± SD of two independent experiments with three replicas each.

2.5. Hematoxicity evaluation

Hematoxicity assays were carried out using fresh and healthy human blood. For the determination of the total hemoglobin concentration in the original blood, a 250-fold dilution of blood was prepared in cyanmethemoglobin reagent, which is also called C reagent (20 mL of blood in 5 mL of C reagent). The C reagent (50 mg potassium ferricyanide, 12.5 mg potassium cyanide, and 35 mg potassium dihydrogen phosphate in 250 mL of distilled water) was prepared in an amber bottle with 250 ml Triton-X, and its pH was adjusted to 7.4. A standard curve for hemoglobin was then established using hemoglobin from bovine blood (see annex Figure B1). For that purpose, a stock solution of the protein (1.5 mg/mL) was prepared using C reagent as the solvent. From this stock solution, serial dilutions were performed to obtain standards of known concentration (0.20, 0.37, 0.54, 0.7, 0.88, 1.05, 1.22, and 1.39 mg/mL), and the absorbance was measured at 550 nm. The C reagent was used as the blank. The purity of the commercial hemoglobin was very good, as assessed by the ratio of absorbance values at 550 nm and 405 nm. The absorbance of the diluted solution of blood was then measured, and its concentration was determined. For the hemotoxicity evaluation of the oxidized dendrimers, the compounds were dissolved in distilled water (30 µM) and diluted to concentrations of 0.1, 1, and 5 µM using PBS solution (Mg^{2+}/Ca^{2+} free). Then, 1 mL of a 10% (v/v) blood solution was prepared in PBS (Mg^{2+}/Ca^{2+} free), and 10 µl of this solution was placed into microcentrifuge tubes, one for each compound and concentration to test, including a positive and negative control. Then, the blood solution was added to 70 µl of each sample and 70 µl of water or PBS for the positive and negative controls, respectively, and incubated for 3 h at 37ºC. Following the incubation period, the mixture was centrifuged at 3800 rpm for 10 min. Then, 40 µl of each supernatant was transferred to 96 well plates, and 160 µl of the C reagent was added. The absorbance values of the supernatants were measured at 550 nm in the microplate reader, and the prepared standard curve was applied to determine their hemoglobin concentrations. The same procedure was performed for the pristine PAMAM dendrimers. Considering the dilutions made throughout the assay, the percentage of hemolysis was then calculated for each situation from the ratio between the hemoglobin concentration in the sample's supernatant and the total value that was initially present multiplied by 100. The results are presented as mean ± SD for three independent assays.

2.6. Fluorescence microscopy studies

The human bone osteosarcoma epithelial (U2OS) cell line was cultured in Dulbecco's modified Eagle's medium (DMEM, high glucose, GlutaMAX) with 10% (v/v) FBS and 1% (v/v) penicillin-streptomycin solution under standard cell culture conditions. Cells were grown at 37°C in a 5% carbon dioxide incubator till 50–80% confluence before being used in the experiments. Cells were then incubated with the APS-treated PAMAM dendrimer G4 for 24 h at 2 μM. Cell culture images were collected using a Cell Observer fluorescence microscope (Zeiss) with a 40x objective, equipped with a black and white photographic camera (Zeiss Axiocam 503 mono) and Zen software image acquisition.

2.7. Encapsulation of DOX

APS-treated PAMAM G4 (10 mg, 0.0007 mmol) was dissolved in 1.5 mL of distilled water. DOX (10 eq. mol) in 300 μL of MeOH and 5μL of triethylamine to neutralize the HCl. Then, the DOX solution was added dropwise into the aqueous solution of APS-treated PAMAM dendrimer G4 and vigorously stirred overnight in the dark. The APS-treated PAMAM dendrimer G4/DOX solution was centrifuged at 7000 rpm for 10 min to remove the free DOX. Then, the precipitated was collected and dissolved in MeOH for UV analysis using a PerkinElmer Lambda 25 UV-Vis spectrometer and the supernatant lyophilized to obtain the APS-treated PAMAM G4/DOX. The absorbance at 483nm was used to calculate the percentage of encapsulated DOX. The same procedure was performed for the non-treated amine-terminated PAMAM dendrimer G4.

2.8. *In vitro* drug release

The DOX release was carried out in PBS (pH 5 and pH 7.4) at 37ºC. APS-treated PAMAM G4/DOX, non-treated PAMAM dendrimer G4, and free DOX were dissolved in 300 μL of UPW and sealed in a mini dialysis device (MWCO 2000 Da). The dialysis device was immersed in 10 mL of PBS at pH 5 and 7.4, respectively. The compounds were weighed according to the DOX amount (2.5 μg). At different time intervals, it was taken out 100 μl of the dialysate to a 96-well opaque plate and replaced with 100 μl of PBS at pH 5 and 7.4. The absorbance of DOX releases was measured using a PerkinElmer VICTOR³™ microplate reader and then determined through a calibration curve for each pH value of PBS (5 and 7.4).

3. Results and discussion

3.1. Structural characterization of dendrimers

Three different generations of PAMAM dendrimers with amine terminal groups (G3, G4, and G5) were oxidized using ammonium persulfate and characterized by ^{1}H-NMR. Comparing each spectrum obtained with the corresponding spectrum of the pristine dendrimer, it is possible to observe a downfield shift of the main NMR signals for the APS-treated PAMAM dendrimers (see Figures E1-E3 in the annex, as well as Table E1).

In fact, it is known that beyond hydrogen peroxide that decomposes originating oxygen, APS hydrolysis also gives rise to other chemical species in solution, such as permonosulfuric acid, peroxymonosulfate, and sulfuric acid[363]. Although the effect of APS on PAMAM dendrimers is still not very well understood, there is evidence that these species confer an acidic environment and cause the protonation of dendrimer's amine groups[121]. Our ^{1}H-NMR results support this finding since the protonated amines will act as electron-withdrawing agents and cause the downfield shift of the signals arising from the protons in the vicinity of both the primary and the tertiary amines. Imae *et al.* also reported the downfield shift of the signal of the methylene protons adjacent to the peripheral amines[119] for APS-treated dendrimers. In our case, a deshielding of the protons surrounding the tertiary amines was observed too. Additionally, the strength of hydrogen bonds between the oxygen in the -C=O moiety and the proton in the -NH moiety increases under acidic conditions, which further contributes to proton deshielding[121]. This behavior was similar for all the tested dendrimer's generations.

The amine-terminated PAMAM dendrimers and APS-treated ones were also studied by FTIR (see the annex, Figures E4 to E6). The spectra of all three generations of pristine dendrimers show the characteristic bands of the amide group (–CONH-)[121,364–366]. The amide A band due to N-H stretching vibration (very sensitive to the strength of hydrogen bonds) appears at 3200-3300 cm^{-1}. Amide B, an overtone of amide II, can be seen around 3080 cm^{-1}. Amide I, an intense band mainly associated with the C=O stretching vibration, arises near 1635 cm^{-1}. Amide II band, mainly resulting from in-plane C-N-H bending and C-N stretching, is also evident near 1550 cm^{-1}. Other amide-associated bands (from III to VI) are also present in the spectra, although more difficult to be analyzed. Methylene groups bands appear at around 2945cm^{-1} (asymmetric C-H methylene stretching), 2850 cm^{-1} (symmetric C-H methylene stretching), and 1435-65 cm^{-1} (H-C-H scissoring and asymmetric deformations). Shoulders at near 1060 cm^{-1} reflect the -C-N stretching band for tertiary amines. Two bands from skeletal C-C stretching at 1130-1150 cm^{-1} can also be seen in the spectra. The primary amines present at the surface of dendrimers should absorb radiation in the region 3250-3400 cm^{-1} (due to two modes of N–H stretching), and the correspondent bands appear overlapped with amide A band and, possibly, with bands related to the presence of traces of water.

The APS treatment has a strong impact on the FTIR spectra of dendrimers, which includes the effect of the generated acidic environment that results in amine protonation, as well as the presence of sulfur-containing chemical species produced during APS hydrolysis. Indeed, Govindachetty Saravanan and Hideki Abe[121] showed by XPS analysis that SO_4^{2-} (sulfur VI) and $S_2O_3^{2-}$/S^{2-} (sulfur II) ions are present in PAMAM dendrimers with hydroxyl termini after APS treatment. These are stable ions that end up interacting with the protonated amine groups. Our results with PAMAM dendrimers with amine termini are generally in line with this work. A broadband is evident above 2400 cm^{-1}, resulting from the overlap of several signals, including those from protonated amines (ammonium groups). Another broadband appears around 1105 cm^{-1} due to the overlapping of the -C-N stretching band of tertiary amines, the bands from skeletal C-C stretching, and also the bands related with the presence of sulfur species (namely the SO_4^{2-} that usually presents a band correspondent to asymmetric stretching around 1090 cm^{-1}). After the oxidative treatment, a sharp band at near 615 cm^{-1} is also revealed, which can be assigned to certain modes of vibration of the amide group (like amide VI band) or,

most probably, to the presence of SO_4^{2-} since this ion shows signals near this frequency caused by out-of-plane bending vibration[367]. The amide I band, which is highly sensitive to small variations in hydrogen bonding, shifted for higher frequencies (from around 1635 cm^{-1} to 1660 cm^{-1}), whereas the signals of methylene groups became weaker. These findings are consistent with a more acidic environment conferred by APS treatment.

3.2. UV-Vis spectroscopy studies

Figure 70 shows the absorbance spectra of pristine and APS-treated PAMAM dendrimers (generations 3, 4, and 5) in aqueous solution. After the oxidative treatment, the slight shoulder that appeared around 280-290 nm in the pristine dendrimers (see Figure 70d that shows the spectra using an expanded scale) became much more intense (a band is clearly seen). Richard Crooks *et al.*[368] performed studies with pristine amine- and hydroxyl-terminated PAMAM dendrimers and concluded that this band is related to radiation absorption by the tertiary amines present in the interior of the dendritic structure. They showed that the intensity of this band increased with the rising in pH and that the process was reversible. Our results with pristine dendrimers also reveal the presence of this band, which increases in intensity with dendrimer's generation, that is, increases with the number of tertiary amines present in the dendrimer's scaffold. However, we show that the same band appears in the spectra of APS-treated PAMAM dendrimers with intensity values of several orders of magnitude higher than those observed in pristine dendrimers (Figure 70e) despite the protonation of tertiary amines in the interior of the dendrimers. In our experiments, both the pristine and the oxidized dendrimers display an absorbance band with a maximum at 280-290 nm, in contrast with the observations made by Abe et al. that reported a red-shift of this band to 360 nm after APS treatment of dendrimers with hydroxyl surface groups[121].

In should, however, be noticed that the absorption spectra of pristine dendrimers reveal the presence of at least two more bands in the range 300-400 nm and 400-500 nm (although having a very low intensity). These bands may also exist in the spectra of APS-treated PAMAM dendrimers through camouflaged by the 280-290 nm band of higher intensity.

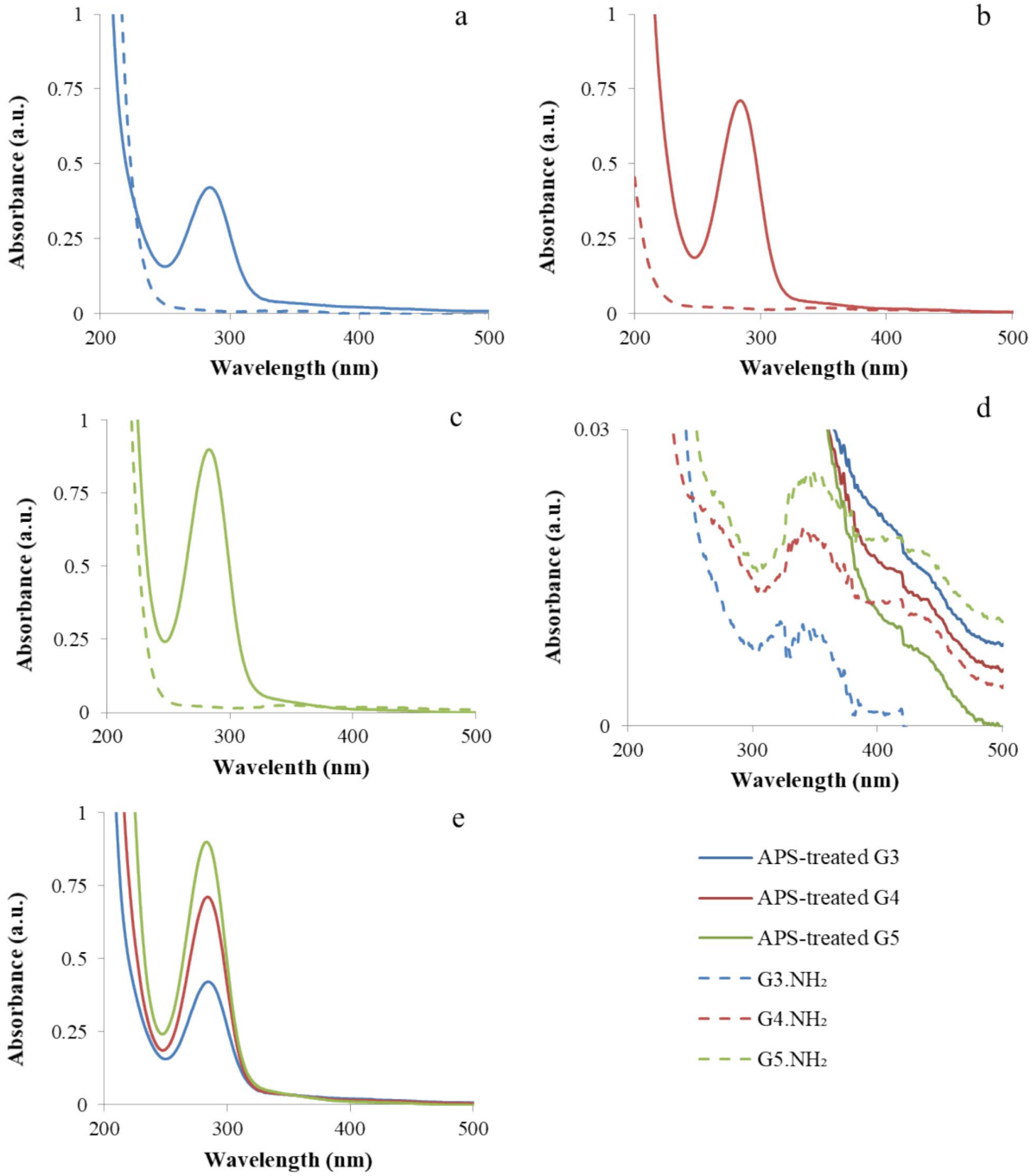

Figure 70: Absorption spectra of pristine and APS-treated PAMAM dendrimers for generations (a) G3, (b) G4, and (c) G5. (d) Absorption spectra are shown on an expanded scale. (e) Comparison of absorption spectra among the three generations of APS-treated PAMAM dendrimers. Spectra were recorded at a concentration of 1x 10^{-5} M in UPW.

The effect of pH on the absorbance of generations 3, 4, and 5 of APS-treated PAMAM dendrimers was then studied by recording absorption spectra in a buffer having the same chemical composition but adjusted to different pH values (Figure 71). In general, the intensity of the band 280-290 nm increases with dendrimer's generation and with the pH value.

When absorbance's intensity at 284 nm is plotted against pH, it is clear an increase after pH≈ 3. At very low pH, for high levels of dendrimer's protonation, the absorbance values are identical for all generations. As the pH rises, the level of dendrimer's protonation is different for each generation, and absorbance values become distinct among them. The absorbance is higher for generation 5, followed by generation 4 and generation 3. Indeed, our results show that the dependency of absorbance at 284 nm on the solution's pH for APS-treated PAMAM dendrimers is identical to what Richard Crooks *et al.* reported for pristine PAMAM dendrimers[368] with both amine or hydroxyl surface termini. Like Richard Crooks *et al*., we had opposite results to Degang Fu *et al.*[369] that made UV-Vis experiments with sectorial PAMAM dendrimers with amine surface groups.

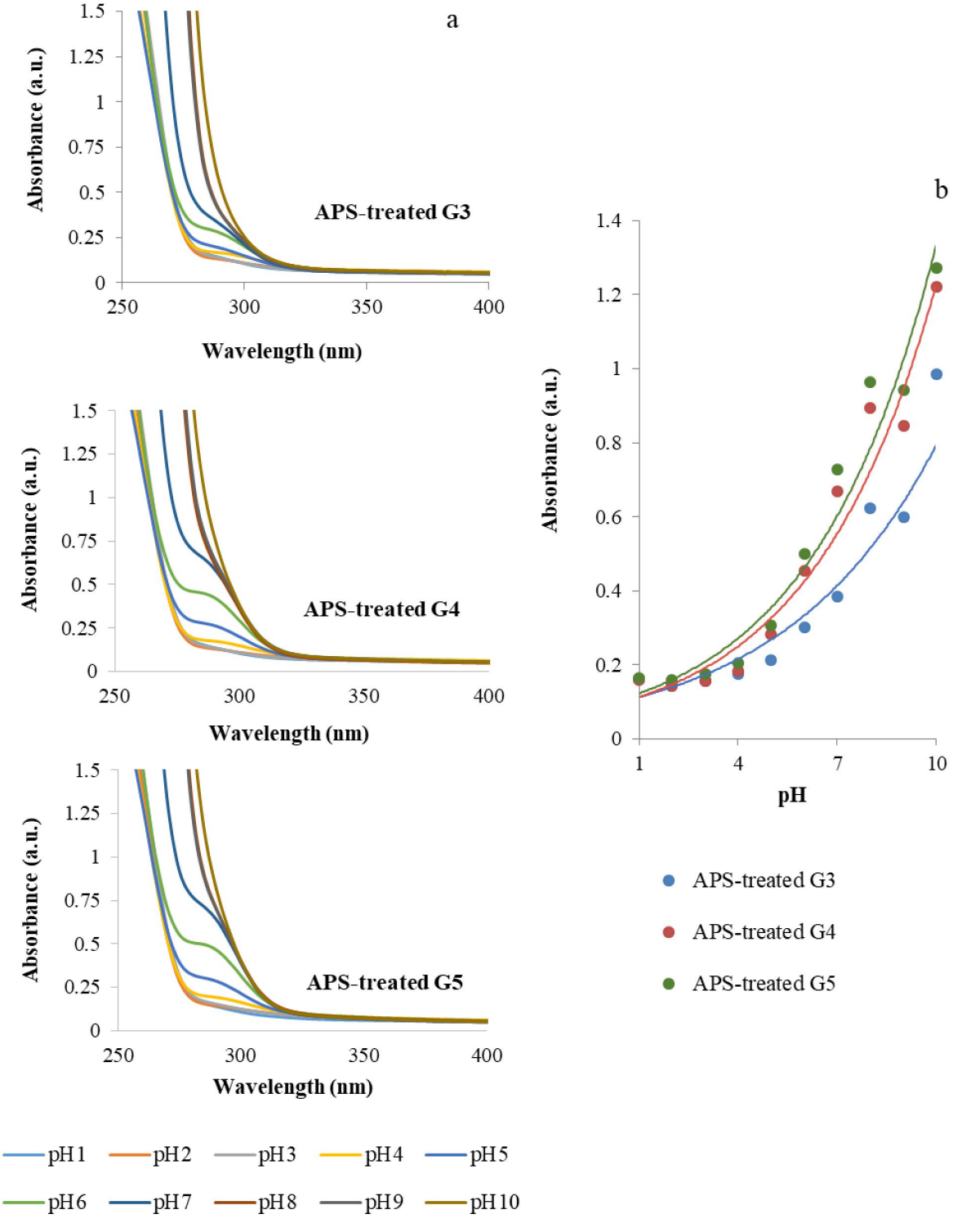

Figure 71: (a) Absorption spectra of APS-treated PAMAM dendrimers recorded in a buffer solution at a concentration of 1 x 10^{-7} M and different pH values; (b) Comparison of absorbance values at 284 nm among the three generations of APS-treated PAMAM dendrimers.

3.3. Photoluminescence studies in solution

The pale-yellow viscous liquids obtained after the synthesis of the APS-treated dendrimers were dissolved in UPW at a concentration of $1x10^{-3}$ M. After irradiation under UV light at 366 nm, a blue luminescence could be observed. Figure 72 qualitatively shows the extent of fluorescence intensity for G3, G4, and G5 dendrimer aqueous solutions prepared at the same concentration (G3>G4>G5). An evident difference in terms of luminescence was clearly seen among the generations (see also the annex, Figure E7).

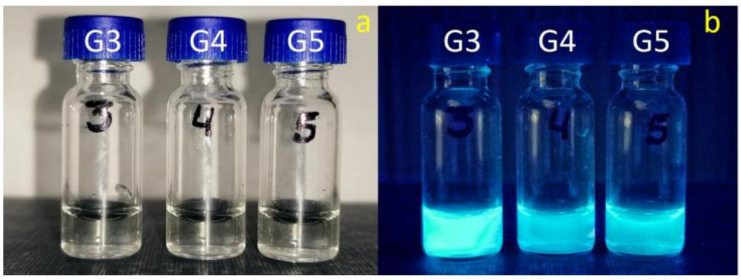

Figure 72: APS-treated PAMAM dendrimers (G3-G5) with a concentration of 1 x 10^{-3} M in UPW without (a) and under UV irradiation (366 nm) (b).

Figure 73 shows the excitation and emission fluorescence spectra of pristine and APS-treated PAMAM dendrimers (generations 3, 4, and 5) in aqueous solution. After excitation at 380 nm, an emission band can be observed for both cases in the blue spectral region with intensity values much higher for the APS-treated dendrimers than for the correspondent pristine ones. Although the excitation spectra revealed another band at *ca.* 250 nm (see annex Figure E8), fluorescence emission intensities were higher when 380 nm was used as excitation wavelength. Interestingly, the excitation spectra show a very weak signal at *ca.* 280-290 nm, which corresponds to the dominant absorption band in the UV-vis spectra. So, the blue fluorescence emitted by the APS-treated dendrimers resulted from excitation in the range 300-425 nm (as mentioned above, radiation absorption in this wavelength range is clearly observable in the UV-vis spectra of pristine dendrimers and is probably hidden by the intense 280-290 nm absorption band in the UV-vis spectra of APS-treated dendrimers).

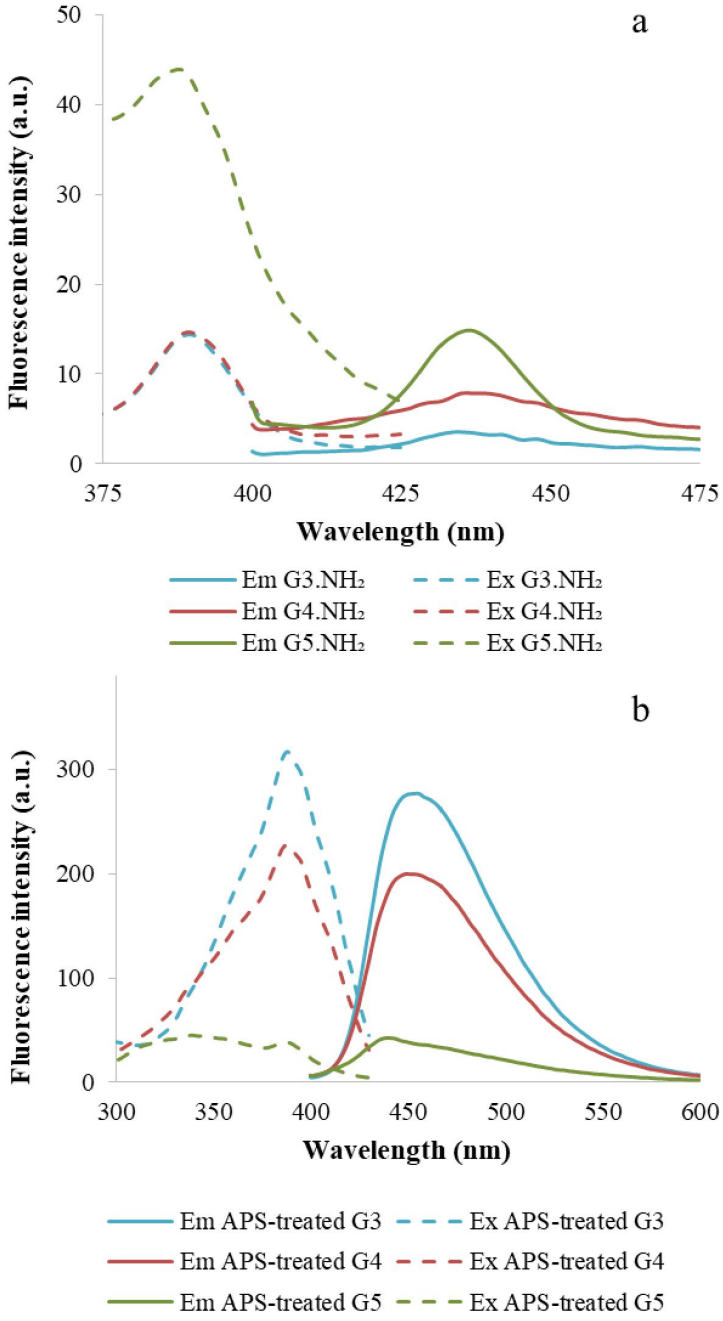

Figure 73: Emission (λ_{ex} = 380 nm) and excitation (λ_{em} = 450 nm) spectra of pristine (a) and APS-treated (b) PAMAM dendrimers. Spectra were recorded at a concentration of 1 x 10^{-5} M in UPW.

The maximum wavelength of fluorescence in the emission spectra had a red-shift from around 437 nm in the pristine dendrimer's spectra to about 450 nm in APS-treated dendrimer's spectra. Moreover, whereas fluorescence intensity increased with generation in pristine dendrimers (Figure 73a), it had an opposite trend in the case of APS-treated dendrimers (Figure 73b). However, it must be noticed that these spectra were all recorded in water. In fact, we could later conclude that the emission of fluorescence by APS-treated dendrimers

was strongly pH-dependent, a characteristic already reported for pristine PAMAM dendrimers[117]. When spectra were recorded in buffer solutions of different pH values (Figure 74a), it was evident that fluorescence intensity was much higher at low pH (Figure 74b), highlighting the role of protonation in the fluorescence behavior of APS-treated dendrimers.

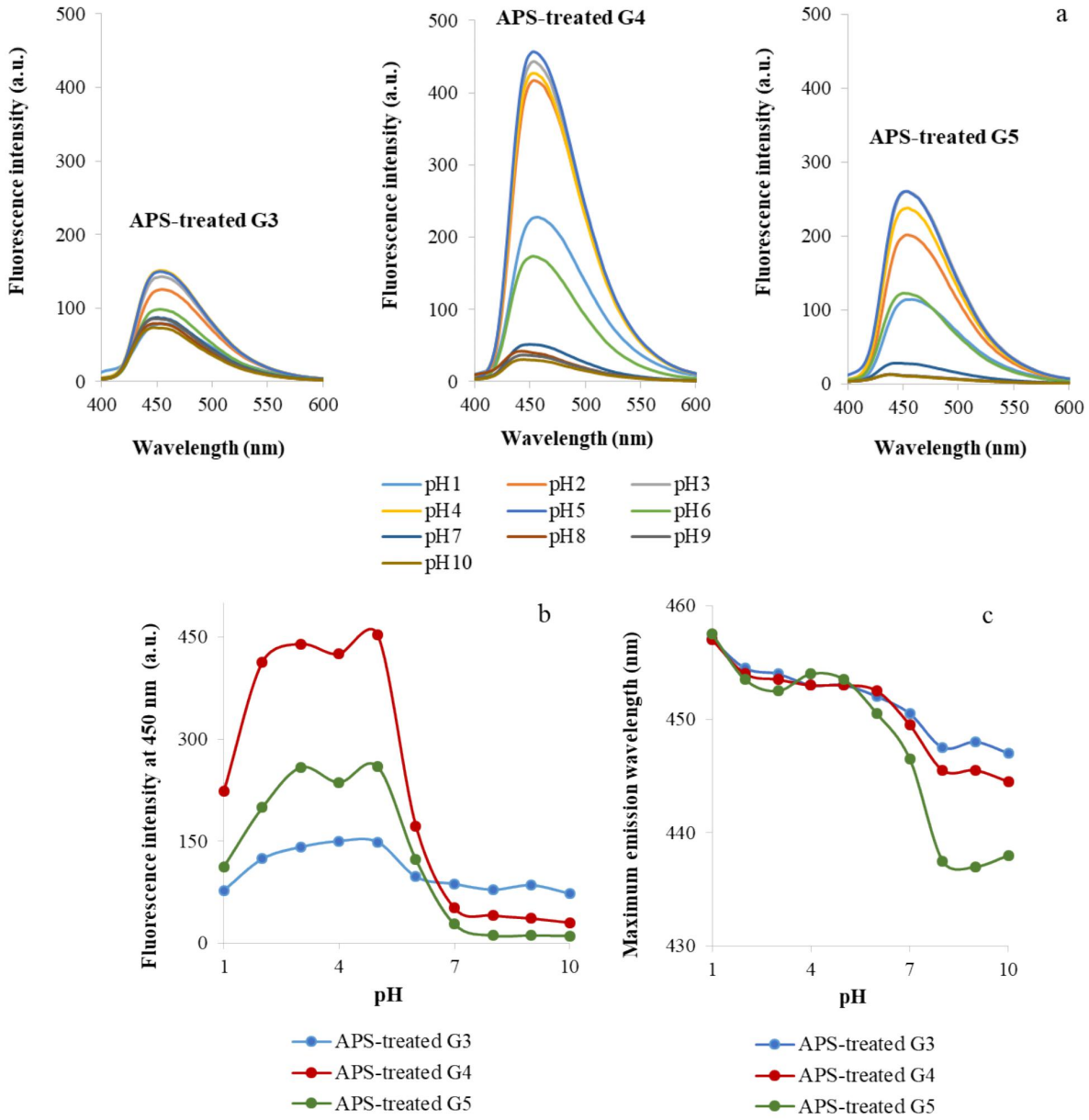

Figure 74: Emission (λ_{ex} = 380 nm) spectra of generation 3, 4 and 5 APS-treated PAMAM dendrimers recorded in a buffer solution at a concentration of 1 x 10^{-6} M and different pH values; (b) Effect of pH on fluorescence intensity at 450 nm; (c) Effect of pH on the maximum wavelength of fluorescence emission.

For all three generations of APS-treated dendrimers, fluorescence intensity significantly increases below pH 7, has maximum values in the 3-5 pH range, and then decreases again at very low pH. Unexpectedly, at a pH lower than 7, generation 4 APS-treated PAMAM dendrimers were the most emissive, followed by generation 5 and only after by generation 3. Indeed, the rise in fluorescence intensity when lowering the pH was much more marked for the highest generations than for generation 3. Another information that comes out from these studies is that the maximum wavelength of fluorescence emission increases with an increase in the concentration of H^+ in solution (pH decrease), as depicted in Figure 74c. Moreover, there is a pronounced jump in this value when decreasing the pH from 7-8 to 6, similarly to what happens with the fluorescence intensities. Interestingly, the pKa of the tertiary amines (around 6.3[368]) is included within this interval of pH. The maximum wavelength of fluorescence emission remains constant in the range of pH 2-6 (low emission zone). These results show that protonation of the tertiary amine groups in APS-treated dendrimers strongly affects fluorescence emission. Indeed, protonation of the tertiary amine groups in the interior of the dendritic structure has been associated with molecular conformational and polarity changes[370]. Moreover, as recognized by other researchers, it will result in high internal repulsion forces among dendrimer branches, thus making the overall structure more rigid[117,121]. Rigidity is also promoted by the increase in the strength of the hydrogen bonds that occurs in an acidic environment[117,371]. In summary, our photoluminescence studies performed with the APS-treated dendrimers in solution support the ideas underlying the NTIL phenomenon described by Donald Tomalia *et al.*[115]. Fluorescence intensity not only depends on the number of HASLs confined in the dendrimer scaffold (that is, on dendrimer generation) but is also enhanced by the scaffold rigidification that occurs as a consequence of APS treatment. Results obtained for the three different generations of dendrimers in Figure 74 should then be a compromise between these two parameters. For example, although APS-treated G4 dendrimers have a lower number of HASLs than their G5 counterparts, they should adopt a more rigid conformation at low pH conditions that promote fluorescence emission. Also, one should notice that, independently of the generation, the emission spectra were not symmetrical. Regarding this observation, there are three possibilities: different HASLs inside the dendrimer structure may exist emitting at different wavelengths; the same HASLs may exist in multiple chemical environments (at least more than one) that modulate fluorescence emission; and, finally, both situations may coexist. In fact, a study using quantum chemical theory methods concluded that there are two potential emitting moieties in pristine PAMAM dendrimers: the imidic acid resonance structure from amide, which formation is promoted at low pH values; and the tertiary ammonium groups formed upon protonation of tertiary amines[365]. Calculations assuming the dendrimers in the gas phase showed that these species could theoretically emit fluorescence at 308 nm (the imidic acid) and 370 nm (the tertiary ammonium group)[365]. Also, a recent work devoted to the study of fluorescence quenching in pristine PAMAM dendrimers points out that there are two distinct fluorescent moieties in their structure with the emission maxima separated by 40 nm[372]. So, it is reasonable to assume that the amide and tertiary amine groups that exist in the dendrimer's scaffold constitute two distinct HASLs with photoluminescence properties that are dependent on the pH environment that is in turn strongly affected by the APS treatment. However, it seems that the APS treatment does not exert its effect to the same extent in both

HASLs as it causes a red shift in the maximum wavelength of fluorescence. In other words, it increases the number of HASLs that emit at a higher wavelength, which, according to the literature[365], should be the tertiary ammonium groups.

The quantum yield of a fluorophore is an important parameter as it informs about the ratio of photons emitted to photons absorbed; that is, it is a measure of the efficiency of the process. Quantum yields were determined for PAMAM dendrimers after the oxidative treatment using pyrene as the reference. Generation 3 APS-treated PAMAM dendrimers were the ones with the highest quantum yield (75%), followed by generation 4 (63%) and generation 5 (15%). Interestingly, Klajnert-Maculewicz *et al.* also find out a decrease in quantum yield with an increase in the generation for pyrrolidone-terminated PAMAM dendrimers[335].

3.4. Photoluminescence studies in lyophilized samples

The absorption spectra of the dendrimers in the lyophilized form were obtained from diffuse reflectance measurements. The results are given in Figure 75.

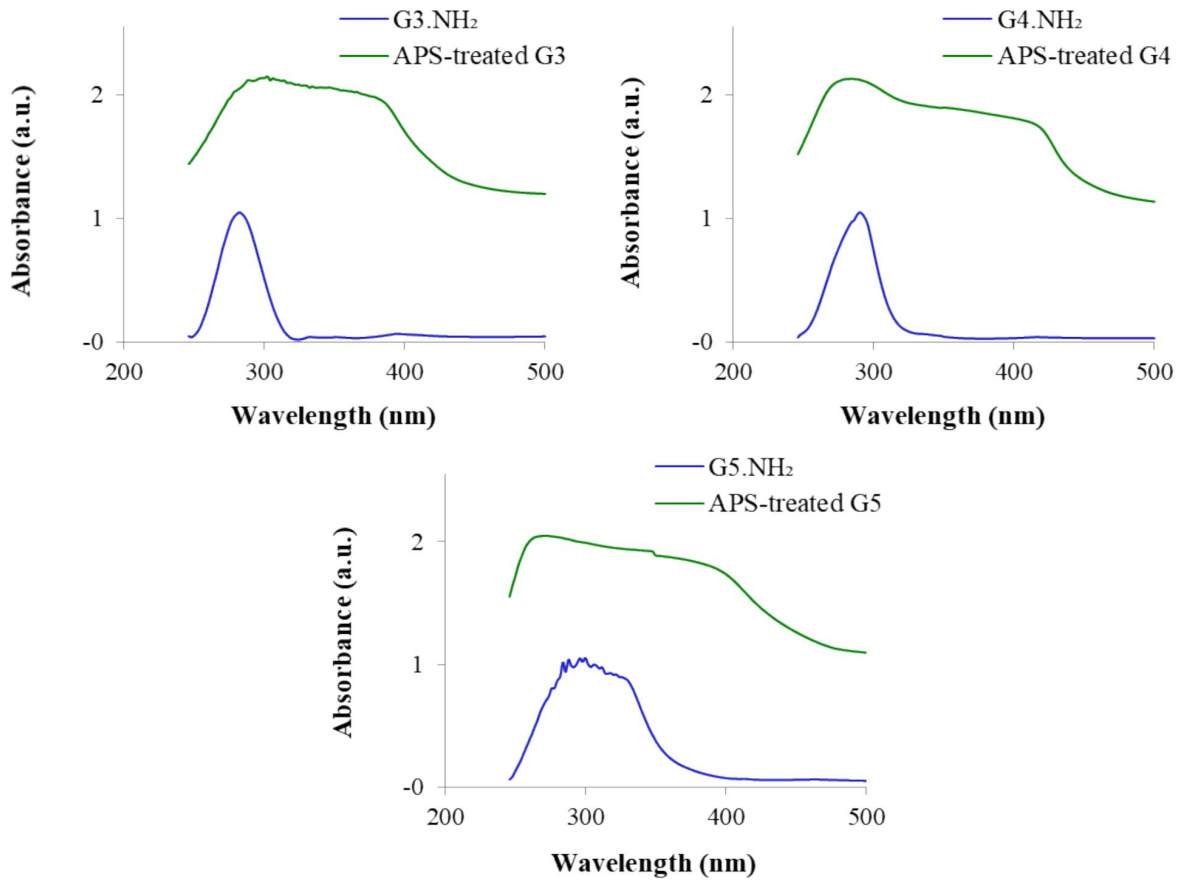

Figure 75: Normalized absorption spectra of pristine PAMAM dendrimers and APS-treated PAMAM dendrimers (G3, G4, and G5) in the lyophilized form.

The absorption spectrum of the G3 pristine PAMAM dendrimers is formed by a band centered at about 280 nm, which is in line with what was observed in the previous UV-vis spectroscopy experiments done in solution. A shoulder appears at the low energy side of the absorption band for pristine G4 and G5 dendrimers, which evidences the effect of the additional shells of the dendrimer on the absorption centers as the generation increases (in fact, very low-intensity absorbance bands in the range 300-400 nm and 400-500 nm were also present in the UV-vis spectra of pristine dendrimers in solution – see Figure 70d). Also, here the APS treatment has a substantial impact on the absorption spectrum. An intense absorption band appears in the 300-400 nm spectral range, which overlaps the one centered at 280 nm. As mentioned before, correspondent absorption bands may be present in the UV-vis spectra of APS-treated dendrimers recorded in solution although camouflaged by the dominant 280-290 nm band (Figure 70d). However, the experiments with the dendrimers in the lyophilized form clearly evidence the existence of absorption at wavelengths above 300 nm.

The emission spectra of the APS-treated and pristine G3, G4, and G5 PAMAM dendrimers were recorded under excitation at 405 nm (Figure 76). In the case of the pristine dendrimers, the emission is formed by two overlapping bands. One is centered at about 445 nm, and the second around 475-480 nm. The relative intensity of the second band increases as the generation of the PAMAM dendrimer is higher. The APS-treated dendrimers present emission spectra formed by the same two overlapping bands, but the relative weight of the second band is more significant. These results are compatible with the hypothesis of the coexistence of more than one type of HASLs emitting in the dendrimer structure and that the APS treatment does not affect the fluorescence intensity of both in the same manner.

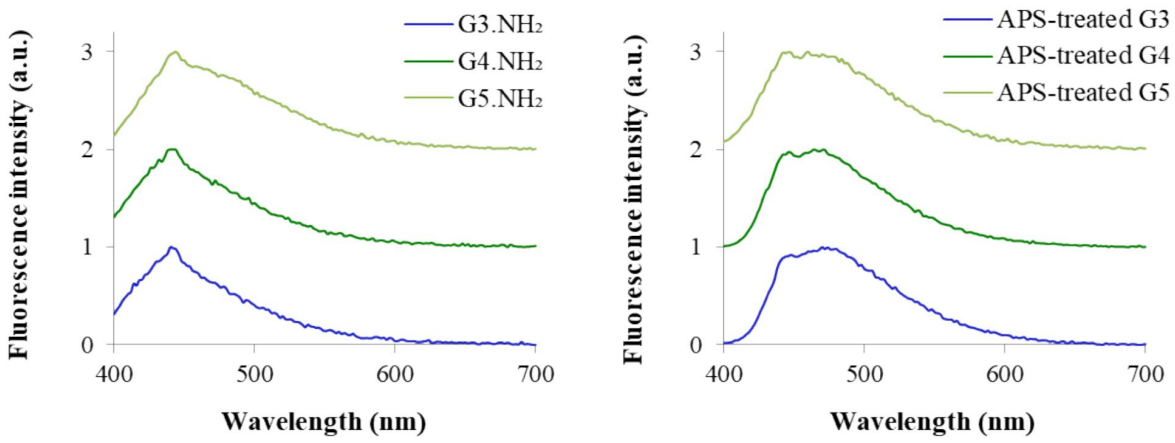

Figure 76: Normalized emission spectra of pristine PAMAM dendrimers and APS-treated PAMAM dendrimers (G3, G4, and G5) in the lyophilized form (λ_{ex} = 405 nm).

A quantitative comparison of the emission intensities in the lyophilized samples remains challenging since differences in the quantity and compactness of the sample directly influence the result. However, one may qualitatively say that emission intensities of the same order of magnitude were obtained in this case for the

APS-treated and the pristine PAMAM dendrimers. This result is quite different from the one observed in the aqueous solution, where the APS-treated dendrimers showed an emission intensity several orders of magnitude higher than the pristine ones (Figure 73). To investigate this finding, time-resolved fluorescence measurements were conducted in G3, G4, and G5 pristine and APS-treated PAMAM dendrimers.

3.5. Time-resolved fluorescence experiments

The decays of the fluorescence of G3, G4, and G5 pristine and APS-treated PAMAM dendrimers were recorded at the maximum of the emission bands when the excitation was tuned at 405 nm. Both lyophilized samples and water solutions at a concentration of 2 x 10^{-5} M were tested and compared (Figure 77). Based on the previous experiments and assuming the existence of two HASLs in the dendrimer's structure, the decay curves were fitted to a double exponential decay equation:

$$I(t) = A_1 e^{-t/\tau_1} + A_2 e^{-t/\tau_2} \quad (5)$$

where 1 and 2 are the decay constants of the fast and slow components, respectively. A_1 and A_2 represent the pre-exponential factors that should correspond to the fraction of each HASLs. An average lifetime (τ_a) is then defined by the equation[361]:

$$< \tau_{av} >= \frac{A_1\tau_1^2 + A_2\tau_2^2}{A_1\tau_1 + A_2\tau_2} \quad . \quad (6)$$

The decay curves were fitted to equation (5), taking into account the reconvolution of the IRF of the experimental setup. Table 24 shows the pre-exponential factors, 1 and 2, and the average lifetime obtained from the fitting procedure. In solution and for the three dendrimers generations, the decay of the APS-treated dendrimers is clearly longer than that of the non-treated precursors, corresponding to higher average lifetimes. When analyzing the pre-exponential factors, one can see that there is a predominance (99-100%) of very fast emitting components (0.01-0.02 ns) in the pristine dendrimers, whereas increased higher average lifetimes (4.92-5.91 ns) are observed in their APS treated counterparts.

Table 24: Fitting parameters and the average lifetime of G3, G4, and G5 pristine and APS-treated PAMAM dendrimers in aqueous solution and in lyophilized form.

	A_1	τ_1 (ns)	A_2	τ_2 (ns)	τ_{av} (ns)
Lyophilized					
APS-treated G3	0.96	0.83	0.04	5.15	1.78
APS-treated G4	0.64	1.52	0.36	6.68	5.19
APS-treated G5	0.70	1.47	0.30	6.99	5.16
$G3.NH_2$	0.89	1.13	0.11	5.30	2.68
$G4.NH_2$	0.82	1.38	0.18	5.58	3.34
$G5.NH_2$	0.86	1.17	0.14	5.48	3.04
Solution					
APS-treated G3	0.81	0.70	0.19	7.05	5.15
APS-treated G4	0.69	1.12	0.31	7.50	5.91
APS-treated G5	0.82	0.93	0.18	7.27	4.92
$G3.NH_2$	0.9999	0.01	0.0001	3.16	0.01
$G4.NH_2$	0.9999	0.01	0.0001	2.68	0.01
$G5.NH_2$	0.999	0.02	0.001	2.8	0.04

The average lifetimes in APS-treated dendrimers result from a combination of fast emitting components (0.70-1.12 ns) with slow emitting ones (7.05-7.50 ns) in a proportion of 69-82% and 18-31%, respectively. These lifetime results agree with the higher emission intensity observed in the APS-treated dendrimers in aqueous solution compared to the pristine ones (Figure 73). Assuming that the HASLs in dendrimers are the imidic acid and the tertiary ammonium groups and based on the previous results and data from literature[365], we propose that the tertiary ammonium groups are the HASLs with longer fluorescence lifetimes. In the lyophilized form, except for G3 PAMAM dendrimers, APS-treated dendrimers still show higher average lifetimes than pristine ones (≈5 ns vs. ≈3 ns), although belonging to the same order of magnitude. This explains the observed qualitatively similar fluorescence intensities for both cases. In APS-treated dendrimers, the characteristics of both slow and fast emitting HASLs are very similar when comparing the results of the fitting parameters obtained for lyophilized and solution samples. Nevertheless, the most notable finding in these studies is when the lyophilized samples of pristine dendrimers are compared with the corresponding solution samples. Much longer average lifetimes (2.68-3.34 ns) are observed in the lyophilized form than in solution (0.01-0.04 ns). This can be explained in light of the NTIL theory that states that NTIL emissions can be enhanced by HASLs aggregation[115]. This property is also observable in many other systems and gives rise to higher fluorescence intensities[115,373]. The mechanism of aggregation-induced emission is very well elucidated by Ben Tang et al. in an excellent review[373] and maybe here applied for the pristine dendrimers. In solution, the dynamic intramolecular motions in dendrimers extinguish their excited-state energy, whereas, in the lyophilized/aggregated form, the restriction of these motions allows the excited state energy to be released by a radiative pathway. This same mechanism can explain why scaffold rigidification can also result in an increase in fluorescence intensity. Most likely, this phenomenon does not occur with APS-treated dendrimers since they

are protonated, and the molecules are less aggregated in the lyophilized sample because of repulsion forces existing among them.

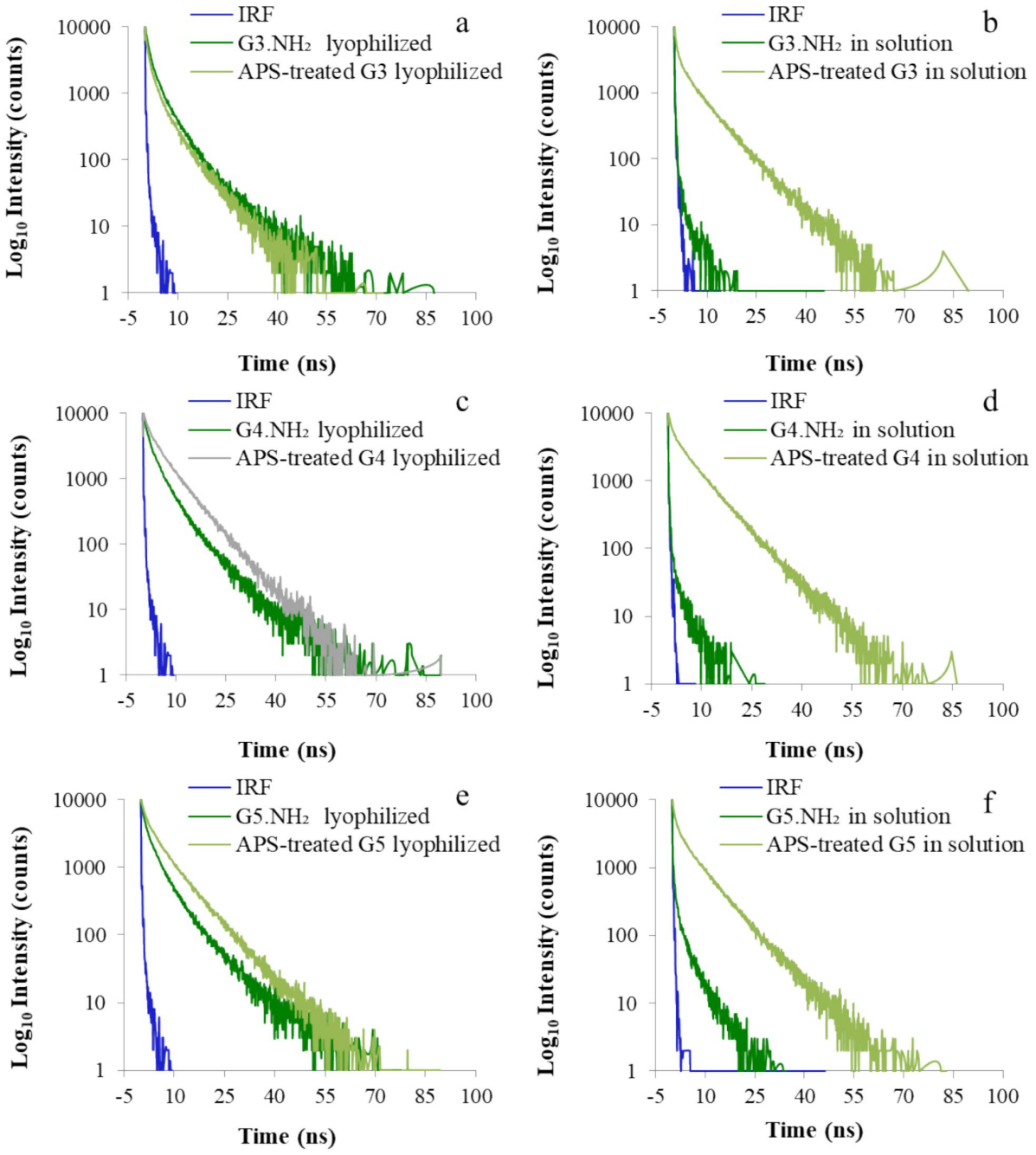

Figure 77: Decay of fluorescence of pristine and APS-treated (a) G3, (c) G4, (e) G5 PAMAM dendrimers in lyophilized form and (d) G3, (e) G4; (f) G5 PAMAM dendrimers in aqueous solution.

3.6. *In vitro* cytotoxicity studies

For the application of dendrimers as bionanomaterials, it is very important to assure that they will not compromise cell viability. In fact, regarding PAMAM dendrimers, it is well known that their toxicity behavior is dependent on the generation, concentration, and type of terminal groups. PAMAM dendrimers with amine termini can be particularly toxic due to their high positive surface charge under physiological conditions[83,105]. As such, we aimed to investigate the cytotoxicity of the APS-treated PAMAM dendrimers and compare it with that of the pristine dendrimers.

The cytotoxicity of dendrimers was then evaluated *in vitro* using NIH 3T3 (mouse fibroblasts) and CAL-72 (human osteosarcoma cells) cell lines. The first cell line was used as a model of normal cells, and the second one as a model of cancer cells as dendrimers are mostly being studied as drug delivery vehicles for cancer-related applications. A metabolic activity assay (the resazurin reduction assay) was used to assess cell viability, and results were obtained after 48 h in culture for different dendrimer concentrations as shown in Figure E9 and E10 in the annex (results are expressed as a percentage of the metabolic activity of the control, that is, cells non exposed to dendrimers). Our results reveal that the viability of NIH 3T3 cells decreased when exposed to pristine amine terminated PAMAM dendrimers, especially for the higher generations at the higher concentrations, which is consistent with the results reported in the literature[83,347]. Similar results were also obtained with the CAL-72 cell line. However, the APS-treated PAMAM dendrimers were much less toxic for both cell lines, especially in the case of G3 and G4 dendrimer generations as can be concluded by the analysis of the IC_{50} values presented in Table 25. These results suggest that the synthesized APS-PAMAM dendrimers could be potentially used for biomedical applications with an advantage over the pristine PAMAM dendrimers since they are less cytotoxic and do not compromise the cell internalization and imaging.

Table 25: IC_{50} values for G3, G4, and G5 pristine and APS-treated PAMAM dendrimers. For IC_{50} determination, experiments were done in the 0-100 μM range.

	IC_{50} ± SD (μM)	
	NIH 3T3 cells	***CAL-72 cells***
$G3.NH_2$	59 ± 5	7.7 ± 0.5
$G4.NH_2$	4.1 ± 0.2	1.7 ± 0.1
$G5.NH_2$	1.6 ±0.1	0.6 ± 0.1
APS-treated G3	> 100	> 100
APS-treated G4	64 ±6	9.7 ± 0.7
APS-treated G5	4.3 ± 0.1	1.1 ± 0.2

3.7. Hematoxicity evaluation

In order to be used as bionanomaterials that need to be administered intravenously, dendrimers should be compatible with blood, namely by not causing the lysis of red cells. Hemolysis was then assessed for APS-treated dendrimers and compared with the results for pristine dendrimers (Figure 78). As expected, results showed that hemolysis increased with the concentration. However, for a concentration of 5 μM or lower, hemoglobin release was always inferior to 10% in both cases and not significantly different from the negative control. In fact, the APS-treated PAMAM dendrimers seem to be slightly less hemotoxic at lower concentrations (0.1 and 1 μM) than the pristine PAMAM dendrimers. In summary, one can consider the APS-treated dendrimers as compatible with blood in what concerns their hemolysis behavior.

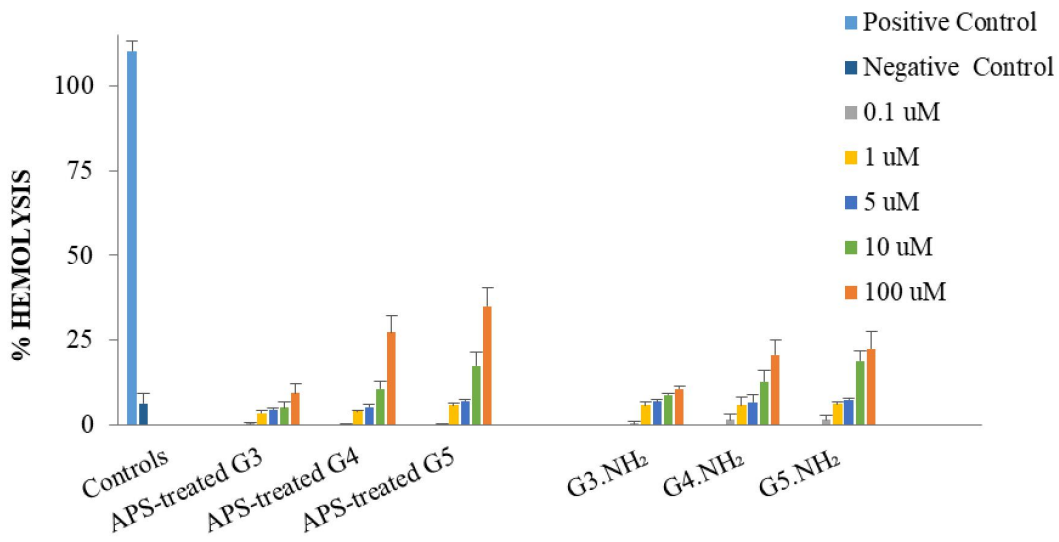

Figure 78: Percentage of hemolysis caused by pristine and APS-treated PAMAM dendrimers at different concentrations after 3 h of incubation at 37ºC. Results are expressed as mean ± SD of three independent experiments with 3 replicas each.

3.8. Visualization of APS-treated PAMAM dendrimers inside cells

A human bone osteosarcoma epithelial cell line (U2OS), known for being easily transfectable, was used to evaluate the possibility of detecting APS-treated PAMAM dendrimers inside cells, that is, to use them as bionanomaterials with traceability capability. G4 APS-treated PAMAM dendrimers were selected to be used in these proof-of-concept assays since, compared to the other dendrimers, they present higher fluorescence emission intensity in the pH range of interest (see Figure 74). It can be seen in Figure 79, these dendrimers were able to be endocytosed by cells and can be detected intracellularly as small fluorescent spots. Importantly, they seem to be present inside cellular vesicles that reside in the cytoplasm. They are probably emitting from acidic vesicles (like the lysosomes or endolysosomes) since, as seen before, their fluorescence emission is higher for acidic pH values. Although further experiments are needed to confirm the localization of APS-

treated dendrimers inside cells, we anticipate that they could possibly be used as fluorescent markers for acidic vesicle staining.

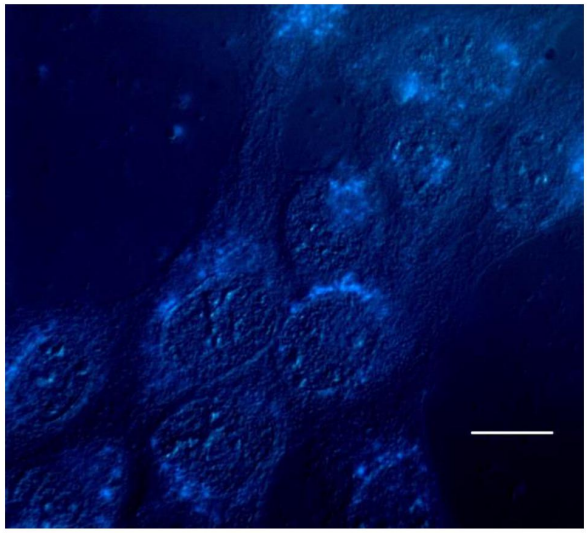

Figure 79: Fluorescence microscopy image of U2OS cells incubated with generation 4 APS-treated PAMAM dendrimers for 24 h (dendrimers were at a concentration of 2 μM). Bar scale = 10 μm.

3.9. Studies with DOX loaded dendrimers

3.9.1. Loading of DOX

DOX, a non-selective anthracycline is one of the most used anticancer drug in the clinic. This drug presents activity on solid and liquid tumors, and is commonly used in nanosystems/nanocarriers for cancer treatment[41]. For that reason, DOX was selected in this work as a model to test the encapsulation and release capacity of the APS-treated PAMAM dendrimer. Considering the previous results from *section 3.3*, we decided on the APS-treated PAMAM dendrimer generation 4 and their respective pristine PAMAM dendrimer to encapsulate DOX. After DOX encapsulation, the loading capacity and loading efficiency were calculated, and the results are presented in Table 26. Based on the obtained results and compared with the pristine PAMAM G4 dendrimer, the loading efficiency and loading capacity were lower on the APS-treated PAMAM G4 dendrimer, with 18% and 5%, respectively. This observed decrease in the loading efficiency and loading capacity of APS-treated PAMAM G4 dendrimer could be because the tertiary and primary amines of the dendrimer treated with APS are protonated, decreasing the interaction with DOX. Nonetheless, the results indicate that DOX could be encapsulated into the APS-treated PAMAM G4 dendrimer. Even with these results, this dendrimer can be relevant for biomedical applications. In fact, this oxidized G4 dendrimer exhibit some benefits when compared with the pristine PAMAM dendrimer, such as less cytotoxicity and enhanced fluorescence.

Table 26: Loading efficiency (EE %) and loading capacity (LC %) of the G4/DOX and APS-treated PAMAM G4 dendrimer/DOX.

	LE%	LC%	Nº of molecules encapsulated[a]
G4.NH$_2$/DOX	76 ± 3.4	26 ± 2.3	8
APS-treated G4/DOX	58 ± 5.6	21 ± 2.3	6

[a]The number of molecules encapsulated was calculated from the following equation,
i= n (drug)/n (dendrimer), where n (drug) = m (encapsulated drug)/MM (drug) and n (dendrimer)= m (dendrimer)/ MM (dendrimer) and *i* is the number of encapsulated molecules.

It is important to highlight that the fluorescence of the encapsulated and non-encapsulated APS-treated PAMAM G4 dendrimer is nearly similar (Figure 80). As such, we can conclude, despite the necessity for further studies, that this APS-treated PAMAM dendrimer is a very promising candidate not only for drug delivery but also for bioimaging applications.

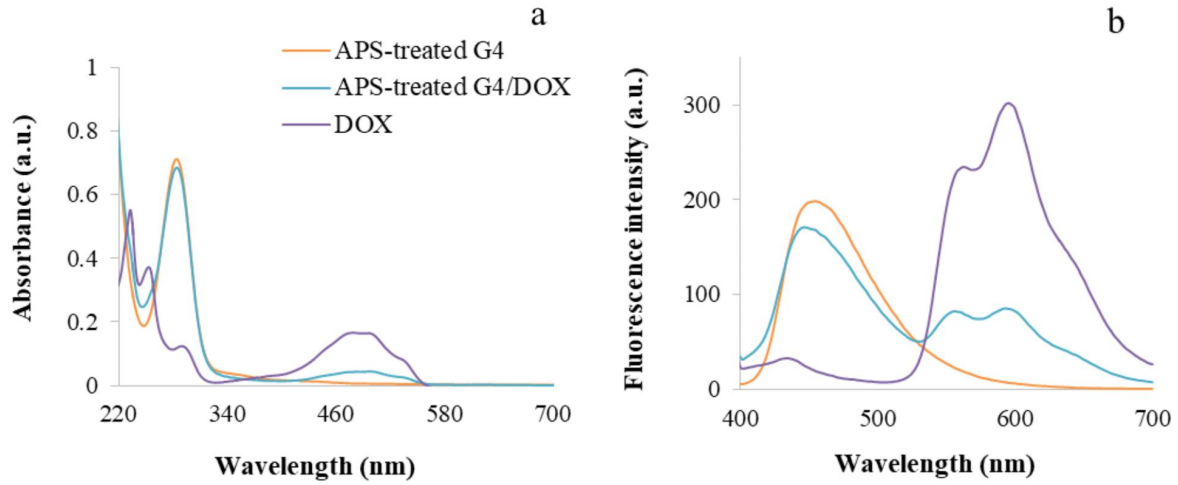

Figure 80: a) Absorbance and b) emission spectra (λ_{ex} = 380 nm) of APS-treated PAMAM G4 dendrimer, APS-treated PAMAM G4/DOX, and DOX with the concentration of 1x10^{-5} M in UPW.

3.9.2. *In vitro* drug release

The drug release profile of DOX from the APS-treated PAMAM G4 dendrimer was studied in two different pHs media (5 and 7.4) at 37ºC and compared with the pristine PAMAM G4 dendrimer and free DOX. In Figure 81, it is observed that DOX was released from the systems more rapidly at pH 5 than at pH 7.4. Comparing the APS-treated PAMAM G4 dendrimer with the pristine PAMAM G4 dendrimer, the behavior in the release profile is quite similar. An initial fast release followed by a sustained release of DOX at pH 5 was noted. A similar release pattern was also observed for both systems at pH 7.4. This release profile pH-dependent shows

that DOX encapsulation in the APS-treated PAMAM dendrimer could be more efficient in cancer tissues (acid pH) than in healthy tissues reducing the drug side effects.

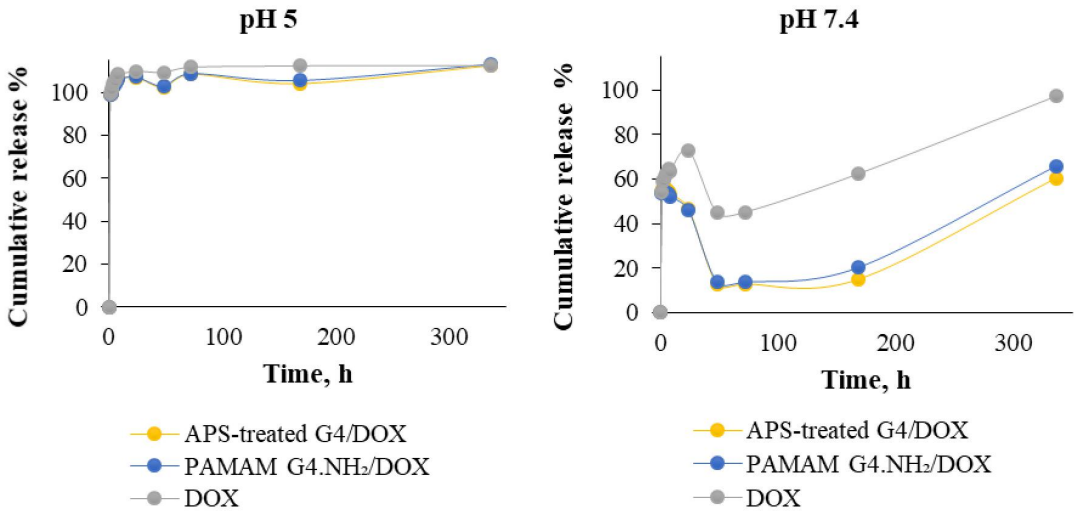

Figure 81: *In vitro* release profile of DOX from APS-treated PAMAM dendrimer G4 and pristine PAMAM dendrimer G4 in different pH media.

4. Conclusions

The spectroscopic behavior of different generations (G3, G4 and G5) of PAMAM dendrimers was evaluated before and after oxidation with ammonium persulfate. The APS treatment clearly resulted in the protonation of the interior of the dendrimer and in an enhancement of their intrinsic fluorescence properties. Globally, the results showed at least two types of emitting electron-rich hetero-atomic subluminophores (HASLs) confined within the dendrimer scaffold with overlapped emission bands. According to our findings and after analysing the data from the literature, we believe that these two HASLs correspond to imidic acid moieties (amide tautomers) and tertiary ammonium groups formed along with the APS treatment. In solution, fluorescence intensity was dependent not only on the pH and on the number of HASLs in the dendrimer scaffold (that is, on dendrimer generation) but also on the rigidification suffered by the dendrimer due to the acidic environment (at a low pH, APS-treated G4 was indeed the most emissive species). Moreover, photoluminescence studies with lyophilized samples confirmed the coexistence of more than one type of HASLs emitting in the dendrimer structure. The APS treatment affected these HASLs to a different extent. In accordance with the observed order of fluorescence intensity, time-resolved fluorescence experiments always showed higher average lifetimes of HASLs for APS-treated dendrimers compared to pristine ones. Interestingly, for pristine dendrimers, average lifetimes were much higher in the lyophilized samples than those in solution, which is evidence of aggregation-induced emission. In contrast, the fraction and lifetimes of HASLs in APS-treated dendrimers were similar in solution and in the lyophilized form, probably because these dendrimers are protonated and cannot approach each other so easily due to the repulsion forces that are established. Importantly, the highly emissive APS-

treated dendrimers presented lower cytotoxicity and hemotoxicity than pristine dendrimers and were also detectable inside cells via fluorescence microscopy. The quantum yield, an important parameter in this type of microscopy, was high, especially for G3 and G4 APS-treated PAMAM dendrimers (75% and 63%, respectively).

To conclude, the easy preparation of these dendrimers, together with their fluorescence and biological properties, may promote their use in more widespread applications as bionanomaterials when compared to traditional PAMAM dendrimers.

CHAPTER V

Conclusions and future perspectives

1. Conclusions and future perspectives

To summarize, PAMAM dendrimers are a versatile nanoplatform for biomedical applications, as drug delivery and bioimaging. The anionic PAMAM dendrimers coordinated with cisplatin and DACHPt improved their solubility and were more toxic against cancer cells when compared with the free drugs. The cationic PAMAM dendrimers, after oxidation, showed strong blue intrinsic fluorescence being less toxic and able for bioimaging applications. In addition, both PAMAM dendrimers (anionic and cationic) could deliver anticancer drugs, increasing their efficacy.

In chapter 2 we described the preparation of low generation anionic PAMAM dendrimers (G0.5-G3.5) functionalized with cisplatin in mono and bidentate forms. These metallodendrimers were characterized by NMR, FTIR, UV-vis and fluorescence spectroscopy, zeta-potential, MS, and EA. After, they were tested in different cancer cell lines and one non-cancer cell line to determine their anticancer activity. The cytotoxicity results indicated that two of these metallodendrimers, (G0.5(COOPt$(NH_3)_2Cl)_8$ and G2.5(COOPt$(NH_3)_2Cl)_{32}$) conjugated with cisplatin in a monodentate form had an efficacy much higher than free cisplatin in all the studied cancer cell lines. However, the remaining metallodendrimers showed an improved efficacy than cisplatin towards a specific cancer cell line. The hemolysis assay showed that the metallodendrimers were not toxic to the blood cells. For further studies, the G0.5(COO(Pt$(NH_3)_2Cl)_8$, G2.5COO(Pt$(NH_3)_2)_{16}$, and G2.5(COOPt$(NH_3)_2Cl)_{32}$ were used to evaluate the interaction with DNA. The DNA binding results indicated a strong interaction of the metallodendrimers compared to free cisplatin. The synergetic effect with a second drug, 5-FU, was performed by encapsulation of 5-FU within the G2.5COO(Pt$(NH_3)_2)_{16}$, and G2.5(COOPt$(NH_3)_2Cl)_{32}$ metallodendrimers. The cytotoxicity assay displayed that the G2.5COO(Pt$((NH_3)_2)_{16}$/5-FU and G2.5(COOPt$(NH_3)_2Cl)_{32}$/5-FU systems were more efficient than the respective metallodendrimer when tested in CACO-2 cells, suggesting a synergetic effect of cisplatin and 5-FU. Furthermore, the *in vitro* drug release studies demonstrated that the encapsulated 5-FU presented a controllable release compared to free 5-FU in pH 7.4 and 5. The metallodendrimers/5-FU systems also proved to be sensitive to pH.

In chapter 3, the preparation of low generations of anionic PAMAM dendrimers (G0.5-G3.5) functionalized with DACHPt and their anticancer activity were evaluated in four cancer cell lines and one non-cancer cell line. The DACHPt-metallodendrimers were characterized by several techniques such as NMR, FTIR, UV-vis and fluorescence spectroscopy, zeta-potential, MS, and EA. They presented to be more cytotoxic in the cancer cell lines study compared to free $DACHPtCl_2$ and oxaliplatin. Their interaction with the human red blood cells was then evaluated. The hemolysis results indicated that the DACHPt-metallodendrimers showed low hematoxicity at the tested concentrations. For further assays, the G2.5COO$(DACHPt)_{16}$ metallodendrimer was used to assess the interaction with DNA. The DNA binding studies with the CT-DNA showed a hyperchromic effect and a strong interaction with DNA compared to oxaliplatin. To increase the potency as an anticancer

drug, the 5-FU was encapsulated into the G2.5COO(DACHPt)$_{16}$. The cytotoxicity results showed that G2.5COO(DACHPt)$_{16}$/5-FU system was 5.5 times more cytotoxic than G2.5COO(DACHPt)$_{16}$ in the A2780CisR cancer cell line. Moreover, this complex released the 5-FU drug gradually compared to the respective metallodendrimer and free drug in pH 7.4 and 5.

In the chapter 4, we prepared fluorescent PAMAM dendrimers (G3-G5) using an oxidative treatment. Afterward, the spectroscopic behavior of the APS-treated was evaluated and compared with the pristine PAMAM dendrimers. The results indicated a protonation in the interior of the dendrimer and consequently an enhancement of intrinsic fluorescence. More specifically, imidic acid moieties and tertiary ammonium groups formed along with the APS treatment that was responsible for their increased fluorescent properties. In solution, the fluorescence intensity was dependent on the pH, the generation, and the dendrimer's rigidification due to the acidic environment. The time-resolved fluorescence studies showed a higher average life-time for the APS-treated compared to the respective pristine dendrimers. The life-time was similar in solution and lyophilized forms of the APS-treated PAMAM dendrimers. The quantum yield was also determined, and the APS-treated PAMAM dendrimer G4 presented a high quantum yield value, 75%. These APS-treated PAMAM dendrimers showed lower cytotoxicity and hematoxicity than pristine PAMAM dendrimers. Their fluorescence were also detectable inside the cells. The APS-treated PAMAM dendrimer G4, after encapsulation with DOX, continued to present fluorescence.

Concluding, the metallodendrimers that showed promising results as anticancer agents can be considered as good candidates as chemotherapeutic agents. The APS-treated PAMAM dendrimers combining their fluorescence with their ability to deliver drugs are promising candidates for the detection and treatment of cancer.

As future perspectives, some complimentary analysis should be performed, such as the determination of the amount of metal present in each dendrimer. Furthermore, other studies are required to understand the mechanism of action of these metallodendrimers, such as the accumulation of reactive oxygen species (ROS), which phase of the cell cycle they act, and the ability to induce apoptosis. Consequently, evaluate *in vivo* the metallodendrimers that presented lower IC_{50} values compared to free drugs. Also, in the long term, side effects studies of the prepared dendrimers/metallodendrimers must be performed to evaluate their efficacy in reducing or eliminating such effects. In addition, more cytotoxic studies with the metallodendrimers/5-FU are necessary to demonstrate if the observed effect is indeed synergetic. Moreover, it is expected to prepare the biodegradable metallodendrimers using the bis-MPA dendrimers and their functionalization with cisplatin and DACHPt. Then, after the biological studies with these bis-MPS dendrimers, compare their anticancer efficacy with the prepared PAMAM cisplatin-metallodendrimers and DACHPt-metallodendrimers.

For the APS-treated PAMAM dendrimers, perform other experiments such as intracellular mechanisms and

cytotoxicity studies to evaluate the effectiveness of the APS-treated PAMAM/DOX systems as an anticancer drug in order to prove their efficacy to be used for bioimaging and cancer treatment. The encapsulation of other drugs like cisplatin and evaluated their potential as another delivery system for cisplatin. Moreover, finally, verify if the prepared compounds could be used to diagnose and treat other diseases.

REFERENCES

References

(1) Sung, H.; Ferlay, J.; Siegel, R. L.; Laversanne, M.; Soerjomataram, I.; Jemal, A.; Bray, F. Global Cancer Statistics 2020: GLOBOCAN Estimates of Incidence and Mortality Worldwide for 36 Cancers in 185 Countries. *CA. Cancer J. Clin.* **2021**, *71*, 209–249. https://doi.org/10.3322/caac.21660.

(2) Organization, W. H. Cancer https://www.who.int/news-room/fact-sheets/detail/cancer (accessed Aug 6, 2021).

(3) The Global Cancer Observatory. *Globocan 2020 - Portugal*; 2020.

(4) American Cancer Society. *Cancer Facts & Figures 2021*; Atlanta, 2021.

(5) Estanqueiro, M.; Amaral, M. H.; Conceição, J.; Sousa Lobo, J. M. Nanotechnological Carriers for Cancer Chemotherapy: The State of the Art. *Colloids Surfaces B Biointerfaces* **2015**, *126*, 631–648. https://doi.org/10.1016/j.colsurfb.2014.12.041.

(6) Pérez-Herrero, E.; Fernández-Medarde, A. Advanced Targeted Therapies in Cancer: Drug Nanocarriers, the Future of Chemotherapy. *Eur. J. Pharm. Biopharm.* **2015**, *93*, 52–79. https://doi.org/10.1016/j.ejpb.2015.03.018.

(7) Torre, L.; Siegal, R.; Jemal, A.; Surveillance & Health Services Research Program. Global Cancer Facts & Figures 3rd Edition. *Am. Cancer Soc.* **2015**, 1–61.

(8) Bidram, E.; Esmaeili, Y.; Ranji-Burachaloo, H.; Al-Zaubai, N.; Zarrabi, A.; Stewart, A.; Dunstan, D. E. A Concise Review on Cancer Treatment Methods and Delivery Systems. *J. Drug Deliv. Sci. Technol.* **2019**, *54*, 101350. https://doi.org/10.1016/j.jddst.2019.101350.

(9) Houts, P. S.; Lenhard, R. E.; Varricchio, C. *Cancer Facts & Figures 2019*; 2019. https://doi.org/10.1046/j.1523-5394.2000.83001.x.

(10) Liang, C.; Xu, L.; Song, G.; Liu, Z. Emerging Nanomedicine Approaches Fighting Tumor Metastasis: Animal Models, Metastasis-Targeted Drug Delivery, Phototherapy, and Immunotherapy. *Chem. Soc. Rev.* **2016**, *45*, 6250–6269. https://doi.org/10.1039/c6cs00458j.

(11) Saharinen, P.; Tammela, T.; Karkkainen, M. J.; Alitalo, K. Lymphatic Vasculature: Development, Molecular Regulation and Role in Tumor Metastasis and Inflammation. *Trends Immunol.* **2004**, *25*, 387–395. https://doi.org/10.1016/j.it.2004.05.003.

(12) Cao, Y.; Zhong, W. Tumor-Derived Lymphangiogenic Factors and Lymphatic Metastasis. *Biomed. Pharmacother.* **2007**, *61*, 534–539. https://doi.org/10.1016/j.biopha.2007.08.009.

(13) Christiansen, A.; Detmar, M. Lymphangiogenesis and Cancer. *Genes and Cancer* **2011**, *2*, 1146–1158. https://doi.org/10.1177/1947601911423028.

(14) Nishida, N.; Yano, H.; Nishida, T.; Kamura, T.; Kojiro, M. Angiogenesis in Cancer. *Vasc. Health Risk Manag.* **2006**, *2*, 213–219. https://doi.org/10.2147/vhrm.2006.2.3.213.

(15) Gay, L. J.; Felding-Habermann, B. Contribution of Platelets to Tumor Metastasis. *Nat. Rev. Cancer* **2011**, *11*, 123–134. https://doi.org/10.1038/nrc3004.

(16) Fernandes, C.; Suares, D.; Yergeri, M. C. Tumor Microenvironment Targeted Nanotherapy. *Front. Pharmacol.* **2018**, *9*, 1–25. https://doi.org/10.3389/fphar.2018.01230.

(17) Navya, P. N.; Kaphle, A.; Srinivas, S. P.; Bhargava, S. K.; Rotello, V. M.; Daima, H. K. Current Trends and Challenges in Cancer Management and Therapy Using Designer Nanomaterials. *Nano Converg.* **2019**, *6*, 1–30. https://doi.org/10.1186/s40580-019-0193-2.

(18) Feng, L.; Dong, Z.; Tao, D.; Zhang, Y.; Liu, Z. The Acidic Tumor Microenvironment: A Target for Smart Cancer Nano-Theranostics. *Natl. Sci. Rev.* **2018**, *5*, 269–286. https://doi.org/10.1093/nsr/nwx062.

(19) Tohme, S.; Simmons, R. L.; Tsung, A. Surgery for Cancer: A Trigger for Metastases. *Cancer Res.* **2017**, *77*, 1548–1552. https://doi.org/10.1158/0008-5472.CAN-16-1536.

(20) Pérez-Herrero, E.; Fernández-Medarde, A. Advanced Targeted Therapies in Cancer: Drug Nanocarriers, the Future of Chemotherapy. *Eur. J. Pharm. Biopharm.* **2015**, *93*, 52–79. https://doi.org/10.1016/j.ejpb.2015.03.018.

(21) Bregoli, L.; Movia, D.; Gavigan-Imedio, J. D.; Lysaght, J.; Reynolds, J.; Prina-Mello, A. Nanomedicine Applied to Translational Oncology: A Future Perspective on Cancer Treatment. *Nanomedicine Nanotechnology, Biol. Med.* **2016**, *12*, 81–103. https://doi.org/10.1016/j.nano.2015.08.006.

(22) Hare, J. I.; Lammers, T.; Ashford, M. B.; Puri, S.; Storm, G.; Barry, S. T. Challenges and Strategies in Anti-Cancer Nanomedicine Development: An Industry Perspective. *Adv. Drug Deliv. Rev.* **2017**, *108*, 25–38. https://doi.org/10.1016/j.addr.2016.04.025.

(23) Bar-Zeev, M.; Livney, Y. D.; Assaraf, Y. G. Targeted Nanomedicine for Cancer Therapeutics: Towards Precision Medicine Overcoming Drug Resistance. *Drug Resist. Updat.* **2017**, *31*, 15–30. https://doi.org/10.1016/j.drup.2017.05.002.

(24) Kaur, D.; Jain, K.; Mehra, N. K.; Kesharwani, P.; Jain, N. K. A Review on Comparative Study of PPI and PAMAM Dendrimers. *J Nanopart Res* **2016**, *18*, 1–14. https://doi.org/10.1007/s11051-016-3423-0.

(25) Zhang, W.; Kohane, D. S. Keeping Nanomedicine on Target. *Nano Lett.* **2021**, *21*, 3–5. https://doi.org/10.1021/acs.nanolett.0c04638.

(26) Li, Z.; Tan, S.; Li, S.; Shen, Q.; Wang, K. Cancer Drug Delivery in the Nano Era: An Overview and Perspectives (Review). *Oncol. Rep.* **2017**, *38*, 611–624. https://doi.org/10.3892/or.2017.5718.

(27) Din, F. ud; Aman, Wa.; Ullah, I.; Qureshi, O. S.; Mustapha, O.; Shafique, S.; Zeb, A. Effective Use of Nanocarriers as Drug Delivery Systems for the Treatment of Selected Tumors. *Int. J. Nanomedicine* **2017**, *12*, 7291–7309. https://doi.org/10.2147/IJN.S146315.

(28) Bae, K. H.; Chung, H. J.; Park, T. G. Nanomaterials for Cancer Therapy and Imaging. *Mol. Cells* **2011**, *31*, 295–302. https://doi.org/10.1007/s10059-011-0051-5.

(29) Hossen, S.; Hossain, M. K.; Basher, M. K.; Mia, M. N. H.; Rahman, M. T.; Uddin, M. J. Smart Nanocarrier-Based Drug Delivery Systems for Cancer Therapy and Toxicity Studies: A Review. *J. Adv. Res.* **2019**, *15*, 1–18. https://doi.org/10.1016/j.jare.2018.06.005.

(30) Park, K. Questions on the Role of the EPR Effect in Tumor Targeting. *J. Control. Release* **2013**, *172*, 391. https://doi.org/10.1016/j.jconrel.2013.10.001.

(31) Golombek, S. K.; May, J. N.; Theek, B.; Appold, L.; Drude, N.; Kiessling, F.; Lammers, T. Tumor Targeting via EPR: Strategies to Enhance Patient Responses. *Adv. Drug Deliv. Rev.* **2018**, *130*, 17–38. https://doi.org/10.1016/j.addr.2018.07.007.

(32) Nichols, J. W.; Bae, Y. H. EPR: Evidence and Fallacy. *J. Control. Release* **2014**, *190*, 451–464. https://doi.org/10.1016/j.jconrel.2014.03.057.

(33) Taurin, S.; Nehoff, H.; Greish, K. Anticancer Nanomedicine and Tumor Vascular Permeability; Where Is the Missing Link? *J. Control. Release* **2012**, *164*, 265–275. https://doi.org/10.1016/j.jconrel.2012.07.013.

(34) Greish, K. Enhanced Permeability and Retention Effect for Selective Targeting of Anticancer Nanomedicine: Are We There Yet? *Drug Discov. Today Technol.* **2012**, *9*, 161–166. https://doi.org/10.1016/j.ddtec.2011.11.010.

(35) Maeda, H. Macromolecular Therapeutics in Cancer Treatment: The EPR Effect and Beyond. *J. Control. Release* **2012**, *164*, 138–144. https://doi.org/10.1016/j.jconrel.2012.04.038.

(36) Lammers, T.; Kiessling, F.; Hennink, W. E.; Storm, G. Drug Targeting to Tumors: Principles, Pitfalls and (Pre-) Clinical Progress. *J. Control. Release* **2012**, *161*, 175–187. https://doi.org/10.1016/j.jconrel.2011.09.063.

(37) Torchilin, V. Multifunctional and Stimuli-Sensitive Pharmaceutical Nanocarriers. *Eur. J. Pharm. Biopharm.* **2009**, *71*, 431–444. https://doi.org/10.1016/j.ejpb.2008.09.026.

(38) Butler, J. S.; Sadler, P. J. Targeted Delivery of Platinum-Based Anticancer Complexes. *Curr. Opin. Chem. Biol.* **2013**, *17*, 175–188. https://doi.org/10.1016/j.cbpa.2013.01.004.

(39) Li, H. J.; Du, J. Z.; Liu, J.; Du, X. J.; Shen, S.; Zhu, Y. H.; Wang, X.; Ye, X.; Nie, S.; Wang, J. Smart Superstructures with Ultrahigh PH-Sensitivity for Targeting Acidic Tumor Microenvironment: Instantaneous Size Switching and Improved Tumor Penetration. *ACS Nano* **2016**, *10*, 6753–6761. https://doi.org/10.1021/acsnano.6b02326.

(40) Jhaveri, A. M.; Torchilin, V. P. Multifunctional Polymeric Micelles for Delivery of Drugs and SiRNA. *Front. Pharmacol.* **2014**, *5*, 1–26. https://doi.org/10.3389/fphar.2014.00077.

(41) Gonçalves, M.; Mignani, S.; Rodrigues, J.; Tomás, H. A Glance over Doxorubicin Based-Nanotherapeutics : From Proof-of-Concept Studies to Solutions in the Market. *J. Control. Release* **2020**, *317*, 347–374.

(42) Park, J.; Choi, Y.; Chang, H.; Um, W.; Ryu, J. H.; Kwon, I. C. Alliance with EPR Effect: Combined Strategies to Improve the EPR Effect in the Tumor Microenvironment. *Theranostics* **2019**, *9*, 8073–8090. https://doi.org/10.7150/thno.37198.

(43) Beltrán-Gracia, E.; López-Camacho, A.; Higuera-Ciapara, I.; Velázquez-Fernández, J. B.; Vallejo-Cardona, A. A. Nanomedicine Review: Clinical Developments in Liposomal Applications. *Cancer Nanotechnol.* **2019**, *10*, 1–40. https://doi.org/10.1186/s12645-019-0055-y.

(44) Baxter. Doxil (doxorubicin HCl liposome injection) for Hospital Care https://www.baxter.com/doxil-doxorubicin-hcl-liposome-injection-hospital-care (accessed Aug 9, 2021).

(45) Drugs, D. F.-A. DOXIL (LIPOSOMAL) https://www.accessdata.fda.gov/scripts/cder/daf/index.cfm?event=overview.process&ApplNo=050718 (accessed Aug 9, 2021).

(46) Acrotech Biopharma, L. Marqibo https://marqibo.com/hcp/about-our-company/ (accessed Aug 9, 2021).

(47) Drugs, D. F.-A. Marqibo kit https://www.accessdata.fda.gov/scripts/cder/daf/index.cfm?event=overview.process&ApplNo=202497.

(48) Kateb, B.; Chiu, K.; Black, K. L.; Yamamoto, V.; Khalsa, B.; Ljubimova, J. Y.; Ding, H.; Patil, R.; Portilla-Arias, J. A.; Modo, M.; Moore, D. F.; Farahani, K.; Okun, M. S.; Prakash, N.; Neman, J.; Ahdoot, D.; Grundfest, W.; Nikzad, S.; Heiss, J. D. Nanoplatforms for Constructing New Approaches to Cancer Treatment, Imaging, and Drug Delivery: What Should Be the Policy? *Neuroimage* **2011**, *54*, S106–S124. https://doi.org/10.1016/j.neuroimage.2010.01.105.

(49) Ke, X. Y.; Lin Ng, V. W.; Gao, S. J.; Tong, Y. W.; Hedrick, J. L.; Yang, Y. Y. Co-Delivery of Thioridazine and Doxorubicin Using Polymeric Micelles for Targeting Both Cancer Cells and Cancer Stem Cells. *Biomaterials* **2014**, *35*, 1096–1108. https://doi.org/10.1016/j.biomaterials.2013.10.049.

(50) Xing, J.; Zhang, D.; Tan, T. Studies on the Oridonin-Loaded Poly(D,L-Lactic Acid) Nanoparticles *in Vitro* and *in Vivo*. *Int. J. Biol. Macromol.* **2007**, *40*, 153–158. https://doi.org/10.1016/j.ijbiomac.2006.07.001.

(51) Yordanov, G. Poly (Alkyl Cyanoacrylate) Nanoparticles as Drug Carriers: 33 Years Later. *Bulg. J. Chem.* **2012**, *1*, 61–73.

(52) Duan, J.; Liu, M.; Zhang, Y.; Zhao, J.; Pan, Y.; Yang, X. Folate-Decorated Chitosan/Doxorubicin Poly(Butyl)Cyanoacrylate Nanoparticles for Tumor-Targeted Drug Delivery. *J. Nanoparticle Res.* **2012**, *14*, 1–9. https://doi.org/10.1007/s11051-012-0761-4.

(53) Gandhi, A.; Paul, A.; Sen, S. O.; Sen, K. K. Studies on Thermoresponsive Polymers: Phase Behaviour, Drug Delivery and Biomedical Applications. *Asian J. Pharm. Sci.* **2015**, *10*, 99–107. https://doi.org/10.1016/j.ajps.2014.08.010.

(54) Maciel, D.; Figueira, P.; Xiao, S.; Hu, D.; Shi, X.; Rodrigues, J.; Tomás, H.; Li, Y. Redox-Responsive Alginate Nanogels with Enhanced Anticancer Cytotoxicity. *Biomacromolecules* **2013**, *14*, 3140–3146. https://doi.org/10.1021/bm400768m.

(55) Khan, I.; Saeed, K.; Khan, I. Nanoparticles: Properties, Applications and Toxicities. *Arab. J. Chem.* **2019**, *12*, 908–931. https://doi.org/10.1016/j.arabjc.2017.05.011.

(56) Chen, Q.; Chen, F.; Yan, Y. Fluorescent Semiconductor Nanocrystals, a Promising Fluorescent Anti-Counterfeiting Material for Specialty Paper. *BioResources* **2013**, *8*, 6–7. https://doi.org/10.15376/biores.8.1.6-7.

(57) Surana, K.; Singh, P. K.; Rhee, H. W.; Bhattacharya, B. Synthesis, Characterization and Application of CdSe Quantum Dots. *J. Ind. Eng. Chem.* **2014**, *20*, 4188–4193. https://doi.org/10.1016/j.jiec.2014.01.019.

(58) Dreaden, E. C.; Austin, L. A.; MacKey, M. A.; El-Sayed, M. A. Size Matters: Gold Nanoparticles in Targeted Cancer Drug Delivery. *Ther. Deliv.* **2012**, *3*, 457–478. https://doi.org/10.4155/tde.12.21.

(59) Amina, S. J.; Guo, B. A Review on the Synthesis and Functionalization of Gold Nanoparticles as a Drug Delivery Vehicle. *Int. J. Nanomedicine* **2020**, *15*, 9823–9857. https://doi.org/10.2147/IJN.S279094.

(60) Martinez-Finkelshtein, A.; Van Assche, W. Gold Nanoparticles: Preparation, Properties, and Applications in Bionanotechnology. *Nanoscale* **2016**, *21*, 1871–1880. https://doi.org/10.1090/noti1430.

(61) Cai, W.; Gao, T.; Hong, H.; Sun, J. Applications of Gold Nanoparticles in Cancer Nanotechnology. *Nanotechnol. Sci. Appl.* **2008**, *1*, 17–32. https://doi.org/10.2147/nsa.s3788.

(62) Chithrani, B. D.; Ghazani, A. A.; Chan, W. C. W. Determining the Size and Shape Dependence of Gold Nanoparticle Uptake into Mammalian Cells. *Nano Lett.* **2006**, *6*, 662–668. https://doi.org/10.1021/nl052396o.

(63) Shi, X.; Wang, S.; Meshinchi, S.; Van Antwerp, M. E.; Bi, X.; Lee, I.; Baker, J. R. Dendrimer-Entrapped Gold Nanoparticles as a Platform for Cancer-Cell Targeting and Imaging. *Small* **2007**, *3*, 1245–1252. https://doi.org/10.1002/smll.200700054.

(64) Mahmoudi, M.; Sant, S.; Wang, B.; Laurent, S.; Sen, T. Superparamagnetic Iron Oxide Nanoparticles (SPIONs): Development, Surface Modification and Applications in Chemotherapy. *Adv. Drug Deliv. Rev.* **2011**, *63*, 24–46. https://doi.org/10.1016/j.addr.2010.05.006.

(65) Vallet-Regí, M.; Colilla, M.; Izquierdo-Barba, I.; Manzano, M. Mesoporous Silica Nanoparticles for Drug Delivery: Current Insights. *Molecules* **2018**, *23*, 1–19. https://doi.org/10.3390/molecules23010047.

(66) Doadrio, A.; Salinas, A.; Sánchez-Montero, J.; Vallet-Regí, M. Drug Release from Ordered Mesoporous Silicas. *Curr. Pharm. Des.* **2015**, *21*, 6213–6819. https://doi.org/10.2174/1381612822666151106121419.

(67) Buhleier, E.; Wehner, W.; Vogtle, F. "Cascade"- and "Nonskid-Chain-like" Syntheses of Molecular Cavity Topologies. *Synthesis* **1978**, *1978*, 155–158. https://doi.org/10.1055/s-1978-24702.

(68) Tomalia, D. A.; Baker, H.; Dewald, J.; Hall, M.; Kallos, G.; Martin, S.; Roeck, J.; Ryder, J.; Smith, P. A New Class of Polymers: Starburst-Dendritic Macromolecules. *Polym. J.* **1985**, *17*, 117–132. https://doi.org/10.1295/polymj.17.117.

(69) Tomalia, D. A.; Baker, H.; Dewald, J.; Hall, M.; Kallos, G.; Martin, S.; Roeck, J.; Ryder, J.; Smith, P. Dendritic Macromolecules: Synthesis of Starburst Dendrimers. *Macromolecules* **1986**, *19*, 2466–2468. https://doi.org/doi.org/10.1021/ma00163a029.

(70) GR, N.; Yao ZQ; GR, B.; VK, G.; PS, R.; Saunders, M. Chemistry of Micelles Series. Part 2. Cascade

Molecules: Synthesis and Characterization of a Benzene [9]3-Arborol. *J Am Chem Soc* **1986**, *108*, 849–850. https://doi.org/10.1021/ja00264a054.

(71) Newkome, G. R.; Yao, Z.; Baker, G. R.; Gupta, V. K. Micelles. Part 1. Cascade Molecules: A New Approach to Micelles. A [27]-Arborol. *J. Org. Chem.* **1985**, *50*, 2003–2004. https://doi.org/10.1021/jo00211a052.

(72) Twibanire, J. D. amou. K.; Grindley, T. B. Polyester Dendrimers. *Polymers* **2012**, *4*, 794–879. https://doi.org/10.3390/polym4010794.

(73) Hawker, C. J.; Fréchet, J. M. J. Preparation of Polymers with Controlled Molecular Architecture. A New Convergent Approach to Dendritic Macromolecules. *J. Am. Chem. Soc.* **1990**, *112*, 7638–7647. https://doi.org/10.1021/ja00177a027.

(74) Mignani, S.; Kazzouli, S. El; Bousmina, M.; Majoral, J. P. Dendrimer Space Concept for Innovative Nanomedicine: A Futuristic Vision for Medicinal Chemistry. *Prog. Polym. Sci.* **2013**, *38*, 993–1008. https://doi.org/10.1016/j.progpolymsci.2013.03.003.

(75) Nanjwade, B. K.; Bechra, H. M.; Derkar, G. K.; Manvi, F. V.; Nanjwade, V. K. Dendrimers: Emerging Polymers for Drug-Delivery Systems. *Eur. J. Pharm. Sci.* **2009**, *38*, 185–196. https://doi.org/10.1016/j.ejps.2009.07.008.

(76) Singh, J.; Jain, K.; Mehra, N. K.; Jain, N. K. Dendrimers in Anticancer Drug Delivery: Mechanism of Interaction of Drug and Dendrimers. *Artif. Cells, Nanomedicine Biotechnol.* **2016**, *44*, 1626–1634. https://doi.org/10.3109/21691401.2015.1129625.

(77) Wu, L. P.; Ficker, M.; Christensen, J. B.; Trohopoulos, P. N.; Moghimi, S. M. Dendrimers in Medicine: Therapeutic Concepts and Pharmaceutical Challenges. *Bioconjug. Chem.* **2015**, *26*, 1198–1211. https://doi.org/10.1021/acs.bioconjchem.5b00031.

(78) Saluja, V.; Mankoo, A.; Saraogi, G. K.; Tambuwala, M. M.; Mishra, V. Smart Dendrimers: Synergizing the Targeting of Anticancer Bioactives. *J. Drug Deliv. Sci. Technol.* **2019**, *52*, 15–26. https://doi.org/10.1016/j.jddst.2019.04.014.

(79) Medina, S. H.; El-Sayed, M. E. H. Dendrimers as Carriers for Delivery of Chemotherapeutic Agents. *Chem. Rev.* **2009**, *109*, 3141–3157. https://doi.org/10.1021/cr900174j.

(80) Kesharwani, P.; Jain, K.; Jain, N. K. Dendrimer as Nanocarrier for Drug Delivery. *Prog. Polym. Sci.* **2014**, *39*, 268–307. https://doi.org/10.1016/j.progpolymsci.2013.07.005.

(81) Pearson, R. M.; Sunoqrot, S.; Hsu, H. J.; Bae, J. W.; Hong, S. Dendritic Nanoparticles: The next Generation of Nanocarriers? *Ther. Deliv.* **2012**, *3*, 941–959. https://doi.org/10.4155/tde.12.76.

(82) Sharma, A. K.; Gothwal, A.; Kesharwani, P.; Alsaab, H.; Iyer, A. K.; Gupta, U. Dendrimer Nanoarchitectures for Cancer Diagnosis and Anticancer Drug Delivery. *Drug Discov. Today* **2017**, *22*, 314–326. https://doi.org/10.1016/j.drudis.2016.09.013.

(83) Janaszewska, A.; Lazniewska, J.; Trzepiński, P.; Marcinkowska, M.; Klajnert-Maculewicz, B. Cytotoxicity of Dendrimers. *Biomolecules* **2019**, *9*, 1–23. https://doi.org/10.3390/biom9080330.

(84) Hsu, H. J.; Bugno, J.; Lee, S. R.; Hong, S. Dendrimer-Based Nanocarriers: A Versatile Platform for

Drug Delivery. *Wiley Interdiscip. Rev. Nanomedicine Nanobiotechnology* **2017**, *9*, 1–21. https://doi.org/10.1002/wnan.1409.

(85) Mittal, P.; Saharan, A.; Verma, R.; Altalbawy, F. M. A.; Alfaidi, M. A.; Batiha, G. E. S.; Akter, W.; Gautam, R. K.; Uddin, M. S.; Rahman, M. S. Dendrimers: A New Race of Pharmaceutical Nanocarriers. *Biomed Res. Int.* **2021**, *2021*, 1–11. https://doi.org/10.1155/2021/8844030.

(86) Bodewein, L.; Schmelter, F.; Di Fiore, S.; Hollert, H.; Fischer, R.; Fenske, M. Differences in Toxicity of Anionic and Cationic PAMAM and PPI Dendrimers in Zebrafish Embryos and Cancer Cell Lines. *Toxicol. Appl. Pharmacol.* **2016**, *305*, 83–92. https://doi.org/10.1016/j.taap.2016.06.008.

(87) Esfand, R.; Tomalia, D. A. Poly(Amidoamine) (PAMAM) Dendrimers: From Biomimicry to Drug Delivery and Biomedical Applications. *Drug Discov. Today* **2001**, *6*, 427–436. https://doi.org/10.1016/S1359-6446(01)01757-3.

(88) Morris, C. J.; Aljayyoussi, G.; Mansour, O.; Griffiths, P.; Gumbleton, M. Endocytic Uptake, Transport and Macromolecular Interactions of Anionic PAMAM Dendrimers within Lung Tissue. *Pharm. Res.* **2017**, *34*, 2517–2531. https://doi.org/10.1007/s11095-017-2190-7.

(89) Winnicka, K.; Bielawski, K.; Rusak, M.; Bielawska, A. The Effect of Generation 2 and 3 Poly(Amidoamine) Dendrimers on Viability of Human Breast Cancer Cells. *J. Heal. Sci.* **2009**, *55*, 169–177.

(90) Mekuria, S. L.; Debele, T. A.; Tsai, H. C. PAMAM Dendrimer Based Targeted Nano-Carrier for Bio-Imaging and Therapeutic Agents. *RSC Adv.* **2016**, *6*, 63761–63772. https://doi.org/10.1039/c6ra12895e.

(91) Esfand, R.; Tomalia, D. A. Laboratory Synthesis of Poly(Amidoamine) (PAMAM) Dendrimers. In *Dendrimers and Other Dendritic Polymers*; Frechet, J. M. J., Tomalia, D. A., Eds.; 2001. https://doi.org/10.1002/0470845821.ch25.

(92) Kirkpatrick, G. J.; Plumb, J. A.; Sutcliffe, O. B.; Flint, D. J.; Wheate, N. J. Evaluation of Anionic Half Generation 3.5-6.5 Poly(Amidoamine) Dendrimers as Delivery Vehicles for the Active Component of the Anticancer Drug Cisplatin. *J. Inorg. Biochem.* **2011**, *105*, 1115–1122. https://doi.org/10.1016/j.jinorgbio.2011.05.017.

(93) Majoros, I. J.; Thomas, T. P.; Mehta, C. B.; Baker, J. R. Poly(Amidoamine) Dendrimer-Based Multifunctional Engineered Nanodevice for Cancer Therapy. *J. Med. Chem.* **2005**, *48*, 5892–5899. https://doi.org/10.1021/jm0401863.

(94) Otto, D. P.; de Villiers, M. M. Poly(Amidoamine) Dendrimers as a Pharmaceutical Excipient. Are We There Yet? *J. Pharm. Sci.* **2018**, *107*, 75–83. https://doi.org/10.1016/j.xphs.2017.10.011.

(95) Menjoge, A. R.; Kannan, R. M.; Tomalia, D. A. Dendrimer-Based Drug and Imaging Conjugates: Design Considerations for Nanomedical Applications. *Drug Discov. Today* **2010**, *15*, 171–185. https://doi.org/10.1016/j.drudis.2010.01.009.

(96) Tomalia, D. A.; Reyna, L. A.; Svenson, S. Dendrimers as Multi-Purpose Nanodevices for Oncology Drug Delivery and Diagnostic Imaging. *Biochem. Soc. Trans.* **2007**, *35*, 61–67.

https://doi.org/10.1042/BST0350061.

(97) Kitchens, K. M.; Kolhatkar, R. B.; Swaan, P. W.; Eddington, N. D.; Ghandehari, H. Transport of Poly(Amidoamine) Dendrimers across Caco-2 Cell Monolayers: Influence of Size, Charge and Fluorescent Labeling. *Pharm. Res.* **2006**, *23*, 2818–2826. https://doi.org/10.1007/s11095-006-9122-2.

(98) Dias, A. P.; da Silva Santos, S.; da Silva, J. V.; Parise-Filho, R.; Igne Ferreira, E.; Seoud, O. El; Giarolla, J. Dendrimers in the Context of Nanomedicine. *Int. J. Pharm.* **2020**, *573*, 118814. https://doi.org/10.1016/j.ijpharm.2019.118814.

(99) Hillaireau, H.; Couvreur, P. Nanocarriers' Entry into the Cell: Relevance to Drug Delivery. *Cell. Mol. Life Sci.* **2009**, *66*, 2873–2896. https://doi.org/10.1007/s00018-009-0053-z.

(100) Vidal, F.; Vásquez, P.; Díaz, C.; Nova, D.; Alderete, J.; Guzmán, L. Mechanism of PAMAM Dendrimers Internalization in Hippocampal Neurons. *Mol. Pharm.* **2016**, *13*, 3395–3403. https://doi.org/10.1021/acs.molpharmaceut.6b00381.

(101) Kitchens, K. M.; El-Sayed, M. E. H.; Ghandehari, H. Transepithelial and Endothelial Transport of Poly (Amidoamine) Dendrimers. *Adv. Drug Deliv. Rev.* **2005**, *57*, 2163–2176. https://doi.org/10.1016/j.addr.2005.09.013.

(102) Fox, L. J.; Richardson, R. M.; Briscoe, W. H. PAMAM Dendrimer - Cell Membrane Interactions. *Adv. Colloid Interface Sci.* **2018**, *257*, 1–18. https://doi.org/10.1016/j.cis.2018.06.005.

(103) Labieniec-Watala, M.; Watala, C. PAMAM Dendrimers: Destined for Success or Doomed to Fail? Plain and Modified PAMAM Dendrimers in the Context of Biomedical Applications. *J. Pharm. Sci.* **2015**, *104*, 2–14. https://doi.org/10.1002/jps.24222.

(104) Luong, D.; Kesharwani, P.; Deshmukh, R.; Mohd Amin, M. C. I.; Gupta, U.; Greish, K.; Iyer, A. K. PEGylated PAMAM Dendrimers: Enhancing Efficacy and Mitigating Toxicity for Effective Anticancer Drug and Gene Delivery. *Acta Biomater.* **2016**, *43*, 14–29. https://doi.org/10.1016/j.actbio.2016.07.015.

(105) Duncan, R.; Izzo, L. Dendrimer Biocompatibility and Toxicity. *Adv. Drug Deliv. Rev.* **2005**, *57*, 2215–2237. https://doi.org/10.1016/j.addr.2005.09.019.

(106) Malik, N.; Wiwattanapatapee, R.; Klopsch, R.; Lorenz, K.; Frey, H.; Weener, J. W.; Meijer, E. W.; Paulus, W.; Duncan, R. Dendrimers: Relationship between Structure and Biocompatibility *in Vitro*, and Preliminary Studies on the Biodistribution of ^{125}I-Labelled Polyamidoamine Dendrimers *in Vivo*. *J. Control. Release* **2000**, *68*, 133–148. https://doi.org/10.1016/S0168-3659(00)00283-2.

(107) Abedi-Gaballu, F.; Dehghan, G.; Ghaffari, M.; Yekta, R.; Abbaspour-Ravasjani, S.; Baradaran, B.; Dolatabadi, J. E. N.; Hamblin, M. R. PAMAM Dendrimers as Efficient Drug and Gene Delivery Nanosystems for Cancer Therapy. *Appl. Mater. Today* **2018**, *12*, 177–190. https://doi.org/10.1016/j.apmt.2018.05.002.

(108) Thomas, T. P.; Choi, S. K.; Li, M.-H.; Kotlyar, A.; Jr., J. R. B. Design of Riboflavin-Presenting PAMAM Dendrimers as a New Nanoplatform for Cancer-Targeted Delivery. *Bioorganic Med. Chem. Lett.* **2010**, *20*, 5191–5194. https://doi.org/10.1016/j.bmcl.2010.07.005.Design.

(109) Zhu, S.; Hong, M.; Zhang, L.; Tang, G.; Jiang, Y.; Pei, Y. PEGylated PAMAM Dendrimer-Doxorubicin Conjugates: *In Vitro* Evaluation and *in Vivo* Tumor Accumulation. *Pharm. Res.* **2010**, *27*, 161–174. https://doi.org/10.1007/s11095-009-9992-1.

(110) Mignani, S.; Rodrigues, J.; Tomas, H.; Roy, R.; Shi, X.; Majoral, J. Bench-to-Bedside Translation of Dendrimers : Reality or Utopia ? A Concise Analysis. *Adv. Drug Deliv. Rev.* **2018**, *136–137*, 73–81. https://doi.org/10.1016/j.addr.2017.11.007.

(111) Trzepiński, P.; Klajnert-Maculewicz, B. Dendrimers for Fluorescence-Based Bioimaging. *J Chem Technol Biotechnol* **2017**, *92*, 1157–1166. https://doi.org/10.1002/jctb.5216.

(112) Noriega-Luna, B.; Godínez, L. A.; Rodríguez, F. J.; Rodríguez, A.; Zaldívar-Lelo De Larrea, G.; Sosa-Ferreyra, C. F.; Mercado-Curiel, R. F.; Manríquez, J.; Bustos, E. Applications of Dendrimers in Drug Delivery Agents, Diagnosis, Therapy, and Detection. *J. Nanomater.* **2014**, *2014*, 1–19. https://doi.org/10.1155/2014/507273.

(113) Jain, K.; Kesharwani, P.; Gupta, U.; Jain, N. K. Dendrimer Toxicity: Let's Meet the Challenge. *Int. J. Pharm.* **2010**, *394*, 122–142. https://doi.org/10.1016/j.ijpharm.2010.04.027.

(114) Scutaru, A. M.; Krüger, M.; Wenzel, M.; Richter, J.; Gust, R. Investigations on the Use of Fluorescence Dyes for Labeling Dendrimers: Cytotoxicity, Accumulation Kinetics, and Intracellular Distribution. *Bioconjug. Chem.* **2010**, *21*, 2222–2226. https://doi.org/10.1021/bc1001906.

(115) Tomalia, D. A.; Klajnert-Maculewicz, B.; Johnson, K. A.-M.; Brinkman, H. F.; Janaszewska, A.; Hedstrand, D. M. Non-Traditional Intrinsic Luminescence: Inexplicable Blue Fluorescence Observed for Dendrimers, Macromolecules and Small Molecular Structures Lacking Traditional/Conventional Luminophores. *Prog. Polym. Sci.* **2019**, *90*, 35–117. https://doi.org/10.1016/j.progpolymsci.2018.09.004.

(116) Wang, D.; Imae, T.; Miki, M. Fluorescence Emission from PAMAM and PPI Dendrimers. *J. Colloid Interface Sci.* **2007**, *306*, 222–227. https://doi.org/10.1016/j.jcis.2006.10.025.

(117) Wang, D.; Imae, T. Fluorescence Emission from Dendrimers and Its PH Dependence. *J. Am. Chem. Soc.* **2004**, *126*, 13204–13205. https://doi.org/10.1021/ja0454992.

(118) Lee, W. I.; Bae, Y.; Bard, A. J. Strong Blue Photoluminescence and ECL from OH-Terminated PAMAM Dendrimers in the Absence of Gold Nanoparticles. *J. Am. Chem. Soc.* **2004**, *126*, 8358–8359. https://doi.org/10.1021/ja0475914.

(119) Tsai, Y. J.; Hu, C. C.; Chu, C. C.; Imae, T. Intrinsically Fluorescent PAMAM Dendrimer as Gene Carrier and Nanoprobe for Nucleic Acids Delivery: Bioimaging and Transfection Study. *Biomacromolecules* **2011**, *12*, 4283–4290. https://doi.org/10.1021/bm201196p.

(120) Larson, C. L.; Tucker, S. A. Intrinsic Fluorescence of Carboxylate-Terminated Polyamido Amine Dendrimers. *Appl. Spectrosc.* **2001**, *55*, 679–683. https://doi.org/10.1366/0003702011952596.

(121) Saravanan, G.; Abe, H. Influence of PH on Dendritic Structure of Strongly Fluorescent Persulfate-Treated Poly(Amidoamine) Dendrimer. *J. Photochem. Photobiol. A Chem.* **2011**, *224*, 102–109. https://doi.org/10.1016/j.jphotochem.2011.09.012.

(122) Chu, C. C.; Imae, T. Fluorescence Investigations of Oxygen-Doped Simple Amine Compared with Fluorescent PAMAM Dendrimer. *Macromol. Rapid Commun.* **2009**, *30*, 89–93. https://doi.org/10.1002/marc.200800571.

(123) Sherje, A. P.; Jadhav, M.; Dravyakar, B. R.; Kadam, D. Dendrimers: A Versatile Nanocarrier for Drug Delivery and Targeting. *Int. J. Pharm.* **2018**, *548*, 707–720. https://doi.org/10.1016/j.ijpharm.2018.07.030.

(124) Huang, D.; Wu, D. Biodegradable Dendrimers for Drug Delivery. *Mater. Sci. Eng. C* **2018**, *90*, 713–727. https://doi.org/10.1016/j.msec.2018.03.002.

(125) Twibanire, J. d. A. K.; Grindley, T. B. Polyester Dendrimers: Smart Carriers for Drug Delivery. *Polymers* **2014**, *6*, 179–213. https://doi.org/10.3390/polym6010179.

(126) Ihre, H.; Hult, A.; Söderlind, E. Synthesis, Characterization, and ^{1}H-NMR Self-Diffusion Studies of Dendritic Aliphatic Polyesters Based on 2,2-Bis(Hydroxymethyl)Propionic Acid and 1,1,1-Tris(Hydroxyphenyl)Ethane. *J. Am. Chem. Soc.* **1996**, *118*, 6388–6395. https://doi.org/10.1021/ja954171t.

(127) Carlmark, A.; Hawker, C.; Hult, A.; Malkoch, M. New Methodologies in the Construction of Dendritic Materials. *Chem. Soc. Rev.* **2009**, *38*, 352–362. https://doi.org/10.1039/b711745k.

(128) Leiro, V.; Garcia, J. P.; Tomás, H.; Pêgo, A. P. The Present and the Future of Degradable Dendrimers and Derivatives in Theranostics. *Bioconjug. Chem.* **2015**, *26*, 1182–1197. https://doi.org/10.1021/bc5006224.

(129) Movellan, J.; González-Pastor, R.; Martín-Duque, P.; Sierra, T.; De La Fuente, J. M.; Serrano, J. L. New Ionic Bis-MPA and PAMAM Dendrimers: A Study of Their Biocompatibility and DNA-Complexation. *Macromol. Biosci.* **2015**, *15*, 657–667. https://doi.org/10.1002/mabi.201400422.

(130) Feliu, N.; Walter, M. V.; Montañez, M. I.; Kunzmann, A.; Hult, A.; Nyström, A.; Malkoch, M.; Fadeel, B. Stability and Biocompatibility of a Library of Polyester Dendrimers in Comparison to Polyamidoamine Dendrimers. *Biomaterials* **2012**, *33*, 1970–1981. https://doi.org/10.1016/j.biomaterials.2011.11.054.

(131) Carlmark, A.; Malmström, E.; Malkoch, M. Dendritic Architectures Based on Bis-MPA: Functional Polymeric Scaffolds for Application-Driven Research. *Chem. Soc. Rev.* **2013**, *42*, 5858–5879. https://doi.org/10.1039/c3cs60101c.

(132) Chirag, M.; Gowda, D. V.; Babu, S.; Famna Roohi, N. K. A Comprehensive Review on Dendrimers in Current Advanced Drug Delivery. *Int. J. Res. Pharm. Sci.* **2020**, *11*, 1055–1066. https://doi.org/10.26452/ijrps.v11i1.1936.

(133) Vogtle, F.; Richardt, G.; Werner, N. Chapter 2- Synthetic Methods for Dendritic Molecules. In *Dendrimer Chemistry*; WILEY-VCH Verlag GmbH & Co. KGaA: Weinheim, 2009; pp 25–48. https://doi.org/10.1002/9783527626953.ch2.

(134) Zeng, X.; Zhang, Y.; Wu, Z.; Lundberg, P.; Malkoch, M.; Nyström, A. M. Hyperbranched Copolymer Micelles as Delivery Vehicles of Doxorubicin in Breast Cancer Cells. *J. Polym. Sci. Part A Polym.*

Chem. **2012**, *50*, 280–288. https://doi.org/10.1002/pola.25027.

(135) Govender, P.; Therrien, B.; Smith, G. S. Bio-Metallodendrimers - Emerging Strategies in Metal-Based Drug Design. *Eur. J. Inorg. Chem.* **2012**, *2012*, 2853–2862. https://doi.org/10.1002/ejic.201200161.

(136) Viñas, C.; Teixidor, F.; Núñez, R. Boron Clusters-Based Metallodendrimers. *Inorganica Chim. Acta* **2014**, *409*, 12–25. https://doi.org/10.1016/j.ica.2013.05.038.

(137) Yan, Y.; Zhang, J.; Ren, L.; Tang, C. Metal-Containing and Related Polymers for Biomedical Applications. *Chem. Soc. Rev.* **2016**, *45*, 5232–5263. https://doi.org/10.1039/c6cs00026f.

(138) Vogtle, F.; Richardt, G.; Werner, N. Chapter 4- Types of Dendrimers and Their Syntheses. In *Dendrimer Chemistry*; WILEY-VCH Verlag GmbH & Co. KGaA: Weinheim, 2009; pp 81–167. https://doi.org/10.1002/9783527626953.ch4.

(139) Newkome, G. R.; Moorefield, C. N.; Baker, G. R.; Saunders, M. J.; Grossman, S. H. Unimolecular Micelles. *Angew. Chemie Int. Ed. English* **1991**, *30*, 1178–1180. https://doi.org/10.1002/anie.199111781.

(140) Denti, G.; Serroni, S.; Ricevuto, V.; Balzani, V. Directional Energy Transfer in a Luminescent Tetranuclear Ru(II) Polypyridine Complex That Contains Two Different Types of Bridging Ligands. *Inorg. Chim. Acta* **1991**, *182*, 127–129.

(141) Denti, G.; Campagna, S.; Serroni, S.; Ciano, M.; Balzani, V. Decanuclear Homo- and Heterometallic Polypyridine Complexes: Syntheses, Absorption Spectra, Luminescence, Electrochemical Oxidation, and Intercomponent Energy Transfer. *J. Am. Chem. Soc.* **1992**, *114*, 2944–2950. https://doi.org/10.1021/ja00044a072.

(142) Valério, C.; Alonso, E.; Ruiz, J.; Blais, J.-C.; Astruc, D. A Polycationic Metallodendrimer with 24 $[Fe(\eta5\text{-}C_5Me_5)(\eta6\text{-N-Alkylaniline})]^+$ Termini That Recognizes Chloride and Bromide Anions. *Angew. Chem. Int. Ed.* **1999**, *38*, 1747–1751. https://doi.org/10.1002/(SICI)1521-3773(19990614)38:12<1747::AID-ANIE1747>3.0.CO;2-G.

(143) Fréchet, J. M. J. Dendrimers and Supramolecular Chemistry. *Supramol. Chem.* **2002**, *99*, 4782–4787. https://doi.org/10.1080/1061027031000073199.

(144) Hwang, S. H.; Shreiner, C. D.; Moorefield, C. N.; Newkome, G. R. Recent Progress and Applications for Metallodendrimers. *New J. Chem.* **2007**, *31*, 1192–1217. https://doi.org/10.1039/b612656c.

(145) J. Jansen, B. A.; van der Zwan, J.; Reedijk, J.; den Dulk, H.; Brouwer, J. A Tetranuclear Platinum Compound Designed to Overcome Cisplatin Resistance. *Eur. J. Inorg. Chem.* **1999**, *1999*, 1429–1433. https://doi.org/10.1002/(sici)1099-0682(1999010.1002/(SICI)1099-0682(199909)1999:9<1429::AID-EJIC1429>3.0.CO;2-8.

(146) Malik, N.; Evagorou, E. G.; Duncan, R. Dendrimer-Platinate: A Novel Approach to Cancer Chemotherapy. *Anticancer. Drugs* **1999**, *10*, 767–776. https://doi.org/10.1097/00001813-199909000-00010.

(147) Gouveia, M.; Figueira, J.; Jardim, M. G.; Castro, R.; Tomás, H.; Rissanen, K.; Rodrigues, J. Poly(Alkylidenimine) Dendrimers Functionalized with the Organometallicmoiety [Ru(η5-

$C_5H_5)(PPh_3)_2]^+$ as Promising Drugs against Cisplatin-Resistant Cancer Cells and Humanmesenchymal Stem Cells. *Molecules* **2018**, *23*, 1–17. https://doi.org/10.3390/molecules23061471.

(148) Ahamad, T.; Mapolie, S. F.; Alshehri, S. M. Synthesis and Characterization of Polyamide Metallodendrimers and Their Anti-Bacterial and Anti-Tumor Activities. *Med. Chem. Res.* **2012**, *21*, 2023–2031. https://doi.org/10.1007/s00044-011-9715-0.

(149) Zhao, X.; Loo, S. C. J.; Lee, P. P. F.; Tan, T. T. Y.; Chu, C. K. Synthesis and Cytotoxic Activities of Chloropyridylimineplatinum(II) and Chloropyridyliminecopper(II) Surface-Functionalized Poly(Amidoamine) Dendrimers. *J. Inorg. Biochem.* **2010**, *104*, 105–110. https://doi.org/10.1016/j.jinorgbio.2009.10.001.

(150) Robilotto, T. J.; Deligonul, N.; Updegraff, J. B.; Gray, T. G. Azido, Triazolyl, and Alkynyl Complexes of Gold(I): Syntheses, Structures, and Ligand Effects. *Inorg. Chem.* **2013**, *52*, 9659–9668. https://doi.org/10.1021/ic4014569.

(151) Parveen, S. Recent Advances in Anticancer Ruthenium Schiff Base Complexes. *Appl. Organomet. Chem.* **2020**, *34*, e5687. https://doi.org/10.1002/aoc.5687.

(152) Chen, L.; Mignani, S.; Caminade, A.-M.; Majoral, J.-P. Metal-Based Phosphorus Dendrimers as Novel Nanotherapeutic Strategies to Tackle Cancers: A Concise Overview. *WIREs Nanomed Nanobiotechnol.* **2019**, *11*, 1577–1588. https://doi.org/10.1002/wnan.1577.

(153) Medici, S.; Peana, M.; Nurchi, V. M.; Lachowicz, J. I.; Crisponi, G.; Zoroddu, M. A. Noble Metals in Medicine: Latest Advances. *Coord. Chem. Rev.* **2015**, *284*, 329–350. https://doi.org/10.1016/j.ccr.2014.08.002.

(154) Mjos, K. D.; Orvig, C. Metallodrugs in Medicinal Inorganic Chemistry. *Chem. Rev.* **2014**, *114*, 4540–4563. https://doi.org/10.1021/cr400460s.

(155) Frezza, M.; Hindo, S.; Chen, D.; Davenport, A.; Schmitt, S.; Tomco, D.; Ping Dou, Q. Novel Metals and Metal Complexes as Platforms for Cancer Therapy. *Curr. Pharm. Des.* **2010**, *16*, 1813–1825. https://doi.org/10.2174/138161210791209009.

(156) Bruijnincx, P. C.; Sadler, P. J. New Trends for Metal Complexes with Anticancer Activity. *Curr. Opin. Chem. Biol.* **2008**, *12*, 197–206. https://doi.org/10.1016/j.cbpa.2007.11.013.

(157) Ndagi, U.; Mhlongo, N.; Soliman, M. E. Metal Complexes in Cancer Therapy - an Update from Drug Design Perpective. *Drug Des. Devel. Ther.* **2017**, *11*, 599–616. https://doi.org/10.2147/DDDT.S119488.

(158) Marques, M. P. M. Platinum and Palladium Polyamine Complexes as Anticancer Agents: The Structural Factor. *ISRN Spectrosc.* **2013**, *2013*, 1–29. https://doi.org/10.1155/2013/287353.

(159) Desoize, B. Metals and Metal Compounds in Cancer Treatment. *Anticancer Res.* **2004**, *24*, 1529–1544.

(160) Bai, L.; Gao, C.; Liu, Q.; Yu, C.; Zhang, Z.; Cai, L.; Yang, B.; Qian, Y.; Yang, J.; Liao, X. Research Progress in Modern Structure of Platinum Complexes. *Eur. J. Med. Chem.* **2017**, *140*, 349–382. https://doi.org/10.1016/j.ejmech.2017.09.034.

(161) Haxton, K. J.; Burt, H. M. Polymeric Drug Delivery of Platinum-Based Anticancer Agents. *J. Pharm.*

Sci. **2009**, *98*, 2299–2316. https://doi.org/10.1002/jps.21611.

(162) Cleare, M. J.; Hydes, P. C.; Malerbi, B. W.; Watkins, D. M. Anti-Tumour Platinum Complexes : Relationships between Chemical Properties and Activity. *Biochimie* **1978**, *60*, 835–850. https://doi.org/10.1016/S0300-9084(78)80568-9.

(163) Lazarević, T.; Rilak, A.; Bugarčić, Ž. D. Platinum, Palladium, Gold and Ruthenium Complexes as Anticancer Agents: Current Clinical Uses, Cytotoxicity Studies and Future Perspectives. *Eur. J. Med. Chem.* **2017**, *142*, 8–31. https://doi.org/10.1016/j.ejmech.2017.04.007.

(164) Kazzouli, S. El; Brahmi, N. El; Mignani, S.; Bousmina, M.; Zablocka, M.; Majoral, J.-P. From Metallodrugs to Metallodendrimers for Nanotherapy in Oncology: A Concise Overview. *Curr. Med. Chem.* **2012**, *19*, 4995–5010. https://doi.org/10.2174/092986731120902499 5.

(165) Rottenberg, S.; Disler, C.; Perego, P. The Rediscovery of Platinum-Based Cancer Therapy. *Nat. Rev. Cancer* **2021**, *21*, 37–50. https://doi.org/10.1038/s41568-020-00308-y.

(166) Kauffman, G. B.; Pentimalli, R.; Doldi, S.; Hall, M. D. Michele Peyrone (1813-1883), Discoverer of Cisplatin. *Platin. Met. Rev.* **2010**, *54*, 250–256. https://doi.org/10.1595/147106710X534326.

(167) Rosenberg, B.; Camp, L. Van; Krigas, T. Inhibition of Cell Division in Escherichia Coli by Electrolysis Products from a Platinum Electrode. *Nature* **1965**, *205*, 698–699. https://doi.org/10.1038/205698a0.

(168) Kelland, L. The Resurgence of Platinum-Based Cancer Chemotherapy. *Nat. Rev. Cancer* **2007**, *7*, 573–584. https://doi.org/10.1038/nrc2167.

(169) Dilruba, S.; Kalayda, G. V. Platinum-Based Drugs: Past, Present and Future. *Cancer Chemother. Pharmacol.* **2016**, *77*, 1103–1124. https://doi.org/10.1007/s00280-016-2976-z.

(170) Rosenberg, B.; VanCamp, L.; Trosko, J. E.; Mansour, V. H. Platinum Compounds: A New Class of Potent Antitumor Agents. *Nature* **1969**, *222*, 385–386. https://doi.org/10.1038/224488a0.

(171) Xian, C.; Chen, H.; Xiong, F.; Fang, Y.; Huang, H.; Wu, J. Platinum-Based Chemotherapy via Nanocarriers and Co-Delivery of Multiple Drugs. *Biomater. Sci.* **2021**, *9*, 6023–6036. https://doi.org/10.1039/d1bm00879j.

(172) Johnstone, T. C.; Suntharalingam, K.; Lippard, S. J. The Next Generation of Platinum Drugs: Targeted Pt(II) Agents, Nanoparticle Delivery, and Pt(IV) Prodrugs. *Chem. Rev.* **2016**, *116*, 3436–3486. https://doi.org/10.1021/acs.chemrev.5b00597.

(173) Ma, P.; Xiao, H.; Li, C.; Dai, Y.; Cheng, Z.; Hou, Z.; Lin, J. Inorganic Nanocarriers for Platinum Drug Delivery. *Mater. Today* **2015**, *18*, 554–564. https://doi.org/10.1016/j.mattod.2015.05.017.

(174) Oun, R.; Moussa, Y. E.; Wheate, N. J. The Side Effects of Platinum-Based Chemotherapy Drugs: A Review for Chemists. *Dalt. Trans.* **2018**, *47*, 6645–6653. https://doi.org/10.1039/c8dt00838h.

(175) Oberoi, H. S.; Nukolova, N. V.; Kabanov, A. V.; Bronich, T. K. Nanocarriers for Delivery of Platinum Anticancer Drugs. *Adv. Drug Deliv. Rev.* **2013**, *65*, 1667–1685. https://doi.org/10.1016/j.addr.2013.09.014.

(176) Mehmood, R. K. Review of Cisplatin and Oxaliplatin in Current Immunogenic and Monoclonal Antibodies Perspective. *Oncol. Rev.* **2014**, *8*, 36–43. https://doi.org/10.4081/oncol.2014.256.

(177) Ciarimboli, G. Membrane Transporters as Mediators of Cisplatin Side-Effects. *Anticancer Res.* **2014**, *34*, 547–550. https://doi.org/10.6064/2012/473829.

(178) Chiorazzi, A.; Semperboni, S.; Marmiroli, P. Current View in Platinum Drug Mechanisms of Peripheral Neurotoxicity. *Toxics* **2015**, *3*, 304–321. https://doi.org/10.3390/toxics3030304.

(179) Dasari, S.; Bernard Tchounwou, P. Cisplatin in Cancer Therapy: Molecular Mechanisms of Action. *Eur. J. Pharmacol.* **2014**, *740*, 364–378. https://doi.org/10.1016/j.ejphar.2014.07.025.

(180) Ghosh, S. Cisplatin: The First Metal Based Anticancer Drug. *Bioorg. Chem.* **2019**, *88*, 102925. https://doi.org/10.1016/j.bioorg.2019.102925.

(181) Gullo, J. J.; Litterst, C. L.; Maguire, P. J.; Sikic, B. I.; Hoth, D. F.; Woolley, P. V. Pharmacokinetics and Protein Binding of Cis-Dichlorodiammine Platinum (II) Administered as a One Hour or as a Twenty Hour Infusion. *Cancer Chemother. Pharmacol.* **1980**, *5*, 21–26. https://doi.org/10.1007/BF00578558.

(182) Visacri, M. B.; Pincinato, E. D. C.; Ferrari, G. B.; Quintanilha, J. C. F.; Mazzola, P. G.; Lima, C. S. P.; Moriel, P. Adverse Drug Reactions and Kinetics of Cisplatin Excretion in Urine of Patients Undergoing Cisplatin Chemotherapy and Radiotherapy for Head and Neck Cancer: A Prospective Study. *DARU, J. Pharm. Sci.* **2017**, *25*, 1–9. https://doi.org/10.1186/s40199-017-0178-9.

(183) Stewart, D. J.; Benjamin, R. S.; Luna, M.; Feun, L.; Caprioli, R.; Seifert, W.; Loo, T. L. Human Tissue Distribution of Platinum after Cis-Diamminedichloroplatinum. *Cancer Chemother. Pharmacol.* **1980**, *10*, 51–54. https://doi.org/10.1007/BF00257239.

(184) Amable, L. Cisplatin Resistance and Opportunities for Precision Medicine. *Pharmacol. Res.* **2016**, *106*, 27–36. https://doi.org/10.1016/j.phrs.2016.01.001.

(185) Hall, M. D.; Okabe, M.; Shen, D.-W.; Liang, X.-J.; Gottesman, M. M. The Role of Cellular Accumulation in Determining Sensitivity to Platinum-Based Chemotherapy. *Annu. Rev. Pharmacol. Toxicol.* **2008**, *48*, 495–535. https://doi.org/10.1146/annurev.pharmtox.48.080907.180426.

(186) Klein, A. V.; Hambley, T. W. Platinum Drug Distribution in Cancer Cells and Tumors. *Chem. Rev.* **2009**, *109*, 4911–4920. https://doi.org/10.1021/cr9001066.

(187) Apps, M. G.; Choi, E. H. Y.; Wheate, N. J. The State-of-Play and Future of Platinum Drugs. *Endocr. Relat. Cancer* **2015**, *22*, 219–233. https://doi.org/10.1530/ERC-15-0237.

(188) Chen, S. H.; Chang, J. Y. New Insights into Mechanisms of Cisplatin Resistance: From Tumor Cell to Microenvironment. *Int. J. Mol. Sci.* **2019**, *20*, 1–21. https://doi.org/10.3390/ijms20174136.

(189) Jo, Y.; Choi, N.; Kim, K.; Koo, H. J.; Choi, J.; Kim, H. N. Chemoresistance of Cancer Cells: Requirements of Tumor Microenvironment-Mimicking *in Vitro* Models in Anti-Cancer Drug Development. *Theranostics* **2018**, *8*, 5259–5275. https://doi.org/10.7150/thno.29098.

(190) Correia, A. L.; Bissell, M. J. The Tumor Microenvironment Is a Dominant Force in Multidrug Resistance. *Drug Resist. Updat.* **2012**, *15*, 1–22. https://doi.org/10.1038/jid.2014.371.

(191) Martinho, N.; Santos, T. C. B.; Florindo, H. F.; Silva, L. C. Cisplatin-Membrane Interactions and Their Influence on Platinum Complexes Activity and Toxicity. *Front. Physiol.* **2019**, *9*, 1–15.

https://doi.org/10.3389/fphys.2018.01898.

(192) Johnstone, T. C.; Suntharalingam, K.; Lippard, S. J. Third Row Transition Metals for the Treatment of Cancer. *Philos. Trans. A* **2015**, *373*, 1–12. https://doi.org/10.1098/rsta.2014.0185.

(193) Wang, D.; Lippard, S. J. Cellular Processing of Platinum Anticancer Drugs. *Nat. Rev. Drug Discov.* **2005**, *4*, 307–320. https://doi.org/10.1038/nrd1691.

(194) Sakhrani, N. M.; Padh, H. Organelle Targeting: Third Level of Drug Targeting. *Drug Des. Devel. Ther.* **2013**, *7*, 585–599. https://doi.org/10.2147/DDDT.S45614.

(195) Wilson, J. J.; Lippard, S. J. Synthetic Methods for the Preparation of Platinum Anticancer Complexes. *Chem. Rev.* **2014**, *114*, 4470–4495. https://doi.org/10.1021/cr4004314.

(196) Crul, M.; van Waardenburg, R. C. A. M.; Beijnen, J. H.; Schellens, J. H. M. DNA-Based Drug Interactions of Cisplatin. *Cancer Treat. Rev.* **2002**, *28*, 291–303. https://doi.org/10.1016/S0305-7372(02)00093-2.

(197) Todd, R. C.; Lippard, S. J. Inhibition of Transcription by Platinum Antitumor Compounds. *Metallomics* **2009**, *1*, 280–291. https://doi.org/10.1039/b907567d.

(198) Awasthi, P.; Foiani, M.; Kumar, A. ATM and ATR Signaling at a Glance. *J. Cell Sci.* **2016**, *129*, 4255–4262. https://doi.org/doi:10.1242/jcs.169730.

(199) O'Grady, S.; Finn, S. P.; Cuffe, S.; Richard, D. J.; O'Byrne, K. J.; Barr, M. P. The Role of DNA Repair Pathways in Cisplatin Resistant Lung Cancer. *Cancer Treat. Rev.* **2014**, *40*, 1161–1170. https://doi.org/10.1016/j.ctrv.2014.10.003.

(200) Brabec, V.; Hrabina, O.; Kasparkova, J. Cytotoxic Platinum Coordination Compounds. DNA Binding Agents. *Coord. Chem. Rev.* **2017**, *351*, 2–31. https://doi.org/10.1016/j.ccr.2017.04.013.

(201) Köberle, B.; Tomicic, M. T.; Usanova, S.; Kaina, B. Cisplatin Resistance: Preclinical Findings and Clinical Implications. *Biochim. Biophys. Acta* **2010**, *1806*, 172–182. https://doi.org/10.1016/j.bbcan.2010.07.004.

(202) Gartel, A. L. Transcriptional Inhibitors, P53 and Apoptoss. *Biochim. Biophys. Acta* **2008**, *1786*, 83–86. https://doi.org/10.1016/j.bbcan.2008.04.004.

(203) Derheimer, F. A.; Chang, C. W.; Ljungman, M. Transcription Inhibition: A Potential Strategy for Cancer Therapeutics. *Eur. J. Cancer* **2005**, *41*, 2569–2576. https://doi.org/10.1016/j.ejca.2005.08.012.

(204) Raymond, E.; Chaney, S. G.; Taamma, A.; Cvitkovic, E. Oxaliplatin: A Review of Preclinical and Clinical Studies. *Ann. Oncol.* **1998**, *9*, 1053–1071. https://doi.org/10.1023/A:1008213732429.

(205) Höfer, D.; Galanski, M.; Keppler, B. K. Synthesis, Characterization, and Time-Dependent NMR Spectroscopy Studies of (SP-4-2)-[(Trans-1R,2R/1S,2S-$^{15}N_2$)-Cyclohexane-1,2-Diamine][($^{13}C_2$)Oxalato]Platinum(II). *Eur. J. Inorg. Chem.* **2017**, *2017*, 2347–2354. https://doi.org/10.1002/ejic.201601503.

(206) Siddik, Z. H.; Ai-baker, S.; Thai, G.; Abdul, R. K. Antitumor Activity of Isomeric 1, 2-Diaminocyclohexane Platinum (IV) Complexes. *Cancer Res. Clin. Oncol.* **1994**, *120*, 409–414. https://doi.org/10.1007/BF01240140.

(207) Galanski, M.; Yasemi, A.; Slaby, S.; Jakupec, M. A.; Arion, V. B.; Rausch, M.; Nazarov, A. A.; Keppler, B. K. Synthesis, Crystal Structure and Cytotoxicity of New Oxaliplatin Analogues Indicating That Improvement of Anticancer Activity Is Still Possible. *Eur. J. Med. Chem.* **2004**, *39*, 707–714. https://doi.org/10.1016/j.ejmech.2004.04.003.

(208) Alcindor, T.; Beauger, N. Oxaliplatin: A Review in the Era of Molecularly Targeted Therapy. *Curr. Oncol.* **2011**, *18*, 18–25. https://doi.org/10.3747/co.v18i1.708.

(209) Abu Ammar, A.; Raveendran, R.; Gibson, D.; Nassar, T.; Benita, S. A Lipophilic Pt(IV) Oxaliplatin Derivative Enhances Antitumor Activity. *J. Med. Chem.* **2016**, *59*, 9035–9046. https://doi.org/10.1021/acs.jmedchem.6b00955.

(210) Li, B.; Meng, Z.; Li, Q.; Huang, X.; Kang, Z.; Dong, H.; Chen, J.; Sun, J.; Dong, Y.; Li, J.; Jia, X.; Sessler, J. L.; Meng, Q.; Li, C. A PH Responsive Complexation-Based Drug Delivery System for Oxaliplatin. *Chem. Sci.* **2017**, *8*, 4458–4464. https://doi.org/10.1039/c7sc01438d.

(211) Graham, M. A.; Lockwood, G. F.; Greenslade, D.; Brienza, S.; Bayssas, M.; Gamelin, E. Clinical Pharmacokinetics of Oxaliplatin: A Critical Review. *Clin. Cancer Res.* **2000**, *6*, 1205–1218. https://doi.org/10.1201/9781420038590.ch1.

(212) Ehrsson, H.; Wallin, I.; Yachnin, J. Pharmacokinetics of Oxaliplatin in Humans. *Med. Oncol.* **2002**, *19*, 261–265. https://doi.org/10.1385/MO:19:4:261.

(213) Quan, X. Q.; Kang, L.; Yin, X. Z.; Jin, Z. H.; Gao, Z. G. Synthesis of PEGylated Hyaluronic Acid for Loading Dichloro(1,2-Diaminocyclohexane)Platinum(II) (DACHPt) in Nanoparticles for Cancer Treatment. *Chinese Chem. Lett.* **2015**, *26*, 695–699. https://doi.org/10.1016/j.cclet.2015.04.024.

(214) Cheng, Q.; Shi, H.; Huang, H.; Cao, Z.; Wang, J.; Liu, Y. Oral Delivery of a Platinum Anticancer Drug Using Lipid Assisted Polymeric Nanoparticles. *Chem. Commun.* **2015**, *51*, 17536–17539. https://doi.org/10.1039/C5CC07853A.

(215) Di Francesco, A. M.; Ruggiero, A.; Riccardi, R. Cellular and Molecular Aspects of Drugs of the Future: Oxaliplatin. *Cell. Mol. Life Sci.* **2002**, *59*, 1914–1927. https://doi.org/10.1007/PL00012514.

(216) Martinez-Balibrea, E.; Martínez-Cardus, A.; Gines, A.; Ruiz De Porras, V.; Moutinho, C.; Layos, L.; Manzano, J. L.; Buges, C.; Bystrup, S.; Esteller, M.; Abad, A. Tumor-Related Molecular Mechanisms of Oxaliplatin Resistance. *Mol. Cancer Ther.* **2015**, *14*, 1767–1776. https://doi.org/10.1158/1535-7163.MCT-14-0636.

(217) Zhang, S.; Lovejoy, K. S.; Shima, J. E.; Lagpacan, L. L.; Shu, Y.; Lapuk, A.; Chen, Y.; Komori, T.; Gray, J. W.; Chen, X.; Lippard, S. J.; Giacomini, K. M. Organic Cation Transporters Are Determinants of Oxaliplatin Cytotoxicity. *Cancer Res.* **2006**, *66*, 8847–8857. https://doi.org/10.1158/0008-5472.CAN-06-0769.

(218) Boulikas, T. Molecular Mechanisms of Cisplatin and Its Liposomally Encapsulated Form , Lipoplatin™. Lipoplatin™ as a Chemotherapy and Antiangiogenesis Drug. *Cancer Ther. Vol Cancer Ther.* **2007**, *5*, 349–376.

(219) Fong, C. W. Platinum Anti-Cancer Drugs: Free Radical Mechanism of Pt-DNA Adduct Formation and

Anti-Neoplastic Effect. *Free Radic. Biol. Med.* **2016**, *95*, 216–229. https://doi.org/10.1016/j.freeradbiomed.2016.03.006.

(220) Cabral, H.; Nishiyama, N.; Okazaki, S.; Koyama, H.; Kataoka, K. Preparation and Biological Properties of Dichloro(1,2-Diaminocyclohexane) Platinum(II) (DACHPt)-Loaded Polymeric Micelles. *J. Control. Release* **2005**, *101*, 223–232. https://doi.org/10.1016/j.jconrel.2004.08.022.

(221) Chaney, S. G.; Campbell, S. L.; Bassett, E.; Wu, Y. Recognition and Processing of Cisplatin- and Oxaliplatin-DNA Adducts. *Crit. Rev. Oncol. Hematol.* **2005**, *53*, 3–11. https://doi.org/10.1016/j.critrevonc.2004.08.008.

(222) Hato, S. V.; Khong, A.; De Vries, I. J. M.; Lesterhuis, W. J. Molecular Pathways: The Immunogenic Effects of Platinum-Based Chemotherapeutics. *Clin. Cancer Res.* **2014**, *20*, 2831–2837. https://doi.org/10.1158/1078-0432.CCR-13-3141.

(223) Wang, Y. J.; Fletcher, R.; Yu, J.; Zhang, L. Immunogenic Effects of Chemotherapy-Induced Tumor Cell Death. *Genes Dis.* **2018**, *5*, 194–203. https://doi.org/10.1016/j.gendis.2018.05.003.

(224) Wu, P.; Zhu, X.; Jin, W.; Hao, S.; Liu, Q.; Zhang, L. Oxaliplatin Triggers Necrosis as Well as Apoptosis in Gastric Cancer SGC-7901 Cells. *Biochem. Biophys. Res. Commun.* **2015**, *460*, 183–190. https://doi.org/10.1016/j.bbrc.2015.03.003.

(225) Lim, S. C.; Choi, J. E.; Kang, H. S.; Si, H. Ursodeoxycholic Acid Switches Oxaliplatin-Induced Necrosis to Apoptosis by Inhibiting Reactive Oxygen Species Production and Activating P53-Caspase 8 Pathway in HepG2 Hepatocellular Carcinoma. *Int. J. Cancer* **2010**, *126*, 1582–1595. https://doi.org/10.1002/ijc.24853.

(226) Selvakumaran, M.; Amaravadi, R. K.; Vasilevskaya, I. A.; O'Dwyer, P. J. Autophagy Inhibition Sensitizes Colon Cancer Cells to Antiangiogenic and Cytotoxic Therapy. *Clin. Cancer Res.* **2013**, *19*, 2995–3007. https://doi.org/10.1158/1078-0432.CCR-12-1542.

(227) Shi, Y.; Tang, B.; Yu, P. W.; Tang, B.; Hao, Y. X.; Lei, X.; Luo, H. X.; Zeng, D. Z. Autophagy Protects against Oxaliplatin-Induced Cell Death via ER Stress and ROS in Caco-2 Cells. *PLOS ONE* **2012**, *7*, 1–8. https://doi.org/10.1371/journal.pone.0051076.

(228) Ding, Z. Bin; Hui, B.; Shi, Y. H.; Zhou, J.; Peng, Y. F.; Gu, C. Y.; Yang, H.; Shi, G. M.; Ke, A. W.; Wang, X. Y.; Song, K.; Dai, Z.; Shen, Y. H.; Fan, J. Autophagy Activation in Hepatocellular Carcinoma Contributes to the Tolerance of Oxaliplatin via Reactive Oxygen Species Modulation. *Clin. Cancer Res.* **2011**, *17*, 6229–6238. https://doi.org/10.1158/1078-0432.CCR-11-0816.

(229) Kalayda, G. V.; Kullmann, M.; Galanski, M.; Gollos, S. A Fluorescent Oxaliplatin Derivative for Investigation of Oxaliplatin Resistance Using Imaging Techniques. *J. Biol. Inorg. Chem.* **2017**, *22*, 1295–1304. https://doi.org/10.1007/s00775-017-1502-z.

(230) Sutton, E. C.; Mcdevitt, C. E.; Prochnau, J. Y.; Yglesias, M. V.; Mroz, A. M.; Yang, M. C.; Cunningham, R. M.; Hendon, C. H.; Derose, V. J. Nucleolar Stress Induction by Oxaliplatin and Derivatives. *J. Am. Chem. Soc.* **2019**, *141*, 18411–18415. https://doi.org/10.1021/jacs.9b10319.

(231) Bruno, P. M.; Liu, Y.; Park, G. Y.; Murai, J.; Koch, C. E.; Eisen, T. J.; Pritchard, J. R.; Pommier, Y.;

Lippard, S. J.; Hemann, M. T. A Subset of Platinum-Containing Chemotherapeutic Agents Kills Cells by Inducing Ribosome Biogenesis Stress. *Nat. Med.* **2017**, *23*, 461–471. https://doi.org/10.1038/nm.4291.

(232) Kasparkova, J.; Vojtiskova, M.; Natile, G.; Brabec, V. Unique Properties of DNA Interstrand Cross-Links of Antitumor Oxaliplatin and the Effect of Chirality of the Carrier Ligand. *Chemistry* **2008**, *14*, 1330–1341. https://doi.org/10.1002/chem.200701352.

(233) Mokhtari, R. B.; Homayouni, T. S.; Baluch, N.; Morgatskaya, E.; Kumar, S.; Das, B.; Yeger, H. Combination Therapy in Combating Cancer. *Oncotarget* **2017**, *8*, 38022–38043. https://doi.org/10.18632/oncotarget.16723.

(234) Saputra, E. C.; Huang, L.; Chen, Y.; Tucker-Kellogg, L. Combination Therapy and the Evolution of Resistance: The Theoretical Merits of Synergism and Antagonism in Cancer. *Cancer Res.* **2018**, *78*, 2419–2431. https://doi.org/10.1158/0008-5472.CAN-17-1201.

(235) Tolcher, A. W.; Mayer, L. D. Improving Combination Cancer Therapy: The CombiPlex® Development Platform. *Futur. Oncol.* **2018**, *14*, 1317–1332. https://doi.org/10.2217/fon-2017-0607.

(236) Chou, T. C. Theoretical Basis, Experimental Design, and Computerized Simulation of Synergism and Antagonism in Drug Combination Studies. *Pharmacol. Rev.* **2006**, *58*, 621–681. https://doi.org/10.1124/pr.58.3.10.

(237) Zhang, R. X.; Wong, H. L.; Xue, H. Y.; Eoh, J. Y.; Wu, X. Y. Nanomedicine of Synergistic Drug Combinations for Cancer Therapy-Strategies and Perspectives. *J. Control. Release* **2016**, *240*, 489–503. https://doi.org/10.1016/j.jconrel.2016.06.012.

(238) Jadia, R.; Scandore, C.; Rai, P.; Program, B. Nanoparticles for Effective Combination Therapy of Cancer. *Int. J. Nanotechnol. Nanomedicine* **2016**, *1*, 1–27. https://doi.org/10.33140/ijnn/01/01/00003.

(239) Weiss, A.; Le Roux-Bourdieu, M.; Zoetemelk, M.; Ramzy, G. M.; Rausch, M.; Harry, D.; Miljkovic-Licina, M.; Falamaki, K.; Wehrle-Haller, B.; Meraldi, P.; Nowak-Sliwinska, P. Identification of a Synergistic Multi-Drug Combination Active in Cancer Cells via the Prevention of Spindle Pole Clustering. *Cancers* **2019**, *11*, 1–22. https://doi.org/10.3390/cancers11101612.

(240) Atyabi, F.; Zahir, F.; Khonsari, F.; Shafiee, A.; Mottaghitalab, F. Chapter 21- Combination Therapy of Macromolecules and Small Molecules: Approaches, Advantages and Limitations. In *Nanostructures for Cancer Therapy*; Elsevier Inc., 2017; pp 541–561. https://doi.org/10.1016/B978-0-323-46144-3/00021-0.

(241) Ardizzoni, A.; Rosso, A.; Salvati, F.; Fusco, V.; Cinquegrana, A.; De Palma, M.; Serrano, J.; Pennucci, M. C.; Soresi, E.; Crippa, M.; Gulisano, M.; Castagneto, B.; Scagliotti, G.; Rinaldi, M.; Santi, L. Doxorubicin and Cisplatin Combination Chemotherapy in Patients With Diffuse Malignant Pleural Mesothelioma. *Am. Cancer Soc.* **1991**, *67*, 2984–2987.

(242) Wang, X.; Plomley, J. B.; Newman, R. A.; Cisneros, A. LC/MS/MS Analyses of an Oleander Extract for Cancer Treatment. *Anal. Chem.* **2000**, *72*, 3547–3552. https://doi.org/10.1021/ac991425a.

(243) Apostolou, P.; Toloudi, M.; Chatziioannou, M.; Ioannou, E.; Knocke, D. R.; Nester, J.; Komiotis, D.;

Papasotiriou, I. Anvirzel™ in Combination with Cisplatin in Breast, Colon, Lung, Prostate, Melanoma and Pancreatic Cancer Cell Lines. *BMC Pharmacol. Toxicol.* **2013**, *14*, 1–6. https://doi.org/10.1186/2050-6511-14-18.

(244) Nessa, M. U.; Beale, P.; Chan, C.; Yu, J. Q.; Huq, F. Synergism from Combinations of Cisplatin and Oxaliplatin with Quercetin and Thymoquinone in Human Ovarian Tumour Models. *Anticancer Res.* **2011**, *31*, 3789–3797.

(245) Saltz, L. B.; Clarke, S.; Díaz-Rubio, E.; Scheithauer, W.; Figer, A.; Wong, R.; Koski, S.; Lichinitser, M.; Yang, T. S.; Rivera, F.; Couture, F.; Sirzén, F.; Cassidy, J. Bevacizumab in Combination with Oxaliplatin-Based Chemotherapy as First-Line Therapy in Metastatic Colorectal Cancer: A Randomized Phase III Study. *J. Clin. Oncol.* **2008**, *26*, 2013–2019. https://doi.org/10.1200/JCO.2007.14.9930.

(246) Rosenberg, A. J.; Rademaker, A.; Hochster, H. S.; Ryan, T.; Hensing, T.; Shankaran, V.; Baddi, L.; Mahalingam, D.; Mulcahy, M. F.; Benson, A. B. Docetaxel, Oxaliplatin, and 5-Fluorouracil (DOF) in Metastatic and Unresectable Gastric/Gastroesophageal Junction Adenocarcinoma: A Phase II Study with Long-Term Follow-Up. *Oncologist* **2019**, *24*, 1039-e642. https://doi.org/10.1634/theoncologist.2019-0330.

(247) Jonker, D.; Rumble, R. B.; Maroun, J. Role of Oxaliplatin Combined with 5-Fluorouracil and Folinic Acid in the First- and Second-Line Treatment of Advanced Colorectal Cancer. *Curr. Oncol.* **2006**, *13*, 173–184. https://doi.org/10.3747/co.v13i5.99.

(248) André, T.; Boni, C.; Mounedji-Boudiaf, L.; Navarro, M.; Tabernero, J.; Hickish, T.; Topham, C.; Zaninelli, M.; Clingan, P.; Bridgewater, J.; Tabah-Fisch, I.; Gramont, A. Oxaliplatin, Fluorouracil and Leucovorin as Adjuvant Treatment for Colon Cancer. *N. Engl. J. Med.* **2011**, *350*, 2343–2351. https://doi.org/10.1007/s11725-011-0275-8.

(249) Longley, D. B.; Harkin, D. P.; Johnston, P. G. 5-Fluorouracil: Mechanisms of Action and Clinical Strategies. *Nature* **2003**, *3*, 330–338. https://doi.org/10.1038/nrc1074.

(250) Miura, K.; Kinouchi, M.; Ishida, K.; Fujibuchi, W.; Naitoh, T.; Ogawa, H.; Ando, T.; Yazaki, N.; Watanabe, K.; Haneda, S.; Shibata, C.; Sasaki, I. 5-FU Metabolism in Cancer and Orally-Administrable 5-FU Drugs. *Cancers* **2010**, *2*, 1717–1730. https://doi.org/10.3390/cancers2031717.

(251) Heidelberger, C.; Chaudhuri, N. K.; Danneberg, P.; Mooren, D.; Griesbach, L.; Duschinsky, R.; Schnitzer, R. J.; Pleven, E.; Scheiner, J. Fluorinated Pyrimidines, a New Class of Tumour-Inhibitory Compounds. *Nature* **1957**, *179*, 663–666. https://doi.org/10.1038/179663a0.

(252) Rutman, R. J.; Cantarow, A.; Paschkis, K. E. The Catabolism of Uracil *in Vivo* and *in Vitro*. *J. Biol. Chem.* **1954**, *210*, 321–329. https://doi.org/10.1016/S0021-9258(18)65456-0.

(253) Handschumacher, R. E.; Welch, A. D. Microbial Studies of 6-Azauracil, an Antagonist of Uracil. *Cancer Res.* **1956**, *16*, 965–969.

(254) Kline, C. L. B.; El-Deiry, W. S. Personalizing Colon Cancer Therapeutics: Targeting Old and New Mechanisms of Action. *Pharmaceuticals* **2013**, *6*, 988–1038. https://doi.org/10.3390/ph6080988.

(255) Arias, J. L. Novel Strategies to Improve the Anticancer Action of 5-Fluorouracil by Using Drug Delivery Systems. *Molecules* **2008**, *13*, 2340–2369. https://doi.org/10.3390/molecules13102340.

(256) Komeda, S.; Casini, A. Next-Generation Anticancer Metallodrugs. *Curr. Top. Med. Chem.* **2012**, *12*, 219–235. https://doi.org/10.2174/156802612799078964.

(257) Anthony, E. J.; Bolitho, E. M.; Bridgewater, H. E.; Carter, O. W. L.; Donnelly, J. M.; Imberti, C.; Lant, E. C.; Lermyte, F.; Needham, R. J.; Palau, M.; Sadler, P. J.; Shi, H.; Wang, F. X.; Zhang, W. Y.; Zhang, Z. Metallodrugs Are Unique: Opportunities and Challenges of Discovery and Development. *Chem. Sci.* **2020**, *11*, 12888–12917. https://doi.org/10.1039/d0sc04082g.

(258) Houdaihed, L.; Evans, J. C.; Allen, C. Overcoming the Road Blocks: Advancement of Block Copolymer Micelles for Cancer Therapy in the Clinic. *Mol. Pharm.* **2017**, *14*, 2503–2517. https://doi.org/10.1021/acs.molpharmaceut.7b00188.

(259) Orient Europharma Co., L. Study of NC-6004 in Combination With 5-FU and Cetuximab in Patients With Head and Neck Cancer https://clinicaltrials.gov/ct2/show/study/NCT02817113 (accessed Aug 11, 2021).

(260) Orient Europharma Co., L. Combination Therapy With NC-6004 and Gemcitabine Versus Gemcitabine Alone in Pancreatic Cancer https://clinicaltrials.gov/ct2/show/record/NCT02043288 (accessed Aug 11, 2021).

(261) Seetharamu, N.; Kim, E.; Hochster, H.; Martin, F.; Muggia, F. Phase II Study of Liposomal Cisplatin (SPI-77) in Platinum-Sensitive Recurrences of Ovarian Cancer. *Anticancer Res.* **2010**, *30*, 541–545.

(262) Poursharifi, M.; Wlodarczyk, M. T.; Mieszawska, A. J. Nano-Based Systems and Biomacromolecules as Carriers for Metallodrugs in Anticancer Therapy. *Inorganics* **2019**, *7*, 1–19. https://doi.org/10.3390/inorganics7010002.

(263) Clinicaltrials.gov. A Study to Determine the Safety of BTP-114 for Treatment in Patients With Advanced Solid Tumors With BRCA Mutations https://clinicaltrials.gov/ct2/show/NCT02950064?cond=Cancer&intr=Cisplatin+Prodrug+BTP-114&draw=2&rank=1 (accessed Jun 9, 2020).

(264) National Cancer Institute. Albumin-binding cisplatin prodrug BTP-114 https://www.cancer.gov/publications/dictionaries/cancer-drug/def/albumin-binding-cisplatin-prodrug-btp-114 (accessed Jun 9, 2020).

(265) Hensing, T. A.; Hanna, N. H.; Gillenwater, H. H.; Camboni, M. G.; Allievi, C.; Socinski, M. A. Phase II Study of BBR 3464 as Treatment in Patients with Sensitive or Refractory Small Cell Lung Cancer. *Anticancer. Drugs* **2006**, *17*, 697–704. https://doi.org/10.1016/S0169-5002(03)00273-3.

(266) Clinicaltrials.gov. BBR 3464 in Treating Patients With Metastatic Small Cell Lung Cancer That Has Not Responded to Previous Treatment https://clinicaltrials.gov/ct2/show/NCT00014547?cond=Cancer&intr=BBR+3464&draw=2&rank=1 (accessed Jun 9, 2020).

(267) Jodrell, D. I.; Evans, T. R. J.; Steward, W.; Cameron, D.; Prendiville, J.; Aschele, C.; Noberasco, C.;

Lind, M.; Carmichael, J.; Dobbs, N.; Camboni, G.; Gatti, B.; De Braud, F. Phase II Studies of BBR3464, a Novel Tri-Nuclear Platinum Complex, in Patients with Gastric or Gastro-Oesophageal Adenocarcinoma. *Eur. J. Cancer* **2004**, *40*, 1872–1877. https://doi.org/10.1016/j.ejca.2004.04.032.

(268) Nowotnik, D. P.; Cvitkovic, E. ProLindac™ (AP5346): A Review of the Development of an HPMA DACH Platinum Polymer Therapeutic. *Adv. Drug Deliv. Rev.* **2009**, *61*, 1214–1219. https://doi.org/10.1016/j.addr.2009.06.004.

(269) National Cancer Institute. DACH polymer platinate AP5346 https://www.cancer.gov/publications/dictionaries/cancer-drug/def/dach-polymer-platinate-ap5346 (accessed Jun 11, 2020).

(270) Starpharma. *Dendrimer-Oxaliplatin Shows Better Anti-Cancer Efficacy and Less Toxicity*; 2013.

(271) Becker, E. D. A Brief History of Nuclear Magnetic Resonance. *Anal. Chem.* **1993**, *65*, 295A-302A. https://doi.org/10.1021/ac00054a716.

(272) Pfeifer, H. A Short History of Nuclear Magnetic Resonance Spectroscopy and of Its Early Years in Germany. *Magn. Reson. Chem.* **1999**, *37*, S154–S159. https://doi.org/10.1002/(sici)1097-458x(199912)37:13<s154::aid-mrc571>3.0.co;2-0.

(273) Fan, T. W. M.; Lane, A. N. Applications of NMR Spectroscopy to Systems Biochemistry. *Prog. Nucl. Magn. Reson. Spectrosc.* **2016**, *92–93*, 18–53. https://doi.org/10.1016/j.pnmrs.2016.01.005.

(274) Gerothanassis, I. P.; Troganis, A.; Exarchou, V.; Barbarossou, K. Nuclear Magnetic Resonance (Nmr) Spectroscopy: Basic Principles and Phenomena, and Their Applications To Chemistry, Biology and Medicine. *Chem. Educ. Res. Pr.* **2002**, *3*, 229–252. https://doi.org/10.1039/b2rp90018a.

(275) Macomber, R. S. *A Complete Introduction to Modern NMR Spectroscopy*; Walsh, E. J., Ed.; John Wiley & Sons: New York, 1998.

(276) Vinje, J.; Sletten, E. NMR Spectroscopy of Anticancer Platinum Drugs. *Anticancer. Agents Med. Chem.* **2008**, *7*, 35–54. https://doi.org/10.2174/187152007779313982.

(277) Berners-Price, S. J.; Ronconi, L.; Sadler, P. J. Insights into the Mechanism of Action of Platinum Anticancer Drugs from Multinuclear NMR Spectroscopy. *Prog. Nucl. Magn. Reson. Spectrosc.* **2006**, *49*, 65–98. https://doi.org/10.1016/j.pnmrs.2006.05.002.

(278) Zou, T.; Sadler, P. J. Speciation of Precious Metal Anti-Cancer Complexes by NMR Spectroscopy. *Drug Discov. Today Technol.* **2015**, *16*, 7–15. https://doi.org/10.1016/j.ddtec.2015.08.002.

(279) De Castro, F.; Benedetti, M.; Del Coco, L.; Fanizzi, F. P. NMR-Based Metabolomics in Metal-Based Drug Research. *Molecules* **2019**, *24*, 1–14. https://doi.org/10.3390/molecules24122240.

(280) Qi, L.; Luo, Q.; Zhang, Y.; Jia, F.; Zhao, Y.; Wang, F. Advances in Toxicological Research of the Anticancer Drug Cisplatin. *Chem. Res. Toxicol.* **2019**, *32*, 1469–1486. https://doi.org/10.1021/acs.chemrestox.9b00204.

(281) Haririan, I.; Alavidjeh, M. S.; Khorramizadeh, M. R.; Ardestani, M. S.; Ghane, Z. Z.; Namazi, H. Anionic Linear-Globular Dendrimer-Cis-Platinum (II) Conjugates Promote Cytotoxicity *in Vitro* against Different Cancer Cell Lines. *Int. J. Nanomedicine* **2010**, *5*, 63–75.

https://doi.org/10.2147/ijn.s8595.

(282) Tran, N. Q.; Nguyen, C. K.; Nguyen, T. P. Dendrimer-Based Nanocarriers Demonstrating a High Efficiency for Loading and Releasing Anticancer Drugs against Cancer Cells *in Vitro* and *in Vivo*. *Adv. Nat. Sci. Nanosci. Nanotechnol.* **2013**, *4*, 1–7. https://doi.org/10.1088/2043-6262/4/4/045013.

(283) Kulhari, H.; Pooja, D.; Singh, M. K.; Chauhan, A. S. Optimization of Carboxylate-Terminated Poly(Amidoamine) Dendrimer-Mediated Cisplatin Formulation. *Drug Dev. Ind. Pharm.* **2015**, *41*, 232–238. https://doi.org/10.3109/03639045.2013.858735.

(284) Kesavan, A.; Ilaiyaraja, P.; Sofi Beaula, W.; Veena Kumari, V.; Sugin Lal, J.; Arunkumar, C.; Anjana, G.; Srinivas, S.; Ramesh, A.; Rayala, S. K.; Ponraju, D.; Venkatraman, G. Tumor Targeting Using Polyamidoamine Dendrimer-Cisplatin Nanoparticles Functionalized with Diglycolamic Acid and Herceptin. *Eur. J. Pharm. Biopharm.* **2015**, *96*, 255–263. https://doi.org/10.1016/j.ejpb.2015.08.001.

(285) Guo, X. L.; Kang, X. X.; Wang, Y. Q.; Zhang, X. J.; Li, C. J.; Liu, Y.; Du, L. B. Co-Delivery of Cisplatin and Doxorubicin by Covalently Conjugating with Polyamidoamine Dendrimer for Enhanced Synergistic Cancer Therapy. *Acta Biomater.* **2019**, *84*, 367–377. https://doi.org/10.1016/j.actbio.2018.12.007.

(286) Nguyen, H.; Nguyen, N. H.; Tran, N. Q.; Nguyen, C. K. Improved Method for Preparing Cisplatin-Dendrimer Nanocomplex and Its Behavior Against NCI-H460 Lung Cancer Cell. *J. Nanosci. Nanotechnol.* **2015**, *15*, 4106–4110. https://doi.org/10.1166/jnn.2015.9808.

(287) International Committee for Standardization in Haematology. International Committee for Standardization in Haematology Recommendations for Reference Method for Haemoglobinometry in Human Blood (ICSH Standard EP 6/2: 1997) and Specifications for International Haemiglobincyanide Reference Preparation (ICSH Standard EP 6/3: 1977). *J. Clin. Pathol.* **1978**, *31*, 139–143.

(288) Sirajuddin, M.; Ali, S.; Badshah, A. Drug-DNA Interactions and Their Study by UV-Visible, Fluorescence Spectroscopies and Cyclic Voltametry. *J. Photochem. Photobiol. B Biol.* **2013**, *124*, 1–19. https://doi.org/10.1016/j.jphotobiol.2013.03.013.

(289) Le, P. N.; Nguyen, N. H.; Nguyen, C. K.; Tran, N. Q. Smart Dendrimer-Based Nanogel for Enhancing 5-Fluorouracil Loading Efficiency against MCF7 Cancer Cell Growth. *Bull. Mater. Sci.* **2016**, *39*, 1493–1500. https://doi.org/10.1007/s12034-016-1274-z.

(290) Howell, B. A.; Fan, D. Poly(Amidoamine) Dendrimer-Supported Organoplatinum Antitumour Agents. *Proc. R. Soc. A* **2010**, *466*, 1515–1526. https://doi.org/10.1098/rspa.2009.0359.

(291) Priqueler, J. R. L.; Butler, I. S.; Rochon, F. D. An Overview of ^{195}Pt Nuclear Magnetic Resonance Spectroscopy. *Appl. Spectrosc. Rev.* **2006**, *41*, 185–226. https://doi.org/10.1080/05704920600620311.

(292) Samide, A.; Grecu, R.; Tutunaru, B.; Tigae, C.; Spînu, C. Cisplatin-Chemotherapeutic Drug Interactions with the Surface of Some Metal Bioimplants in Physiological Serum. *Int. J. Electrochem. Sci.* **2017**, *12*, 11316–11329. https://doi.org/10.20964/2017.12.66.

(293) Othayoth, R.; Mathi, P.; Bheemanapally, K.; Kakarla, L.; Botlagunta, M. Characterization of Vitamin-Cisplatin-Loaded Chitosan Nano-Particles for Chemoprevention and Cancer Fatigue. *J.*

Microencapsul. **2015**, *32*, 578–588. https://doi.org/10.3109/02652048.2015.1065921.

(294) Yellepeddi, V. K.; Vangara, K. K.; Palakurthi, S. Poly(Amido)Amine (PAMAM) Dendrimer-Cisplatin Complexes for Chemotherapy of Cisplatin-Resistant Ovarian Cancer Cells. *J. Nanoparticle Res.* **2013**, *15*, 1–15. https://doi.org/10.1007/s11051-013-1897-6.

(295) Allison, M.; Caramés-méndez, P.; Christopher, M. P.; Phillips, R. M.; Lord, R. M.; Patrick, C. M. Bis(Bipyridine)Ruthenium(II) Ferrocenyl Beta-Diketonate Complexes: Exhibiting Nanomolar Potency against Human Cancer Cell Lines. *Chem. A Eur. J.* **2020**, *27*, 1–10. https://doi.org/10.1002/chem.202004024.

(296) Badisa, R. B.; Darling-Reed, S. F.; Joseph, P.; Cooperwood, J. S.; Latinwo, L. M.; Goodman, C. B. Selective Cytotoxic Activities of Two Novel Synthetic Drugs on Human Breast Carcinoma MCF-7 Cells. *Anticancer Res.* **2009**, *29*, 2993–2996.

(297) Oliveira, P. F.; Alves, J. M.; Damasceno, J. L.; Oliveira, R. A. M.; Júnior Dias, H.; Crotti, A. E. M.; Tavares, D. C. Cytotoxicity Screening of Essential Oils in Cancer Cell Lines. *Rev. Bras. Farmacogn.* **2015**, *25*, 183–188. https://doi.org/10.1016/j.bjp.2015.02.009.

(298) Mandal, R.; Kalke, R.; Li, X. F. Interaction of Oxaliplatin, Cisplatin, and Carboplatin with Hemoglobin and the Resulting Release of a Heme Group. *Chem. Res. Toxicol.* **2004**, *17*, 1391–1397. https://doi.org/10.1021/tx049868j.

(299) Han, M.; Chen, J.; Wang, J.; Chen, S.; Wang, X. Blood Compatibility of Polyamidoamine Dendrimers and Erythrocyte Protection. *J. Biomed. Nanotechnol.* **2010**, *6*, 82–92. https://doi.org/10.1166/jbn.2010.1096.

(300) Pages, B. J.; Ang, D. L.; Wright, E. P.; Aldrich-Wright, J. R. Metal Complex Interactions with DNA. *Dalt. Trans.* **2015**, *44*, 3505–3526. https://doi.org/10.1039/c4dt02700k.

(301) Wang, Z.; Wu, M.; Gou, S. Toward a Better Understanding of the Oxaliplatin Mode of Action upon the Steric Hindrance of 1,2-Diaminocyclohexane and Its Analogue. *J. Inorg. Biochem.* **2016**, *157*, 1–7. https://doi.org/10.1016/j.jinorgbio.2016.01.011.

(302) Johnstone, T. C.; Wilson, J. J.; Lippard, S. J. Monofunctional and Higher-Valent Platinum Anticancer Agents. *Inorg. Chem.* **2013**, *52*, 12234–12249. https://doi.org/10.1021/ic400538c.

(303) Alotaibi, S.; Momen, A. A. Anticancer Drugs' Deoxyribonucleic Acid (DNA) Interactions. In *Interactions, Biophysical Chemistry - Advance Applications*; IntechOpen, 2019; pp 1–23. https://doi.org/10.5772/intechopen.85794.

(304) Wang, Q.; Yang, L.; Wu, J.; Wang, H.; Song, J.; Tang, X. Four Mononuclear Platinum(II) Complexes: Synthesis, DNA/BSA Binding, DNA Cleavage and Cytotoxicity. *BioMetals* **2017**, *30*, 17–26. https://doi.org/10.1007/s10534-016-9984-7.

(305) Shahabadi, N.; Kashanian, S.; Fatahi, A. Identification of Binding Mode of a Platinum (II) Complex, PtCl 2 (DIP), and Calf Thymus DNA. *Bioinorg. Chem. Appl.* **2011**, *2011*, 1–7. https://doi.org/10.1155/2011/687571.

(306) Dey, D.; Kumar, S.; Maiti, S.; Dhara, D. Stopped-Flow Kinetic Studies of Poly(Amidoamine)

Dendrimer-Calf Thymus DNA to Form Dendriplexes. *J. Phys. Chem. B* **2013**, *117*, 13767–13774. https://doi.org/10.1021/jp406973t.

(307) Ibrahim, R. A. A. Z.; Suhail, F. S. A.; Al-Hakeim, H. K. Stability of Anticancer Drug 5-Fluorouracil in Aqueous Solution: An Assessment of Kinetic Behavior. *Nano Biomed. Eng.* **2018**, *10*, 224–234. https://doi.org/10.5101/nbe.v10i3.p224-234.

(308) Rengaraj, A.; Subbiah, B.; Haldorai, Y.; Yesudhas, D.; Yun, H. J.; Kwon, S.; Choi, S.; Han, Y. K.; Kim, E. S.; Hema Shenpagam, N.; Huh, Y. S. PAMAM/5-Fluorouracil Drug Conjugate for Targeting E6 and E7 Oncoproteins in Cervical Cancer: A Combined Experimental/: In Silico Approach. *RSC Adv.* **2017**, *7*, 5046–5054. https://doi.org/10.1039/c6ra26511a.

(309) Choudhary, S.; Gupta, L.; Rani, S.; Dave, K.; Gupta, U. Impact of Dendrimers on Solubility of Hydrophobic Drug Molecules. *Front. Pharmacol.* **2017**, *8*, 1–23. https://doi.org/10.3389/fphar.2017.00261.

(310) Shirasaka, T.; Shimamoto, Y.; Ohshimo, H.; Saito, H.; Fukushima, M. Metabolic Basis of the Synergistic Antitumor Activities of 5-Fluorouracil and Cisplatin in Rodent Tumor Models *in Vivo*. *Cancer Chemother. Pharmacol.* **1993**, *32*, 167–172. https://doi.org/10.1007/BF00685830.

(311) Yim, E. K.; Lee, S. B.; Lee, K. H.; Kim, C. J.; Park, J. S. Analysis of the *in Vitro* Synergistic Effect of 5-Fluorouracil and Cisplatin on Cervical Carcinoma Cells. *Int. J. Gynecol. Cancer* **2006**, *16*, 1321–1329. https://doi.org/10.1111/j.1525-1438.2006.00551.x.

(312) Gupta, A.; Dubey, S.; Mishra, M. Unique Structures, Properties and Applications of Dendrimers. *J. Drug Deliv. Ther.* **2018**, *8*, 328–339. https://doi.org/10.22270/jddt.v8i6-s.2083.

(313) Aurelia Chis, A.; Dobrea, C.; Morgovan, C.; Arseniu, A. M.; Rus, L. L.; Butuca, A.; Juncan, A. M.; Totan, M.; Vonica-Tincu, A. L.; Cormos, G.; Muntean, A. C.; Muresan, M. L.; Gligor, F. G.; Frum, A. Applications and Limitations of Dendrimers in Biomedicine. *Molecules* **2020**, *25*, 1–41. https://doi.org/10.3390/molecules25173982.

(314) Wang, N.; Cheng, X.; Li, N.; Wang, H.; Chen, H. Nanocarriers and Their Loading Strategies. *Adv. Healthc. Mater.* **2019**, *8*, 1–26. https://doi.org/10.1002/adhm.201801002.

(315) Gonçalves, R. F. S.; Martins, J. T.; Duarte, C. M. M.; Vicente, A. A.; Pinheiro, A. C. Advances in Nutraceutical Delivery Systems: From Formulation Design for Bioavailability Enhancement to Efficacy and Safety Evaluation. *Trends Food Sci. Technol.* **2018**, *78*, 270–291. https://doi.org/10.1016/j.tifs.2018.06.011.

(316) Tokarczyk, K.; Jachimska, B. Characterization of G4 PAMAM Dendrimer Complexes with 5-Fluorouracil and Their Interactions with Bovine Serum Albumin. *Colloids Surfaces A Physicochem. Eng. Asp.* **2019**, *561*, 357–363. https://doi.org/10.1016/j.colsurfa.2018.10.080.

(317) Buczkowski, A.; Sekowski, S.; Grala, A.; Palecz, D.; Milowska, K.; Urbaniak, P.; Gabryelak, T.; Piekarski, H.; Palecz, B. Interaction between PAMAM-NH_2 G4 Dendrimer and 5-Fluorouracil in Aqueous Solution. *Int. J. Pharm.* **2011**, *408*, 266–270. https://doi.org/10.1016/j.ijpharm.2011.02.014.

(318) Devarakonda, B.; Otto, D. P.; Judefeind, A.; Hill, R. A.; de Villiers, M. M. Effect of PH on the

Solubility and Release of Furosemide from Polyamidoamine (PAMAM) Dendrimer Complexes. *Int. J. Pharm.* **2007**, *345*, 142–153. https://doi.org/10.1016/j.ijpharm.2007.05.039.

(319) Chinnathambi, S.; Karthikeyan, S.; Kesherwani, M.; Velmurugan, D.; Hanagata, N. Underlying the Mechanism of 5-Fluorouracil and Human Serum Albumin Interaction: A Biophysical Study. *J. Phys. Chem. Biophys.* **2016**, *6*, 1–9. https://doi.org/10.4172/2161-0398.1000214.

(320) Wielińska, J.; Nowacki, A.; Liberek, B. 5-Fluorouracil-Complete Insight Into Its Neutral and Ionised Forms. *Molecules* **2019**, *24*, 1–19. https://doi.org/10.3390/molecules24203683.

(321) Olukman, M.; Şanlı, O.; Solak, E. K. Release of Anticancer Drug 5-Fluorouracil from Different Ionically Crosslinked Alginate Beads. *J. Biomater. Nanobiotechnol.* **2012**, *3*, 469–479. https://doi.org/10.4236/jbnb.2012.34048.

(322) Chandran, S. P.; Natarajan, S. B.; Chandraseharan, S.; Mohd Shahimi, M. S. B. Nano Drug Delivery Strategy of 5-Fluorouracil for the Treatment of Colorectal Cancer. *J. Cancer Res. Pract.* **2017**, *4*, 45–48. https://doi.org/10.1016/j.jcrpr.2017.02.002.

(323) Villarreal-Gómez, L. J.; Serrano-Medina, A.; José Torres-Martínez, E.; Lizeth Perez-González, G.; Manuel Cornejo-Bravo, J. Polymeric Advanced Delivery Systems for Antineoplasic Drugs: Doxorubicin and 5-Fluorouracil. *E-Polymers* **2018**, *18*, 359–372. https://doi.org/10.1515/epoly-2017-0202.

(324) Entezar-Almahdi, E.; Mohammadi-Samani, S.; Tayebi, L.; Farjadian, F. Recent Advances in Designing 5-Fluorouracil Delivery Systems: A Stepping Stone in the Safe Treatment of Colorectal Cancer. *Int. J. Nanomedicine* **2020**, *15*, 5445–5458. https://doi.org/10.2147/IJN.S257700.

(325) Ly, T. U.; Tran, N. Q.; Hoang, T. K. D.; Phan, K. N.; Truong, H. N.; Nguyen, C. K. Pegylated Dendrimer and Its Effect in Fluorouracil Loading and Release for Enhancing Antitumor Activity. *J. Biomed. Nanotechnol.* **2013**, *9*, 213–220. https://doi.org/10.1166/jbn.2013.1479.

(326) Khattak, M. A. Calcium and Magnesium Prophylaxis for Oxaliplatin-Related Neurotoxicity: Is It a Trade-off between Drug Efficacy and Toxicity? *Oncologist* **2011**, *16*, 1780–1783. https://doi.org/10.1634/theoncologist.2011-0227.

(327) Cid, N. P.; Novas, M. J.; Tomei, A. A. Process for Preparation of 1,2-Dianimo-Cyclohexane-Platinum (II) Complexes. USOO8637692B2, 2014.

(328) Williams, K. M.; Poynter, A. D.; Hendrie, J. D.; Jackson, D. C.; Martin, V. K. Comparison of N-Acetylmethionine Reactivity between Oxaliplatin and an Oxaliplatin Derivative with Chiral (S,S) Amine Nitrogen Atoms. *Inorganica Chim. Acta* **2013**, *401*, 64–69. https://doi.org/10.1016/j.ica.2013.03.008.

(329) Zhang, D.; Zhang, J.; Jiang, K.; Li, K.; Cong, Y.; Pu, S.; Jin, Y.; Lin, J. Preparation, Characterization and Antitumour Activity of β-, γ- And HP-β-Cyclodextrin Inclusion Complexes of Oxaliplatin. *Spectrochim. Acta - Part A Mol. Biomol. Spectrosc.* **2016**, *152*, 501–508. https://doi.org/10.1016/j.saa.2015.07.088.

(330) Aderibigbe, B. A.; Mugogodi, A.; Nwamadi, M.; Ray, S. S.; Steenkamp, V.; Balogun, M. O.; Matshe,

W. M. R. Polyamidoamine - Drug Conjugates Containing Metal - Based Anticancer Compounds. *J. Inorg. Organomet. Polym. Mater.* **2020**, *30*, 1503–1518. https://doi.org/10.1007/s10904-019-01325-7.

(331) Haruko, I.; Junnosuke, F.; Kazuo, S. Absorption Spectra and Circular Dichroisms of Metal Complexes. I. Platinum(II)-, Palladium(II)- and Gold(III)-Complexes Containing Optically Active Diamines. *Bull. Chem. Soc. Jpn.* **1967**, *40*, 2584–2591. https://doi.org/10.1246/bcsj.40.2584.

(332) Howell, B. A.; Fan, D. Poly(Amidoamine) Dendrimer-Supported Organoplatinum Antitumour Agents. *Proc. R. Soc. A* **2010**, *466*, 1515–1526. https://doi.org/10.1098/rspa.2009.0359.

(333) Still, B. M.; Kumar, P. G. A.; Aldrich-Wright, J. R.; Price, W. S. 195Pt NMR - Theory and Application. *Chem. Soc. Rev.* **2007**, *36*, 665–686. https://doi.org/10.1039/b606190g.

(334) Avaji, P. G.; Park, J. H.; Lee, H. J.; Jun, Y. J.; Park, K. S.; Lee, K. E.; Choi, S.-J.; Lee, H. J.; Sohn, Y. S. Design of a Novel Theranostic Nanomedicine: Synthesis and Physicochemical Properties of a Biocompatible Polyphosphazene–Docetaxel Conjugate. *Int. J. Nanomedicine* **2016**, *11*, 837–851. https://doi.org/10.2147/IJN.S140073.

(335) Studzian, M.; Pułaski, Ł.; Tomalia, D. A.; Klajnert-Maculewicz, B. Non-Traditional Intrinsic Luminescence (NTIL): Dynamic Quenching Demonstrates the Presence of Two Distinct Fluorophore Types Associated with NTIL Behavior in Pyrrolidone-Terminated PAMAM Dendrimers. *J. Phys. Chem. C* **2019**, *123*, 18007–18016. https://doi.org/10.1021/acs.jpcc.9b02725.

(336) Lemma, T.; Pawliszyn, J. Human Serum Albumin Interaction with Oxaliplatin Studied by Capillary Isoelectric Focusing with the Whole Column Imaging Detection and Spectroscopic Method. *J. Pharm. Biomed. Anal.* **2009**, *50*, 570–575. https://doi.org/10.1016/j.jpba.2008.10.028.

(337) Rafi, M.; Cabral, H.; Kano, M. R.; Mi, P.; Iwata, C.; Yashiro, M.; Hirakawa, K.; Miyazono, K.; Nishiyama, N.; Kataoka, K. Polymeric Micelles Incorporating (1,2-Diaminocyclohexane)Platinum (II) Suppress the Growth of Orthotopic Scirrhous Gastric Tumors and Their Lymph Node Metastasis. *J. Control. Release* **2012**, *159*, 189–196. https://doi.org/10.1016/j.jconrel.2012.01.038.

(338) Spyropoulos-Antonakakis, N.; Sarantopoulou, E.; Trohopoulos, P. N.; Stefi, A. L.; Kollia, Z.; Gavriil, V. E.; Bourkoula, A.; Petrou, P. S.; Kakabakos, S.; Semashko, V. V.; Nizamutdinov, A. S.; Cefalas, A. C. Selective Aggregation of PAMAM Dendrimer Nanocarriers and PAMAM/ZnPc Nanodrugs on Human Atheromatous Carotid Tissues: A Photodynamic Therapy for Atherosclerosis. *Nanoscale Res. Lett.* **2015**, *10*, 1–19. https://doi.org/10.1186/s11671-015-0904-5.

(339) Enciso, A. E.; Neun, B.; Rodriguez, J.; Ranjan, A. P.; Dobrovolskaia, M. A.; Simanek, E. E. Nanoparticle Effects on Human Platelets *in Vitro*: A Comparison between PAMAM and Triazine Dendrimers. *Molecules* **2016**, *21*, 1–7. https://doi.org/10.3390/molecules21040428.

(340) Vidal, F.; Vásquez, P.; Cayumán, F. R.; Díaz, C.; Fuentealba, J.; Aguayo, L. G.; Yévenes, G. E.; Alderete, J.; Guzmán, L. Prevention of Synaptic Alterations and Neurotoxic Effects of PAMAM Dendrimers by Surface Functionalization. *Nanomaterials* **2018**, *8*, 1–12. https://doi.org/10.3390/nano8010007.

(341) N'Soukpo-Kossi, C. N.; Descôteaux, C.; Asselin, É.; Tajmir-Riahi, H. A.; Bérubé, G. DNA Interaction

with Novel Antitumor Estradiol-Platinum(II) Hybrid Molecule: A Comparative Study with Cisplatin Drug. *DNA Cell Biol.* **2008**, *27*, 101–107. https://doi.org/10.1089/dna.2007.0669.

(342) Zou, Y.; Biao, L.; Xu, F.; Liu, R.; Liu, Z.; Fu, Y. Structural Study on the Interactions of Oxaliplatin and Linear DNA. *Scanning* **2016**, *38*, 880–888. https://doi.org/10.1002/sca.21337.

(343) Sato, S.; Itamochi, H.; Kigawa, J.; Oishi, T.; Shimada, M.; Sato, S.; Naniwa, J.; Uegaki, K.; Nonaka, M.; Terakawa, N. Combination Chemotherapy of Oxaliplatin and 5-Fluorouracil May Be an Effective Regimen for Mucinous Adenocarcinoma of the Ovary: A Potential Treatment Strategy. *Cancer Sci.* **2009**, *100*, 546–551. https://doi.org/10.1111/j.1349-7006.2008.01065.x.

(344) Oberoi, H. S.; Nukolova, N. V.; Zhao, Y.; Cohen, S. M.; Kabanov, A. V.; Bronich, T. K. Preparation and In Vivo Evaluation of Dichloro(1,2-Diaminocyclohexane)Platinum(II)-Loaded Core Cross-Linked Polymer Micelles . *Chemother. Res. Pract.* **2012**, *2012*, 1–10. https://doi.org/10.1155/2012/905796.

(345) Liu, G.; Gao, H.; Zuo, Y.; Zeng, X.; Tao, W.; Tsai, H. I.; Mei, L. DACHPt-Loaded Unimolecular Micelles Based on Hydrophilic Dendritic Block Copolymers for Enhanced Therapy of Lung Cancer. *ACS Appl. Mater. Interfaces* **2017**, *9*, 112–119. https://doi.org/10.1021/acsami.6b11917.

(346) Oberoi, H. S.; Nukolova, N. V.; Bronich, T. K. Dichloro(1,2-Diaminocyclohexane)Platinum(II) (DACHPt) Loaded Polymer Micelles with Cross-Linked Core: Preparation and Characterization. *PMSE Prepr.* **2011**, *104*, 1–7. https://doi.org/10.1038/jid.2014.371.

(347) Gonçalves, M.; Maciel, D.; Capelo, D.; Xiao, S.; Sun, W.; Shi, X.; Rodrigues, J.; Tomás, H.; Li, Y. Dendrimer-Assisted Formation of Fluorescent Nanogels for Drug Delivery and Intracellular Imaging. *Biomacromolecules* **2014**, *15*, 492–499. https://doi.org/10.1021/bm401400r.

(348) Mignani, S.; Rodrigues, J.; Tomás, H.; Zablocka, M.; Shi, X.; Caminade, A.-M.; Majoral, J.-P. Dendrimers in Combination with Natural Products and Analogues as Anti-Cancer Agents. *Chem. Soc. Rev.* **2018**, *47*, 514–532. https://doi.org/10.1039/c7cs00550d.

(349) Trzepinski, P.; Klajnert-Maculewicz, B. Dendrimers for Fluorescence-Based Bioimaging. *J Chem Technol Biotechnol* **2017**, *92*, 1157–1166. https://doi.org/10.1002/jctb.5216.

(350) Mukherjee, S. P.; Davoren, M.; Byrne, H. J. *In Vitro* Mammalian Cytotoxicological Study of PAMAM Dendrimers – Towards Quantitative Structure Activity Relationships. *Toxicol. Vitr.* **2010**, *24*, 169–177. https://doi.org/10.1016/j.tiv.2009.09.014.

(351) Wang, G.; Fu, L.; Walker, A.; Chen, X.; Lovejoy, D. B.; Hao, M.; Lee, A.; Chung, R.; Rizos, H.; Irvine, M.; Zheng, M.; Liu, X.; Lu, Y.; Shi, B. Label-Free Fluorescent Poly(Amidoamine) Dendrimer for Traceable and Controlled Drug Delivery. *Biomacromolecules* **2019**, *20*, 2148–2158. https://doi.org/10.1021/acs.biomac.9b00494.

(352) Dougherty, C. A.; Vaidyanathan, S.; Orr, B. G.; Banaszak Holl, M. M. Fluorophore:Dendrimer Ratio Impacts Cellular Uptake and Intracellular Fluorescence Lifetime. *Bioconjug. Chem.* **2015**, *26*, 304–315. https://doi.org/10.1021/bc5005735.

(353) Janaszewska, A.; Studzian, M.; Petersen, J. F.; Ficker, M.; Paolucci, V.; Christensen, J. B.; Tomalia, D. A.; Klajnert-maculewicz, B. Modified PAMAM Dendrimer with 4-Carbomethoxypyrrolidone

Surface Groups-Its Uptake, Efflux , and Location in a Cell. *Colloids Surfaces B Biointerfaces* **2017**, *159*, 211–216. https://doi.org/10.1016/j.colsurfb.2017.07.052.

(354) Zhang Yuan, W.; Zhang, Y. Nonconventional Macromolecular Luminogens with Aggregation-Induced Emission Characteristics. *J. Polym. Sci. Part A Polym. Chem.* **2017**, *55*, 560–574. https://doi.org/10.1002/pola.28420.

(355) Wang, D.; Imae, T. Morphological Dependence of Fluorescence Emitted from PbS/PAMAM Dendrimer Nanocomposite. *Chem. Lett.* **2005**, *34*, 640–641. https://doi.org/10.1246/cl.2005.640.

(356) Yemul, O.; Imae, T. Synthesis and Characterization of Poly(Ethyleneimine) Dendrimers. *Colloid Polym. Sci.* **2008**, *286*, 747–752. https://doi.org/10.1007/s00396-007-1830-6.

(357) Gouveia, M.; Figueira, J.; Jardim, M. G.; Castro, R.; Tomás, H.; Rissanen, K.; Rodrigues, J. Poly(Alkylidenimine) Dendrimers Functionalized with the Organometallic Moiety $[Ru(\eta5\text{-}C_5H_5)(PPh_3)_2]^+$ as Promising Drugs Against Cisplatin-Resistant Cancer Cells and Human Mesenchymal Stem Cells. *Molecules* **2018**, *23*, 1–17. https://doi.org/10.3390/molecules23061471.

(358) Maciel, D.; Guerrero-beltrán, C.; Ceña-diez, R.; Tomás, H.; Muñoz-fernández, M. Á.; Rodrigues, J. New Anionic Poly(Alkylideneamine) Dendrimers as Microbicide Agents against HIV-1 Infection. *Nanoscale* **2019**, *11*, 9679–9690. https://doi.org/10.1039/c9nr00303g.

(359) Mignani, S.; Rodrigues, J.; Roy, R.; Shi, X.; Ceña, V.; Kazzouli, S. El; Majoral, J. Exploration of Biomedical Dendrimer Space Based on *In-Vitro* Physicochemical Parameters : Key Factor Analysis (Part 1). *Drug Discov. Today* **2019**, *24*, 1176–1183. https://doi.org/10.1016/j.drudis.2019.02.014.

(360) Mignani, S.; Rodrigues, J.; Tomas, H.; Caminade, A.; Laurent, R.; Shi, X.; Majoral, J.-P. Recent Therapeutic Applications of the Theranostic Principle with Dendrimers in Oncology. *Sci. China Mater.* **2018**, *61*, 1367–1386. https://doi.org/10.1007/s40843-018-9244-5.

(361) Lakowicz, J. R. *Principles of Fluorescence Spectroscopy*, third edit.; Springer: New York, 2006. https://doi.org/10.1007/978-0-387-46312-4.

(362) Berlman, I. B. *Handbook of Fluorescence Spectra of Aromatic Molecules*, second edi.; Academic Press, INC. (London) LTD.: New York, 1971. https://doi.org/10.1016/B978-0-12-092656-5.X5001-1.

(363) Gall, J. F.; Church, G. L.; Brown, R. L. Solubility of Ammonium Persulfate in Water and in Solutions of Sulfuric Acid and Ammonium Sulfate. *J. Phys. Chem* **1943**, *47*, 645–649. https://doi.org/10.1021/j150432a003.

(364) Deutsch, D. S.; Siani, A.; Fanson, P. T.; Hirata, H.; Matsumoto, S.; Williams, C. T.; Amiridis, M. D. FT-IR Investigation of the Thermal Decomposition of Poly(Amidoamine) Dendrimers and Dendrimer-Metal Nanocomposites Supported on Al_2O_3 and ZrO_2. *J. Phys. Chem. C* **2007**, *111*, 4246–4255. https://doi.org/10.1021/jp065853d.

(365) Ji, Y.; Yang, L. X.; Qian, Y. Poly-Amidoamine Structure Characterization: Amide Resonance Structure of Imidic Acid (HO–C=N) and Tertiary Ammonium. *RSC Adv.* **2014**, *4*, 49535–49540. https://doi.org/10.1039/C4RA09081K.

(366) Kong, J.; Yu, S. Fourier Transform Infrared Spectroscopic Analysis of Protein Secondary Structures.

Acta Biochim. Biophys. Sin. **2007**, *39*, 549–559. https://doi.org/10.1111/j.1745-7270.2007.00320.x.

(367) Yuhua, S.; Chuanhao, L. I.; Xuemei, Z.; Anjian, X.; Lingguang, Q.; Jinmiao, Z. Study on the Preparation and Formation Mechanism of Barium Sulphate Nanoparticles Modified by Different Organic Acids. *J. Chem. Sci.* **2007**, *119*, 319–324. https://doi.org/10.1007/s12039-007-0043-3.

(368) Pande, S.; Crooks, R. M. Analysis of Poly(Amidoamine) Dendrimer Structure by UV-Vis Spectroscopy. *Langmuir* **2011**, *27*, 9609–9613. https://doi.org/10.1021/la201882t.

(369) Wang, Y.; Niu, S.; Zhang, Z.; Xie, Y.; Yuan, C.; Wang, H.; Fu, D. Reversible PH Manipulation of the Fluorescence Emission from Sectorial Poly(Amidoamine) Dendrimers. *J. Nanosci. Nanotechnol.* **2010**, *10*, 4227–4233. https://doi.org/10.1166/jnn.2010.2195.

(370) Chen, W.; Tomalia, D. A.; Thomas, J. L. Unusual PH-Dependent Polarity Changes in PAMAM Dendrimers: Evidence for PH-Responsive Conformational Changes. *Macromolecules* **2000**, *33*, 9169–9172. https://doi.org/10.1021/ma000791p.

(371) Malyarenko, D. I.; Vold, R. L.; Hoatson, G. L. Solid State Deuteron NMR Studies of Polyamidoamine Dendrimer Salts. 1. Structure and Hydrogen Bonding. *Macromolecules* **2000**, *33*, 1268–1279. https://doi.org/10.1021/ma9916178.

(372) Konopka, M.; Janaszewska, A.; Klajnert-Maculewicz, B. Intrinsic Fluorescence of PAMAM Dendrimers - Quenching Studies. *Polymers* **2018**, *10*, 1–8. https://doi.org/10.3390/polym10050540.

(373) Mei, J.; Leung, N. L. C.; Kwok, R. T. K.; Lam, J. W. Y.; Tang, B. Z. Aggregation-Induced Emission: Together We Shine, United We Soar! *Chem. Rev.* **2015**, *115*, 11718–11940. https://doi.org/10.1021/acs.chemrev.5b00263.

ANNEX

Annex

Instrumentation/Characterization techniques- Chapters II and III

a. NMR

Nuclear Magnetic Resonances (NMR) experiments were recorded with a Bruker Avance II+ UltraShield™ 400 Plus Ultra Long Hold NMR spectrometer at room temperature (probe temperature) at 400, 100, and 86 MHz in D_2O as a solvent. The software used for the NMR plots was Bruker® Topspin 3.6.1. Chemical shifts (δ) are reported in ppm and referenced relatively to the residual deuterated solvent peaks, with the exception in the ^{195}Pt-NMR were it was used as an external reference the K_2PtCl_4 at -1631ppm. The ^{1}H-NMR spectra were recorded with a spectral width of 6009.615 Hz with 64K data points and a relaxation delay of 1 s. The ^{13}C-NMR it was used a spectral width of 24038.461 Hz with 64K data points and a relaxation delay of 2 s. And for the ^{195}Pt-NMR a spectral with of 131578.953 and 300000 Hz were used, using 16384 scans with a relaxation delay of 4 s and a line broadening of 30 Hz.

b. FTIR

The Fourier transformed infrared spectra (FTIR) were recorded using a PerkinElmer Spectrum Two™ spectrometer on KBr pellets in the range of 4000-400 cm^{-1}. The plots were obtained using the software PerkinElmer Spectrum IR 10.6.0. Only the significant bands are reported.

c. Microplate reader

The *in vitro* cytotoxicity and the hemolysis assay were measured using a Perkin Elmer VICTOR³™ Multilabel Reader. The software used to treat the data was Wallac 1420 workstation 2.0.

d. Ultraviolet-Visible

UV-Vis and drug release studies were performed using a PerkinElmer UV-Vis spectrometer Lambda with a cm quartz cuvettes. For software used was UV Winlab 5.2.0. The solutions were prepared in ultrapure water.

e. Fluorescence

Photoluminescence (PL) studies were carried out by using a PerkinElmer LS 55 fluorescence spectrometer with a 1cm quartz cuvettes. The software was FL WinLab software 4.00.03. The excitation wavelength used was 380 nm. The solutions were also prepared in ultrapure water.

f. Zeta-potential

The zeta-potential of the compounds was checked by the technique Dynamic light scattering through the equipment Malvern, Zetasizer Nano ZS. And with the Zetasizer software 7.12. The solutions were prepared in ultrapure water with a concentration of 0.3 mg/mL, and the obtained results were obtained from three

independent measurements. The ultrapure water used was filtered before its use with a filter of 0.2 μm.

g. Mass Spectroscopy

The Mass Spectroscopy (MS) was performed by using the MALDI ionization technique with a ULTRAFLEX III TOF/TOF equipment from Bruker and ESI, electrospray ionization technique, in positive mode, by QTOF hybrid analyzer model MAXIS II from Bruker. These analyses were made through the Mass Spectrometry Unit at Interdepartmental Investigation Service at *Universidad Autónoma de Madrid*. And by the Bruker Autoflex maX MALDI TOF/TOF Mass Spectrometer at Centro de Química da Madeira in University of Madeira. Accordingly, the G2.5COO($Pt(NH_3)_2)_{16}$ metallodendrimer was characterized by MALDI in the linear mode using the matrix trans-2-[3-(4-tert-Butylphenyl)-2-methyl-2-propenylidene]malononitrile (DCTB). The remaining cisplatin-metallodendrimers were characterized by ESI in the positive mode. The compounds were dissolved in water and the methanol was used as ionizing phase. Regarding to DACHPt-metallodendrimers, the G0.5COO$(DACHPt)_4$ and G3.5COO$(DACHPt)_{32}$ metallodendrimers were characterized by MALDI with the matrix, α-cyano-4-hydroxycinnamic acid (ACC). However, in the metallodendrimer G3.5COO$(DACHPt)_{32}$ was used in the reflector mode. The metallodendrimers G1.5COO$(DACHPt)_8$ and G2.5COO$(DACHPt)_{16}$ were characterized by ESI in the positive mode. For G1.5COO$(DACHPt)_8$, a direct infusion of a 1:10 dilution in methanol with 0.1% formic acid of the initial sample solution was performed and for the G2.5COO$(DACHPt)_{16}$ was performed in the exact mass with methanol and 0.1% formic acid as ionizing phase.

h. Elemental analysis

Elemental analysis (EA) were performed by the Elemental Analysis Unit at Interdepartmental Research Service in *Universidad Autónoma de Madrid*, through the equipment LECO-CHNS 932.

i. Flow Cytometry

The Flow Cytometer analysis were performed by Flow Cytometer Novocyte® 3000 with fluidics station (NovoCyte) and autosampler, NovoSampler® Pro (ACEA Bioscience). The acquisition per sample was 10000 events, and the data were treated with NovoExpress™ Flow Cytometer Software 1.2.4.

A. Characterization of starting materials

- Anionic PAMAM dendrimers (G0.5-G3.5)

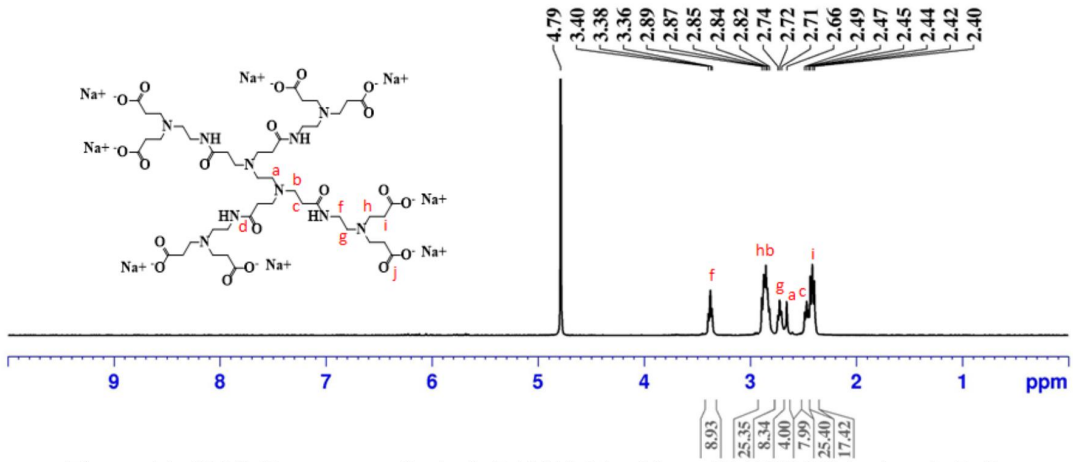

Figure A1: ^{1}H-NMR spectrum of anionic PAMAM dendrimer G0.5(COONa)$_8$ done in D_2O.

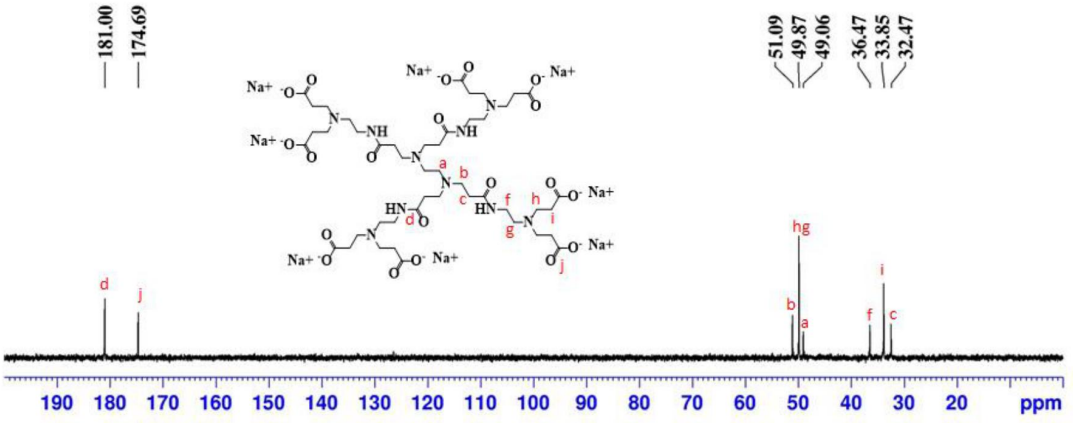

Figure A2: ^{13}C-NMR spectrum of anionic PAMAM dendrimer G0.5(COONa)$_8$ done in D_2O.

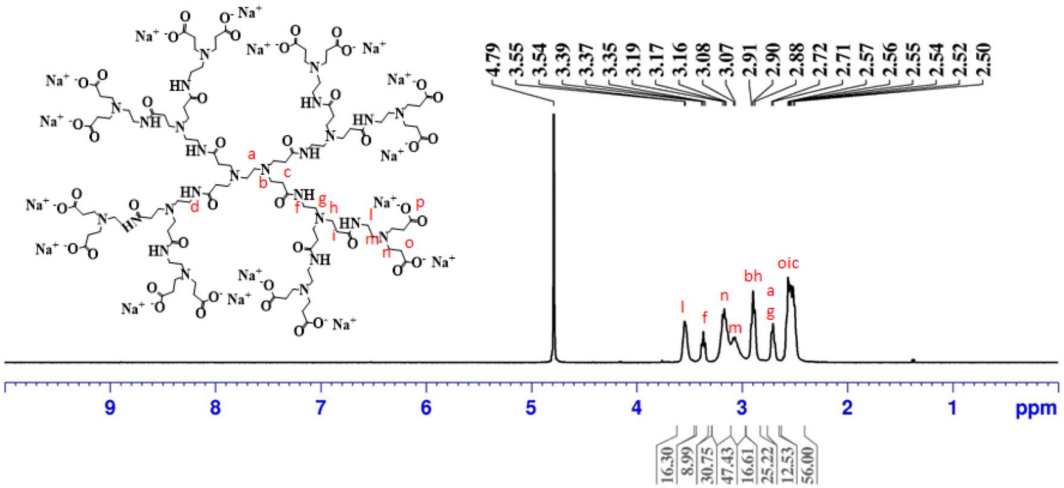

Figure A3: ^{1}H-NMR spectrum of anionic PAMAM dendrimer G1.5(COONa)$_{16}$ done in D_2O.

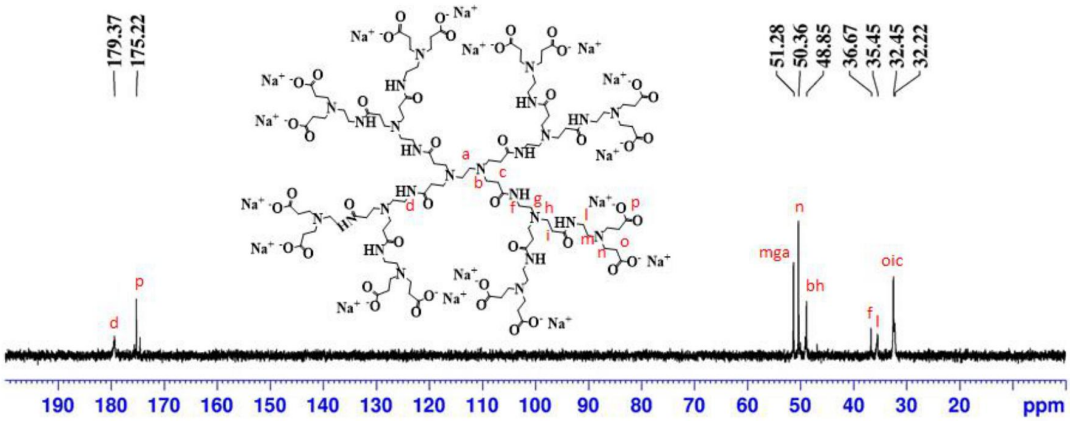

Figure A4: ^{13}C NMR spectrum of anionic PAMAM dendrimer G1.5(COONa)$_{16}$ done in D_2O.

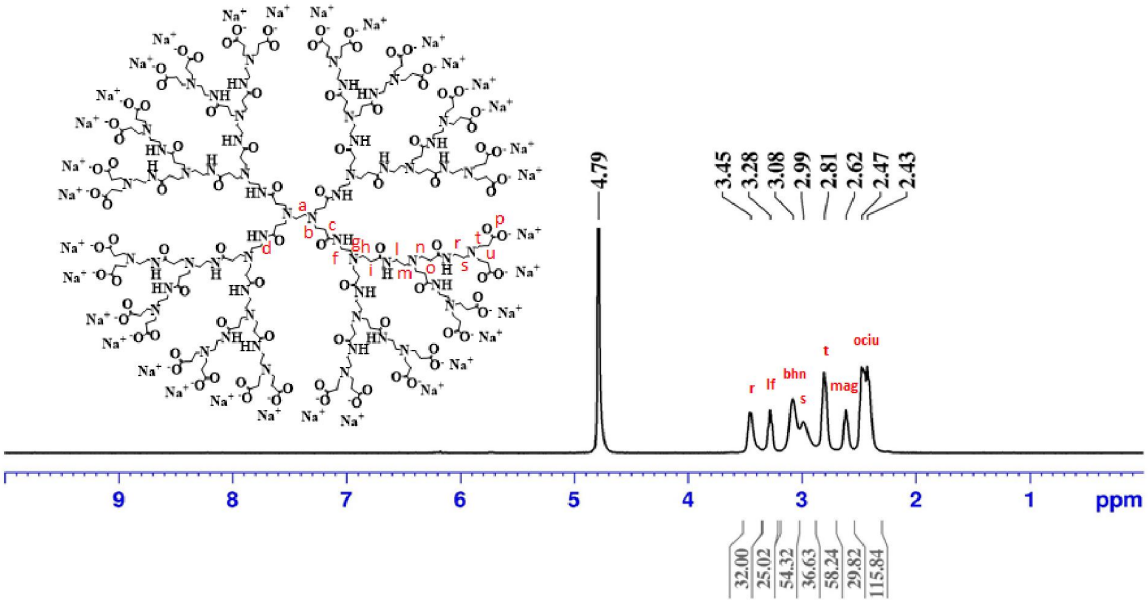

Figure A5: ^{1}H-NMR spectrum of anionic PAMAM dendrimer G2.5(COONa)$_{32}$ done in D_2O.

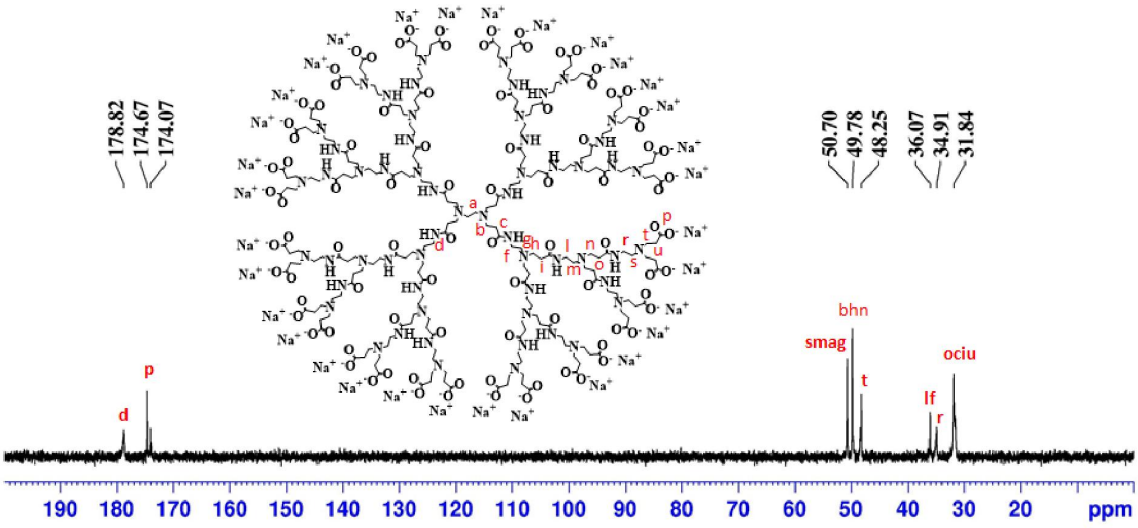

Figure A6: ^{13}C-NMR spectrum of anionic PAMAM dendrimer G2.5(COONa)$_{32}$ done in D_2O.

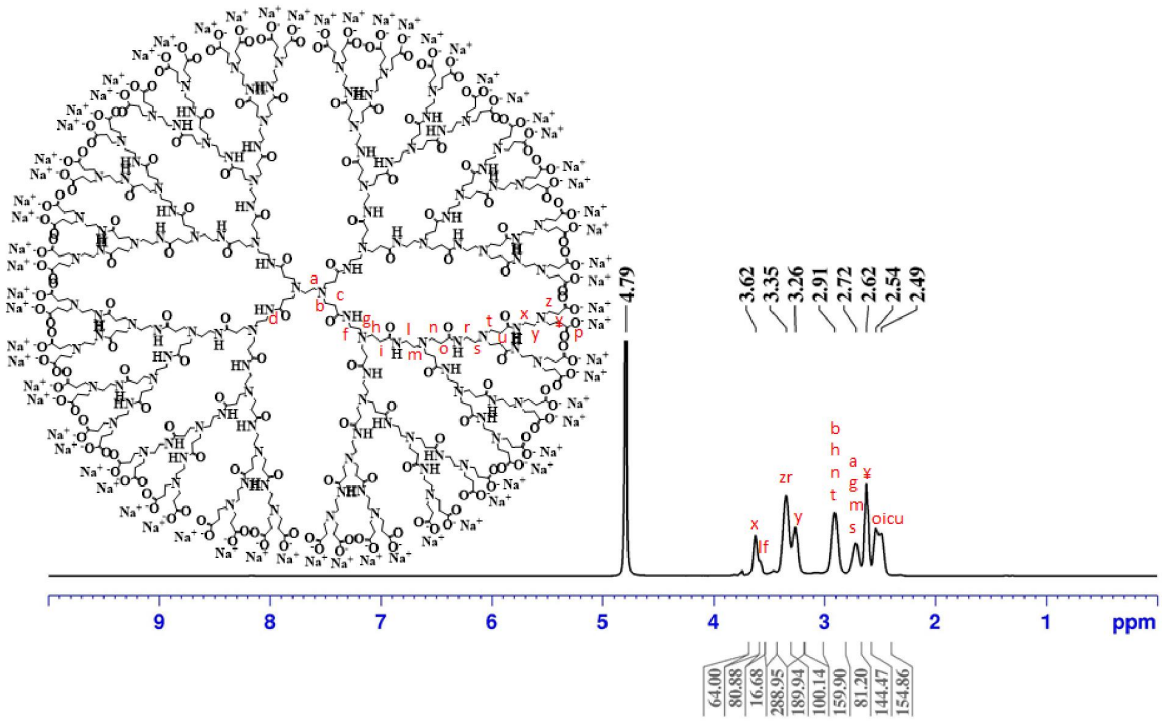

Figure A7: ^{1}H-NMR spectrum of anionic PAMAM dendrimer G3.5(COONa)$_{64}$ done in D_2O.

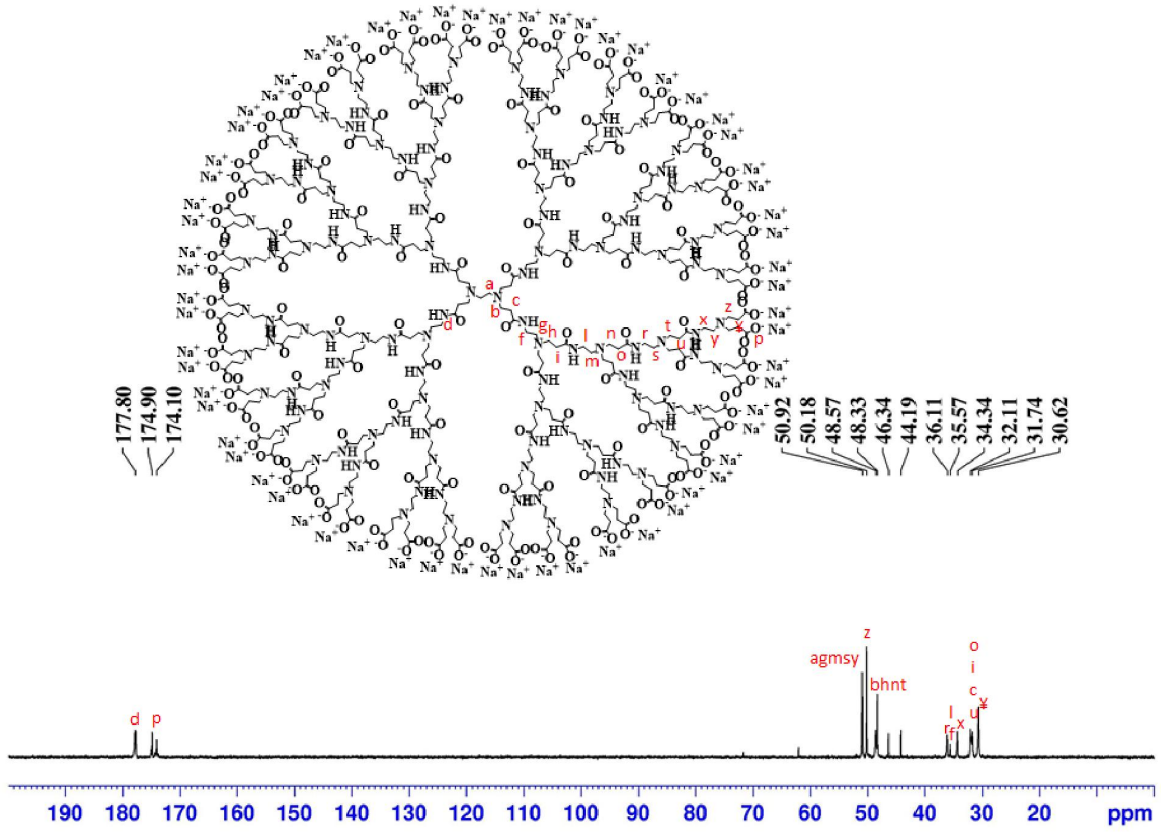

Figure A8: ^{13}C-NMR spectrum of anionic PAMAM dendrimer G3.5(COONa)$_{64}$ done in D_2O.

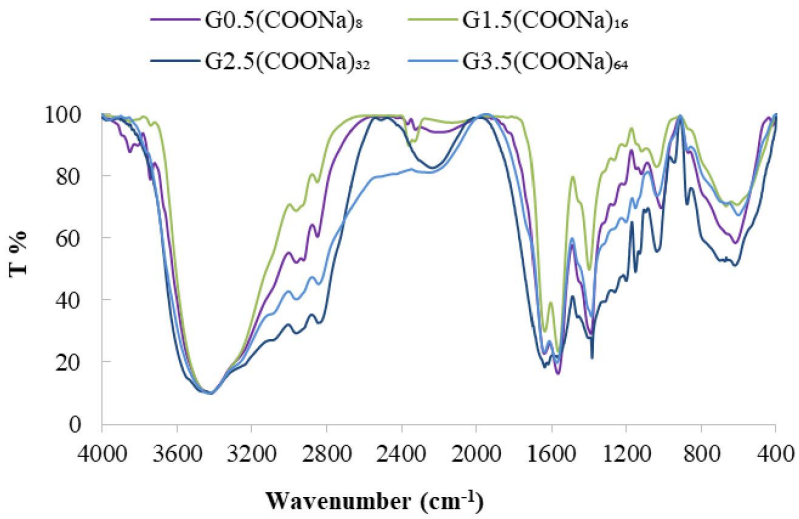

Figure A9: FTIR spectra of different generations of anionic PAMAM dendrimers (G0.5-G3.5) in KBr pellet.

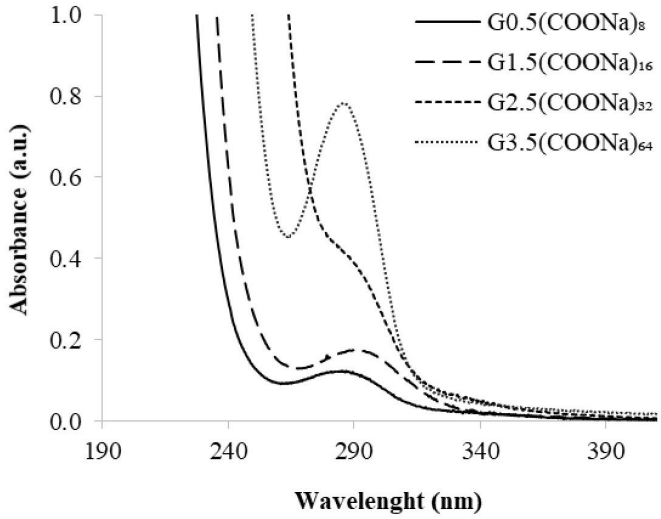

Figure A10: UV-Vis spectra of anionic PAMAM dendrimers at a concentration of 500 µM in ultrapure water.

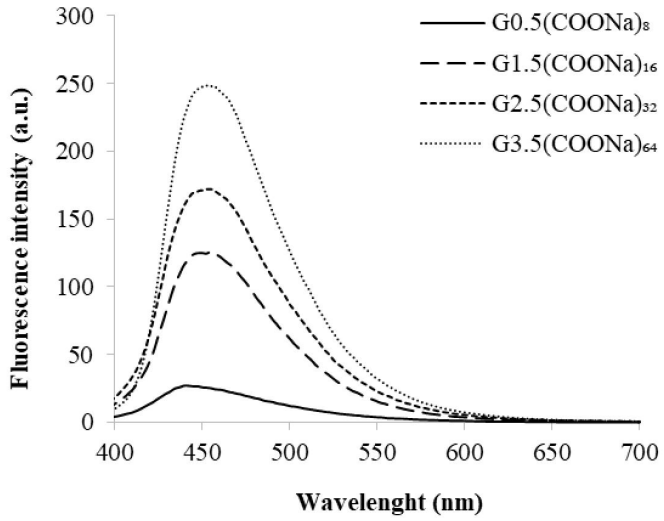

Figure A11: Emission (λ_{ex} = 380 nm) of anionic PAMAM dendrimers at a concentration of 500 µM in ultrapure water.

- Cisplatin

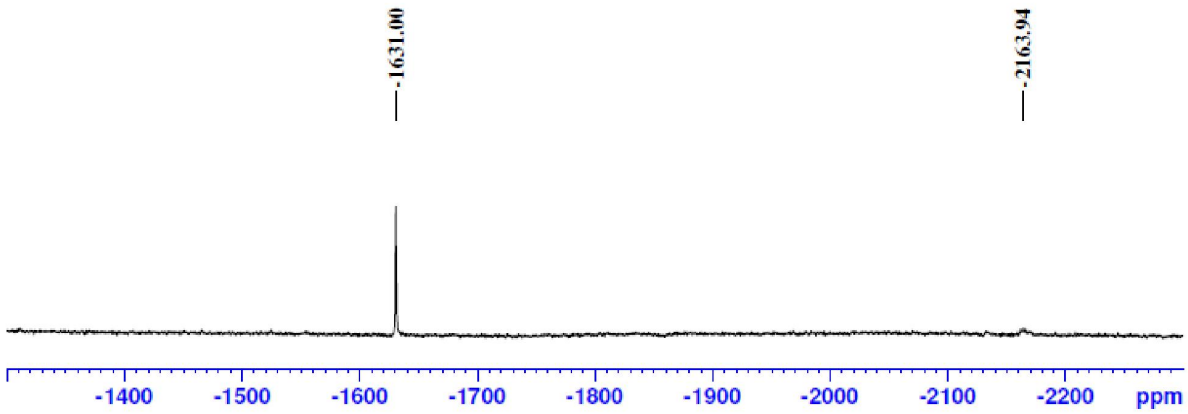

Figure A12: ^{195}Pt-NMR spectrum of cisplatin performed in D_2O, with K_2PtCl_4 as an external reference (-1631 ppm).

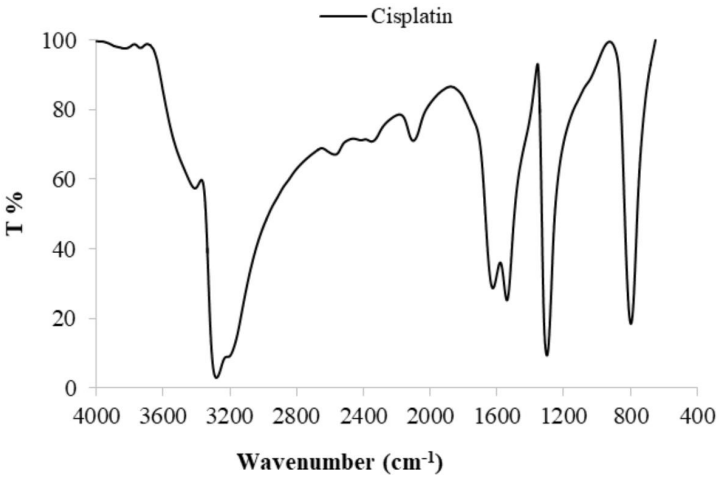

Figure A13: FTIR spectra of cisplatin in KBr pellet.

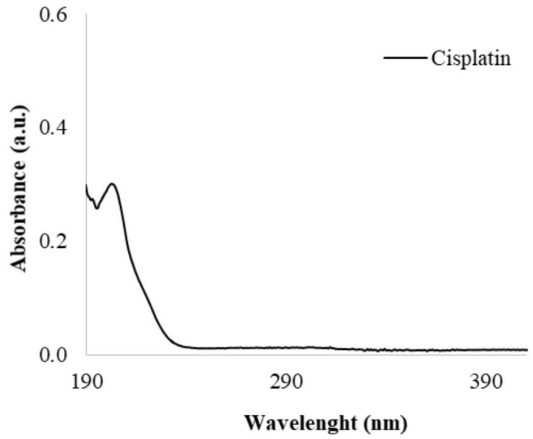

Figure A14: UV-Vis spectra of cisplatin at a concentration of 40 μM in ultrapure water.

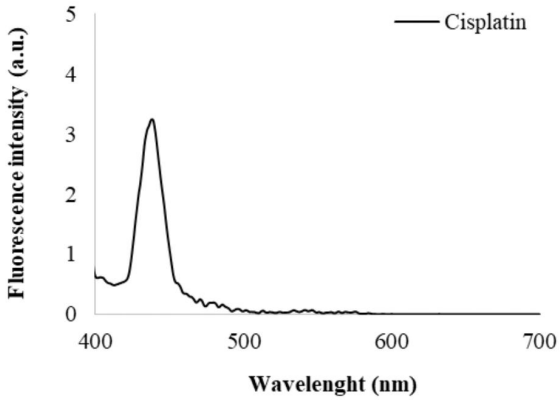

Figure A15: Emission (λ_{ex} = 380 nm) of cisplatin at a concentration of 500 μM in ultrapure water.

- 5-Fluorouracil (5-FU)

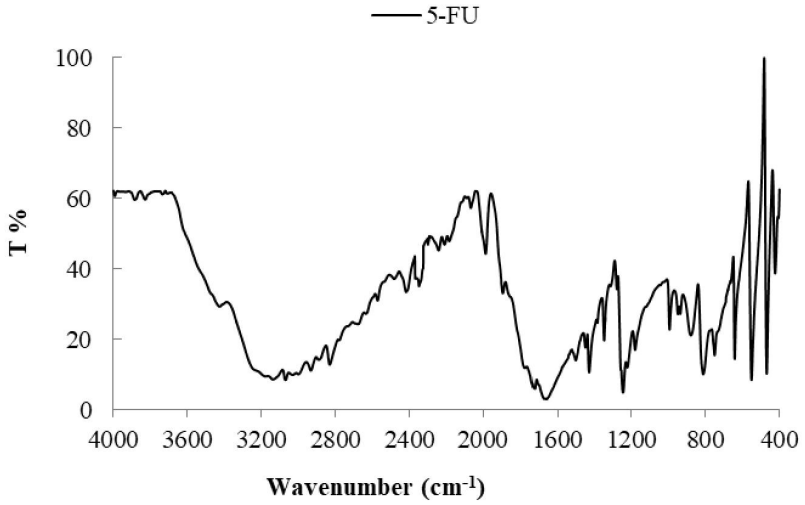

Figure A16: FTIR spectra of 5-fluorouracil in KBr pellet.

- DNA

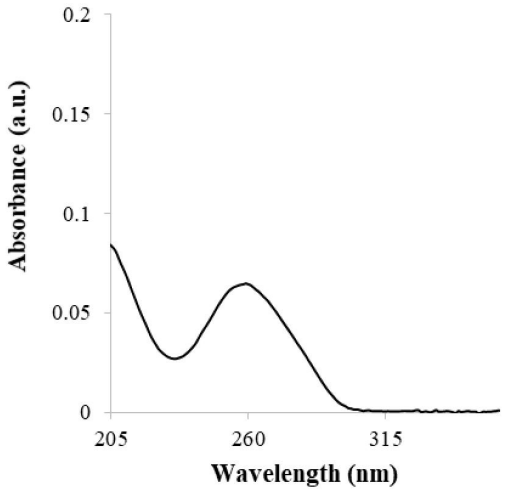

Figure A17: UV-Visible of DNA (10 μM) in Tris-HCl buffer at pH 7.4 buffer.

B. General – Calibration curves

- Hematoxicity

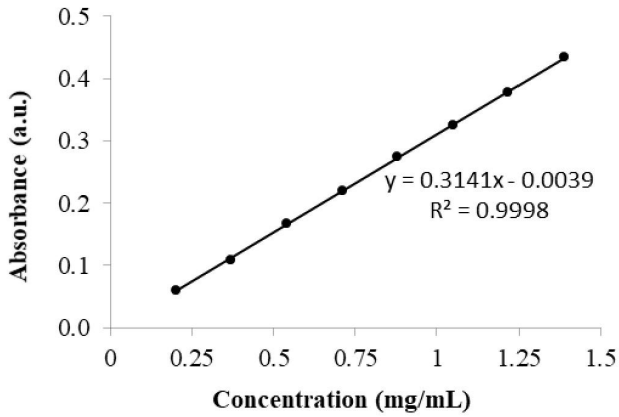

Figure B1: Standard curve of Hg using several dilutions: 0.2; 0.37; 0.54; 0.71; 0.88; 1.05; 1.22 and 1.39 mg/mL. The absorbance was measured at 550 nm.

- Encapsulation

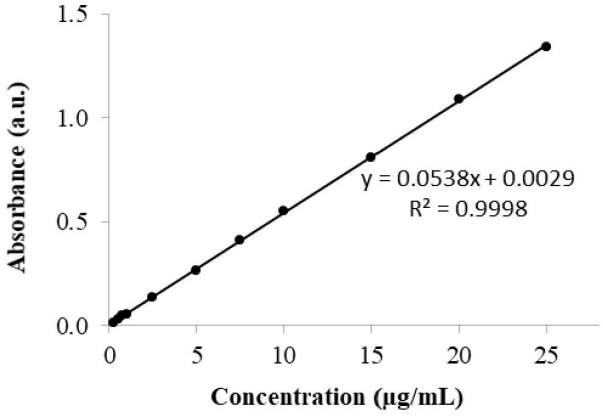

Figure B2: Standard curve of 5-Fluorouracil in ultrapure water using different concentrations: 0.25, 0.5, 0.75, 1, 2.5, 5, 7.5, 10, 15, 20 and 25 µg/mL. The absorbance was measured at 266 nm.

-

- *In vitro* release

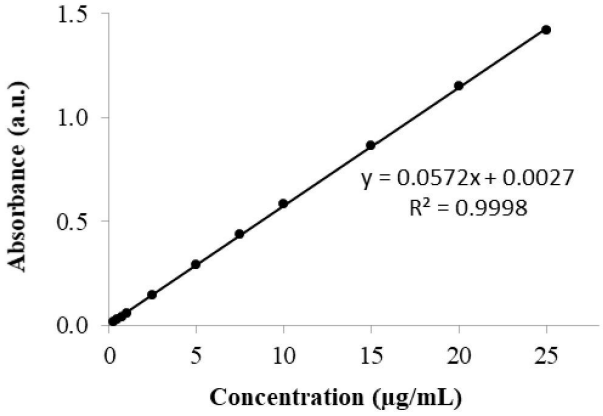

Figure B3: Standard curve of 5-Fluorouracil in PBS 5 using different concentrations: 0.25, 0.5, 0.75, 1, 2.5, 5, 7.5, 10, 15, 20 and 25 µg/mL. The absorbance was measured at 266 nm.

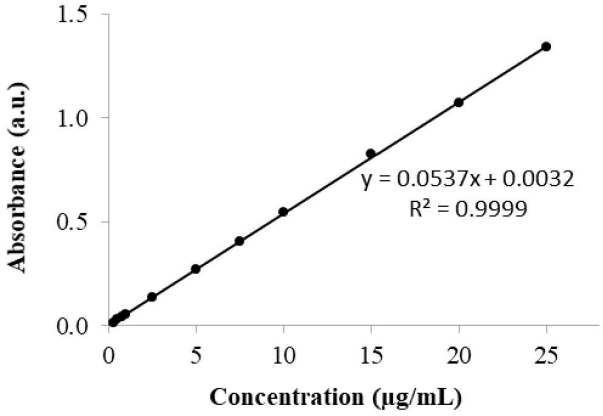

Figure B4: Standard curve of 5-Fluorouracil in PBS 7.4 using different concentrations: 0.25, 0.5, 0.75, 1, 2.5, 5, 7.5, 10, 15, 20 and 25 µg/mL. The absorbance was measured at 266 nm.

C. Chapter II: Cisplatin-based metallodendrimers as anticancer drug

- Characterization

  - **Monodentate form**

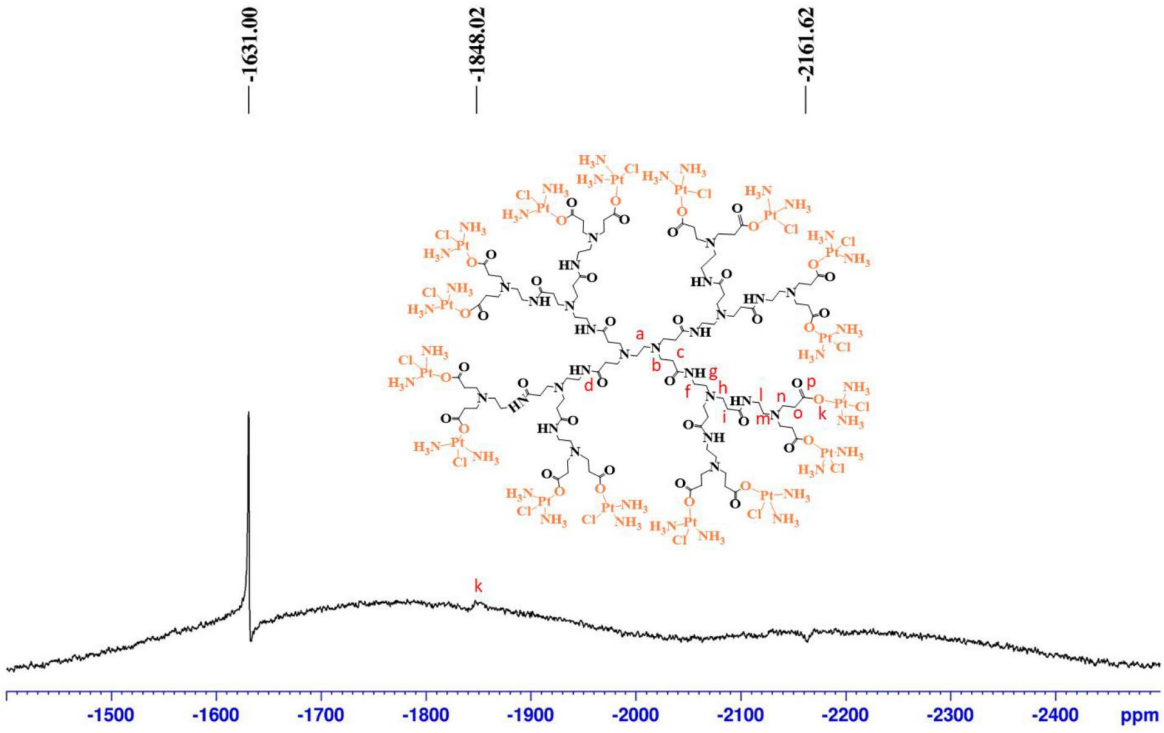

Figure C1: ^{195}Pt-NMR spectrum of G1.5(COOPt$(NH_3)_2Cl)_{16}$ performed in D_2O, with K_2PtCl_4 as an external reference (-1631 ppm).

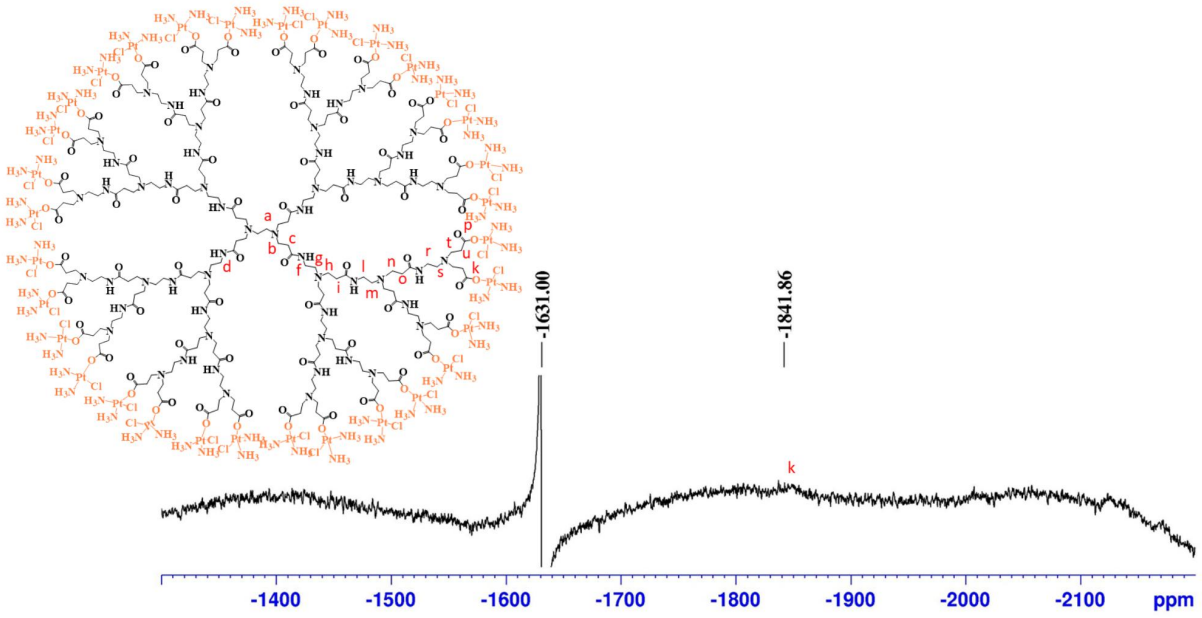

Figure C2: ^{195}Pt-NMR spectrum of G2.5(COOPt(NH$_3$)$_2$Cl)$_{32}$ performed in D_2O, with K_2PtCl_4 as an external reference (-1631 ppm).

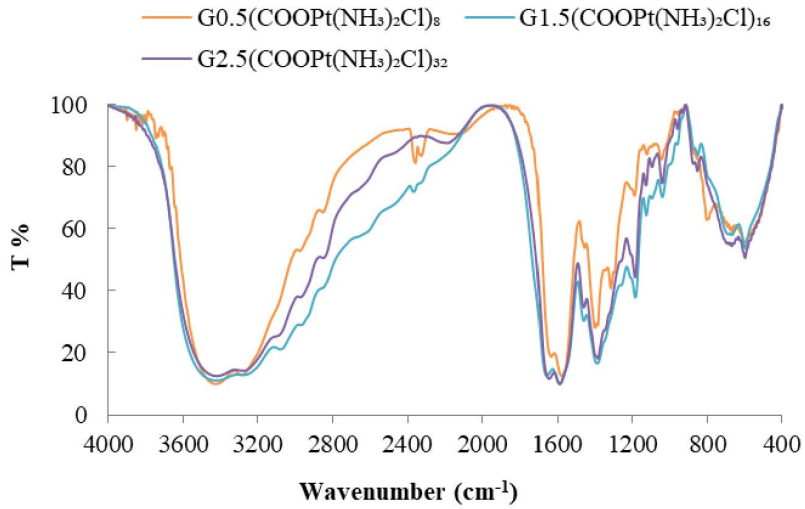

Figure C3: FTIR spectra of metallodendrimers conjugated with cisplatin in monodentate form. The spectra was performed in KBr pellet.

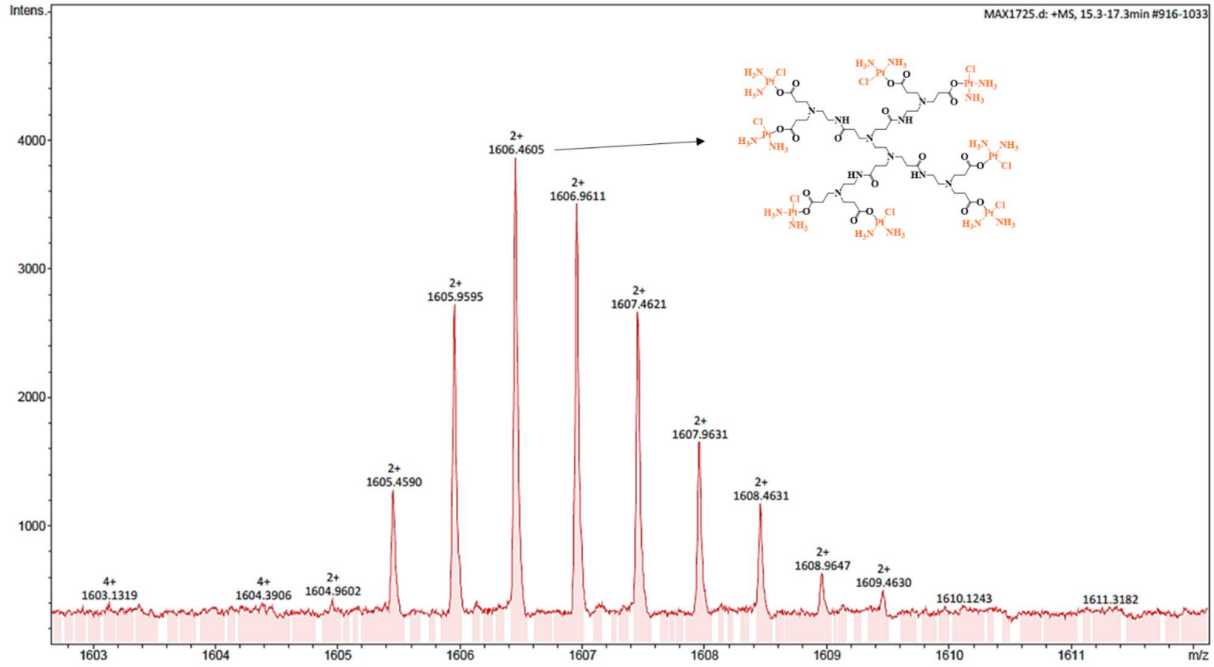

Figure C4: TOF-MS (ESI +) mass spectrum of G0.5(COOPt$(NH_3)_2Cl)_8$ metallodendrimer.

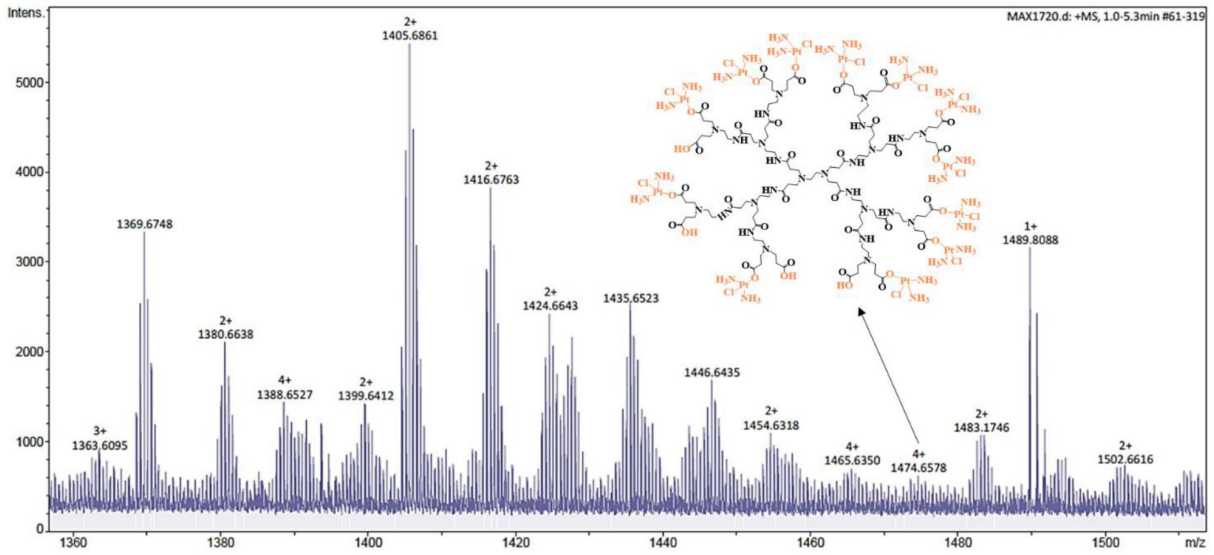

Figure C5: TOF-MS (ESI +) mass spectrum of G1.5(COOPt$(NH_3)_2Cl)_{16}$ metallodendrimer.

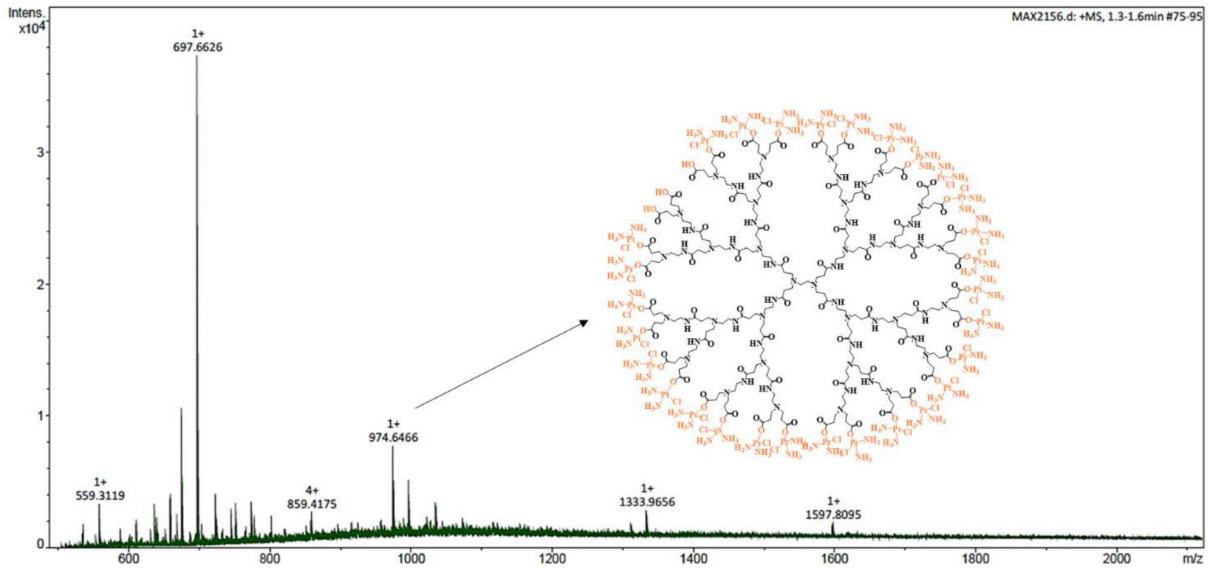

Figure C6: TOF-MS (ESI +) mass spectrum of G2.5(COOPt$(NH_3)_2Cl)_{32}$ metallodendrimer.

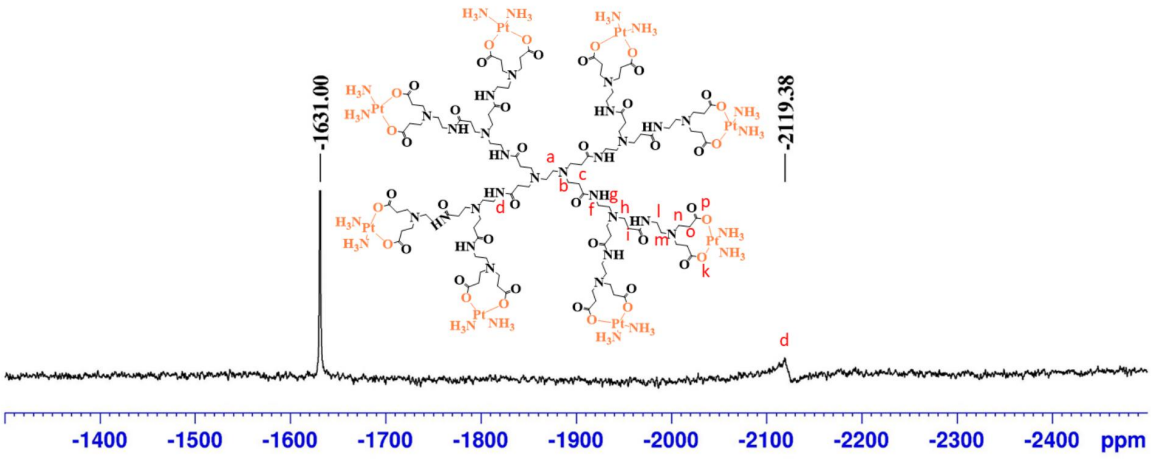

Figure C7: ^{195}Pt-NMR spectrum of G1.5COO$(Pt(NH_3)_2)_8$ performed in D_2O, with K_2PtCl_4 as an external reference (-1631 ppm).

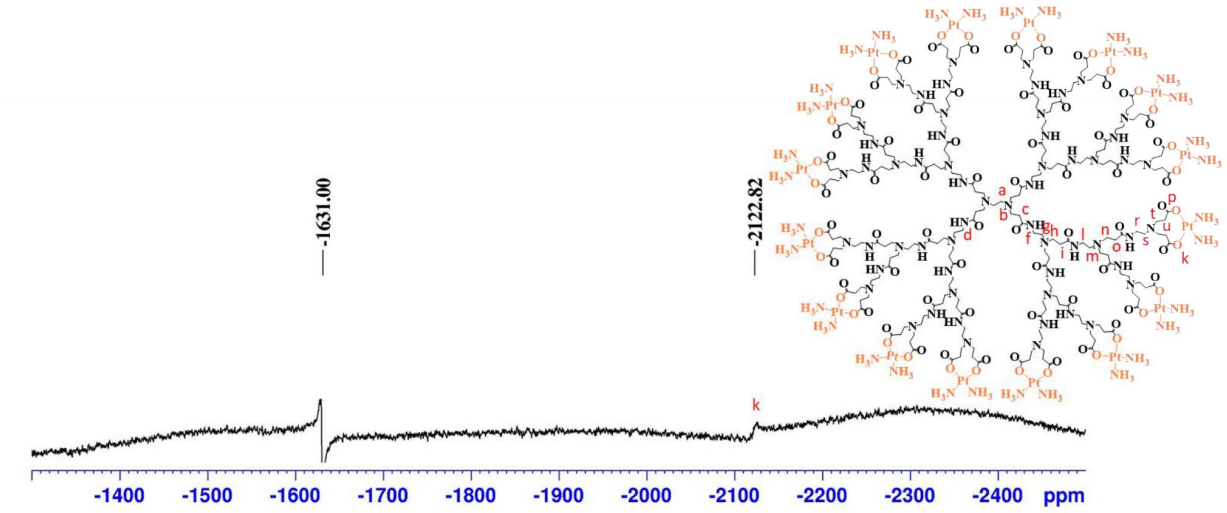

Figure C8: ^{195}Pt-NMR spectrum of G2.5COO(Pt(NH$_3$)$_2$)$_{16}$ performed in D_2O, with K_2PtCl_4 as an external reference (-1631 ppm).

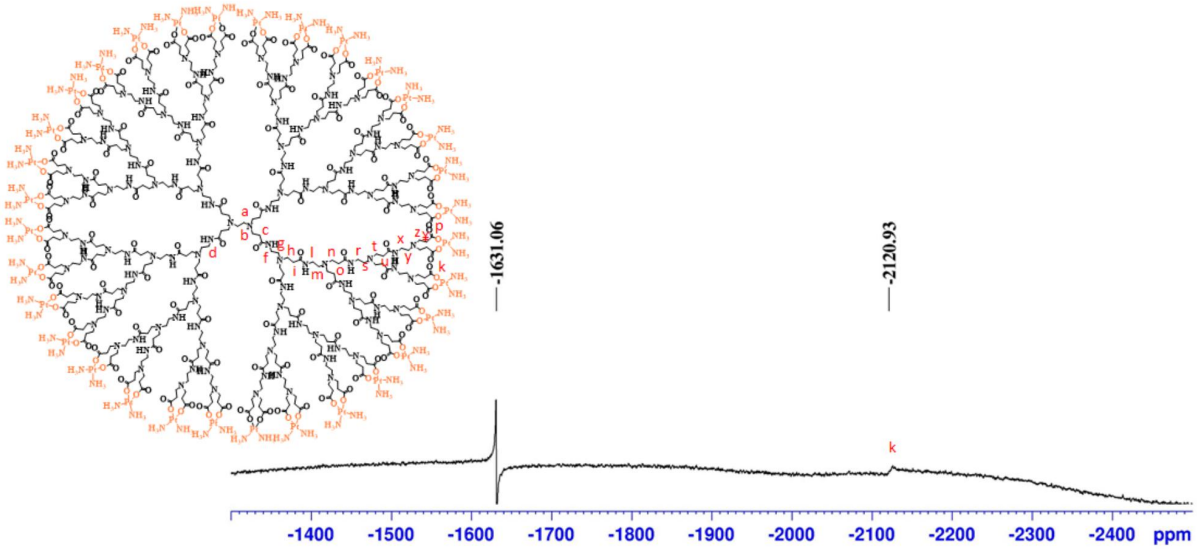

Figure C9: ^{195}Pt-NMR spectrum of G3.5COO(Pt(NH$_3$)$_2$)$_{32}$ performed in D_2O, with K_2PtCl_4 as an external reference (-1631 ppm).

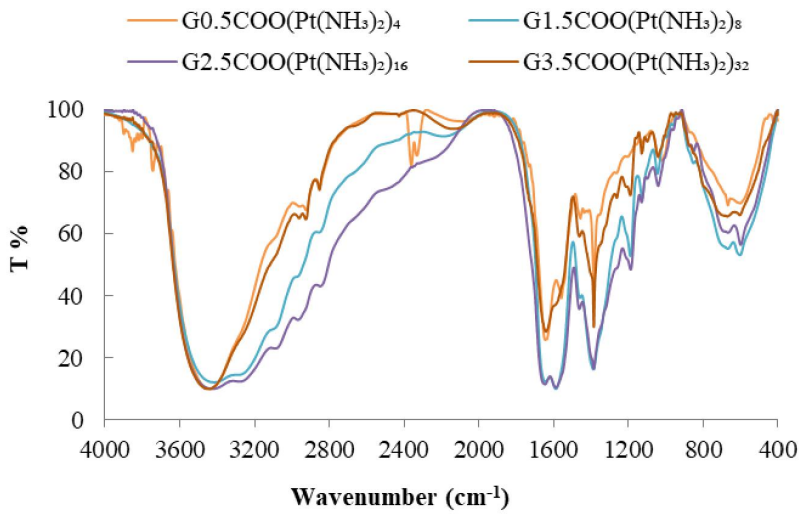

Figure C10: FTIR spectrum of metallodendrimers conjugated with cisplatin in bidentate form. The spectrum was performed in KBr pellets.

- **Bidentate form**

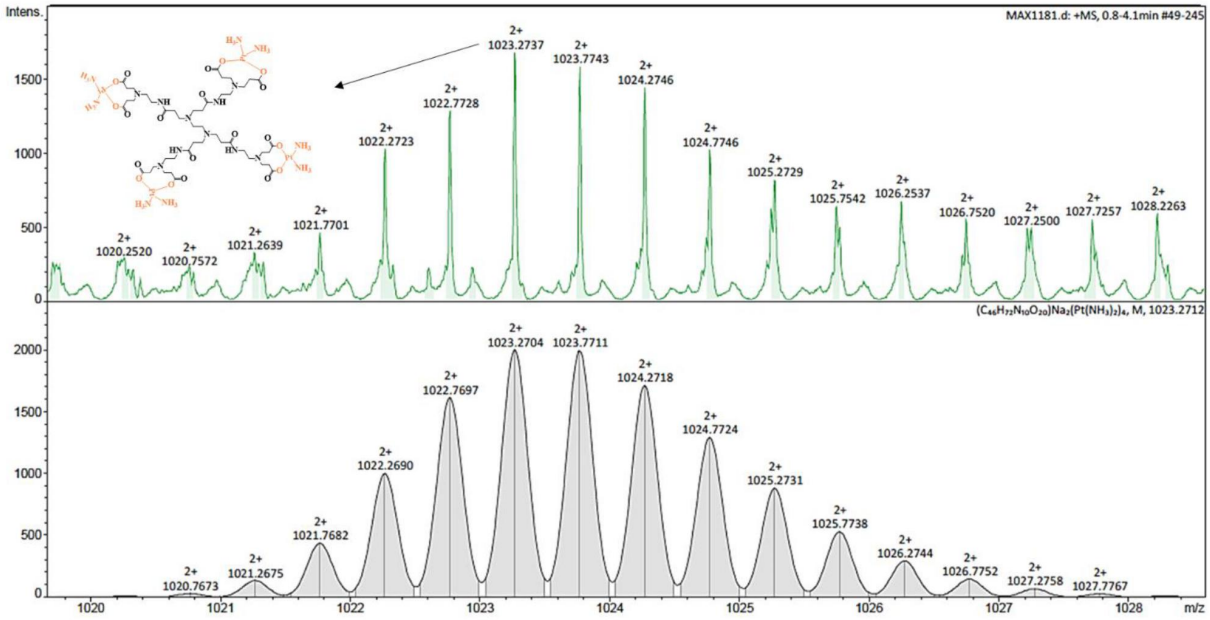

Figure C11: TOF-MS (ESI +) mass spectrum of G0.5COO(Pt(NH3)2)4 metallodendrimer.

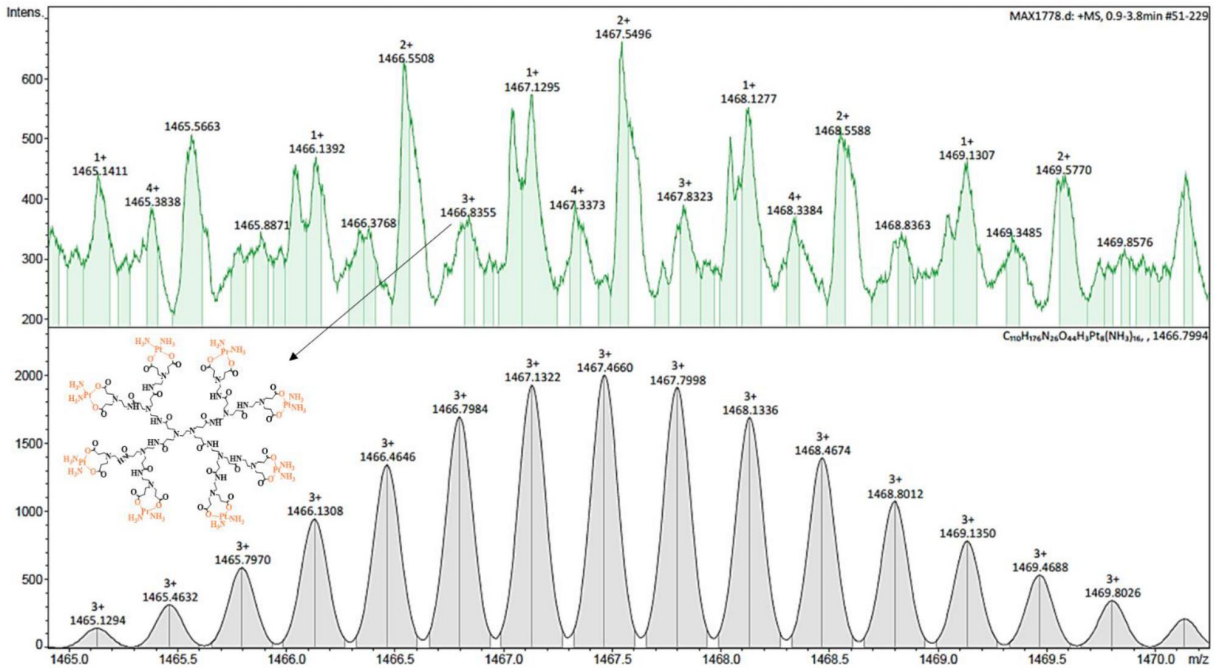

Figure C12: TOF-MS (ESI +) mass spectrum of G1.5COO($Pt(NH_3)_2)_8$ metallodendrimer.

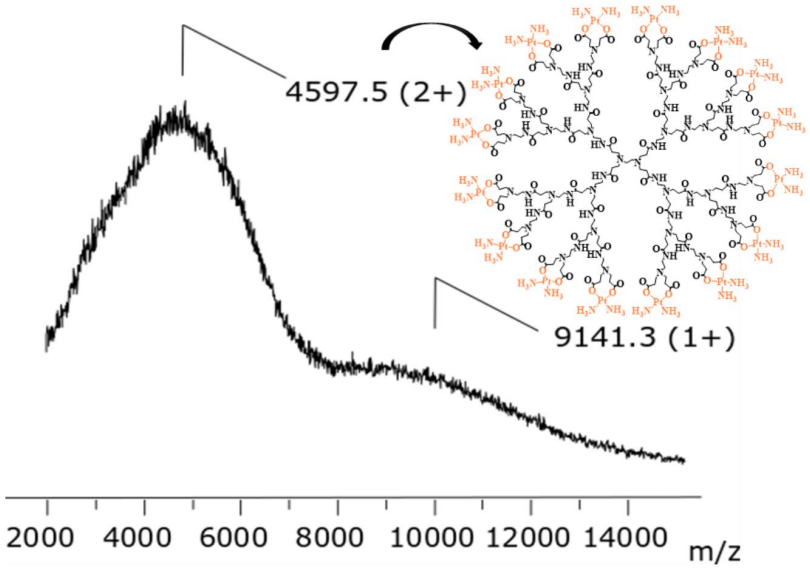

Figure C13: TOF-MS (MALDI) mass spectrum of G2.5COO($Pt(NH_3)_2)_{16}$ metallodendrimer.

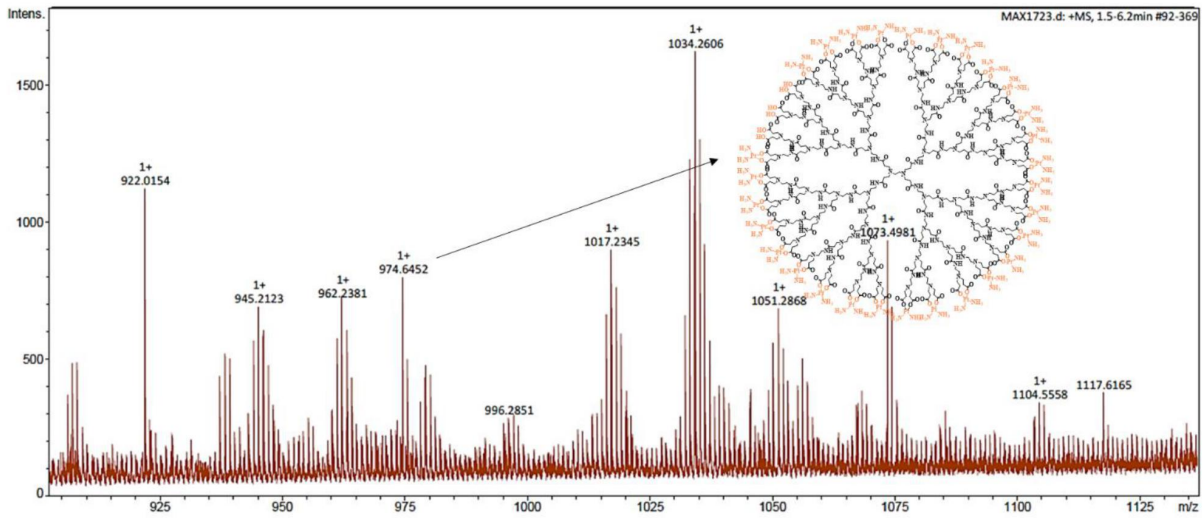

Figure C14: TOF-MS (ESI +) mass spectrum of G3.5COO$(Pt(NH_3)_2)_{32}$ metallodendrimer.

- Cytotoxicity assay

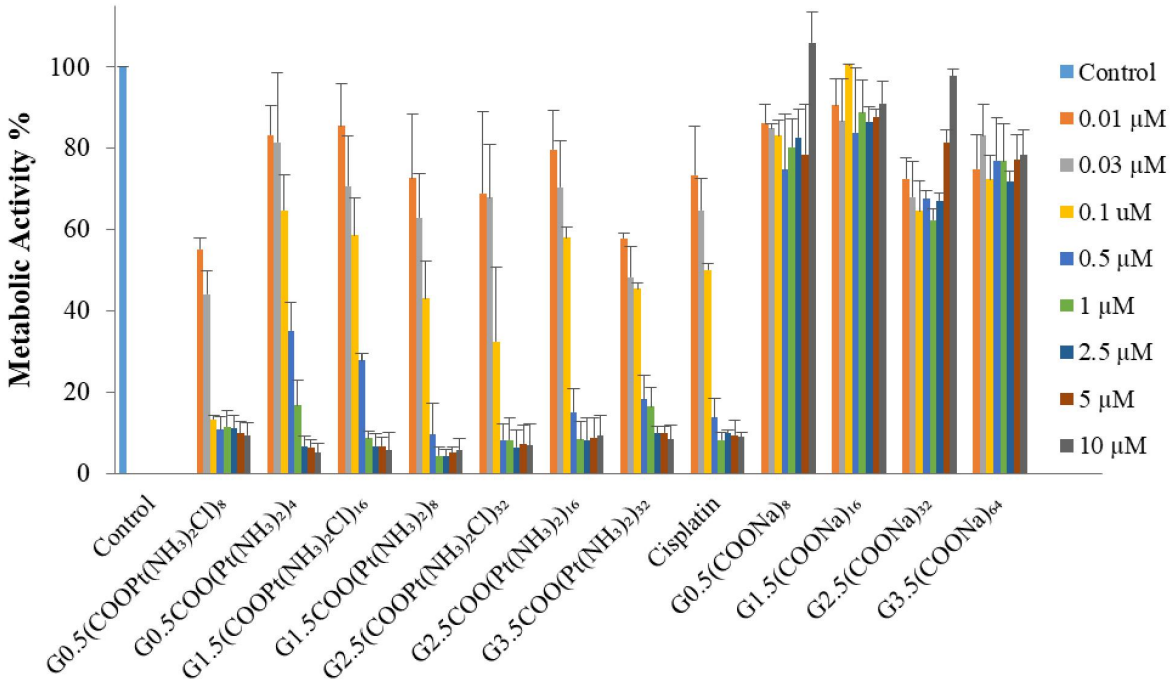

Figure C15: *In vitro* cytotoxicity studies of the cisplatin-metallodendrimers and anionic PAMAM dendrimers with different generations (0.5-3.5) on A2780 cell line. The cells were treated for 72 h with a concentration range from 0.01 µM to 10 µM. The results are expressed as mean ± SD three independent experiments performed in triplicate.

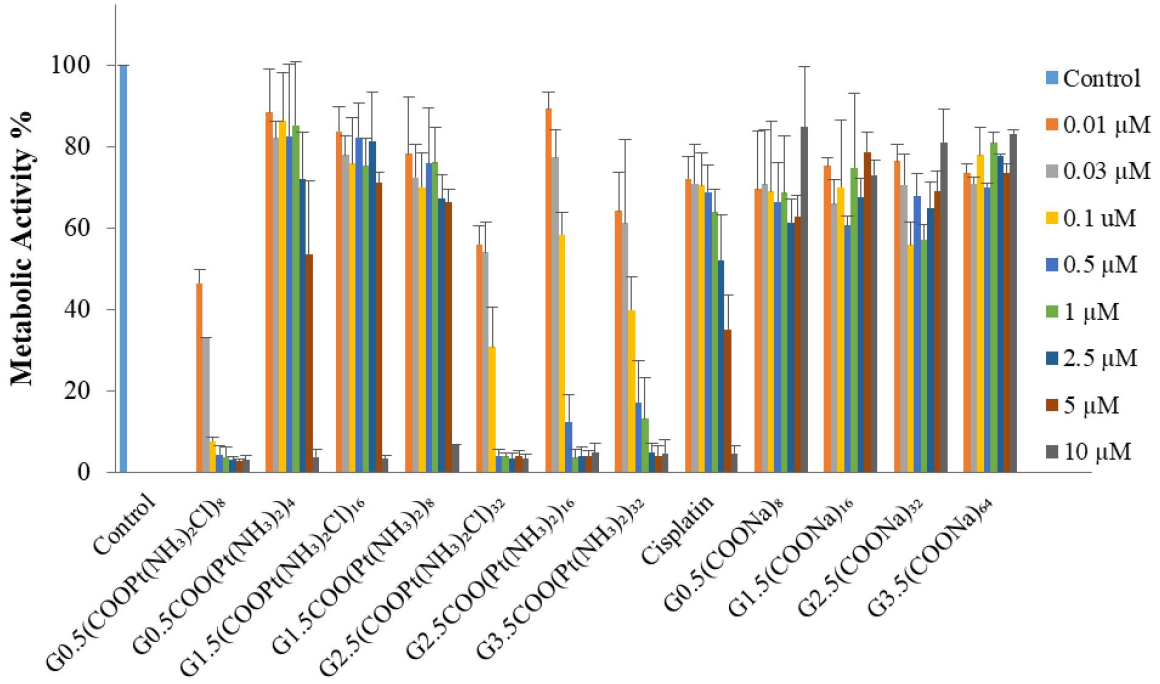

Figure C16: *In vitro* cytotoxicity studies of the cisplatin-metallodendrimers and anionic PAMAM dendrimers with different generations (0.5-3.5) on A2780CisR cell line. The cells were treated for 72 h with a concentration range from 0.01 µM to 10 µM. The results are expressed as mean ± SD three independent experiments performed in triplicate.

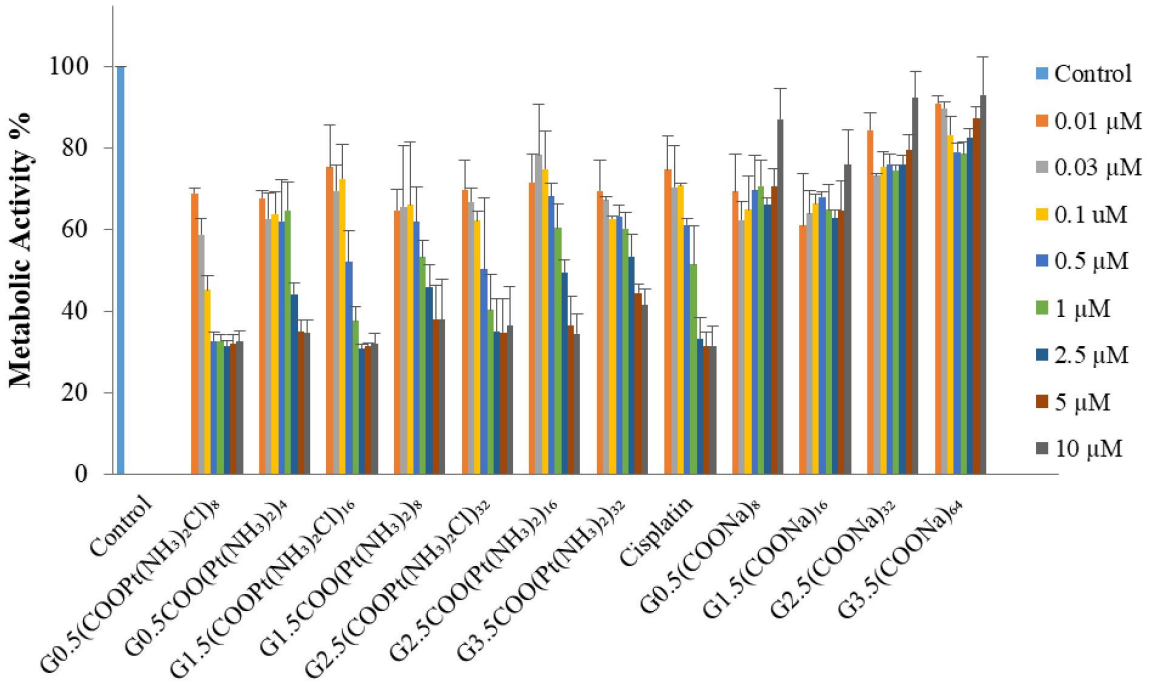

Figure C17: *In vitro* cytotoxicity studies of the cisplatin-metallodendrimers and anionic PAMAM dendrimers with different generations (0.5-3.5) on MCF-7 cell line. The cells were treated for 72 h with a concentration range from 0.01 µM to 10 µM. The results are expressed as mean ± SD three independent experiments performed in triplicate.

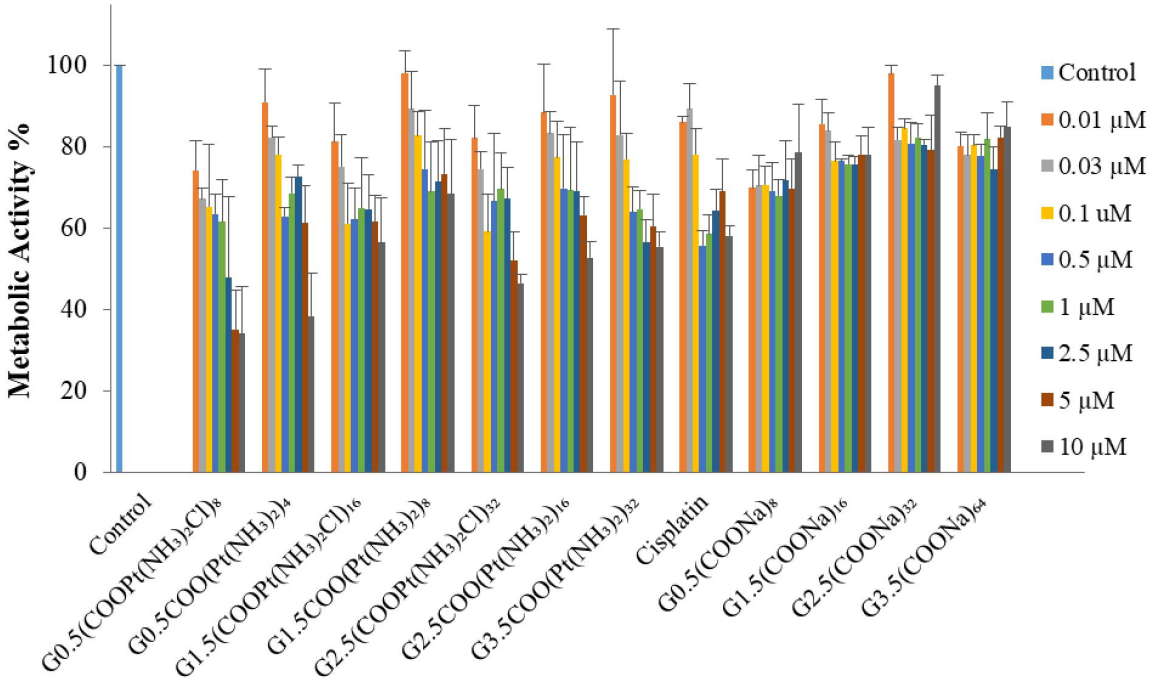

Figure C18: *In vitro* cytotoxicity studies of the cisplatin-metallodendrimers and anionic PAMAM dendrimers with different generations (0.5-3.5) on CACO-2 cell line. The cells were treated for 72 h with a concentration range from 0.01 µM to 10 µM. The results are expressed as mean ± SD three independent experiments performed in triplicate.

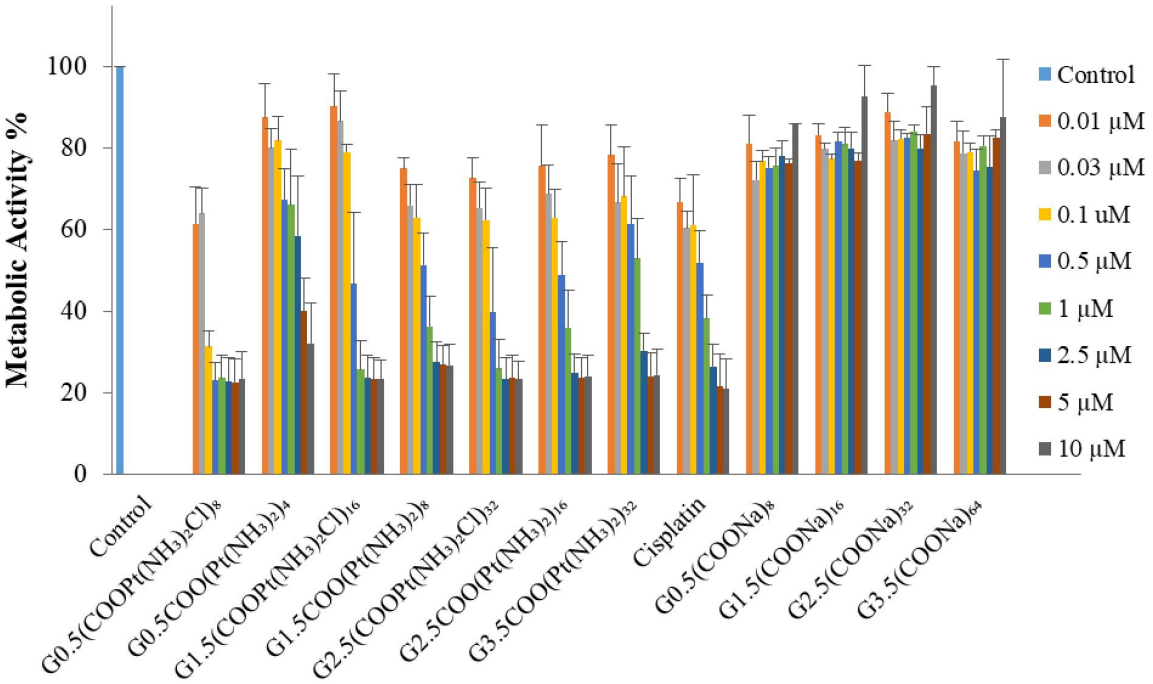

Figure C19: *In vitro* cytotoxicity studies of the cisplatin-metallodendrimers and anionic PAMAM dendrimers with different generations (0.5-3.5) on BJ cell line. The cells were treated for 72 h with a concentration range from 0.01 µM to 10 µM. The results are expressed as mean ± SD three independent experiments performed in triplicate.

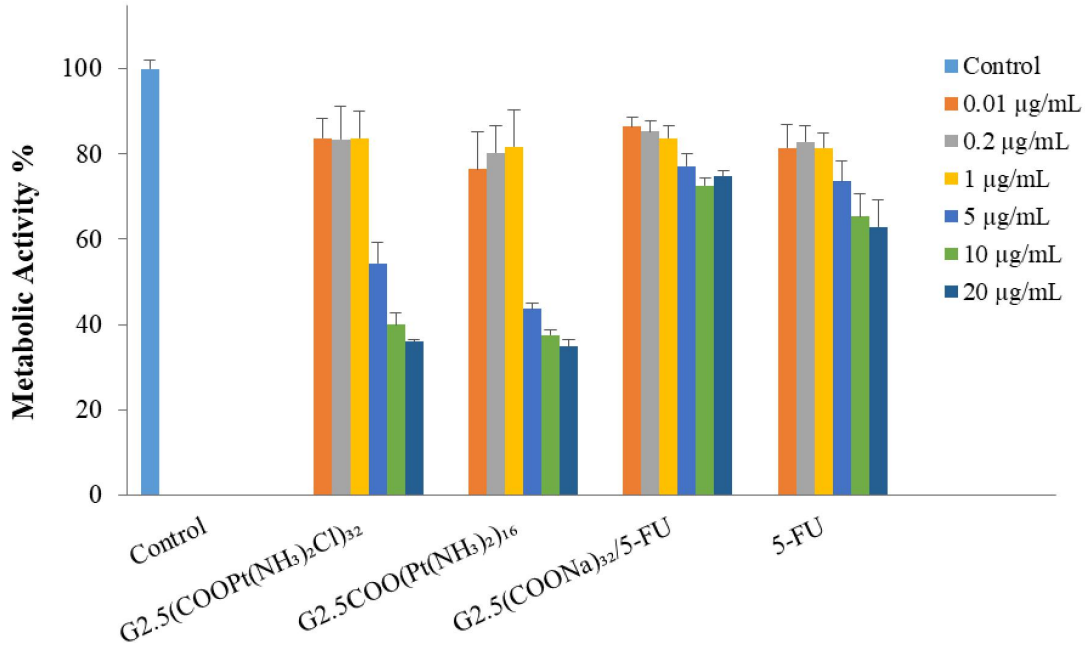

Figure C20: *In vitro* cytotoxicity studies of the complexes cisplatin-metallodendrimers/5-FU, G2.5(COONa)$_{32}$/5-FU and 5-FU on A2780CisR cell line. The cells were treated for 72 h with a concentration range from 0.01 µg/mL to 20 µg/mL. The results are expressed as mean ± SD three independent experiments performed in triplicate.

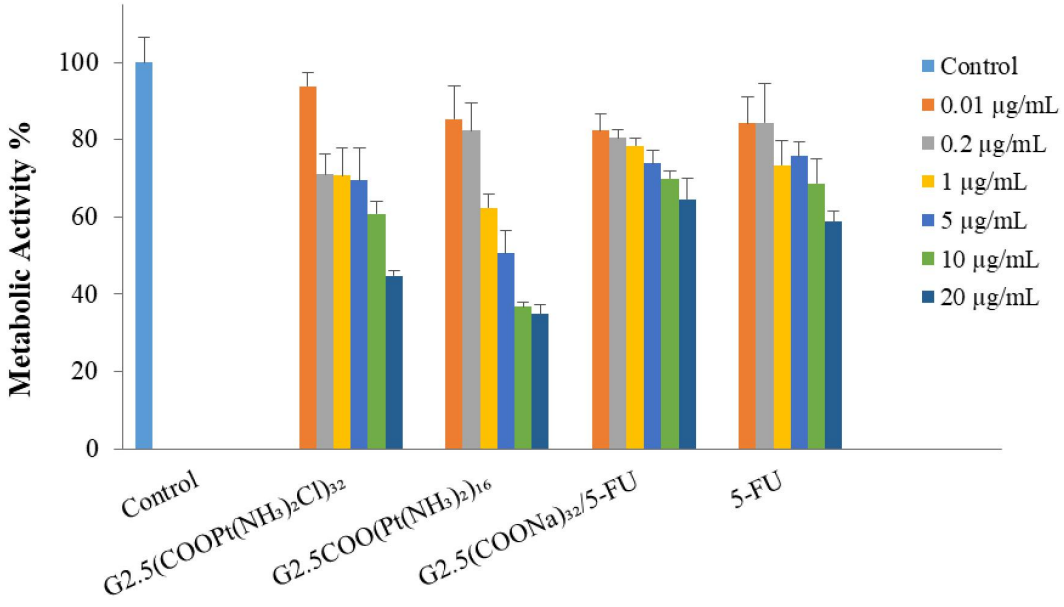

Figure C21: *In vitro* cytotoxicity studies of the complexes cisplatin metallodendrimers/5-FU, G2.5(COONa)$_{32}$/5-FU and 5-FU on CACO-2 cell line. The cells were treated for 72 h with a concentration range from 0.01 µg/mL to 20 µg/mL. The results are expressed as mean ± SD three independent experiments performed in triplicate.

- DNA binding studies

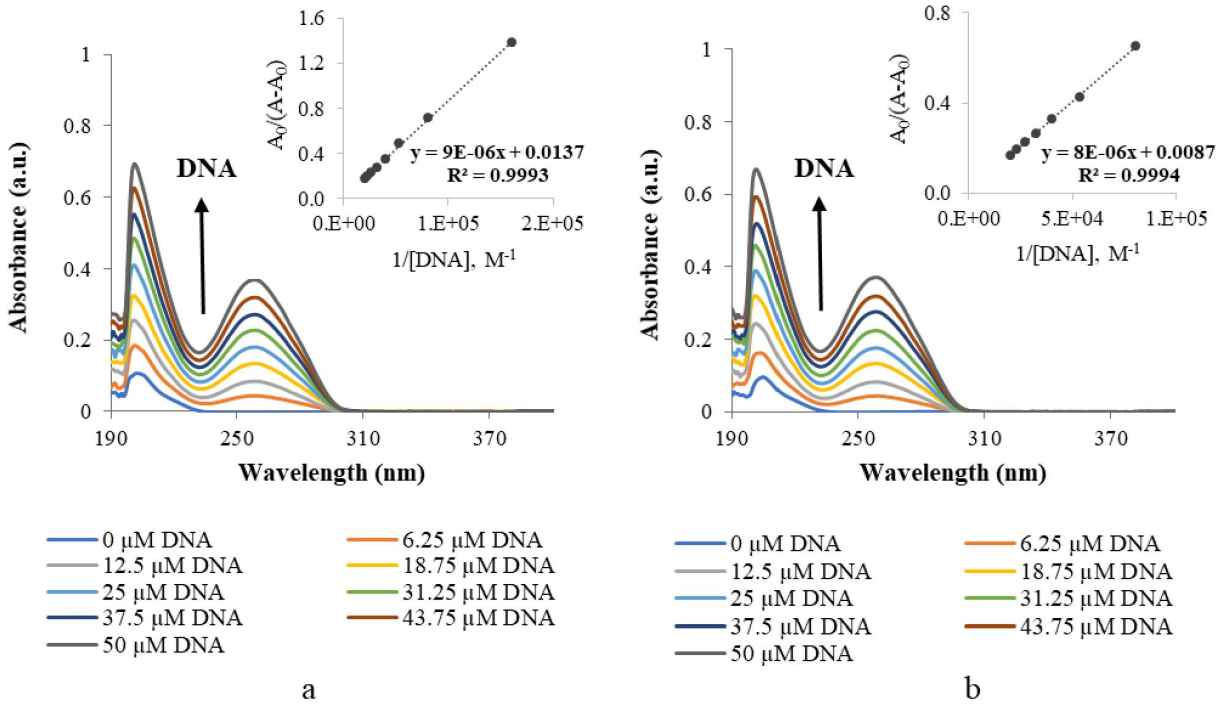

Figure C22: UV-visible spectra of cisplatin a) 1st trial b) 2nd trial with increasing concentration of CT-DNA (0, 6.25, 12.5, 18.75, 25, 31.25, 37.5, 43.75 and 50 µM) in 5 mM Tris-HCl/50 mM NaCl at pH 7.4. The inset corresponds to the plot of $A_0/(A-A_0)$ versus 1/[DNA], which is used to determine the binding constant. The arrow indicates the direction of increasing the concentration of DNA.

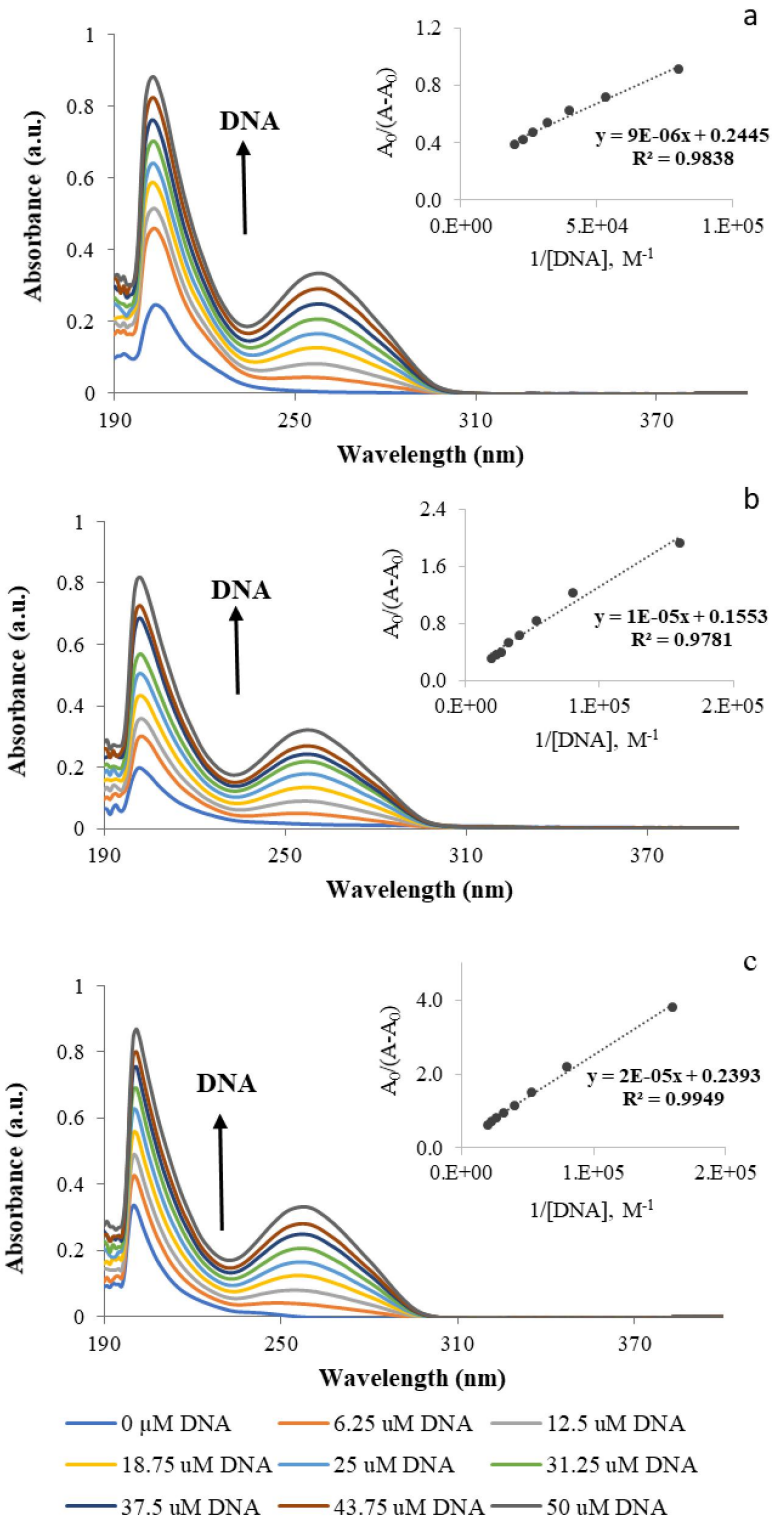

Figure C23: UV-visible spectra 2nd trial of a)G0.5(COOPt$(NH_3)_2Cl)_8$ b)G2.5(COOPt$(NH_3)_2Cl)_{32}$ c)G2.5COO(Pt$(NH_3)_2)_{16}$ with increasing concentration of CT-DNA (0, 6.25, 12.5, 18.75, 25, 31.25, 37.5, 43.75 and 50 µM) in 5 mM Tris-HCl/50 mM NaCl at pH 7.4. The inset corresponds to the plot of $A_0/(A-A_0)$ versus 1/[DNA], which is used to determine the binding constant. The arrow indicates the direction of increasing the concentration of DNA.

- Complexes - characterization

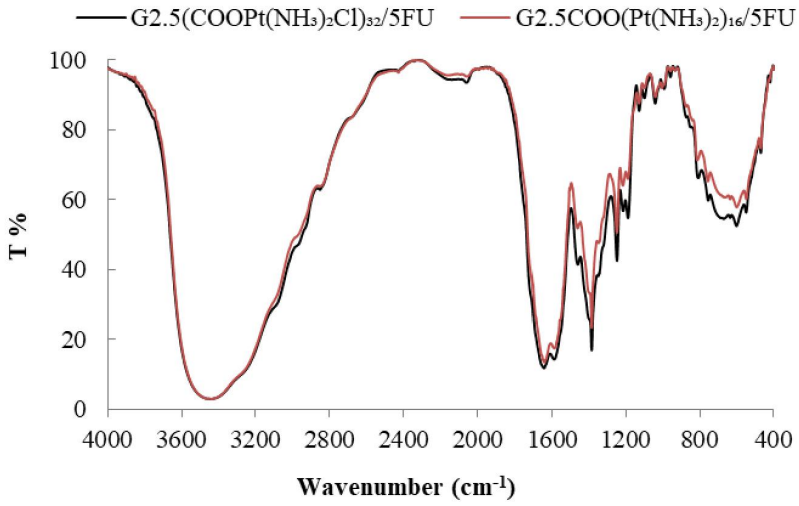

Figure C24: FTIR spectra of G2.5(COOPt(NH$_3$)$_2$Cl)$_{32}$/5FU and G2.5COO(Pt(NH$_3$)$_2$)$_{16}$/5FU in KBr pellet.

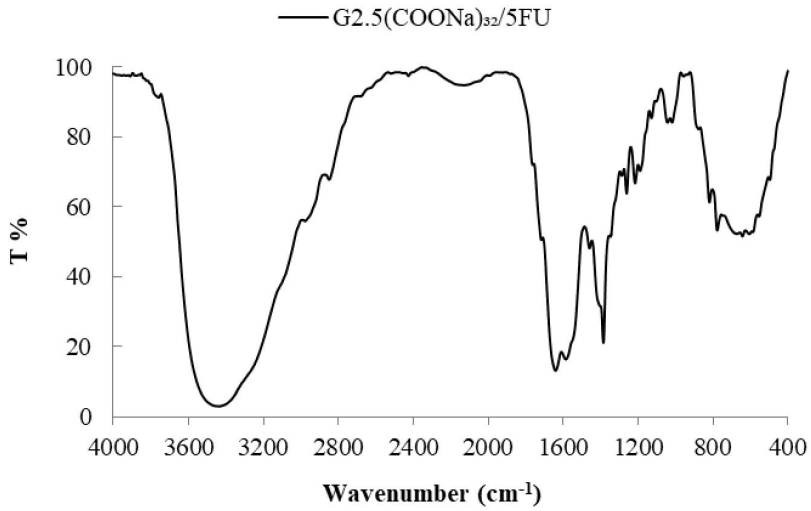

Figure C25: FTIR spectra of G2.5(COONa)$_{32}$/5-FU in KBr pellet.

D. Chapter III: Improving the efficacy of DACHPt and 5-FU anticancer drugs using anionic PAMAM dendrimers as drug delivery system

- Characterization

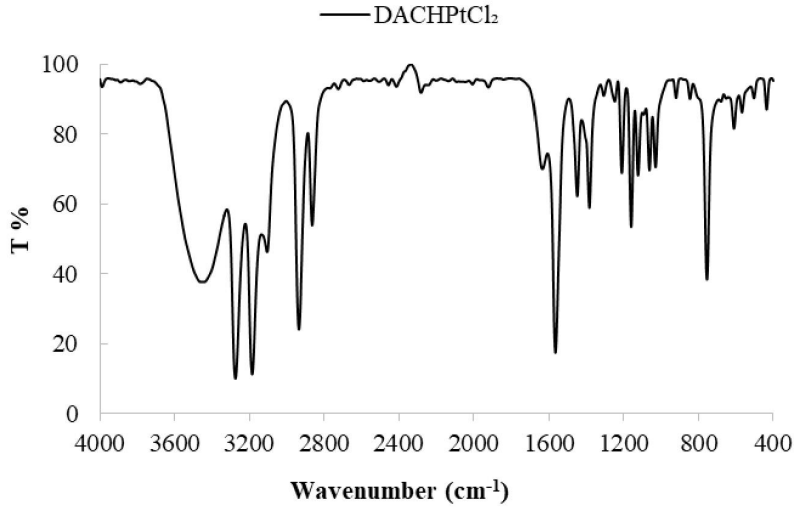

Figure D1: FTIR spectra of $DACHPtCl_2$ in KBr pellet.

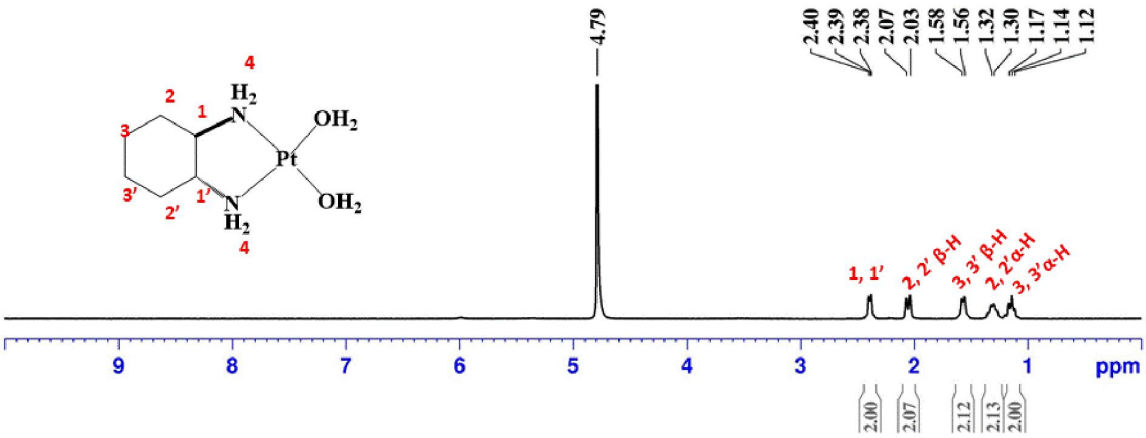

Figure D2: ^{1}H-NMR spectrum of bis-aquated DACHPt done in D_2O.

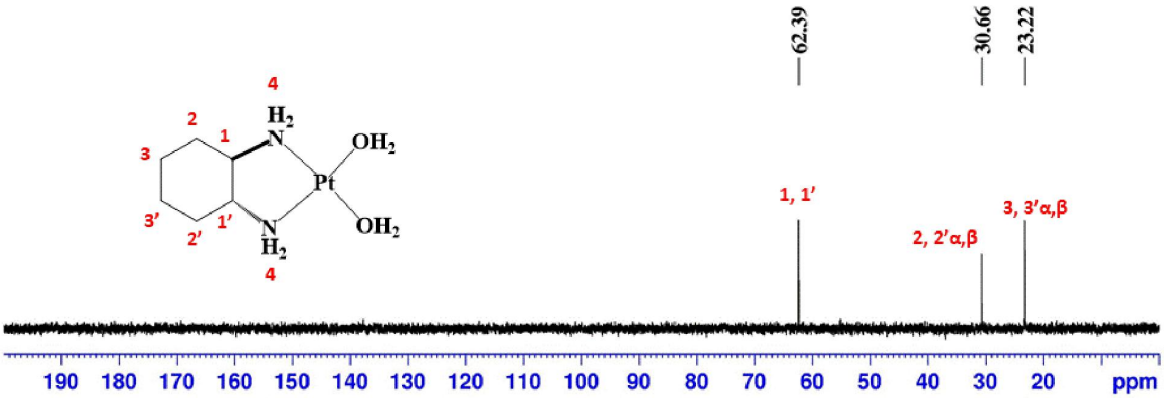

Figure D3: ^{13}C-NMR spectrum of bis-aquated DACHPt done in D_2O.

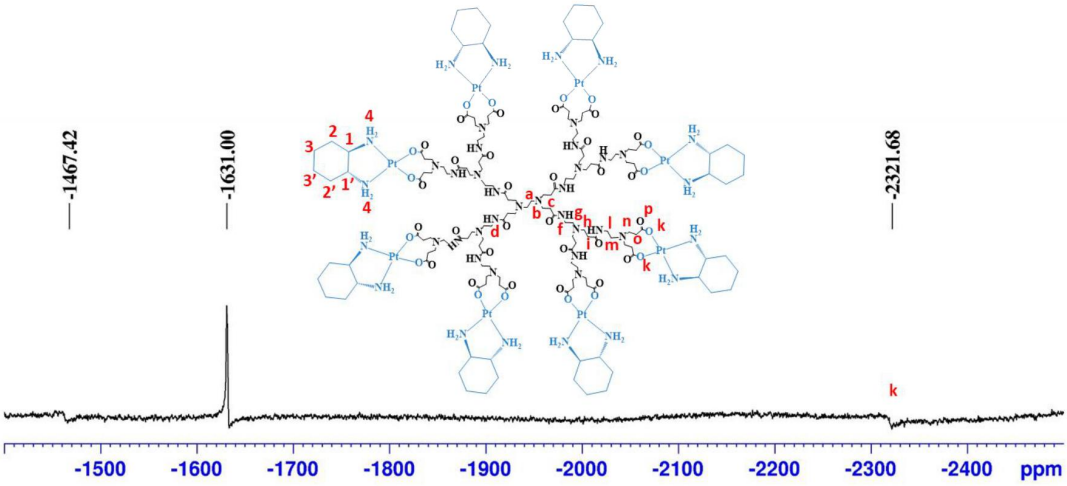

Figure D4: ^{195}Pt-NMR spectrum of G1.5COO(DACHPt)$_8$ performed in D_2O, with K_2PtCl_4 as an external reference (-1631 ppm).

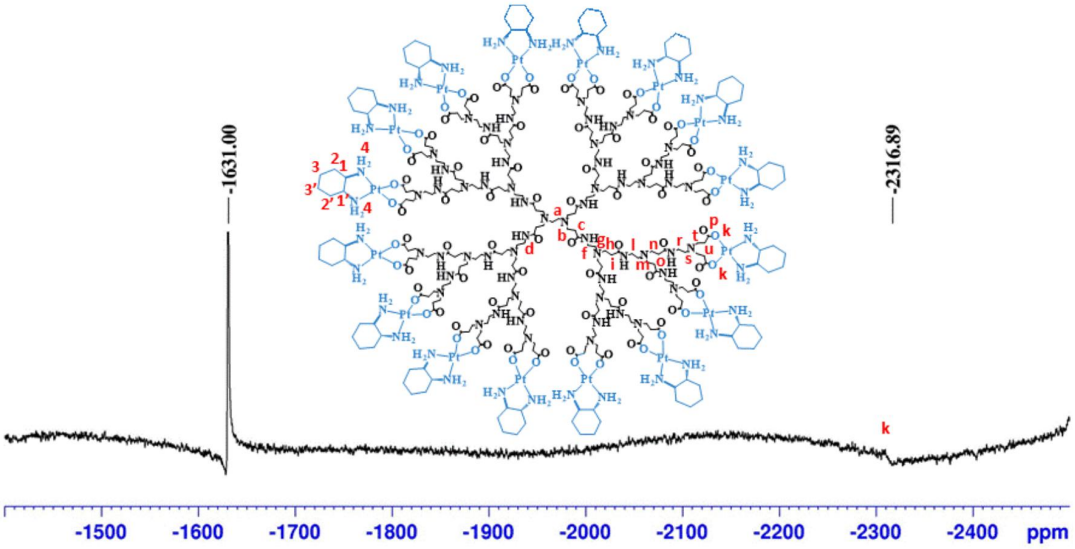

Figure D5: ^{195}Pt-NMR spectrum of G2.5COO(DACHPt)$_{16}$ performed in D_2O, with K_2PtCl_4 as an external reference (-1631 ppm).

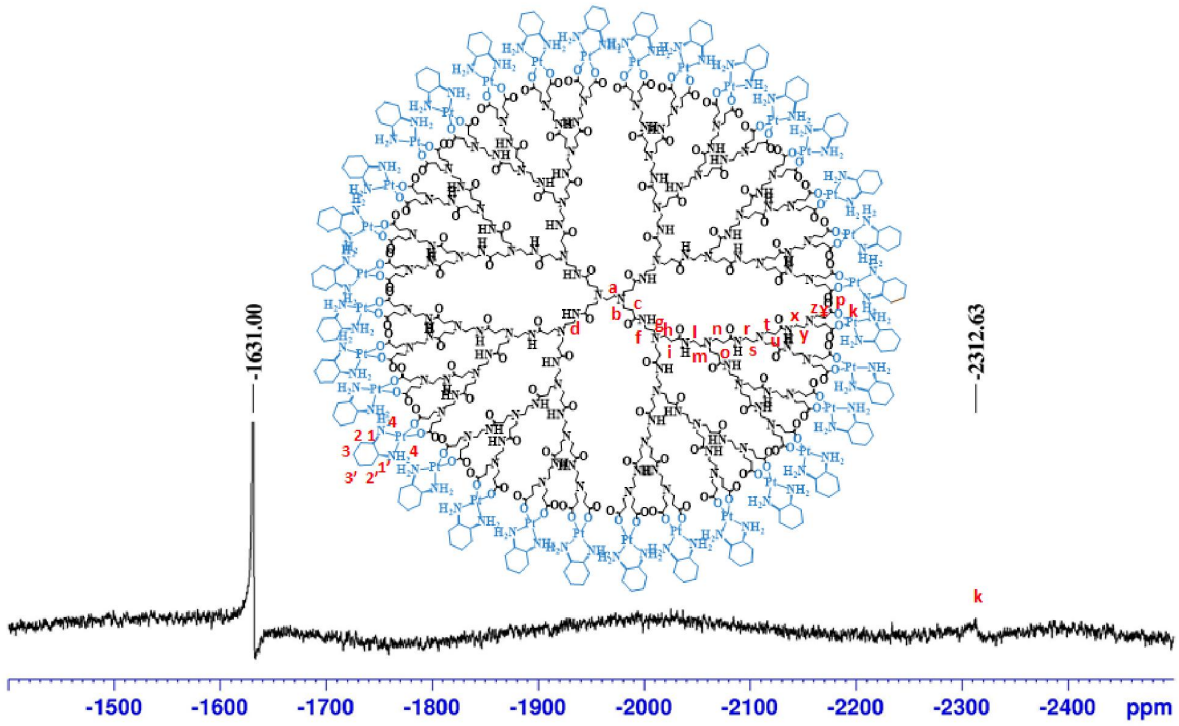

Figure D6: ^{195}Pt-NMR spectrum of G3.5COO(DACHPt)$_{32}$ performed in D_2O, with K_2PtCl_4 as an external reference (-1631 ppm).

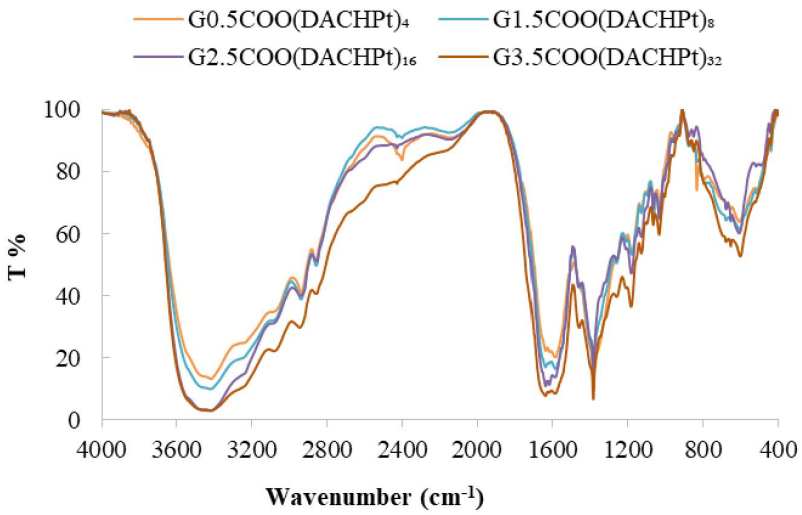

Figure D7: FTIR spectra of DACHPt-metallodendrimers in KBr pellet.

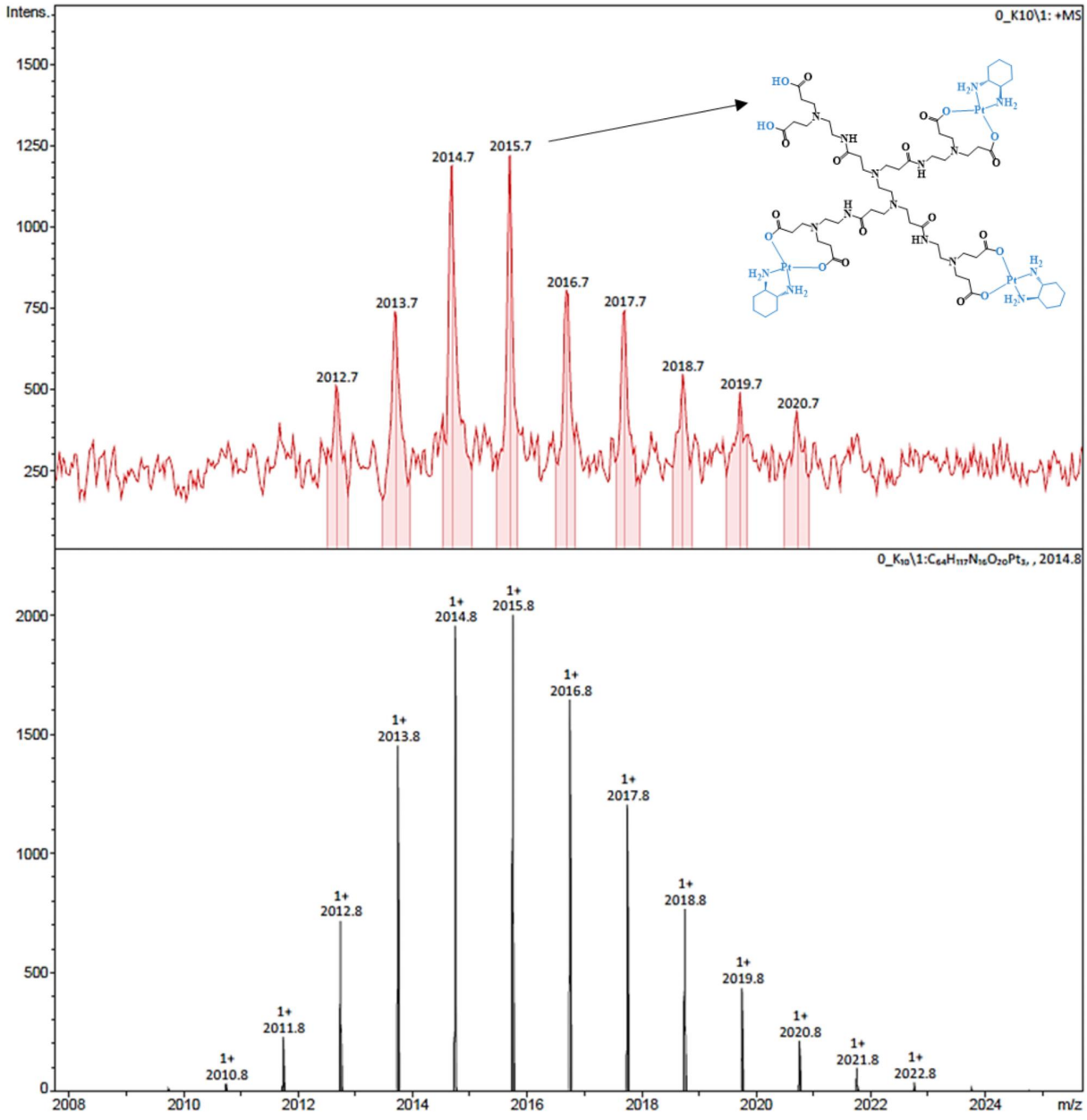

Figure D8: TOF-MS (MALDI) mass spectrum of G0.5COO(DACHPt)$_4$ metallodendrimer.

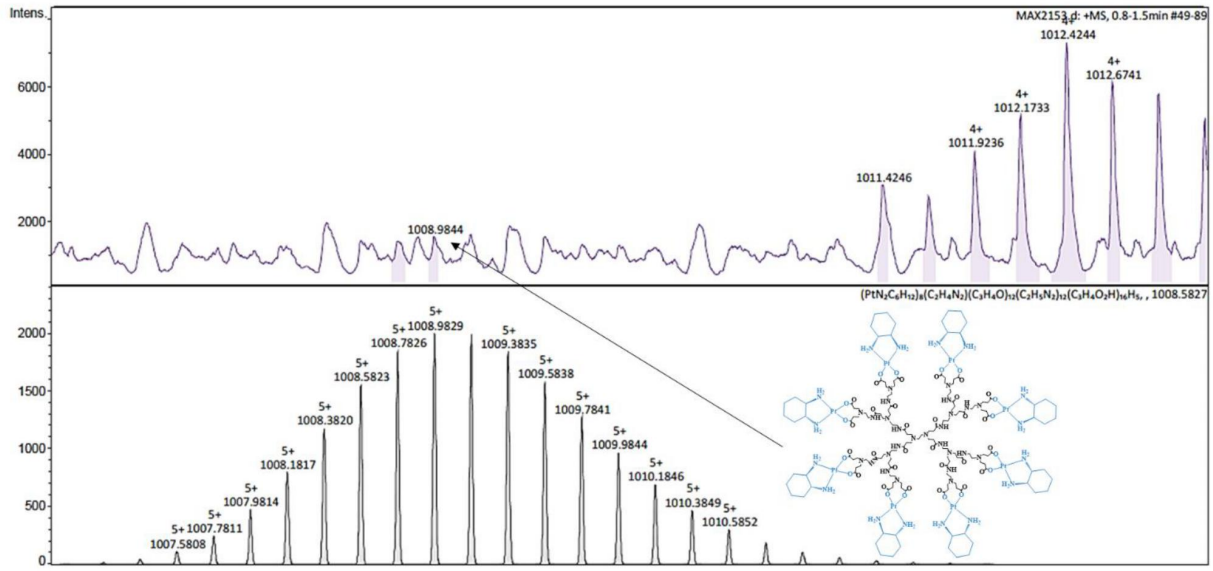

Figure D9: TOF-MS (ESI +) mass spectrum of G1.5COO(DACHPt)$_8$ metallodendrimer.

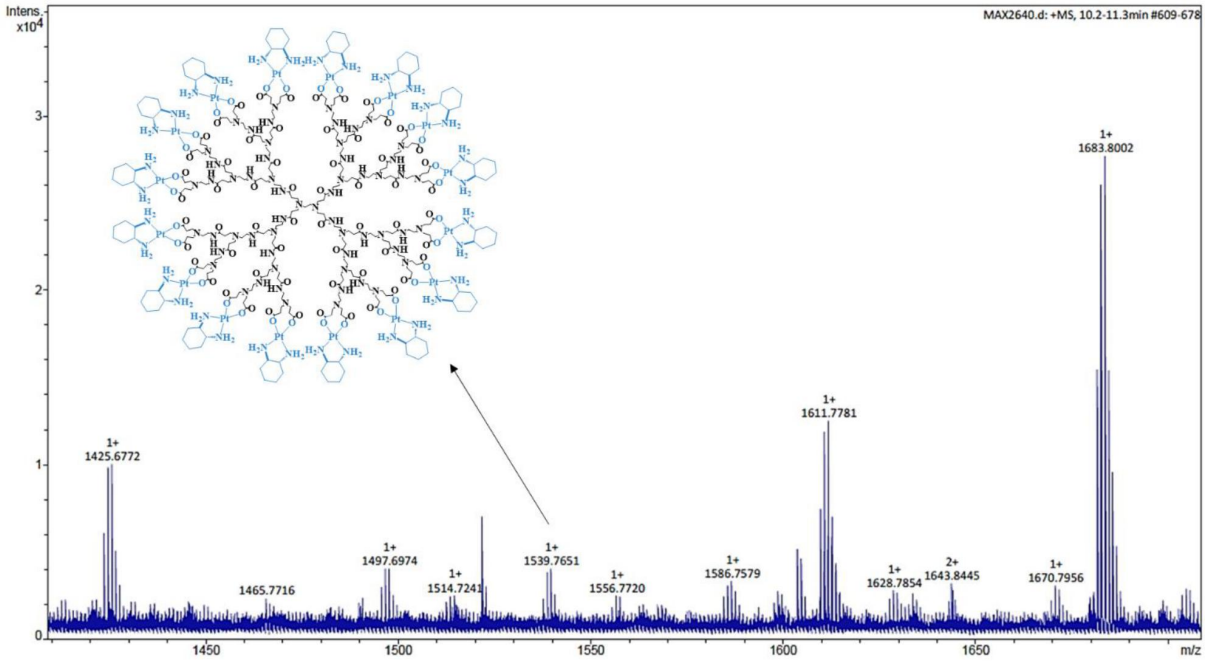

Figure D10: TOF-MS (ESI +) mass spectrum of G2.5COO(DACHPt)$_{16}$ metallodendrimer.

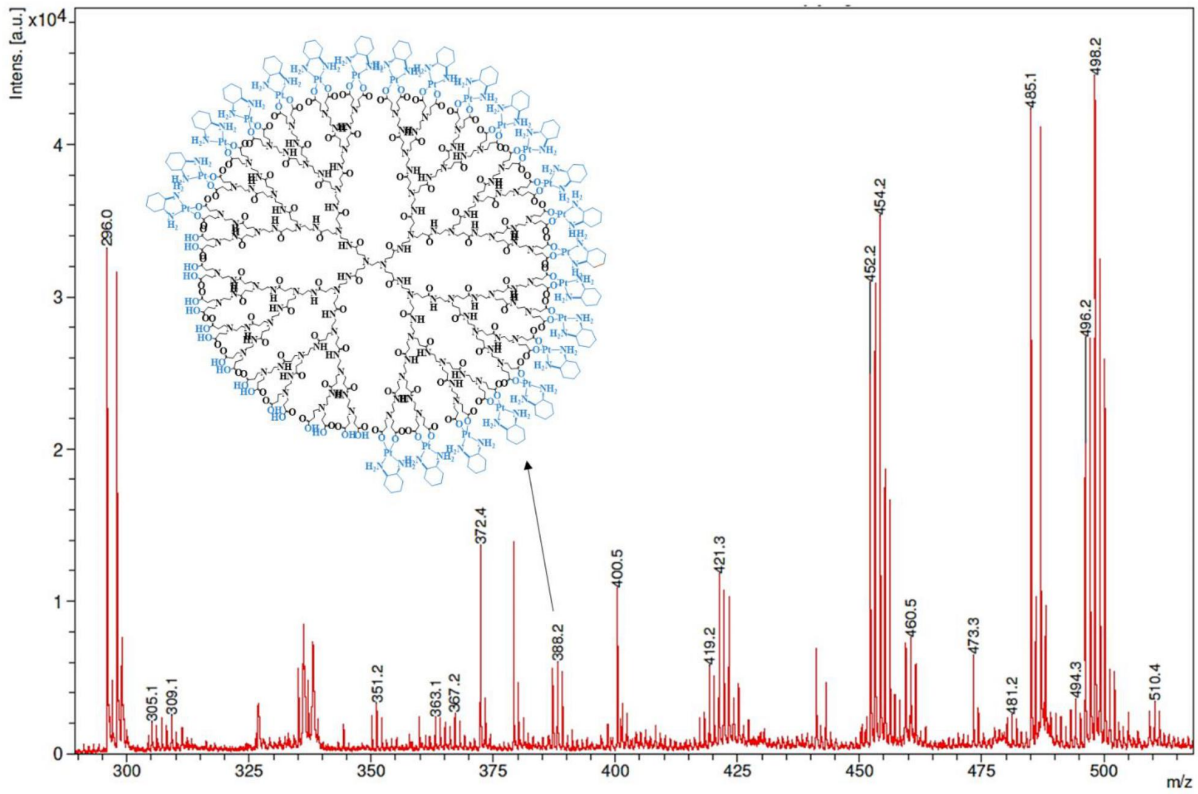

Figure D11: TOF-MS (MALDI) mass spectrum of G3.5COO(DACHPt)$_{32}$ metallodendrimer.

- Cytotoxicity assay

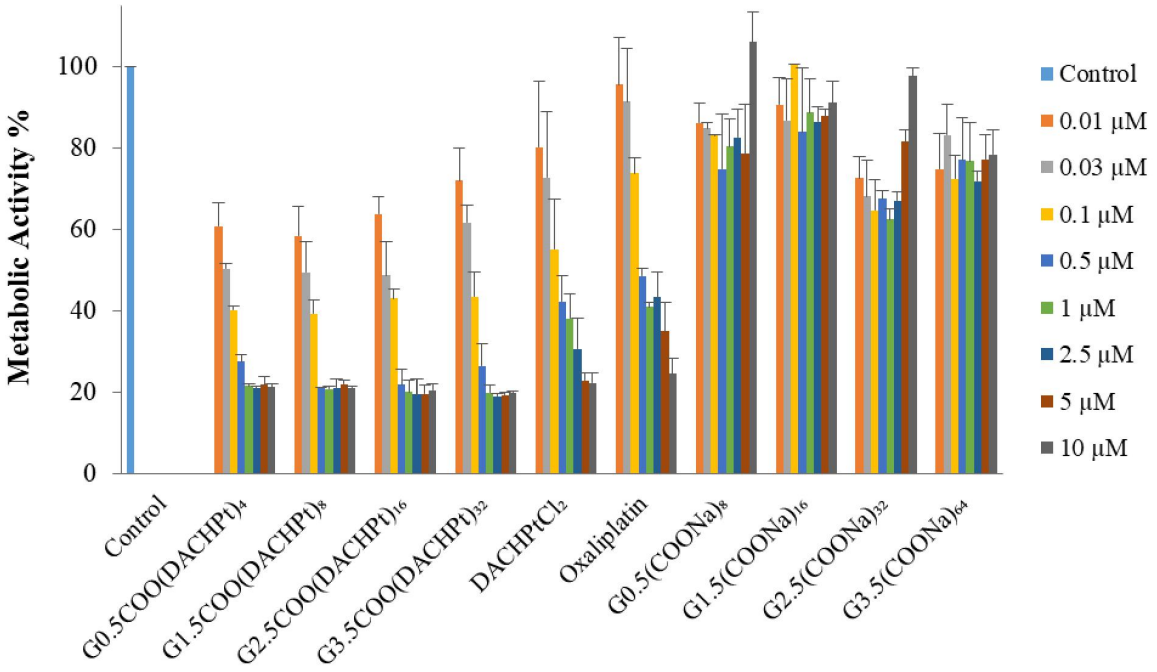

Figure D12: *In vitro* cytotoxicity studies of the DACHPt-metallodendrimers and anionic PAMAM dendrimers with different generations (0.5-3.5) on A2780 cancer cell line. The cells were treated for 72 h with a concentration range from 0.01 µM to 10 µM. The results are expressed as mean ± SD three independent experiments performed in triplicate.

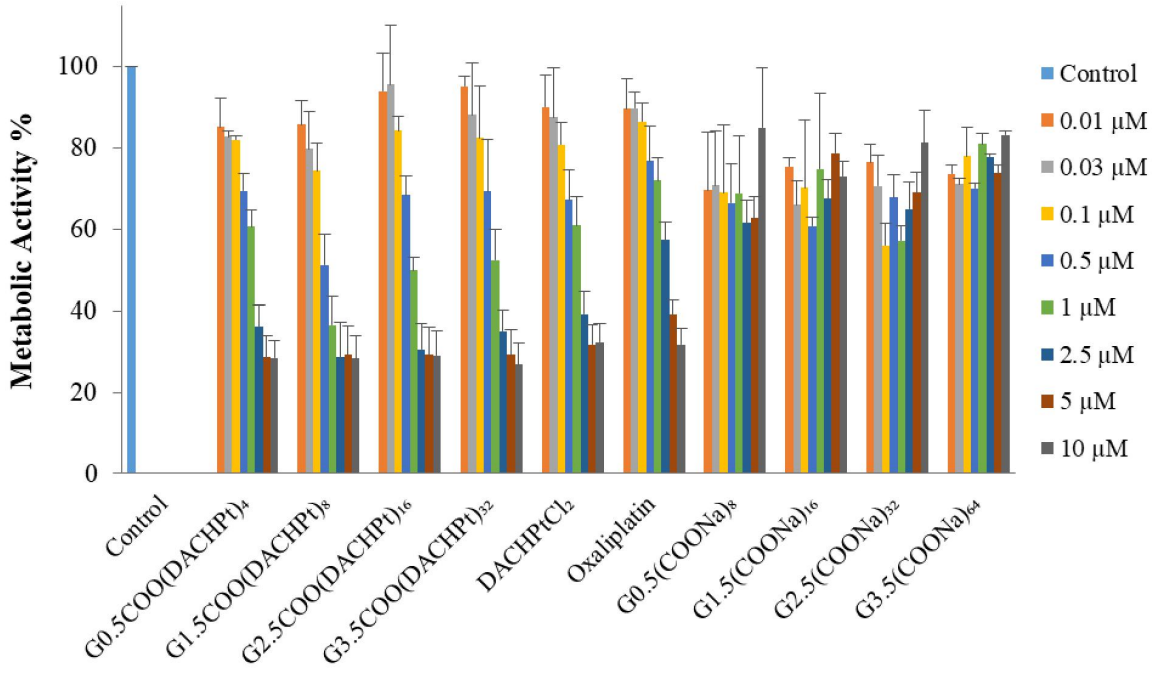

Figure D13: *In vitro* cytotoxicity studies of the DACHPt-metallodendrimers and anionic PAMAM dendrimers with different generations (0.5-3.5) on A2780CisR cancer cell line. The cells were treated for 72 h with a concentration range from 0.01 µM to 10 µM. The results are expressed as mean ± SD three independent experiments performed in triplicate.

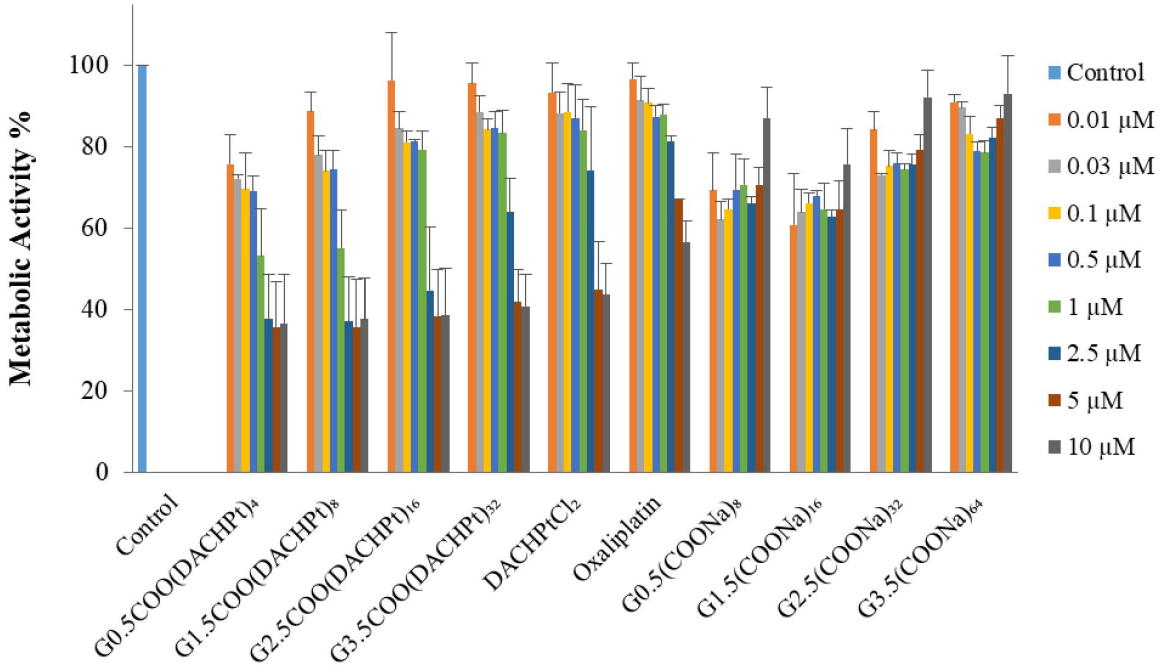

Figure D14: *In vitro* cytotoxicity studies of the DACHPt-metallodendrimers and anionic PAMAM dendrimers with different generations (0.5-3.5) on MCF-7 cancer cell line. The cells were treated for 72 h with a concentration range from 0.01 µM to 10µM. The results are expressed as mean ± SD three independent experiments performed in triplicate.

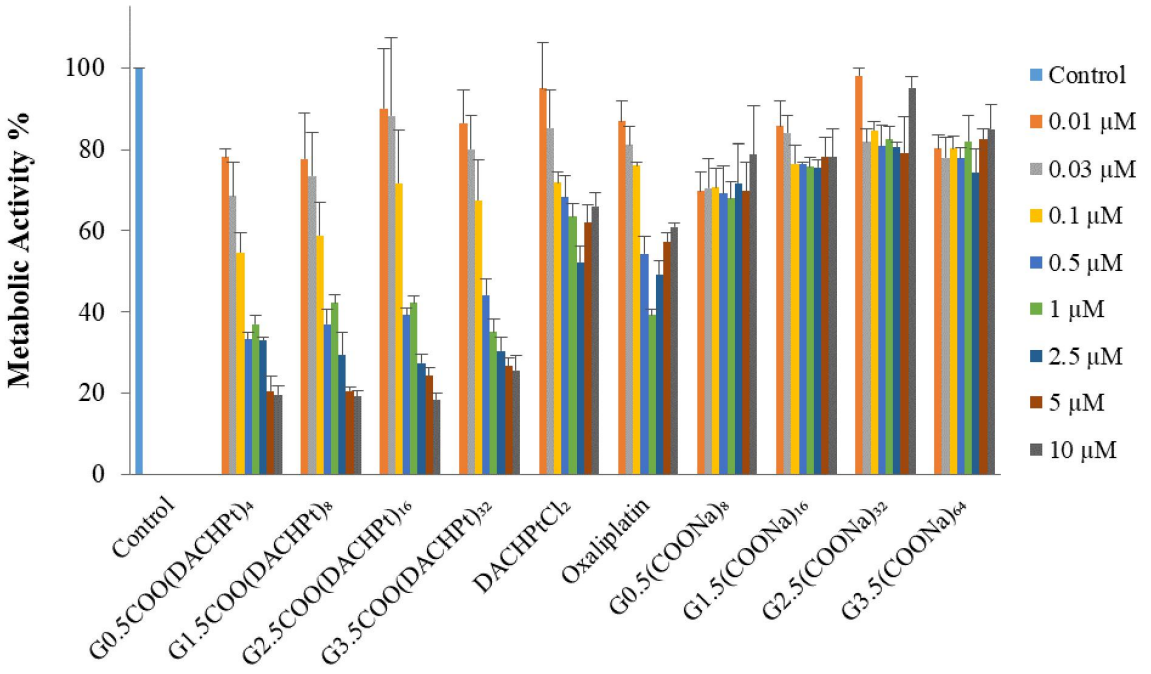

Figure D15: *In vitro* cytotoxicity studies of the DACHPt-metallodendrimers and anionic PAMAM dendrimers with different generations (0.5-3.5) on CACO-2 cancer cell line. The cells were treated for 72 h with a concentration range from 0.01 µM to 10 µM. The results are expressed as mean ± SD three independent experiments performed in triplicate.

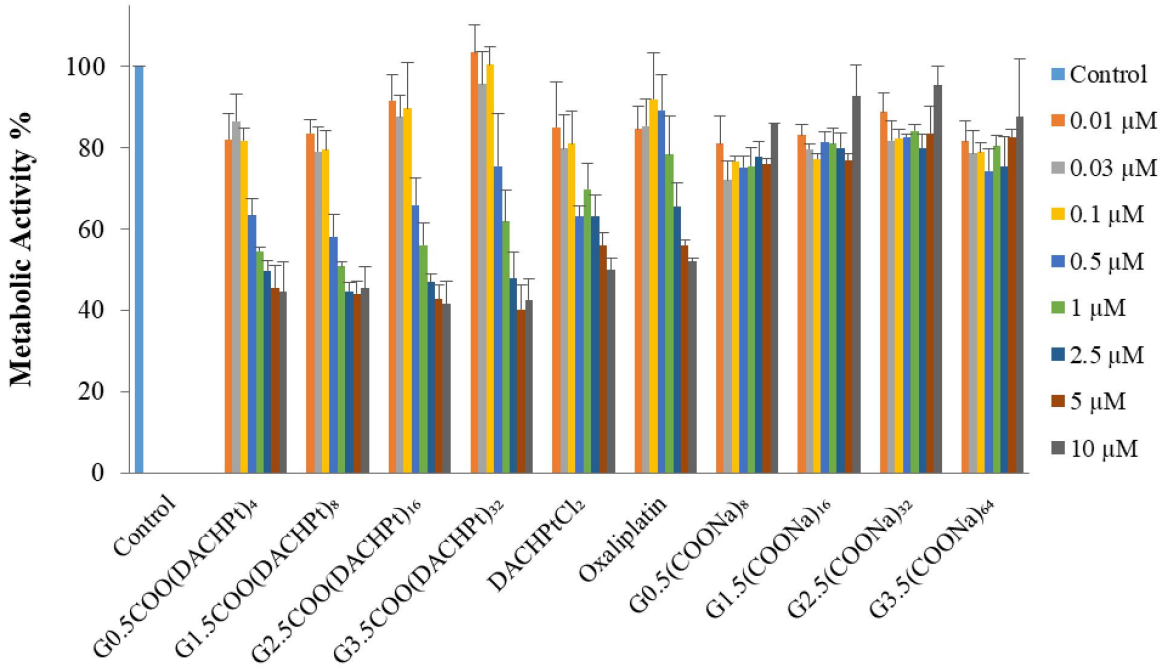

Figure D16: *In vitro* cytotoxicity studies of the DACHPt-metallodendrimers and anionic PAMAM dendrimers with different generations (0.5-3.5) on BJ cell line. The cells were treated for 72 h with a concentration range from 0.01 µM to 10 µM. The results are expressed as mean ± SD three independent experiments performed in triplicate.

Table D1: Relative potency (RP) of the DACHPt-metallodendrimers calculated from the division of the IC_{50} value of $DACHPtCl_2$ by the IC_{50} value of metallodendrimers.

Relative potency (RP)	**A2780**	**A2780CisR**	**MCF-7**	**CACO-2**
$G0.5COO(DACHPt)_4$	9.3	1	3.4	**> 55.6**
$G1.5COO(DACHPt)_8$	7	**2.9**	3.4	**> 40**
$G2.5COO(DACHPt)_{16}$	7	**1.6**	1.8	**> 28.6**
$G3.5COO(DACHPt)_{32}$	3.5	1.4	1.3	**> 25.6**

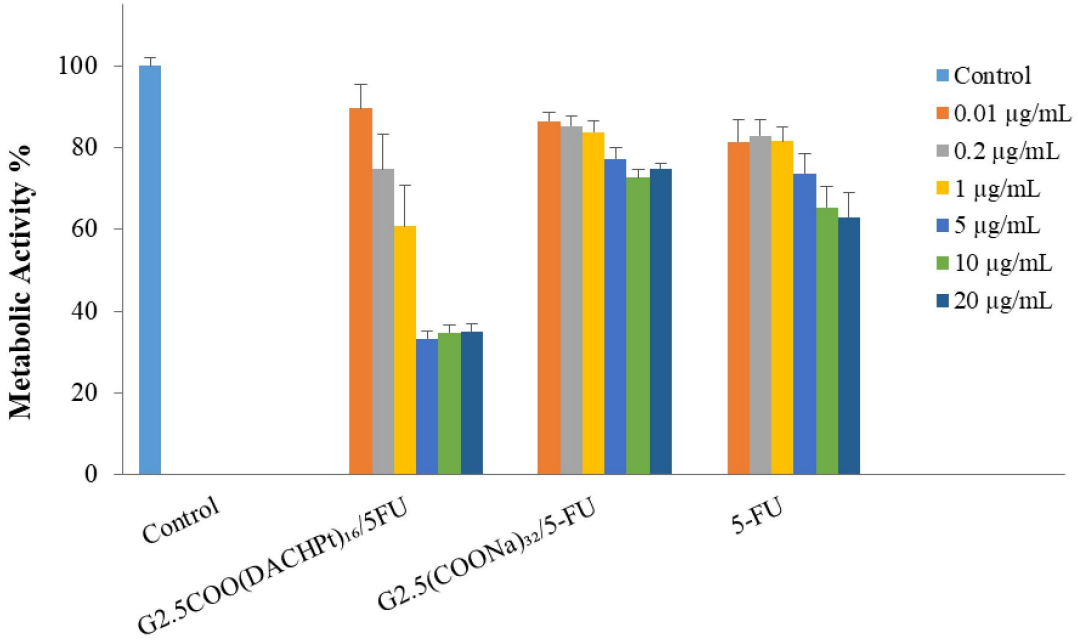

Figure D17: *In vitro* cytotoxicity studies of the complexes G2.5COO(DACHPt)$_{16}$/5-FU and G2.5(COONa)$_{32}$/5-FU and 5-FU on A2780CisR cell line. The cells were treated for 72 h with a concentration range from 0.01 µg/mL to 20 µg/mL. The results are expressed as mean ± SD three independent experiments performed in triplicate.

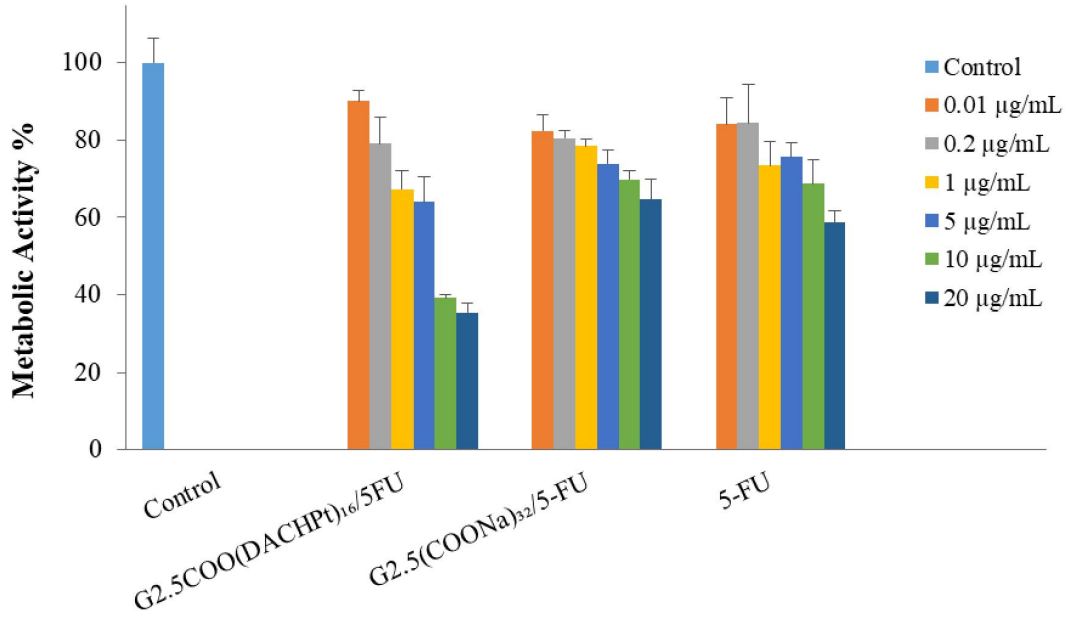

Figure D18: *In vitro* cytotoxicity studies of the complexes G2.5COO(DACHPt)$_{16}$/5-FU and G2.5(COONa)$_{32}$/5-FU and 5-FU on CACO-2 cell line. The cells were treated for 72 h with a concentration range from 0.01 µg/mL to 20 µg/mL. The results are expressed as mean ± SD three independent experiments performed in triplicate.

- DNA Binding studies

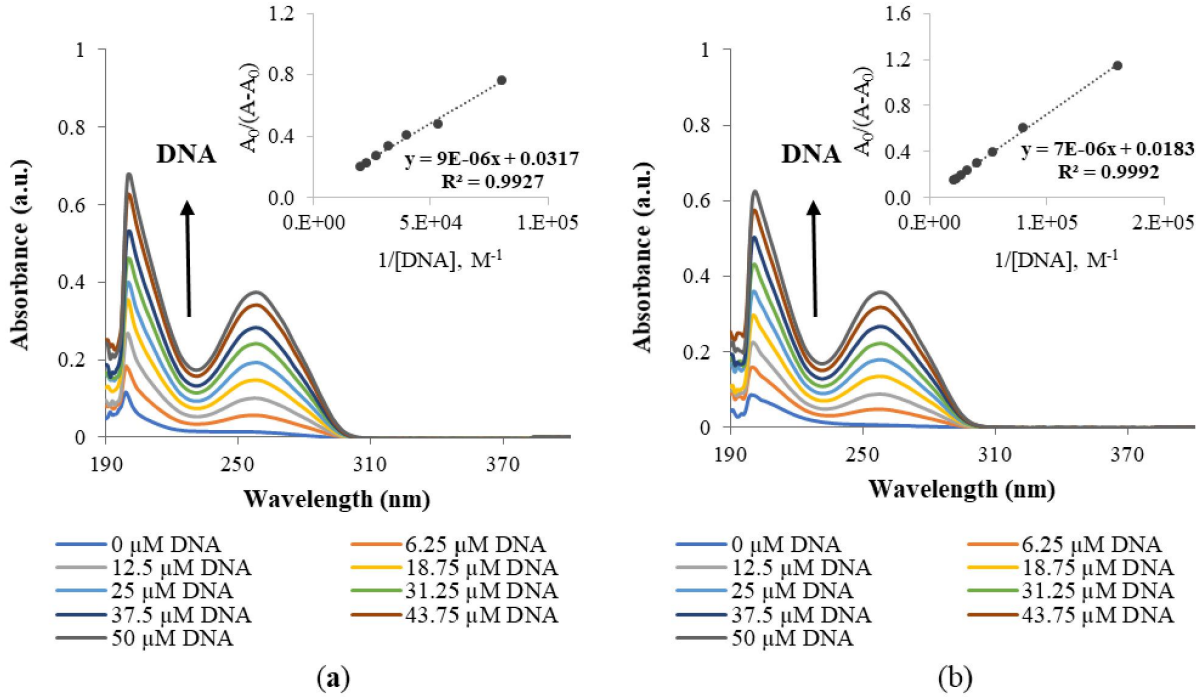

Figure D19: UV-visible spectra of oxaliplatin of a) 1st trial b) 2nd trial with increasing concentration of CT-DNA (0, 6.25, 12.5, 18.75, 25, 31.25, 37.5, 43.75 and 50 µM) in 5 mM Tris-HCl/50 mM NaCl at pH 7.4. The inset corresponds to the plot of $A_0/(A-A_0)$ versus 1/[DNA], which is used to determine the binding constant. The arrow indicates the direction of increasing the concentration of DNA.

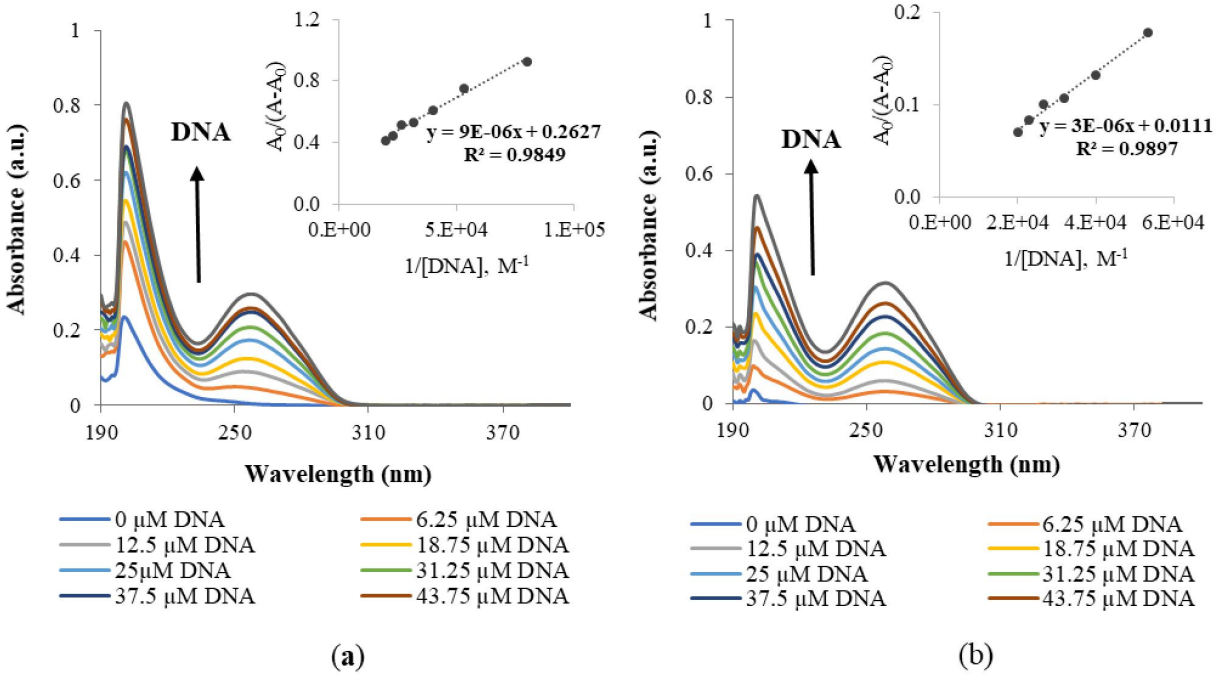

Figure D20: UV-visible spectra of 2nd trial a) G2.5COO(DACHPt)$_{16}$ and b) DACHPtCl$_2$ with increasing concentration of CT-DNA (0, 6.25, 12.5, 18.75, 25, 31.25, 37.5, 43.75 and 50 µM) in 5 mM Tris-HCl/50 mM NaCl at pH 7.4. The inset corresponds to the plot of $A_0/(A-A_0)$ versus 1/[DNA], which is used to determine the binding constant. The arrow indicates the direction of increasing the concentration of DNA.

- Complexes - characterization

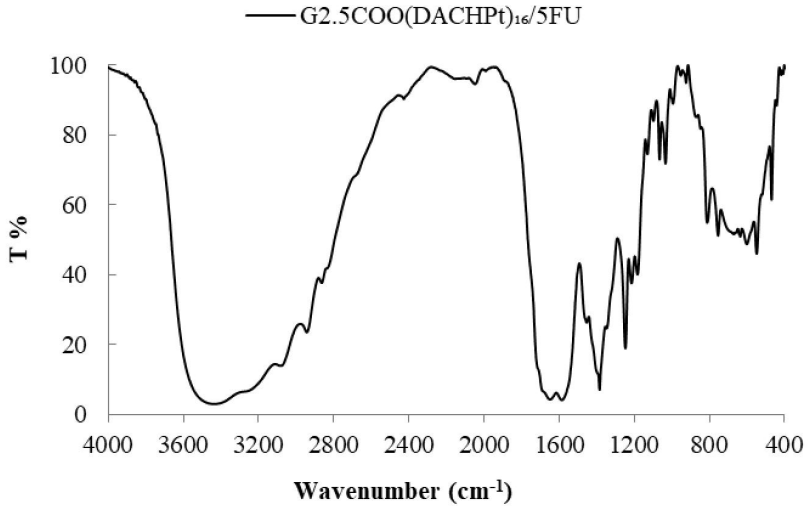

Figure D21: FTIR spectra of G2.5COO(DACHPt)$_{16}$/5-FU in KBr pellet.

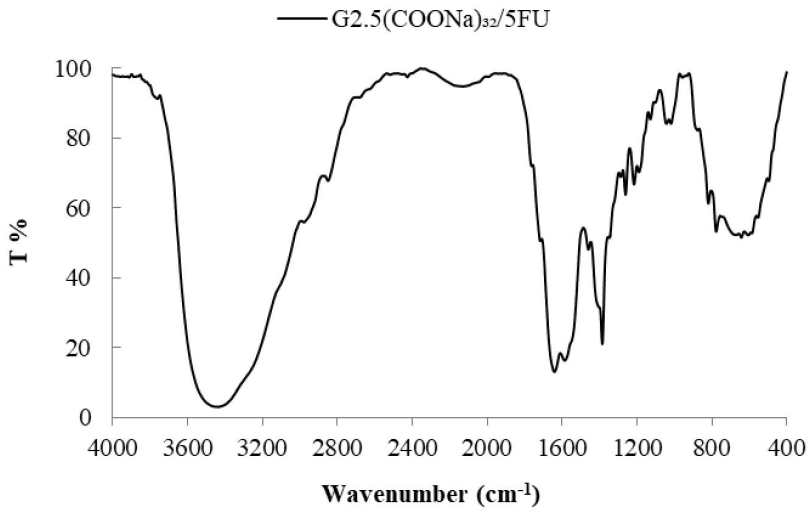

Figure D22: FTIR spectra of G2.5(COONa)$_{32}$/5-FU in KBr pellet.

E. Chapter IV: Intrinsic Blue fluorescence of oxidized PAMAM dendrimers

- Characterization of amine-terminated PAMAM dendrimers and APS-treated PAMAM dendrimers

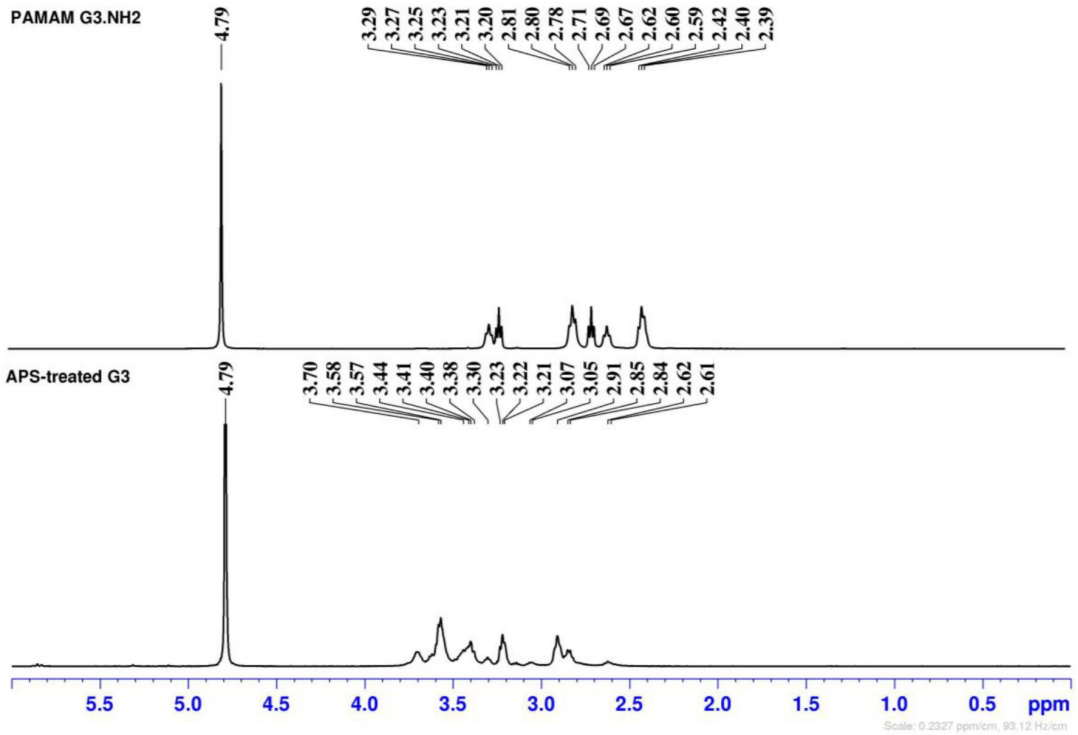

Figure E1: ^{1}H-NMR spectra of a) G3.NH_2 PAMAM dendrimer and b) APS-treated G3 in D_2O.

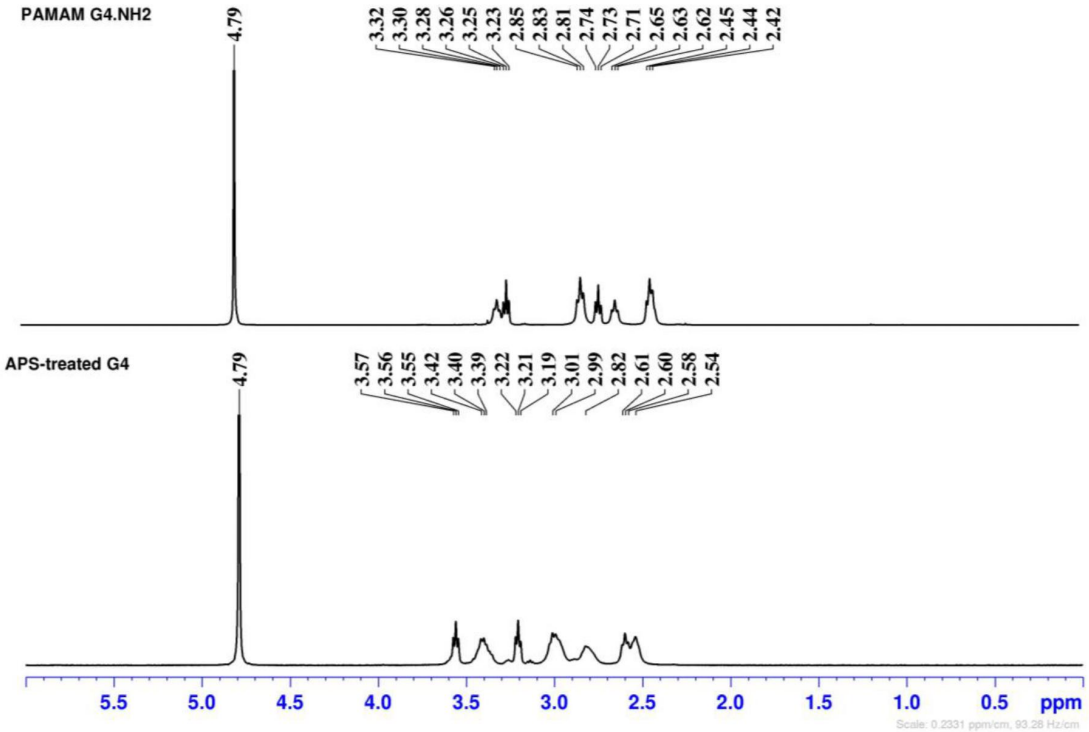

Figure E2: ^{1}H-NMR spectra of a) G4.NH_2 PAMAM dendrimer and b) APS-treated G4 in D_2O.

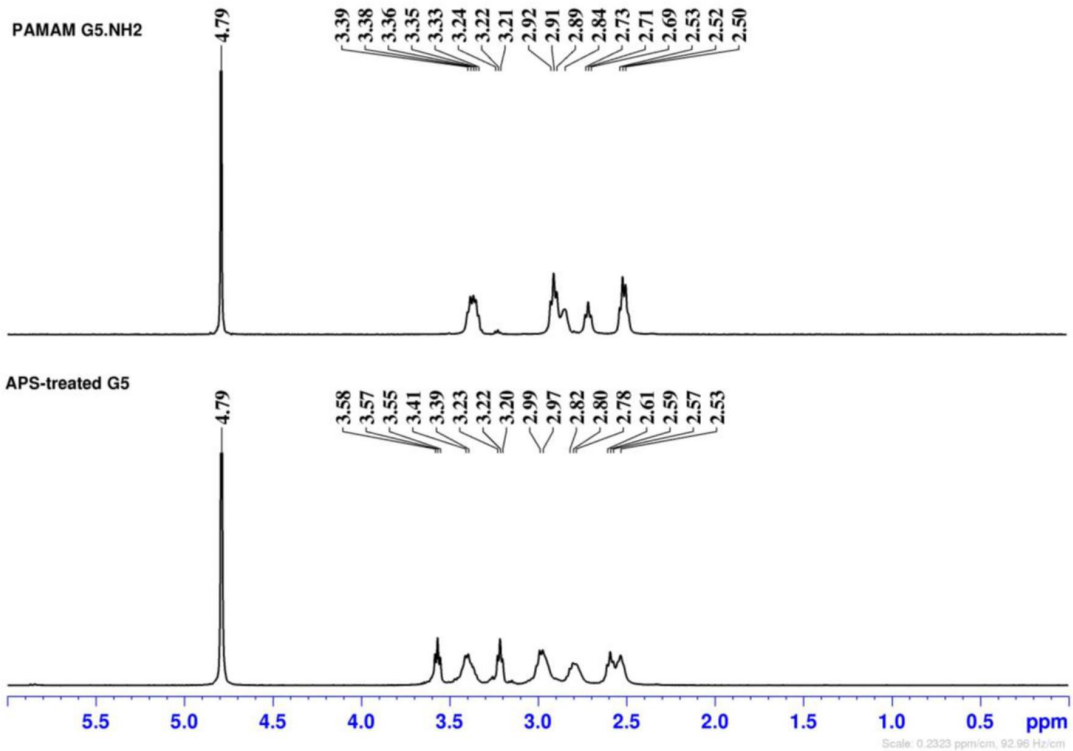

Figure E3: ^{1}H-NMR spectra of a) G5.NH_2 PAMAM dendrimer and b) APS-treated G5 in D_2O.

Table E1: Chemical structure of the APS-treated/pristine PAMAM dendrimers and the corresponding chemical shifts (in ppm) obtained by ^{1}H-NMR (in D_2O).

Chemical structure	***G3.NH₂***	***APS-treated G3.NH₂***	***G4.NH₂***	***APS-treated G4.NH₂***	***G5.NH₂***	***APS-treated G5.NH₂***
*-NCH₂C**H₂**CONH-*	2.40	2.85	2.43	2.59	2.51	2.57
*-CONHCH2C**H₂**N-*	2.60	3.22	2.63	2.87	2.71	2.80
*-CONHCH₂C**H₂**NH₂*	2.69	**3.40**	2.73	**3.20**	2.84	**3.21**
*-NC**H₂**CH₂CONH-*	2.80	**3.30**	2.83	**3.04**	2.90	**2.97**
*-CONHC**H₂**CH₂NH₂*	3.21	**3.69**	3.25	**3.56**	3.36*	**3.58**
*-CONHC**H₂**CH₂N-*	3.27	**3.57**	3.28	**3.40**	3.36*	**3.39**

*Signals are overlapping.

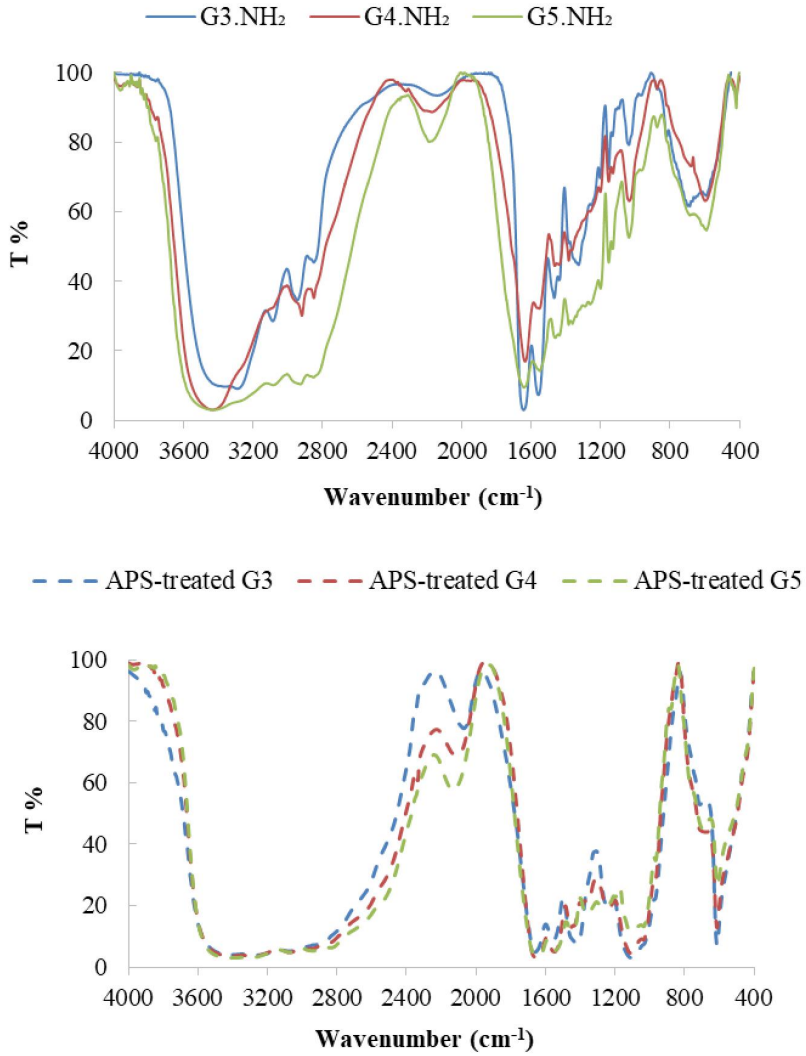

Figure E4: FTIR spectra of generations 3, 4, and 5 of the pristine/APS-treated PAMAM dendrimers (recorded in KBr pellets) – full scale.

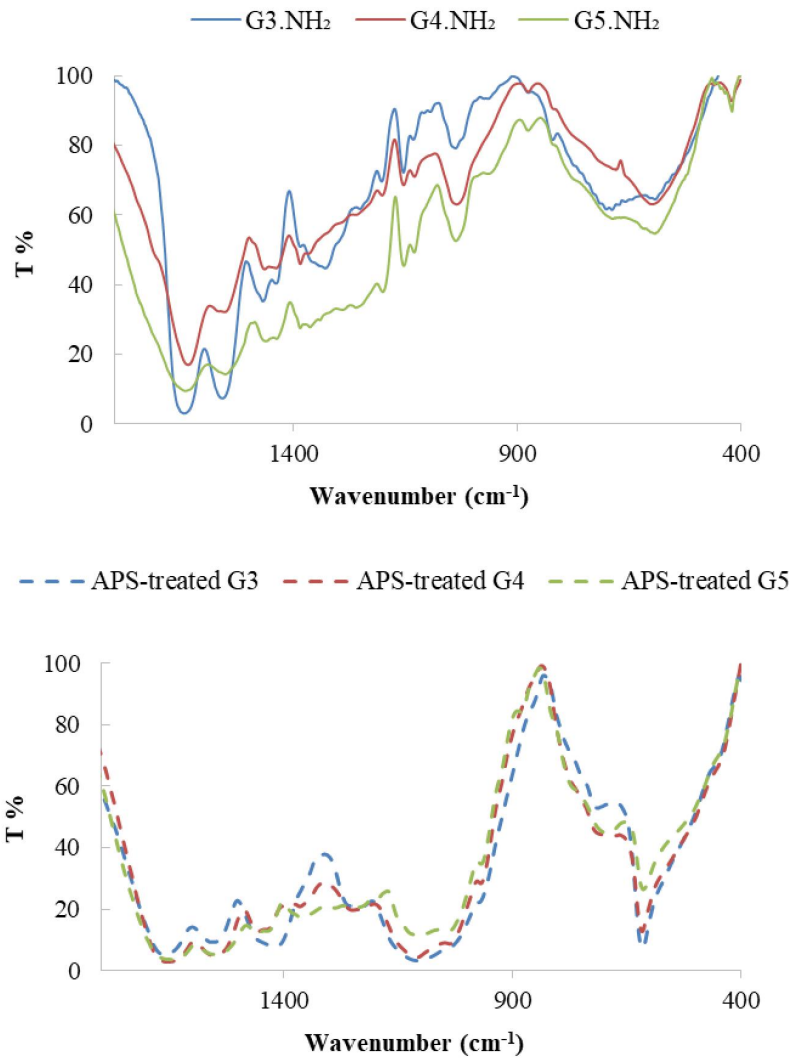

Figure E5: FTIR spectra of generations 3, 4, and 5 of the pristine/APS-treated PAMAM dendrimers (recorded in KBr pellets) – enlarged scale.

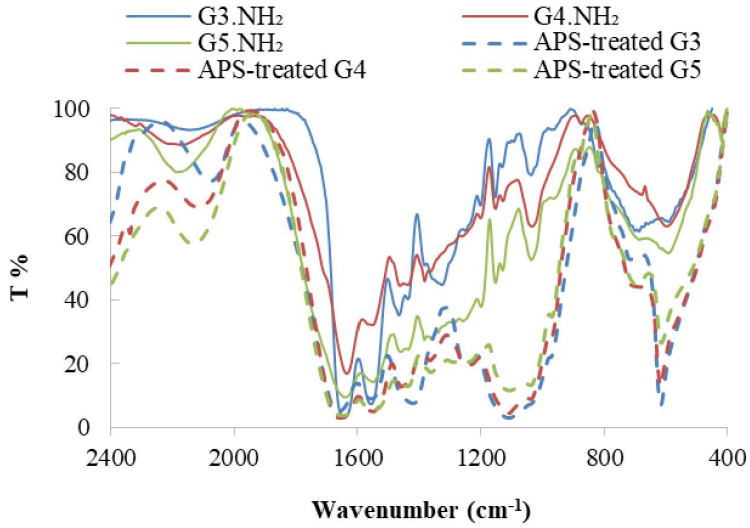

Figure E6: FT-IR spectra of generations 3, 4, and 5 of the pristine/APS-treated PAMAM dendrimers (recorded in KBr pellets) – enlarged scale (comparison among spectra).

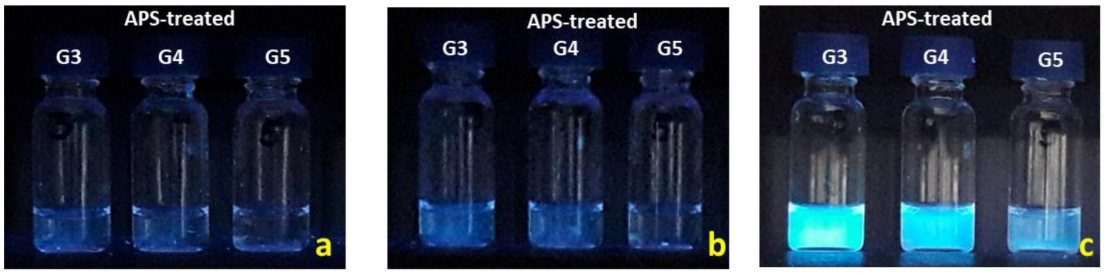

Figure E7: APS-treated PAMAM dendrimers under UV irradiation at 366 nm with a concentration of a) 1 x 10^{-6} M, b) 1 x 10^{-5} M, and c) 4.3 mg/600 µL (APS-treated G3: 1 x 10^{-3} M, APS-treated G4: 5 x 10^{-4} M and APS-treated G5: 2.5 x 10^{-4} M) in ultrapure water.

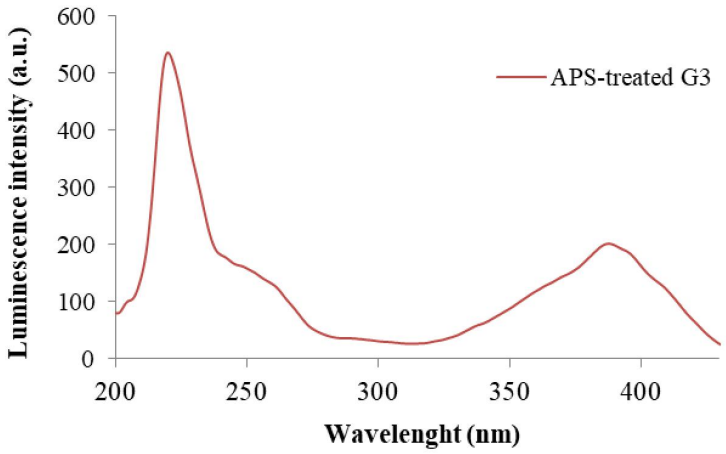

Figure E8: Enlarged excitation spectrum of generation 3 APS-treated dendrimers (λ_{em}= 450 nm) showing a band *ca.* 250 nm. The sharp band at 225 nm is due to second-order scattering. The spectrum was recorded at a 1 x 10^{-5} M concentration in ultrapure water.

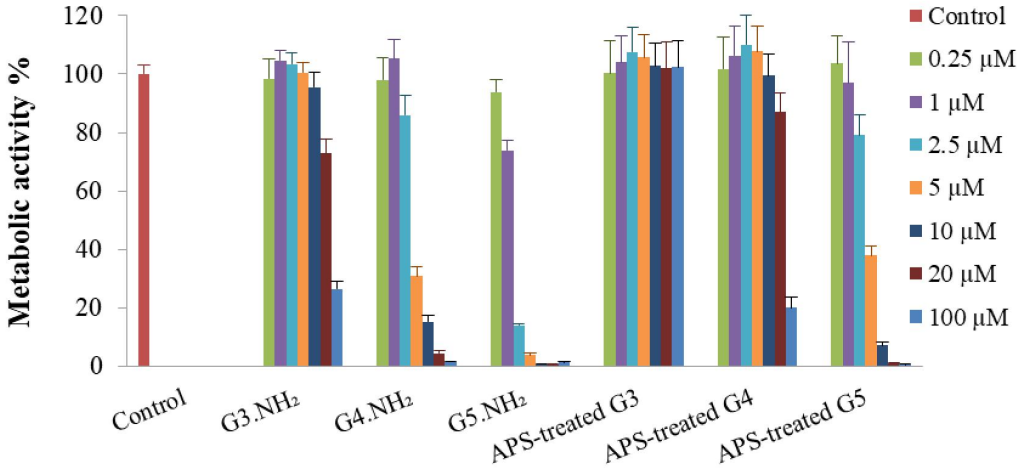

Figure E9: Cytotoxicity of pristine and APS-treated PAMAM dendrimers after 48 h of incubation using NIH 3T3 cell lines. The results are expressed as the mean ± SD of three in independent experiments with three replicas each.

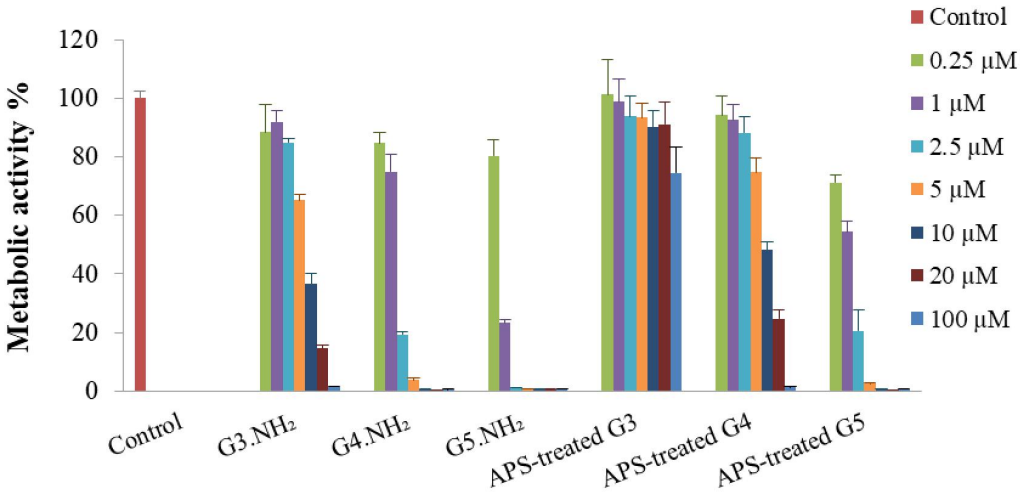

Figure E10: Cytotoxicity of pristine and APS-treated PAMAM dendrimers after 48 h of incubation using CAL-72 cell lines. The results are expressed as the mean ± SD of three independent experiments with three replicas each.

FCT Fundação para a Ciência e a Tecnologia
MINISTÉRIO DA CIÊNCIA, TECNOLOGIA E ENSINO SUPERIOR

Base Fund UIDB/00674/2020
Programmatic Fund UIDP/00674/2020

M1420-01-0145-FEDER-000005 - CQM+
(Madeira 14-20 Program)

Projet M1420 - 09-5369-FSE-000001- PhD Grant

Doctoral Program in Nuclear Magnetic Resonance Applied
to Chemistry, Materials and Biosciences (PTNMR PhD)

Cofinanciado por:

A Nossa Universidade

Colégio dos Jesuítas
Rua dos Ferreiros - 9000-082, Funchal

Tel: +351 291 209400
Fax: +351 291 209410
Email: gabinetedareitoria@uma.pt

Cofinanciado por:

MADEIRA 14-20 · REGIÃO AUTÓNOMA DA MADEIRA · PORTUGAL 2020 · UNIÃO EUROPEIA Fundo Social Europeu · arditi